The role of the strange quark in chiral symmetry breaking

Sebastien Descotes-Genon

Faculté des Sciences d'Orsay

Mémoire d'Habilitation à Diriger les Recherches
présenté

par

Sébastien Descotes-Genon

Le rôle du quark étrange dans la brisure de la symétrie chirale

le 12 octobre 2011 devant la Commission d'Examen

Mme	B.	Bloch-Devaux	Examinateur
MM.	M.	Davier	Président
	M.	Knecht	Rapporteur
	U.-G.	Meißner	Rapporteur
	Ch.	Sachrajda	Examinateur
	A.	Pich	Rapporteur

Laboratoire de Physique Théorique, Bat 210, F-91406 Orsay Cedex, France.
– Unité Mixte de Recherche 8627 CNRS/Univ. Paris-Sud 11 –

Contents

What is the use of a book, without pictures or conversations?

Alice

1 Invitation

1.1 The enigma of the strongly coupled regime of QCD

After a century trying to understand matter at the smallest possible distances, physicists have obtained a remarkably efficient description of its structure and dynamics. The Standard Model of particle physics is not only a very satisfying phenomenological description of physics at the subatomic scales, but it is also the proof that quantum mechanics and relativity, combined in quantum field theories, are essential to provide accurate predictions concerning elementary particles [1–4]. Among the most remarkable proofs are the very high accuracy up to which theory and experiment agree concerning the electroweak precision tests performed at the Z-pole [5] and the determination of the anomalous moment of charged leptons [6–9].

However, this very satisfying situation has a less-than-satisfying corollary: the very structure of quantum field theories imply the running of the couplings when the scales change. This yield the fact that theories, at least in some energy range, are strongly coupled and cannot be tackled with the theorists' favourite tool, namely perturbation theory. If this issue is not particularly pressing in the electroweak sector of the Standard Model – the energy range where the problem would occur are so high that we expect other, new phenomena to set in much before – it is an essential feature of the strong interaction, which at low energies binds the quarks and gluons of the theory into the experimentally observed hadrons [10–13].

Our limited understanding of strongly coupled theories is a problem within the Standard Model, as we lack the dictionary to describe the hadronisation relating both worlds. This problem is for instance acute when one wants to describe weak transitions between quarks and extract the the Cabibbo-Kobayashi-Maskawa matrix elements from experimental data [14]. Moreover, this limitation hinders the exploration of strongly coupled theories for models of New Physics (for instance, alternatives to the Higgs model of electroweak symmetry breaking [15–17]), which are generally assumed to be weakly coupled not for fundamental reasons, but mainly because of the difficulties faced by theorists otherwise.

One can turn the tables and consider Quantum Chromodynamics as the best playground to understand strongly coupled gauge theories. And before understanding such a theory, one must be able to describe it. In the limit where the light quarks become massless, the low-energy dynamics of QCD is governed by the spontaneous breakdown of a global symmetry, chiral symmetry, and by the dynamics of its corresponding Goldstone bosons, which correspond to the pions, kaons and eta meson. The presence of very light degrees of freedom whose dynamics obeys an underlying symmetry makes low-energy QCD particularly appealing for the use of effective field theory.

The programme is very similar to the general objectives of quantum field theory, but with restrictions on the degrees of freedom and the range of energies relevant for the problem at hand [3, 18, 19]. The effective theory is then organised as an expansion in powers of small parameters, based on a power counting related to the hierarchy of the scales involved. This concept of effective theory has proved particularly fertile in many different areas (heavy quark systems, jet physics, technicolor models of electroweak symmetry breaking...), and it has even modified our view of the Standard Model, now considered "only" as the effective description of a more fundamental theory, yet to be discovered.

Chiral perturbation theory [20–22] follows this program by providing the low-energy expansion of QCD correlators of vector and axial currents as well as pseudoscalar and scalar densities, as series in powers of momenta and quark masses. The unknown low-energy dynamics of QCD is embedded in low-energy constants that proliferate as one goes to higher and higher orders in the expansion. However, if one sticks to a given order of the expansion (i.e., hopefully, to a given accuracy), one has to deal to a finite number of unknown constants to be fixed from

experiment or other theoretical computations (lattice simulations, analytic models...). These low-energy constants are also related to (generally non-local) chiral order parameters. Chiral perturbation theory can be seen as the most efficient way to organise and hopefully reduce our ignorance on low-energy QCD according to the symmetries known to operate in the domain of energy that we are interested in.

One can consider such a theory under several angles: *a)* on the theoretical side, to determine the pattern of chiral symmetry breaking from experiment or from specific models (resonance saturation [23–28], Nambu-Jona-Lasinio [29,30], AdS/QCD models [31–33]...), *b)* on the phenomenological side, to make predictions on some observables by reexpressing them in terms of other, already measured, quantities, *c)* as a tool to perform extrapolations in quark masses, for instance for lattice simulations performed at values higher than the physical ones. These three avenues have generated a lot of activities over the last decades.

One of the main difficulties in this game comes from the fact that not all low-energy constants are "born equal": some can be determined quite easily (those related to the energy dependence of form factors, for instance), whereas others are much more difficult to pin down (those related to the quark-mass dependence of quantities, or involving scalar densities). This explains that the situation remains still unclear concerning the values of some of the low-energy constants, and more generally concerning the pattern of chiral symmetry breaking.

In this picture, the strange quark is known to play a particular role, due to its intermediate mass. It is light enough for a chiral expansion in powers of m_s/Λ_H (where Λ_H is the typical hadronic scale of order 1 GeV) to make sense, at least in principle. On the other hand, it is sufficiently close to the perturbative scale Λ_{QCD} (a few hundred MeV) so that the impact of the sea $s\bar{s}$ pairs on the structure of the QCD vacuum are not negligible, but difficult to assess. In view of this, it makes sense to discuss and compare two different chiral limits of potential phenomenological interest, namely the $N_f = 2$ chiral limit, where only the u and d quarks are taken as massless, and the $N_f = 3$ where the strange quark mass is also sent to zero.

The differences induced in the pattern of chiral symmetry breaking by the variation of the strange quark mass affect the three aspects discussed above *a)* theoretically, a substantial difference between the two chiral limits is an indication of the role played by massive quarks on the chiral structure of QCD vacuum, *b)* phenomenologically, the matching between $N_f = 2$ and $N_f = 3$ chiral perturbation theories is often performed to improve the accuracy of their respective predictions thanks to sharpened estimates of the low-energy constants of both theories, based on the assumption that the patterns of symmetry breaking are not very different, and *c)* the chiral extrapolations for lattice quantities might have to be revisited since they often rely on a $N_f = 3$ chiral perturbation theory, in particular to extrapolate matrix elements involving kaons and η.

What is the role of the strange quark in chiral symmetry ? Are the patterns of chiral symmetry breaking similar or different in the two- and three-flavour chiral limits ? A part of my work has been devoted to these questions, with interesting hints that this role is important, ant that they might be significant differences between the chiral order parameters describing these two chiral limits. The present document is an attempt to summarise my efforts on this subject. As indicated earlier, the comparison with experimental data and with lattice results is obviously essential here, and I tried as much as possible to recall the context in which these issues are discussed, with the ultimate hope of understanding some features of the dynamics strongly-coupled gauge theories.

1.2 A hitchhiker's guide to this manuscript

An Habilitation à Diriger les Recherches is one of these formal exercises that the French seem to be fond of, like the *dissertation* for the Baccalauréat, or the *note de synthèse* for the *concours de la fonction publique* to become a civil servant, up to the point that its form may matter more than its content or purpose. In the particular case of the Habilitation, the expectations are sometimes unclear, and the answers range from the raw collection of papers to the little encyclopedia or a scientist's memoirs. I have tried to consider the exercise as an opportunity to gather several works that are connected by a single line of research but were interspersed with other activities in particle physics over time. This is the main purpose of the present manuscript, where I have tried to clean up and make more consistent some of the discussions that can be found in my articles, and I have decided to focus on the question of the role of the strange quark in this document to keep an internal consistency in its development. It is clear that it represents only a particular section of my research activities, which has been concerned with various aspects of flavour physics – not only concerned with strangeness, but also with charm and beauty, as well as the global analysis of flavour transitions within and beyond the Standard Model. This choice has the drawback of requiring more space (and more details) than a simple collection of papers, and probably more time to the reader. I hope that he/she will however appreciate my efforts to structure the discussion, and to save his/her time thanks to the present overview.

Each of the chapter can be seen as the summary of one or several articles, which I will recall in the introduction of each chapter:

- *Ch. 2: Chiral symmetry breaking and the number of light flavours* discusses general features of chiral symmetry breaking in QCD. A representation of chiral order parameters in terms of the Euclidean Dirac operator is then introduced, highlighting the role of the fermion determinant, as well as the potential dependence of the order parameters on vacuum light-quark loops and on the number of massless fermions of the theory. In particular, a bound on the eigenvalues of the Dirac operator, derived by Vafa and Witten, shows that the order parameters should decrease when one goes from $N_f = 2$ to $N_f = 3$ chiral limits. Connections with the structure of the scalar sector, that shares the same quantum numbers as the vacuum, are then discussed. I end with a speculative discussion of the evolution of the pattern of chiral symmetry breaking as the number of light (or massless) quarks increases.

  [A] SDG, L. Girlanda, and J. Stern, *Paramagnetic effect of light quark loops on chiral symmetry breaking*, JHEP 0001 (2000) 041 [34]

  [B] SDG, *Finite volume analysis of N_f-induced chiral phase transitions*, Phys. Rev. D 62 (2000) 054011 [35]

- *Ch. 3: Chiral perturbation theory and its limits* recalls basics of the effective descriptions of low-energy QCD in terms of the pseudo-Goldstone bosons associated to chiral symmetry breaking. I discuss in particular the current situation concerning the determination of the low-energy constants. The issue of the convergence of three-flavour χPT is raised, and I discuss the conditions under which the chiral expansions of pseudoscalar masses and decay constants are saturated by their leading order. Next-to-leading order low-energy constants, suppressed by the Zweig rule but enhanced by the large value of the strange quark, are shown to play an essential role in the discussion. If they deviate from very specific values, this might lead to a significant competition between formal

leading- and next-to-leading orders in the three-flavour chiral expansions. I discuss also the two-flavour chiral expansions, and show that the matching with three-flavour chiral series provide interesting correlations between $N_f = 2$ order parameters and the quark mass ratio $r = 2m_s/(m_u + m_d)$.

[C] SDG and J. Stern, *Vacuum fluctuations of $q\bar{q}$ and values of low-energy constants*, Phys. Lett. B488 (2000) 274 [36]

[D] SDG, L. Girlanda, and J. Stern, Chiral order and fluctuations in multi-flavor QCD, Eur. Phys. J. C27 (2003) 115 [37]

[E] SDG, N. Fuchs, L. Girlanda, and J. Stern, *Resumming QCD vacuum fluctuations in three-flavor chiral perturbation theory*, Eur. Phys. J. C34 (2004) 201 [38]

- *Ch. 4: The m_s-dependence of the quark condensate* estimates the two-point correlator $\langle(\bar{u}u)(\bar{s}s)\rangle$ that assesses the dependence of the $N_f = 2$ chiral condensate on the strange-quark mass. This correlator is determined from rapidly convergent sum rules, which are saturated by pion and kaon scalar form factors. The latter, which cannot be determined experimentally, are reconstructed from models of scattering between $\pi\pi$ and $K\bar{K}$ states. However, the normalisation of these scalar form factors is unknown, but can be related to the quark-mass dependence of the kaon and pion masses. The sum rule yields finally constraints between the values of three-flavour order parameters and the quark mass ratio r, indicating a significant suppression of the quark condensate from the two- to the three-flavour chiral limits.

  [F] SDG, *Zweig rule violation in the scalar sector and values of low-energy constants*, JHEP 0103 (2001) 002 [39]

- *Ch. 5: An alternative treatment of three-flavour chiral series* considers how to treat chiral series when the pattern of chiral symmetry breaking yields a numerical competition between leading- and next-to-leading-order chiral perturbation theory. We propose a framework to treat chiral series in such a situation, and apply it to the case of several form factors of phenomenological interest (pion and kaon electromagnetic ones, $K_{\ell 3}$ vector and scalar form factors). We confront these chiral expansions to lattice determinations of the masses, decay constants, and form factors by two collaborations (RBC/UKQCD and JLQCD). We then extract information on the three-flavour chiral order parameters and compare the fits obtained with our formulae to alternative procedures.

  [G] SDG, *The Role of strange sea quarks in chiral extrapolations on the lattice*, Eur. Phys. J. C40 (2005) 81 [40]

  [H] V. Bernard, SDG, and G. Toucas, *Chiral dynamics with strange quarks in the light of recent lattice simulations*, JHEP 1101 (2011) 107 [41]

- *Ch. 6: $\pi\pi$ scattering : experimental and dispersive constraints* turns to experimental constraints on the pattern of two-flavour chiral symmetry breaking. I first describe the main tool of analysis, the solutions of the dispersive constraints obeyed by the $\pi\pi$ scattering amplitude in the isospin limit and known as Roy equations. Then I describe the extraction of two-flavour chiral order parameters from $K_{\ell 4}$ data, considering first the E865 data as an illustration of the method, before turning to the more recent and more accurate phase shifts provided by the NA48/2 collaboration. I discuss the importance of isospin corrections and provide a sketch of a dispersive estimate of these corrections,

before giving updated results for the $N_f = 2$ pattern of chiral symmetry breaking from these data.

[I] SDG, N. Fuchs, L. Girlanda, and J. Stern, Analysis and interpretation of new low-energy $\pi\pi$ scattering data, Eur. Phys. J. C24 (2002) 469 [42]

[J] SDG, M. Knecht, V. Bernard, in preparation [43]

- *Ch. 7: πK scattering : experimental and dispersive constraints* turns to experimental constraints on the pattern of three-flavour chiral symmetry breaking. I recall how two sets of dispersion relations (fixed-t and hyperbolic) can be jointly used to constrain low-energy πK scattering from information extracted at higher energy. These Roy-Steiner equations have a more complicated structure than the Roy equations, as the crossed channel involves $\pi\pi \to K\bar{K}$ transitions which is not related to πK scattering. The two subtraction parameters needed are chosen as the two S-wave scattering lengths, which are found to be larger than the NLO χPT estimates. I also recall how the existence and the parameters of the κ resonance can be inferred from the same dispersion relations extended to the complex energy plane.

  [K] P. Büttiker, SDG, and B. Moussallam, *A new analysis of πK scattering from Roy and Steiner type equations*, Eur. Phys. J. C33 (2004) 409 [44]

  [L] SDG and B. Moussallam, *The $K^*0(800)$ scalar resonance from Roy-Steiner representations of πK scattering*, Eur.Phys.J. C33 (2004) 409-432 [45]

- *Ch.8 : Three-flavour chiral symmetry breaking according to $\pi\pi$ and πK scatterings* provides combines the two previous chapters. After reconstructing the $\pi\pi$ and πK amplitudes in the subthreshold region (below the opening of physical channels), I match them to chiral representations allowing for a competition between leading and next-to-leading order. The extraction of the values of the various low-energy constants is obtained within a frequentist approach yielding confidence intervals for the three-flavour chiral order parameters as well as the quark mass ratio r.

  [M] SDG, *Low-energy $\pi\pi$ and πK scatterings revisited in three-flavour resummed chiral perturbation theory*, Eur. Phys. J. C52 (2007) 141 [46]

Some sections/subsections are essentially repetitions/slight updates of the above article(s). In this case, the heading will exhibit in brackets the corresponding references, to save the reader's time in the case that he/she knows already the content of the paper. In the same spirit, the introduction and the conclusion should provide the main ingredients/arguments of the chapter, and should be self-sufficient for a first approach and quick browsing through this document. In the same spirit, the last chapter *Outlook* recalls the main conclusions of the present manuscript, before discussing some further perspectives.

Let me see: four times five is twelve, and four times six is thirteen, and four times seven is – oh dear! I shall never get to twenty at that rate !

Alice

2

Chiral symmetry breaking and the number of light flavours

Chiral symmetry and its spontaneous breakdown are known to govern low-energy QCD. This phenomenon justifies the mass gap between the pseudoscalar mesons (identified to Goldstone bosons of the broken symmetries) and the rest of the spectrum. In principle, the mass hierarchy between the various light quarks allows one to consider two different chiral limits of interest, with $m_{u,d} \to 0$, but m_s either kept at its physical value or sent to zero, a.k.a., $N_f = 2$ and $N_f = 3$ chiral limits (N_f denoting the number of massless flavours). In each limit, one can define several order parameters to describe the pattern of chiral symmetry breaking, among which the best known are the quark condensate and the pseudoscalar decay constant. Depending on the pattern of chiral symmetry breaking, the quark condensate can be large or small compared to the other scales of the theory, but the decay constant, describing the coupling of the Goldstone bosons to the axial currents, must be non-vanishing for chiral symmetry to be broken.

One can gain further insight into these order parameters by considering QCD on an Euclidean torus. Correlators are then expressed as averages over gluonic configurations of functions of the Dirac operator eigenvectors and eigenvalues. Chiral order parameters turn out to be dominated by the accumulation of low eigenvalues around zero as the volume of the torus becomes large, but the quark condensate and the pseudoscalar decay constant are not sensitive to the same kind of accumulation, opening the possibility of having two different chirally broken phases (with or without a quark condensate). Moreover, one can expect that such infrared-dominated quantities are particularly sensitive to the low Dirac eigenvalues coming from the fermionic determinant contained in the average over gluonic configurations. A bound derived by Vafa and Witten leads to the fact that the fermionic determinant suppresses infrared-dominated quantities, all the more efficiently that there are more light (or massless) flavours in the theory.

This observation yields naturally the question whether this suppression is weak or strong in the transition from $N_f = 2$ to $N_f = 3$, i.e. when the strange quark mass is shifted from its physical value down to zero. In the case of the quark condensate, one can express the difference between $\Sigma(2)$ and $\Sigma(3)$ as an m_s-enhanced correlator violating the Zweig rule (or suppressed in the large-N_c limit) in the scalar sector, where it is known to be badly satisfied. There is therefore a tantalising connection between the well-known issues raised by the wide and elusive scalar resonances and the m_s-dependence of the chiral structure of QCD vacuum which has the same quantum numbers. It turns out that a rather natural scenario with significant fluctuations of small Dirac eigenvalues could yield to a strong suppression of $N_f = 3$ order parameters compared to their $N_f = 2$ counterparts. We conclude by some considerations on the dependence of the pattern of chiral symmetry breaking if one adds more and more light flavours, including the possibility a chirally-broken phase with a vanishing quark condensate [1].

2.1 Chiral symmetry of strong interactions

2.1.1 The QCD Lagrangian

The well-established light mesons and baryons can be organised in multiplets with very similar masses. The first example is provided by isospin multiplets $(n,\ p)$, $(\pi^-,\ \pi^0,\ \pi^+)$, $(\Delta^-,\ \Delta^0,$

[1] This chapter is based on the following articles:

[A] SDG, L. Girlanda, and J. Stern, *Paramagnetic effect of light quark loops on chiral symmetry breaking*, JHEP 0001 (2000) 041 [34]

[B] SDG, *Finite volume analysis of N_f-induced chiral phase transitions*, Phys. Rev. D 62 (2000) 054011 [35]

Δ^+, Δ^{++})... This symmetry is satisfied experimentally with a high accuracy (typical isospin-violating corrections are rarely above a few %). These isospin multiplets themselves can be organised in octets such as (π, K, η) and decuplets like $(\Delta, \Sigma, \Xi, \Omega)$ collecting both strange and non-strange particles. The mass differences are more significant, from 10 to 30 %. An approximate flavour symmetry, $\mathrm{SU}_V(3)$, putting the three light quarks u, d, s on the same footing, can account for this spectrum – some of its irreducible representations correspond to the observed octets and decuplets. In addition, the octet of lightest pseudoscalar mesons (pions, kaons, eta) stands out because of their masses[2] significantly lower than the typical hadronic scale of 1 GeV, but also the masses of other resonances (vector and axial mesons, excited pseudoscalar states, baryons). If this octet had a vanishing mass, its elements would be identified with Goldstone bosons from the spontaneous breakdown of a global continuous symmetry. As suggested above, a residual symmetry group $\mathrm{SU}_V(3)$ would be responsible for the degeneracy of the hadronic spectrum according to octets and decuplets.

These observations were actually the starting point for the quark model proposed by Gell-Mann and Zweig [47, 48]. It was amended later by Han, Nambu, Greenberg and Gell-Mann [49–51] through the introduction of colour to cope with the incompatibilities between the baryon spectrum (and in particular the Δ^{++}) with the spin-statistics theorem. Subsequent progress led finally to the now accepted quantum field theory for strong interactions, Quantum Chromodynamics (QCD) [1–4]. It is based on a local colour symmetry group $\mathrm{SU}_C(3)$, generated by the Gell-Mann matrices T^α ($\alpha = 1 \dots 8$) following the commutation relations $[T^a, T^b] = i f^{abc} T^c$, with f^{abc} the corresponding structure constants defining the Lie algebra. The quarks transform under the fundamental representation of this group, whereas the gauge bosons of the interaction, the gluons, transform under the adjoint representation. We can split the QCD Lagrangian into several parts:

$$\mathcal{L}_{\mathrm{QCD}} = \mathcal{L}_g + \mathcal{L}_q + \mathcal{L}_m + \mathcal{L}_f, \qquad \mathcal{L}_g = -\frac{1}{4} G^{\alpha;\mu\nu} G^\alpha_{\mu\nu} - \frac{g^2}{32\pi^2} \theta \, \tilde{G}^{\alpha;\mu\nu} G^\alpha_{\mu\nu}, \quad (2.1)$$

$$\mathcal{L}_q = \sum_Q \bar{Q}(i\not{D} - M_Q)Q + \sum_q \bar{q} i \not{D} q, \qquad \mathcal{L}_m = -m_u \bar{u}u - m_d \bar{d}d - m_s \bar{s}s. \quad (2.2)$$

The gluonic tensor is $G^a_{\mu\nu} = \partial_\mu A^a_\nu - \partial_\nu A^a_\mu + g f^{abc} A^b_\mu A^c_\mu$, and the covariant derivative is $\not{D} = \gamma^\mu D_\mu = \gamma^\mu(\partial_\mu - i g G^\alpha_\mu T^\alpha)$. $\mathcal{L}_g$ collects the pure gauge terms: the kinetic gluonic part and a topological term involving the vacuum angle θ [52, 53] and the dual of the gluonic tensor: $\tilde{G}^{\alpha;\rho\sigma} = \epsilon^{\mu\nu\rho\sigma} G^\alpha_{\mu\nu}/2$. This topological term induces $\mathcal{P}$ et $\mathcal{T}$ violation, and measurements on the dipole electric moment of the neutron constrain the vacuum angle θ to be very small, below 10^{-10} [52–54] [3]. $\mathcal{L}_f$ contains the gauge-fixing term and the associated Fadeev-Popov ghosts. $\mathcal{L}_m$ singles out the mass terms for the light quarks. The other fermionic terms are collected in $\mathcal{L}_q$, where Q denotes the heavy quarks (c, b, t) and q the light quarks (u, d, s). The separation between light and heavy quarks reflect the strong hierarchy among the masses, and the fact that only three of them are light compared to the typical QCD scale.

[2] Unless specified otherwise, we always take for the pseudoscalar masses and decay constants (see sec. 3.5.1 for more detail):

$$M_\pi = 0.13957 \text{ GeV}\,, M_K = 0.4957 \text{ GeV}\,, M_\eta = 0.5478 \text{ GeV}\,, F_\pi = 0.0922 \text{ GeV}\,, F_K/F_\pi = 1.19\,, \mu = 0.770 \text{ GeV}\,.$$

Apart from some sections in ch. 6, we work in the isospin limit at all time.

[3] The smallness of this CP-violating quantity is not explained in the Standard Model, and has led many proposals of extensions to justify it, in particular, the Peccei-Quinn symmetry with the occurrence of axion particles [55, 56].

This Lagrangian exhibits for each quark flavour a global phase symmetry $U(1)$. But $\mathcal{L}_q$, which describes the light quarks in the chiral limit of $N_f = 3$ massless quarks $m_u = m_d = m_s = 0$ has a larger symmetry group, which can be highlighted by projecting the quarks over their right and left chiralities

$$q_R = \frac{1+\gamma_5}{2}q, \qquad q_L = \frac{1-\gamma_5}{2}q. \tag{2.3}$$

In the limit of a massless fermion, chirality can be identified with helicity (the projection of spin along the momentum) and the left and right sectors decouple:

$$\mathcal{L}_q = \sum_Q \bar{Q}(i\not{D} - M_Q)Q + \sum_q \bar{q}_R i\not{D} q_R + \sum_q \bar{q}_L i\not{D} q_L \tag{2.4}$$

This decomposition brings the chiral symmetry group: $G = \mathrm{SU}_L(3) \otimes \mathrm{SU}_R(3) \otimes \mathrm{U}_V(1)$, a global symmetry group acting in the flavour-chirality space. $\mathrm{U}_V(1)$ is a vector phase group, which acts identically on the two chiralities:

$$q_L \to e^{i\delta} q_L, \qquad q_R \to e^{i\delta} q_R. \tag{2.5}$$

The flavour triplets transform under the non-Abelian part of G as:

$$\psi_L = \begin{pmatrix} u_L \\ d_L \\ s_L \end{pmatrix} \to V_L \psi_L, \qquad \psi_R = \begin{pmatrix} u_R \\ d_R \\ s_R \end{pmatrix} \to V_R \psi_R. \tag{2.6}$$

At the classical level, there is a further flavour-singlet axial symmetry: $\psi_L \to e^{i\delta}\psi_L, \psi_R \to e^{-i\delta}\psi_R$, but the Noether current corresponding to this axial symmetry $U_A(1)$, $A_\mu = \bar{\psi}\gamma_\mu\gamma_5\psi$, is not conserved due to quantum effects: $\partial^\mu A_\mu = 3g^2/(16\pi^2) \times \tilde{G}^{\alpha;\mu\nu} G^\alpha_{\mu\nu}$. This actually shows the connection between this symmetry and the winding number density $\omega = g^2/(32\pi^2) \times \tilde{G}^{\alpha;\mu\nu} G^\alpha_{\mu\nu}$, conjugate quantity of the vacuum angle θ [4]. For the time being, we will focus mainly on the $\mathrm{SU}_L(3) \otimes \mathrm{SU}_R(3)$ symmetry of the theory.

Let us notice that the mass term for light quarks, $\mathcal{L}_m$, mixes the two chiralities:

$$\mathcal{L}_m = -m_u(\bar{u}_L u_R + \bar{u}_R u_L) - m_d(\bar{d}_L d_R + \bar{d}_R d_L) - m_s(\bar{s}_L s_R + \bar{s}_R s_L)\,, \tag{2.7}$$

and thus breaks chiral symmetry explicitly. The chiral limit, where the light quark masses vanish, yields an extension of the symmetries of the Lagrangian. We can expect the chiral limit to be an appropriate simplification to discuss the dynamics of low-energy QCD, since the three light quark have masses that are much smaller (m_u, m_d) or smaller (m_s) than the typical hadronic scale (1 GeV).

2.1.2 Currents and charges

In the three-flavour chiral limit, we can define the currents associated with $\mathrm{SU}_L(3) \otimes \mathrm{SU}_R(3)$, which are conserved both at the classical and quantum levels:

$$(J_L)^a_\mu = \bar{\psi_L}\gamma_\mu\lambda^a\psi_L, \qquad (J_R)^a_\mu = \bar{\psi_R}\gamma_\mu\lambda^a\psi_R. \tag{2.8}$$

[4] Once electromagnetism is included, a similar anomaly affects not only the singlet axial current, but also the diagonal components of the axial multiplet, leading to the anomalous processes $\pi^0 \to 2\gamma$, $\eta \to 2\gamma$.

where the Gell-Mann matrices λ^a ($a = 1 \dots 8$) are the generators of the two SU(3) subgroups, normalised by $\langle \lambda_a \lambda_b \rangle = \delta_{ab}/2$ (the trace over flavour indices is denoted $\langle\rangle$). One can also consider the vector and axial currents:

$$V_\mu^a = (J_R + J_L)_\mu^a = \bar{\psi}\gamma_\mu \lambda^a \psi, \qquad A_\mu^a = (J_R - J_L)_\mu^a = \bar{\psi}\gamma_\mu\gamma_5 \lambda^a \psi. \tag{2.9}$$

Another conserved current stems from $\mathrm{U}_V(1)$, linked with the baryonic number: $V_\mu = \bar{\psi}\gamma_\mu\psi$, which can be written $V_\mu = V_\mu^0$, if λ^0 is defined as the matrix proportional to identity (equals to $1/\sqrt{6}$).

The light-quark masses break chiral symmetry in an explicit way, so that vector and axial currents are only partially conserved out of the chiral limit:

$$\partial^\mu V_\mu^a = i\bar{\psi}[M, \lambda^a]\psi, \qquad \partial^\mu A_\mu^b = i\bar{\psi}\{M, \lambda^b\}\gamma_5\psi, \tag{2.10}$$

where M is the light-quark mass matrix, $a = 0 \dots 8$ and $b = 1 \dots 8$. These equations involve the scalar and pseudoscalar densities:

$$\partial^\mu V_\mu^a = f^{abc} M^b S^c, \quad \partial^\mu A_\mu^a = d^{abc} M^b P^c, \qquad S^a = \bar{\psi}\lambda^a\psi, \quad P^b = \bar{\psi} i\gamma_5 \lambda^b \psi, \tag{2.11}$$

with $M^a = \langle M\lambda^a \rangle$. These relationships involve the SU(3) structure functions, both antisymmetric f^{abc} and symmetric d^{abc}: $[\lambda_a, \lambda_b] = if^{abc}\lambda_c$ and $\{\lambda_a, \lambda_b\} = \delta^{ab}/3 + d^{abc}\lambda^c$.

If one defines the charges Q_V^a et Q_A^a associated with vector and axial currents, one has the commutation relations:

$$\left[Q_V^a, Q_V^b\right] = if^{abc}Q_V^c, \quad \left[Q_V^a, Q_A^b\right] = if^{abc}Q_A^c, \quad \left[Q_A^a, Q_A^b\right] = if^{abc}Q_V^c. \tag{2.12}$$

The vector charges Q_V^a ($a = 1 \dots 8$) close in a sub-algebra coming from the diagonal subgroup $\mathrm{SU}_V(3)$. They account for the degeneracies of the hadronic spectrum mentioned to at the beginning of the chapter. On the contrary, the same spectrum does not exhibit the same agreement with the whole chiral symmetry group. In particular, the parity operation provides a connection between "left" and "right" charges, and a hadronic spectrum respecting chiral symmetry should exhibit, for each hadron multiplet, a second multiplet with the same mass and opposite parity. This is not the case, especially for mesons, since the lowest pseudoscalar octet (π, K, η) has no clear counterpart in the scalar sector, and vector and axial mesons have quite different masses.

2.2 Spontaneous breakdown of chiral symmetry

2.2.1 Realisation of chiral symmetry

The above considerations indicate that chiral symmetry is not realised in the usual Wigner mode, but rather undergoes a Nambu-Goldstone realisation [57–61]. The Lagrangian is invariant under the symmetry group, but the fundamental state is not – together with the rest of the spectrum. The symmetry is broken spontaneously, and according to Goldstone theorem [62,63], the spectrum of the theory exhibits as many massless scalar particles (called Goldstone bosons) as broken directions. In the chiral limit, $G = \mathrm{SU}_L(3) \otimes \mathrm{SU}_R(3) \otimes \mathrm{U}_V(1)$ is broken spontaneously, which can be expressed as [5]:

$$Q_V^a|0\rangle = 0, \qquad Q_A^b|0\rangle \neq 0. \tag{2.13}$$

[5] This presentation is simplified, since $Q_A^b|0\rangle$ cannot be interpreted with a meaningful modulus. In order to describe the spontaneous breakdown of the symmetry in a correct way, one must find a local (or multilocal) order parameter $\mathcal{O}$, such that: $\langle 0|[\mathcal{O}, Q_V^a]|0\rangle = 0$ and $\langle 0[\mathcal{O}, Q_A^b]|0\rangle \neq 0$.

with $a = 0 \dots 8$ et $b = 1 \dots 8$. The fundamental state $|0\rangle$ has a residual symmetry group $H = \mathrm{SU}_V(3)$. One will have 8 pseudoscalar Goldstone bosons $|\pi^b(p)\rangle$, organised as an octet according to H:

$$Q_V^a|\pi^b(p)\rangle = if^{abc}|\pi^c(p)\rangle, \tag{2.14}$$

which are coupled to axial currents through a single decay constant:

$$\langle 0|A_\mu^a(x)|\pi^b(p)\rangle = i\delta^{ab}F(3)p_\mu e^{ip\cdot x}, \tag{2.15}$$

where the bracketed (3) keeps track of the relevant chiral limit: $m_u, m_d, m_s \to 0$. The light quark masses correspond to a small explicit breaking of chiral symmetry, and in particular, they have the effect of defining which of the degenerate vacua is to be chosen as the fundamental state of the theory (the so-called "vacuum alignment") [3]. Once they are put back, the 8 Goldstone bosons will be become massive but light – they can be identified with pions, kaons and η, whose dynamics will be governed by the spontaneous breakdown of chiral symmetry.

General theorems constrain the pattern of chiral symmetry breaking. In the framework of vector-like theories, Vafa and Witten [64] showed that vector symmetries could not be broken if the vacuum angle θ vanishes, based on Weingarten inequalities [65] that are discussed in sec. A.1.2. On the other hand, in $\mathrm{SU}_C(3)$ gauge theory with $N_f \geq 3$ fermions, anomalous Ward identities impose that some three-point correlators exhibit poles at zero momentum. If the theory is confining (without coloured states in the spectrum), one must be able to reproduce these long-distance singularities by the presence of massless hadrons This suggests strongly the breakdown of chiral symmetry if the theory is confining (with the corollary that the restoration of chiral symmetry restoration an absence of confinement) [3, 66–68].

General theorems on Goldstone bosons indicate that the latter do not interact in the limit of vanishing momenta [62,63,69]. This result can be recovered by studying the processes between low-energy mesons, starting from the current algebra outlined in sec. 2.1.2 and adding three hypotheses [70]:

- Goldstone bosons are the only massless particles arising in the spectrum of asymptotic states.
- At low energies, Green functions are dominated by poles due to the exchange of theses bosons (pion pole dominance).
- The vertices describing the interactions of these bosons can be Taylor expanded in powers of the momenta.

With the help of these hypotheses, one can determine the structure of the leading term of any interaction among Goldstone bosons. An inductive proof shows that the interactions among an arbitrary number of mesons disappear in the limit of vanishing momenta.

At this stage, Quantum Chromodynamics and the effective description of Goldstone bosons exhibit opposite features: when the involved momenta are reduced, the coupling of quarks and gluons increase, whereas the coupling of mesons decrease. This feature will prove particularly useful to build a perturbative framework to describe low-energy QCD.

2.2.2 Notion of order parameter

The spontaneous breakdown of a global symmetry is a very common issue in physics, and we can obviously borrow many ideas from other fields to study the mechanism responsible for the spontaneous breakdown of chiral symmetry. A useful analogy is provided by ferromagnetic

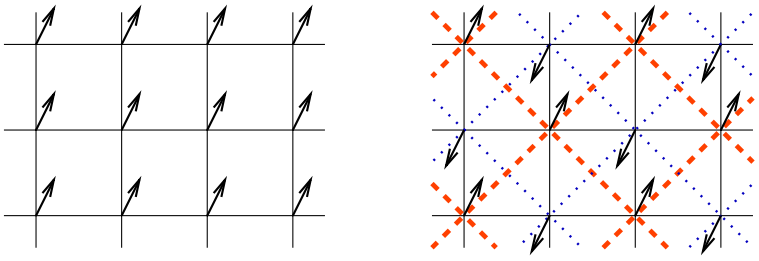

Figure 2.1: *Sketch of the fundamental state for ferromagnetic spin system (left) and anti-ferromagnetic (right), under the Curie temperature.*

systems, which can be modeled as a lattice of interacting spins. Under a the (critical) Curie temperature, an ordered phase appears, featuring a nonzero spontaneous magnetisation $\vec{M}$ (defined as the normalised sum over all the spins of the systems) due to a macroscopic alignment of the spins of the system. Above the critical temperature, the order disappears and the spontaneous magnetisation vanishes. A simplified model for such system would be provided by a Hamiltonian where interactions among spins are of the form $\vec{S}_i \cdot \vec{S}_j$. This Hamiltonian is thus invariant under any global rotation belonging to $O(3)$. But under the critical temperature, this rotational symmetry is broken by the fundamental state, which defines a privileged axis. Indeed, its spontaneous magnetisation transforms as a vector under the rotation generators L_i ($i = 1, 2, 3$). At zero temperature, only the fundamental state contributes to the statistical average of $\vec{M}$, and we have:

$$\langle M_i \rangle_{T=0} = \langle 0|M_i|0\rangle = -\frac{i}{2}\epsilon_{ijk}\langle 0|[L_j, M_k]|0\rangle \,. \tag{2.16}$$

If the fundamental state $|0\rangle$ is invariant, it is annihilated by the generators of $O(3)$ L_i, and the spontaneous magnetisation vanishes. Conversely, if the spontaneous magnetisation is different from zero, the fundamental state breaks the symmetry of the Hamiltonian. If $\mathcal{O}$ is an order parameter, it satisfies the implication:

$$\mathcal{O} \neq 0 \Rightarrow \text{Symmetry breaking.} \tag{2.17}$$

There is an infinity of order parameters *in principle*. They can be obtained by computing the vacuum expectation value of operators transforming under a (generally reducible) representation of the symmetry group, whose decomposition in irreducible representations do not contain the trivial representation. But the reciprocal of eq. (2.17) is not correct: the spontaneous breakdown of a symmetry does not constrain *every* order parameter to acquire a non-vanishing value. For instance, in anti-ferromagnetic systems, the low-temperature phase exhibits a long-range order with anti-parallel spins. This order breaks the rotational invariance. However the spontaneous magnetisation remains zero, and the breakdown of the symmetry is flagged by other order parameters, such as the difference of magnetisation on the two sub-lattices $\vec{A} = \vec{M}_{\text{dotted lattice}} - \vec{M}_{\text{dashed lattice}}$, cf. Fig. 2.1). The relevance of an order parameter is related to the mechanism responsible for symmetry breaking. Conversely, the study of order parameters should shed light on the nature of this mechanism, and in the long run, provide hints of a model describing dynamically the breaking of this symmetry – as would be the long-term goal of a study of the breakdown of chiral symmetry.

2.2.3 Chiral order parameters

In the chiral limit, one can build different order parameters transforming under representation of $\mathrm{SU}_L(3) \otimes \mathrm{SU}_R(3)$ excluding the trivial representation. Some are Green functions of the axial and vector currents A^a_μ, V^a_μ and of the scalar and pseudoscalar densities S^a, P^a, such as:

$$\Pi^{ab}_{\mu\nu}(q) = i \int d^4x \; e^{iq\cdot x} \langle 0|T[V^a_\mu(x)V^b_\nu(0) - A^a_\mu(x)A^b_\nu(0)]|0\rangle \,. \tag{2.18}$$

If we denote (n_L, n_R) the representations de $\mathrm{SU}_L(3) \otimes \mathrm{SU}_R(3)$, Π transforms as $(8, 8)$ in the chiral limit for any value of the flowing momentum q, and in particular, does not feature the trivial representation.

Let us assume that chiral symmetry is broken and consider Π in the chiral limit. The correlator has poles corresponding to one-particle states:

$$\Pi^{ab}_{\mu\nu}(q) = q_\mu q_\nu \left[-\sum_P \frac{F(3)^2}{q^2} - \sum_V \frac{F_V^2}{M_V^2 - q^2} + \sum_A \frac{F_A^2}{M_A^2 - q^2} \right] + \dots \tag{2.19}$$

where the first term comes from Goldstone bosons due to the breakdown of chiral symmetry, and the second and third terms correspond to massive (vector and axial) resonances (the ellipsis denoting non-holomorphic structures arising at higher energies). We have introduced the couplings (or decay constants) of the one-particle states F to the vector and axial currents. At vanishing momentum ($q_\mu = 0$), only the Goldstone bosons contribute:

$$\Pi^{ab}_{\mu\nu}(0) = -\frac{1}{4} g_{\mu\nu} \delta^{ab} F^2(3), \tag{2.20}$$

We can use eq. (2.20) as a definition for $F^2(3)$, which is different from zero if chiral symmetry is broken. Conversely, if $F^2(3) \neq 0$, the chiral order parameter $\Pi^{ab}_{\mu\nu}(0)$ is different from 0 and the fundamental state of the theory is not symmetric under the chiral symmetry group, as discussed in the previous section. According to Goldstone theorem, the spectrum of the theory contains massless spin-0 states. Since the broken directions cannot belong to the vector sector [67], the Goldstone bosons must couple to axial currents. $F^2(3)$ can thus be identified with the decay constant of Goldstone bosons in the chiral limit [6].

$\Pi(0)$ plays therefore a very particular role among order parameters of chiral symmetry, since the implication (2.17) is replaced by the equivalence for this single order parameter:

$$\Pi^{ab}_{\mu\nu}(0) \neq 0 \Leftrightarrow F_0 \neq 0 \Leftrightarrow \text{Chiral symmetry breaking.} \tag{2.21}$$

Due to this peculiar role, F^2 defined in eq. (2.20) and corresponding to the decay constant of the pion in the chiral limit could be called *the* order parameter of chiral symmetry.

There are also local order parameters, such as the quark condensate: $\langle \bar{q}q \rangle^{(3)} = \langle 0|\bar{u}u|0\rangle^{(3)} = \langle 0|\bar{d}d|0\rangle^{(3)} = \langle 0|\bar{s}s|0\rangle^{(3)}$ which transforms as $(3^*, 3) \oplus (3, 3^*)$. One can also think of other order parameters, such as the mixed condensate $\langle 0|\bar{q}^i \sigma^{\mu\nu} G^\alpha_{\mu\nu} T^\alpha_{ij} q_j|0\rangle^{(3)}$, or four-quark condensates such as $\langle 0|(\bar{q}\Gamma_1 q)(\bar{q}\Gamma_2 q)|0\rangle^{(3)}$, which are often discussed in the framework of QCD sum

[6] The Goldstone theorem is generally stated for a local non-trivial operator whose vacuum expectation value does not vanish. Following the same line of thought, it can be proven that Goldstone bosons arise in the case of multilocal operators depending on several points $(x_1, x_2, \dots x_n)$ localised in a finite volume. In particular, one can consider the correlator $\langle 0|T[V^a_\mu(x)V^b_\nu(0) - A^a_\mu(x)A^b_\nu(0)]|0\rangle$ at x finite, but large. If the value of this correlator does not vanish, there is indeed a spontaneous breakdown of chiral symmetry, and the contribution of Goldstone bosons to the correlator is leading.

rules [71, 71, 72]. Let us remark that all these order parameters probe the chiral structure of the fundamental state of QCD, a feature that cannot be probed by perturbative QCD, as the latter performs its expansion in powers of the strong coupling constant around a trivial vacuum (in particular, the order parameters discussed here, such as Π, would all vanish if evaluated perturbatively in the chiral limit).

2.2.4 The quark condensate and the pseudoscalar decay constant

In practice, two order parameters play a prominent role in the study of chiral symmetry breaking. We have seen that pseudoscalar decay constant $F^2(3)$ was the non-ambiguous signature of chiral symmetry breaking. The quark condensate plays also an important role. For instance, it arises in the expansion of the mass of the pseudoscalar mesons in the quark masses:

$$F_\pi^2 M_\pi^2 = 2m\Sigma(3) + O(m_q^2), \tag{2.22}$$

$$F_K^2 M_K^2 = (m + m_s)\Sigma(3) + O(m_q^2), \tag{2.23}$$

$$F_\eta^2 M_\eta^2 = \frac{2}{3}(m + 2m_s)\Sigma(3) + O(m_q^2), \tag{2.24}$$

with the quark condensate in the chiral limit $\mathrm{SU}_L(3)\otimes\mathrm{SU}_R(3)$: $\Sigma(3) = -\langle 0|\bar{u}u|0\rangle^{(3)}$. The terms quadratic in quark masses are denoted $O(m_q^2)$, whereas isospin breaking effects are neglected (electromagnetic corrections and difference $m_u - m_d$) – in particular $m = m_u = m_d$.

These equations relate the masses of the pseudoscalar mesons (due to the explicit breaking of chiral symmetry) and the quark condensate in the chiral limit (which is an order parameter of the spontaneous breakdown of the same symmetry). The quark condensate induces a linear response to the perturbation due to the quark masses, in a similar way to the spontaneous magnetisation of ferromagnet systems in the presence of an exterior electrical field. The quark condensate must be negative (or zero), otherwise the mesons would acquire negative masses for very small quark masses (condition of vacuum stability).

How to exploit eqs. (2.22)-(2.24) ? It is often assumed that the corrections of higher orders are negligible not only in the chiral limit $m_u = m_d = m_s = 0$, but also for physical quark masses. This leads to a scenario where the spontaneous breakdown of chiral symmetry is caused by a significant condensation of quark-antiquark pairs in the vacuum: $\langle\bar{q}q\rangle^3 \sim -(230\ \mathrm{MeV})^3$ [20, 21, 71, 73]. The quark condensate would then play an essential role to describe the consequences of chiral symmetry breaking, whereas other order parameters would describe only marginally relevant aspects of the phenomenon. The main object of our Such a scenario, usually accepted, could turn out to be oversimplified, and we are going to explore some alternatives now.

2.2.5 Two chiral limits of interest

Due to the mass hierarchy $m_u \sim m_d \ll m_s \ll \Lambda_{\mathrm{QCD}}$, one can consider two different chiral limits of interest (see fig. 2.2):

- $N_f = 3$ chiral limit: $m_u, m_d, m_s = 0$ with an octet of Goldstone bosons, identified with (π, K, η),
- $N_f = 2$ chiral limit: $m_u, m_d = 0$ but m_s physical, with a triplet of Goldstone bosons, identified with the pions.

Up to now, we have discussed mainly the $N_f = 3$ chiral limit. But all the above discussion can be adapted to the $N_f = 2$ chiral limit with the $\mathrm{SU}_L(2) \otimes \mathrm{SU}_R(2)$ group. In this chiral limit,

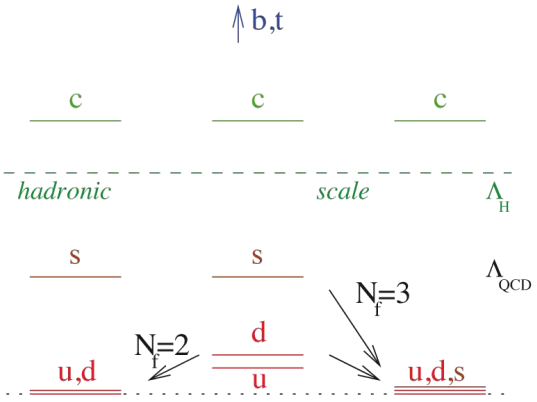

Figure 2.2: *The mass hierarchy among the quarks in the Standard Model, and the two chiral limits discussed in this chapter.*

where the masses of the u and d quarks go to zero, but the s quark remains at its physical mass, the breakdown of chiral symmetry can be understood in terms of $\mathrm{SU}_L(2)\otimes\mathrm{SU}_R(2)$ order parameters, which contain an implicit dependence on m_s. Let us notice that in the $N_f = 2$ limit, there are fewer order parameters than for the $N_f = 3$ chiral limit, since the conjugate representations 2 et 2^* are equivalent (whereas 3 and 3^* are not). Some products of these representations will contain the trivial representation, whereas the same products for 3 and 3^* would not. Among the various order parameters of interest, and in agreement with the previous discussion, we can define the pseudoscalar decay constant and the quark condensate in both chiral limits:

$$F^2(2) = \lim_{m_u,m_d\to 0} F_\pi^2\,, \qquad F^2(3) = \lim_{m_u,m_d,m_s\to 0} F_\pi^2\,, \qquad \lim_{m_s\to 0} F^2(2) = F^2(3)\,, \tag{2.25}$$

$$\Sigma(2) = \lim_{m_u,m_d\to 0} -\langle 0|\bar{u}u|0\rangle\,, \qquad \Sigma(3) = \lim_{m_u,m_d,m_s\to 0} -\langle 0|\bar{u}u|0\rangle\,, \qquad \lim_{m_s\to 0} \Sigma(2) = \Sigma(3)\,. \tag{2.26}$$

Both limits are relevant for phenomenological studies, and differ by the variation of a single QCD parameter (the strange quark mass). The chiral structure of QCD vacuum may or may not be strongly affected when one changes the mass of the strange quark, depending on the role played by the the strange sea-quark pairs populating the (non-trivial) fundamental state of the theory. A better understanding of the role played by the strange quark can be reached by considering an alternative representation of chiral order parameters, through the spectrum of the Euclidean Dirac operator.

2.3 Chiral symmetry and spectrum of the Euclidean Dirac operator

2.3.1 Euclidean QCD on a torus

Due to the vector-like nature of QCD, interesting statements can be inferred after a Wick rotation is performed in order to change from a Minkowski metric to an Euclidean one:

$$x_0 = -i\bar{x}_0\,, \qquad x^2 = x_0^2 - \vec{x}^2 \to -\bar{x}_0^2 - \vec{\bar{x}}^2 = -\bar{x}^2. \tag{2.27}$$

The QCD Lagrangian in the Euclidean metric reads:

$$\mathcal{L}^e_{\text{QCD}} = \frac{1}{4} G^{\alpha;\mu\nu} G^\alpha_{\mu\nu} + i \frac{g^2}{32\pi^2} \tilde{\theta}\ \tilde{G}^{\alpha;\mu\nu} G^\alpha_{\mu\nu} + \bar{\psi}(-i\not{D} + M)\psi. \tag{2.28}$$

where some aspects related to the treatment of fermions are covered in sec. A.1.1. We will set the vacuum angle $\tilde{\theta} = 0$, unless specified otherwise.

Since we are interested in the long-distance, infrared properties of the theory, it is useful to introduce an infrared regulator by considering this Euclidean theory in a finite volume, whose sides are identified to yield a four-dimension Euclidean torus of size $L \times L \times L \times L$. The identification between x and $x + a$ can be done directly for the gluon field, up to a gauge transformation [74], whereas the anti-periodicity of fermionic fields is required:

$$G_\mu(x + N) = \Omega_N G_\mu(x) \Omega_N^\dagger - i \Omega_N \partial_\mu \Omega_N^\dagger\,, \qquad q(x + N) = (-1)^{n_0+n_1+n_2+n_3} \Omega_N(x) q(x), \tag{2.29}$$

with $N = (n_0, n_1, n_2, n_3) \cdot L$, $\{n_i\}$ integers, and $\Omega_a = \Omega_a(x) \in \text{SU}(N_C)$. These two conditions constrain the transition function:

$$\Omega_{N+P}(x) = \Omega_P(x + N)\Omega_N(x). \tag{2.30}$$

These constraints of (anti-)periodicity on the torus allow one to treat an Euclidean field theory in a finite volume as a system of statistical mechanics at finite temperature (the "time" dimension playing the role of the inverse of temperature) [75, 76].

At finite volume, the gauge configurations can be classified according to a topological invariant, the winding number:

$$\nu[G] = \frac{1}{32\pi^2} \int d^4x\ \tilde{G}^\alpha_{\mu\nu} G^\alpha_{\mu\nu}, \tag{2.31}$$

whose values belong to a discrete set [7]. On the torus, this topological invariant can be reexpressed as a function for the transition function Ω, and the condition eq. (2.30) constrained ν to be an integer [74].

2.3.2 Spectrum of the Euclidean Dirac operator

In the Euclidean metric, the Dirac operator $H = \gamma_\mu D_\mu$ combines two antihermitian operators and is thus hermitian. For each gauge configuration G, it can be diagonalised:

$$\not{D}\psi_n = \lambda_n \psi_n, \tag{2.32}$$

where $\{\psi_n\}$ is a complete basis of orthonormal states:

$$\int d^4x\ \psi_n^\dagger(x)\psi_m(x) = \delta_{mn}, \qquad \sum_n \psi_n(x)\psi_n^\dagger(y) = \delta^{(4)}(x - y). \tag{2.33}$$

This basis and the corresponding spectrum are obtained for a given gluonic configuration. Let us notice that this spectrum is symmetric with respect to 0 (see fig. 2.3), as γ_5 and H anticommute:

$$H\psi_n = \lambda_n \psi_n \Rightarrow H\gamma_5\psi_n = -\gamma_5 H\psi_n = -\lambda_n \gamma_5 \psi_n. \tag{2.34}$$

[7] In order to give a finite Euclidean action, the strength tensor $G_{\mu\nu}$ must decrease sufficiently quickly at infinity. The gluonic field must thus go to a pure gauge potential at infinity: $G_\mu \to -i(\partial_\mu \omega)\omega^\dagger$. The gluon configurations can be sorted according to the value reached by ω in each space direction n_μ ($n^2 = 1$). This defines an application from the sphere S^3 into the gauge group. For any simple Lie group G, such an application exhibits an infinite number of topological classes, indexed by an integer: $\pi_3(G) = Z$ [76].

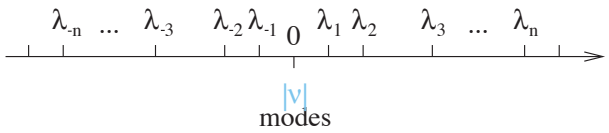

Figure 2.3: *Spectrum of the Dirac operator. As the volume of the torus L^4 grows, the eigenvalues tend to decrease and accumulate around zero like a power of $1/L$.*

For each eigenvector ψ_n with a non-vanishing eigenvalue, $\gamma_5\psi_n$ is also an eigenvector, with eigenvalue $-\lambda_n$. We can sort the strictly positive eigenvalues in increasing order (for $n \geq 1$), and we define $\psi_{-n} = \gamma_5\psi_n$ and $\lambda_{-n} = -\lambda_n$ for negative indices. In the subspace for $\lambda = 0$, we can choose a basis consisting of chirality eigenstates, with n_+ right-handed states and n_- left-handed ones. The Atiyah-Singer index theorem [77] links the degeneracy of the zero eigenvalue with the winding number of the gluonic configuration considered: $\nu = n_+ - n_-$.

Vafa and Witten have shown the existence of a uniform bound on the Dirac eigenstates [67]:

$$|\lambda_n[G]| < C\frac{n^{1/d}}{L} \equiv \omega_n, \tag{2.35}$$

whee $d(=4)$ is the space-time dimension, and C is a constant, independent of the gluonic configuration $G_\mu(x)$, the integer n and the volume $V = L^d$ (but C depends on the space-time geometry). The upper bound ω_n is essentially equivalent to what is obtained in the free theory (up to the constant C), where the solutions are plane waves of the form:

$$\psi_n(x) = e^{+i\bar{p}_n\cdot\bar{x}}u(\bar{p}_n)\,, \qquad \psi_n(x) = e^{-i\bar{p}_n\cdot\bar{x}}v(\bar{p}_n)\,, \tag{2.36}$$

with u, v solutions of the Euclidean Dirac equation for the mass $m^2 = \bar{p}^2$. The antiperiodic boundary conditions imposed on the torus require the momentum $\bar{p}_n$ to be "half-integer":

$$\bar{p}_n = \frac{2\pi}{L}(n_0 + 1/2, n_1 + 1/2, n_2 + 1/2, n_3 + 1/2) \qquad \vec{n} \in Z^4 \tag{2.37}$$

so that these solutions correspond to eigenvalues of the form:

$$\not{D}\psi_n = \not{p}_n\psi_n = \pm\frac{2\pi}{L}\sqrt{\sum_i \left(n_i + \frac{1}{2}\right)^2}\psi_n\,. \tag{2.38}$$

This behaviour of eigenvalues going as $1/L$ is also expected in the presence of a gluonic field at the ultraviolet end of the Dirac spectrum, where the role of gluonic configurations is less and less relevant. On the other hand, let us remark that eq. (2.35) implies that there should be eigenvalues accumulating around 0 in the large-volume limit. We will see that this accumulation is related to properties of chiral symmetry breaking in the following sections. The bound (2.35) can be interpreted as the paramagnetic response of the Euclidean spectrum under an external gauge field [78–80]. Once the field applied, the energy of the system "decreases". This paramagnetic behaviour of fermions is opposite to that of scalars: indeed, the spectrum of the Klein-Gordon operator has a diamagnetic behaviour, as its eigenvalues increase once a field is applied [81].

The fermion integral can be performed formally and expressed in terms of $\det(-i\not{D} + M)$, leaving an average over gluonic configurations, as is done in lattice gauge theory to evaluate

correlators by Monte-Carlo methods [82, 83]. One can follow the same idea by projecting the fermion fields on the eigenstate basis:

$$q^f(x) = \sum_n a_n^f \psi_n(x), \qquad \bar{q}^f(x) = \sum_n \bar{b}_n^f \psi_n^\dagger(x)\,, \tag{2.39}$$

where f is a flavour index, and $\{a_n^f\}$ and $\{\bar{b}_n^f\}$ are independent Grassmann families. The eigenstate basis $\{\psi_n\}$ is orthonormal, so that the change from the variables $\{q^f, \bar{q}^f\}$ to the variables $\{a_n^f, \bar{b}_n^f\}$ has a unity Jacobian [8]. The vacuum expectation value of an operator $\mathcal{Y}$ can then be written:

$$\begin{aligned}\langle\Omega|\mathcal{Y}|\Omega\rangle &= \int [dG][d\bar{q}][dq] e^{-S_g[G]} e^{-S_f[G,q,\bar{q}]} \mathcal{Y} \\ &= \int [dG] e^{-S_g[G]} \int \prod_{n,f} d\bar{b}_n^f da_n^f \exp\left[-\bar{b}_n^f (m_f - i\lambda_n) a_n^f\right] \bar{\mathcal{Y}},\end{aligned} \tag{2.40}$$

where S_g is the pure Yang-Mills action and $\bar{\mathcal{Y}}$ is the expression of $\mathcal{Y}$, once the fermion fields are projected over the Dirac eigenstates. In this framework, we can express the correlator of bilinear operators of the form: $\mathcal{O}_i(x) = \bar{\psi}(x)\Gamma_i\psi(x)$, with Γ_i a combination of Dirac and flavour matrices. We obtain:

$$\begin{aligned}\langle\Omega|\mathcal{O}_1(x)\mathcal{O}_2(y)|\Omega\rangle &= Z^{-1} \int [dG][d\bar{q}][dq] e^{-S_g[G]} e^{-S_f[G,q,\bar{q}]} \bar{\psi}(x)\Gamma_1\psi(x)\bar{\psi}(y)\Gamma_2\psi(y) \\ &= - \ll \mathrm{Tr}[\Gamma_1 S(x,y|G)\Gamma_2 S(y,x|G)] \gg,\end{aligned} \tag{2.41}$$

where the propagator of light quarks in a given gauge configuration appears:

$$S(x,y|G) = \sum_n \frac{\psi_n(x)\psi_n^\dagger(y)}{M - i\lambda_n}, \tag{2.42}$$

with M the light-quark mass matrix. The average over gluonic configurations $\ll\gg$ is defined as:

$$\ll \mathcal{O} \gg = \frac{\int [dG] e^{-S_g[G]} \Delta[G] \mathcal{O}}{\int [dG] e^{-S_g[G]} \Delta[G]}\,. \tag{2.43}$$

As described in more detail in app. A.1.1, the integration of the Grassmann variables yields the following expression of the fermion determinant:

$$\Delta(G) = \prod_i \Delta(m_i|G)\,, \qquad \Delta(m|G) = m^{|\nu|} \prod_{n>0} \frac{m^2 + \lambda_n^2[G]}{m^2 + \omega_n^2}\,, \tag{2.44}$$

where we have exploited the symmetry of the Dirac spectrum with respect to 0, and introduced a normalisation through ω_n which is independent of the gluon configuration. The average can be seen as a statistical average over the gauge configurations, weighted with the positive measure $\Delta[G]\exp(-S_g[G])$ (for a vanishing vacuum angle).

[8] We will not discuss the axial anomaly that results from the non-invariance of the fermion measure under axial rotations $U_A(1)$ [2, 3].

2.3.3 Infrared-dominated order parameters

Chiral order parameters can be studied within this framework. Let us take the $\mathrm{SU}_L(N_f) \otimes \mathrm{SU}_R(N_f)$ chiral limit, keeping the remaining N_h "heavy" quarks at their mass:

$$m_1 = m_2 = \ldots = m_{N_f} = m \to 0, \qquad m_j \neq 0,\ N_f < j \leq N_f + N_h. \tag{2.45}$$

If we denote $-\Sigma(N_f)$ the quark condensate $\langle \bar{u}u \rangle$ in this limit, we get:

$$\Sigma(N_f) = \lim \frac{1}{L^4} \ll \int dx\ \mathrm{Tr}\ S(x,x|G) \gg_{N_f} = \lim \frac{1}{L^4} \ll \sum_n \frac{m}{m^2 + \lambda_n^2} \gg_{N_f} . \tag{2.46}$$

where lim denotes the large-volume limit $L \to \infty$ followed by the chiral limit $\mathrm{SU}(N_f) \times \mathrm{SU}(N_f)$ (2.68). The average over gluon configurations weighted by the fermion determinant and the Yang-Mills action is defined in eq. (2.43):

$$\ll \Gamma \gg_{N_f} = Z^{-1} \int d\mu[G]\ \Gamma\ \Delta^{N_f}(m|G) \prod_{j>N_f}^{N_f+N_h} \Delta(m_j|G) \exp\{-S_g[G]\}. \tag{2.47}$$

Z is a normalisation factor ensuring $\ll 1 \gg_{N_f} = 1$. We have

$$\Sigma(N_f) = \lim \frac{1}{L^4} \ll \sum_n \frac{m}{m^2 + \lambda_n^2} \gg_{N_f} = \lim_{m \to 0} \int_{-\infty}^{\infty} d\epsilon \frac{m}{m^2 + \epsilon^2} \lim_{L \to \infty} \frac{1}{L^4} \ll \sum_n \delta(\epsilon - \lambda_n) \gg_{N_f} \tag{2.48}$$

$$= 2 \lim \int_0^{\infty} \frac{du}{1+u^2} \frac{1}{L^4} \ll \rho(mu) \gg_{N_f}, \tag{2.49}$$

relating the quark condensate to the density of eigenvalues ρ defined as:

$$\rho(\epsilon) = \sum_n \delta(\epsilon - \lambda_n). \tag{2.50}$$

Eqs. (2.18) et (2.20) yield the decay constant in the same way [84]:

$$F^2(N_f) = \lim \frac{1}{L^4} \ll \sum_{k,n} \frac{m}{m^2 + \lambda_k^2} \frac{m}{m^2 + \lambda_n^2} J_{kn} \gg_{N_f}, \tag{2.51}$$

with:

$$J_{kn} = \frac{1}{4} \sum_{\mu} \left| \int dx\ \psi_k^{\dagger}(x) \gamma_\mu \psi_n(x) \right|^2 . \tag{2.52}$$

Since the eigenstate basis for each gluon configuration is complete, one has $\sum_n J_{kn} = 1$.

One can see that these two order parameters are linked to the accumulation of eigenstates around 0. In particular, we recover the Banks-Casher relation between the quark condensate and the eigenvalue density around 0 [85]. One can indeed rewrite these order parameters as:

$$\Sigma(N_f) = \pi \lim_{\epsilon \to 0} \lim_{L \to \infty} \rho(\epsilon, L), \qquad F^2(N_f) = \pi^2 \lim_{\epsilon \to 0} \lim_{L \to \infty} L^4 J(\epsilon, L) \rho^2(\epsilon, L), \tag{2.53}$$

with the "density" and the "mobility" [84]:

$$\rho(\epsilon, L) = \frac{1}{2\epsilon L^4} \ll \sum_n^{\epsilon} \gg_{N_f} = \frac{1}{2\epsilon L^4} N(\epsilon, L)\,, \quad J(\epsilon, L) = \frac{1}{N^2(\epsilon, L)} \ll \sum_{n,k}^{\epsilon} J_{nk} \gg_{N_f} . \tag{2.54}$$

$\sum_n^\epsilon$ denotes the sum over the eigenvalues $|\lambda_n| < \epsilon$. The quark condensate $\Sigma(N_f)$ and the decay constant $F^2(N_f)$ are not sensitive to the same features of the infrared end of the Dirac spectrum. In particular, comparing the powers of the factors $m/(m^2+\lambda^2)$ and $1/L^4$ in eqs. (2.48) and (2.51) suggests that the quark condensate gets a non-vanishing value if the eigenvalues accumulate around 0 like $1/L^4$, whereas a behaviour like $1/L^2$ is needed to obtain $F^2 \neq 0$ [84] (one notices that the eigenvalues corresponding to the perturbative regime $O(1/L)$ do not contribute to these two chiral order parameters, in agreement with the non-perturbative nature of chiral symmetry breaking).

Finally, one should mention a further feature of the Dirac spectrum, obtained by considering the correlator of two scalar densities: the density of Dirac eigenvalues exhibits a cusp structure of the form [86]:

$$\lim_{L\to\infty} \rho(\epsilon, L) = \frac{1}{\pi}\Sigma(N_f) + \frac{N_f^2-4}{32\pi^2}\frac{\Sigma(N_f)^2}{F^2(N_f)}|\epsilon| + O(\epsilon)\,. \tag{2.55}$$

2.3.4 Chiral symmetry breaking at finite volume

The previous discussion might seem a bit surprising, since we are discussing properties of chiral order parameters describing the spontaneous breakdown of chiral symmetry, by considerations of the Dirac spectrum at finite volume. But it is known that the spontaneous breakdown of a global symmetry cannot occur at finite volume. We can illustrate this point by considering a theory with a discrete symmetry $\phi \to -\phi$ (also exhibited by the effective action $\Gamma[\phi]$), with a state minimising $-\Gamma[\phi]$ for a constant vacuum expectation value $\phi(x) = \bar{\phi} \neq 0$. We have then two states $|\Omega,+\rangle$ and $|\Omega,-\rangle$ with respective vacuum expectations $\bar{\phi}$ and $-\bar{\phi}$ corresponding to the same minimal vacuum energy. But the presence of these two states does not mean that the symmetry is necessarily broken, since we do not know what is the actual fundamental state chosen by the theory: $|\Omega,+\rangle$ or $|\Omega,-\rangle$ (breaking the discrete symmetry), or $|\Omega,+\rangle + |\Omega-,\rangle$ or $|\Omega,+\rangle - |\Omega,-\rangle$ (satisfying the discrete symmetry) ? The form of the Hamiltonian between the two states is very simple, due to the symmetry between $|\Omega,+\rangle$ and $|\Omega-\rangle$:

$$H = \begin{bmatrix} a & b \\ b & a \end{bmatrix} \qquad \text{for} \qquad \begin{bmatrix} |\Omega,+\rangle \\ |\Omega-\rangle \end{bmatrix}, \tag{2.56}$$

with eigenstates $|\Omega,+\rangle + |\Omega,-\rangle$ and $|\Omega,+\rangle - |\Omega,-\rangle$ of energies $a \pm |b|$ respecting the symmetry of the theory. One would thus expect for a completely isolated system to have a symmetric ground state. However, b corresponds to the tunelling from $|\Omega,+\rangle$ to $|\Omega,-\rangle$ and would thus be suppressed by an exponential penetration factor of the form $\exp(-C\cdot V)$. Therefore, the two states are actually almost degenerate for a macroscopic system. Any (even small) external perturbation H' breaking the symmetry by having, say, $\langle\Omega,+|H'|\Omega,+\rangle < \langle\Omega,-|H'|\Omega,-\rangle$, will have matrix elements much larger than b and will cause the fundamental state of the system to be aligned almost entirely along $|\Omega,+\rangle$ rather than close to one of the symmetric states $|\Omega,+\rangle + |\Omega,-\rangle$ and $|\Omega,+\rangle - |\Omega,-\rangle$.

This argument can be extended to more general cases [3], stressing the importance of considering the thermodynamical limit (sending $L \to \infty$ before taking the chiral limit) in order to obtain a system exhibiting a spontaneous breakdown of chiral symmetry. Indeed, swapping the large-volume and small-mass limits in eqs (2.48) and (2.51) yields a vanishing value for these order parameters – one must take the correct order of limits to obtain a dense Dirac spectrum around 0 which will contribute to the condensate and/or the decay condensate. But the above arguments suggests that one does not need an infinite volume to see chiral symmetry

breaking effects, only a volume and a perturbation both large enough for the system to select a non-symmetric fundamental state [87–89].

Let us consider the situation where the quark condensate does not vanish. One expects that the low eigenvalues will have a mean spacing of eigenvalues going like:

$$\Sigma : \qquad \Delta\lambda \simeq \frac{1}{V\rho_1(\lambda)} \sim \frac{1}{V\Sigma(N_f)}\,, \tag{2.57}$$

from eqs. (2.53) and (2.54), taking into account that $\ll \sum_n{}^{\epsilon} \gg_{N_f} \simeq \epsilon/\Delta\lambda$. If $m \gg \Delta\lambda$, i.e., $mV\Sigma(N_f) \gg 1$, eq. (2.48) will yield a non-vanishing value for $\Sigma(N_f)$ even at finite volume, so that chiral symmetry is broken by $\Sigma(N_f) \neq 0$. The pseudoscalar decay constant can be discussed in similar terms, with the mean spacing:

$$F^2 : \qquad \Delta\lambda \simeq \frac{1}{V\rho_2(\lambda)} \sim \frac{1}{L^2F(N_f)}\,, \tag{2.58}$$

so that $mL^2F(N_f) \gg 1$ is the condition for spontaneous breakdown of chiral symmetry to occur at finite volume through $F^2(N_f) \neq 0$.

A simplified description of the distribution of the Dirac eigenvalues, based on a breakdown of chiral symmetry driven by the quark condensate solely, can be found in the framework of Chiral Random Matrix Theory [90–92]. This approach describes the low-energy partition function of QCD as a random matrix model assumed to belong to the same universality class provided that the Dirac matrix can be replaced by a random matrix with the same global symmetries, chiral symmetry is broken spontaneously in the limit of infinitely large random matrices, and the random matrix elements do not have any spacetime dependence [9]. Information on the distribution of the lowest Dirac eigenvalues has been derived within this framework, which has also been used to study the effect of finite temperature and chemical potential. By definition, these models are focused on the effect of the quark condensate on the Dirac spectrum and thus are not able to derive correlations among Dirac eigenvalues/eigenvectors related to more complicated order parameters (and more elaborate patterns of chiral symmetry breaking).

More features of the spectrum can be studied thanks to the Leutwyler-Smilga sum rules [74] obtained by matching the QCD and LO effective generating functionals, and providing the behaviour of inverse moments of the Dirac eigenvalues $\sum_{n>0}(1/\lambda_n)^k$, averaged over a topological sector of fixed winding number in terms of the quark condensate and pseudoscalar decay constant. These relationships have been discussed in the case of more complicated patterns of chiral symmetry breaking [35] and recovered in the framework of the Chiral Random Matrix Theory [90–92].

The microscopic Dirac eigenvalue distribution, the Leutwyler-Smilga sum rules as well as other related quantities (such as the topological susceptibility, i.e., the average of the squared winding number) are currently investigated in lattice simulations as an alternative determination of the quark condensate [93–97]. Let us however emphasize that these works actually determine an effective condensate embedding mass corrections involving other chiral order parameters [10].

[9] The content of this model is therefore close to leading-order Chiral Perturbation Theory for constant fields, and their predictions in this domain comparable.

[10] In the language of three-flavour Chiral Perturbation Theory described in the next chapter, the NLO expressions for these quantities involve the counterterm L_6, which may contribute significantly (and as much as the quark condensate) to the effective condensate determined in these computations [98–101]. Studies of the low-lying Dirac eigenvalues including these effects [102] point indeed toward a significant contribution from NLO, as commented in sec. 2.5.1.

2.4 The role of the number of light flavours

2.4.1 Paramagnetic effect of light-quark loops [A]

Let us consider get back to the situation described in sec. 2.3.3, with N_f light quarks and N_h more massive ones. We assume that the lightest of the massive quarks, denoted s, has a non-zero mass which is small compared to the scale of the theory – QCD is obviously equivalent to the case $N_f = 2$. The average eq. (2.47) exhibits an explicit dependence on N_f related to the fermion determinant, which can be isolated for infrared-dominated order parameters:

$$\ll \Gamma \gg_{N_f} = Z^{-1} \int d\mu[G]\ \Gamma\ \Delta^{N_f}(m|G)\Delta(m_s|G) \prod_{j>N_f}^{N_f+N_h} \Delta(m_j|G) \exp\{-S_g[G]\}. \tag{2.59}$$

Let us choose a cut-off Λ and define the integer K so that $\omega_K = \Lambda$ (let us notice that this definition is independent from the gluonic configuration chosen). We can write down the fermion determinant for one quark flavour as:

$$\Delta(m|G) = m^{|\nu|}\Delta_{\rm IR}(m|G)\Delta_{\rm UV}(m|G), \tag{2.60}$$

where we have divided the spectrum of the Dirac operator into two parts, infrared and ultraviolet. The infrared part reads:

$$\Delta_{\rm IR}(m|G) = \prod_{n=1}^{K} \frac{m^2 + \lambda_n^2[G]}{m^2 + \omega_n^2} < 1, \tag{2.61}$$

where the bound comes from eq. (2.35). This separation is indeed gauge invariant: K does not depend on G, and the eigenvalues of the Dirac operator are invariant under gauge transformations (they just perform a redefinition of the eigenvector basis through a rotation). In $\Delta_{\rm UV}$, the eigenvalues λ_n should become close to the free-theory bound ω_n. In addition, the factors $\Delta(m_j, G)$ related to massive quarks contain a heavy mass m_j unaffected by the chiral limit which provides a natural infrared cut-off, making these factors insensitive to small eigenvalues $\lambda \ll m_j$. For order parameters that are dominated by small eigenvalues, we expect thus $\Delta_{\rm IR}$ to play a prominent role in the average eq. (2.59). Since $\Delta_{\rm IR}$ is an increasing function of the quark mass:

$$m < m_s \Longrightarrow \Delta_{\rm IR}(m|G) < \Delta_{\rm IR}(m_s|G)\,, \tag{2.62}$$

we expect that taking the limit $m_s \to 0$ together with $m \to 0$ (chiral limit for $N_f + 1$ flavours) should lead to a decrease of the chiral order parameters compared to the chiral limit for N_f flavours:

$$\Sigma(N_f + 1) < \Sigma(N_f)\,, \qquad F^2(N_f + 1) < F^2(N_f)\,. \tag{2.63}$$

The significance of this paramagnetic effect depends on the sensitivity of each parameter to the lowest Dirac eigenvalues, in the large-volume and small-mass limits. This may suggest that Σ could undergo a stronger suppression than F^2 as N_f grows. Let us stress that this effect should affect mainly quantities dominated by the infrared end of the Dirac spectrum – other kinds of observables (spectrum and dynamics of vector mesons, string tension…) should have a rather limited sensitivity to the number of light-quark fermions (in particular, the large-N_c limit could prove quite useful to discuss such quantities).

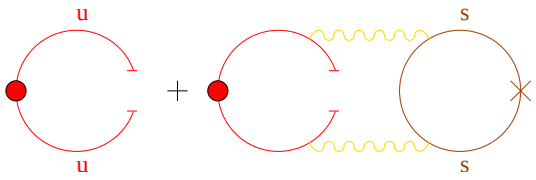

Figure 2.4: *Diagrammatic representation in perturbation theory of the "genuine" $\Sigma(N_f+1)$ and "induced" $\mathcal{Z}_s(m_s)$ condensates contributing to the quark condensate $\Sigma(N_f)$, due to the presence of massive $s\bar{s}$ pairs in the sea.*

The quark condensate $\Sigma(N_f)$ is a function of m_s, and its derivative with respect to this parameter brings down a strange scalar density from the action:

$$\begin{aligned}\frac{\partial}{\partial m_s}\Sigma(N_f) &= \lim_{m\to 0}\int dx\langle T\bar{u}u(x)\ \bar{s}s(0)\rangle^c \ \equiv\ \Pi_Z(m_s) \\ &= \lim \frac{1}{L^4} \ll \left(\sum_k \frac{m}{m^2+\lambda_k^2}\right)\left(\sum_n \frac{m_s}{m_s^2+\lambda_n^2}\right) \gg^c_{N_f},\end{aligned} \tag{2.64}$$

where c denotes the connected component of the correlator. Since $\Sigma(N_f)$ tends to $\Sigma(N_f+1)$ when $m_s \to 0$, we have:

$$\Sigma(N_f) = \Sigma(N_f+1) + \int_0^{m_s} d\mu\ \Pi_Z(\mu) = \Sigma(N_f+1) + m_s\mathcal{Z}_s(m_s) + O(m_s^2\log m_s). \tag{2.65}$$

A third order parameter arises at this stage, in addition to the quark condensate Σ and the decay constant F^2: the two-point correlator Π_Z, which is $1/N_c$-suppressed and violates the Zweig rule in the scalar sector [11]. One can interpret $\Sigma(N_f)$ as receiving two different contributions, one from the "genuine" condensate $\Sigma(N_f+1)$ and another from an "induced" condensate $\mathcal{Z}_s(m_s)$ coming from the effect of $s\bar{s}$ sea pairs, as illustrated in the diagrams of perturbation theory in fig. 2.4. The presence of this extra contribution means that one cannot identify the condensates in the N_f and N_f+1 chiral limits immediately.

A similar discussion holds in the case of the pseudoscalar decay constant, relating the difference between $F^2(N_f)$ et $F^2(N_f+1)$ to the three-point correlator (and a fourth chiral order parameter of interest):

$$i\int d^4x\ d^4y\ e^{iq\cdot(x-y)}\langle T[V_\mu^a(x)V_\nu^b(y) - A_\mu^a(x)A_\nu^b(y)](\bar{s}s)(0)\rangle\,. \tag{2.67}$$

Let us remark that the 0^{++} channel plays here a privileged role, since it has the quantum numbers of the vacuum. The variation of a chiral order parameter from N_f to N_f+1 must be given by a correlator that violates the Zweig rule in the $J^{PC}=0^{++}$ channel (the $1/N_c$ counting of the various correlators considered here is discussed in more details in app. A.2.2), and for this reason, often assumed to be small. We are going to investigate in more detail this assertion.

[11] Π_Z is an order parameter for $\mathrm{SU}_L(N_f)\otimes\mathrm{SU}_R(N_f)$, whereas the correlator:

$$\lim_{m\to 0}\int dx e^{iq\cdot x}\langle T[\bar{u}u(x)\bar{s}s(0)rangle^c\,, \tag{2.66}$$

at $q^2\neq 0$ is an order parameter for both $\mathrm{SU}_L(N_f)\otimes\mathrm{SU}_R(N_f)$ and $\mathrm{SU}_L(N_f+1)\otimes\mathrm{SU}_R(N_f+1)$ theories.

2.4.2 The case of multi-flavour QCD [D]

Due to the quark mass hierarchy, the above discussion is limited to the comparison between $N_f = 2$ and $N_f = 3$ chiral limits for phenomenological applications, since the masses of the other quarks are too large compared to the typical hadronic scales. It is however interesting to discuss a larger framework, which can be called multi-flavour QCD, where more and more massless flavours are added to the theory [34]. Let us assume that we take a QCD-like theory with a large number of heavy quarks which decouple from long-distances, and that we send the masses of N_f of these quarks to zero:

$$m_1 = m_2 = \ldots = m_{N_f} = m \to 0, \qquad m_j \gg \Lambda_H,\ j > N_f. \tag{2.68}$$

We can define order parameters for $\mathrm{SU}_L(N_f) \otimes \mathrm{SU}_R(N_f)$ chiral symmetry:

$$\sigma(N_f) = \lim_{m\to 0} -\langle|\bar{u}u|0\rangle\,, \qquad f^2(N_f) = \lim_{m\to 0} F_\pi^2\,. \tag{2.69}$$

and we study their dependence on N_f [12]. The same argument still holds: considering the gluonic average eq. (2.59), we see that the normalisation of the infrared part of the determinant yields $\Delta_{\mathrm{IR}}(m|G) < 1$, which is exponentiated to the N_f-th power in the average over gluonic configurations, leading to a more and more efficient suppression as N_f grows. One should therefore expect a paramagnetic suppression of chiral order parameters also in this situation:

$$\sigma(N_f + 1) < \sigma(N_f)\,, \qquad f^2(N_f + 1) < f^2(N_f)\,. \tag{2.70}$$

As before, the question remains how strong the suppression is as one moves from N_f to $N_f + 1$. A comment is in order here. We have denoted the chiral order parameters in a different way from those in the physical case Σ and F^2 since the fermion determinant, and thus the average over the gluonic configurations, is in principle different:

- the difference between $\sigma(3)$ and $\Sigma(3)$ amounts to including (or not) heavy-quark loops (charm, bottom, top) and is probably small for chiral order parameters sensitive to the infrared end of the Dirac spectrum
- $\sigma(2)$ would correspond to decoupling the strange quark (and thus to have $m_s \to \infty$) whereas $\Sigma(2)$ takes m_s at its physical mass : in other words, $\Sigma(2)$ corresponds somehow to $\sigma(N_f)$ with N_f between 2 and 3.

A similar discussion holds for F^2 and f^2. A sketch of the situation is described in fig. 2.5.

One can give a more precise description of the situation where $m_s \to \infty$ by using ref. [103], where the problem of matching two QCD-like theories which differ by the integration of one massive quark (sufficiently massive for perturbation theory to hold) is considered. One has the equivalence between the full QCD action (with a dynamical heavy quark) and the effective one (where the dynamical quark has been integrated out):

$$Z = \int [DG][D\psi][D\bar{\psi}][Dh][D\bar{h}] \exp[iS(G, \psi, \bar{\psi}, h, \bar{h}; g, m, m_h)] \tag{2.71}$$

$$\sim_{\,m_h\to\infty} \int [DG][D\psi][D\bar{\psi}] \exp[iS^{\mathrm{eff}}(G, \psi, \bar{\psi}; g', m'; m_h)]\,, \tag{2.72}$$

[12] We keep the fundamental scale Λ_{QCD} (defined in a mass-independent scheme) at a fixed value (say its value at a scale below the charm threshold in the physical case), in order to be able to compare the different theories.

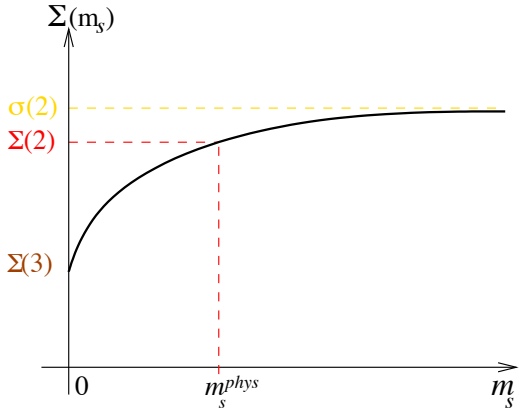

Figure 2.5: *Dependence on m_s of the quark condensate Σ, and its relation with σ.*

with the effective action

$$S^{\rm eff}(G,\psi,\bar\psi;g',m';m_h) = S(\sqrt{z_3}G,\sqrt{z_2}\psi,\sqrt{z_2}\bar\psi,0,0;z_g g,z_m m,0)+\sum_n \int d^4x \frac{z_n O_n(x)}{m_h^{d_n-4}}\,, \quad (2.73)$$

where z's are renormalisation factors, O_n are the (tower of) operators induced by the integration of the heavy quark and m' is the effective light quark mass including effects from the (integrated out) heavy quark. As far as the quark condensate is concerned, one obtains:

$$\langle\bar u u\rangle^{(N_f+1)} = \frac{\partial}{\partial m} Z|_{m=0} \sim_{m_h\to\infty} \frac{\partial}{\partial m}\int [DG][D\psi][D\bar\psi]\exp[iS^{\rm eff}(G,\psi,\bar\psi;g',m';m_h)] \quad (2.74)$$

$$\sim_{m_h\to\infty} \frac{\partial m'}{\partial m}\times \langle\bar u u\rangle^{(N_f)}\Big|_{m=0} + O\left(\frac{1}{m_h}\right). \quad (2.75)$$

The conversion factor for the light quark mass between the full (m) and the effective (m') actions is known up to two loops (see eq.(93) in ref. [103]):

$$\Sigma(2) \sim_{m_s\to\infty} \sigma(2)\left[1+\left(\frac{\alpha_s(\mu)}{\pi}\right)^2\left(\frac{89}{432}+\frac{5}{36}\log\frac{m_s^2}{\mu^2}+\frac{1}{12}\log^2\frac{m_s^2}{\mu^2}\right)+O(\alpha_s^3)\right]+O\left(\frac{1}{m_s}\right), \quad (2.76)$$

where m_s denotes the heavy quark masses defined in the $\bar MS$-scheme considered at the scale μ. As expected, the limit $m_s\to\infty$ sends $\Sigma(2)$ to $\sigma(2)$ up to logarithmic and power-suppressed corrections.

2.5 The N_f-sensitivity of the pattern of chiral symmetry breaking

2.5.1 From 2 to 3 flavours [A]

The dependence of chiral order parameters on N_f is often assumed to be negligible, because it is related to the role of light-quark loops in these parameters, and the related weight of the fermionic determinant. Indeed, the effect of these loops is suppressed according to the Zweig rule and to the limit of a large number of colours. Both are often considered as good approximations of QCD [104–107]. This idea was applied in the sector of the lightest pseudoscalar mesons

to provide models for the associated correlators [25, 108–114] and to determine counterterms of their effective theory [23, 27, 115–119]. More recently, the same Lagrangians were extended to higher orders under the name of Resonance Chiral Theory, taking into account the OPE constraints on the high-energy behaviour of the QCD correlators to describe the dynamics of light resonances, and thus reach the energy region between 1 and 2 GeV [26, 28, 120–126]. The overall agreement with data can be considered as a global test of the validity of the large-N_c limit underlying this approach.

In another domain, for a long time, many lattice QCD computations were performed within quenched QCD (a non-unitary Yang-Mills theory where the fermion determinant is set 1), with an overall decent agreement with experimental data. This was often taken as a further proof of the limited influence of the fermion determinant. However, recent improvements in lattice simulations have paved the way for unquenched simulations with three light dynamical (or sea) quarks. Even though these simulations are still at an early stage, their results are already very instructive, especially when one is interested in the low-energy dynamics of strong interactions. Indeed several groups have observed significant variations between the chiral limit of $N_f = 2$ and $N_f = 3$ massless flavours, for instance studies based on the light-meson masses and decay constants found: PACS-CS [127] and MILC [128, 129] found:

$$\text{PACS}-\text{CS}: \frac{F(2)}{F(3)} = 1.089 \pm 0.045\,, \qquad \frac{\Sigma(2)}{\Sigma(3)} = 1.245 \pm 0.010\,, \tag{2.77}$$

$$\text{MILC}: \frac{F(2)}{F(3)} = 1.15 \pm 0.05 \begin{pmatrix} +0.10 \\ -0.03 \end{pmatrix}, \qquad \frac{\Sigma(2)}{\Sigma(3)} = 1.52 \pm 0.17 \begin{pmatrix} +0.38 \\ -0.15 \end{pmatrix}. \tag{2.78}$$

whereas a JLQCD and TWQCD lattice study of the distribution of low-lying Dirac eigenvalues obtained [102]:

$$\text{JLQCD/TWQCD}: \frac{\Sigma(2)}{\Sigma(3)} = 1.30 \pm 0.54\,. \tag{2.79}$$

In addition, the large-N_c limit is known to be a bad approximation for the scalar sector 0^{++}. This can be seen for instance in the decays $J/\Psi \to VPP$, with $V = \phi, \omega$ and $P = \pi^{\pm}, K^{\pm}$, whose dynamics in the S-wave indicate a significant violation of the Zweig rule [130, 131]. This remark has a direct implication on Π_Z defined in eq. (2.64) and the resulting variation of the quark condensate. Indeed, scalar states, singlets of SU(N_f), strongly coupled to the first N_f quarks and to the scalar density $\bar{s}s$, could yield an "induced" condensate of comparable size to the "genuine" condensate in eq. (2.65). Such a variation would thus be related to the puzzling features of the spectrum of scalar resonances, departing from the conventional situation of nonets with an ideal mixing [13].

Indeed, in contrast to the vector and tensor mesons, the identification of the scalar mesons is a long-standing puzzle [132]. Many scalar resonances are difficult to resolve because of their large decay widths leading to a significant overlap with the background, with several decay channels opening up within short mass intervals. In addition, light non-$q\bar{q}$ scalar are expected (glueballs, multiquark), blurring even more the quark-model picture guiding the discussion of

[13] For instance, in the vector channel, one has an ideal mixing between the ω and ϕ resonances, leading to an almost exact quark assignment for the neutral, non-strange vector mesons:

$$|\rho^0\rangle = \frac{|u\bar{u}\rangle - |d\bar{d}\rangle}{\sqrt{2}}\,, \qquad |\omega\rangle = \frac{|u\bar{u}\rangle + |d\bar{d}\rangle}{\sqrt{2}}\,, \qquad |\phi\rangle = |s\bar{s}\rangle\,, \tag{2.80}$$

so that none of these resonances would contribute significantly to the spin 1 analogue of the two-point correlator Π_Z, because none couple to both operators at the same time.

I	Name	Mass (MeV)	Width (MeV)	Sources
$I=0$	$f_0(600)$	400-1200	600-1000	$\pi\pi$ S-wave analysis of πN and $K_{\ell 4}$
	$f_0(980)$	980 ± 10	40-100	$\pi^- p \to \pi^0\pi^0 n, \phi \to f_0\gamma$
				$\gamma\gamma \to \pi\pi, J/\psi \to \phi^+\phi^-, D_s$ decays
	$f_0(1370)$	1200-1500	200-500	4π in $p\bar{p}$ and $p\bar{n}/n\bar{p}$
	$f_0(1500)$	1505 ± 6	109 ± 7	$\pi\pi, K\bar{K}, \eta\eta, \eta\eta', 4\pi$ in $p\bar{p}$ and $p\bar{n}/n\bar{p}$
$I=1/2$	$K_0^*(800)$	672 ± 40	550 ± 34	See sec. 7.6
	$K_0^*(1430)$	1425 ± 50	270 ± 80	$K\pi$ final state in Kp production
$I=1$	$a_0(980)$	980 ± 20	50-100	$K\bar{K}$ and $\pi\eta$ in $p\bar{p}$ annihilation, $\phi \to a_0\gamma$
	$a_0(1450)$	1474 ± 19	265 ± 13	$p\bar{p}$ annihilation, $D^\pm \to K^+K^-\pi^\pm$

Table 2.1: *Light scalar resonances listed in ref. [137].*

other channels. This means that most scalar resonances cannot be identified as sharp resonances well separated and with little mixing, which will described by narrow Breit-Wigners, and that more involved tools must be used, in particular the analytic continuation of scattering/decay amplitudes to identify the position of the poles in unphysical sheets of the complex energy plane [45,133], unitarised amplitude methods to understand their large-N_c behaviour [134,135], or their behaviour in lattice simulations [136].

The Particle Data Group [137] list several resonances as clearly identified, collected in tab. 2.1. Their interpretation is subject to even more controversies than their identification [138]. $f_0(980)$ and $a_0(980)$ are often considered as $K\bar{K}$ molecules due to the proximity of their masses to this threshold. Another popular model consists in putting $f_0(980)$, $a_0(980)$, $f_0(600)$, $K_0^*(800)$ in a nonet of four-quark states, whereas $f_0(1370)$, $f_0(1500)$, $K_0^*(1430)$, $a_0(1450)$ would form another nonet from $q\bar{q}$ states. One main difficulty for such unambiguous theoretical interpretation comes from the mixing of the various states among themselves, as well as with pure glue states (glueballs) which should also appear in the spectrum above 1 GeV. At any rate, it is quite striking the low-energy scalar spectrum, directly connected to the structure of the vacuum through its quantum numbers, presents a rather complicated pattern, very different from other channels. This feature could have an impact on the discussion of the m_s-dependence of chiral order parameters.

2.5.2 For large N_f [B,D]

Other approaches, investigating the case of multi-flavour QCD, see sec. 2.4.2, support also that there should be some sensitivity of these order parameters on the number of massless flavours. Chiral phase transitions are thus expected to occur for sufficiently large N_f/N_c [139], leading to the restoration of chiral symmetry. Indeed, if we consider the β-function in perturbative QCD [10], we know that asymptotic freedom will be lost for large values of N_f (above 16 if we remain at the one-loop level). The theory exhibits then a non-Abelian QED-like behaviour, where neither confinement nor chiral symmetry breaking are expected. If the number of flavours decreases, one expects to encounter a conformal window where the theory is asymptotically free in the ultraviolet, but present a non-trivial infrared fixed point. In such a scale-invariant theory, the theory cannot confined and chiral symmetry must remain unbroken. Finally, as we decrease the number of flavours, the infrared fixed-point becomes non-perturbative and the coupling constant becomes large, triggering a breakdown of chiral symmetry. Just below the

boundary, one may expect early signs of the restoration of chiral symmetry, such as an almost parity doubling spectrum [140, 141].

Analytic studies of the QCD conformal window based on perturbative arguments [142] suggest that chiral symmetry is restored for $N_f \sim 10$ (for $N_c = 3$). Gap equations in the same window yield a slightly different limit [143], with a critical value for N_f above 12. In addition, the instanton liquid model [144] predicts that instantons do not contribute to chiral symmetry breaking any more for $N_f > 6$ [145, 146].

Lattice simulations have been used to investigate this conformal window as a function of the number of flavours and the representation of the fermions, in relation with extended technicolor scenarios. They identify the conformal-invariant nature of Yang-Mills theory through different features such as the power-like dependence of the whole spectrum on the quark masses (no mass gap) or the running of the coupling constant (from the comparison of lattices of different sizes, the potential between static charges, or the study of the renormalisation group flow of the coupling constants). Indications from several collaborations indicate that the lower end of the conformal window should be somewhere around $N_f = 9$ or 10 for fermions in the fundamental representation [147]. In all cases, we see that there should be some not-so-large value of N_f above which chiral symmetry should be restored.

2.5.3 Chiral phase transitions in multi-flavour QCD [D]

As discussed above, one may expect several phases when one increases the number of light flavours in the theory, with a restoration of chiral symmetry for some critical value of N_f. One question is whether there are further phase transitions within the chirally broken phase, as some of the order parameters vanish as the number of flavour increases. There is in particular a situation where a strong dependence of the quark condensate on the number of light-quark flavours would find a natural explanation. If σ is particularly sensitive to the suppressing effect of light-quark loops, as suggested by the fact that they are not sensitive to the same kind of accumulation of small Dirac eigenvalues around zero as other chiral order parameters, it could vanish earlier than f^2. Three phases could then occur:

- For $N_f < n_{\text{crit}}(N_c)$, chiral symmetry is broken and the quark condensate does not vanish.
- For $n_{\text{crit}}(N_c) \leq N_f \leq N_{\text{crit}}(N_c)$, chiral symmetry is broken, but the condensate vanishes.
- Above $N_{\text{crit}}(N_c)$, chiral symmetry is restored.

The transition at $N_f = n_{\text{crit}}(N_c)$ could be related to the extension of the residual symmetry group, such as: $\text{SU}_L(N_f) \otimes \text{SU}_R(N_f) \to \text{SU}_V(N_f) \times Z_A(N_f)$. Indeed the discrete axial symmetry $Z_A(N_f)$ forces some chiral order parameters to vanish, such as Σ [148]. As discussed in app. A.1.2, Weingarten inequalities [65] do not hinder the existence of an intermediate chirally-broken phase with a vanishing quark condensate. However, the two transitions could occur simultaneously $n_{\text{crit}}(N_c) = N_{\text{crit}}(N_c)$, so that the vanishing of the quark condensate coincide with the restoration of chiral symmetry. The qualitative argument suggesting a decrease of order parameters does not allow us to quantify this effect.

However, in a three-phase scenario, a strong variation of $\Sigma(N_f)$ would find a natural explanation just below the critical value $n_{\text{crit}}(N_c)$ where the quark condensate vanishes. Let us take a theory with N_f flavours with $N_f + 1 < n_{\text{crit}}(N_c) \leq N_f + 2$, and let us call m_s the $N_f + 1$-th quark and define $\Sigma(N_f + 1)$ and $\Sigma(N_f + 2)$ in analogy with the discussion for $N_f = 2$. In that case, $\Sigma(N_f + 1)$ differs from zero but it is already small. According to eq. (2.49), a small condensate would indicate the suppression of the average density of states $\ll \rho(\lambda) \gg_{N_f} /L^4$ for

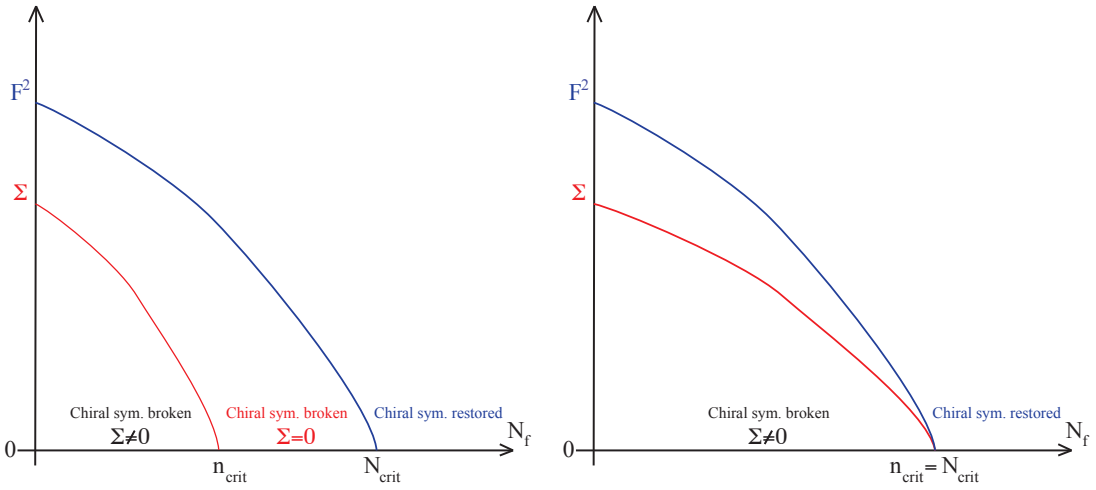

Figure 2.6: *Two different scenarios of chiral symmetry breaking and restoration, depending on the presence of an intermediate phase breaking chiral symmetry but with a vanishing quark condensate.*

$\lambda \sim m$. On the other hand, close to a phase transition, the fluctuations of this density of states and/or the density-density correlation $\ll \rho(\lambda)\rho(\lambda') \gg^c_{N_f} /L^4$ for $\lambda \sim \lambda' \sim m$ are expected to increase. Actually, the difference between $\Sigma(N_f+1)$ and $\Sigma(N_f)$ is related to this correlation through eq. (2.64):

$$\Pi_Z(m_s) = 4 \lim \int_0^\infty \frac{du}{1+u^2} \frac{dv}{1+v^2} \frac{1}{L^4} \ll \rho(mu)\rho(m_s v) \gg^c_{N_f} . \tag{2.81}$$

Therefore, slightly below the critical point $n_{\rm crit}(N_c)$, the suppression of the density of states and the increase in density-density correlations could yield a competition between the first two terms in the m_s-expansion in eq. (2.65) [34].

It is interesting to study the large-N_c limit of the three-phase scenario. The quark loops are suppressed, and the chiral order parameters become independent of N_f. The critical point $n_{\rm crit}(N_c)$, where σ vanishes, would thus tend to infinity in this limit [14]. The $1/N_c$-expansion would thus converge slowly close to critical point, and would be unable to reproduce properly the phase above $n_{\rm crit}(N_c)$. One can in particular recall the study of Weiberg-like sum rules for vector and axial mesons in the large N_c limit in ref. [108], which connected the spectrum of spin-1 mesons with the condensates arising in the Operator Product Expansion of the $VV-AA$ correlator. A vanishing quark condensate would require a complicated pattern of cancellation in these sum rules between the vector and axial resonances in the chiral limit, which does not seem realised phenomenologically. This is in agreement with the expectation that $\lim_{N_c\to\infty} n_{\rm crit}(N_c) = \infty$, so that the phase above $n_{\rm crit}(N_c)$ cannot be reached easily within a large-N_c framework.

2.6 Summary

Low-energy QCD is governed by the breakdown of chiral symmetry, which can be described through chiral order parameters. Two parameters play a particular role: the quark condensate

[14] Such a behaviour would be in agreement with many perturbative computations where N_f and N_c arise only through the ratio N_f/N_c.

Σ (most simple order parameter) and the decay constant F^2 (unambiguous signature of chiral symmetry breaking) The mass hierarchy $m_u, m_d \ll m_s \ll \Lambda_H \sim 1$ GeV suggests two different chiral limits. The first one consists in keeping m_s at its physical mass whereas $m_u, m_d \to 0$. This limit of $N_f = 2$ massless flavours is particularly useful to analyse $\pi\pi$ scattering at threshold. The second limit corresponds to $N_f = 3$ massless flavours: m_u, m_d and m_s go to 0, where K and η dynamics is also included.

One may wonder about the role played by the number of light flavours: does the chiral structure of the QCD vacuum evolve significantly when N_f increases ? Chiral symmetry is expected to be restored at very large N_f, indicating some sensitivity of the vacuum to light-quark loops, in constrast with the Zweig rule and the large-N_c limit. The issue can be studied through the spectrum of the Dirac operator $\not{D}$ on an Euclidean torus. Indeed, the pattern of chiral symmetry breaking is reflected by the accumulation of small eigenvalues around zero when the volume of the torus tend to infinity. In particular, chiral order parameters such as $\Sigma(N_f)$ and $F^2(N_f)$ are dominated by these small eigenvalues. Due to Vafa-Witten's paramagnetic bound on the latter, one expects the fermion determinant to suppress such order parameters more and more as more and more light flavours become massless. Σ and F^2 are thus expected to decrease from $N_f = 2$ to $N_f = 3$ massless flavours. The same argument suggests that the same effect would occur by adding more and more massless flavours to the theory while keeping Λ_{QCD} to a fixed value.

The speed of this decrease can be measured through chiral order parameters that violate the Zweig rule in the scalar sector 0^{++}. This sector is known no to comply with the Zweig rule and the large-N_c limit, so that order parameters like Σ and F^2 could depend strongly on N_f. In addition, Σ and F^2 are not sensitive to the same features in the accumulation of small eigenvalues around 0 when the volume of the torus goes to infinity. Σ could thus decrease more quickly than F^2. This suggests a more speculative scenario of two chiral phase transitions occurring one after the other as N_f increases. We start from a phase where the quark condensate is different from zero and chiral symmetry is spontaneously broken. When N_f increases, Σ would decrease more quickly than F^2 and would vanish for a critical number of flavours $n_{\rm crit}(N_c)$. The pseudoscalar decay constant would still be different from zero and it would vanish only later, for a second critical value $N_{\rm crit}(N_c)$. The phase $n_{\rm crit}(N_c) < N_f < N_{\rm crit}(N_c)$ features a vanishing quark condensate, but chiral symmetry is still broken since $F^2(N_f) \neq 0$. Chiral symmetry restoration occurs only once the number of massless flavours is larger than $N_{\rm crit}(N_c)$. This scenario exhibits interesting possibilities near the first critical point. Indeed, $\Sigma(N_f)$ can be interpreted as the density of Dirac eigenvalues, whereas the difference $\Sigma(N_f + 1) - \Sigma(N_f)$, related to the violation of the Zweig rule in the scalar sector, corresponds to correlations between eigenvalues. At the vicinity of a critical point, we would expect a suppression of the density of states and an increase in the fluctuations. A significant decrease of the quark condensate from 2 to 3 flavours could be explained due to the fact that $n_{\rm crit}(N_c)$ is close to 3, in relation with the observed violation of the Zweig rule in the scalar sector 0^{++}.

This scenario is only a possible scheme for such chiral phase transition – we could also imagine that there is no such intermediary phase, so that the vanishing of the quark condensate and the restoration of chiral symmetry occur for the same number of flavours. Experimental data, lattice simulations or more elaborated models of spontaneous chiral symmetry breaking should provide elements to decide which scenario is favoured.

Begin at the beginning and go on till you come to the end: then stop.

The King

3

Chiral perturbation theory and its limits

After the general discussion of chiral order parameters and their dependence on the strange quark mass, it is time to discuss the effective theory of low-energy QCD that embeds chiral symmetry breaking, namely Chiral Perturbation Theory (χPT). This effective theory exploits in an optimal way our knowledge of chiral symmetry to provide the generic form of QCD correlators at low energies as an expansion of masses and momenta. This is obtained by matching the generating functional of QCD to that of the effective theory, and ensuring that the symmetries of the former are obeyed by the latter – more precisely, that the Ward identities encoding chiral symmetry are obeyed by the mass and momentum expansion of the correlators provided by the effective theory. The latter involves the chiral order parameters discussed previously under the form of low-energy constants, that are unknown and should be determined from experiment or lattice simulations. One can design different versions of χPT in the chiral limits of $N_f = 2$ and $N_f = 3$ massless flavours, involving either only very soft pions, or moderately soft π, K, η. The two theories can be matched in the regime where they overlap.

Due to the non-renormalisable character of this effective theory, these low-energy constants proliferate as the order of the expansion increases. If the leading-order (LO) constants amount to the two chiral order parameters discussed in the previous chapter, next-to-leading-order (NLO) constants are already difficult to determine, and one must rely on models to determine a significant fraction of next-to-next-to-leading (NNLO) constants, as they cannot be realistically all determined from experiment or lattice simulations. We perform a brief overview of some of the determination of the NLO low-energy constants of $N_f = 2$ and $N_f = 3$ χPT, based either on dispersive considerations or on lattice simulations. Some of the $N_f = 3$ constants are particularly difficult to pin down, like L_4 and L_6, which are large-N_c suppressed and encode the quark-mass dependence of observables like the masses and decay constants of the pseudoscalar mesons. It turns out that these low-energy constants also encode the N_f-dependence of the quark condensate and the pseudoscalar decay constant, and thus are related to the discussion of the previous chapter. Depending on the values of L_4 and L_6, one may expect a numerical competition between the (suppressed) leading-order contribution and the (m_s-enhanced) next-to-leading order contributions. In that case, one has to be careful with some usual reexpressions of χPT counterterms in terms of physical observables (for instance m_s/m in terms of M_K^2/M_π^2), since these reexpressions are only valid at leading order, and thus may suffer from large higher-order corrections.

We start from identities for the masses and decay constants of the pseudoscalar mesons, supposed to exhibit good convergence properties at NNLO to draw some conclusions on relations between low-energy constants and pattern of chiral symmetry breaking. A small shift of L_6 and L_4 from very particular ("critical") values is enough create a very strong suppression of the quark condensate and the pseudoscalar decay constant from $N_f = 2$ to $N_f = 3$. We discuss some further features of the two-flavour order parameters, which are essentially correlated with the value of the quark mass ratio $r = m_s/m$. Some differences in the structure of the $N_f = 2$ and $N_f = 3$ theories allow us to expect a suppression only in the latter case, whereas the former one should be protected from vacuum fluctuations of quark pairs. We finally discuss the connection with the condensates at finite quark mass involved in the Operator Product Expansion of QCD correlators at high energies [1].

[1] This chapter is based on the following articles:

[C] SDG and J. Stern, *Vacuum fluctuations of $q\bar{q}$ and values of low-energy constants*, Phys. Lett. B488 (2000) 274 [36]

[D] SDG, L. Girlanda, and J. Stern, Chiral order and fluctuations in multi-flavor QCD, Eur. Phys. J. C27 (2003) 115 [37]

[E] SDG, N. Fuchs, L. Girlanda, and J. Stern, *Resumming QCD vacuum fluctuations in three-flavor chiral*

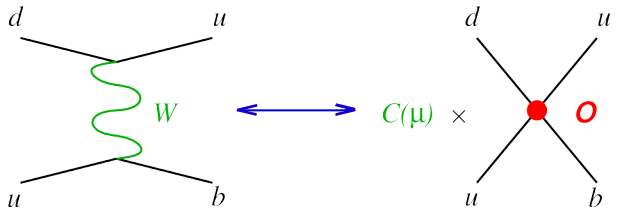

Figure 3.1: *From the Fermi theory of weak interactions to the Standard Model and back.*

3.1 Effective field theory

Quantum Chromodynamics at low energies cannot be analysed in terms of quarks and gluons, since they interact strongly and are confined inside hadrons. However, the spectrum of the bound states suggest to exploit approximate symmetries of the theory and to build an effective theory in terms of the relevant degrees of freedom. This is a rather general problem in physics: low-energy computations in the framework of a theory known at high energies but fairly complicated can be performed more efficiently through a simplified, approximate, theory [19, 22, 69, 70, 149–151]. If we perform experiments at higher and higher energies, new degrees of freedom will emerge, and some particles which were considered elementary will become bound states of more fundamental fields. Inversely, if the energy of the processes is lowered, some degrees of freedom will disappear from the observable spectrum of the theory and can be integrated out of the functional integral. Obviously, this programme can be achieved only if the processes occurring at different energies decouple enough for this separation to make sense, so that the accuracy at which the effective description mirrors the fundamental theory can be estimated through ratios of significantly different scales.

A prominent example of such approach is provided by the effective Hamiltonian that is used to analyse weak decays of mesons and baryons [152]. Indeed, in the Standard Model, this multi-scale problem, involving at the same time the electroweak scale (weak gauge bosons and top quark, around 100 GeV) and the hadronic scale (mass of the bound states involving b, c or s quarks, around a few GeV at most). Integrating out the heavy degrees of freedom yields an effective Hamiltonian that corresponds to a factorised expression, with local operators involving only light dynamical fields (describing the low-energy dynamics of the theory, identical to that of the Standard Model) multiplied by Wilson coefficients (encoding the high-energy dynamics of the Standard Model). The latter can be evaluated perturbatively if the separation scale Λ between low and high energies is not too small, and radiative corrections can still be determined using perturbation theory if the separation scale lies in the perturbative domain of QCD. One may think that this treatment is a step backwards, as one goes back from the electroweak theory down to an extended Fermi theory of weak interactions, but this effective treatment of the Standard Model has several advantages: it allows one to separate neatly the different scales in the problem and the difficulties specific to each energy region (content and dynamics of the electroweak sector on one side, nonperturbative effects of strong interactions through weak matrix elements on the other side), and an RGE approach can be used to resum the large logarithms occurring in the Wilson coefficients as one integrates out the degrees of freedom from the electroweak scale down to the hadronic scale of the problem.

The weak effective Hamiltonian is an example of a decoupling effective theory, since all

perturbation theory, Eur. Phys. J. C34 (2004) 201 [38]

the effect of the heavy fields is encoded in the Wilson coefficients, whereas the light degrees of freedom are the same as (the low-momentum modes of) the fields of the underlying theory $(u, d, s, \gamma \ldots)$. The effective Lagrangian has a general form after integrating out degrees of freedom heavier than Λ:

$$\mathcal{L}_{\text{eff}} = \mathcal{L}_{d\leq 4} + \sum_{d>4} \frac{1}{\Lambda^{d-4}} \sum_{i_d} C_{i_d} \mathcal{O}_{i_d} \,, \tag{3.1}$$

where $\mathcal{L}_{d\leq 4}$ containing the potentially renormalisable terms with operator dimension $d \leq 4$, the coefficients C_{i_d} are dimensionless Wilson coefficients and $\mathcal{O}_{i_d}$ are local operators of light fields with dimension d. Other effective theories consist of the Euler-Heisenberg theory for QED at energies much below the electron mass, or the Standard Model itself. In the latter case, we do not know the relevant scale or the underlying theory, even though there are many contenders (e.g., supersymmetry, GUT, extra-dimensional gauge theories. . .) and we have only vague hints of the terms involved in the effective Lagrangian for $d > 4$.

But one can also consider non-decoupling effective theories, where the light degrees of freedom of the effective theory are different from those of the underlying one, because of a phase transition occurring as one decreases the energy. This phase transition comes from the spontaneous breakdown of a symmetry, generating Goldstone bosons that are definitely light degrees of freedom. Since a spontaneously broken symmetry can be used to relate processes with different numbers of Goldstone bosons, the dimensional separation eq. (3.1) is not meaningful. In general, the effective Lagrangian is non-renormalisable, which does not prevent if from being a well-defined and consistent framework. Because of the phase transition occurring as one lowers the energy, we cannot determine the structure of the theory, and in particular the values of the Wilson coefficients, through a perturbative computation as an expansion of the gauge coupling constants, as we could do in the decoupling case.

We will therefore adopt a slightly less ambitious approach to determine the effective theory of low-energy QCD that falls in this non-decoupling category. We aim at a theory of strong interactions, valid at low energies where Goldstone bosons are the relevant degrees of freedom, following the principles of quantum field theory: isolate the relevant degrees of freedom, determine the underlying symmetries and build the most general field theory in agreement with those. According to Weinberg's conjecture [18, 69, 149, 153], computing a matrix element with this Lagrangian to any given order of perturbation theory will yield the most general S-matrix element consistent with analyticity, perturbative unitarity, cluster decomposition and the assumed symmetry principles. An important feature here is the nature of the degrees of freedom: we deal with pseudo-Goldstone bosons, whose interactions becomes weaker and weaker as the momentum decreases, as recalled in sec. 2.2.1. Therefore, a perturbative expansion can be considered even for low-energy QCD, if the effective theory is expressed in terms of the lightest pseudoscalar octet and if the expansion parameter is the energy rather than the gauge coupling.

Since we perform a low-energy expansion of Green functions, we will build a tower of Lagrangians contributing to a given power $(E/\Lambda)^k$ to the observables, with operators of increasing degree. We will organise the low-energy theory with growing k and we will stop at a given accuracy (i.e. for a given power). The theory will thus involve a growing number of unknown parameters (the coefficients of the operators) since we cannot follow Wilson's ideas up to their conclusion in the case of QCD. This may seem rather discouraging at first sight: a non-decoupling effective theory cannot pretend to compute a large number of processes from a limited set of parameters with a high accuracy. But it is able to assess the symmetry relations between different processes quantitatively. It provides a structure for our theoretical knowledge (and ignorance) to exploit experimental data optimally, and as such, it is the appropriate framework to obtain information on the dynamics of QCD in the non-perturbative regime.

3.2 The effective theory of low-energy QCD

3.2.1 QCD generating functional

We want to build an effective theory of QCD, where the degrees of freedom are the pseudoscalar mesons (π, K, η), taking chiral symmetry into account. With the help of this theory, we will study processes by computing Green functions of axial ad vector currents and of scalar and pseudoscalar densities, before using the LSZ reduction formula to extract amplitudes for incoming and outgoing states of pseudoscalar mesons. The full set of connected Green functions for this problem can be derived from their generating functional:

$$e^{i\Gamma[v,a,s,p,\theta]} = \langle 0|T \exp\left\{ i \int d^4x \; \bar{\psi}[\gamma^\mu(v_\mu + \gamma_5 a_\mu) - (s - i\gamma_5 p)]\psi - \frac{g^2}{32\pi^2}\theta \; \tilde{G}^{\alpha;\mu\nu} G^\alpha_{\mu\nu} \right\} |0\rangle \,, \tag{3.2}$$

where v, a, s, p, θ are classical sources. The Green functions are obtained by taking derivatives of Γ with respect to this sources, then setting $v = a = s = p = 0$ et $\theta = \theta_0$ (if we consider a non-vanishing vacuum angle). Γ can be reexpressed through the functional integral:

$$e^{i\Gamma[v,a,s,p,\theta]} = \int [DG][D\psi][D\bar{\psi}] \quad \exp\left\{ i \int d^4x \mathcal{L}_{\rm QCD} \right\}_{\theta=0} \tag{3.3}$$

$$\times \exp\left\{ i \int d^4x \bar{\psi}[\gamma^\mu(v_\mu + \gamma_5 a_\mu) - s + \gamma_5 p)]\psi - \frac{g^2}{32\pi^2}\theta \; \tilde{G}^{\alpha;\mu\nu} G^\alpha_{\rho\sigma} \right\} \tag{3.4}$$

$$= \int [DG][D\psi][D\bar{\psi}] \exp\left\{ i \int d^4x \mathcal{L}_{\rm QCD}[v,a,s,p,\theta] \right\}, \tag{3.5}$$

with the QCD Lagrangian in the presence of sources:

$$\mathcal{L}_{\rm QCD}[v,a,s,p,\theta] = \mathcal{L}_f + \sum_Q (i\not{D} - M_Q)Q - \frac{1}{4} G^{\alpha;\mu\nu} G^\alpha_{\mu\nu} - \frac{g^2}{32\pi^2}\theta \; \tilde{G}^{\alpha;\mu\nu} G^\alpha_{\mu\nu}$$

$$+ \sum_q \bar{\psi}[\gamma^\mu(iD_\mu + v_\mu + \gamma_5 a_\mu) - \tilde{s} + \gamma_5 p]\psi,$$

where $\tilde{s}(x) = s(x) + M$, with the light-quark mass matrix M. We will actually replace $\tilde{s}$ by s in the last expression and we will compute the different derivatives of the generating functional at the point $v = a = p = 0$, $s = M$ and $\theta = \theta_0$.

3.2.2 Ward identities

Our effective theory will involve only the pseudoscalar mesons (collected in a matrix U) as degrees of freedom, and it must obey the constraints from chiral symmetry. Its generating functional will be:

$$e^{i\Gamma_{\rm eff}[v,a,s,p,\theta]} = \int [dU] \exp\left\{ i \int d^4x \; \mathcal{L}_{\rm eff}[U,v,a,s,p,\theta] \right\} = e^{i\Gamma[v,a,s,p,\theta]} + \ldots \tag{3.6}$$

where the ellipsis recall us that the equality between the QCD and effective generating functionals must be understood, up to a given order in a low-energy expansion that we will define in the following. Chiral symmetry will constrain the structure of the Green functions by imposing Ward identities among them, and this requirement can be expressed in a very simple way in the

framework of the generating functional. The whole set of Ward identities can be reexpressed by requiring that Γ is invariant under local transformations (depending on space-time) of the external sources $\mathcal{S} = v, a, s, p$:

$$\Gamma[\mathcal{S}'] = \Gamma[\mathcal{S}], \qquad \mathcal{S}' = T(g)\mathcal{S}, \tag{3.7}$$

with $g(x) \in \mathrm{SU}_L(N_f) \otimes \mathrm{SU}_R(N_f)$ and $T(g)$ its representation for the sources $\mathcal{S}$ (more detail can be found in app. A.2.1). We could include Green functions of the singlet axial and vector currents in this framework. One must then consider transformations under $\mathrm{U}_L(N_f) \times \mathrm{U}_R(N_f)$ ($\langle\alpha\rangle \neq 0$ and $\langle\beta\rangle \neq 0$). However, the constraints stemming from symmetries at the classical level cannot be all fulfilled simultaneously at the quantum level, due to the impossibility to define the integration measure over fermions in a way that is both gauge- and chiral-invariant under the whole chiral group [154]. It manifests itself as ambiguities in the one-loop evaluation of correlators involving both axial and vector currents. Fixing these ambiguities amounts to allowing for anomalous Ward identities, meaning that some of the symmetry constraints must be abandoned once one goes at the quantum level (in practice, one warrants the conservation of vector currents, which are gauged once QCD is embedded in the Standard Model, and puts all the burden of anomalous non-conservation on the axial currents [155]). This issue modifies eq. (3.7) and requires a particular treatment, detailed in app. A.2.1. Γ must be split in two parts:

$$\Gamma[\mathcal{S}] = \Gamma^0[\mathcal{S}] + \Gamma^{WZ}[\mathcal{S}], \tag{3.8}$$

where Γ^{WZ} collects terms corresponding to the anomalous identities (it corresponds to finding a particular solution to the equation for the anomalous terms eq. (A.43)) and Γ^0 is the general solution for the invariance equation:

$$\Gamma^0[\mathcal{S}'] = \Gamma^0[\mathcal{S}]\,. \tag{3.9}$$

Any Lagrangian fulfilling the Ward identifies of chiral symmetry (detailed in app. A.2.1) will obey the decomposition (3.8). Wess and Zumino [156], and Witten [156] built an explicit Lagrangian accounting for anomalous Ward identities, expressed in terms of U, v_μ and a_μ, which can describe Γ^{WZ}. At this stage, it remains to build the general solution Γ^0.

3.2.3 Description of Goldstone bosons

In QCD, the chiral symmetry group G acts on the quarks as:

$$q_R \xrightarrow{g} V_R q_R, \qquad q_L \xrightarrow{g} V_L q_L. \tag{3.10}$$

The effective theory deals with Goldstone bosons, which transform under a representation of G:

$$\phi^a \xrightarrow{g} \theta^a(g, \phi). \tag{3.11}$$

It turns out that the representation θ is constrained tightly by the composition law [70]:

$$\theta(g_1, \theta(g_2, \phi)) = \theta(g_1 g_2, \phi). \tag{3.12}$$

We can start by defining the subgroup that leaves the origin stable: $H = \{h, \theta(g, 0) = 0\}$. Let us notice that $\theta(gh, 0) = \theta(g, 0)$ for all $g \in G$ and $h \in H$. $\theta(g, 0)$ is thus an application from the quotient space G/H obtained by identifying in G the elements g and g' such as $g' = gh$ with $h \in H$. This application of G/H in G is invertible: if $\theta(g_1, 0) = \theta(g_2, 0)$, one has $g_1 g_2^{-1} \in H$, so

that g_1 and g_2 correspond to the same element in G/H. We can thus identify the Goldstone boson fields to the coordinates of the quotient space G/H.

Let us choose a representant n in each equivalence class $\{gh, h \in H\}$, in order to decompose any element of G as $g = nh$ in a unique way. The composition law eq. (3.12) shows that the image n' of n under the action of $g \in G$ is obtained by decomposing the product gn in $n'h$, which corresponds to the action of G on G/H. Here, $G = \mathrm{SU}_L(N_f) \otimes \mathrm{SU}_R(N_f)$ and $H = \mathrm{SU}_V(N_f)$, so that $g = (V_R, V_L)$, whereas H consists in pairs (V, V). We can choose as a representant of each class $n = (U, \mathbf{1}) \in G/H$. The composition law is expressed as:

$$gn = (V_R, V_L)(U, \mathbf{1}) = (V_R U, V_L) = (V_R U V_L^\dagger, \mathbf{1})(V_L, V_L) = n'h. \tag{3.13}$$

so that the Goldstone bosons transform as:

$$U'(x) = V_R U(x) V_L^\dagger. \tag{3.14}$$

One can choose any parametrisation of the coordinates for the unitary matrix U. A popular representation is (the first equality holds for arbitrary N_f, the second one for $N_f = 3$):

$$U = \exp\left[i \sum_{a=1}^{N_f^2-1} \frac{\phi_a \lambda^a}{F(N_f)} \right], \qquad \frac{1}{\sqrt{2}}\phi_a\lambda^a = \begin{pmatrix} \frac{\pi^0}{\sqrt{2}} + \frac{\eta}{\sqrt{6}} & \pi^+ & K^+ \\ \pi^- & -\frac{\pi^0}{\sqrt{2}} + \frac{\eta}{\sqrt{6}} & K^0 \\ K^- & \bar{K^0} & -\frac{2\eta}{\sqrt{6}} \end{pmatrix}. \tag{3.15}$$

We will see later that we can identify the various fields with the corresponding mesons at the lowest order of the theory in the isospin limit.

Let us notice that eq. (3.14) can be extended without difficulty to local transformations $V_R(x)$ and $V_L(x)$. On the other hand, if we want to include the singlet axial and vector currents in our analysis, the $U_A(1)$ chiral rotations require a modification of the formalism since they do not obey $\det U(x) = 1$ [20, 21]. On must replace this constraint by :

$$\det U(x) = e^{-i\theta(x)}, \tag{3.16}$$

in order to fulfill eq. (3.14) for any element in $U_L(N_f) \times U_R(N_f)$. Our expression in terms of pseudoscalar mesons is still valid, as long as one multiplies the matrix (3.15) by a phase $\exp(-i\theta(x)/N_f)$.

3.2.4 Effective Lagrangian

We look for an effective Lagrangian, function of Goldstone bosons and not of quarks and gluons, which satisfies the same Ward identities as QCD. According to sec. 3.2.2, these identities are verified if and only if the action is invariant under a local transformation of the sources, up to a term describing anomalous Ward identities. We will thus look for the most general expression of $\mathcal{L}_{\text{eff}}[U, \mathcal{S}]$:

$$e^{i\Gamma^0[\mathcal{S}]} = \int [DU] \exp\left\{ i \int d^4x \; \mathcal{L}_{\text{eff}}[U, \mathcal{S}] \right\}, \tag{3.17}$$

with Γ^0 invariant under the local transformations of $\mathcal{S}$. Since the measure $[DU]$ is itself invariant under these transformations, we must determine the most effective Lagrangian invariant under local transformations of the sources and of the meson matrix, expressed in terms of U, θ, v_μ, a_μ, s, p, and their derivatives.

We introduce the covariant derivatives:

$$D_\mu U = \partial_\mu U - i(v_\mu + a_\mu)U + iU(v_\mu - a_\mu), \qquad D_\mu\theta = \partial_\mu\theta + 2\langle a_\mu\rangle, \tag{3.18}$$

and the curvature tensors, associated with a_μ et v_μ and exhibiting the appropriate covariance properties: [20, 21]:

$$F^I_{\mu\nu} = \partial_\mu F^I_\nu - \partial_\nu F^I_\mu - i[F^I_\nu, F^I_\mu] \quad (I = R \text{ ou } L), \qquad F^{R,L}_\mu = v_\mu \pm a_\mu\,. \tag{3.19}$$

Since we look for an invariant action, we could also consider the more general case of a Lagrangian density invariant up to a divergence. But an invariance theorem derived for relativistic effective Lagrangians [149] shows that one can always come back to the determination of a strictly invariant Lagrangian density, up to a change of coordinates in U. In addition, one can prove that any invariant effective Lagrangian under the chiral transformations can be built only from the fields and their covariant derivatives. We have thus all the bricks needed to build our effective Lagrangian.

We can also use the fact that s, p, θ do no have independent transformation laws. The quark mass matrix can be diagonalised with real positive eigenvalues. By an appropriate chiral transformation, we can always get down to:

$$s + ip = M,\ \theta \quad \rightarrow \quad s = \mathcal{M},\ p = 0,\ \theta = \bar\theta, \tag{3.20}$$

where M is the quark mass matrix in any basis, $\mathcal{M}_q$ the diagonal matrix with real positive eigenvalues m_u, m_d, m_s, and $\bar\theta$ the chirally invariant vacuum angle $\theta + \arg\det(s + ip)$. Thus $\Gamma[s, p, \theta]$ depends only on the eigenvalues of the mass matrix and on the invariant vacuum angle $\bar\theta$. Conversely, this transformation allow us to fix $\theta = 0$, up to a rotation of the mass matrix:

$$s + ip = M_q,\ \theta \quad \rightarrow \quad s + ip = M\exp(i\theta/N_f),\ \theta = 0. \tag{3.21}$$

We can thus consider the (more simple) situation where the vacuum angle vanishes identically. In the effective Lagrangian, $U(x)$ belongs then to $\mathrm{SU}(N_f)$, M is replaced by $M\exp(i\theta/N_f)$ and $\langle a_\mu\rangle$ by $(D_\mu\theta)/2$ to account for the source associated with the winding number density $\tilde G G$ [157]. We will not consider here correlators containing $G\tilde G$ or A^0_μ and we assume $\langle a_\mu\rangle = 0$ and θ constant. The study of Γ for any value of the vacuum angle can thus be simplified to the case where $\theta = 0$.

3.2.5 Power counting

The effective Lagrangian contains an infinite number of terms, since one can construct an infinite number of invariants from the elementary building blocks presented above. We want to compute various hadronic processes at low energies, and we know that they vanish in the limit of vanishing incoming momenta and quark masses. If q is the typical external momentum in a process, the leading order will be given, say, by q^2, with additional corrections in q^4, $q^6\ldots$. The Lagrangian should thus be truncated to the desired momentum power: $\mathcal{L}_{\text{eff}} = \sum \mathcal{L}_n$, where $\mathcal{L}_n$ contains *all* the terms that are invariant under chiral transformations and contributing to the power q^n. The problem becomes finite, as long as one sticks to a fixed power of external momenta. In addition to vertices, the pions can also contribute through loops, which must be included in the analysis to comply with unitarity. Let us take an arbitrary graph with L loops connected through n_k interaction vertices coming from $\mathcal{L}_k$ (some examples of such diagrams for $\pi\pi$ scattering are represented in fig. 3.2), leading to:

$$\int (d^4l)^L \frac{1}{(l^2)^I} \prod_k (l^k)^{n_k}\,, \tag{3.22}$$

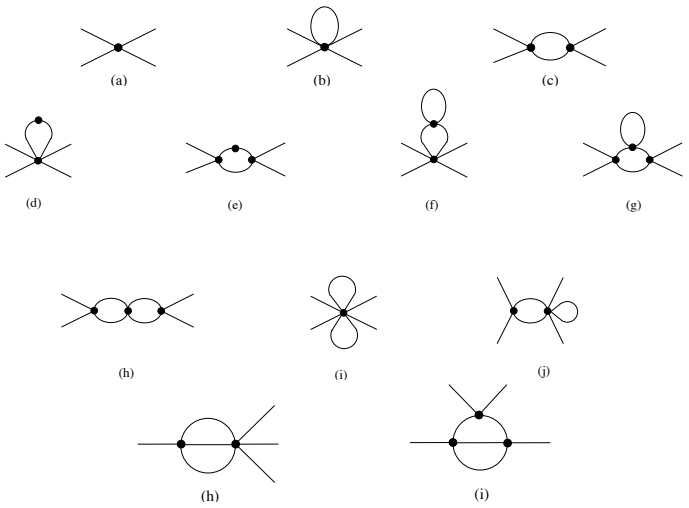

Figure 3.2: *Examples of contributions to $\pi\pi$ scattering at leading order and next-to-leading order (first line), next-to-next-to-leading order (following lines). The dots represent LO or NLO vertices.*

where I denotes the number of internal lines of the graph. Each loop requires an integration over a moment, each boson on an internal line provides a propagator in $1/l^2$, and each vertex of $\mathcal{L}_k$ yields a contribution like l^k by construction. If we use a regularisation preserving chiral symmetry and a mass-independent subtraction scheme (for instance, dimension regularisation associated with a minimal subtraction scheme), the external momenta q are the only dimensionful parameters of the problem. The amplitude must scale like p^D, with

$$D = 4L - 2I + \sum_k k n_k = 2 + 2L + \sum_k (k-2) n_k \tag{3.23}$$

from the usual geometrical relations $V - I + L = 1$ and $\sum_k n_k = V$. Since the Lagrangian start with its kinetic term, the lowest term starts at q^2, so that $k \geq 2$. A graph with N loops is thus suppressed by a factor q^{2N} with respect to tree graphs. For instance, if we want to compute a process up to q^4 order, the involved graphs are: $L = 0,\ m_4 = 1\ , m_{k>4} = 0$ and $L = 1,\ m_{k>2} = 0$, i.e., a tree graph with a vertex from $\mathcal{L}_4$ or a loop with vertices from $\mathcal{L}_2$. Such a loop yields divergences to be renormalised. Since we choose a regularisation that preserves chiral symmetry, the renormalisation of this loop requires counterterms of order q^4 that are local and respect the symmetries of the Lagrangian. But $\mathcal{L}_4$ provides a complete catalogue of these terms: the loop divergences can be absorbed by the counterterms already present.

More generally, if we stop at a given power q^n of momenta, we can always absorb the divergences from loops containing vertices with $\mathcal{L}_{m<n}$ in the counterterms present in $\mathcal{L}_n$. Our theory is thus renormalisable in its modern sense: if we stop at a given order, the divergences can be absorbed by a finite number of counterterms that arise necessarily in the Lagrangian at this order. The structure of the divergences (i.e., the UV behaviour of the theory) is also constrained by the symmetries of the theory, We will thus apply the following power counting:

$$U,\ \theta \sim 1\,, \qquad v_\mu,\ a_\mu,\ D_\mu U,\ D_\mu \theta \sim q\,, \tag{3.24}$$

and each additional derivative (covariant for U, ordinary for external sources) is counted like one power of momentum (the anomalous Wess-Zumino Lagrangian starts then at q^4).

3.3 Chiral Perturbation Theory

3.3.1 Three-flavour Lagrangian

Up to now, we have not considered the quark masses. Away from the chiral limit, the effective Lagrangian consists of an infinite tower of invariants:

$$\mathcal{L}_{\text{eff}} = \sum_{k,l} \mathcal{L}_{k,l}, \qquad \mathcal{L}_{k,l} \sim q^k m_q^l. \tag{3.25}$$

This double expansion must be organised according to a single index. The masses of the quarks are related to scalar and pseudoscalar sources, for which no obvious counting exists. We must compare m_q and $q \sim M_\pi$. If the quark condensate contributes significantly to the meson masses, a linear dependence of M_π^2 on the quark masses is a good first-order approximation:

$$s,\ p\ \sim\ q^2\,, \tag{3.26}$$

leading to the following expansion of the effective Lagrangian:

$$\mathcal{L}_{\text{eff}} = \mathcal{L}_2 + \mathcal{L}_4 + \mathcal{L}_6 + \ldots \qquad \mathcal{L}_n = \sum_{k+2l=d} \mathcal{L}_{k,l}. \tag{3.27}$$

This counting yields Chiral Perturbation Theory (χPT) proposed by Gasser and Leutwyler [20, 21, 158] [2]. The first-order Lagrangian corresponds to $O(q^2)$:

$$\mathcal{L}_2 = \frac{1}{4} F_0^2 \left[\langle D_\mu U^\dagger D^\mu U \rangle + \langle U^\dagger \chi + \chi^\dagger U \rangle \right], \tag{3.28}$$

where $\chi = 2B_0(s + ip)$. B_0 and F_0 are low-energy constants yet to be determined. If we consider this Lagrangian in the isospin limit $m_u = m_d = m$, we can expand the meson matrix U up to the second order in the meson fields, leading to:

$$\begin{aligned} \mathcal{L}_2 \to\ & \frac{1}{2}\partial_\mu \pi^0 \partial^\mu \pi^0 + \partial_\mu K^+ \partial^\mu K^- + \partial_\mu \bar{K}^0 \partial^\mu K^0 + \partial_\mu \pi^+ \partial^\mu \pi^- + \frac{1}{2}\partial_\mu \eta \partial^\mu \eta \\ & - mB\pi^0\pi^0 - 2mB\pi^+\pi^- - (m+m_s)B_0 \bar{K}^0 K^0 - (m+m_s)B_0 K^+ K^- - \frac{1}{3}(m+2m_s)B_0 \eta\eta\,. \end{aligned} \tag{3.29}$$

We see that we obtain expressions for meson masses at leading order:

$$M_\pi^2 = 2mB_0 + O(m_q^2)\,, \quad M_K^2 = (m+m_s)B_0 + O(m_q^2)\,, \quad M_\eta^2 = \frac{4}{3}M_K^2 - \frac{1}{3}M_\pi^2 + O(m_q^2) \tag{3.30}$$

the last one corresponding to the Gell-Mann–Okubo relation, satisfied at the leading order in the chiral expansion. We can identify the two low-energy constants arising in the Lagrangian by taking either a derivative with respect to the axial source $a_{\mu,21}$, or with respect to the scalar source $s_1 1$, leading respectively to:

$$\langle 0|\bar{d}\gamma_\mu\gamma_5 u|\pi^+(p)\rangle = i\left[\frac{F_0}{\sqrt{2}} + O(m_q)\right] p_\mu\,, \qquad \langle \bar{u}u \rangle = -F_0^2 B_0 + O(m_q)\,, \tag{3.31}$$

[2] An alternative counting, known as Generalized χPT [159], was introduced later to cope with the possibility of a small condensate, introducing a different power counting ($B_0 \sim m \sim q$), leading to an even larger number of counterterms than χPT. However, this framework did not consider the role of fluctuations encoded in NLO counterterms violating the Zweig rule in the scalar sector. We will come comment on this issue in the next chapters.

so that we have the identifications of the low-energy constants with the three-flavour order parameters:

$$F_0 = F(3)\,, \qquad B_0 = \frac{\Sigma(3)}{F(3)^2}\,, \tag{3.32}$$

We thus recover eqs. (2.22)-(2.24), corresponding to the famous Gell-Mann-Oakes-Renner relation [160]. We can introduce the following quantities:

$$X(3) = \frac{2m\Sigma(3)}{F_\pi^2 M_\pi^2}\,, \qquad Z(3) = \frac{F(3)^2}{F_\pi^2}\,, \qquad Y(3) = \frac{X(3)}{Z(3)} = \frac{2mB_0}{M_\pi^2}\,. \tag{3.33}$$

which correspond to the quark condensate and the decay constant, as well as their ratio, in dimensionless units. These quantities provide the relative contribution of the LO term to the chiral expansion of $F_\pi^2 M_\pi^2$, F_π^2 and M_π^2: all of them would be exactly 1 if the LO Lagrangian saturated the chiral expansion. The next order, $O(q^4)$, reads:

$$\begin{aligned}
\mathcal{L}_4 = \frac{1}{4}F_0^2[&L_0\langle D_\mu U^\dagger D_\nu U D^\mu U^\dagger D^\nu U\rangle + L_1\langle D_\mu U^\dagger D^\mu U\rangle^2 + L_2\langle D_\mu U^\dagger D_\nu U\rangle\langle D^\mu U^\dagger D^\nu U\rangle \\
&+L_3\langle D_\mu U^\dagger D^\mu U D_\nu U^\dagger D^\nu U\rangle + L_4\langle D_\mu U^\dagger D^\mu U\rangle\langle \chi^\dagger U + U^\dagger\chi\rangle + L_5\langle D_\mu U^\dagger D^\mu U(\chi^\dagger U + U^\dagger\chi)\rangle \\
&+L_6\langle \chi^\dagger U + U^\dagger\chi\rangle^2 + L_7\langle \chi^\dagger U - U^\dagger\chi\rangle^2 + L_8\langle \chi^\dagger U\chi^\dagger U + U^\dagger\chi U^\dagger\chi\rangle \\
&-iL_9\langle F_{\mu\nu}^R D^\mu U D^\nu U^\dagger + F_{\mu\nu}^L D^\mu U^\dagger D^\nu U\rangle + L_{10}\langle U^\dagger F_{\mu\nu}^R U F^{L;\mu\nu}\rangle \\
&+H_1\langle F_{\mu\nu}^R F^{R;\mu\nu} + F_{\mu\nu}^L F^{L;\mu\nu}\rangle + H_2\langle\chi^\dagger\chi\rangle].
\end{aligned} \tag{3.34}$$

This NLO Lagrangian holds for an arbitrary number of flavours, but for $N_f = 3$, the operator associated with L_0 can be re-absorbed into other operators thanks to Cayley-Hamilton identities [20,21]. The 10 L_i's are Low-Energy Constants (LECs), whose values should be determined from experimental data. They are renormalised by one-loop diagrams occurring at the same order in the chiral expansion. H_1 and H_2 are called high-energy counterterms, multiplying operators allowed by chiral symmetry, but without dynamical fields. They do not occur in physical low-energy processes, but can arise in quantities that depend on ultraviolet regularisation (such as the condensates away from the chiral limit), and correspond to the divergences present in some Green functions (the structure of these divergences is indeed constrained by chiral symmetry). At NNLO, the Lagrangian contains 94 counterterms, with 90 LECs denoted C_i (and 4 high-energy counterterms). At this stage, it is impossible to determine all counterterms from experiment, and one must determine most of them either from analytic estimates, such as resonance saturation, or from lattice determination.

At this stage, even though we focus only on low-energy dynamics of pseudoscalar mesons, we should add that there are other implementations of chiral effective theories:

- for other systems interacting with soft pions, such as baryons [22, 161–164] or heavy mesons [165],
- with a different fermion content from QCD, for instance quenched and partially quenched theories with different valence and sea-quark contents [166–169] or supersymmetric theories [74, 170, 171],
- in presence of other explicit sources of chiral symmetry breaking, in particular for lattice formulations of fermion actions [172, 173],

- in finite volumes, with different regimes depending on which light degrees of freedom are relevant or with different boundary conditions [87–89, 174, 175],
- for weak decays, in particular for the analysis of $K \to \pi\pi$ decays [176–179],
- for other strongly interacting non-Abelian gauge theories, for instance for Technicolor-like theories [17, 180, 181].

Each of these theories does only involve the Lagrangian described here, but also new LECs (and operators) describing the interaction of Goldstone bosons in a new environment.

3.3.2 Generating functional at one loop

Let us come back to the Lagrangian describing low-energy π, K, η interactions, which can be dealt with in two different ways. A first approach consists in deriving Feynman rules for the various vertices and propagators, spelling out the relevant diagrams and computing the corresponding integrals for each particular process. This is the path followed for the analyses performed at the two-loop level [158], where the large number of low-energy constants compared to the number of accessible processes would make a completely general analysis of the generating functional of limited use.

On the other hand, such an analysis is very useful at the one-loop level where the number of LECs is limited. One can actually integrate the degrees of freedom collected in U, to express the generating functional only in terms of its sources and of propagators with a known structure. Since the integration is performed at the level of the generating functional, one does not need to evaluate any further diagrams, but just to perform functional derivatives with respect to the appropriate sources. For three flavours, this one-loop generating functional reads [21]:

$$Z = Z_t + Z_u + Z_A + \dots \tag{3.35}$$

where the ellipsis stands for NNLO contributions. The three terms of the one-loop generating functional are:

- Z_t is the sum of $O(p^2)$ and $O(p^4)$ tree graphs, and of tadpole contributions:

$$Z_t = \sum_P \int dx \frac{F_0^2}{6} \left\{ 1 - \frac{3}{16\pi^2} \frac{\overset{\circ}{M}{}_P^2}{F_0^2} \log \frac{\overset{\circ}{M}{}_P^2}{\mu^2} \right\} \sigma^{\Delta}_{PP} \tag{3.36}$$

$$+ \sum_P \int dx \frac{3F_0^2}{6} \left\{ 1 - \frac{3}{6\pi^2} \frac{\overset{\circ}{M}{}_P^2}{F_0^2} \log \frac{\overset{\circ}{M}{}_P^2}{\mu^2} \right\} \sigma^{\chi}_{PP} + \int dx \; \mathcal{L}_4^r \,,$$

  σ^{Δ} and σ^{χ} collect source terms for vector / axial currents and scalar / pseudoscalar densities, and $\mathcal{L}_4^r$ is the $O(p^4)$ chiral Lagrangian with renormalised constants L_i^r and H_i^r. $\overset{\circ}{M}{}_P^2$ denotes the $O(p^2)$ contribution to the (squared) mass of the Goldstone boson P:

$$\overset{\circ}{M}{}_\pi^2 = Y(3) M_\pi^2 \,, \qquad \overset{\circ}{M}{}_K^2 = \frac{r+1}{2} Y(3) M_\pi^2 \,, \qquad \overset{\circ}{M}{}_\eta^2 = \frac{2r+1}{3} Y(3) M_\pi^2 \,. \tag{3.37}$$

- Z_u collects unitarity corrections corresponding to one-loop graphs with two $O(p^2)$ vertices:

$$Z_u = \sum_{P,Q} \int dx \; dy \Big[\{ \{ \partial_{\mu\nu} - g_{\mu\nu} \Box \} M^r_{PQ}(x-y) - g_{\mu\nu} L_{PQ}(x-y) \} \hat{\Gamma}^{\mu}_{PQ}(x) \hat{\Gamma}^{\nu}_{QP}(y) \tag{3.38}$$

$$- \partial_\mu K_{PQ}(x-y) \hat{\Gamma}^{\mu}_{PQ}(x) \bar{\sigma}_{QP}(y) + \frac{1}{4} J^r(x-y) \bar{\sigma}_{PQ}(x) \bar{\sigma}_{QP}(y) \Big]$$

where J, K, L, M are (renormalised) functions defined from the one-loop scalar integral with mesons P and Q propagating in the loop (with the LO masses eq. (3.37)), and $\hat{\Gamma}^\mu$ and $\bar{\sigma} = \sigma^\Delta + \sigma^\chi$ collect source terms.

- Z_A is the Wess-Zumino functional collecting anomalous contributions.

These three terms involve the solution $\bar{U}$ of the equation of motion in presence of (axial, pseudoscalar and vacuum angle) sources. When one wants a specific correlator, one has just to perform the derivatives of the generating functional with respect to the various sources.

The dependence on the renormalisation scale form the tadpole and unitarity corrections cancel exactly that of the NLO counterterms introduced in $\mathcal{L}_4$, so that the generating functional (and the derived correlators) are independent of the renormalisation scale. This scale, typically chosen of the order of the first non-Goldstone hadronic excitation ($\mu = M_\rho$), corresponds to the separation between the low-energy dynamics, encoded in the operators, and the high-energy dynamics, subsumed in the values of the LECs.

3.3.3 Analytic determinations of three-flavour low-energy constants

In principle, the LECs should be determined from experimental measurements, combined with assumptions concerning the appropriate convergence of the effective theory. One can easily state some of the observables associated to each $O(p^4)$ LEC that are simple to determine on lattice simulations and/or to extract from experiment:

- L_1, L_2, L_3: $K_{\ell 4}$ form factors ($F_\pi^2 F_K f, F_\pi^2 F_K g, F_\pi^2 F_K h$),
- L_4, L_5: π, K decay constants (F_π^2, F_K^2),
- L_6, L_8: π, K masses ($F_\pi^2 M_\pi^2, F_K^2 M_K^2$),
- L_7: η mass and decay constant ($F_\eta^2, F_\eta^2 M_\eta^2$),
- L_9: Pion electromagnetic form factor ($F_\pi^2 F_V^\pi$),
- L_{10}: $\pi \to e\nu\gamma$ form factor ($F_\pi A_{VAP}$) [3].

One should distinguish LECs involve only derivatives of the meson field, which are easier to access experimentally by studying the energy-dependence of form factors or scattering amplitudes (at NLO, $L_{1,2,3,9,10}$), and those involving also quark masses, which are much more difficult to probe experimentally but can be accessed through lattice simulations by varying quark masses (at NLO, $L_{4,5,6,7,8}$).

At the time when one-loop χPT was introduced, the determination of the LECs was obviously rather crude. The original determination in ref. [21] is recalled in the first columns of tab. 3.1. In particular, the Zweig rule was used to pin down some of the LECs that were impossible to determine otherwise. Indeed, applying the large-N_c counting rules, recalled in app. A.2.2, one obtains:

$$L_7 = O(N_c^2)\,, \qquad L_{1,2,3,4,5,6,8,9,10}, H_{1,2} = O(N_c)\,, \qquad 2L_1 - L_2, L_4, L_6 = O(1)\,. \tag{3.39}$$

Indeed, L_7 is the only NLO LEC to receive a contribution from the η' meson going like $F(3)^2/M_{\eta'}^2$. For the other LECs, operators with several flavour traces are $1/N_c$-suppressed

[3] It is also possible to extract this LEC from τ spectral functions through a sum rule on the correlator $VV - AA$ [182].

i	[21]	Source	10 iso $O(p^6)$ [183]	All $O(p^6)$ [183]	$O(p^4)$ [183]	IAM [184]
1	0.7 ± 0.3	$K_{\ell 4}$, D-wave $\pi\pi$, Zweig r.	0.39 ± 0.12	0.88 ± 0.09	1.12	0.56 ± 0.10
2	1.3 ± 0.7	$K_{\ell 4}$, D-wave $\pi\pi$, Zweig r.	0.73 ± 0.12	0.61 ± 0.20	1.23	1.21 ± 0.10
3	-4.4 ± 2.5	$K_{\ell 4}$, D-wave $\pi\pi$, Zweig r.	-2.34 ± 0.37	-3.04 ± 0.43	-3.98	-2.79 ± 0.14
4	-0.3 ± 0.5	Zweig rule	0 ± 0	0.75 ± 0.75	1.50	-0.36 ± 0.17
5	1.4 ± 0.5	F_K/F_π	0.97 ± 0.11	0.58 ± 0.13	1.21	1.4 ± 0.5
6	-0.2 ± 0.3	Zweig rule	0 ± 0	0.29 ± 0.85	1.17	0.07 ± 0.08
7	-0.4 ± 0.15	GMO, L_5, L_8	-0.30 ± 0.15	-0.11 ± 0.15	-0.36	-0.44 ± 0.15
8	0.9 ± 0.3	$M^2_{K^0} - M^2_{K^+}$, L_5, $\frac{m_s - \hat{m}}{m_d - m_u}$	0.60 ± 0.20	0.18 ± 0.18	0.62	0.78 ± 0.18
9	6.9 ± 0.7	$\langle r^2 \rangle^\pi_V$	5.9 ± 0.5	5.9 ± 0.5	5.9	-
10	-5.5 ± 0.7	$\pi \to e\nu\gamma$	-4.1 ± 0.4	-4.1 ± 0.4	4.1	-

Table 3.1: *Values of the $N_f = 3$ NLO low-energy constants $L_i(M_\rho) \cdot 10^3$ given in refs. [21] (initial NLO estimates), [183] (fits to NLO and NNLO expressions) and [184] (Inverse Amplitude method). The Fit 10 iso in ref. [183] includes only a subset of the inputs used for Fit All, including the expressions either at $O(p^4)$ or at $O(p^6)$.*

compared to operators with a single trace, as they correspond to non-planar diagrams (hence $L_{4,6}$ suppressed compared to $L_{5,8}$). A Cayley-Hamilton identity allows one to rewrite L_1 and L_2 operators in term of operators with single flavour traces and one with two flavour traces, proportional to $2L_1 - L_2$. It was thus supposed that the two LECs L_4 and L_6 could be set to zero on the ground of the Zweig rule/large-N_c suppression, indicating that there is only a small m_s-dependence of chiral order parameters. But at which scale M_{ZR} should one set $L^r_{4,6}(M_{ZR}) = 0$? In ref. [21], the η-mass scale was chosen, even though it has become fairly standard to use the ρ-mass as the central scale for resonance saturation later on. Since these two LECs are renormalisation-scale dependent, the choice implies some variation for the estimate of the LECs at $\mu = M_\rho$:

$$M_{ZR} = M_\eta : \qquad L^r_6(M_\rho) = -0.17 \cdot 10^{-3}\,, \qquad L^r_4(M_\rho) = -0.27 \cdot 10^{-3}\,, \tag{3.40}$$

$$M_{ZR} = M_\rho : \qquad L^r_6(M_\rho) = 0\,, \qquad L^r_4(M_\rho) = 0\,, \tag{3.41}$$

$$M_{ZR} = 1 \text{ GeV} : \qquad L^r_6(M_\rho) = 0.13 \cdot 10^{-3}\,, \qquad L^r_4(M_\rho) = 0.21 \cdot 10^{-3}\,. \tag{3.42}$$

In sec. 3.5.3, we will see that the values obtained with the choice $M_{ZR} = M_\eta$ are close to the values corresponding to a complete equality between two-flavour and three-flavour chiral order parameters. On the other hand, the a priori equivalent choices $M_{ZR} = M_\rho$ or $M_Z = 1$ GeV would lead to a significant suppression of $\Sigma(3)$ and $F(3)$.

The next step consisted in computing measured processes up to NNLO, both in $N_f = 2$ and $N_f = 3$ χPT: masses and decay constants [185, 186], $\pi\pi$ scattering [187], πK scattering [188], form factors (electromagnetic, $K_{\ell 3}$, $K_{\ell 4}$, scalar) [189–192]. The same group has proceeded to global fits of the corresponding available data for pseudoscalar masses and decay constants, quark mass ratio, $K_{\ell 4}$ form factors. Later were added observables corresponding to $\pi\pi$ and πK scatterings as well as scalar form factors [183]. Models of resonance saturation were used in order to fix the values of the C_i's in both vector and scalar channels. The results of several fits are collected in tab. 3.1, in overall agreement with the data apart from the slope of the $K_{\ell 4}$ form factor f_s.

If the first fits [186] set L_4 and L_6 to zero on similar grounds to ref. [21], this constraint was relaxed afterwards [183], and one can observe indeed that the fits prefer values of L_4 and L_6 that are positive. The other large-N_c suppressed combination $2L_1 - L_2$ is also found quite large. These results yield a significant decrease of $F_0 = 65$ MeV compared to $F_\pi = 92.2$ MeV, and a

Relative contribution	LO	NLO	NNLO
M_π^2	1.035	-0.084	0.049
M_K^2	1.106	-0.181	0.075
M_η^2	1.186	-0.224	0.038
F_π	0.705	0.220	0.127
F_K	0.589	0.260	0.216

Table 3.2: *Pattern of convergence for pseudoscalar observables at the best solution of Fit All $O(p^6)$ in ref. [183]. All contributions are indicated relatively to the physical value.*

peculiar pattern of convergence for masses and decay constants (for Fit All $O(p^6)$) recalled in tab. 3.2. NLO and NNLO contributions are of similar size and cancel each other for some of the contributions. Some of the problems encountered in refs. [187,188] were reassessed in ref. [193], in particular the determination of NNLO LECs. Following ref. [116], the many $O(p^6)$ LECs are often estimated using resonance saturation. In ref. [193], the specific resonance Lagrangian used in refs. [187,188] was shown to provide values for vector-dominated LECs rather far away from the expectations based on πK dispersion relations, but other resonance Lagrangians failed also to reproduce these same results.

This is a long-standing issue in the building of resonances satisfying all the short-distance constraints required by OPE as well as having a satisfying coupling to the light degrees of freedom of the theory, and there is no unique solution for all correlators/processes that one can consider [23,24,26,28,72,110,111,116,120–126]. In addition, it remains to be clarified whether a large-N_c approach is appropriate for all channels, including the scalar one, following the discussion in sec. 2.5.1. Therefore, one may wonder whether the problems of convergence seen in refs. [187,188] could stem from two different sources. *i)* the use of resonance saturation to fix NNLO counterterms, which is already delicate in spin-1 channels and certainly questionable in the scalar sector, *ii)* the observed slow convergence of chiral expansions, which contradicts the starting assumptions of the NNLO analysis.

In ref. [183], the dependence of these results on the models for the NNLO counterterms was investigated, by opting for alternative models to the resonance saturation (chiral quark model, randomly selected values). It was shown that indeed the actual values obtained for the LECs L_i's were quite dependent on the assumptions made on the C_i's, with equal goodness of fit, including cases where NNLO contributions were small, but with a numerical competition between LO and NLO. No firm conclusions were drawn on a preferred model for the C_i's, nor the actual convergence range or rate of three-flavour χPT.

There have been several attempts to extend the range of validity of the chiral series. The first one consists in building a Resonance Chiral Theory, taking the resonances as dynamical fields and combining the large-N_c and chiral counting together with the constraints from OPE to obtain a consistent picture of correlators of phenomenological interest [25–28]. The results for the correlators dominated by spin-1 mesons yield values of the chiral LECs in good agreement with other estimates. Another possibility consists in unitarising their expression, for instance through the Inverse Amplitude Method. A fit to the available data on meson-meson scattering up to 1.2 GeV [184] provides values of the low-energy constants that in overall agreement with the original estimates in ref. [21]. It is however difficult to assess precisely the impact of higher orders in this resummed approach, and thus whether these values can be compared directly to the NLO estimates presented in tab. 3.1. Moreover, some of the channels considered exhibit a

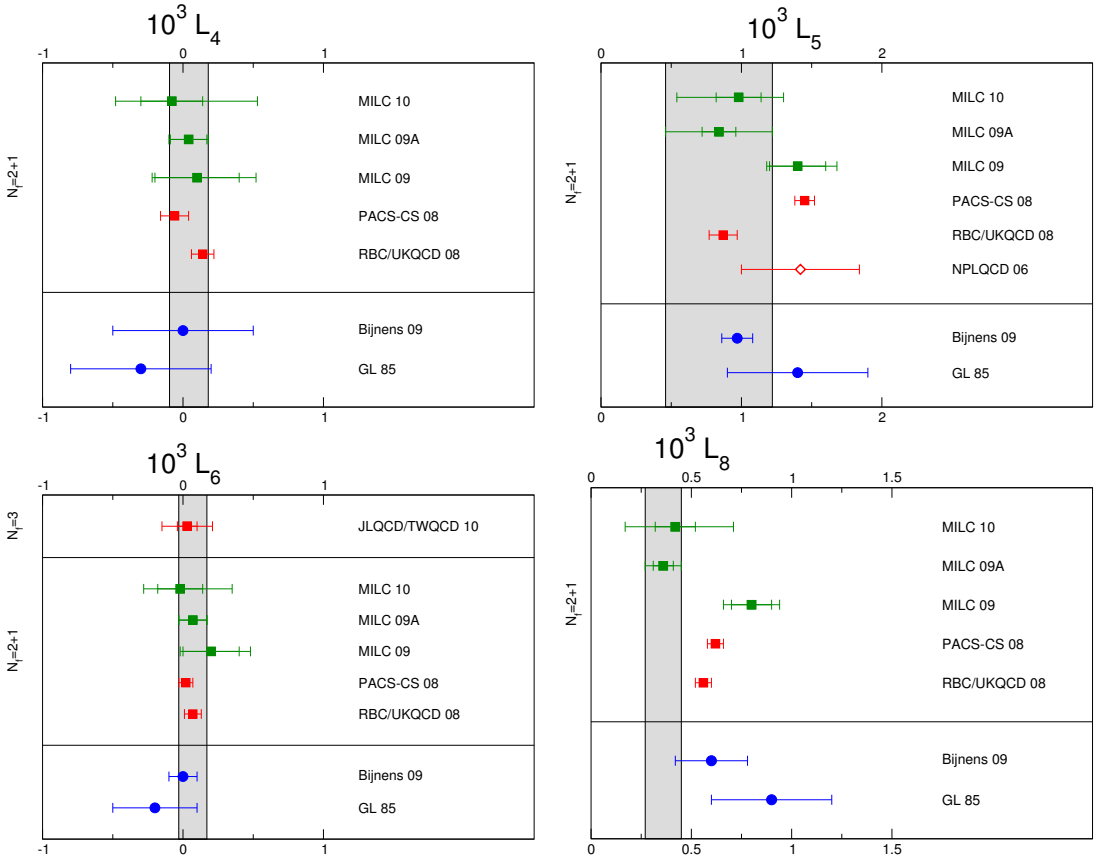

Figure 3.3: *Summary of the various lattice determinations of $N_f = 3$ LECs at the scale $\mu = M_\rho$. From ref. [82].*

very large dispersion in their data.

3.3.4 Lattice determinations of three-flavour low-energy constants

Lattice simulations have also been used to determine the values of the LECs, with the added interest that they can determine the chirally-breaking contributions proportional to the quark masses in a much more transparent way than the phenomenological analyses. Conversely, once these LECs are determined, the chiral series can be used to perform the extrapolation, including non-analytic curvature effects related to chiral logarithms, as illustrated in fig. 3.4.

The effects discussed here are related to strange sea-quarks, and can be tackled only with (2+1) dynamical fermions with light masses. Fermions with the most interesting properties with respect to chiral symmetry (Ginsparg-Wilson, domain-wall, twisted-mass) have begun to include all three light flavours as dynamical quarks [194–196], and corresponding chiral Lagrangians have been determined to include chiral-symmetry breaking effects at finite lattice spacing. On the other hand, staggered fermions [197] have been exploited for simulations with (2+1) dynamical quarks, but their use is under much debate [198–202]. The presence of the fourth root of the fermion determinant yields non-localities which are still to be understood and recovering QCD requires taking the various continuum limits in a careful way [203]. A staggered version of χPT [204] has been developed to extract chiral LECs from the pseudoscalar spectrum. It attempts at reproducing the fourth-rooting of the fermion determinant and includes many

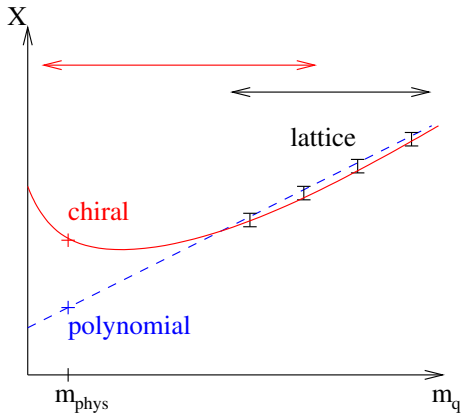

Figure 3.4: *Illustration of the complementarity between lattice and chiral computations for a given observable. The lattice computations are often performed at values of quark masses large compared to those where chiral logarithms set in, but can be used to constrain the value of the low-energy constants, if there is an overlap between lattice simulations and χPT.*

other effects (lattice spacing, finite-volume effects, taste-breaking terms), leading to a number of LECs much larger than in continuum un-staggered χPT. The hope is that the LECs common to both theories should be identical because QCD ought to be recovered as a limit of lattice QCD with fourth-rooted staggered fermions. In practice [205], chiral fits to staggered data on the pseudoscalar spectrum must include a large number of parameters and thus are highly non-trivial. Mixed actions with domain-wall valence quarks and staggered sea quarks have also been considered to reduce the number of LECs involved in the associated chiral Lagrangian at the price of losing unitarity in addition to locality [206].

A recent review [82] provides a detailed summary of the various lattice determinations for the low-energy constants, and we recall the corresponding figures in fig. 3.3. We see that slightly positive values of L_4 and L_6 are favoured by all lattice determinations, and higher than the original estimates [21]. It turns out that several collaborations performing simulations with 2+1 dynamical quarks reported difficulties when fitting their data with $N_f = 3$ next-to-leading-order chiral expansions for pseudoscalar masses, decay constants, and $K_{\ell 3}$ form factors [127,207–209], forcing some of the collaborations to rely on $N_f = 2$ chiral expansions only (for instance using on Heavy-Kaon χPT to perform their extrapolations [210, 211]). Among the difficulties were the absence (or the weakness) of curvature in the dependence of the observables on the quark masses, even though such a curvature, related to the chiral logarithms, was expected to set in, considering the light quark masses involved. Other collaborations, performing NNLO fits on data for staggered fermions [129, 205], obtained decent fits, but with a size of NNLO contributions much larger than the NLO ones.

Assuming that there are no intrinsic problems with the lattice data, these results can be interpreted in different ways. It may be that some lattice systematics (artefacts due to lattice spacing, renormalisation of operators...) hide the presence of chiral logarithms, but it may also be a problem of convergence of $N_f = 3$ chiral series. These series may not converge quickly, because their LO term in the chiral counting is not numerically dominant and competes with (formally) higher-order contributions, the strange quark mass used in the simulations (and close to the physical value) is too large for a good convergence of three-flavour χPT, and the region of overlap between lattice and χPT has not been reached yet.

i	[20]	Source	10 iso [183]	All [183]	IAM [212]
1	-2.3 ± 3.7	D-wave $\pi\pi$ scattering lengths	-0.6	-1.9	-0.3
2	6.0 ± 1.3	D-wave $\pi\pi$ scattering lengths	5.7	5.3	4.1
3	2.9 ± 2.4	$M^2_{K^0} - M^2_{K^+}$, $\frac{2m_s - m_u - m_d}{m_d - m_u}$	1.3	4.2	3.0
4	4.6 ± 0.9	$\langle r^2 \rangle^\pi_S$	4.0	4.8	4.5
5	14	Sum rule vector and axial mesons	-	-	-
6	16.5 ± 1.1	$\langle r^2 \rangle^\pi_V$	-	-	-

Table 3.3: *Values of the $N_f = 2$ NLO low-energy constants $\bar{\ell}_i$ given in refs. [20] (NLO estimates), [183] (fits to $N_f = 3$ NNLO expansions, and matching to $N_f = 2$ χPT) and [212] (Inverse Amplitude Method applied to $\pi\pi$ data and lattice results).*

3.3.5 $N_f = 2$ chiral perturbation theory

The previous discussion can also be adapted to the case of $\mathrm{SU}_L(2) \otimes \mathrm{SU}_R(2)$, i.e., very low energies, where only pions are the appropriate degrees of freedom [20]. In that case, the chiral Lagrangian has a much simpler form, as Cayley-Hamilton identities relate some of the operators in eq. (3.34). Similarly to what was done in the previous case, two LECs arise at LO, related to the two-flavour condensate $\Sigma(2)$ and decay constant $F(2)$. At NLO, one encounter 7 low-energy constants, denoted $\bar{\ell}_i$, and 3 high-energy counterterms, denoted $\bar{h}_i$, whereas NNLO brings 54 LECs and 4 high-energy counterterms. All these LECs are defined in the $N_f = 2$ chiral limit, and similarly to $F^2(2)$ and $\Sigma(2)$, they still exhibit a dependence on the strange quark mass, which is kept at its physical mass. One can match the two- and three-flavour theories order by order in the chiral expansion in their common domain of application, i.e. observables with very soft pions. One could do it in principle by computing all the possible processes at a given order in both theories, but it proves much more efficient, and much more elegant, to perform the matching at the level of the generating functional, which guarantees that all relevant processes will be considered at once. Doing so at one loop, one obtains for the LO LECs [20]:

$$F(2)^2 = F(3)^2 - 2F(3)^2\bar{\mu}_K + 16m_s\frac{\Sigma(3)}{F(3)^2}L^r_4\,, \tag{3.43}$$

$$\Sigma(2) = \Sigma(3) - 2F(3)^2\bar{\mu}_K - \frac{1}{3}\bar{\mu}_\eta + 32m_s\frac{\Sigma(3)}{F(3)^2}L^r_6\,, \tag{3.44}$$

$$\bar{\mu}_P = \lim_{m_s\to 0}\frac{M_P^2}{32\pi^2F_0^2}\log\frac{M_P^2}{\mu^2} = \frac{1}{F_0^2}\left[\nu_P - \frac{1}{32\pi^2}\right]\,, \tag{3.45}$$

which are the translations of the statements in sec. 2.4.1 on the N_f dependence of chiral order parameters: L_4 is related to $\langle(\bar{s}s)(VV-AA)\rangle$ and L_6 to $\langle(\bar{u}u)(\bar{s}s)\rangle$. We have for the NLO LECs relationships such as (for those involved in the u, d quark-mass dependence of the pion mass and decay constant):

$$\ell^r_3 = -8L^r_4 - 4L^r_5 + 16L^r_6 + 8L^r_8 - \frac{1}{18}\nu_\eta\,, \qquad \ell^r_4 = 8L^r_4 + 4L^r_5 - \frac{1}{2}\nu_K\,, \tag{3.46}$$

A matching at two loops has been recently completed [213, 214], allowing to assess the corrections from the C_i's LECs to the previous relationships. One can also match the two approaches in the kaon sector. One has then to build a heavy-kaon χPT, treating the K meson as a heavy

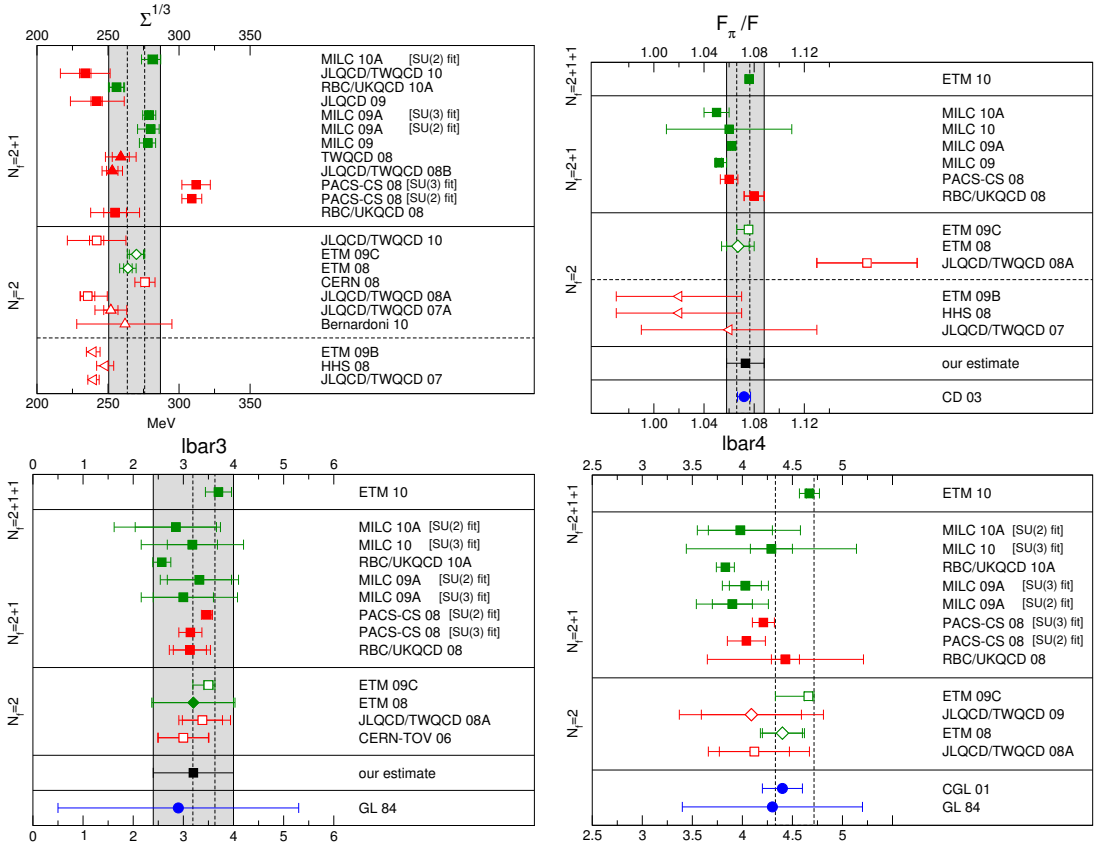

Figure 3.5: *Summary of the various lattice determinations of $N_f = 2$ LECs. From ref. [82].*

(static) object, and determine the value of the LECs of this new theory in terms of the L_i's and C_i's introduced here [211, 215].

The values for the $N_f = 2$ LECs have been determined originally combining estimates of $N_f = 3$ χPT with information on pion observables, as indicated in tab. 3.3, as well as results obtained by matching the $N_f = 2$ theory on NNLO $N_f = 3$ fits [183]. Lattice can also provide relevant information, even though the range of simulated masses is still a bit high compared to the physical ones. A recent review [82] provides a detailed summary of the situation in fig. 3.5. We see that the values of the $N_f = 2$ quark condensate and decay constants are in good agreement among the different collaborations and indicate that the quark condensate is the dominant parameter for $N_f = 2$ chiral symmetry breaking. In a similar way, the LECs $\bar{\ell}_3$ and $\bar{\ell}_4$ governing the quark-mass dependence of the pion mass and decay constant are found with similar values to those obtained from phenomenology. Moreover, several lattice studies indicate a curvature in agreement with the expectations of two-flavour χPT concerning NLO chiral logarithms [127, 205, 207, 216, 217], even though there are still some cases where this curvature does not arise, even for very light up and down quark masses [208, 209].

Another approach consisted in unitarising $N_f = 2$ chiral expansions up to two loops, and to perform a joint fit on experimental data on $\pi\pi$ scattering (up to 1 GeV) and lattice data (for values of M_π up to 350 MeV) [212]. The results are in good agreement with earlier estimates. Taken altogether results seem to indicate a good convergence of $N_f = 2$ chiral series for pion observables, contrary to the situation for $N_f = 3$ expansions.

3.4 Convergence and instabilities of $N_f = 3$ chiral expansion

At this stage, we have several hints that vacuum fluctuations of $\bar{s}s$ pairs as well as problems of convergence [34] could possibly show up in $N_f = 3$ chiral expansions. In the rest of this chapter, we will discuss the link existing between these two issues.

3.4.1 The bare χPT series [C,E]

χPT is expected to provide an adequate representation of the generating function of QCD eq.(3.6) at low energies. Therefore, it is natural to take as primary objects for the expansion in powers of m_u, m_d, m_s the connected QCD correlation functions of quark currents (V, A, S, P) with external momenta fixed in a low-energy region away from the singularities generated by Goldstone bosons. We will take as a working hypothesis that the usual low-energy observables, e.g., Goldstone boson masses, decay constants, form factors and scattering amplitudes (at particular kinematical points) exhibit good convergence properties when they are linearly expressed through such QCD correlation functions (values or residues at given kinematical points). While a similar assumption is implicitly made in the standard off-shell formulation of χPT [20, 21], we will see that in the presence of important vacuum fluctuations, this assumption should be understood as a restriction: observables that are not *linearly* expressible in terms of QCD correlators, e.g., *ratios* of Goldstone boson masses, need not admit a well convergent perturbative treatment and they should be treated with a particular care. We will see in the following that this selects for instance $F_\pi^2 M_\pi^2$, F_π^2 and $F_\pi^2 F_K^2 A_{\pi K}$ (where $A_{\pi K}$ denotes the πK-scattering amplitude), but rules out M_π^2.

The chiral expansion of symmetry-breaking observables in terms of the three lightest quark masses m_u, m_d, m_s is actually not a genuine power series expansion, due to the presence of chiral logarithms, which reflect infrared singularities characteristic of the chiral limit. One can nevertheless give an unambiguous scale-independent meaning to the renormalised coefficients of each power of individual quark masses. An energy-independent observable [4] can generally be represented as a formal series:

$$A = \sum_{j,k,l} m_u^j m_d^k m_s^l A_{jkl}[m_u, m_d, m_s; B_0, F_0; L_1^r(\mu) \dots L_{10}^r(\mu); C_1^r(\mu) \dots C_{90}^r(\mu); \dots], \qquad (3.47)$$

where the coefficients A_{jkl} are defined in terms of the constants contained in the effective Lagrangian (B_0, F_0, $L_i^r(\mu)$, $C_i^r(\mu)$ ...) In addition, the A_{jkl} depend logarithmically on the quark masses through the Goldstone boson masses in the loops, and this dependence is such that for each jkl the coefficient A_{jkl} is independent of the scale μ. We refer to the expansion expressed in the form (3.47) as a *bare expansion*, to emphasize that it is entirely written in terms of the parameters of the effective Lagrangian – no reexpression of the latter in terms of observable quantities has been performed. Even before one starts rewriting and reordering the series (3.47) in powers of Goldstone boson masses, the full renormalisation of the bare expansion (3.47) can be performed order by order in quark masses. Consequently, the coefficients A_{jkl} are finite as well as cut-off and renormalisation scale-independent for all values of quark masses and of (renormalised) LECs in the effective Lagrangian.

In view of the previous discussion, we are concerned with practical questions related to the convergence properties of the bare χPT expansion (3.47) in QCD. The latter will depend on the values of running quark masses and on the values of the LECs at the typical hadronic scale $\Lambda_H \sim M_\rho$ set by the masses of non-Goldstone hadrons. In particular, one should question

[4] Energy-dependent quantities, such as form factors and scattering amplitude will be addressed in ch. 5.

the convergence of the bare chiral expansion for the actual values of quark masses and not just in the infinitesimal vicinity of the chiral limit. In the real world, all three quarks *uds* are sufficiently light,

$$m_u(\Lambda_H), m_d(\Lambda_H) \ll m_s(\Lambda_H) \ll \Lambda_H \,, \tag{3.48}$$

to expect a priori some (at least asymptotic) convergence of the three-flavour bare χPT series.

We have argued that fluctuations of $\bar{s}s$ pairs lead to a partial suppression of the three-flavour condensate $\Sigma(3)$, reducing the relative importance of the first term in the bare expansion of the Goldstone boson masses. The importance of such pairs is measured by the strength of the effective QCD coupling; i.e., comparing m_s with Λ_{QCD}, rather than with the hadronic scale Λ_H. Furthermore, the impact of these fluctuations is proportional to m_s. Hence, instabilities due to fluctuations of vacuum quark-antiquark pairs turn out to be particularly relevant for strange quarks and could manifest themselves when two- and three-flavour chiral expansions are compared. We can consider for instance the Ward identity related to the mass of the pion:

$$F_\pi^2 M_\pi^2 = 2m\Sigma(3) + 64(r+2)m^2 B_0^2 \Delta L_6 + 64 m^2 B_0^2 \Delta L_8 + F_\pi^2 M_\pi^2 d_\pi \,. \tag{3.49}$$

The parameters ΔL_6 and ΔL_8 are defined in terms of the LECs $L_6(\mu), L_8(\mu)$ and logarithms of Goldstone boson masses (their expression is given in sec. 3.5.1). Vacuum fluctuations of $\bar{s}s$-pairs show up in the term $m_s B_0^2 \Delta L_6$. For the physical value of $m_s \sim \Lambda_{QCD}$, the corresponding $O(p^4)$ contribution proportional to ΔL_6 can be as important [34, 36, 218, 219] as the LO condensate term $2m\Sigma(3)$. Even then, the remainder d_π, which collects all $O(p^6)$ and higher contributions, can still be small: $d_\pi \ll 1$. In other words, vacuum fluctuations need not affect the *overall* convergence of the bare chiral expansions such as (3.47) or (3.49) at least for some well-defined selected class of observables.

3.4.2 The role of higher-order remainders [E]

Let us write a generic bare expansion (3.47) in a concise form:

$$A = A_{\rm LO} + A_{\rm NLO} + A\,\delta A. \tag{3.50}$$

Eq. (3.50) is an identity: $A_{\rm LO}$ collects leading powers in quark masses in the bare expansion (3.47) (e.g., the condensate term in eq. (3.49)), $A_{\rm NLO}$ consists of all next-to-leading contributions (the second and third terms in eq. (3.49)), whereas $A\,\delta A$ stands for the sum of all remaining terms starting with the next-to-next-to-leading order (NNLO). In eq. (3.49), the latter is denoted as $\delta(F_\pi^2 M_\pi^2) \equiv d_\pi$.

With this setting, A can be identified with the exact (experimental) value of the observable A. Usually, $A_{\rm LO}$ corresponds to the $O(p^2)$ contribution, $A_{\rm NLO}$ to $O(p^4)$ and $A\,\delta A$ collects all higher orders starting with $O(p^6)$ [5]. δA will be referred to as a *higher-order remainder*. A precise definition of δA involves some convention in writing $A_{\rm NLO}$, and we will define it in detail in ch. 5. For the present discussion of energy-independent quantities at NLO, involving only the tree and tadpole contributions of Z_t in the generating functional eq. (3.35), we emphasise that we keep the expressions as they stand, with in particular LO masses as arguments of the chiral logarithms.

Not much is known about the size of higher-order remainders despite the fact that complete $SU(3) \times SU(3)$ two-loop calculations do exist for many observables [158] and the general structure of the generating functional is known to this order [220–222]. Following this line, the

[5] The case of a quantity whose expansion only starts at $O(p^4)$ or higher, requires particular care.

bare expansion can be pushed further and the higher-order remainder δA can be represented as

$$A\,\delta A = \Delta^A_{2L}(\mu) + \Delta^A_{1L}(\mu) + \Delta^A_{\rm tree}(\mu) + \dots\,, \tag{3.51}$$

where the ellipsis stands for $O(p^8)$ and higher contributions. The splitting of the $O(p^6)$ part [220–222] into the genuine two-loop contribution Δ_{2L} (containing only $O(p^2)$ vertices), the one-loop contribution Δ_{1L} (with the insertion of a single $O(p^4)$ vertex) and the tree $O(p^6)$ contribution $\Delta_{\rm tree}$ depends on the renormalisation scale and scheme.

Several ingredients are actually needed to estimate δA from the representation (3.51). The first two terms (loop contributions) depend respectively on $O(p^2)$ parameters mB_0, m_sB_0, F_0 and on $O(p^4)$ LECs $L^r_i(\mu)$. Furthermore, the tree-level counterterms $\Delta^A_{\rm tree}(\mu)$ are built up from the 90 LECs $C^r_i(\mu)$ that define the $O(p^6)$ effective Lagrangian. Even if some of them can presumably be determined from the momentum dependence of form factors, decay distributions and scattering amplitudes (e.g., quadratic slopes), the remaining unknown $O(p^6)$ constants, which merely describe the higher-order dependence on quark masses, are probably much more numerous than the observables that one can hope to measure experimentally. At this stage some models (resonance saturation, large-N_c approaches, NJL...) and/or lattice determinations are required, but the large number of terms contributing to a given $\Delta^A_{\rm tree}$ makes the resulting uncertainty in δA delicate to estimate (we discuss some of these aspects in sec. 8.3.3). Finally, it is worth stressing that only the sum of the three components shown in eq. (3.51) is meaningful. An estimate of the size of higher-order remainders is therefore not possible without a precise knowledge of the $O(p^2)$ and $O(p^4)$ constants mB_0, F_0 and the L_i's.

We will not address the problem of determining higher-order remainders on the basis of eq. (3.51). We are going to show that interesting non-perturbative conclusions can be reached, even if we do not decompose higher-order remainders and investigate the behaviour of the theory as a function of their size. We start with a simple theoretical assumption about higher orders: the bare chiral expansion of "good observables" as defined at the beginning of sec. 3.35, is *globally convergent*, i.e. the higher-order remainder δA in the identity (3.50) is small compared to 1:

$$\delta A \ll 1\,, \tag{3.52}$$

for the physical values of the quark masses and for the actual size of $O(p^2)$ and $O(p^4)$ parameters. On general grounds, one expects $\delta A = O(m^2_{\rm quark})$. In the worst case, its size should be $\delta A = O(m_s^2) \sim (30\%)^2 = 0.1$, but in many situations δA turns out to be $O(m_s m)$ or even $O(m^2)$ and is therefore more suppressed [6]. These cases are usually identified as a consequence of $SU(2)\times SU(2)$ low-energy theorems. (Such suppressions are not claimed from arguments based on the Zweig rule, since we never assume the latter.) However the higher-order remainders will not be neglected or used as small expansion parameters in the following.

On the other hand, no particular hierarchy will be assumed between the leading and next-to-leading components of (3.50). By definition, for infinitesimally small quark masses m_u, m_d, m_s one should have

$$A_{\rm NLO} \ll A_{\rm LO}\,, \qquad X_A \equiv \frac{A_{\rm LO}}{A} \sim 1\,. \tag{3.53}$$

However, due to vacuum fluctuations of $\bar qq$ pairs, the condition (3.53) can be easily invalidated for physical value of $m_s \sim \Lambda_{QCD}$: as discussed in eq. (Re eq:genuineinduced), the three-flavour condensate $\Sigma(3)$ in eq. (3.49) may be of a comparable size to – or even smaller than – the term m_sZ^s, reflecting the vacuum effects of massive $\bar ss$ pairs. At the same time, vacuum fluctuations

[6] We take as order of magnitudes 10 % for $O(m)$ contributions and 30 % for $O(m_s)$ terms. This can be related to the typical sizes of violation for $SU(2)\times SU(2)$ and $SU(3)\times SU(3)$ flavour symmetries.

need not affect the overall convergence of the bare chiral expansion (3.49), i.e., the condition (3.52) can still hold for "good observables" such as $F_\pi^2 M_\pi^2$. We will call *conditionally convergent* an observable for which $\delta A \ll 1$ but the hierarchy condition (3.53) does not hold.

Once a numerical competition is allowed between LO and NLO in the chiral expansions, one may wonder whether this could also occur at higher orders, so that the NNLO or higher remainders would actually be large. One cannot exclude logically such a possibility, even though this means that the underlying assumptions of χPT (consistent expansion of the generating functional of QCD) do not hold, and that the hope of an effective theory of QCD should be dismissed. One should add however that naive dimensional arguments, based on resonance saturation, suggest that each order of the chiral expansion should be suppressed by M_P^2/Λ_H^2, where M_P is the mass of the Goldstone bosons and Λ_H the mass of the lightest resonance states, and thus that there should be some numerical hierarchy between the orders of the chiral expansion. However, this argument does not hold between LO and NLO, as there is no possibility to estimate the LO contribution from the condensate using such resonance arguments (there is no coloured state able to saturate $\langle \bar{u}u \rangle$).

As stated before, if we have similar contributions from all orders of χPT, the whole chiral approach should be dismissed. We do not want to go to such extremes (yet), and will only allow for a numerical competition between LO and NLO. The comparison with data should ultimately tell us what the actual situation is, and in which mass/energy window the chiral expansions can be exploited in a meaningful way.

3.4.3 Instabilities in chiral series [E]

The usual treatment of χPT consists of two different steps.

1. The first step coincides with what has been described above as the "bare expansion" in powers of quark masses and external momenta. The coefficients of this expansion are unambiguously defined in terms of parameters of the effective Lagrangian $B_0, F_0, L_i \ldots$, independently of the convergence properties of the bare expansion. At NLO, they can be obtained from the generating functional eq. (3.35).

2. The second step consists in rewriting the bare expansion as an expansion in powers of Goldstone boson masses, by eliminating order by order the quark masses m and m_s and the three-flavour order parameters $\Sigma(3), F(3)$ in favour of the physical values of Goldstone boson masses M_P^2 and decay constants F_P^2. For this aim one inverts the expansion of Goldstone boson masses:

$$2mB_0 = M_\pi^2 \left(1 + \sum_P c_P^B M_P^2 + \ldots \right) , \tag{3.54}$$

where c_P^B contains the low-energy constants L_i and the chiral logarithms. A similar "inverted expansion" is worked out for F_0^2:

$$F_0^2 = F_\pi^2 \left(1 + \sum_P c_P^F M_P^2 + \ldots \right) , \tag{3.55}$$

and for the quark mass ratio

$$\frac{m_s + m}{2m} = \frac{M_K^2}{M_\pi^2} \left(1 + \sum_P c_P^r M_P^2 + \ldots \right) . \tag{3.56}$$

As a result of these two steps, observables other than M_π^2, M_K^2, F_π^2 (already used in eqs. (3.54), (3.55) and (3.56)) are expressed as expansions in powers of M_P^2 and $\log M_P^2$ with their coefficients depending on the constants L_i, C_i, etc. Large vacuum fluctuations of $\bar{s}s$ pairs could represent a serious impediment to the second step, i.e., to the perturbative reexpression of order parameters. This may happen if the bare expansion (3.50) of Goldstone boson masses and decay constants is only conditionally convergent: the leading and next-to-leading contributions are then of comparable size $A_{\rm LO} \sim A_{\rm NLO}$, despite a good global convergence $\delta A \ll 1$. In such a case, it is not a good idea to replace in higher orders of the bare expansion $X(3)$ by 1, $2mB_0$ by M_π^2, F_0^2 by F_π^2, etc. Indeed, consider a generic (conditionally convergent) observable A with its bare expansion eq. (3.50). The latter unambiguously defines the coefficients of the formal chiral expansion for any observable $F = f(A)$ as $F = F_{LO} + F_{NLO} + F\delta F$, with

$$F_{LO} = f(A_{LO})\,, \quad F_{NLO} = A_{NLO} f'(A_{LO})\,, \quad \delta F = 1 - \frac{f(A_{LO})}{f(A)} - \frac{f'(A_{LO})}{f(A)}[A - A_{LO} - A\delta A]\,. \tag{3.57}$$

Depending on the value of $X_A = A_{LO}/A$, i.e., the saturation of the chiral expansion of A by its first term, the chiral series of F may or may not converge well. One has in particular the two limiting behaviours:

$$X_A \to 1:\ \delta F \to -\frac{f'(A)}{f(A)} A\delta A\,, \qquad X_A \to 0 : \delta F \to 1 - \frac{f(0)}{f(A)} - \frac{f'(0)}{f(A)} A + \frac{f'(0)}{f(A)} A\delta A\,. \tag{3.58}$$

In the first case, a bound on δA implies a bound on δF, meaning that F converges well provided that A does. But in the second case, the size of δF is by no means driven by that of δA. As an illustration, if we take the "observables" $B = 1/A$ and $C = \sqrt{A}$, we obtain:

$$\delta B = \frac{(1 - X_A)^2}{X_A^2} - \frac{\delta A}{X_A^2}\,, \quad \delta C = 1 - \frac{1}{2\sqrt{X_A}} - \frac{1}{2}\sqrt{X_A} - \frac{1}{2\sqrt{X_A}}\delta A\,. \tag{3.59}$$

Even if we set $\delta A = 0$, we would need $X_A = A_{LO}/A$ above 41% to ensure that $|\delta B| < 10\%$, and X_A above 76% to ensure that $|\delta C| < 10\%$. Therefore, if the chiral expansions of some of the observables considered are not saturated by their LO term, we cannot take an arbitrary function of these observables, consider its chiral expansion, and assume that it will converge. This explains the origin of instabilities and large coefficients in the inverted expansion such as (3.54) or (3.55).

3.5 Constraints from Goldstone boson masses and decay constants

3.5.1 Pions and kaons [E]

We have now to discuss the implications of a numerical competition between LO and NLO for specific observables. The first example consists in pseudoscalar decay constants and masses. The pion and kaon masses are well known experimentally.As far as the decay constants are concerned, F_π and F_K are accessible at a high precision through leptonic decays (π_{l2} and K_{l2} respectively [137]) which provide in the framework of the Standard Model (SM) [223]:

$$|V_{us}/V_{ud}| \times F_K/F_\pi = 0.2758 \pm 0.0005\,, \tag{3.60}$$

which can be combined with the very accurate determination of the first element of the CKM matrix V_{ud} from super-allowed $0^+ \to 0^+$ nuclear beta decays [224]

$$|V_{ud}| = 0.97425 \pm 0.00022\,, \tag{3.61}$$

the unitarity of the CKM matrix and the smallness of the $|V_{ub}|$ matrix element to get:

$$F_\pi|_{SM} = 92.2 \pm 0.3 \text{ MeV} \qquad F_K/F_\pi|_{SM} = 1.192 \pm 0.006\,, \tag{3.62}$$

Due to our suspicion of instabilities in chiral expansion, we decided to consider only observables derived from correlators of axial/vector currents and scalar/pseudoscalar densities. This selects naturally the two-point axial correlator [7], with the structure (for $a, b = 1 \dots 3$):

$$\Pi^{ab}_{AA;\mu\nu} = i \int d^4x e^{ip(x-y)} \langle 0|T[A^a_\mu(x) A^b_\nu(0)]|0\rangle \tag{3.63}$$

$$= \delta^{ab} \left[\frac{p_\mu p_\nu F_\pi^2}{M_\pi^2 - p^2} + g_{\mu\nu} F_\pi^2 + (p_\mu p_\nu - g_{\mu\nu}) \Pi^T_{AA}(p^2) + p_\mu p_\nu \Pi^L_{AA}(p^2) \right] \tag{3.64}$$

where the longitudinal and transverse pieces Π^L_{AA} and Π^T_{AA} are regular at low p^2 [20,185]. The related observables can be obtained from values of Π^{ab}_{AA} at particular values or its residues:

$$F_\pi^2 \delta^{ab} = \frac{1}{4} \Pi_{AA;\mu\mu}(0)\,, \qquad F_\pi^2 M_\pi^2 \delta^{ab} = \lim_{p^2 \to M_\pi^2} (M_\pi^2 - p^2) \Pi_{AA;\mu\mu}(p^2)\,, \tag{3.65}$$

which are expected to have good (if conditional) convergence properties. The usual χPT expressions (sec. 10 in ref. [21]) can be recast in the following form:

$$F_\pi^2 = F_\pi^2 Z(3) + 8(r+2) Y(3) M_\pi^2 \Delta L_4 + 8 Y(3) M_\pi^2 \Delta L_5 + F_\pi^2 e_\pi\,, \tag{3.66}$$

$$F_K^2 = F_\pi^2 Z(3) + 8(r+2) Y(3) M_\pi^2 \Delta L_4 + 4(r+1) Y(3) M_\pi^2 \Delta L_5 + F_K^2 e_K\,, \tag{3.67}$$

$$F_\pi^2 M_\pi^2 = F_\pi^2 M_\pi^2 X(3) + 16(r+2) Y^2(3) M_\pi^4 \Delta L_6 + 16 Y^2(3) M_\pi^4 \Delta L_8 + F_\pi^2 M_\pi^2 d_\pi\,, \tag{3.68}$$

$$F_K^2 M_K^2 = \frac{r+1}{2} F_\pi^2 M_\pi^2 X(3) \tag{3.69}$$

$$+ 8(r+2)(r+1) Y^2(3) M_\pi^4 \Delta L_6 + 4(r+1)^2 Y^2(3) M_\pi^4 \Delta L_8 + F_K^2 M_K^2 d_K\,,$$

We take as free parameters the $N_f = 3$ quark condensate and pseudoscalar decay constant expressed in physical units, as well as their ratio and the quark mass ratio:

$$X(3) = \frac{2m\Sigma(3)}{F_\pi^2 M_\pi^2}\,, \quad Z(3) = \frac{F^2(3)}{F_\pi^2}\,, \quad Y(3) = \frac{X(3)}{Z(3)} = \frac{2mB_0}{M_\pi^2}\,, \quad r = \frac{m_s}{m}\,. \tag{3.70}$$

We have introduced the higher-order remainders d_π, e_π, d_K and e_K, and$\Delta L_i = L_i^r(\mu) - \hat{L}_i(\mu)$ combine the (renormalised and quark-mass independent) constants $L_{4,5,6,8}$ and chiral logarithms so that they are independent of the renormalisation scale μ:

$$32\pi^2 \hat{L}_4(\mu) = \frac{1}{8} \log \frac{\overset{\circ}{M}{}_K^2}{\mu^2} - \frac{1}{8(r-1)(r+2)} \left[(4r+1) \log \frac{\overset{\circ}{M}{}_K^2}{\overset{\circ}{M}{}_\pi^2} + (2r+1) \log \frac{\overset{\circ}{M}{}_\eta^2}{\overset{\circ}{M}{}_K^2} \right]\,, \tag{3.71}$$

[7] One could also use two-point correlators of pseudoscalar densities, with the same result concerning the "good" observables related to the pion mass and decay constant.

$$32\pi^2\hat{L}_5(\mu) = \frac{1}{8}\left[\log\frac{\overset{\circ}{M}{}_K^2}{\mu^2} + 2\log\frac{\overset{\circ}{M}{}_\eta^2}{\mu^2}\right] + \frac{1}{8(r-1)}\left[3\log\frac{\overset{\circ}{M}{}_\eta^2}{\overset{\circ}{M}{}_K^2} + 5\log\frac{\overset{\circ}{M}{}_K^2}{\overset{\circ}{M}{}_\pi^2}\right], \tag{3.72}$$

$$32\pi^2\hat{L}_6(\mu) = \frac{1}{16}\left[\log\frac{\overset{\circ}{M}{}_K^2}{\mu^2} + \frac{2}{9}\log\frac{\overset{\circ}{M}{}_\eta^2}{\mu^2}\right] - \frac{1}{16}\frac{r}{(r+2)(r-1)}\left[3\log\frac{\overset{\circ}{M}{}_K^2}{\overset{\circ}{M}{}_\pi^2} + \log\frac{\overset{\circ}{M}{}_\eta^2}{\overset{\circ}{M}{}_K^2}\right] \tag{3.73}$$

$$32\pi^2\hat{L}_8(\mu) = \frac{1}{16}\left[\log\frac{\overset{\circ}{M}{}_K^2}{\mu^2} + \frac{2}{3}\log\frac{\overset{\circ}{M}{}_\eta^2}{\mu^2}\right] + \frac{1}{16(r-1)}\left[3\log\frac{\overset{\circ}{M}{}_K^2}{\overset{\circ}{M}{}_\pi^2} + \log\frac{\overset{\circ}{M}{}_\eta^2}{\overset{\circ}{M}{}_K^2}\right]. \tag{3.74}$$

As indicated in sec. 3.4.1, we have kept the LO values of the pseudoscalar masses eq. (3.37) in the chiral logarithms. The values of the logarithms are only mildly dependent on r and $Y(3)$; for $r = 25$ and $Y(3) = 1$,

$$\Delta L_4 = L_4^r(M_\rho) + 0.50\cdot 10^{-3}, \qquad \Delta L_5 = L_5^r(M_\rho) + 0.57\cdot 10^{-3}, \tag{3.75}$$

$$\Delta L_6 = L_6^r(M_\rho) + 0.25\cdot 10^{-3}, \qquad \Delta L_8 = L_8^r(M_\rho) + 0.18\cdot 10^{-3}. \tag{3.76}$$

Since F_π, F_K, M_π and M_K are rather accurately known, we can use these expressions to eliminate the $O(p^4)$ LECs above in the chiral expansion of other observables. This is rather different from the usual χPT trading, since we keep explicitly higher-order terms that would have been neglected in the usual (perturbative) treatment of chiral series.

From the masses and decay constants (3.66)-(3.69), we get the equivalent set of equations providing some $O(p^4)$ LECs in terms of physical masses and decay constants, $r, X(3), Y(3)$ and NNLO remainders:

$$Y^2(3)\Delta L_6 = \frac{1}{16(r+2)}\frac{F_\pi^2}{M_\pi^2}[1 - \epsilon(r) - X(3) - d], \tag{3.77}$$

$$Y^2(3)\Delta L_8 = \frac{1}{16}\frac{F_\pi^2}{M_\pi^2}[\epsilon(r) + d'], \tag{3.78}$$

$$Y(3)\Delta L_4 = \frac{1}{8(r+2)}\frac{F_\pi^2}{M_\pi^2}[1 - \eta(r) - Z(3) - e], \tag{3.79}$$

$$Y(3)\Delta L_5 = \frac{1}{8}\frac{F_\pi^2}{M_\pi^2}[\eta(r) + e']. \tag{3.80}$$

with

$$\epsilon(r) = 2\frac{r_2 - r}{r^2 - 1}, \qquad \eta(r) = \frac{2}{r-1}\left(\frac{F_K^2}{F_\pi^2} - 1\right), \qquad r_2 = 2\frac{F_K^2 M_K^2}{F_\pi^2 M_\pi^2} - 1 \simeq 35, \tag{3.81}$$

and the following linear combinations of higher-order remainders arise:

$$d = \frac{r+1}{r-1}d_\pi - \left(\epsilon(r) + \frac{2}{r-1}\right)d_K, \qquad d' = d - d_\pi, \tag{3.82}$$

$$e = \frac{r+1}{r-1}e_\pi - \left(\eta(r) + \frac{2}{r-1}\right)e_K, \qquad e' = e - e_\pi. \tag{3.83}$$

The above identities are algebraically exact, but they are useful only as long as higher-order remainders are small. The estimation of the size of the higher-order remainders is in principle rather non trivial. As proposed in sec. 3.4.2, we take:

$$d, e = O(m_s^2) \sim 10\% \,, \qquad d', e' = O(m m_s) \sim 3\% \,, \tag{3.84}$$

with the rule of thumb that NNLO corrections of size $O(m_s^2)$ should not exceed $(30\%)^2 \simeq 10\%$ of the contribution to the observable while $O(m_s m)$ terms would be less than $30\% \cdot 10\% \simeq 3\%$. We will propose in ch. 5 a different but compatible way of dealing with this issue.

In eqs. (3.77)-(3.80), the presence of powers of $Y(3)$, i.e., B_0, follows from the normalisation of the scalar and pseudoscalar sources in ref. [21]: these powers arise only for $O(p^4)$ LECs related to explicit chiral symmetry breaking (two powers for L_6, L_7, L_8, one for L_4 and L_5), and are absent for LECs associated with purely derivative terms. We can also combine these equations to obtain two relations for the order parameters:

$$X(3) = 1 - \epsilon(r) - [Y(3)]^2 \rho/4 - d, \qquad Z(3) = 1 - \eta(r) - Y(3)\lambda/4 - e. \tag{3.85}$$

where the LECs L_6 and L_4 enter the discussion through the combinations related to fluctuations of small Dirac eigenvalues (see sec. 2.5.3):

$$\lambda = 32 \frac{M_\pi^2}{F_\pi^2}(r+2)\Delta L_4 \,, \qquad \rho = 64 \frac{M_\pi^2}{F_\pi^2}(r+2)\Delta L_6 \,. \tag{3.86}$$

The remaining two equations (3.78)-(3.80) can be reexpressed as a relation between $\epsilon(r)$ and L_8 on one hand and between $\eta(r)$ and L_5 on the other hand:

$$\epsilon(r) = 16 \frac{M_\pi^2}{F_\pi^2}[Y(3)]^2 \Delta L_8 - d' \,, \qquad \eta(r) = 8 \frac{M_\pi^2}{F_\pi^2} Y(3) \Delta L_5 - e' \,. \tag{3.87}$$

3.5.2 Perturbative reexpression of order parameters [E]

The four exact equations eqs. (3.85) and (3.87)-(3.87) can be used to illustrate explicitly the instabilities which may arise in the perturbative expression of $X(3)$ and $Z(3)$ in powers of M_P^2 given by eqs. (3.54) and (3.55). In the perturbative treatment of three-flavour χPT [21], one uses the fact that $Y(3) = 1 + O(M_P^2)$ to set systematically $Y(3) = 1$ whenever it appears in the NLO term. One first uses eq. (3.87) to express F_K^2/F_π^2 and $r = m_s/m$ in terms of ΔL_5 and ΔL_8, neglecting higher-order terms. In these equations, the quark mass ratio r appearing in the expressions for ΔL_i has to be replaced by its leading order value:

$$r_0 = 2 \frac{M_K^2}{M_\pi^2} - 1 \sim 24 \,. \tag{3.88}$$

The result reads:

$$\frac{F_K^2}{F_\pi^2} = 1 + 8 \frac{M_K^2 - M_\pi^2}{F_\pi^2} \Delta L_5 + \ldots \qquad r + 1 = 2 \frac{M_K^2}{M_\pi^2} \left(1 + 8 \frac{M_K^2 - M_\pi^2}{F_\pi^2} [\Delta L_5 - 2 \Delta L_8] + \ldots \right) . \tag{3.89}$$

Strictly speaking, eq. (3.89) does not get any direct contribution from the vacuum fluctuation of $\bar{s}s$ pairs which violate the Zweig rule and are tracked by L_6 and L_4. The situation is quite different in the case of the identities eq. (3.85) for $X(3)$ and $Z(3)$, where the terms describing

fluctuations are potentially dangerous. Expressing them perturbatively thanks to eq. (3.89), one gets:

$$X(3) = 1 - 16\frac{M_\pi^2}{F_\pi^2}\Delta L_8 - 16\frac{2M_K^2 + M_\pi^2}{F_\pi^2}\Delta L_6 + \dots \tag{3.90}$$

$$Z(3) = 1 - 8\frac{M_\pi^2}{F_\pi^2}\Delta L_5 - 8\frac{2M_K^2 + M_\pi^2}{F_\pi^2}\Delta L_4 + \dots \tag{3.91}$$

The large coefficients characteristic of the perturbative treatment of $1/(F_\pi^2 M_\pi^2)$ – and to some extent also of $1/F_\pi^2$ – now become visible. Eqs. (3.90) and (3.91) lead numerically to:

$$X(3) = 1 - 37\Delta L_8 - 950\Delta L_6 + \dots \qquad Z(3) = 1 - 18\Delta L_5 - 475\Delta L_4 + \dots \tag{3.92}$$

In eqs. (3.90) and (3.91), the main NLO contribution comes from the M_K^2-enhanced term proportional to the $O(p^4)$ Zweig-rule violating LECs L_6 and L_4. If the latter stay close to their critical values (corresponding to $\Delta L_4 \sim \Delta L_6 \sim 0$, i.e., $L_4(M_\rho) \simeq -0.50 \cdot 10^{-3}$ and $L_6^r(M_\rho) \simeq -0.25 \cdot 10^{-3}$ for $r = 25$ and $Y(3) = 1$), the NLO contributions remain small. As explained in the following chapters, the dispersive estimates of these low-energy constants are rather different from the critical values.

For illustrative purposes, let us take $L_6^r(M_\rho) = (0.6 \pm 0.2) \cdot 10^{-3}$, $L_4^r(M_\rho) = (0.2 \pm 0.3) \cdot 10^{-3}$, and let us study the convergence of the previous perturbative expansions. If we take $L_5^r(M_\rho) = 1.4 \cdot 10^{-3}$ and $L_8^r(M_\rho) = 0.9 \cdot 10^{-3}$ [20], the numerical evaluation of eqs. (3.90)-(3.91) leads to the decomposition:

$$\begin{aligned} \text{Qty} &= \text{LO} + [\text{fluct} + \text{other}] + \text{NNLO} \\ \\ X(3) \equiv \frac{2m\Sigma(3)}{F_\pi^2 M_\pi^2} &= 1 - [0.82 + 0.04] + O(p^4)\,, \\ \\ Z(3) \equiv \frac{F(3)^2}{F_\pi^2} &= 1 - [0.34 + 0.04] + O(p^4)\,, \\ \\ (r+1)\frac{M_\pi^2}{2M_K^2} &= 1 - [0.00 + 0.06] + O(p^4)\,. \end{aligned} \tag{3.93}$$

For each quantity, the right-hand side is the sum of the leading term (1), the NLO term (the sum in brackets) and higher-order terms. The NLO term is decomposed into its two contributions: the first one comes from the fluctuation term (proportional to ΔL_4 or ΔL_6) and the second one collects all other NLO contributions. Fluctuation contributions have a dramatic effect on the convergence – they are the only terms enhanced by a factor of M_K^2 in eqs. (3.90) and (3.91).

3.5.3 Non-perturbative elimination of low-energy constants [E]

We have just seen that the perturbative treatment of chiral series fails if vacuum fluctuations of $\bar{q}q$ pairs are large, resulting in instabilities in the chiral expansions. In this case, the nonlinearities in eq. (3.85), relating order and fluctuation parameters, are crucial, and we must not linearize these relations (hence the inadequacy of a perturbative treatment). We should therefore treat eq. (3.85) without performing any approximation. As indicated in ref. [37], we

can reexpress eq (3.85) as a non-linear system for $Y(3)$ and $Z(3)$, with two solutions for the ratio of order parameters $Y(3) = X(3)/Z(3)$:

$$Y(3) = \frac{X(3)}{Z(3)} = \frac{2[1-\epsilon(r)-d]}{1-\eta(r)-e+\sqrt{[1-\eta(r)-e]^2+[\rho-\lambda][1-\epsilon(r)-d]}}\,. \tag{3.94}$$

$$\left(\text{or } = \frac{2[1-\epsilon(r)-d]}{1-\eta(r)-e-\sqrt{[1-\eta(r)-e]^2+[\rho-\lambda][1-\epsilon(r)-d]}}\right) \tag{3.95}$$

The nonlinear character of the system (3.85) in $X(3), Z(3)$ results in the (non-perturbative) square root. We see that the behaviour of $Y(3)$ is controlled by the parameter $\rho - \lambda$, i.e., $2L_6 - L_4$ as can be seen from eqs. (3.86). The first branch eq. (3.94) corresponds to $Y(3)$ between 0 and 2, whereas the second branch eq. (3.95) yield $Y(3)$ above 2 (and potentially up to infinity, corresponding to the situation where the quark condensate is sizeable, but the decay constant very small). The properties of these two solutions were discussed in more detail in ref. [37] in the context of QCD-like theories with a large number of flavours. In the following, we will focus on the first branch eq. (3.94) which embeds the value $Y(3) = 1$ in the small fluctuation limit $\rho - \lambda \ll 1$.

The perturbative treatment sketched in the previous section corresponds to linearising eq. (3.94), assuming that the fluctuation parameter $\rho - \lambda \ll 1$:

$$Y(3) = \frac{X(3)}{Z(3)} = 2\frac{1-\epsilon(r)-d}{1-\eta(r)-e}\left[1 - \frac{\rho-\lambda}{4}\frac{1-\epsilon(r)-d}{(1-\eta(r)-e)^2} + \frac{(\rho-\lambda)^2}{16}\left(\frac{1-\epsilon(r)-d}{(1-\eta(r)-e)^2}\right)^2 + \dots\right] \tag{3.96}$$

where ρ and λ contain L_6 and L_4 (see eq. (3.86)), whereas $\epsilon(r)$ and $\eta(r)$ can be reexpressed in terms of L_8 and L_5 (see eq. (3.87)). We see therefore that the non-perturbative expression eq. (3.94) resums a tower of contributions from the fluctuation parameters ρ and λ. In particular, the expansion eq. (3.96) is invalid if large fluctuations occur: ρ and/or λ are then numerically of order 1, although they count as $O(p^2)$ in the chiral limit, and thus the above series does not converge. One need not very large values of the Zweig-suppressed constants L_4 and L_6 to achieve this, due to the m_s-enhanced factor of λ and ρ. If we take $r = 25$ and $Y(3) = 1$, one gets:

$$\rho - \lambda \simeq 1980 \cdot (2\Delta L_6 - \Delta L_4)\,, \tag{3.97}$$

so that a shift of $2L_6 - L_4$ of only a fraction of 10^{-3} from the value $2\hat{L}_6 - \hat{L}_4$ (which almost vanishes for $r = 25$, $Y(3) = 1$, is enough to generate a large value of $\rho - \lambda$ and thus to suppress significantly $Y(3)$. Eq. (3.94) leads to the suppression of $Y(3)$, which would contribute to a stabilisation of eq. (3.85) by reducing the contribution proportional to the fluctuation parameters ρ and λ. This is illustrated in fig. 3.6, where one can see that the value $Y(3) = 1$ corresponds to a line where $\rho = \lambda$, i.e. $2L_6 = L_4$. There is also a region where eq. (3.94) does not admit real solutions, corresponding to L_4 significantly larger than L_6.

A similar discussion can be held separately for $X(3)$ with ρ and L_6, and for $Z(3)$ with λ and L_4. In each case, values of the Zweig-rule suppressed LECs slightly shifted from $\hat{L}_4$ and $\hat{L}_6$ towards positive values are enough to provide a significant suppression of the chiral order parameters, so that they cannot reach "very" large values (a few 10^{-3}) without leading to a very significant suppression. This is illustrated in fig. 3.7 for particular values of r and $Y(3)$. We recall that even a naive estimate based on the Zweig rule eq. (3.40) is able to provide $L_6^r(M_\rho) \simeq 0.12 \cdot 10^{-3}$ and $L_6^r(M_\rho) \simeq 0.20 \cdot 10^{-3}$, corresponding to a sizable decrease of $X(3)$ and $Z(3)$ compared to their $N_f = 2$ counterparts. One understands better the results of the NNLO fits gathered in tabs. 3.1 and 3.2, as $L_4^r(M_\rho)$ and $L_6^r(M_\rho)$ are both positive and above 10^{-3},

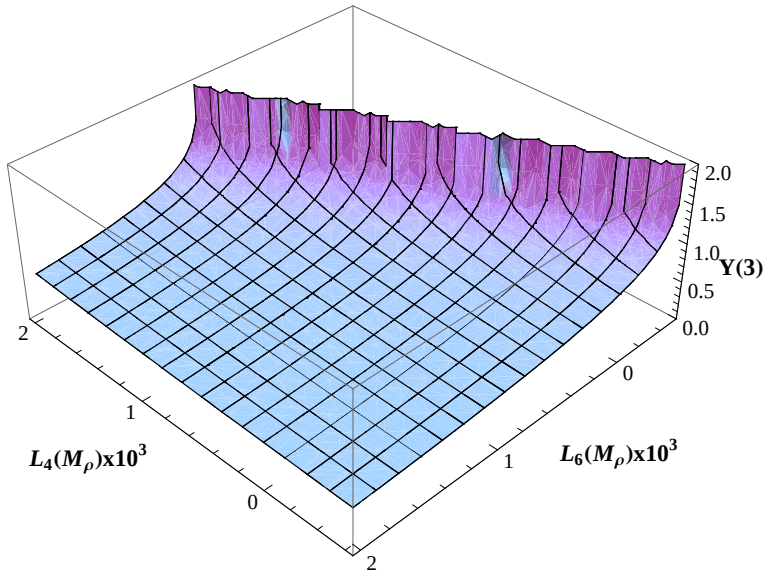

Figure 3.6: $Y(3) = 2mB_0/M_\pi^2$ *as a function of* $L_4(M_\rho)$ *and* $L_6(M_\rho)$ *for* $r = 25$ *(and remainders* $e = d = 0$*). The frontier delimits the region where* ρ *and* λ *do not yield solutions for eq. (3.94).*

leading to a significant suppression of LO contributions to F_P^2 and $F_P^2 M_P^2$, and potentially to the problems of convergence advocated in the previous sections.

As an illustration of the lattice determinations of the LECs in sec. 3.3.4, one can also quote the following values [129] obtained by comparing lattice simulations with staggered quarks with the staggered version of χPT [204]:

$$[\text{MILC}]: \qquad r = 27.2(4)\,, \quad [2L_6^r - L_4^r](M_\eta) = 0.5(1)(2)\cdot 10^{-3} \quad L_4^r(M_\eta) = 0.1(2)(2)\cdot 10^{-3}\,. \tag{3.98}$$

Combining the errors in quadrature and using eq. (3.94) as well the other results in sec. 3.5.2, $X(3)$ would stand between 0.55 and 0.95, $Z(3)$ between 0.57 and 1.04, and $Y(3)$ between 0.67 and 1.08. Obviously, if the values of $X(3)$ and $Z(3)$ are on the smaller end of these ranges, i.e., if L_6 and L_4 are in the upper end of the range in ref. [129], the assumption of small vacuum fluctuations is not correct, and the extraction of the LECs by the means of staggered χPT [204] should be reassessed more carefully. Similar conclusion hold for most of the lattice determinations gathered in fig. 3.3. As discussed extensively in ref. [37], different behaviours of the fluctuation parameters can result in a rather varied range of patterns of chiral symmetry breaking.

We would like to extract information about $N_f = 3$ chiral symmetry breaking from physical observables, even in the event that the perturbative expansion breaks down. We will thus take as independent quantities the parameters:

$$X(3) = \frac{2m\Sigma(3)}{F_\pi^2 M_\pi^2}\,, \qquad Z(3) = \frac{F^2(3)}{F_\pi^2}\,, \qquad r = \frac{m_s}{m}\,. \tag{3.99}$$

We should emphasize that this corresponds to a different choice from that adopted in the perturbative treatment of chiral series where $X(3)$, $Z(3)$, r, F_K/F_π are iteratively expressed in terms of L_4, L_5, L_6, L_8. In contrast, we start by the same four identities and express non-perturbatively L_4, L_5, L_6, L_8 in terms of $X(3)$, $Z(3)$, r, F_K/F_π; this is a sensible treatment provided that both LO and NLO terms are considered.

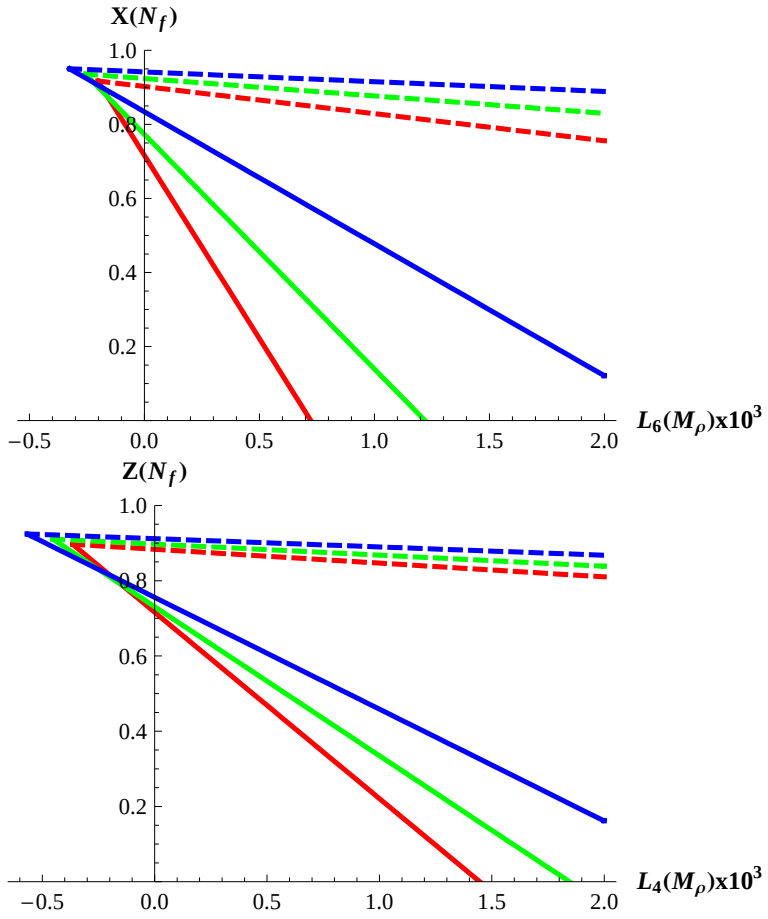

Figure 3.7: *Top:* $X(2)$ *(dashed lines) and* $X(3)$ *(solid lines) as functions of* $L_6(M_\rho)$ *for different values of* $Y(3) = 0.6$ *(blue), 0.8 (green) and 1 (red). Bottom:* $Z(2)$ *(dashed lines) and* $Z(3)$ *(solid lines) as functions of* $L_4(M_\rho)$ *for different values of* $Y(3) = 0.6$ *(blue), 0.8 (green) and 1 (red). In each case, the remainders have been set to zero for the sake of clarity.*

Keeping in mind that LO and NLO contributions can have a similar size, we treat as exact identities the expansions of good observables in powers of quark masses, and exploit the mass and decay constant identities to reexpress $O(p^2)$ and $O(p^4)$ LECs in terms of r, $X(3)$, $Z(3)$, observables quantities and higher-order remainders. This leads to eqs. (3.77)-(3.80). Plugging these identities into χPT expansions corresponds therefore to a resummation of vacuum fluctuations encoded in ρ and λ, as opposed to the usual (iterative and perturbative) treatment of the same chiral series. We can then reexpress observables in terms of the three parameters of interest $X(3)$, $Z(3)$, r and higher-order remainders. We will come back to this approach in ch. 5.

3.5.4 The η-mass and the Gell-Mann–Okubo formula [E]

It remains for us to discuss the mass and decay constant of the η meson as constrained by Ward identities for two-point functions of the eighth component of the axial current and of its divergence. The corresponding identities involve one new NLO constant L_7 and two extra

higher-order remainders d_η and e_η :

$$F_\eta^2 = F_\eta^2 Z(3) + 8(r+2)Y(3)M_\pi^2\Delta L_4 + \frac{8}{3}(2r+1)Y(3)M_\pi^2\Delta L_5 \tag{3.100}$$
$$+\frac{1}{48\pi^2}\left[(2r+1)\log\frac{\overset{\circ}{M}{}_\eta^{\,2}}{\overset{\circ}{M}{}_K^{\,2}} - \log\frac{\overset{\circ}{M}{}_K^{\,2}}{\overset{\circ}{M}{}_\pi^{\,2}}\right] + F_\eta^2 e_\eta\,,$$

$$F_\eta^2 M_\eta^2 = \frac{2r+1}{3}F_\pi^2 M_\pi^2 X(3) + \frac{16}{3}(2r+1)(r+2)Y^2(3)M_\pi^4\Delta L_6 \tag{3.101}$$
$$+\frac{16}{3}(2r^2+1)Y^2(3)M_\pi^4\Delta L_8 + \frac{32}{3}(r-1)^2Y^2(3)M_\pi^4 L_7 + F_\eta^2 M_\eta^2 d_\eta\,.$$

These two identities will be used to reexpress the LEC L_7 in terms of order parameters and quark mass ratio, and to eliminate the decay-constant F_η, which is not directly accessible experimentally. This new discussion is closely related to the old question [225, 226] whether the remarkable accuracy of the Gell-Mann-Okubo (GMO) formula for Goldstone bosons finds a natural explanation within χPT and what it says about the size of the three-flavour condensate.

The combination:

$$D_{GMO} = 3F_\eta^2 M_\eta^2 - 4F_K^2 M_K^2 + F_\pi^2 M_\pi^2\,, \tag{3.102}$$

does not receive any $O(p^2)$ contribution from the genuine condensate $\Sigma(3)$. The η-mass identity (3.100) leads to the following simple formula for D_{GMO}, expressed in units $F_\pi^2 M_\pi^2$:

$$\Delta_{GMO} \equiv \frac{D_{GMO}}{F_\pi^2 M_\pi^2} = 16\frac{M_\pi^2}{F_\pi^2}(r-1)^2[Y(3)]^2(2L_7 + \Delta L_8) + d_{GMO}\,. \tag{3.103}$$

Similarly, the identity for F_η can be put into the form:

$$\frac{F_\eta^2}{F_\pi^2} = 1 + \frac{4}{3}\left(\frac{F_K^2}{F_\pi^2} - 1\right) + \frac{1}{48\pi^2}\frac{M_\pi^2}{F_\pi^2}Y(3)\left[(2r+1)\log\frac{\overset{\circ}{M}{}_\eta^{\,2}}{\overset{\circ}{M}{}_K^{\,2}} - \log\frac{\overset{\circ}{M}{}_K^{\,2}}{\overset{\circ}{M}{}_\pi^{\,2}}\right] + e_{GMO}\,. \tag{3.104}$$

Eqs. (3.103) and (3.104) are exact as long as the NNLO remainders:

$$d_{GMO} = 3\frac{F_\eta^2 M_\eta^2}{F_\pi^2 M_\pi^2}d_\eta - 4\frac{F_K^2 M_K^2}{F_\pi^2 M_\pi^2}d_K + d_\pi\,, \qquad e_{GMO} = \frac{F_\eta^2}{F_\pi^2}e_\eta + \frac{4}{3}\frac{F_K^2}{F_\pi^2}e_K - \frac{e_\pi}{3}\,, \tag{3.105}$$

are included. If one follows sec. 3.5.2 and treats the exact formulae (3.103) and (3.104) perturbatively, one reproduces the $O(p^4)$ expressions given in ref. [21], as expected.

Remarkably, the identities (3.103) and (3.104) are simpler and more transparent than their perturbative version, and we find them useful to make a few numerical estimates which may be relevant for a discussion of the GO formula. For this purpose we shall use the value $r \sim 24$ of the quark mass ratio and neglect for a moment the higher-order remainders d_{GMO} and e_{GMO}, as well as error bars related to the experimental inputs on masses and decay constants. For this exercise, we also disregard isospin breaking and electromagnetic corrections. First, the dependence of F_η on $Y(3) = 2mB_0/M_\pi^2$ is negligibly small [8]:

$$\frac{F_\eta^2}{F_\pi^2} = 1.555 + 0.052\cdot Y(3)\,. \tag{3.106}$$

[8] This is obtained for $r = r_0$ – the coefficient of $Y(3)$ varies between 0.010 and 0.079 in the range $r_1 \le r \le r_2$ defined in sec. 3.6.1.

We estimate $\Delta_{GMO} = D_{GMO}/F_\pi^2 M_\pi^2$, using $F_\eta^2/F_\pi^2 = 1.565$ (obtained for $Y(3) = 1$ and corresponding to $F_\eta = 115$ MeV, and find:

$$\Delta_{GMO} = 72.34 - 71.45 + 1 = 1.89\,. \tag{3.107}$$

We have split the result into the three contributions corresponding respectively to η, K and π, in order to emphasize the accuracy of the formula. If we drop the decay constants in Δ_{GMO}, we obtain:

$$\tilde{\Delta}_{GMO} = \frac{3M_\eta^2 - 4M_K^2 + M_\pi^2}{M_\pi^2} = 46.21 - 50.46 + 1 = -3.24\,. \tag{3.108}$$

Hence, apart from a change of sign, this more familiar definition of the GO discrepancy is of a comparable magnitude as Δ_{GMO}. For the reasons already stressed, the interpretation in terms of QCD correlation functions is more straightforward when $F_P^2 M_P^2$ is used.

If the origin of the GO formula were to be naturally explained by the dominance of the $O(p^2)$ condensate term in the expansion of $F_P^2 M_P^2$, the order of magnitude of the estimate (3.107) should be reproduced by eq. (3.103) for a typical order of magnitude of the $O(p^4)$ LECs L_8 and L_7 without any fine tuning of their values. Using eq. (3.87) and neglecting the higher-order remainder d', one gets:

$$16\frac{M_\pi^2}{F_\pi^2}(r-1)^2[Y(3)]^2\Delta L_8 = (r-1)^2[\epsilon(r) + d'] = 19.3 \qquad [r = r_0]\,. \tag{3.109}$$

Hence, the typical $O(p^4)$ contribution ΔL_8 to Δ_{GMO} happens to be nearly one order of magnitude bigger than the estimate (3.107): the latter can only be reproduced by tuning very finely the LEC L_7:

$$[Y(3)]^2(\Delta L_8 + 2L_7) \simeq 0.1 \times 10^{-3}\,, \tag{3.110}$$

to be compared with the above estimate $[Y(3)]^2\Delta L_8 \simeq 1.0 \times 10^{-3}$. All this of course does not reveal any contradiction, but it invalidates the customary "explanation" of the GO formula and the standard argument against a possible suppression of the three-flavour condensate $\Sigma(3)$. Therefore, the fact that the GO formula is satisfied so well remains unexplained independently of the size of $\Sigma(3)$ and of the vacuum fluctuations. The last point can be explicitly verified: the genuine condensate contribution $\Sigma(3)$ as well as the induced condensate $m_s Z^s$, which represents an $O(p^4)$ contribution to $F_P^2 M_P^2$, both drop out of the GO combination (3.102).

We now return to our framework: we do not assume a particular hierarchy between LO and NLO contributions to chiral series, and we do not neglect any longer the higher-order remainders (in the case of the η-meson, d_{GMO} and e_{GMO} might be sizeable and should be kept all the way through). It is possible to use the previous formulae to reexpress L_7 in a similar way to eqs. (3.77)-(3.80):

$$[Y(3)]^2 L_7 = \frac{1}{32(r-1)^2}\frac{F_\pi^2}{M_\pi^2}\left[\frac{3F_\eta^2 M_\eta^2 - 4F_K^2 M_K^2 + F_\pi^2 M_\pi^2}{F_\pi^2 M_\pi^2}\right. \tag{3.111}$$
$$\left. -(r-1)^2[\epsilon(r) + d'] - \frac{3F_\eta^2 M_\eta^2 d_\eta - 4F_K^2 M_K^2 d_K + F_\pi^2 M_\pi^2 d_\pi}{F_\pi^2 M_\pi^2}\right].$$

This expression should be used to reexpress non-perturbatively L_7 in terms of chiral order parameters (F_η^2 is given by eq. (3.104)). We can already notice that in eq. (3.111), the first contribution, which corresponds to Δ_{GMO}, is 5 to 10 times suppressed with respect to the second term $(r-1)^2[\epsilon(r) + d']$.

3.6 Relations between two- and three-flavour chiral perturbation theory

3.6.1 Constraints on leading-order parameters [D,E]

As indicated before, in presence of only conditionally convergent quantities, we must abandon the assumption that the LO parameters are close to their values: $X(3) \simeq 1$, $Z(3) \simeq 1$ and $r \simeq 2M_K^2/M_\pi^2 - 1$. The first two values corresponded to the assumption that $\rho \ll 1$ and $\lambda \ll 1$, and the third one came from the assumption that meson masses are saturated by their LO term. But even in absence of a saturation by LO parameters, we can still bound these parameters.

The first requirement comes from the vacuum stability: the three-flavour quark condensate cannot be negative, or the squared meson masses would be negative for very small but finite quark masses, where the Gell-Mann-Oakes Renner relations eqs. (2.22)-(2.24) would be very well satisfied. Similarly, the squared decay constant cannot be negative, and it cannot be zero for chiral symmetry to be broken, so that we have the positivity conditions:

$$\text{Positivity } (N_f = 3): \qquad X(3) \geq 0\,, \qquad Z(3) > 0\,. \tag{3.112}$$

On the other hand, we have the paramagnetic inequalities requiring $X(2)$ and $Z(2)$ to be larger than their three-flavour counterparts. By considering the $N_f = 3$ chiral expansions of $F_\pi^2 M_\pi^2$ and F_π^2, eqs. (3.66) and (3.68), in the two-flavour limit $m_{u,d} \to 0$ but m_s physical, one can obtain the expansion of the two-flavour chiral order parameters, for instance:

$$\Sigma(2) = \lim_{m\to 0} \frac{F_\pi^2 M_\pi^2}{2m} = \Sigma(3) + 32B_0^2 m_s \overline{\Delta L}_6 + \Sigma(2)\bar{d}_\pi\ , \tag{3.113}$$

using a bar to indicate that a quantity is evaluated in the $N_f = 2$ chiral limit. Once converted in the of interest in physical units, we obtain:

$$X(2)(1-\bar{d}_\pi) = X(3) + \frac{r}{r+2}\left[1 - X(3) - \epsilon(r) - d - Y(3)^2 f_1\right]\ , \tag{3.114}$$

$$Z(2)(1-\bar{e}_\pi) = Z(3) + \frac{r}{r+2}\left[1 - Z(3) - \eta(r) - e - Y(3) g_1\right]\ , \tag{3.115}$$

as can be seen from eq. (3.113), using eq. (3.77) to replace $\overline{\Delta L}_6$ by its expression in term of $X(3)$, and similarly for $Z(3)$. f_1 and g_1 are the (small) combinations of chiral logarithms:

$$f_1 = \frac{M_\pi^2}{32\pi^2 F_\pi^2}\left[\frac{r}{r-1}\left(3\log\frac{\overset{\circ}{M}{}_K^2}{\overset{\circ}{M}{}_\pi^2} + \log\frac{\overset{\circ}{M}{}_\eta^2}{\overset{\circ}{M}{}_K^2}\right) - (r+2)\left(\log\frac{\overset{\circ}{M}{}_K^2}{\overset{\circ}{\bar{M}}{}_K^2} + \frac{2}{9}\log\frac{\overset{\circ}{M}{}_\eta^2}{\overset{\circ}{\bar{M}}{}_\eta^2}\right)\right] \tag{3.116}$$

$$g_1 = \frac{M_\pi^2}{32\pi^2 F_\pi^2}\left[\frac{4r+1}{r-1}\log\frac{\overset{\circ}{M}{}_K^2}{\overset{\circ}{M}{}_\pi^2} + \frac{2r+1}{r-1}\log\frac{\overset{\circ}{M}{}_\eta^2}{\overset{\circ}{M}{}_K^2} - (r+2)\log\frac{\overset{\circ}{M}{}_K^2}{\overset{\circ}{\bar{M}}{}_K^2}\right]\ , \tag{3.117}$$

We have $f_1 \sim 0.05$ and $g_1 \sim 0.07$ for $r = 25$ and $Y(3) = 1$. In these expressions, the dependence of the two-flavour chiral order parameters on the three-flavour ones is rather weak, since they are essentially given by:

$$X(2) = \frac{r}{r+2}[1-\epsilon(r)] - \frac{2}{r+2}X(3) + \ldots \qquad Z(2) = \frac{r}{r+2}[1-\eta(r)] - \frac{2}{r+2}Z(3) + \ldots\,. \tag{3.118}$$

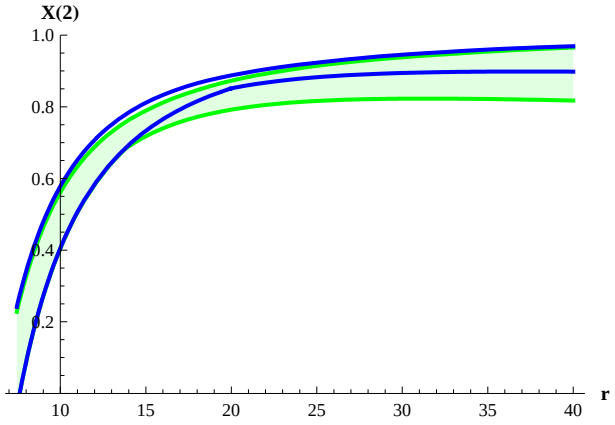

Figure 3.8: $X(2)$ *as a function of* r*: the region in green corresponds to the range of variation for* $70 \leq F_0 \leq 80$ *MeV, and the domain between the blue lines corresponds to the range of variation for* $80 \leq F_0 \leq 90$ *MeV. In each case, we have assumed* $d = \bar{d}_\pi = O(10\%)$*,* $0 \leq X(3) \leq 1$*,* $0 \leq Y(3) \leq 2$*.*

where the ellipsis denote small quantities (chiral logarithms, higher-order remainders) to be neglected in the following discussion [9]. This correlation between two-flavour order parameters and r stems from the use of the mass and decay constant identities eq. (3.66)-(3.69) and the fact that we know the pion and kaon masses and decay constants very accurately, enforcing strong correlations between LO and NLO low-energy constants. This correlation is illustrated in figs. 3.8 and 3.9. The very weak relation between $X(2)$ and $X(3)$ on one side, and between $Z(2)$ and $Z(3)$ on the other side, is also seen in fig. 3.7, where the two-flavour order parameters are essentially independent of the value of the low-energy constants L_6 and L_4, contrary to their three-flavour counterparts.

We see that the vacuum stability condition for the two-flavour condensate (and thus the positivity of the squared pion mass at small m_u, m_d) imposes that r is larger than the value r_1 so that $\epsilon(r_1) = 1$:

$$\text{Positivity } (N_f = 2): \qquad r \geq r_1 = 2\frac{F_K M_K}{F_\pi M_\pi} - 1 \simeq 8\,. \tag{3.119}$$

On the other hand, the paramagnetic inequalities yield:

$$0 \leq X(2) - X(3) = \frac{r}{r+2}[1 - X(3) - \epsilon(r)] + \ldots \tag{3.120}$$

$$0 \leq Z(2) - Z(3) = \frac{r}{r+2}[1 - Z(3) - \eta(r)] + \ldots \tag{3.121}$$

We have the conditions $X(3) \leq 1 - \epsilon(r)$ and $Z(3) \leq 1 - \eta(r)$. $\eta(r)$ is always positive, whereas $\epsilon(r)$ becomes slightly negative (between 0 and -0.01) for $r > r_2$, so that:

$$\text{Paramagnetic}: \qquad X(3) \leq X(2) \leq 1\,, \qquad Z(3) \leq Z(2) \leq 1\,, \tag{3.122}$$

[9] Notice that there is a difference between the role of $X(3)$ and $Z(3)$ here. The chiral logarithms that we neglect in eqs. (3.114)-(3.114) are multiplied by $Y(3) = X(3)/Z(3)$: their contributions will remain small for any value of $0 \leq X(3) \leq 1$, but they can explode if $Z(3)$ gets close to zero. We have however assumed that the pattern of three-flavour chiral symmetry breaking remains in the first branch eq. (3.94) for $Y(3)$, so that $Y(3) \leq 2$ and these logarithms are indeed small.

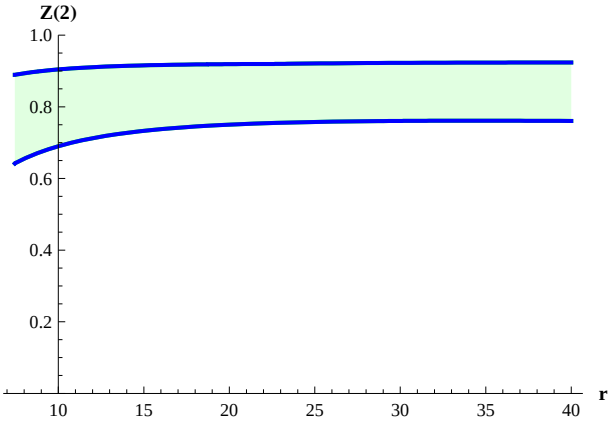

Figure 3.9: $Z(2)$ *as a function of* r*: the region in green corresponds to the range of variation for* $0.5 \leq X(3) \leq 0.75$*, and the domain between the blue lines corresponds to the range of variation for* $0.75 \leq X(3) \leq 1$ *(the two regions overlap fully). In each case, we have assumed* $e = \bar{e}_\pi = O(10\%)$*,* $0 < Z(3) \leq 1$*,* $0 \leq Y(3) \leq 2$*.*

where we have also used eq. (3.118). We see that in principle, nothing prevents $r = m_s/m$ to be very large, or even to be sent to infinity (as for instance in the $N_f = 2$ chiral limit). We will however in the following assume that $\epsilon(r) \geq 0$, in analogy with $\eta(r)$, leading to the condition $r \leq r_2$. Finally, as discussed in sec. 3.5.3, it is clear from eq. (3.94) that $Y(3)$ varies between 0 and 2.

As a summary, we obtain the following ranges of variation (up to small corrections from the terms neglected in the previous discussion):

$$0 \leq X(3) \leq X(2) \leq 1\,, \qquad 0 < Z(3) \leq Z(2) \leq 1\,, \qquad 0 \leq Y(3) \leq 2\,, \qquad r_1 \leq r \leq r_2\,. \tag{3.123}$$

3.6.2 The case of two-flavour Chiral Perturbation Theory [D]

The outcome of the previous analysis is the persistence of a large two-flavour condensate $\Sigma(2)$ even when the three-flavour condensate $\Sigma(3)$ is suppressed. We have seen that $X(3)$ could be well below 1, indicating that the expansion of $F_\pi^2 M_\pi^2$ in powers of m_u, m_d and m_s need not be dominated by the genuine condensate term $(m_u + m_d)\Sigma(3)$. We see that $Z(2)$ will remain close to 1, and is essentially correlated with r, but the situation is more complicated for $X(2)$, and we may encounter three different situations:

- $r \simeq r_1 \simeq 8$, $X(2)$ is small and so is $X(3)$, due to the paramagnetic inequalities. One has small and almost identical two- and three-flavour condensates (small Zweig-rule violation),
- $r \geq 15$, $X(2)$ is close to 1, and so is $X(3)$. One has large and almost identical two- and three-flavour condensates (small Zweig-rule violation),
- $r \geq 15$, $X(2)$ is close to 1, but $X(3)$ is significantly smaller. One has significantly different two- and three-flavour condensates (large Zweig-rule violation).

The first possibility corresponds to the so-called Generalised χPT, which dealt with the possibility of a small quark condensate for both two and three flavours [159], organising the double

tower of operators eq. (3.25) with a different counting ($B_0 \sim m_q \sim p$), but assuming that Zweig rule violation allowed to neglect the counterterms associated with L_4 and L_6. At that time, the conclusion was that the measurement of a small condensate through $\pi\pi$ scattering (probed through $K_{\ell 4}$ or τ decays) was related to a small value of the quark mass ratio. We see that we should modify this conclusion by considering that $\pi\pi$ scattering probes the two-flavour condensate. Therefore, a small value of the two-flavour quark condensate imposes both a value of r close to r_1 and a small value of the three-flavour condensate. On the other hand, a large value of the two-flavour condensate $X(2) \simeq 1$ provides only weak information on r (greater than, say, 15), and it does not allow us to determine the value of $X(3)$ if we have no extra information on the amount of Zweig-rule violation from the $\langle(\bar{u}u)(x)(\bar{s}s)(0)\rangle$ correlator.

In order to gain more insight into the different behaviour of two- and three-flavour chiral dynamics, it is convenient to rewrite the $N_f = 2$ Ward identities generating the expansion of $F_\pi^2 M_\pi^2$ and of F_π^2 in a form as close as possible to sec. 3.5.1. They involve the condensate $\Sigma(2)$, the decay constant $F^2(2)$ and the two $O(p^4)$ symmetry-breaking scale-independent LECs $\bar{\ell}_3$ and $\bar{\ell}_4$ [20]:

$$F_\pi^2 M_\pi^2 = 2m\Sigma(2) + \frac{m^2 B^2(2)}{8\pi^2}(4\bar{\ell}_4 - \bar{\ell}_3) + F_\pi^2 M_\pi^2 \delta\,, \quad F_\pi^2 = F^2(2) + \frac{mB(2)}{4\pi^2}\bar{\ell}_4 + F_\pi^2 \varepsilon\,. \quad (3.124)$$

Here $B(2) = \Sigma(2)/F^2(2)$ and the higher-order remainders δ and ε (not be confused with the function $\epsilon(r)$) are $O(m^2)$, expected to be of order 1%. The analogy with the three-flavour case can be pushed further by rewriting eq. (3.124) in the form of eqs. (3.85):

$$X(2) = 1 - \delta - Y(2)^2\bar{\rho}/4\,, \qquad Z(2) = 1 - \varepsilon - Y(2)\bar{\lambda}/4\,, \quad (3.125)$$

$$\bar{\rho} = \frac{1}{8\pi^2}\frac{M_\pi^2}{F_\pi^2}(4\bar{\ell}_4 - \bar{\ell}_3)\,, \qquad \bar{\lambda} = \frac{1}{8\pi^2}\frac{M_\pi^2}{F_\pi^2}4\bar{\ell}_4\,. \quad (3.126)$$

Even though their structure is similar, the two- and three-flavour cases are expected to behave differently because the corresponding parameters ρ and λ are of a different origin. In Chapter 2, we have discussed the connection of the three-flavour parameters L_4 and L_6 with the correlations between vacuum strange and non-strange $\bar{q}q$ pairs and with the fluctuations of small Euclidean Dirac eigenvalues. We do not know much about the importance of these fluctuations from first principles, but we do understand why in the $N_f \geq 3$ theory such fluctuations manifest themselves through important OZI-rule violations in the vacuum channel $J^P = 0^+$. Hence, if the quark pairs in the vacuum are strongly correlated and/or the low-energy Dirac spectrum is subjected to large fluctuations, ρ, λ are likely large and the perturbative solution of the system (3.85) breaks down. On the other hand, in a $N_f = 2$ theory and in the presence of massive ($m_s \sim \Lambda_{QCD}$) strange quarks in the sea, the same cause does not produce the same effect. In this case, the fluctuations of small Dirac eigenvalues are much harder to relate to low-energy observables: the OZI-rule is inoperative in this case, and the scalar correlator $\langle(\bar{u}u)(\bar{d}d)\rangle$ is chirally invariant and not simply related to an observable order parameter. The different nature of parameters $\bar{\rho}$ and $\bar{\lambda}$ is further illustrated by a different behaviour in the large-N_c limit: whereas the multi-flavour fluctuation parameters ρ, λ are suppressed as $O(1/N_c)$, $\bar{\rho}$ and $\bar{\lambda}$ behave as $O(1)$ since the constants $\bar{\ell}_3$ and $\bar{\ell}_4$ behave like $O(N_c)$ (see eq. (3.46)).

3.6.3 Operator Product Expansion condensates [E]

One of our aims is to pin down chiral order parameters that govern the low-energy behaviour of QCD correlators. Related though different quantities arise when the high-energy limit of

the same correlation functions is studied through the operator product expansion (OPE) [71, 72, 227, 228]. Local condensates appear then, and those with the lowest dimension are:

$$\Sigma_u = -\langle 0|\bar{u}u|0\rangle\,, \quad \Sigma_d = -\langle 0|\bar{d}d|0\rangle\,, \quad \Sigma_s = -\langle 0|\bar{s}s|0\rangle\,, \tag{3.127}$$

where the physical vacuum of the theory is denoted $|0\rangle$ with all the quarks carrying their physical masses: no chiral limit is taken.

These OPE quark condensates occur in various sum rules for two-point correlators and could thus be determined in this framework. First, they arise (multiplied by a mass term) in the high-energy tail of the correlators as dimension-4 operators [71, 228]. Next, in some sum rules, normal-ordered condensates of the type (3.127) appear through chiral Ward identities. For instance, in the case of the divergence of the strangeness-changing vector current [229, 230], the strange-quark mass is determined via a sum rule with no subtraction, but another sum rule can be written with the subtraction constant $(m_s - m_u)(\Sigma_s - \Sigma_u)$, providing in principle some information on the OPE quark condensates. Unfortunately, the high-energy tail of the (Borel transformed) two-point function involved in this case has a QCD expansion which behaves quite badly and prevents an accurate determination. Lastly, the OPE quark condensates arise when factorisation is invoked to reexpress higher-dimensional four-quark operators as the square of $\bar{q}q$ vacuum expectation values. Typical values considered in sum rules are [71, 72, 227, 228]:

$$0.6 \times [-225\ \text{MeV}]^3 \leq \Sigma_{u,d} \leq 1.5 \times [-225\ \text{MeV}]^3\,, \qquad \Sigma_s/\Sigma_{u,d} = 0.75 \pm 0.12\,. \tag{3.128}$$

for the non-normal ordered condensates in the $\overline{MS}$ scheme. We stress that the OPE quark condensates $\Sigma_u, \Sigma_d, \Sigma_s$ have a different definition (and thus value) from the chiral condensates that we have considered up to now:

$$\Sigma(2) \equiv -\lim_{m_u,m_d\to 0}\langle 0|\bar{u}u|0\rangle = \lim_{m_u,m_d\to 0}\Sigma_u = \lim_{m_u,m_d\to 0}\Sigma_d\,, \tag{3.129}$$

$$\Sigma(3) \equiv -\lim_{m_u,m_d,m_s\to 0}\langle 0|\bar{u}u|0\rangle = \lim_{m_u,m_d,m_s\to 0}\Sigma_u = \lim_{m_u,m_d,m_s\to 0}\Sigma_d = \lim_{m_u,m_d,m_s\to 0}\Sigma_s \tag{3.130}$$

In particular, $\Sigma_u, \Sigma_d, \Sigma_s$ exhibit an ultraviolet divergence that must be renormalised; therefore, their definition and their value depend on the renormalisation convention applied. It is possible to relate them to $\Sigma(3)$ using $N_f = 3$ χPT. For instance, if we take their NLO expression, eq. (9.1) in ref. [21] in the isospin limit, we get:

$$\begin{aligned} X_{u,d} &\equiv \frac{2m\Sigma_{u,d}}{F_\pi^2 M_\pi^2} = X(3) + [Y(3)]^2\frac{M_\pi^2}{F_\pi^2}\left[16(r+2)\Delta L_6 + 4(2\Delta L_8 + \Delta H_2)\right] + d_{\Sigma;u,d} \\ &= 1 - \frac{1}{2}\epsilon(r) + 4[Y(3)]^2\frac{M_\pi^2}{F_\pi^2}\Delta H_2 - d + \frac{1}{2}d' + d_{\Sigma;u,d}\,, \end{aligned} \tag{3.131}$$

$$\begin{aligned} X_s &\equiv \frac{2m\Sigma_s}{F_\pi^2 M_\pi^2} = X(3) + [Y(3)]^2\frac{M_\pi^2}{F_\pi^2}\left[16(r+2)\Delta L_6 + 4r(2\Delta L_8 + \Delta H_2)\right] + d_{\Sigma;s} \\ &= 1 + \frac{r-2}{2}\epsilon(r) + 4r[Y(3)]^2\frac{M_\pi^2}{F_\pi^2}\Delta H_2 - d + \frac{r}{2}d' + d_{\Sigma;s}\,, \end{aligned} \tag{3.132}$$

where higher-order remainders are denoted $d_{\Sigma;u,d}$ and $d_{\Sigma;s}$, and the $O(p^4)$ high-energy counterterm H_2^r arises in the combination:

$$\Delta H_2 = H_2^r(\mu) - \frac{1}{128\pi^2}\left(\frac{1}{2}\log\frac{\overset{\circ}{M}{}_K^2}{\mu^2} + \frac{1}{3}\log\frac{\overset{\circ}{M}{}_\eta^2}{\mu^2}\right) - \frac{1}{256\pi^2(r-1)}\left(3\log\frac{\overset{\circ}{M}{}_K^2}{\overset{\circ}{M}{}_\pi^2} + \log\frac{\overset{\circ}{M}{}_\eta^2}{\overset{\circ}{M}{}_K^2}\right). \tag{3.133}$$

The value of such high-energy counterterms cannot be fixed by low-energy data only, and their presence in the chiral expansions is merely a manifestation of the renormalisation-scheme dependence of the OPE quark condensates.

An interesting relation, free from high-energy counterterms, exists between the OPE condensates:

$$\frac{rX_{u,d} - X_s}{r-1} = 1 - \epsilon(r) - d + \frac{r}{r-1} d_{\Sigma;u,d} - \frac{1}{r-1} d_{\Sigma;s} \,. \tag{3.134}$$

Two conclusions can be drawn from this relation. First, for r larger than 15, eq. (3.134) shows that $X_{u,d}$ is close to $[1 - \epsilon(r) - d]$, while we see from eq. (3.118) that $X(2)(1 - \bar{d}_\pi)$ equals $[1 - \epsilon(r) - d]$ up to $1/r$-suppressed corrections. $\Sigma_{u,d}$ should thus be very close to $\Sigma(2)$, which was expected since the u, d quarks are very light and the physical world is near the $N_f = 2$ chiral limit. The second conclusion is that $X_s - X_{u,d}$ can hardly be obtained from such a relation, since $X_{u,d}$ and $1 - \epsilon(r) - d$ largely cancel. Thus, very accurate knowledge of r and $X_{u,d}$ would be needed to determine X_s this way. More generally, the possibility of significant vacuum fluctuations of $s\bar{s}$ pairs makes it difficult to relate in a quantitative way $\Sigma(3)$ and the OPE quark condensates $\Sigma_{u,d}$ and Σ_s.

3.7 Summary

It is possible to exploit the ideas of effective field theories to describe QCD at low energies. The resulting framework, Chiral Perturbation Theory, providing a generating functional for the QCD correlators of axial/vector currents and scalar/pseudoscalar densities, taking pions, kaons and eta mesons as dynamical degrees of freedom and yielding their expansion in powers of momenta and quark masses. The parameters of the expansion are unknown low-energy constants, describing the pattern of chiral symmetry breaking and embedding the effects of more massive degrees of freedom (resonances) that have been integrated out and are not dynamical in the effective theory. Their number grows as one goes to higher and higher orders in the chiral expansion. The features of this expansion are strongly constrained by chiral symmetry and its breakdown. First of all, this expansion is perturbative, because the degrees of freedom chosen are pseudo-Goldstone bosons of chiral symmetry breaking and thus interact weakly at low energies. Moreover, chiral symmetry provides relationships (Ward identities) between different correlators, and thus between the Low-Energy Counterterms arising in the latter. There remain however a large number of counterterms to be determined either from experiment or from lattice simulations.

One can start from the $N_f = 3$ chiral limit, taking π, K, η as degrees of freedom, and build χPT order by order. One then encounters 2 low-energy constants at leading order (equivalent to the quark condensate and the pseudoscalar decay constant), 10 at next-to-leading order and more than a hundred at next-to-next-to-leading order. One can also consider the $N_f = 2$ chiral limit, taking only pions as dynamical at even lower energies. We can then translate the discussion of the previous chapter, comparing the order parameters in these two chiral limits and discussing the decrease of the quark condensate and the decay constant as m_s varies from its physical mass to zero. At next-to-leading order, the amount of variation is described by the two counterterms L_6 and L_4, which are Zweig suppressed but m_s-enhanced in the chiral expansion. Exploiting the well-known values of the π and K masses and decay constants and their chiral expansion, one can see that the values of L_6 and L_4 must be finely tuned to critical values (around $L_4^r(M_\rho) = -0.25 \cdot 10^{-3}$ and $L_6^r(M_\rho) = -0.50 \cdot 10^{-3}$) for their contribution to remain small. Otherwise, the NLO contribution become enhanced while the LO chiral parameters, i.e., the three-flavour quark condensate and decay constant, must be suppressed.

Confronted with the numerical competition between LO and NLO terms in chiral series (or instabilities), one could dismiss the theory as non-convergent. However, the situation is certainly more subtle, as $N_f = 3$ χPT yields sensible order-of-magnitude estimates for most of the processes. Arguments based on resonance saturation yield a hierarchy in counterterms, so that NNLO contributions should indeed be suppressed compared to NLO, but these argument cannot be used for LO, and thus to determine the relative weight of LO and NLO contributions. One may therefore hope that the chiral series are still *conditionally convergent*, with a small contribution from NNLO and higher-order contributions, but a numerical competition between LO and NLO. If one wants to take this direction, one has to face several issues with the treatment of chiral series. Since the series are not saturated by their first term, one cannot trade LO low-energy constants $(F_0, 2mB_0)$ for physical observables (F_π, M_π^2) up to small corrections. Moreover, one has to define which observables are expected to be conditionally convergent, as an arbitrary function of a conditionally convergent observable (for instance its inverse) may not have a well-convergent Taylor expansion. The underlying construction of χPT singles out the generating functional as the relevant framework for this discussion, leading us to choose the correlators of axial/vector currents and scalar/pseudoscalar densities as conditionally convergent quantities.

In particular, this procedure selects F_P^2 and $F_P^2 M_P^2$ (with $P = \pi, K, \eta$) as observables of interest, which can be used to reexpress some of the NLO low-energy constants ($L_{4,5,6,7,8}$) in terms of the $N_f = 3$ LO quantities:

$$r = \frac{m_s}{m}\,, \qquad X(3) = \frac{2m\Sigma(3)}{F_\pi^2 M_\pi^2}\,, \qquad Z(3) = \frac{F(3)^2}{F_\pi^2}\,, \tag{3.135}$$

as well as remainders collecting (small) contributions coming from NNLO and higher orders. One can then check that $X(3)$ and $Z(3)$ are very significantly suppressed if $L_6^r(M_\rho)$ and $L_4^r(M_\rho)$ have positive values (and get down to zero if these low-energy constants are above 10^{-3}). On the other hand, L_5 and L_8 are mainly correlated to the quark mass ratio r

One can also consider the $N_f = 2$ chiral order parameters $X(2)$ and $Z(2)$ (as well as the quark condensates in presence of massive quarks considered for the Operator Product Expansion). Our knowledge on F_P^2 and $F_P^2 M_P^2$ (with $P = \pi, K$) allows us to reexpress these order parameters in terms of $N_f = 3$ LO quantities, to observe that $X(2)$ and $Z(2)$ are essentially correlated with r, and one can consider three different scenarios: *a)* $r \simeq 10$ and both $X(2)$ and $X(3)$ are small, *b)* $r \geq 15$, $X(2)$ and $X(3)$ are both close to 1, *c)* $r \geq 15$, $X(2)$ is close to 1 and $X(3)$ is small. In the following, we will provide pieces of information favouring scenario *c)*, based on

- A sum-rule evaluation of the low-energy constant L_6^r, indicating a significant difference between $X(2)$ and $X(3)$ for $r \geq 15$ (and thus disfavouring scenario *b)*
- A study of $\pi\pi$ scattering from $K_{\ell 4}$ decays, indicating that $X(2)$ is close to 1 (and thus disfavouring scenario *a)*
- A dispersive analysis of $K\pi$ scattering data, suggesting that $X(3)$ is not close to 1 (and thus disfavouring scenario *b)*

Finally, we will combine information obtained on $\pi\pi$ and πK scatterings in a statistical framework to provide some quantitative statements on the values of the LO parameters eq. (3.135).

- What size do you want to be?
- Oh, I'm not particular as to size, only one doesn't like changing so often, you know.

The Caterpillar and Alice

4

The m_s-dependence of the quark condensate

We have seen the masses and decay constants of the Goldstone bosons do not provide enough information to estimate the actual size of the fluctuations of $s\bar{s}$ pairs in QCD, if we allow for a numerical competition between LO and NLO. To reach this goal, several references [218, 219] have proposed a sum rule to estimate L_6, or equivalently, $\Sigma(2) - \Sigma(3)$, by estimating the two-point correlator $\langle 0|(\bar{u}u)(\bar{s}s)|0\rangle$ at vanishing momentum. Even though this correlator assesses the violation of the Zweig rule in the scalar sector and is thus difficult to estimate precisely from experiment, it is possible to write down a convergent sum rule for this correlator, which can be expressed in terms of the scalar (strange and non-strange) form factors of the pion of the kaon. The latter can be obtained at low energies by solving coupled-channel equations involving the $\pi\pi$ and the $K\bar{K}$ $I = \ell = 0$ channels, and their transition matrix. However, the normalisation at zero of these form factors is not determined by these equations, but it can be related (through the Feynman-Hellman theorem) to the (derivatives) of the pion and kaon masses.

Assuming that the two- and three-flavor condensates are large and similar sizes, ref. [218] ended up with a ratio $\Sigma(3)/\Sigma(2) \sim 1/2$ once NLO where included to estimate $\Sigma(2)$. A careful study of models of resonance saturation for the $O(p^6)$ scalar contributions in ref. [219] confirmed a large decrease of the quark condensate when NNLO were taken into account. Even though these results suggest a significant variation in the pattern of chiral symmetry breaking from $N_f = 2$ to $N_f = 3$, it seemed necessary to reevaluate this sum rule without any supposition about the size of the condensates. This modifies in particular the discussion of the normalisation of the form factors. Moreover, additional sum rules combined with the Operator Product Expansion can be used to assess more precisely the (small) contribution from the high-energy part of the sum rule.

Considering three different models for $\pi\pi$ and $K\bar{K}$ scattering in the $I = \ell = 0$ channel, we obtain an estimate of $X(2) - X(3)$ that depends on r, but is generally larger than 0.2, indicating a significant suppression of the quark condensate from two to three flavours. We can use further low-energy theorems to determine simultaneously the three-flavour quark condensate and decay constant, indicating a significant suppression for both quantities for r around 25. Incidentally, one can use the same formalism to estimate the scalar radius of the pion, which proves an interesting constraint for the extraction of two-flavour chiral order parameters from $\pi\pi$ scattering. [1]

4.1 Sum rule for $X(2) - X(3)$

4.1.1 Zweig-rule-suppressed correlator of two scalar densities [F]

In relation to eq. (2.64), we introduce the correlator [218, 219]:

$$\Pi(p^2) = i\frac{mm_s}{M_\pi^2 M_K^2} \lim_{m\to 0} \int d^4x \; e^{ip\cdot x} \; \langle 0|T\{\bar{u}u(x) \; \bar{s}s(0)\}|0\rangle, \tag{4.1}$$

that is invariant under the QCD renormalization group, violates the Zweig rule in the 0^{++} channel and whose value at 0 is related to the difference between the two- and three-flavour quark condensates. For $m_s \neq 0$, Π is a $\mathrm{SU}_L(2) \otimes \mathrm{SU}_R(2)$ order parameter, related to the

[1] This chapter is based on the following article:

[F] SDG, *Zweig rule violation in the scalar sector and values of low-energy constants*, JHEP 0103 (2001) 002 [39]

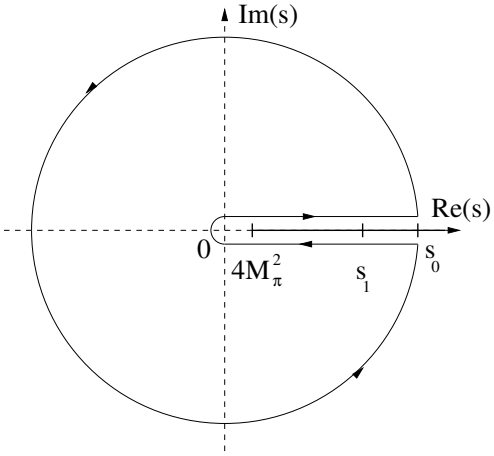

Figure 4.1: *Contour of the integral used in the sum rule for the correlator* $\langle \bar{u}u\ \bar{s}s \rangle$.

derivative of $\Sigma(2)$ with respect to m_s:

$$m m_s \partial\Sigma(2)/\partial m_s = M_\pi^2 M_K^2 \Pi(0) \tag{4.2}$$

We can use the relation eq. (3.113) between r, $X(3)$ and $X(2)$ to compute $\partial\Sigma(2)/\partial m_s$. This leads to an equation involving $\Pi(0)$:

$$X(2)-X(3) = \frac{2M_K^2}{F_\pi^2}\Pi(0)+\frac{r[X(3)]^2}{32\pi^2}\frac{F_\pi^2 M_\pi^2}{F_0^4}\left(\bar{\lambda}_K + \frac{2}{9}\bar{\lambda}_\eta\right)+\frac{m}{F_\pi^2 M_\pi^2}\left(1 - m_s\frac{\partial}{\partial m_s}\right)\lim_{m\to 0}\frac{F_\pi^2 M_\pi^2 d_\pi}{m}, \tag{4.3}$$

with the logarithmic derivatives [2]: $\bar{\lambda}_P = m_s \cdot \partial(\log \bar{M}_P^2)/\partial m_s$. We are going to exploit experimental information to evaluate $\Pi(0)$ through the pinched weight sum rule:

$$\begin{aligned}\Pi(0) = &\frac{1}{\pi}\int_0^{s_1} ds\ \mathrm{Im}\ \Pi(s)\ \frac{1}{s}\left(1-\frac{s}{s_0}\right) \\ &+\frac{1}{\pi}\int_{s_1}^{s_0} ds\ \mathrm{Im}\ \Pi(s)\ \frac{1}{s}\left(1-\frac{s}{s_0}\right) + \frac{1}{2i\pi}\int_{|s|=s_0} ds\ \Pi(s)\ \frac{1}{s}\left(1-\frac{s}{s_0}\right).\end{aligned} \tag{4.4}$$

The three terms will be estimated in different ways, following techniques of sum rules [71, 72,227,228] commonly used for the determination of α_s from hadronic τ spectral function [231–235]:

- For $0 \leq \sqrt{s} \leq \sqrt{s_1} \sim 1.2$ GeV, the spectral function Im Π is obtained by solving Omnès-Muskhelishvili equations for two coupled channels, using several T-matrix models in the scalar sector.

[2] For simplicity, we reproduce here the results of refs. [36, 39], where the chiral logarithms were expressed in terms of the physical masses, rather than in terms of the leading-order (LO) masses, as done in the other chapters, and in particular in eq. (3.113). Using the logarithmic derivatives with LO masses in the logarithms $\overset{\circ}{\bar{\lambda}}_K = 1$, $\overset{\circ}{\bar{\lambda}}_\eta = 4/3$ rather than those with physical masses, $\bar{\lambda}_K$ and $\bar{\lambda}_\eta$, would amount to a redefinition of the remainder $\bar{d}_\pi$. It would actually increase the difference $X(2) - X(3)$ by a slightly positive shift (between 0 and 0.1), for the values of F_0 and r considered here. Moreover, we used the following values for the pseudoscalar decay constants: $F_\pi = 0.0924$ GeV, $F_K/F_\pi = 1.22$, in contrast with the values used in the other chapters.

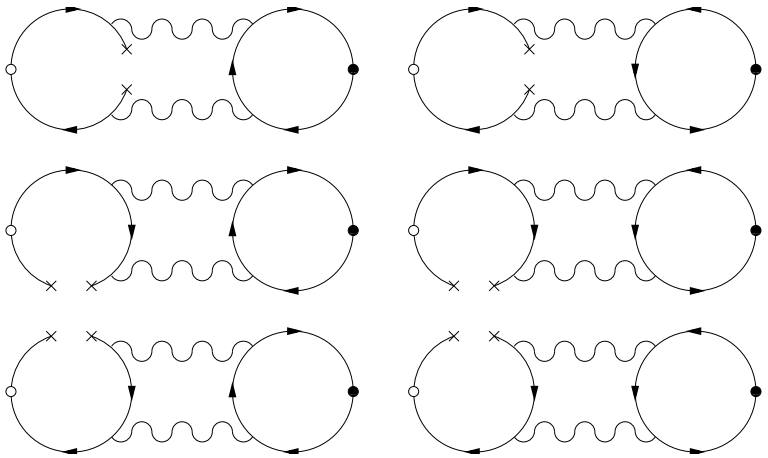

Figure 4.2: *Feynman diagrams contributing to* $m_s\langle\bar{u}u\rangle$ *in OPE of* Π *(lowest order in* α_s*). The white (black) circle is the scalar source* $\bar{u}u$ *(*$\bar{s}s$*).*

- For $\sqrt{s_1} \leq \sqrt{s} \leq \sqrt{s_0} \sim 1.5$ GeV, another sum rule is exploited in order to bound the contribution of this integral.
- For $|s| = s_0$, we estimate the integral through Operator Product Expansion (OPE).

4.1.2 Asymptotic behavior [F]

Π can be expanded using OPE:

$$\Pi(p^2) = i\frac{mm_s}{M_\pi^2 M_K^2} \lim_{m\to 0} \int d^4x\, e^{ip\cdot x}\, \langle 0|T[\bar{u}u(x)\, \bar{s}s(0)]|0\rangle \underset{P^2\to\infty}{\sim} \frac{mm_s}{M_\pi^2 M_K^2} \sum_{n\geq 4} \frac{1}{(P^2)^{n/2-1}} C^{(n)}(t)\langle 0|\mathcal{O}_n|0\rangle, \tag{4.5}$$

with $P^2 = -p^2$, μ a renormalization scale, $t = P^2/\mu^2$, and $\mathcal{O}_n$ a combination of n-dimensional operators. Π transforms chirally as $(\bar{u}u)(\bar{s}s)$ and we take the chiral limit $m \to 0$. Hence, the lowest-dimension operator is $\mathcal{O}_4 = m_s\bar{u}u$, associated to a decrease of $O(1/P^2)$, and the contributing diagrams include at least two gluonic lines, so that $C^{(4)}(t) \propto \alpha_s^2(P^2)$ [218]. For large P, the LO contribution decreases therefore faster than $1/P^2$ (due to the factor of logarithmic suppression α_s^2), so that one can write two sum rules:

$$\int_0^\infty ds\ \mathrm{Im}\ \Pi(s) = 0\,, \qquad \int_0^\infty \frac{ds}{s} \mathrm{Im}\ \Pi(s) = \Pi(0)\,, \tag{4.6}$$

so that the finite-energy equivalent eq. (4.4) should be sensitive mainly to the low-energy part of the spectral function.

We will work in dimensional regularization ($d = 4-2\omega$) to determine the leading coefficient $C^{(4)}$. In the class of t'Hooft's gauges, the gluon propagator reads:

$$\frac{-i}{k^2+i\epsilon}\left(g_{\mu\nu} - (1-\xi)\frac{k_\mu k_\nu}{k^2+i\epsilon}\right)\delta_{ab}, \tag{4.7}$$

with ξ a free real parameter. The Wilson coefficient of $m_s\bar{u}u$ (at the leading order) is obtained by adding 6 two-loop integrals. It is easy to see that the contributions of ξ and ξ^2 cancel in this sum of integrals, and the Wilson coefficient of $m_s\bar{u}u$ at the leading order is independent

of the chosen gauge (in the class of t'Hooft's gauges). We need the large-P^2 limit of integrals like:

$$g_s^4 \mu^{4\omega} m_s \langle \bar{u}u \rangle \frac{1}{p^2} \int \frac{d^4q}{(2\pi)^d} \frac{d^4k}{(2\pi)^d} \mathcal{P}(p^2, q^2, k^2, p\cdot q, p\cdot k, q\cdot k, m_s^2) \tag{4.8}$$
$$\times \frac{1}{[(p-q)^2 - m_0^2]^{n_2} [q^2 - m_0^2]^{n_3}} \frac{1}{[(k+p)^2 - m_s^2]^{n_4} [(k+q)^2 - m_s^2]^{n_5} [k^2 - m_s^2]^{n_6}},$$

where $\mathcal{P}$ is a polynomial of degree 2. m_0 corresponds at the same time to $m = m_u = m_d$ for fermion propagators in the loop of $u-d$ quarks, and to a fictitious mass to regularize infrared gluonic divergences (we take at the end the limit $m_0 \to 0$).

Using Passarino-Veltman reduction identities like $2(k\cdot q) = [(k+q)^2 + m_s^2] - [k^2 + m_s^2] - q^2$, we can reexpress the sum in terms of scalar integrals:

$$\frac{1}{p^{2\nu_0}} \int \frac{d^4q\ d^4k}{[q^2 - m_0^2]^{\nu_1} [k^2 - m_s^2]^{\nu_2}} \frac{1}{[(k+q)^2 - m_s^2]^{\nu_3} [(p-q)^2 - m_0^2]^{\nu_4} [(k+p)^2 - m_s^2]^{\nu_5}}, \tag{4.9}$$

with $m_1 = m_4 = m_0$ and $m_2 = m_3 = m_5 = m_s$. These integrals are formally identical to the ones arising for two-loop self-energies. The behavior of such integrals at large external momentum has already been studied. The basic idea consists in following the flux of the large external momentum through the Feynman diagrams, in order to Taylor expand the propagators [236]. This procedure, based on the asymptotic expansion theorem [237], was described in detail in ref. [39]. Rather lengthy computations lead to the first term arising in the OPE of the correlator. Some integrals contain ultraviolet poles in $1/\omega$, but these divergences cancel when all the contributions are summed (this cancellation is a non-trivial check of the procedure). The first term in OPE is:

$$i \frac{m m_s}{M_\pi^2 M_K^2} \lim_{m\to 0} \int d^4x\ e^{ip\cdot x}\ \langle 0|T\{\bar{u}u(x)\ \bar{s}s(0)\}|0\rangle \underset{P^2\to\infty}{\sim} -\frac{18[1-2\zeta(3)]}{P^2} \left(\frac{\alpha_s}{\pi}\right)^2 \frac{m_s^2}{M_\pi^2 M_K^2} m\langle \bar{u}u\rangle. \tag{4.10}$$

where the involved condensate should be the two-flavor one, since we work in the $N_f = 2$ chiral limit ($m \to 0$, $m_s \neq 0$).

4.1.3 Contribution for $s \leq s_1$: pion and kaon scalar form factors [F]

In order to compute the integral:

$$\mathcal{I} = \frac{1}{\pi} \int_0^{s_1} ds\ \text{Im}\ \Pi(s)\ \frac{1}{s} \left(1 - \frac{s}{s_0}\right), \tag{4.11}$$

we have to know Im Π between 0 and s_1 ($\sqrt{s}_1 \sim 1.2$ Gev). The procedure is explained in detail in refs. [218, 219], and we shall merely sketch its main features for completeness. In the range of energy between 0 and s_1, the $\pi\pi$- and $K\bar{K}$- channels should dominate the spectral function [130, 218, 238]. If we denote these channels respectively 1 and 2, the spectral function is:

$$\text{Im}\ \Pi(s) = \frac{m m_s}{M_\pi^2 M_K^2} \frac{1}{16\pi} \sum_{i=1,2} \sqrt{\frac{s - 4M_i^2}{s}} [n_i F_i(s)][n_i G_i^*(s)] \theta(s - 4M_i^2), \tag{4.12}$$

with the scalar form factors for the pion and the kaon:

$$\vec{F}(s) = \begin{pmatrix} \langle 0|\bar{u}u|\pi\pi\rangle \\ \langle 0|\bar{u}u|K\bar{K}\rangle \end{pmatrix}, \qquad \vec{G}(s) = \begin{pmatrix} \langle 0|\bar{s}s|\pi\pi\rangle \\ \langle 0|\bar{s}s|K\bar{K}\rangle \end{pmatrix}, \tag{4.13}$$

with $M_1 = M_\pi$ and $M_2 = M_K$. $n_1 = \sqrt{3/2}$ and $n_2 = \sqrt{2}$ are numerical factors related to the normalization of the states $|\pi\pi\rangle$ and $|K\bar{K}\rangle$.

The form factors are analytic functions in the complex energy plane, with the exception of a right cut along the real axis. According to perturbative QCD arguments [239, 240], these form factors should have the asymptotic behaviour $F_i(s) \sim 1/s$ when $s \to \infty$, and verify a dispersion relation with no subtraction. Obviously, when s increases, new channels open, and the two-channel approximation is no more sufficient: if the 4π channel is chirally suppressed at low energies and does not seem to couple significantly to the $f_0(980)$ meson, it couples to heavier scalar mesons (around 1.5 GeV). However, we will need $\vec{F}$ and $\vec{G}$ only for $s \leq s_1$, where $\pi\pi$ and $K\bar{K}$ are the dominant channels, and we will suppose that the two-channel approximation holds for any energies (up to corrections that will not affect the low-energy behaviour of the spectral function that we are interested in). We have the discontinuity along the cut:

$$S_{ij} = \delta_{ij} + 2i\sigma_i^{1/2} T_{ij} \sigma_j^{1/2} \theta(s - 4M_i^2)\theta(s - 4M_j^2), \tag{4.14}$$

$$\text{Im } F_i(s) = \sum_{j=1}^{n} T_{ij}^*(s)\sigma_j(s)F_j(s)\theta(s - 4M_j^2), \qquad \sigma_i = \sqrt{\frac{s - 4M_i^2}{s}}. \tag{4.15}$$

In addition, we will suppose that the two-channel T-matrix model impose the correct asymptotic behaviour for $\vec{F}$ and $\vec{G}$. Under these assumptions, $\vec{F}$ and $\vec{G}$ satisfy separately a set of coupled Omnès-Muskhelishvili equations [218, 238, 241, 242]:

$$F_i(s) = \frac{1}{\pi} \sum_{j=1}^{n} \int_{4M_\pi^2}^{\infty} ds' \frac{1}{s' - s} T_{ij}^*(s') \sqrt{\frac{s' - 4M_j^2}{s'}} \theta(s' - 4M_j^2) F_j(s'), \tag{4.16}$$

with the condition that the T matrix leads to the expected decrease of the form factors for $s \to \infty$. Ref. [218] has proved a condition of existence and unicity for the solution of eq. (4.16): $\Delta(\infty) - \Delta(4M_\pi^2) = 2\pi$, where $\Delta(s) = \delta_1 + \delta_2$ is the sum of the $\pi\pi$ and $K\bar{K}$ phase shifts:

$$S = \begin{bmatrix} \eta e^{2i\delta_1} & i(1-\eta^2)^{1/2} e^{i(\delta_1+\delta_2)} \\ i(1-\eta^2)^{1/2} e^{i(\delta_1+\delta_2)} & \eta e^{2i\delta_2} \end{bmatrix}, \tag{4.17}$$

In that case, the set of linear equations admits a unique solution, once the values at a given energy are fixed [219]. All the solutions are thus linear combinations of a basis, for instance the solutions $\vec{A}(s)$ and $\vec{B}(s)$ such as: $\vec{A}(0) = \binom{1}{0}$ and $\vec{B}(0) = \binom{0}{1}$. $\vec{F}$ and $\vec{G}$ can therefore be written as:

$$\vec{F}(s) = F_1(0)\vec{A}(s) + F_2(0)\vec{B}(s), \qquad \vec{G}(s) = G_1(0)\vec{A}(s) + G_2(0)\vec{B}(s). \tag{4.18}$$

The numerical solutions A and B of the system (4.16) were studied in ref. [218], by writing the integral equations in a discretised form, with the main difficulty of computing the principal-value integrals in eq. (4.16) with a high accuracy. The integration region was split into several sub-intervals, each mapped to $[-1, 1]$, and the integrand was expanded over a basis of Legendre polynomials. A Gauss-Legendre quadrature was then used to compute the integral in eq. (4.16) using only values of the integrand at particular points $\{s'_j\}$. In this manner, the functional equation (4.16) for an arbitrary s got transformed into a linear equations. Writing down this equation for $s \in \{s'_j\}$ allows one to write down a homogeneous system for the values of the form factors at the points $\{s'_j\}$, which could be solved numerically using a singular-value decomposition of the linear system.

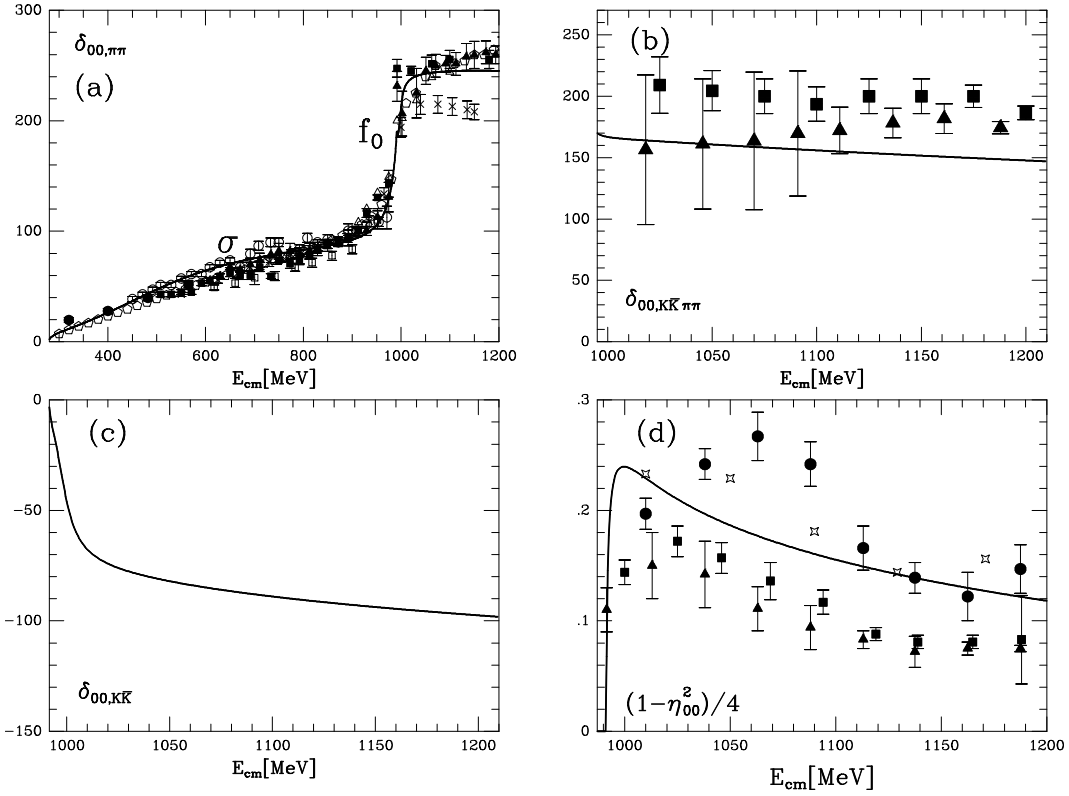

Figure 4.3: *Compilation of experimental results from ref. [244]. The solid line corresponds to the T-matrix model used in this reference Form left to right and top to bottom: $\pi\pi \to \pi\pi$ δ_1 phase shift, $\pi\pi \to K\bar{K}$ $\delta_1 + \delta_2$ phase shift, $K\bar{K} \to K\bar{K}$ δ_2 phase shift and inelasticity $(1-\eta^2)/4$.*

Once A and B are determined for a particular model of T-matrix, one has still to compute the value of the form factors at zero is related to the derivatives of the pseudoscalar masses with respect to the quark masses:

$$F_1(0) = \frac{1}{2}\left(\frac{\partial M_\pi^2}{\partial m}\right)_{m=0}, \; F_2(0) = \frac{1}{2}\left(\frac{\partial M_K^2}{\partial m}\right)_{m=0}, \; G_1(0) = \left(\frac{\partial M_\pi^2}{\partial m_s}\right)_{m=0} = 0, \; G_2(0) = \left(\frac{\partial M_K^2}{\partial m_s}\right)_{m=0}. \tag{4.19}$$

Up to now, we have followed the same line as refs. [218,238]. But in these papers, the value of the scalar form factors at zero was derived supposing that the three-flavour quark condensate dominates the expansion of the pseudoscalar masses. We are going to allow a competition between the terms linear and quadratic in quark masses, so that the normalization of the form factors may become rather different from what is considered in refs. [218, 238]. In a similar way, the form factors that we will obtain could differ from the ones obtained by a matching with χPT one-loop expressions [130, 243].

We consider here three models of T-matrix, proposed respectively by Oller, Oset and Pelaez in ref. [244], by Au, Morgan and Pennington in ref. [247], and by Kaminski, Lesniak and Maillet in refs. [245, 246]. These models fit correctly the available data in the scalar sector under 1.3 Gev, as discussed in refs. [218, 238, 244]. However, they have to be corrected for very low and very high energies, as discussed in ref. [218]: chiral symmetry constrains the $\pi\pi$ phase shifts near the threshold, and the asymptotic behaviour of the phases shifts has to be changed to to insure existence and unicity for the solution of eq. (4.16).

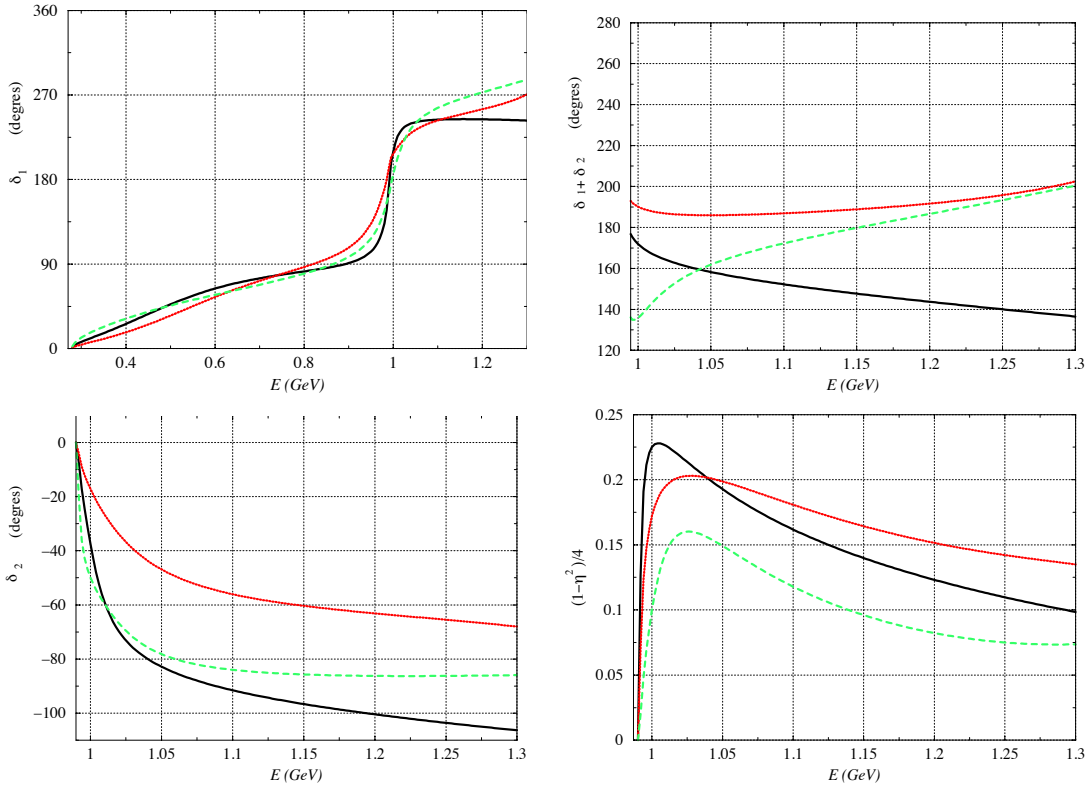

Figure 4.4: *Models of T-matrix considered: ref. [244] (solid, black), refs. [245, 246] (dotted, red) and ref. [247] (dashed, green). From left to right and top to bottom: $\pi\pi \to \pi\pi$ δ_1 phase shift, $\pi\pi \to K\bar{K}$ $\delta_1 + \delta_2$ phase shift, $K\bar{K} \to K\bar{K}$ δ_2 phase shift and inelasticity $(1-\eta^2)/4$.*

If we put eq. (4.18) into eq. (4.12), we obtain the spectral function as the sum of two contributions:

$$\text{Im } \Pi(s) = \gamma_\pi \lambda_K \left[\frac{\sqrt{3}}{32\pi} \sum_{i=1,2} \sqrt{\frac{s-4M_i^2}{s}} A_i(s) B_i^*(s) \theta(s-4M_i^2) \right] \tag{4.20}$$

$$+\gamma_K \lambda_K \frac{M_K^2}{M_\pi^2} \left[\frac{1}{16\pi} \sum_{i=1,2} \sqrt{\frac{s-4M_i^2}{s}} B_i(s) B_i^*(s) \theta(s-4M_i^2) \right],$$

where the logarithmic derivatives of the masses are denoted:

$$\lambda_P = \frac{m_s}{M_P^2} \left(\frac{\partial M_P^2}{\partial m_s} \right)_{m=0} = \frac{m_s}{M_P^2} \frac{\partial \bar{M}_P^2}{\partial m_s}, \qquad \gamma_P = \frac{m}{M_P^2} \left(\frac{\partial M_P^2}{\partial m} \right)_{m=0}. \tag{4.21}$$

The two bracketed functions in eq. (4.20) can be plotted: the first one is called "type AB^*", the second one "type BB^*". It is also interesting to study how these two contributions cancel each other inside the spectral function, by taking the estimates corresponding to a saturation of the mass identities by the quark condensate: $\gamma_\pi = 1$, $\lambda_K = 1 - M_\pi^2/(2M_K^2)$ and $\gamma_K = M_\pi^2/(2M_K^2)$. A peak, corresponding to the narrow resonance $f_0(980)$ (see sec. 2.5.1), arises with a height depending on the models: ref. [244] leads to a smaller peak than refs. [247] and [245, 246].

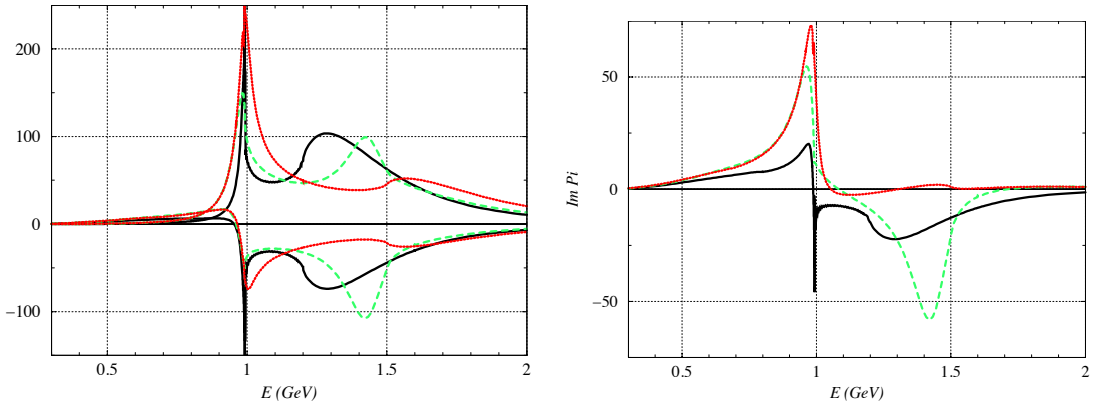

Figure 4.5: *Left: Contributions of type BB^* (positive) and type AB^* (negative) to the spectral function. Right: example of spectral function, obtained with $\gamma_\pi = 1$, $\lambda_K = 1 - M_\pi^2/(2M_K^2)$ and $\gamma_K = M_\pi^2/(2M_K^2)$. In both cases, we plot the results for the T-matrix models of ref. [244] (solid lines, black), ref. [247] (dotted, red) and refs. [245, 246] (dashed, green).*

The integral between 0 and s_1 in the sum rule eq. (4.4) can be written, using eq. (4.20):

$$\frac{1}{\pi}\int_0^{s_1} ds\ \mathrm{Im}\ \Pi(s)\ \frac{1}{s}\left(1-\frac{s}{s_0}\right) = \gamma_\pi\lambda_K\mathcal{I}_{AB} + \gamma_K\lambda_K\frac{M_K^2}{M_\pi^2}\mathcal{I}_{BB}, \tag{4.22}$$

where $\mathcal{I}_{XY} = \mathcal{M}_{XY}^{(-1)} - \mathcal{M}_{XY}^{(0)}/s_0$ involves the moments:

$$\mathcal{M}_{AB}^{(k)} = \frac{\sqrt{3}}{32\pi^2}\int_0^{s_1} ds\ s^k \sum_{i=1,2}\sqrt{\frac{s-4M_i^2}{s}}A_i(s)B_i^*(s)\theta(s-4M_i^2), \tag{4.23}$$

$$\mathcal{M}_{BB}^{(k)} = \frac{1}{16\pi^2}\int_0^{s_1} ds\ s^k \sum_{i=1,2}\sqrt{\frac{s-4M_i^2}{s}}B_i(s)B_i^*(s)\theta(s-4M_i^2). \tag{4.24}$$

Notice that we solve the Omnès-Muskhelishvili equations to obtain the scalar form factors of the pion and the kaon in the limit $m \to 0$ (and m_s fixed at its physical value). But we consider T-matrix models fitting experimental data, with up and down quarks with their physical masses. The limit $m \to 0$ sets the $\pi\pi$-threshold to zero[3], changes $\pi\pi$ phase shifts near the threshold and shifts slightly the $K\bar{K}$ threshold. Such modifications should not alter significantly the general shape of the spectral function. In particular, the integral of the spectral function, dominated by the $f_0(980)$ peak, should be affected only marginally when $T_{m\neq 0}$ is considered instead of $T_{m\to 0}$.

4.1.4 Second sum rule : $s_1 \leq s \leq s_0$ [F]

The contribution of the integral below s_1 is positive and dominated by the $f_0(980)$ peak. But according to sec. 4.1.2, Π is superconvergent, and the integral of the spectral function from 0

[3]For $m \to 0$, the cut along the real axis starts at $s = 0$. However, the integral $\int_0^{s_0} ds\ (1 - s/s_0)\cdot \mathrm{Im}\ \Pi(s)/s$ is convergent, since for $s \to 0$: $F_1(s) \to F_1(0)$ and $G_1(s) \sim G_1'(0)\cdot s$, leading to:

$$\mathrm{Im}\ \Pi(s) \sim \frac{3}{32\pi}\frac{mm_s}{M_\pi^2 M_K^2}F_1(0)G_1'(0)\cdot s. \tag{4.25}$$

to infinity vanishes. Im $\Pi(s)$ should therefore become negative in some range of energy. In particular, negative peaks should naturally appear in the spectral function, in relation with higher-mass scalar resonances like $f_0(1370)$ and $f_0(1500)$ (see sec. 2.5.1).

This remark will be useful to estimate the contribution from the region $s_1 \leq s \leq s_0$, since in this region we cannot rely on the two-channel approximation used in the previous section [4]. Let us suppose that the spectral function is negative for $s_1 \leq s \leq s_0$.[5] The contribution from the intermediate region in eq. (4.3) can be estimated from:

$$\frac{1}{s_0}\mathcal{J}' \leq -\frac{1}{\pi}\int_{s_1}^{s_0} ds\ \text{Im}\ \Pi(s)\ \frac{1}{s}\left(1-\frac{s}{s_0}\right) \leq \frac{1}{s_1}\mathcal{J}', \tag{4.26}$$

where $\mathcal{J}'$ is the integral:

$$\mathcal{J}' = \frac{1}{\pi}\int_{s_1}^{s_0} ds\ \text{Im}\ \Pi(s)\ \left(1-\frac{s}{s_0}\right), \tag{4.27}$$

which satisfies the sum rule:

$$\frac{1}{\pi}\int_0^{s_1} ds\ \text{Im}\ \Pi(s)\ \left(1-\frac{s}{s_0}\right) + \mathcal{J}' + \frac{1}{2i\pi}\int_{|s|=s_0} ds\ \Pi(s)\ \left(1-\frac{s}{s_0}\right) = 0\,. \tag{4.28}$$

The first integral in eq. (4.28) can be computed from the spectral function obtained in the previous section, since it is evaluated in the low-energy region where the two-channel approximation should be valid:

$$\frac{1}{\pi}\int_0^{s_1} ds\ \text{Im}\ \Pi(s)\ \left(1-\frac{s}{s_0}\right) = \gamma_\pi\lambda_K\mathcal{I}'_{AB} + \gamma_K\lambda_K\frac{M_K^2}{M_\pi^2}\mathcal{I}'_{BB}, \tag{4.29}$$

with $\mathcal{I}'_{XY} = \mathcal{M}^{(0)}_{XY} - \mathcal{M}^{(1)}_{XY}/s_0$ involving the moments eqs. (4.23)-(4.24).

The contribution from the complex circle [third integral in eq. (4.28)] can be estimated through OPE, using the method described in the following section:

$$\begin{aligned}\frac{1}{2i\pi}\int_{|s|=s_0} ds\ \Pi(s)\ \left(1-\frac{s}{s_0}\right) &= 9[1-2\zeta(3)]\frac{F_\pi^2}{M_K^2}X(2)m_s^2(s_0)a^2(s_0) \\ &\times\left\{1+\frac{\beta_0\gamma}{2}a(s_0)+\left[\frac{\beta_1\gamma}{2}-\frac{\gamma(\gamma+1)}{8}\left(\frac{\pi^2}{3}-2\right)\beta_0^2\right]a^2(s_0)\right\}+\ldots \\ &= 9[1-2\zeta(3)]\frac{F_\pi^2}{M_K^2}X(2)m_s^2(s_0)a^2(s_0)[1+6.5\cdot a(s_0)-25.125\cdot a^2(s_0)].\end{aligned} \tag{4.30}$$

4.1.5 High-energy contribution : $|s| = s_0$ [F]

We still have to determine the contribution of the integral on the large circle:

$$\mathcal{K} = \frac{1}{2i\pi}\int_{|s|=s_0} ds\ \Pi(s)\ \frac{1}{s}\left(1-\frac{s}{s_0}\right) = \frac{1}{2\pi}\int_{-\pi}^{\pi} d\theta\ (1+e^{i\theta})\ \Pi(p^2=-s_0e^{i\theta}). \tag{4.31}$$

The factor $(1-s/s_0)$ suppresses the contribution stemming from the time-like region around s_0, so that we can use in this integral the Operator Product Expansion of Π [231–235, 248].

[4] in ref. [218], models with a third, effective, two-body channel, were discussed, leading to similar conclusions as in the two-channel case as far as $\Pi(0)$ was concerned.

[5] If the spectral function is partially positive in this range, our hypothesis will end up with an estimate for the second integral that will be smaller than its actual value. In that case, we would underestimate the difference $X(2) - X(3)$.

Once Renormalization Group Improvement is applied to eq. (4.10), the QCD renormalization group invariant $m_s\langle\bar{u}u\rangle$ gets the coefficient:

$$a^2(P^2)m_s^2(P^2) = a^2(s_0)m_s^2(s_0) \times \left[\frac{a(P^2)}{a(s_0)}\right]^{8/b_0+2}, \tag{4.32}$$

with $a(s) = \alpha_s(s)/\pi$ and $b_0 = 11 - 2N_f/3 = 9$. The integral eq. (4.31) becomes:

$$\mathcal{K} = \frac{9[1-2\zeta(3)]}{2\pi}\frac{F_\pi^2}{M_K^2}X(2)\frac{m_s^2(s_0)}{s_0}[a(s_0)]^{-\frac{8}{b_0}}\int_{-\pi}^{\pi} ds\ (1+e^{-i\theta})\ a^\gamma(s_0e^{i\theta}), \tag{4.33}$$

with $\gamma = 2 + 8/b_0 = 2 + 8/9$. To compute this integral, we expand $a(P^2 = s_0e^{i\theta})$ in powers of $a(s_0)$ [this corresponds to Fixed-Order Perturbation Theory in the language used ot extract α_s from the τ spectral functions [231–235]]. The expansion of $a(s_0e^{i\theta})$ is:

$$a(s_0e^{i\theta}) = a(s_0) - \frac{i}{2}\beta_0\theta a^2(s_0) + \left[\frac{i}{2}\beta_1\theta - \frac{1}{4}\theta\beta_0^2\theta^2\right]a^3(s_0) + O(a^4), \tag{4.34}$$

$$\beta_0 = \frac{33-2N_f}{6} = \frac{9}{2}, \qquad \beta_1 = \frac{306-38N_f}{24} = 8. \tag{4.35}$$

leading to

$$\begin{aligned}\mathcal{K} &= 9[1-2\zeta(3)]\frac{F_\pi^2}{M_K^2}X(2)\frac{m_s^2(s_0)}{s_0}a^2(s_0) \\ &\quad\times\left\{1 - \frac{\beta_0\gamma}{2}a(s_0) - \left[\frac{\beta_1\gamma}{2} + \frac{\gamma(\gamma+1)}{8}\left(\frac{\pi^2}{3}-2\right)\beta_0^2\right]a^2(s_0)\right\} + \ldots \\ &= 9[1-2\zeta(3)]\frac{F_\pi^2}{M_K^2}X(2)\frac{m_s^2(s_0)}{s_0}a^2(s_0)[1 - 6.5\cdot a(s_0) + 48.236\cdot a^2(s_0) + \ldots].\end{aligned} \tag{4.36}$$

which converges reasonably well as $a(s_0) = \alpha_s(s_0)/\pi$ is very small. This negative contribution is strongly suppressed by α_s^2 and m_s^2/s_0. We have considered here $m_s \sim 200$ MeV, but the contribution of this integral is so small that the error due to m_s and α_s can be neglected. Notice that duality is not supposed to arise in the scalar sector for as low energies as in other channels, due to a probably large contribution from direct instantons in this sector [73].

4.2 Results

4.2.1 Estimate of $X(3)$ [F]

The logarithmic derivatives of the masses are obtained from the expansions of F_P^2 and $F_P^2M_P^2$ [6]:

$$\lambda_P = \frac{m_s}{M_P^2}\left(\frac{\partial M_P^2}{\partial m_s}\right)_{m=0} = \frac{m_s}{M_P^2}\frac{\partial \bar{M}_P^2}{\partial m_s}, \qquad \gamma_P = \frac{m}{M_P^2}\left(\frac{\partial M_P^2}{\partial m}\right)_{m=0}. \tag{4.37}$$

The corresponding expressions can be easily obtained starting from the chiral expansion of the masses and decay constants eqs. (3.66)-(3.69). We have $\lambda_\pi = 0$ since it is proportional to the derivative of M_π^2 with respect to m_s in the limit $m \to 0$.

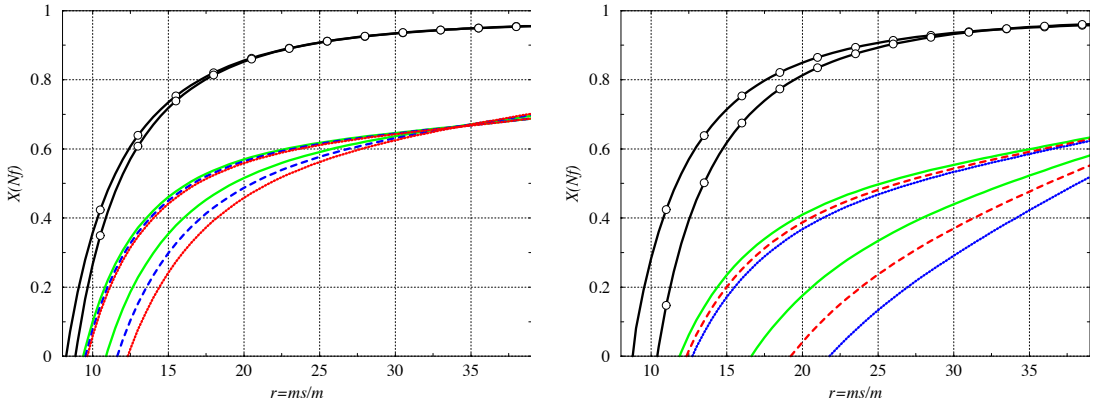

Figure 4.6: *Sum rule : Range for $X(3)$ as a function of $r = m_s/m$ for F_0=85 MeV, with the T-matrix models of refs. [244] (left) and [247] (right). The results are plotted for s_1=1.2 GeV and s_0=1.5 GeV (solid lines, green), 1.6 GeV (dashed lines, red) and 1.7 GeV (dotted lines, blue). The lines with white circles show the corresponding range for $X(2)$.*

Two different estimates of $X(2) - X(3)$ are available: the first one is the relation between $X(2)$ and $X(3)$ [eq. (3.114)], the second one consists of the relation between $X(2) - X(3)$ and $\Pi(0)$ [eq. (4.3)] and the sum rule for $\Pi(0)$ [eq. (4.4)]. In both cases, the difference $X(2) - X(3)$ can be expressed as a function of the observables and of $r, X(3), F(3)$. This overdetermination can be viewed as a constraint fixing $X(3)$ in terms of r and $F(3)$, see figs. 4.6-4.7.

This analysis contains 3 sources of errors. *i)* First, we have neglected higher-order remainders in the expansions of pseudoscalar masses and decay constants. Their effect is easy to control in the relations between $X(2)$ and $X(3)$ [eq. (3.114)] or $F(2)$ and $F(3)$ [eq. (3.115)], but the situation gets more complicated for the sum rule eq. (4.3) and for the logarithmic derivatives λ_P and γ_P. The authors of ref. [185] noticed that the dependence on m_s of $\Sigma(2)$ is not really affected by two-loop effects. In addition, these effects have the same sign as one-loop contributions: if they were significant, they would increase (and not decrease) the gap between $X(2)$ and $X(3)$. A similar conclusion was drawn in ref. [219]. The higher remainders are supposed here to be small, and they are not included in the results.

ii) The evaluation of the sum rule eq. (4.4) relies on an estimate of the integral between s_1 and s_0. If we choose a couple (F_0, r), we will not end up with one value for $X(3)$, but rather a range of acceptable values that will also depend on the separators $s_1 < s_0$. In figs. 4.6-4.7, the upper bound for $X(3)$ remains stable for $\sqrt{s_0} > 1.5$ GeV, whereas the lower bound depends strongly on s_0. When s_0 increases, the lower bound of eq. (4.26) is too loose to be saturated. A more stringent lower bound would be welcome.

iii) The third source of error is the T-matrix used to build the spectral function eq. (4.20) for $s < s_1$. Three different models of T-matrix have been used [244–247]. The central element is the shape of the $f_0(980)$ peak. Ref. [244] leads to the least pronounced effect. The two other models [245–247] lead to a higher $f_0(980)$ peak, a larger value for $\Pi(0)$, and a smaller value for $X(3)$.

The range for $X(3)$ is much narrower for large values of r, and can be even reduced to one

[6] We recall that we present here the results obtained in ref. [36, 39], where we used the physical masses in the argument of the chiral logarithms, instead of their LO expressions as in the other chapters. The difference between the two prescriptions is rather small, and should not have a strong impact on the discussion presented here.

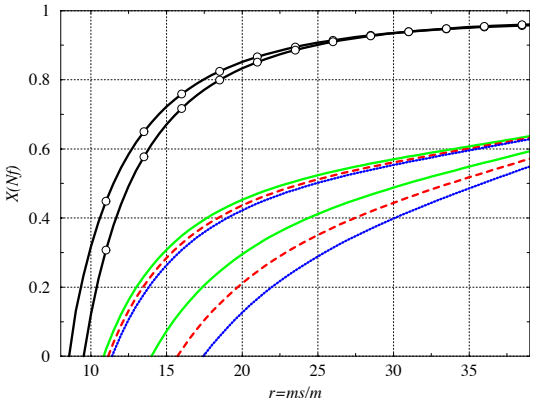

Figure 4.7: *Sum rule : Range for $X(3)$ as a function of $r = m_s/m$ for F_0=85 MeV, with the T-matrix models of refs. [245, 246]. The results are plotted for s_1=1.2 GeV and s_0=1.5 GeV (solid lines, green), 1.6 GeV (dashed lines, red) and 1.7 GeV (dotted lines, blue). The lines with white circles show the corresponding range for $X(2)$.*

value in the case of ref. [244]. This range should be broadened if we took into account the errors related to higher orders in the expansion of pseudoscalar masses and decay constants. The value of F_0 has no major influence on the constraint for $[X(3), r]$. For instance, choosing F_0=75 MeV would slightly shift the curves for $X(3)$ towards the left of the graphs ($r \to r-2$). Similarly, a change of $\sqrt{s_1}$ around 1.2 GeV does not affect strongly the results. If we choose $\sqrt{s_1}$=1.3 GeV, the convergence of the upper bound is slightly less good, but its values remain very close to figs. 4.6-4.7. One observes a significant gap between the two- and three-flavour condensate. For small values of r, the gap between $X(2)$ and $X(3)$ becomes smaller, but at the price of having an almost vanishing $X(3)$. For $r \sim 25$, the values of $X(3)$ correspond then to the half of $X(2)$. We end up with a similar result to the one obtained in refs. [218, 219], but without relying on the hypothesis $X(3) \sim 1$.

4.2.2 Slope of the strange scalar form factor of the pion [F]

Additional information about the decay constants is provided by the scalar form factors through a low-energy theorem [218, 219, 238]:

$$\frac{\partial F^2(2)}{\partial m_s} = 2F^2(2) \lim_{q^2 \to 0} \frac{G_1(q^2)}{q^2}\,, \qquad \frac{m_s}{F(2)} \frac{\partial F(2)}{\partial m_s} = m_s G_1'(0). \tag{4.38}$$

This low-energy theorem provides a relation between the logarithmic derivative of $F(2)$ with respect to m_s, and the slope of the strange scalar form factor of the pion for a vanishing momentum. We can exploit the solutions of Omnès-Muskhelishvili equations to determine the slope of the form factor according to eq. (4.18) :

$$m_s G_1'(0) = m_s G_2(0) B_1'(0) = m_s \frac{\partial \bar{M}_K^2}{\partial m_s} B_1'(0) = \lambda_K M_K^2 B_1'(0). \tag{4.39}$$

$B_1'(0)$ is computed by taking the derivative with respect to s at 0 of eq. (4.16):

$$B_1'(0) = \frac{1}{\pi} \sum_{j=1}^{2} \int_{4M_\pi^2}^{\infty} ds' \frac{1}{s'^2} T_{1j}^*(s') \sqrt{\frac{s' - 4M_j^2}{s'}} \theta(s' - 4M_j^2) B_j(s'). \tag{4.40}$$

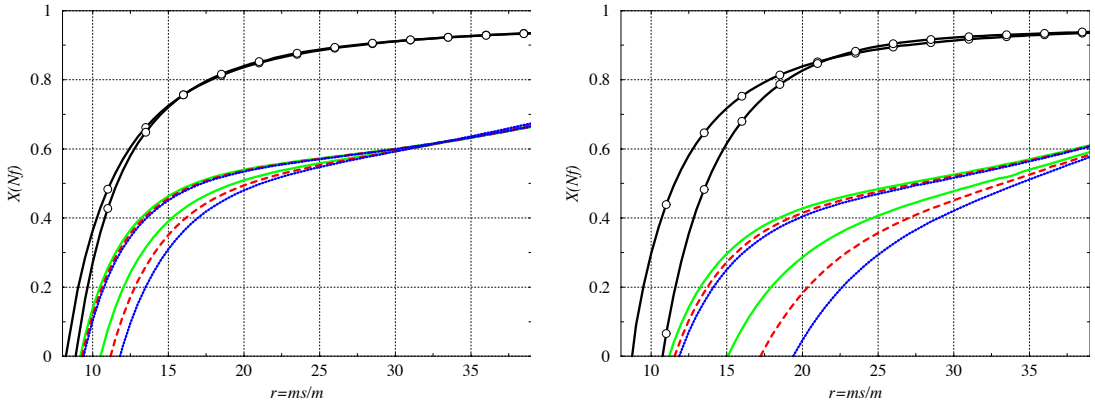

Figure 4.8: *Sum rule and slope of the strange form factor of the pion : Range for $X(3)$ as a function of $r = m_s/m$ with the T-matrix models of refs. [244] (left) and [247] (right). The intervals are plotted for s_1=1.2 GeV and s_0=1.5 GeV (solid lines, green), 1.6 GeV (dashed lines, red) and 1.7 GeV (dotted lines, blue). The lines with white circles show the corresponding range for $X(2)$.*

The numerical resolution of Omnès-Muskhelishvili equations eq. (4.16) yields the values of $\vec{B}(s)$ at the points of integration used for the Gauss-Legendre quadrature [218]. Hence, we can compute directly the integral eq. (4.40) by the same integration method.

On the other hand, eq. (3.66) leads to:

$$\frac{m_s}{2F^2(2)}\frac{\partial F^2(2)}{\partial m_s} = \frac{1}{\bar{F}_\pi^2}\left[m_s B_0\left[L_4(\mu) - \frac{1}{256\pi^2}\log\frac{M_K^2}{\mu^2}\right] - \frac{rX(3)}{64\pi^2}\frac{F_\pi^2 M_\pi^2}{F_0^2}\left(\log\frac{\bar{M}_K^2}{M_K^2} + \frac{M_K^2}{\bar{M}_K^2}\lambda_K\right)\right]. \tag{4.41}$$

We see that eq. (4.38) is an additional constraint, different from the sum rule eq. (4.4). From the analysis of the pseudoscalar spectrum, we have concluded that all the quantities could be expressed (at the NLO) as functions of masses, decay constants, and 3 parameters $r, X(3), F(3)$. The sum rule was a first constraint, fixing a range for $X(3)$ depending on r and $F_0 \equiv F(3)$. If we exploit the second constraint eq. (4.38), we can obtain ranges for $F(3)$ and $X(3)$ as functions of r, plotted respectively in figs. 4.8-4.9 and figs. 4.10-4.11. The values of $X(3)$ are close to the ones obtained by the only application of the sum rule eq. (4.4). The results obtained then for $X(3)$ were not very sensitive to the valued chosen for F_0. We see also that the slope of the strange scalar form factor of the pion leads to rather small values for $F(3)$ (around 70 MeV) for $r \sim 25$. This result is in agreement with the small *positive* values obtained for $L_4(M_\rho)$ in different works described in the previous chapter. It is also interesting to compare these findings with the results of refs. [130, 131], where the scalar form factors of the pion and the kaon were investigated in the S-wave component of the decays $J/\psi \to VPP$, with $V = \phi, \omega$ and $P = \pi^\pm, K^\pm$. Indeed, a fit of (unitarised) χPT to the BES data in these channels [131] provides values of $L_4^r(M_\rho) = (0.84\pm0.07)\cdot10^{-3}$ and $L_6^r(M_\rho) = (0.03\pm0.16)\cdot10^{-3}$, indicating a similar pattern of suppression of the quark condensate and the decay constant as in our case (the results should be compared to our values for $r \simeq 25$).

Let us add that two constraints used here do not demand the same accuracy for the scalar form factors. The sum rule involves the integral of the spectral function Im Π up to 1.2 GeV, which is dominated by the $f_0(980)$ peak. The global shape of the spectral function (and more precisely around 1 GeV) is the crucial element. The low-energy theorem eq. (4.39) focuses on the slope of a form factor at zero, i.e. its detailed behaviour at low energy. The resulting

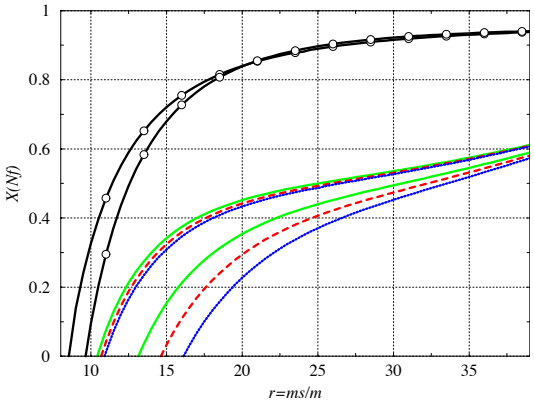

Figure 4.9: *Sum rule and slope of the strange form factor of the pion : Range for $X(3)$ as a function of $r = m_s/m$ with the T-matrix models of refs. [245, 246]. The intervals are plotted for s_1=1.2 GeV and s_0=1.5 GeV (solid lines, green), 1.6 GeV (dashed lines, red) and 1.7 GeV (dotted lines, blue). The lines with white circles show the corresponding range for $X(2)$.*

constraint may be less stable than the sum rule, so that we split the analysis in two parts: the first one dealing only with the sum rule, the second one exploiting both constraints at the same time.

4.2.3 Scalar radius of the pion [F]

The scalar radius of the pion $\langle r^2\rangle_s^\pi$ can also be obtained from the scalar form factors of the pion, considered out of the chiral limit [i.e. with the physical masses m_s and $m = (m_u + m_d)/2$]:

$$F_1(s) = F_1(0)\left[1 + \frac{1}{6}\langle r^2\rangle_s^\pi s + c_\pi s^2 + \ldots\right], \tag{4.42}$$

If we project $\vec{F}$ on the two solutions $\vec{A}$ and $\vec{B}$, we obtain:

$$\langle r^2\rangle_s^\pi = 6\frac{F_1'(0)}{F_1(0)} = 6\left[A_1'(0) + \frac{M_K^2}{M_\pi^2}\frac{\tilde{\gamma}_K}{\tilde{\gamma}_\pi}B_1'(0)\right], \tag{4.43}$$

where a third kind of logarithmic derivatives is involved (considered out of the chiral limit): $\tilde{\gamma}_P = \partial[\log M_P^2]/\partial[\log m]$, which are easy to express using the expressions of the masses and decay constants

We are interested in a quantity describing the non-strange pion form factor around the threshold. It should be possible to neglect the $K\bar{K}$ channel with no major change in the results. This point of view is supported by a numerical estimate: $B_1'(0)/A_1'(0) \sim 0.1$ and $(M_K^2/M_\pi^2)\times(\tilde{\gamma}_K/\tilde{\gamma}_\pi) \sim 1/2$. If we restricted our analysis to the $\pi\pi$ channel, only the first term (the solution $\vec{A}$) would appear on the right side of eq. (4.43). The scalar radius of the pion would be independent of r, $X(3)$ and F_0 in that case. Actually, the second term on the right side of eq. (4.43), related to the $K\bar{K}$ channel, is responsible for a weak dependence of $\langle r^2\rangle_s^\pi$ on r, $X(3)$, F_0. We can use the previous results, where $X(3)$ and F_0 are functions of r, in order to study the range of variation for the pion scalar radius:

0.537 – 0.588 fm^2	Oller-Oset-Pelaez	ref. [244],
0.567 – 0.630 fm^2	Au-Morgan-Pennington	ref. [247],
0.592 – 0.650 fm^2	Kaminski-Lesniak-Maillet	refs. [245, 246],

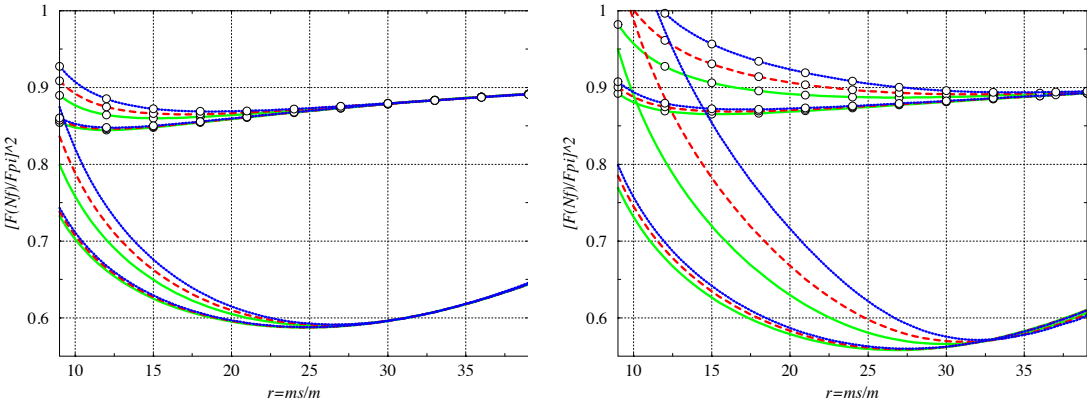

Figure 4.10: *Sum rule and slope of the strange form factor of the pion : Ranges for* $[F(3)/F_\pi]^2$ *(no symbol) and* $[F(2)/F_\pi]^2$ *(white circles) as functions of* $r = m_s/m$ *with the T-matrix models of refs. [244] (left) and [247] (right). The intervals are plotted for* s_1*=1.2 GeV and* s_0*=1.5 GeV (solid lines, green), 1.6 GeV (dashed lines, red) and 1.7 GeV (dotted lines, blue).*

to be compared to the estimates: 0.6 ± 0.2 fm^2 [249], 0.55 ± 0.15 fm^2 [20, 21], 0.55 to 0.61 fm^2 [243], 0.57 to 0.61 fm^2 [250] and 0.61 ± 0.04 fm^2 [251]. The importance on inelastic channels in these dispersive estimates was discussed in refs. [252, 253], ultimately confirming these values, within the assumptions made on the asymptotic behaviour of the form factors to obtain unique solutions to the system of coupled Omnès-Muskhelishvili equations. As we will discuss in ch. 6, some analyses attempting to extract information on $\pi\pi$ scattering from experimental data rely strongly on the value of the scalar radius of the pion. For this chapter, information about the scalar radius of the pion could be seen as an additional constraint on our system, since $\langle r^2 \rangle_s^\pi$ is related to $2L_4 + L_5$. The situation is similar to the previous section: this constraint could rather easily be affected by higher-order corrections, and in addition, the value of the scalar radius cannot be measured directly and must be determined by a dispersive analysis very similar to that performed here. It seems therefore wiser not to use this constraint for the time being.

4.3 Summary

The pseudoscalar spectrum (masses and decay constants) by itself does not contain enough information to pin down the size of $s\bar{s}$ fluctuations. This effect can however be estimated from experimental data in the scalar channel. Indeed, the difference between $X(2)$ and $X(3)$ is related to the correlator Π of two scalar densities $\bar{u}u$ and $\bar{s}s$ at vanishing momentum. It can be expressed in terms of a sum rule consisting of three distinct integrals. *a)* We compute the first one, involving the spectral function Im Π up to energies around 1.2 GeV, by solving coupled Omnès-Muskhelishvili equations for the scalar form factors of the pion and the kaon. The solutions depend on the T-matrix model used to describe the interactions between $\pi\pi$- and $\bar{K}K$ $I = \ell = 0$ channels, and on a normalization of the form factors related to the derivatives of M_π and M_K with respect to m and m_s. *b)* The second integral corresponds to the contribution of the spectral function Im Π between 1.2 and 1.6 GeV, where we cannot trust the two-channel approximation anymore. A second sum rule is used to estimate roughly this integral. *c)* The third integral is performed on a large complex circle, with a large enough radius to rely on the

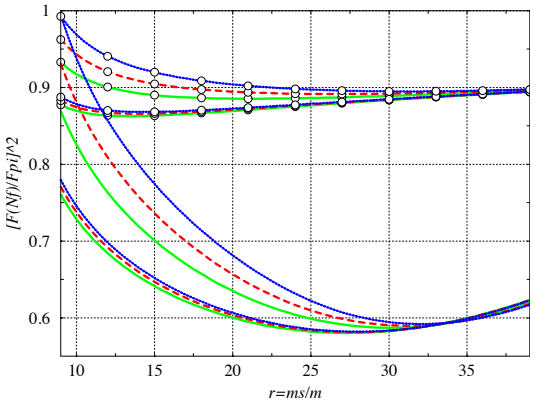

Figure 4.11: *Sum rule and slope of the strange form factor of the pion : Ranges for* $[F(3)/F_\pi]^2$ *(no symbol) and* $[F(2)/F_\pi]^2$ *(white circles) as functions of* $r = m_s/m$ *with the T-matrix model of refs. [245, 246]. The intervals are plotted for* s_1*=1.2 GeV and* s_0*=1.5 GeV (solid lines, green), 1.6 GeV (dashed lines, red) and 1.7 GeV (dotted lines, blue).*

Operator Product Expansion (OPE) of Π.

The most significant contribution stems from the first integral: the $f_0(980)$-peak leads to a large value for $\Pi(0)$, and therefore to an important splitting between $X(2)$ and $X(3)$. If we fix $X(3)$, r and $F(3)$, we know $X(2)$ and the LECs $L_{i=4\ldots8}$, using our previous analysis of the pseudoscalar spectrum. The derivatives of M_π and M_K with respect to m and m_s can then be directly computed, since they involve $X(3)$, r, $F(3)$ and LECs. The sum rule eq. (4.4) can therefore be seen as a constraint, giving $X(3)$ as a function of r and $F(3)$. Several sources of errors could affect this sum rule : the higher-order remainders in the expansions of $F_P^2 M_P^2$ and F_P^2, the rough estimate of the integral in the intermediate energy range, the T-matrix model. The three models considered here support nevertheless a large decrease of $X(3)$ with respect to $X(2)$, corresponding to positive values of $L_6(M_\rho)$. The size of the splitting between the quark condensates depends on the height of the $f_0(980)$ peak in the spectral function. In the particular case $r \sim 25$, $F(3) = 85$ MeV, the results of ref. [218] are confirmed: $X(3)$ can hardly reach more than one half of $X(2)$ for the three considered models.

The scalar form factors of the pion and the kaon can be exploited in several ways. For instance, L_4 [i.e. $F(3)$] is related to the slope of the scalar form factor of the pion at zero. This second constraint may be used to fix $X(3)$ and F_0 as functions of r. If the conclusions for $X(3)$ remain unchanged, positive values of $L_4(M_\rho)$ are obtained, leading to a significant decrease from $F(2)$ to $F(3)$ (20 to 30%). The Zweig rule would be violated strongly for L_4 and L_6. However, this second constraint is sensitive to fine details of a form factor (slope at zero), whereas the sum rule depends on the general shape of the spectral function Im Π [and especially on the presence of a high peak corresponding to the $f_0(980)$ resonance]. The scalar radius of the pion has also been computed, in agreement with former estimates.

At large values of r (above 15), these results disfavour the scenario where the two- and three-flavour condensates and decay constants are close. At small values of r (around 10), one gets closer (but small) values of the quark condensates in two and three chiral limits. Obviously this result is quite dependent on several layers of theoretical assumptions (asymptotic behaviour of the form factors, models of $\pi\pi$ and $K\bar{K}$ scatterings in the scalar channel), and should be confirmed by experimental data or further theoretical estimates. This is the purpose of the following chapters.

- Would you tell me, please, which way I ought to go from here?
- That depends a good deal on where you want to get to.
- I don't much care where.
- Then it doesn't much matter which way you go.
- . . . so long as I get somewhere.
- Oh, you're sure to do that, if only you walk long enough.

Alice and the Cheshire Cat

5

An alternative treatment of three-flavour chiral series

We have seen that significant vacuum fluctuations of $s\bar{s}$ pairs may lead to instabilities in chiral expansions, where instabilities are defined as a numerical competition between the terms considered as leading and next-to-leading in the chiral counting. This effect would be related to a large violation of the Zweig rule in the scalar sector, indicated by values of the $O(p^4)$ LECs L_4 and L_6 significantly different from specific, small and negative values. Our dispersive estimates of L_6 and L_4 suggest indeed larger values than their large-N_c expressions, with a correlated suppression of the three-flavour leading chiral order parameters.

A pessimistic way of considering the problem would consist in dismissing the whole χPT as soon as problems of convergence arise. A less restrictive point of view was adopted in sec. 3.5, assuming that:

- only some ("good") observables have convergent expansions, when expressed in terms of the couplings arising in the chiral Lagrangian.
- one may trade these couplings for physical quantities only when physical arguments indicate that the convergence of the series will be improved (location of nonanalytic structures imposed by unitarity at the physical poles, thresholds...)
- a series is considered as convergent when the sum of LO and NLO terms is large compared to the remaining part of the series.
- the resulting formulae must be treated analytically, without neglecting higher-order corrections when reexpressing low-energy constants in terms of observables.

Following this procedure (and taking the isospin limit $m_u = m_d = m$), observables can be expressed in terms of LO quantities:

$$X(3) = \frac{2m\Sigma(3)}{F_\pi^2 M_\pi^2}\,, \qquad Z(3) = \frac{F^2(3)}{F_\pi^2}\,, \qquad r = \frac{m_s}{m}\,, \tag{5.1}$$

as well as NLO LECs and remainders. The first two quantities in eq. (5.1) are of particular relevance, since they express two main order parameters of $N_f = 3$ chiral symmetry breaking, the quark condensate and the pseudoscalar decay constant, in physical units. They also assess the saturation of the chiral expansion of $F_\pi^2 M_\pi^2$ and F_π^2 by their leading order. The third quantity measures the relative size of the quark masses in a framework where the strange quark is supposed to play a peculiar role in the chiral structure of QCD vacuum.

Exploiting the fact that some quantities describing the dynamics of pseudoscalar mesons are well measured and inverting the relationships between these observables and LECs, we can express the NLO LECs in terms of low-energy observables (masses, decay constants, form factors... described in sec. 3.3.3), the three leading-order (LO) parameters in eq. (5.1), and higher-order remainders (associated to each observable and assumed to be small). These expressions can be exploited in the chiral expansions of other convergent observables, in order to express the latter quantities in terms of LO quantities and remainders only. The comparison with experimental information should then provide more information on the pattern of chiral symmetry breaking in the $N_f = 3$ chiral limit.

We have already applied this procedure in sec. 3.5 to masses and decay constants. It allows one to resum higher-order contributions in chiral series from L_4 and L_6 low-energy constants, which encode the effect of $s\bar{s}$ pairs on the structure of the chiral vacuum. It may induce a significant m_s -dependence in the pattern of chiral symmetry breaking and can generate a numerical competition between LO and NLO in $N_f = 3$ chiral series. This feature is related to the name of Resummed Chiral Perturbation Theory (ReχPT) chosen to describe this particular

treatment of chiral expansions. This framework is compatible with the usual treatment of chiral series in the limit where the latter are saturated by their LO term, but it allows for a consistent treatment of the series even if there is a significant competition of LO and NLO contributions for some of the observables.

We will illustrate our procedure to energy-dependent quantities, namely form factors, such as the electromagnetic form factors of pions and kaons, as well as those for $K_{\ell 3}$ decays. We use the same framework to deal with masses, decay constants and form factors simulated on the lattice for 2+1 dynamical flavours (in the unitary limit where valence and sea quarks have the same masses). The interest is threefold. First, the lattice simulations probe the m_s-sensitivity of observables, hard to estimate from continuum measurements, but with deep connection with the pattern of $N_f = 3$ chiral symmetry breaking. Second, lattice simulations [RBC/UKQCD [207–209], PACS-CS [127]] have encountered difficulties in their fits of NLO $N_f = 3$ chiral expansions, which could be explained by instabilities and numerical competitions between LO and NLO contributions to the series. Finally, the same LECs are involved as in the continuum, so that one can exploit the same relationships both on the lattice and in the continuum, without additional assumptions (the only issue being the scaling of the higher-order remainders as one changes the values of the quark masses). This will allow us to extract information on the pattern of three-flavour chiral symmetry breaking from lattice data. [1]

5.1 One-loop expansion of QCD Green functions [H,M]

We start from the one-loop generating functional for three-flavour χPT [21]:

$$Z = Z_t + Z_u + Z_A + \dots \tag{5.2}$$

where the ellipsis stands for NNLO contributions. The three terms of the one-loop generating functional were described in sec. 3.3.2: Z_t is the sum of $O(p^2)$ and $O(p^4)$ tree graphs, Z_u collects unitarity corrections corresponding to one-loop graphs with two $O(p^2)$ vertices and Z_A is the Wess-Zumino functional collecting anomalous contributions. The one-loop functional eq. (3.35) has been derived using the propagators and couplings of the $O(p^2)$ chiral Lagrangian [21], and therefore it is expressed only in terms of chiral couplings: F_0 and B_0, $L_i \dots$ In particular, the Goldstone degrees of freedom have masses truncated at $O(p^2)$, denoted $\overset{\circ}{M}{}^2_P$ and defined in eq. (3.37). Large fluctuations should induce significant differences between this quantity and the physical mass M_P^2. Therefore, we want to replace $\overset{\circ}{M}{}^2_P$ by M_P^2 only when justified by physics arguments, since this replacement may have an important impact when comparing chiral expansions with experimental data.

- The anomalous contribution Z_A corresponds to local couplings for vector and axial currents, and is not affected by our discussion.
- For the unitarity corrections Z_u, were we to consider higher and higher orders of the chiral expansion, we should obtain that the masses occurring in the one-loop scalar integrals $\bar{J}$

[1] This chapter is based on the following articles:

[G] SDG, *The Role of strange sea quarks in chiral extrapolations on the lattice*, Eur. Phys. J. C40 (2005) 81 [40]

[H] V. Bernard, SDG, and G. Toucas, *Chiral dynamics with strange quarks in the light of recent lattice simulations*, JHEP 1101 (2011) 107 [41]

and $\bar{\bar{J}}$ are physical masses, in order to get the low-mass two-particle cuts at the physical positions. Therefore, we write those functions with the physical masses of the Goldstone bosons. On the contrary, we keep the multiplying factors Γ^μ and $\bar{\sigma}$ expressed in terms of parameters of the effective Lagrangian (m_q, $B_0 \dots$).

- In the same spirit, for two-point functions of axial or pseudoscalar functions, we should reexpress the chiral expansion so that the pole of the Goldstone boson propagator is located at the physical value of the meson, and not its LO expression $\overset{\circ}{M}{}^2_P$.

- The tadpole contributions present in Z_t are derived using the $O(p^2)$ contribution to the Goldstone boson masses $\overset{\circ}{M}{}^2_P$ and will be kept as such

- Physical S-matrix elements are obtained from the Green functions derived with the generating functional by applying the LSZ reduction formula. The external legs corresponding to incoming and outgoing particles must be put on the mass shell. In the process, the products of external momenta are translated into the well-known Mandelstam variables. These kinematical relations are valid for physical masses, and we will use the latter (and not the $O(p^2)$ truncated masses $\overset{\circ}{M}{}^2_P$) whenever we reexpress products of external momenta. This prescription is consistent with the use of physical masses in the one-loop scalar integral $\bar{J}$ present in the unitarity term Z_u.

As indicated in sec. 3.4.1, we call "bare expansion" the chiral expansion treated according to our prescription, because of we prefer keeping original couplings of the chiral Lagrangian to trading them for physical masses and decay constants. We sum up our method to obtain the expansions of Green functions in Resummed χPT:

1. Consider a subset of observables suitable for a chiral expansion, such as the linear space of connected QCD correlators of axial/vector currents and their derivatives away from kinematic singularities.

2. Extract the bare expansion of the observables using the one-loop generating functional eq. (3.35): in Z_u, use the physical masses for the function $\bar{J}$ defined from the one-loop scalar integral, and ensure that the pole for single Goldstone boson exchange is located at its physical value.

3. Use physical masses to reexpress scalar products of external momenta in terms of the Mandelstam variables.

4. Keep track of the higher-order contributions by introducing remainders, i.e. NNLO quantities which have an unknown value but are assumed small enough for the chiral series to converge.

5. Exploit algebraically the resulting relations, and never trade the couplings of the chiral Lagrangian for observables while neglecting higher-order terms.

The main differences from the usual treatment of three-flavour chiral series consists in the choice of a particular subset of observables, the distinction between physical meson masses and their $O(p^2)$ parts, and the algebraic use of chiral expansions while keeping track of higher-order terms explicitly.

We will now illustrate this procedure to energy-dependent quantities, such as the electromagnetic form factors of pions and kaons (denoted F_V^P), as well as those for $K_{\ell 3}$ decays (denoted f_+ and f_0):

$$F_\pi^2, F_K^2 = \mathcal{F}(X(3), Z(3), r; \Delta L_4, \Delta L_5; \text{remainders}) \tag{5.3}$$

$$F_\pi^2 M_\pi^2, F_K^2 M_K^2 = \mathcal{F}(X(3), Z(3), r; \Delta L_6, \Delta L_8; \text{remainders}) \tag{5.4}$$

$$F_\pi^2 F_V^\pi, F_K^2 F_V^{K^+}, F_K^2 F_V^{K^0}, F_\pi F_K f_+ = \mathcal{F}(t; X(3), Z(3), r; \Delta L_4, \Delta L_5; \text{remainders}) \tag{5.5}$$

$$F_\pi F_K f_- = \mathcal{F}(t; X(3), Z(3), r; \Delta L_4, \Delta L_5, \Delta L_9; \text{remainders}) \tag{5.6}$$

where the factors of F_π and F_K come from the wave-function renormalisation in the LSZ reduction of the axial currents to obtain pion and kaon external states. In principle, we could then perform a global fit of the observables to determine the LO and NLO low-energy constants $(r, X(3), Z(3), L_{4,5,6,8,9})$ assuming that the higher-order remainders remain small. But one can also use the fact that some of these observables are known rather accurately experimentally to invert the corresponding relations, and reexpress the NLO LECs in terms of the three fundamental parameters $r, X(3), Z(3)$, measured quantities (indicated in sec. 3.3.3) and higher-order remainders. This proved quite useful to highlight correlations in sec. 3.6.1 to determine the correlation between the two-flavour condensate $X(2)$ and the ratio of quark masses r due to the strong constraint coming from the pion and kaon masses and decay constants.

We thus use this approach to reexpress $\Delta L_4, \Delta L_5$ in terms of F_π^2, F_K^2, $\Delta L_6, \Delta L_8$ in terms of $F_\pi^2 M_\pi^2, F_K^2 M_K^2$, and ΔL_9 in terms of $\langle r^2 \rangle_\pi^V$. These expressions can be reinjected in the remaining bare expansions, so that one has:

$$F_V^{K^+}(t), F_V^{K^0}(t), f_+(t), f_-(t) = \mathcal{F}(t; X(3), Z(3), r; F_\pi^2, F_K^2, F_\pi^2 M_\pi^2, F_K^2 M_K^2, \langle r^2 \rangle_\pi^V; \text{remainders}) \tag{5.7}$$

Comparison these expressions with experimental measurements yields information on the fundamental parameters $X(3), Z(3), r$. One can also consider lattice simulations, where the same observables are considered at different values of the quark masses.

5.2 Electromagnetic form factor

5.2.1 Definition [H]

We will now illustrate our procedure with the example of the electromagnetic pion form factor:

$$\langle \pi^+ | j_\mu | \pi^+ \rangle = (p + p')^\mu F_V^\pi(t)\,, \tag{5.8}$$

where the electromagnetic current is $j_\mu = V_\mu^3 + V_\mu^8/\sqrt{3}$, p (p') is the momentum of the incoming (outgoing) pion, and $t = (p' - p)^2$. As explained in sec. 5.1, we obtain this form factor in χPT from the correlator $\langle (A_{\pi^+}^\mu)^\dagger A_{\pi^+}^\nu j^\mu \rangle$, leading to the product $F_\pi^2 F_V^\pi$ through the LSZ reduction formula. In the case of the electromagnetic form factor, "good" observables are thus obtained from $F_\pi^2 F_V^\pi$ at low energies away from singularities, i.e., the right-hand cuts, starting from $t \geq 4M_\pi^2$.

We obtain the following bare expansion, in agreement with refs. [190, 243, 254]:

$$F_\pi^2 F_V^\pi(t) = F_\pi^2 Z(3) + M_\pi^2 Y(3)[8(r+2)L_4^r + 8L_5^r] - \frac{1}{32\pi^2} M_\pi^2 Y(3) \left[4 \log \frac{\overset{\circ}{M}{}_\pi^2}{\mu^2} + (r+1) \log \frac{\overset{\circ}{M}{}_K^2}{\mu^2} \right]$$

$$+t\left[2L_9^r - \frac{1}{32\pi^2}\left[\frac{1}{3}\log\frac{\overset{\circ}{M}{}_\pi^2}{\mu^2} + \frac{1}{6}\log\frac{\overset{\circ}{M}{}_K^2}{\mu^2} + \frac{1}{6}\right]\right]$$

$$+\frac{1}{6}[t - 4M_\pi^2 Y(3)]\bar{J}_{\pi\pi}(t) + \frac{1}{12}[t - 2(r+1)M_\pi^2 Y(3)]\bar{J}_{KK}(t) + \Re F_\pi^2 F_V^\pi(t)\,, \qquad (5.9)$$

with the nonanalytic pieces from the two-meson channels encoded in the $\bar{J}$ function [21], and $Y(3) = X(3)/Z(3) = 2mB_0/M_\pi^2$. We have added the higher-order remainder function $\Re F_\pi^2 F_V^\pi(t)$, a polynomial function of t collecting remainders:

$$\Re F_\pi^2 F_V^\pi(t) = (\Re F_\pi^2 F_V^\pi)_0 + \frac{t}{F_\pi^2}(\Re F_\pi^2 F_V^\pi)_1 + O(t^2)\,, \qquad (5.10)$$

with $(\Re F_\pi^2 F_V^\pi)_0 = O(m_q^2)$ and $(\Re F_\pi^2 F_V^\pi)_1 = O(m_q)$.

At next-to-leading order in the chiral expansion, the nonanalytic dependence on quark masses and momenta arises through the unitarity function $\bar{J}_{PQ}$. Following our prescription, we compute the functions $\bar{J}$ (and $\bar{\bar{J}} = \bar{J} - s\bar{J}'(0)$) with the physical values of M_π^2, M_K^2, M_η^2, rather than their LO expansion, i.e. we define the chiral expansion in ReχPT as eq. (5.9) with:

$$\bar{J}_{PP}(t) = \frac{s}{16\pi^2}\int_{4M_P^2}^\infty \frac{dx}{x(x-s)}\sqrt{1 - \frac{4M_P^2}{x}} = \frac{1}{16\pi^2}\left[\sigma\log\frac{\sigma-1}{\sigma+1} + 2\right]\,, \qquad \sigma = \sqrt{1 - \frac{4M_P^2}{t}}\,, \qquad (5.11)$$

so that our expansion of the form factor eq. (5.9) features a unitarity cut from the two-pion channel starting at $t = 4M_\pi^2$ (id. for the two-kaon channel). Indeed, from general arguments of unitarity, we know that the higher-order corrections will shift the start of the right-hand cut from $4\overset{\circ}{M}{}_P^2$ to $4M_P^2$. Unfortunately, unitarity does not provide us more information on the structure of the cut (and in particular the coefficient multiplying the $\bar{J}$ function) due to the perturbative nature of the chiral expansion.

When needed, we will obtain the ReχPT expansion of other observables by performing the same replacement for the functions $\bar{J}$ and $\bar{\bar{J}}$ occurring in the definition of the loop integrals K_{PQ}, L_{PQ} and M_{PQ}^r in ref. [21]. As indicated in the previous section, we do *not* perform any further replacement neither in the unitary functions nor in the rest of the expressions: for instance, we have not modified the functions multiplying the $\bar{J}$ functions, nor the chiral logarithms coming from the tadpole terms in eq. (5.9), since we have no way of determining if the latter modifications would improve or spoil the convergence of the series [2]. Adopting a dispersive point of view, we can say that the position of the cuts are imposed by unitarity, but not the value of the induced imaginary parts at low energies and that of the subtraction constants (polynomials).

One checks easily that the NLO chiral expansion of the electromagnetic form factor in ref. [254] can be recovered:

$$F_V^\pi(t) = 1 + 2H_{\pi\pi}(t) + H_{KK}(t) + O(p^4)\,, \qquad (5.12)$$

[2] This procedure is slightly different from the approach taken in refs. [38,46,255], where this substitution was performed everywhere in the unitarity functions J, K, L, M and in the tadpole logarithms. It turns out that the difference is usually very small: the unitarity functions yield only a small contribution below the first threshold, and there is only a logarithmic difference in the case of the tadpole (either M_P is close to its $O(p^2)$ term and the change is trivially justified, or $\overset{\circ}{M}{}_P^2$ is much smaller than M_P^2 and the whole tadpole contribution is very small).

with:

$$H_{PP}(t) = \frac{1}{F_0^2}\left[\frac{1}{12}\left(t - 4M_P^2\right)\bar{J}_{PP}(t) - \frac{t}{6}\frac{1}{32\pi^2}\left(\log\frac{M_P^2}{\mu^2} + 1\right) + \frac{t}{288\pi^2}\right] + \frac{2t}{3F_0^2}L_9^r\,. \quad (5.13)$$

In the case where $F_0 \equiv F(3)$ is small compared to F_π, $F_\pi^2 F_V^\pi(t)$ is expected to exhibit a better convergence than $F_V^\pi(t)$ in our framework according to eqs. (5.12)-(5.13). Similar expressions hold for other observables: good observables will generally come multiplied by powers of physical pseudoscalar decay constants (one for each external pseudoscalar meson involved).

5.2.2 Pion electromagnetic square radius [H]

The electromagnetic square radius of the pion is the low-energy observable associated with F_V^π:

$$F_\pi^2\langle r^2\rangle_V^\pi = 6F_\pi^2\frac{dF_V^\pi}{dt}(0)\,. \quad (5.14)$$

Following the previous discussion of the form factor, the product of F_π^2 and $\langle r^2\rangle_V^\pi$ is the quantity expected to exhibit a good convergence in our framework. eq. (5.9) yields the corresponding expansion of $\langle r^2\rangle_V^\pi$:

$$\langle r^2\rangle_V^\pi = \frac{6}{F_\pi^2}\left[2\Delta L_9 - \frac{1}{32\pi^2}\left[\frac{1}{6} + \frac{2}{9}Y(3) + \frac{M_\pi^2}{18M_K^2}(r+1)Y(3)\right]\right] + \langle r^2\rangle_V^\pi e_V^\pi\,, \quad (5.15)$$

where we have introduced the scale-independent combination $\Delta L_9 = L_9^r(\mu) - \hat{L}_9^r(\mu)$, and the higher-order remainder e_V^π:

$$\hat{L}_9^r(\mu) = \frac{1}{32\pi^2}\left[\frac{1}{6}\log\frac{\overset{\circ}{M}{}_\pi^2}{\mu^2} + \frac{1}{12}\log\frac{\overset{\circ}{M}{}_K^2}{\mu^2}\right], \qquad e_V^\pi = \frac{6}{F_\pi^4}\frac{(\Re F_\pi^2 F_\pi^V)_1}{\langle r^2\rangle_V^\pi}\,. \quad (5.16)$$

The pion electromagnetic square radius is well determined experimentally, and it is expected to suffer only mildly from higher-order corrections, being an observable involving pions (the curvature of the form factor, would also provide an interesting observable, but is beyond our next-to-leading-order (NLO) framework [256]). We will thus use this observable to express L_9:

$$\Delta L_9 = \frac{F_\pi^2}{12}\langle r^2\rangle_V^\pi[1 - e_V^\pi] + \frac{1}{32\pi^2}\left[\frac{1}{12} + \frac{1}{9}Y(3) + \frac{M_\pi^2}{36M_K^2}(r+1)Y(3)\right]. \quad (5.17)$$

Equivalent relations for other LECs, namely $L_{4,5,6,8}$ were discussed in eqs. (3.79)-(3.78). $L_9(M_\rho)$ can thus be estimated as a function of $r, Y(3)$ and NNLO remainder. For instance, if we take $Y(3) = 1$ and $r = 2M_K^2/M_\pi^2 - 1$ (corresponding to LO estimates holding in the case of a fast convergence) and the central experimental value [137]:

$$\langle r^2\rangle_V^\pi = 0.451 \pm 0.031\ \text{fm}^2\,, \quad (5.18)$$

we obtain $L_9^r(M_\rho) = 6.77 \cdot 10^{-3}$ in the ball park of usual estimates of this LEC (see tab. 3.1).

5.3 Kaon electromagnetic form factors

The method described in the previous section can easily be generalized to other observables. Of particular interest are the kaon electromagnetic form factors and the $K\pi$ form factors which will be discussed in the following sections.

5.3.1 Definition [H]

The kaon vector form factors [190, 254] are defined as:

$$\langle K^+|j_\mu|K^+\rangle = (p+p')^\mu F_V^{K^+}(t)\,, \qquad \langle K^0|j_\mu|K^0\rangle = (p+p')^\mu F_V^{K^0}(t)\,, \tag{5.19}$$

with the same convention as in the case of the pion electromagnetic form factor. All of them are associated with the P-wave projection of the crossed channel. Following the discussion in 5.1, we expect $F_K^2 F_V^{K^+}$ and $F_K^2 F_V^{K^0}$ to have good convergence properties away from the singularities (opening thresholds...). Expanding these form factors and reexpressing some couplings in terms of $r, Y(3)$ and $Z(3)$, we obtain the bare expansion of the vector form factors:

$$\begin{aligned}\frac{F_K^2}{F_\pi^2}F_V^{K^0}(t) = &-\frac{t}{192\pi^2F_\pi^2}\log\frac{\overset{\circ}{M}{}_K^2}{\overset{\circ}{M}{}_\pi^2} - \frac{1}{12F_\pi^2}[t-4M_\pi^2Y(3)]\bar{J}_{\pi\pi}(t) \\ &+\frac{1}{12F_\pi^2}[t-2(r+1)M_\pi^2Y(3)]\bar{J}_{KK}(t) + \frac{1}{F_\pi^2}\Re F_K^2F_V^{K^0}(t)\,,\end{aligned} \tag{5.20}$$

$$\begin{aligned}\frac{F_K^2}{F_\pi^2}F_V^{K^+}(t) = &\, Z(3) + \frac{M_\pi^2}{F_\pi^2}[Y(3)][8(r+2)L_4^r + 4(r+1)L_5^r] \\ &-\frac{1}{32\pi^2}\frac{M_\pi^2}{F_\pi^2}Y(3)\left[\frac{3}{2}\log\frac{\overset{\circ}{M}{}_\pi^2}{\mu^2} + \frac{3}{2}(r+1)\log\frac{\overset{\circ}{M}{}_K^2}{\mu^2} + \frac{1}{2}(2r+1)\log\frac{\overset{\circ}{M}{}_\eta^2}{\mu^2}\right] \\ &+\frac{t}{F_\pi^2}\left[2L_9^r - \frac{1}{32\pi^2}\left[\frac{1}{6}\log\frac{\overset{\circ}{M}{}_\pi^2}{\mu^2} + \frac{1}{3}\log\frac{\overset{\circ}{M}{}_K^2}{\mu^2} + \frac{1}{6}\right]\right] \\ &+\frac{1}{12F_\pi^2}[t-4M_\pi^2Y(3)]\bar{J}_{\pi\pi}(t) + \frac{1}{6F_\pi^2}[t-2(r+1)M_\pi^2Y(3)]\bar{J}_{KK}(t) + \frac{1}{F_\pi^2}\Re F_K^2F_V^{K^+}(t)\,,\end{aligned} \tag{5.21}$$

where $\Re F_K^2 F_V^{K^0}(t)$ and $\Re F_K^2 F_V^{K^+}(t)$ are polynomial functions of t collecting remainders:

$$\Re F_K^2F_V^{K^0}(t) = \frac{t}{F_K^2}(\Re F_K^2F_V^{K^0})_1 + O(t^2)\,, \tag{5.22}$$

$$\Re F_K^2F_V^{K^+}(t) = (\Re F_K^2F_V^{K^+})_0 + \frac{t}{F_K^2}(\Re F_K^2F_V^{K^+})_1 + O(t^2)\,, \tag{5.23}$$

with $(\Re F_V^K)_0 = O(m_q^2)$ and $(\Re F_V^K)_1 = O(m_q)$. We have divided the expressions of the form factors eqs. (5.21)-(5.20) by a numerical factor F_π^2 for sole purpose of convenience, in order to deal with dimensionless quantities. We can follow the program advocated in sec. (5.1), so that the expressions of the $O(p^4)$ LECs eqs. (3.79)-(3.78) and (5.17) yield:

$$\begin{aligned}\frac{F_K^2}{F_\pi^2}F_V^{K^+}(t) = &\, 1 + \frac{r-1}{2}\eta(r) + \frac{r+1}{2}e' - e \\ &+t\left[\frac{1}{12}\langle r^2\rangle_V^\pi[1-e_V^\pi] + \frac{1}{32\pi^2F_\pi^2}\left[\frac{1}{12} + \frac{1}{9}Y(3) + \frac{M_\pi^2}{32M_K^2}(r+1)Y(3)\right]\right] \\ &+\frac{M_\pi^2}{F_\pi^2}[Y(3)][8(r+2)\hat{L}_4^r + 4(r+1)\hat{L}_5^r] + \frac{t}{F_\pi^2}\left[2\hat{L}_9^r - \frac{1}{32\pi^2}\left[\frac{1}{6}\log\frac{\overset{\circ}{M}{}_\pi^2}{\mu^2} + \frac{1}{3}\log\frac{\overset{\circ}{M}{}_K^2}{\mu^2} + \frac{1}{6}\right]\right]\end{aligned} \tag{5.24}$$

$$-\frac{1}{32\pi^2}\frac{M_\pi^2}{F_\pi^2}Y(3)\left[\frac{3}{2}\log\frac{\overset{\circ}{M}{}_\pi^2}{\mu^2}+\frac{3}{2}(r+1)\log\frac{\overset{\circ}{M}{}_K^2}{\mu^2}+\frac{1}{2}(2r+1)\log\frac{\overset{\circ}{M}{}_\eta^2}{\mu^2}\right]$$

$$+\frac{1}{12F_\pi^2}[t-4M_\pi^2Y(3)]\bar{J}_{\pi\pi}(t)+\frac{1}{6F_\pi^2}[t-2(r+1)M_\pi^2Y(3)]\bar{J}_{KK}(t)+\frac{1}{F_\pi^2}\Re F_K^2F_V^{K^+}(t)\,, \quad (5.25)$$

where $\hat{L}_i^r$ are just combinations of chiral logarithms, depending on $Y(3)$ and r. $F_V^{K^0}(t)$ is still given by eq. (5.20). It is interesting to notice that none of the two form factors actually provide information on $F(3)$, and they are functions of r and $Y(3)$ only.

In the limit where all the observables are saturated by their leading order, the standard NLO chiral expansions of the vector form factors [190, 254] can be recovered by expanding the ratio F_π^2/F_K^2 at next-to-leading order and replacing the leading order masses by the physical ones:

$$F_V^{K^0}(t)=-H_{\pi\pi}(t)+H_{KK}(t)+O(p^4)\,,\qquad F_V^{K^+}(t)=F_V^{\pi}(t)+F_V^{K^0}(t)+O(p^4)\,, \quad (5.26)$$

with H_{PQ} defined as:

$$H_{PQ}(t)=\frac{1}{F_0^2}\left[\frac{1}{12}\left(t-2\Sigma_{PQ}+\frac{\Delta_{PQ}^2}{t}\right)\bar{J}_{PQ}(t)-\frac{\Delta_{PQ}^2}{3t}\,\bar{\bar{J}}_{PQ}\,(t)-\frac{t}{6}k_{PQ}+\frac{t}{288\pi^2}\right]+\frac{2t}{3F_0^2}L_9^r\,, \quad (5.27)$$

involving $\Sigma_{PQ}=M_P^2+M_Q^2$ and $\Delta_{PQ}=M_P^2-M_Q^2$, and $\bar{\bar{J}}_{PQ}\,(t)=\bar{J}_{PQ}(t)-t\bar{J}'_{PQ}(t)$.

5.3.2 Kaon electromagnetic radii [H]

In a similar way to the pion form factor, the K^+ electromagnetic square radius is given by

$$\langle r^2\rangle_V^{K^+}=\frac{6}{F_K^2}\left[2\Delta L_9-\frac{1}{32\pi^2}\left(\frac{1}{6}\log\frac{\overset{\circ}{M}{}_K^2}{\overset{\circ}{M}{}_\pi^2}+\frac{1}{6}+\frac{1}{9}Y(3)+\frac{M_\pi^2}{9M_K^2}(r+1)Y(3)\right)\right]+\langle r^2\rangle_V^{K^+}e_V^{K^+}\,, \quad (5.28)$$

with the remainder:

$$e_V^{K^+}=\frac{6}{F_K^4}\frac{(\Re F_K^2F_{K^+}^V)_1}{\langle r^2\rangle_V^{K^+}}\,. \quad (5.29)$$

Replacing ΔL_9 by its value in terms of the pion radius, eq.(5.17), leads to the following relation:

$$F_K^2\langle r^2\rangle_V^{K^+}(1-e_V^{K^+})-F_\pi^2\langle r^2\rangle_V^{\pi}(1-e_V^{\pi})=\frac{1}{32\pi^2}\left[-\log\frac{\overset{\circ}{M}{}_K^2}{\overset{\circ}{M}{}_\pi^2}+\frac{2}{3}Y(3)-\frac{M_\pi^2}{3M_K^2}(r+1)Y(3)\right]\,, \quad (5.30)$$

where the right-hand side is a very small correction for any reasonable value of r and $Y(3)$, so that the electromagnetic square radius of the charged kaon is essentially predicted to be $\langle r^2\rangle_V^{K^+}\simeq F_\pi^2/F_K^2\times\langle r^2\rangle_V^{\pi}\simeq 0.32$ fm^2. Two experiments (NA47 and Fermilab) have measured this radius, leading to the average [137]:

$$\langle r^2\rangle_V^{K^+}=0.314\pm0.035\ \text{fm}^2\,. \quad (5.31)$$

The square radius of the neutral kaon reads:

$$F_K^2\langle r^2\rangle_V^{K^0}(1-e_V^{K^0})=\frac{1}{32\pi^2}\left[-\log\frac{\overset{\circ}{M}{}_K^2}{\overset{\circ}{M}{}_\pi^2}+\frac{2}{3}Y(3)-\frac{M_\pi^2}{3M_K^2}(r+1)Y(3)\right] \quad (5.32)$$

with the remainder:

$$e_V^{K^0} = \frac{6}{F_K^2}\frac{(\Re F_{K^0}^V)_1}{\langle r^2\rangle_V^{K^0}}\,, \tag{5.33}$$

The current experimental average is [137]:

$$\langle r^2\rangle_V^{K^0} = -0.077 \pm 0.010 \text{ fm}^2\,. \tag{5.34}$$

Eqs. (5.30) and (5.32) yield the following relation between the electromagnetic radii:

$$\langle r^2\rangle_V^{\pi}(1-e_V^{\pi}) = \frac{F_K^2}{F_\pi^2}\left(\langle r^2\rangle_V^{K^+}(1-e_V^{K^+}) - \langle r^2\rangle_V^{K^0}(1-e_V^{K^0})\right)\,. \tag{5.35}$$

which is fulfilled using the experimental values of the radii and the SM value of F_K/F_π (the remainders must be on the large side of their allowed value according to the dimensional estimation discussed in sec. 5.5.3).

5.4 $K\pi$ form factors

5.4.1 Definition [H]

Among the quantities that can be determined from lattice simulations, one can single out the $K_{\ell 3}$ form factors defined as:

$$\sqrt{2}\langle K^+|\bar{u}\gamma_\mu s|\pi^0\rangle = (p'+p)^\mu f_+(t) + (p'-p)^\mu f_-(t)\,. \tag{5.36}$$

f_+ corresponds to P-wave projection of the $K_{\ell 3}$ transition, whereas its S-wave part comes from

$$f_0(t) = f_+(t) + \frac{t}{\Delta_{K\pi}} f_-(t)\,, \tag{5.37}$$

where $\Delta_{PQ} = M_P^2 - M_Q^2$. Following the discussion in sec.5.1, $F_\pi F_K f_+$ and $F_\pi F_K f_-$ are expected to have good convergence properties away from the singularities (opening thresholds...). As before, their chiral expansions can be expressed in terms of $r, X(3), Z(3)$, NLO low-energy constants (L_4, L_5 and L_9) and remainders. Reexpressing L_4 and L_5 using eqs. (3.79)-(3.80) yields the following expansions of the $K_{\ell 3}$ form factors:

$$\begin{aligned} F_\pi F_K f_+(t) = {} & \frac{F_\pi^2 + F_K^2}{2} + \frac{3}{2}[tM_{K\pi}^r(t) + tM_{K\eta}^r(t) - L_{K\pi}(t) - L_{K\eta}(t)] \\ & + 2tL_9^r + F_\pi F_K d_+ + te_+\,, \end{aligned} \tag{5.38}$$

$$\begin{aligned} F_\pi F_K f_-(t) = {} & \frac{F_K^2 - F_\pi^2}{2} - \frac{3}{2}(M_K^2 - M_\pi^2)[M_{K\pi}^r(t) + M_{K\eta}^r(t)] \\ & + \frac{1}{4}K_{K\pi}(t)\left[5(t - M_\pi^2 - M_K^2) + \frac{3}{2}(r+3)M_\pi^2 Y(3)\right] \\ & - \frac{1}{4}K_{K\eta}(t)\left[3(t - M_\pi^2 - M_K^2) + \frac{1}{2}(r+3)M_\pi^2 Y(3)\right] \\ & - 2(M_K^2 - M_\pi^2)L_9^r + F_\pi F_K(d_- - d_+) + t(e_- - e_+)\,, \end{aligned} \tag{5.39}$$

where $d_\pm = O(m_q^2)$ and $e_\pm = O(m_q)$ combine the remainders from the form factors and the decay constants:

$$F_\pi F_K d_+ = (\Re F_\pi F_K f_+)_0 - \frac{F_\pi^2 e_\pi + F_K^2 e_K}{2}\,, \tag{5.40}$$

$$F_\pi F_K (d_- - d_+) = (\Re F_\pi F_K f_-)_0 + \frac{F_\pi^2 e_\pi - F_K^2 e_K}{2}\,, \tag{5.41}$$

$$F_\pi F_K e_+ = (\Re F_\pi F_K f_+)_1\,, \tag{5.42}$$

$$F_\pi F_K (e_- - e_+) = (\Re F_\pi F_K f_+)_1\,. \tag{5.43}$$

The remainders in $F_\pi F_K(\Re f_\pm)(t)$ are defined as before. When performing our fits to lattice data, we will also express L_9 in terms of the pion radius using eq. (5.17). Inserting eqs. (5.38)-(5.39) into eq. (5.37) leads to the following expression for the scalar form factor:

$$\begin{aligned} F_\pi F_K f_0(t) = {} & \frac{F_K^2 + F_\pi^2}{2} + \frac{t}{\Delta_{K\pi}}\frac{F_K^2 - F_\pi^2}{2} - \frac{3}{2}L_{K\pi}(t) - \frac{3}{2}L_{K\eta}(t) \\ & + \frac{t}{4\Delta_{K\pi}}K_{K\pi}(t)\left[5(t - M_\pi^2 - M_K^2) + \frac{3}{2}(r+3)M_\pi^2 Y(3)\right] \\ & - \frac{t}{4\Delta_{K\pi}}K_{K\eta}(t)\left[3(t - M_\pi^2 - M_K^2) + \frac{1}{2}(r+3)M_\pi^2 Y(3)\right] \\ & + (F_\pi F_K d_+ + t e_+)\left(1 - \frac{t}{\Delta_{K\pi}}\right) + (F_\pi F_K d_- + t e_-)\frac{t}{\Delta_{K\pi}}\,. \end{aligned} \tag{5.44}$$

In the limit where all expansions are saturated by their LO contribution, the well-known expression for the vector form factor is recovered:

$$f_+^{K\pi}(t) = 1 + \frac{3}{2}H_{K\pi}(t) + \frac{3}{2}H_{K\eta}(t) + O(p^4)\,, \tag{5.45}$$

as well as that for $f_-^{K\pi}$ [254].

5.4.2 The Callan-Treiman point and its soft kaon analog [H]

According to the Callan-Treiman theorem [257], in the soft-pion limit ($p'^2 = M_\pi^2 = 0$), the scalar form factor at $t = \Delta_{K\pi} \equiv M_K^2 - M_\pi^2$ (Callan-Treiman point) should be equal to F_K/F_π. This implies that $F_K F_\pi f_0(\Delta_{K\pi}) - F_K^2$ vanishes in the $N_f = 2$ chiral limit. There is a soft-kaon analog of this theorem holding at $t = \tilde{\Delta}_{K\pi} \equiv -\Delta_{K\pi}$, stating that $F_K F_\pi f_0(\tilde{\Delta}_{K\pi}) - F_\pi^2$ vanishes in the $N_f = 3$ chiral limit. At these particular points, eq. (5.44) reads:

$$\begin{aligned} F_\pi F_K f_0(\Delta_{K\pi}) = {} & F_K^2 - \frac{3}{2}L_{K\pi}(\Delta_{K\pi}) - \frac{3}{2}L_{K\eta}(\Delta_{K\pi}) + \frac{1}{4}K_{K\pi}(\Delta_{K\pi})\left[-10M_\pi^2 + \frac{3}{2}(r+3)M_\pi^2 Y(3)\right] \\ & - \frac{1}{4}K_{K\eta}(\Delta_{K\pi})\left[-5M_\pi^2 + \frac{1}{2}(r+3)M_\pi^2 Y(3)\right] + F_\pi F_K d_- + \Delta_{K\pi} e_-\,, \end{aligned}$$

$$\begin{aligned} F_\pi F_K f_0(-\Delta_{K\pi}) = {} & F_\pi^2 - \frac{3}{2}L_{K\pi}(-\Delta_{K\pi}) - \frac{3}{2}L_{K\eta}(-\Delta_{K\pi}) - \frac{1}{4}K_{K\pi}(-\Delta_{K\pi})\left[-10M_K^2 + \frac{3}{2}(r+3)M_\pi^2 Y(3)\right] \\ & + \frac{1}{4}K_{K\eta}(-\Delta_{K\pi})\left[-6M_K^2 + \frac{1}{2}(r+3)M_\pi^2 Y(3)\right] + F_\pi F_K(2d_+ - d_-) - \Delta_{K\pi}(2e_+ - e_-)\,. \end{aligned}$$

One can check explicitely that these expressions fulfill the Callan-Treiman theorem and its soft-kaon analog (the K and L contributions canceling each other) provided the following constraints on the higher-order remainders

$$d_- = O(mm_s)\,, \qquad e_- = O(m)\,, \tag{5.46}$$

meaning that d_- and e_- are $1/r$-suppressed compared to d_+ and e_+.

We can define the discrepancies from the Callan-Treiman theorem(s):

$$\Delta_{CT} = f_0(\Delta_{K\pi}) - \frac{F_K}{F_\pi}\,, \qquad \tilde{\Delta}_{CT} = f_0(-\Delta_{K\pi}) - \frac{F_\pi}{F_K}\,. \tag{5.47}$$

These NLO quantities can be expressed from eqs. (5.46)-(5.46), embedding the fact that Δ_{CT} is $1/r$-suppressed compared to $\tilde{\Delta}_{CT}$. For comparison, these quantities have been calculated in one-loop χPT in the isospin limit [254]:

$$\Delta_{CT} = -3.5 \cdot 10^{-3}\,, \qquad \tilde{\Delta}_{CT} = 0.03\,. \tag{5.48}$$

It has in fact been shown in refs. [258, 259] that a precise assessment of the scalar form factor at the Callan-Treiman points could probe physics beyond the Standard Model in the strange quark sector, in particular right-handed couplings of quarks to W bosons. The pioneering work [258] led to a reanalysis of $K_{\ell 3}$ data by several collaborations [260–263], which at present show a good/marginal agreement with the Standard Model.

The $K_{\ell 3}$ vector form factor at zero momentum transfer is another quantity of interest. Indeed, the measurement of $K_{\ell 3}$ decays can be analysed in the framework of the Standard Model to determine the product $|V_{us} f_+(0)|$, and thus the CKM matrix element $|V_{us}|$. A recent fit to $|V_{ud}|$ (from super-allowed $0^+ \to 0^+$ nuclear decays), $|V_{us}| f_+(0)$ (from $K_{\ell 3}$), and $|V_{us}/V_{ud}| F_K/F_\pi$ (from $\pi_{\ell 2}$ and $K_{\ell 2}$) together with the unitarity of the CKM matrix led to [223]:

$$f_+(0)|_{SM} = 0.959 \pm 0.005\,, \tag{5.49}$$

and a value of $F_K/F_\pi|_{SM}$ in full agreement with eq.(3.62) (with a strong correlation between these two quantities).

Deviation of $f_+(0)$ from this value would be an indication of new physics, so that this quantity plays a particularly important role to test the Standard Model in the light quark sector. A direct determination of these quantities on the lattice as well as a well-controlled method to extrapolate lattice data down to the physical quark masses are naturally crucial to get a proper assessment of the uncertainties (from statistical, but also systematic origins).

5.5 Observables for lattice simulations at different quark masses

As detailed in sec. 3.3.4, lattice simulations have the potential to determine the LECs encoding the pattern of three-flavour chiral symmetry breaking. However, the extraction of the LECs is generally performed by fitting the quark mass dependence of various observables, taking chiral series where the LO is already expected to saturate the expansion. As an alternative to such extractions, which rely strongly on the usual (perturbative) treatment of chiral series, we proposed a lattice test of the size of $s\bar{s}$ vacuum fluctuations based on ReχPT in ref. [255]. We considered simulations with (2+1) flavours, with a strange quark mass at its physical value $\tilde{m}_s = m_s$, but two u, d light quarks with identical masses $\tilde{m}$ larger than their physical values m and smaller than m_s. The larger values of the u, d masses enhanced the impact of the vacuum

fluctuations encoded in L_4 and L_6 on observables such as the masses and decay constants of pions and kaons. This led to a difference in the curvatures of F_P^2 and $F_P^2 M_P^2$ ($P = \pi, K$) as functions of $q = \tilde{m}/\tilde{m}_s$, depending on the size of $X(3)$ and $Z(3)$. The effect was less pronounced in the case of M_P^2, obtained as the ratio of the two former observables, leading to a fairly linear behaviour as a function of q. We proposed in the same reference a test of the size of $X(3)$ on the lattice from the pion and kaon spectrum, by considering the dependence of the ratios on q:

$$R_\pi = \frac{\tilde{F}_\pi^2 \tilde{M}_\pi^2}{q F_\pi^2 M_\pi^2} \qquad R_K = \frac{2\tilde{F}_K^2 \tilde{M}_K^2}{(q+1) F_K^2 M_K^2} \tag{5.50}$$

where $\tilde{F}_\pi^2$ and $\tilde{M}_\pi^2$ denote quantities computed on the lattice with u, d quarks of mass $\tilde{m}$.

The recent $2+1$ dynamical simulations provide new and relevant information on the impact of $s\bar{s}$ fluctuations related to the presence of strange quarks in the sea [82, 83, 264]. Conversely, ReχPT can provide a more appropriate treatment of chiral extrapolations if the hints of suppressed $N_f = 3$ quark condensate and decay constants are confirmed. In principle, this analysis would require lattice data performed with several u, d, s quark masses (whose renormalized values are known) and transfer momenta (in the case of form factors, scattering amplitudes), but where the continuum and infinite-volume limit have already been performed ($a \to 0, L \to \infty$). Unfortunately, such data sets are not (yet) available. Some collaborations [e.g., MILC [128,129]] provide numbers directly in the physical limit, performing the chiral extrapolation at the same time as the continuum limit. This prevents one from testing different alternatives concerning chiral extrapolation, even though the results sometimes contradict the usual assumptions made when exploiting chiral series (for instance their saturation by the quark condensate and the decay constant, see secs. 3.3.4 and 3.5.3). Others [BMW [265, 266], ETMC [267], TWQCD-JLQCD [196]] do not provide the decay constants and the renormalized quark masses mandatory for such a study. Finally, some collaborations [RBC/UKQCD [207–209], PACS-CS [127]] have performed their analysis only at one particular lattice spacing and/or one particular volume, without always being able to estimate the systematics associated with the continuum and infinite-volume limits fully.

In view of this situation, we will restrict ourselves to the studies made by RBC/UKQCD [207–209] and PACS-CS [127], described in more detail in apps. A.3.1 and A.3.2. The fact that only statistical errors are quoted in both cases prevents us from using a full-fledged statistical treatment [46]. As explained in the previous section, we can use the relations eqs. (3.79)-(3.80) (decay constants), eqs. (3.77)-(3.78) (masses), eq. (5.17) (pion electromagnetic square radius)... to express NLO LECs in terms of r, $X(3)$, $Z(3)$, accurately measured observables and remainders. These relations can be inserted in the chiral expansions of other observables (such as kaon or $K_{\ell 3}$ form factors, or meson-meson scattering), which can be used to constrain r, $X(3)$ and $Z(3)$. For each new observable, one or several remainders are introduced, which are assumed to be small but nevertheless limit the accuracy of the chiral series. Contrary to the discussions of the previous chapters, we will not fix the value of F_K/F_π, since simulations are expected to be the main source of information on this quantity.

Fitting these data will offer us the opportunity to extract relevant information on chiral symmetry breaking and to check the consistency of our picture concerning the numerical competition between LO and NLO terms. We consider simulations with 3 dynamical flavours $(\tilde{m}, \tilde{m}, \tilde{m}_s)$ and denote $\tilde{X}$ the values for the lattice quantities (and X the corresponding value for physical quark masses). We introduce the ratios:

$$p = \frac{\tilde{m}_s}{m_s}\,, \qquad q = \frac{\tilde{m}}{\tilde{m}_s}\,, \tag{5.51}$$

in addition to the ratio of physical quark masses r and the chiral parameters arising in the LO Lagrangian in eq. (5.1).

5.5.1 Masses and decay constants [H]

Proceeding as before in this new setting, we obtain the following expansions for the lattice value of the decay constants:

$$\frac{\tilde{F}_\pi^2}{F_\pi^2} = Z(3) + \frac{M_\pi^2}{F_\pi^2} pqrY(3) \left[8\left(\frac{1}{q}+2\right) L_4^r + 8L_5^r \right] \tag{5.52}$$
$$- \frac{M_\pi^2}{F_\pi^2} \frac{1}{32\pi^2} pqrY(3) \left[4\log\frac{\overset{\tilde{\circ}}{M}{}_\pi^2}{\mu^2} + \left(\frac{1}{q}+1\right)\log\frac{\overset{\tilde{\circ}}{M}{}_K^2}{\mu^2} \right] + \frac{\tilde{F}_\pi^2}{F_\pi^2}\tilde{e}_\pi \,,$$

$$\frac{\tilde{F}_K^2}{F_\pi^2} = Z(3) + \frac{M_\pi^2}{F_\pi^2} pqrY(3) \left[8\left(\frac{1}{q}+2\right) L_4^r + 4\left(\frac{1}{q}+1\right) L_5^r \right] \tag{5.53}$$
$$- \frac{M_\pi^2}{F_\pi^2} \frac{1}{32\pi^2} pqrY(3) \left[\frac{3}{2}\log\frac{\overset{\tilde{\circ}}{M}{}_\pi^2}{\mu^2} + \frac{3}{2}\left(\frac{1}{q}+1\right)\log\frac{\overset{\tilde{\circ}}{M}{}_K^2}{\mu^2} + \frac{1}{2}\left(\frac{2}{q}+1\right)\log\frac{\overset{\tilde{\circ}}{M}{}_\eta^2}{\mu^2} \right] + \frac{\tilde{F}_K^2}{F_\pi^2}\tilde{e}_K \,,$$

where the LO contributions to the simulated pseudoscalar masses are involved:

$$\overset{\tilde{\circ}}{M}{}_\pi^2 = pqrM_\pi^2 Y(3)\,, \qquad \overset{\tilde{\circ}}{M}{}_K^2 = \frac{pqr}{2}\left(\frac{1}{q}+1\right) M_\pi^2 Y(3)\,, \qquad \overset{\tilde{\circ}}{M}{}_\eta^2 = \frac{pqr}{3}\left(\frac{2}{q}+1\right) M_\pi^2 Y(3)\,, \tag{5.54}$$

and $\tilde{e}_P$ are remainders of $O(\tilde{m}_q^2)$ ($\tilde{m}_q$ denotes either $\tilde{m}_s$ or $\tilde{m}$). We have divided by the physical value of F_π^2 in order to deal with dimensionless quantities. In a similar way, we obtain the bare expansions of the masses:

$$\frac{\tilde{F}_\pi^2 \tilde{M}_\pi^2}{F_\pi^2 M_\pi^2} = pqr \Bigg\{ X(3) + \frac{M_\pi^2}{F_\pi^2} pqr[Y(3)]^2 \left[16\left(\frac{1}{q}+2\right) L_6^r + 16L_8^r \right] \tag{5.55}$$
$$- \frac{M_\pi^2}{F_\pi^2} \frac{1}{32\pi^2} pqr[Y(3)]^2 \left[3\log\frac{\overset{\tilde{\circ}}{M}{}_\pi^2}{\mu^2} + \left(\frac{1}{q}+1\right)\log\frac{\overset{\tilde{\circ}}{M}{}_K^2}{\mu^2} + \frac{1}{9}\left(\frac{2}{q}+1\right)\log\frac{\overset{\tilde{\circ}}{M}{}_\eta^2}{\mu^2} \right] \Bigg\} + \frac{\tilde{F}_\pi^2 \tilde{M}_\pi^2}{F_\pi^2 M_\pi^2}\tilde{d}_\pi \,,$$

$$\frac{\tilde{F}_K^2 \tilde{M}_K^2}{F_\pi^2 M_\pi^2} = \frac{pqr}{2}\left(\frac{1}{q}+1\right) \Bigg\{ X(3) + \frac{M_\pi^2}{F_\pi^2} pqr[Y(3)]^2 \left[16\left(\frac{1}{q}+2\right) L_6^r + 8\left(\frac{1}{q}+1\right) L_8^r \right] \tag{5.56}$$
$$- \frac{M_\pi^2}{F_\pi^2} \frac{1}{32\pi^2} pqr[Y(3)]^2 \left[\frac{3}{2}\log\frac{\overset{\tilde{\circ}}{M}{}_\pi^2}{\mu^2} + \frac{3}{2}\left(\frac{1}{q}+1\right)\log\frac{\overset{\tilde{\circ}}{M}{}_K^2}{\mu^2} + \frac{5}{18}\left(\frac{2}{q}+1\right)\log\frac{\overset{\tilde{\circ}}{M}{}_\eta^2}{\mu^2} \right] \Bigg\} + \frac{\tilde{F}_K^2 \tilde{M}_K^2}{F_\pi^2 M_\pi^2}\tilde{d}_K \,,$$

where $\tilde{d}_P$ are remainders of $O(\tilde{m}_q^2)$. We have divided by the physical value of $F_\pi^2 M_\pi^2$ in order to deal with dimensionless quantities. As explained before, we use eqs. (3.79)-(3.78) to express the (mass-independent) chiral couplings $L_{4,5,6,8}$ in terms of $r, X(3), Z(3)$ and the physical masses and decay constants.

5.5.2 $K_{\ell 3}$ form factors [H]

We obtain for the lattice form factors:

$$\tilde{F}_\pi \tilde{F}_K \tilde{f}_+(t) = \frac{\tilde{F}_\pi^2 + \tilde{F}_K^2}{2} + \frac{3}{2}[t\tilde{M}^r_{K\pi}(t) + t\tilde{M}^r_{K\eta}(t) - \tilde{L}_{K\pi}(t) - \tilde{L}_{K\eta}(t)] + 2tL_9^r + \tilde{F}_\pi \tilde{F}_K \tilde{d}_+ + t\tilde{e}_+ \quad (5.57)$$

$$\begin{aligned}\tilde{F}_\pi \tilde{F}_K \tilde{f}_0(t) = {} & \frac{\tilde{F}_K^2 + \tilde{F}_\pi^2}{2} + \frac{t}{\tilde{\Delta}_{K\pi}} \frac{\tilde{F}_K^2 - \tilde{F}_\pi^2}{2} - \frac{3}{2}\tilde{L}_{K\pi}(t) - \frac{3}{2}\tilde{L}_{K\eta}(t) \\ & + \frac{t}{4\tilde{\Delta}_{K\pi}} \tilde{K}_{K\pi}(t) \left[5(t - \tilde{M}_\pi^2 - \tilde{M}_K^2) + \frac{3}{2}\left(\frac{1}{q} + 3\right) pqr M_\pi^2 Y(3) \right] \\ & - \frac{t}{4\tilde{\Delta}_{K\pi}} \tilde{K}_{K\eta}(t) \left[3(t - \tilde{M}_\pi^2 - \tilde{M}_K^2) + \frac{1}{2}\left(\frac{1}{q} + 3\right) pqr M_\pi^2 Y(3) \right] \\ & + (\tilde{F}_\pi \tilde{F}_K \tilde{d}_+ + t\tilde{e}_+)\left(1 - \frac{t}{\tilde{\Delta}_{K\pi}}\right) + (\tilde{F}_\pi \tilde{F}_K \tilde{d}_- + t\tilde{e}_-)\frac{t}{\tilde{\Delta}_{K\pi}}\,, \end{aligned} \quad (5.58)$$

where $\tilde{L}_{PQ}$, $\tilde{K}_{PQ}$, $\tilde{M}_{PQ}$ are evaluated with the LO pseudoscalar masses at the simulated quark masses using eq. (5.54), apart from the $\bar{J}_{PQ}$ function which is evaluated at the simulated ("physical") pion and kaon masses using eqs. (5.55)-(5.56). In the above formulae, the decay constants on the right-hand side arise from the reexpression of L_4 and L_5, and should be understood as a short-hand notation of the full expressions in eqs. (5.52)-(5.53). For the vector form factor, we can trade L_9 for the pion electromagnetic square radius using eq. (5.17).

5.5.3 Remainders [H]

The expressions for the simulated masses, decay constants, form factors and electromagnetic square radius involve unknown remainders. These remainders collect all the contributions coming from NNLO, NNNLO and higher orders. They can be evaluated by resonance saturation [23], involving a hadronic scale Λ_H only mildly affected by the actual value of the quark masses (mass of the $\rho, K^* \ldots$). In order to keep track of the scaling of the remainders with the quark masses, we take the following NNLO estimates which involves the hadronic scale at the fourth power:

$$d, e, d_K, e_K, d_+ = O\left(\frac{M_K^4}{\Lambda_H^4}\right), \qquad e_+ = O\left(\frac{F_\pi^2 M_K^2}{\Lambda_H^4}\right), \qquad e_\pi^V = O\left(\frac{6}{\langle r^2\rangle_V^\pi}\frac{M_K^2}{\Lambda_H^4}\right), \quad (5.59)$$

$$d', e', d_- = O\left(\frac{2M_\pi^2 M_K^2}{\Lambda_H^4}\right), \qquad e_- = O\left(\frac{2F_\pi^2 M_\pi^2}{\Lambda_H^4}\right), \quad d_\pi = d - d', \quad e_\pi = e - e' \quad (5.60)$$

where M_π^2 and M_K^2 follow the known dependence of the remainders on m and m_s, whereas F_π^2 is inserted when a dimensionful constant with no dependence on m_q is required.

A typical order of magnitude for $O(m_s^2)$ remainders so that the chiral series converge is 10% so that $\Lambda_H \simeq 0.8$ GeV. The corresponding size σ of the remainders is given in tab. 5.1, and the remainders will be required to stay in the range $[-\sigma, \sigma]$ in our fits to lattice data if necessary. In the specific case of the electromagnetic square radius of the pion, we have combined the uncertainty on the experimental measurement of the square radius with the theory uncertainty on the remainder in quadrature (the range for the kaon radii would be the same). We can then use the leading scaling of the remainders to perform a rough extrapolation to the simulated

Remainder	σ
d, e, d_+	0.148
d', e', d_-	0.024
e_+	0.005
e_-	0.001
e_π^V	0.318

Table 5.1: *Size of the NNLO remainders allowed in our fits, based on a dimensional estimate.*

quark masses:

$$\tilde{d}_\pi = p^2 d - p^2 qrd' , \qquad \tilde{d}_K = \left(\frac{F_K M_K}{F_\pi M_\pi}\right)^2 p^2 \frac{r+1}{2}\left(d - \frac{r+1}{2} qrd'\right) , \quad (5.61)$$

$$\tilde{e}_\pi = p^2 e - p^2 qre' , \qquad \tilde{e}_K = \left(\frac{F_K}{F_\pi}\right)^2 p^2 \left(e - \frac{r+1}{2} qre'\right) , \quad (5.62)$$

$$\tilde{d}_+ = p^2 d_+ , \qquad \tilde{e}_+ = p e_+ , \qquad \tilde{d}_- = p^2 qrd_- , \qquad \tilde{e}_- = pqre_- . \quad (5.63)$$

5.6 Fit to lattice values

5.6.1 Data and parameters [H]

We are now in a position to build the χ^2 function to be minimised for the sets of data that we will consider. The inputs are the following ones, as recalled in apps. A.3.1 and A.3.2:

- $\tilde{F}_\pi^2, \tilde{F}_K^2, \tilde{F}_\pi^2\tilde{M}_\pi^2, \tilde{F}_K^2\tilde{M}_K^2$ for known values of the quark masses $(\tilde{m}, \tilde{m}_s)$ (RBC/UKQCD and PACS-CS)
- $\tilde{F}_\pi\tilde{F}_K\tilde{f}_+$ and $\tilde{F}_\pi\tilde{F}_K\tilde{f}_0$ for several transfer momenta (RBC/UKQCD)
- We consider the quantities given by these collaborations corresponding to light quark masses and small momenta where chiral perturbation theory is expected to be valid.

The uncertainties on these quantities were obtained by combining the uncertainties in quadrature: no correlation between the various observables is provided in the articles of both collaborations, and we have only the statistical errors (no estimate of the systematic uncertainties was available for the quantities of interest here). The parameters entering the fit are:

- Quantities from the LO chiral Lagrangian $X(3)$, $Z(3)$, r,
- Higher-order remainders: d, d', e, e' (in all cases), $d_+, e_+, d_-, e_-, e_\pi^V$ (for $K_{\ell 3}$ form factors),
- The value of the ratio of decay constants F_K/F_π,
- The value of $p_{ref} = \tilde{m}_{s,ref}/m_s$ for a lattice set of reference, providing the equivalence between lattice and physical quark masses (when possible).

The last quantity is estimated by both collaborations, but we found it interesting to keep this parameter free in the fit, in order to take partially into account systematic effects related to lattice spacing (notice that we do not include any uncertainty on the determination of the lattice spacing by the two collaborations in our analysis). Since the quark masses are expressed in a mass-independent scheme involving only multiplicative renormalisation, we can determine the value of $p = \tilde{m}_s/m_s$ for any lattice set once we know p for a given reference set using $\tilde{m}_s = (\tilde{m}_s/\tilde{m}_{s,ref}) \cdot p_{ref}$. We had to fix the last two parameters in the case of RBC/UKQCD fits, due to the limited number of unitarity (unquenched) points available for the masses and decay constants (only 2 different pairs of quark masses).

When computing the values of the observables from NLO chiral expansions, we need the values of the masses and decay constants for the simulated quark masses (for instance in the unitarity functions $\bar{J}$). In such a case, we computed systematically the values of the decay constants and masses from their chiral expansions (5.52)-(5.56), rather than plugging in their "measured" values on the lattice. This distinction may have some importance for the $K_{\ell 3}$ form factors eqs. (5.38) and (5.44), where we have reexpressed L_4 and L_5 in terms of $\tilde{F}_\pi^2$ and $\tilde{F}_K^2$, but where the latter quantities stand for their chiral expansion in terms of LECs (the fits to RBC/UKQCD would be slightly improved compared to the ones presented here if we used the measured values of $\tilde{F}_\pi^2$ and $\tilde{F}_K^2$ rather than the computed ones).

In addition, the mass $\tilde{M}_\eta$ and decay constant $\tilde{F}_\eta$ of the η are needed for the evaluation of the loop integral $\bar{J}_{PQ}$ (and related unitarity functions). They are obtained at a sufficient accuracy for our purposes using the two following LO formulae reminiscent of the Gell-Mann-Okubo relation:

$$\tilde{F}_\eta^2 = \frac{4}{3}\tilde{F}_K^2 - \frac{1}{3}\tilde{F}_\pi^2\,, \qquad \tilde{F}_\eta^2\tilde{M}_\eta^2 = \frac{4}{3}\tilde{F}_K^2\tilde{M}_K^2 - \frac{1}{3}\tilde{F}_\pi^2\tilde{M}_\pi^2\,. \tag{5.64}$$

We constrain the remainders in the ranges indicated in tab. 5.1. Once the (MINUIT-powered) fit has converged, we can estimate a large body of quantities: NLO LECs, $N_f = 2$ chiral order parameters, values of the $K_{\ell 3}$ scalar form factor at zero momentum transfer, at the Callan-Treiman point and its soft kaon analog, test of the convergence of the series. We have propagated the errors exploiting the covariance matrix provided by MINOS, assuming that all uncertainties follow a Gaussian distribution.

5.6.2 Low-energy constants [H]

Our results are summarised in tabs. 5.2 and 5.3. The first series of rows corresponds to the outcome of the fit, whereas the lower rows are quantities derived from the results of the fit (LO LECs, NLO LECs, quantities in the $N_f = 2$ chiral limit, $K_{\ell 3}$ quantities, relative fraction of LO/NLO/remainders contributions at the minimum for several observables), and the last row is the χ^2 per degree of freedom.

The fit of RBC/UKQCD results includes only a limited number of data points for the masses and decay constants, which forces us to fix one of the parameters of the fit, namely the simulated strange quark mass [3] and to impose some bounds on the size of the higher-order remainders, based on a simple estimate from resonance saturation described in sec. 5.5.3. Indeed, some of these remainders are pushed to the limits of their range when the set of data is too small, because there is not enough information for MINUIT to choose a particular value

[3] Letting all parameters free gives comparable results for the central values, but some parameters get very large uncertainties, larger than their allowed range. Propagating the errors in such a situation would be meaningless, and reporting the results of this fit would not provide much more information than the constrained fit that we present here.

for these remainders (keeping them free would lead to a larger contribution from higher orders and to a further decrease of the LO contribution).

The ratio of decay constants F_K/F_π (left free in our fit) comes out slightly larger (smaller) for PACS-CS (RBC/UKQCD) than its Standard Model value eq.(3.62) in the fits of the masses and decay constants. We obtain also values of simulated strange quark masses and of the physical strange quark mass in good agreement with the results obtained by the two collaborations, as recalled in apps. A.3.1 and A.3.2 (the discrepancy between RBC/UKQCD and PACS-CS is due to the different choice of renormalisation procedure, which explains the low value obtained by the PACS-CS collaboration [268]).

The decay constant in the $N_f = 3$ chiral limit is found to be rather low, in agreement with other recent works [183, 269]. This pattern of chiral symmetry breaking (with low quark condensate and decay constant) is reflected by the values obtained for the low-energy constants L_4 and L_6, which are both positive and do not show any sign of Zweig suppression, in agreement with the discussion in the previous chapters. It is thus not surprising to witness a strong suppression from the $N_f = 2$ chiral limit to the $N_f = 3$ one. The two-flavour quark condensate and decay constants, obtained from eqs. (3.114) and (3.115) saturate the chiral expansions, indicating that two-flavour χPT is appropriate to describe pion dynamics, as we will see also in ch. 6 from the analysis of the recent data on $K_{\ell 4}$ decays. The other LECs $L_{5,8,9}$ have values in agreement with conventional estimates (this was expected in particular for L_9 since our framework induces modifications that are only sub-leading for vector quantities such as the pion electromagnetic form factor).

The $K_{\ell 3}$ form factor at zero momentum transfer, $f_+(0) = f_0(0)$, involves only LECs related to decay constants and masses, eq. (5.38). In principle, it can be predicted from a fit of the latter quantities up to the determination of the remainder d_+. We quote the corresponding results in tabs. 5.2 and 5.3, where the central value for $f_+(0)$ corresponds to remainders set to zero. The uncertainty on this quantity includes the maximal size allowed for the remainders d_+ based on dimensional estimation (see tab. 5.1), as well as the uncertainties coming from the parameters of the fit. Clearly, the higher-order remainder d_+ hinders any accurate determination of $f_+(0)$, unless their value is also precisely determined from the fit, which is possible once data on $K_{\ell 3}$ form factors themselves is included. The values obtained for $f_0(0)$ are somewhat larger than the Standard Model value eq.(5.49), as well as those obtained from the RBC/UKQCD collaboration (see app. A.3.1) using different forms for the extrapolation in quark masses [208, 209].

Once the $K_{\ell 3}$ form factors are included in our fits, L_9 can be determined even though the fit does not constrain for this particular LEC tightly. In tabs. 5.2 and 5.3, the deviations from the Callan-Treiman relation at $t = \Delta_{K\pi}$ and its soft kaon analog at $-\Delta_{K\pi}$ are given. Their values are of the expected size for $SU(N_f)$ chiral-symmetry breaking quantities for $N_f = 2, 3$ flavours respectively, and thus compatible with the one obtained in standard χPT. The values of the square radii of the charged and neutral kaons have rather large uncertainties and are thus within the experimental error bars.

5.6.3 Convergence of three-flavour chiral series [H]

In the last lines of our tables, we have indicated for each fit the contribution from LO, NLO and remainders to pseudoscalar decay constants and masses for values of the parameters at the minimum of the fit. We can see that the series converge well on overall (remainder much smaller than LO+NLO), but that the LO term is far from saturating the series. The values of $Y(3)$ obtained is smaller than 1, reducing the contribution from chiral logarithms compared to that from the NLO LECs. Indeed, tadpole diagrams generate chiral logarithms of the form

	PACS − CS Without $K_{\ell 3}$	RBC/UKQCD With $K_{\ell 3}$
r	26.5 ± 2.3	23.2 ± 1.5
$X(3)$	0.59 ± 0.21	0.20 ± 0.14
$Y(3)$	0.90 ± 0.22	0.43 ± 0.30
$Z(3)$	0.66 ± 0.09	0.46 ± 0.04
F_K/F_π	1.237 ± 0.025	1.148 ± 0.015
Rem. at limit	none	d, e
$\tilde{m}_{s,ref}/m_s$	1.24 ± 0.08	$1.15^\star$
$m_s(2\text{ GeV})$[MeV]	70 ± 4	107
$m(2\text{ GeV})$[MeV]	2.6 ± 0.3	4.6 ± 0.3
$B_0(2\text{ GeV})$[GeV]	3.34 ± 1.18	0.92 ± 0.67
F_0[MeV]	74.8 ± 4.9	62.2 ± 2.5
$L_4(\mu) \cdot 10^3$	-0.1 ± 0.2	2.4 ± 2.0
$L_5(\mu) \cdot 10^3$	1.8 ± 0.4	1.8 ± 1.6
$L_6(\mu) \cdot 10^3$	0.1 ± 0.4	4.7 ± 7.1
$L_8(\mu) \cdot 10^3$	0.8 ± 0.7	4.4 ± 7.1
$L_9(\mu) \cdot 10^3$	$\times$	4.4 ± 2.8
F_π^2	$0.66 + 0.22 + 0.12$	$0.45 + 0.69 - 0.14$
F_K^2	$0.44 + 0.48 + 0.08$	$0.34 + 0.76 - 0.10$
$F_\pi^2 M_\pi^2$	$0.60 + 0.30 + 0.10$	$0.20 + 0.95 - 0.15$
$F_K^2 M_K^2$	$0.42 + 0.50 + 0.08$	$0.14 + 0.97 - 0.11$
$F_\pi F_K f_+(0)$	$\times$	$0.40 + 0.75 - 0.15$
χ^2/N	0.9/3	4.4/8

Table 5.2: *Results of fits performed on the data from the PACS-CS [127] and RBC/UKQCD [207–209] collaborations on pseudoscalar masses and decay constants, and $K_{\ell 3}$ form factors in the case of RBC/UKQCD. In all cases, we considered only data with light pions and only statistical errors are shown. In the RBC/UKQCD case, we fixed the lattice strange quark mass (marked with a star). The LECs are given at the scale $\mu = m_\rho$. The penultimate set of rows collects the relative fractions of LO/NLO/remainders for decay constants, masses and $K_{\ell 3}$ form factor at vanishing transfer momentum (for RBC/UKQCD) at the minimum.*

$M_P^2 \log(M_P^2/\mu^2)$ which can prove quite troublesome to fit. For instance, the RBC/UKQCD collaboration [207–209] finds a better agreement of their data on decay constants with polynomial fits than with chiral series. In our treatment, these chiral logarithms always involve the LO mass $\overset{\circ}{M}{}_P^2$. Therefore, the limit of a small $Y(3)$ tames the chiral logarithms in our expansions, so that these logarithms become hard to distinguish from a polynomial at the numerical level on the range of masses where χPT could be valid. Furthermore large contributions from NLO LECs, and in particular from L_4 and L_6 as just discussed, will enhance the quadratic depen-

	PACS − CS Without $K_{\ell 3}$	RBC/UKQCD With $K_{\ell 3}$
$X(2)$	0.90 ± 0.01	0.90 ± 0.02
$Y(2)$	1.04 ± 0.02	1.00 ± 0.03
$Z(2)$	0.87 ± 0.02	0.90 ± 0.02
$B(2\text{ GeV})$[GeV]	3.83 ± 0.50	2.09 ± 0.19
F[MeV]	85.8 ± 0.7	87.7 ± 0.8
$\bar{\ell}_3$	5.0 ± 2.1	-0.6 ± 3.7
$\bar{\ell}_4$	4.5 ± 0.5	3.3 ± 0.5
Σ/Σ_0	1.51 ± 0.51	4.52 ± 2.83
B/B_0	1.15 ± 0.26	2.28 ± 1.39
F/F_0	1.15 ± 0.08	1.41 ± 0.06
$f_+(0)$	1.004 ± 0.149	0.985 ± 0.008
$\Delta_{CT} \cdot 10^3$	$\times$	-0.2 ± 12.1
$\Delta'_{CT} \cdot 10^3$	$\times$	-126 ± 104
$\langle r^2 \rangle_V^{K^+}$[fm^2]	$\times$	0.248 ± 0.156
$\langle r^2 \rangle_V^{K^0}$[fm^2]	$\times$	-0.027 ± 0.106

Table 5.3: *Results of fits performed on the data from the PACS-CS [127] and RBC/UKQCD [207–209] collaborations on pseudoscalar masses and decay constants, and $K_{\ell 3}$ form factors in the case of RBC/UKQCD. In all cases, we considered only data with light pions and only statistical errors are shown. In the PACS-CS case, the $K_{\ell 3}$ form factor at zero momentum transfer is a prediction of the fit (with an error combining those obtained from the fit and the maximal contribution allowed for the remainder from dimensional estimation).*

dence on the quark masses and thus our chiral expressions will mimic a polynomial dependence on the quark masses that cannot be reproduced in the more usual treatment of chiral expansions. These mechanisms could explain why chiral logarithms are often difficult to identify in lattice data, in addition to other effects (heavy strange quark mass, lattice systematics...).

We can compare these results with those from a fit of the same observables, where the NLO and higher contributions (chiral logarithms μ_P, LECs L_i, remainders) are computed replacing $2mB_0$, $(m+m_s)B_0$ and F_0 by the physical pion and kaon masses and the pion decay constant. This is exactly equivalent to performing the same fit as before with the following replacements in the NLO and higher-order contributions:

$$r \to 2\frac{M_K^2}{M_\pi^2} - 1, \qquad q \to \frac{\tilde{M}_\pi^2}{2\tilde{M}_K^2 - \tilde{M}_\pi^2}, \qquad p \to \frac{2\tilde{M}_K^2 - \tilde{M}_\pi^2}{2M_K^2 - M_\pi^2}, \qquad Y(3) \to 1, \tag{5.65}$$

$$\eta(r) \to \eta(r_0), \qquad \epsilon(r) \to \epsilon(r_0) - 2X(3)\frac{r - r_0}{r_0^2 - 1}, \qquad \log\frac{\overset{\circ}{M}{}_P^2}{\mu^2} \to \log\frac{M_P^2}{\mu^2}, \tag{5.66}$$

both for the observables that we consider, eqs. (5.52)-(5.58), and the equations allowing the determination of $L_{4,5,6,8,9}$, eqs. (5.17) and (3.71)-(3.74). For PACS-CS, this leads to $\chi^2/N =$

1.1/3 (compared to our result 0.9/3), with very similar values for the fundamental parameters $r, X(3), Y(3), Z(3)$. For RBC/UKQCD, the fitting procedure yields $\chi^2/N = 9.5/8$ (compared to our result 4.4/8), with much more uncertain values of the fundamental parameters (e.g., $r = 14.9 \pm 12.1$, $X(3) = 0.30 \pm 0.26$, $Y(3) = 0.68 \pm 0.60$). This is not particularly surprising since our fits to the PACS-CS data led to values of r and $Y(3)$ in good agreement with eq. (5.65), but not the RBC/UKQCD ones. The corresponding convergence of the pseudoscalar masses and decay constants is then (the relative contribution for LO, NLO and higher orders is given here):

$$\begin{array}{rll} \text{PACS}-\text{CS [NLO phys. masses]} & F_\pi^2 : 0.64 + 0.26 + 0.10, & F_\pi^2 M_\pi^2 : 0.67 + 0.24 + 0.09, \\ & F_K^2 : 0.42 + 0.51 + 0.07 & F_K^2 M_K^2 : 0.50 + 0.44 + 0.06, \\ \text{RBC/UKQCD [NLO phys. masses]} & F_\pi^2 : 0.45 + 0.70 - 0.15 & F_\pi^2 M_\pi^2 : 0.31 + 0.81 - 0.12, \\ & F_K^2 : 0.34 + 0.76 - 0.10, & F_K^2 M_K^2 : 0.15 + 0.94 - 0.11. \end{array} \tag{5.67}$$

There is no saturation of the series by their leading order. We see that our formulae yields results that are in good agreement with those obtained after reexpressing the NLO contributions in terms of F_π, M_π, M_K in the PACS-CS case, where $Y(3)$ is close to 1. On the other hand, when $Y(3)$ is not close to 1 (for instance in the RBC/UKQCD case), our formulae provide more efficient and accurate fits (lower χ^2, smaller error bars). From a more methodological point of view, we avoid a perturbative reexpression of LECs in terms of F_π, M_π, M_K in a regime where it is not justified.

These trends can be compared interestingly with the fits done by the lattice collaborations themselves, with a different treatment of the chiral series than ours. For instance, the MILC collaboration [129] observed from fits with staggered χPT that M_π^2 received NNLO corrections of the same size as NLO contributions, canceling each other to a large extent, with small NNNLO corrections (the latter being taken as analytic in quark masses and lattice spacings), whereas F_π exhibited no problems of convergence. On the other hand, the RBC/UKQCD collaboration [207] experienced difficulties in fitting F_π both in $N_f = 2$ and $N_f = 3$ theories. They also noticed that fits to M_K^2 and F_K using the $N_f = 3$ chiral expansion led to very significant NLO contributions (of order 50%) when data up to the kaon mass scale was included, and they conclude that higher-order corrections could be very significant (up to 30%). Let us remark that the inclusion of NNLO terms for $K_{\ell 3}$ form factors and F_K/F_π to fits of the RBC/UKQCD data seems to solve convergence issues for these particular quantities assuming no Zweig-rule violation in the scalar sector [269]: a good χ^2 is obtained with a rather good convergence of the chiral series with NNLO terms of the expected size (ref. [269] did not discuss the extrapolation of F_π itself).

A particular attention was paid in ref. [209] to the structure of the chiral expansion of $f_+(0) = 1 + f_2 + f_4$, where f_2 is the NLO contribution, which involves only a combination of chiral logarithms *divided by* F_0^2:

$$f_2 = -\frac{3}{256\pi^2 F_0^2}\left[(M_K^2 + M_\pi^2)\, h\!\left(\frac{M_\pi^2}{M_K^2}\right) + (M_K^2 + M_\eta^2)\, h\!\left(\frac{M_\eta^2}{M_K^2}\right)\right], \qquad h(x) = 1 + \frac{2x}{1-x^2}\log x\,. \tag{5.68}$$

f_2 is often said to be free from LECs and thus known precisely from Chiral Perturbation Theory. This statement is not totally correct for the following reasons. One usually assumes that the value of F_0 is close to that of F_π, so that it can be replaced in actual calculations by the physical value of the pion decay constant leading to the estimate $f_2 \simeq -0.023$. Since the difference between the two quantities is a higher-order effect, one can always perform this replacement.

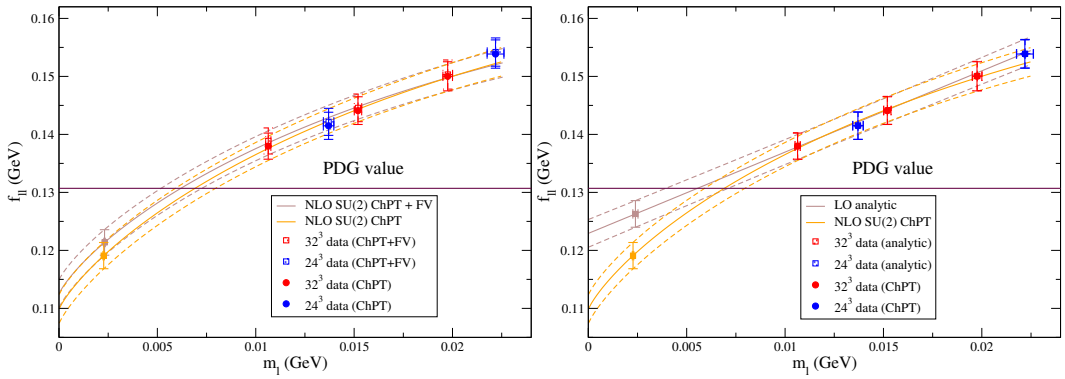

Figure 5.1: *Unitary data for F_π adjusted to the continuum limit using each of the fit ansätze. The horizontal solid line indicates the PDG value $F_\pi = 130.4$ MeV [i.e., $F_\pi = 92.2$ with our normalisation, differing by a factor $\sqrt{2}$ from the one used for these plots]. The left panel compares the infinite-volume and finite-volume forms of the NLO $N_f = 2$ fit (showing that finite-volume effects are not responsible for this discrepancy), while the right panel compares the analytic fit to the infinite-volume NLO $N_f = 2$ fit. Taken from ref. [194].*

However, one has to determine how large the NNLO term f_4 can be with such a prescription, and consequently how well the chiral series for f_+ converges. If F_0 is significantly lower than F_π, the convergence is expected to be rather slow, forcing us to treat the NLO contribution to $f_+(0)$ more carefully. The MILC collaboration has faced similar discussions on which decay constant should be chosen for NLO fits of the pseudoscalar spectrum, concluding that F_0 was not an appropriate choice due to its smallness [205]. In the present chapter, we advocated that correlators of vector and axial currents yields observables with good convergence properties, selecting $F_\pi F_K f_0(0)$. In the case of $K_{\ell 3}$, we should replace F_0^2 by $F_\pi F_K$ in the evaluation of eq. (5.68), as can be checked in our expression for f_+, eq. (5.38). Our procedure provides a prescription to determine the appropriate combination of decay constants to be used for NLO chiral formulae.

5.6.4 Update of RBC/UKQCD results

Since the publication of ref. [41], new data from RBC/UKQCD have been issued with a new volume and different quark masses [194] (see app. A.3.3). Our approach is however unlikely to solve the problems caused by the observed linearity of F_π as a function of $m_{u,d}$, see fig. 5.1, which contradicts the expected curvature due to chiral logarithms in $N_f = 2$ χPT. One could in principle imagine to decrease the size of $B(2) = \Sigma(2)/F^2(2)$ that governs the two-flavour chiral logarithms, so that the chiral behaviour of F_π at small $\tilde{m}_{u,d}$ would mimic a straight line. However this would require a value of r close to its lower bound (see figs. 3.8 and 3.9) in contradiction with the rest of the RBC/UKQCD data, as well as with the experimental evidence gathered on $\pi\pi$ scattering (to be detailed in ch. 6).

Indeed, if we perform a fit to the RBC/UKQCD data previously considered in the $24^3 \times 64$ ($a^{-1} = 1.78(3)$ GeV) and adding the values of pseudoscalar and masses obtained in the $32^3 \times 64$ volume ($a^{-1} = 2.28(3)$ GeV), we obtain a rather poor fit of χ^2/d.o.f.=40.6/19, corresponding to a 3.0 σ discrepancy. The poor fit is due to the tension between the lattice data for F_π, the curvature required in $N_f = 2$ χPT and the physical value of F_π. If the value of F_π is let free, one obtains a good fit (χ^2/d.o.f.=17.4/18) but for a very low value of $F_\pi = 84.2 \pm 0.1$ MeV, in

	RBC/UKQCD Constrained a	RBC/UKQCD Free a
r	23.6 ± 0.8	25.8 ± 0.8
$X(3)$	0.37 ± 0.06	0.33 ± 0.04
$Y(3)$	0.63 ± 0.11	0.86 ± 0.13
$Z(3)$	0.58 ± 0.04	0.38 ± 0.07
F_K/F_π	1.17 ± 0.01	1.22 ± 0.02
Rem. at limit	d, e	d, e, e_V^π
$\tilde{m}_{s,ref}/m_s$	1.20 ± 0.04	1.52 ± 0.04
$a^{-1}[(24)^3]/[1.73\text{ GeV}]$	1.02 ± 0.09	1.09 ± 0.01
$a^{-1}[(32)^3]/[2.28\text{ GeV}]$	1.02 ± 0.09	1.10 ± 0.01
$m_s(2\text{ GeV})[\text{MeV}]$	91.2 ± 3.0	72.2 ± 1.8
$m(2\text{ GeV})[\text{MeV}]$	3.9 ± 0.2	2.8 ± 0.1
$B_0(2\text{ GeV})[\text{GeV}]$	1.58 ± 0.34	3.00 ± 0.51
$F_0[\text{MeV}]$	70.5 ± 2.3	57.1 ± 5.2
$L_4(\mu) \cdot 10^3$	1.1 ± 0.3	1.0 ± 0.2
$L_5(\mu) \cdot 10^3$	1.7 ± 0.4	1.7 ± 0.2
$L_6(\mu) \cdot 10^3$	1.6 ± 0.8	0.7 ± 0.3
$L_8(\mu) \cdot 10^3$	2.2 ± 1.0	1.0 ± 0.4
$L_9(\mu) \cdot 10^3$	4.8 ± 2.4	6.4 ± 2.8
F_π^2	$0.58 + 0.56 - 0.14$	$0.38 + 0.72 - 0.10$
F_K^2	$0.42 + 0.68 - 0.10$	$0.26 + 0.81 - 0.07$
$F_\pi^2 M_\pi^2$	$0.37 + 0.78 - 0.15$	$0.33 + 0.82 - 0.15$
$F_K^2 M_K^2$	$0.26 + 0.85 - 0.11$	$0.24 + 0.87 - 0.11$
$F_\pi F_K f_+(0)$	$0.50 + 0.64 - 0.14$	$0.32 + 0.79 - 0.11$
χ^2/N	31.3/19	17.3/17

Table 5.4: *Results of fits performed on the data from the RBC/UKQCD [194, 207–209] collaborations on pseudoscalar masses and decay constants, as well as $K_{\ell 3}$ form factors, for volumes of $24^3 \times 64$ ($a^{-1} = 1.78(3)$ GeV) and $32^3 \times 64$ ($a^{-1} = 2.28(3)$ GeV). In all cases, we considered only data with light pions and only statistical errors are shown. The LECs are given at the scale $\mu = m_\rho$. The penultimate set of rows collects the relative fractions of LO/NLO/remainders for decay constants, masses and $K_{\ell 3}$ form factor at vanishing transfer momentum at the minimum.*

agreement with the observations made in ref. [194] using $N_f = 2$ chiral extrapolations.

At this stage, we do not perform better than NLO χPT since the problem seems rooted in a question (the $m_{u,d}$-dependence of F_π) related to the $N_f = 2$ pattern of chiral symmetry breaking. But one should also note another underlying issue, i.e., the determination of the lattice spacing in ref. [194] which is performed at the same time as that of the quark masses through a fit to the π, K and Ω masses, using either $N_f = 3$ NLO χPT or an analytic ansatz.

	RBC/UKQCD Constrained a	RBC/UKQCD Free a
$X(2)$	0.90 ± 0.01	0.89 ± 0.01
$Y(2)$	1.00 ± 0.01	1.03 ± 0.01
$Z(2)$	0.90 ± 0.01	0.87 ± 0.02
$B(2\text{ GeV})$[GeV]	2.52 ± 0.14	3.58 ± 0.12
F[MeV]	87.3 ± 0.4	85.8 ± 0.8
$\bar{\ell}_3$	0.6 ± 1.3	3.9 ± 1.1
$\bar{\ell}_4$	3.5 ± 0.3	4.5 ± 0.5
Σ/Σ_0	2.44 ± 0.40	2.69 ± 0.34
B/B_0	1.59 ± 0.27	1.19 ± 0.18
F/F_0	1.24 ± 0.04	1.50 ± 0.13
$f_+(0)$	0.987 ± 0.006	0.989 ± 0.004
$\Delta_{CT} \cdot 10^3$	1.8 ± 10.7	1.8 ± 10.2
$\Delta'_{CT} \cdot 10^3$	-86.2 ± 95.5	-74.9 ± 96.3
$\langle r^2\rangle_V^{K^+}$[fm^2]	0.237 ± 0.139	0.263 ± 0.140
$\langle r^2\rangle_V^{K^0}$[fm^2]	-0.026 ± 0.101	-0.026 ± 0.094

Table 5.5: *Results of fits performed on the data from the RBC/UKQCD [194, 207–209] collaborations on pseudoscalar masses and decay constants, as well as $K_{\ell 3}$ form factors, for volumes of $24^3 \times 64$ ($a^{-1} = 1.78(3)$ GeV) and $32^3 \times 64$ ($a^{-1} = 2.28(3)$ GeV). In all cases, we considered only data with light pions and only statistical errors are shown.*

Both methods yield almost identical answers for the lattice spacing, but it might be interesting to consider the impact of additional (yet undetected) systematics.

We can allow the lattice spacings a for the two volumes $24^3 \times 64$ and $32^3 \times 64$ to differ from their central values (either adding a χ^2 built from the uncertainties quoted in ref. [194] or letting them free within a 10% range), to obtain the results quoted in tabs. 5.4 and 5.5. We see that the quality of the fits improves significantly, suggesting a systematic shift of the lattice spacing by a few % in the same direction for both volumes would be able to restore the agreement between the lattice data and the measured value of F_π in our framework. In the case where the two lattice spacings are left free, some quantities acquire larger error bars, but it is interesting to notice that there is no obvious problem with some of the quantities (we recall that these fits are built so that $F_\pi = 92.2$ MeV at the physical point). With this idea in mind, it might prove interesting to perform the determination of a, m, m_s following the same method as the one presented in ref. [194], using the present ReχPT formulae to determine if there are differences in the estimates of these parameters.

5.7 Summary

In the previous chapters, we have discussed the possibility of a numerical competition in chiral series between leading-order contributions – from the decay constant and/or the condensate in

the $N_f = 3$ chiral limit ($m_u = m_d = m_s = 0$) – and next-to-leading-order contributions – in particular from L_4 and L_6, related to the Zweig-rule violation in the scalar sector, enhanced by m_s and not accurately known. If there is such a competition, one must decide which observables are expected to have a good overall convergence (small higher-order contributions). According to the assumed equivalence of the χPT and QCD generating functionals at low energies, it seems reasonable to consider observables derived from correlators of axial and vector currents as well as pseudoscalar and scalar densities, as done here. For these observables, one must treat chiral series with a particular care, avoiding the perturbative reexpression of LECs in terms of observables while neglecting higher orders (this can be done by introducing remainders corresponding to NNLO and higher contributions) and choosing how unitarity contributions should be treated to define the structure of the chiral expansion and its splitting into leading, next-to-leading and higher-order terms. Such a set of prescriptions was introduced some time ago under the name of Resummed Chiral Perturbation Theory. We have applied this approach to observables related to pseudoscalar masses, decay constants, and kaon and pion form factors (electromagnetic and $K_{\ell 3}$ ones). This allows us to illustrate how $O(p^4)$ LECs $L_{4,5,6,8,9}$ can be reexpressed in terms of the leading-order quantities $X(3), Z(3), r$ as well as experimental values of observables (pion and kaon decay constants and masses, square electromagnetic radius of the pion) and associated remainders.

Then we have turned to 2+1 lattice simulations where these observables were obtained for several sets of quark masses: PACS-CS (decay constants and masses only) [127] and RBC/UKQCD (decay constants, masses, $K_{\ell 3}$ form factors) [207–209]. We performed fits to data corresponding only to light quark masses and small momenta, but checked the stability of our procedure by considering also fits to all data available (unitary points). Since only statistical uncertainties (without correlations) are available for each of the points, we performed naive fits with Gaussian errors, in order to determine the leading-order parameters of the chiral Lagrangian as well as higher-order remainders and the ratio of decay constants. The obtained fits were of good quality, favouring a suppression of LO contributions compared to NLO ones in the chiral series. At this point, we should emphasize that our framework does not contain any bias concerning the size of $X(3)$, $Y(3)$ and $Z(3)$ or on the relative size of the LO and NLO contributions. It is compatible with the usual assumptions that chiral series of decay constants, squared masses... are saturated by their LO contribution, but it can also accommodate situations where there is a numerical competition between LO and NLO terms. The interesting point here is that the same low-energy constants are involved for the physical quantities and those simulated on the lattice for different quark masses: one can thus exploit the previous discussions, and incorporate information on the physical values of the observables in the fit to reexpress the NLO LECs exactly as before.

It turns out that the lattice data set from the RBC/UKQCD and PACS-CS collaborations favour values for the three quantities $X(3), Y(3), Z(3)$ smaller than 1, with a χ^2/d.o.f. which ranges from fairly good to excellent. Our results confirm the difficulties reported by the two collaborations to fit $N_f = 3$ NLO chiral expressions when a saturation by LO is assumed, and highlights the improvement provided by our ReχPT formulae for the extrapolations in quark masses of these quantities. Our fits are generally of a good quality. This allows one to determine the values of the LO quantities as well as the higher-order remainders, with a good accuracy in the case of PACS-CS, with a more limited precision for RBC/UKQCD because of the restricted number of low-mass points. One observes that the decay constant and the quark condensate in the $N_f = 3$ limit ($m_u = m_d = m_s = 0$) are both small and suppressed compared to the $N_f = 2$ case ($m_u = m_d = 0$ and m_s physical), and the low-energy constants L_4 and L_6 do not follow the Zweig rule suppression generally advocated to set them to zero. On the

other hand, the other low-energy constants L_5, L_8 and L_9 have values in good agreement with previous estimates.

The ratio of quark masses r remains quite close to the most simple estimate from pseudoscalar masses, and $N_f = 2$ chiral order parameters are in good agreement with the values extracted from $K_{\ell 4}$ decays (see next chapter). When the sets of data are large enough, the higher-order remainders remain in the expected range from a naive dimensional estimate, whereas the expected numerical competition between LO and NLO chiral expansions indeed occurs for F_π^2, F_K^2, $F_\pi^2 M_\pi^2$ and $F_K^2 M_K^2$. Beyond this description of the pattern of $N_f = 3$ chiral symmetry breaking and its implication for the convergence of chiral expansions, we can also make a few predictions. The values obtained for the kaon electromagnetic radii are in good agreement with experimental data. In the case of RBC/UKQCD, the value obtained for $f_+(0)$ with our fits is slightly larger than the ones quoted by the collaboration, relying on different formulae for the chiral expansion of the $K_{\ell 3}$ form factors. This issue has naturally an impact on the determination of $|V_{us}|$, considering the level of accuracy achieved in $K_{\ell 3}$ decays [223].

We have also briefly discussed new results from the RBC/UKQCD collaborations with a new volume and lattice spacing [194], where the $m_{u,d}$-dependence of the decay constant F_π was indicated not to follow the curvature expected from $N_f = 2$ χPT. We confirmed the presence of this problem, which cannot be solved directly within our framework. We have however discussed the impact of a systematic effect in the determination of the lattice spacing(s). It seems that a good fit of masses, decay constants and $K_{\ell 3}$ form factors can be achieved with a moderate (a few %) shift of the values of the lattice spacings in the same direction.

After this discussion on lattice indications for the pattern of chiral symmetry breaking, confirming the suppression of three-flavour chiral order parameters already hinted at by our dispersive estimates of $\langle 0|(\bar{u}u)(\bar{s}s)|0\rangle$, we will turn to the comparison of $\pi\pi$ and πK scatterings from the analysis of experimental data.

Sentence first – verdict afterwards.

The Queen

6

$\pi\pi$ scattering: experimental and dispersive constraints

As a first step in our comparison of the patterns of $N_f = 2$ and $N_f = 3$ chiral symmetry breaking, we focus on the two-flavour chiral limit where $m_u = m_d = 0$ but m_s is kept at its physical value. The degrees of freedom of $N_f = 2$ Chiral Perturbation Theory (χPT) are restricted to pions, and thus the main test/source of information comes from $\pi\pi$ scattering. Experimentally, one can access this amplitude via two main ways, i.e., production experiments of the form $\pi N \to \pi\pi N$ choosing the transferred momentum to be close to the pion pole, and rescattering effects in form factors or decay amplitudes involving two-pion states. In both cases, the low partial waves (S and P waves) dominate completely the low-energy $\pi\pi$ dynamics.

For a long time, $\pi\pi$ scattering remained rather poorly known, with very limited information from $\pi N \to \pi\pi N$ data as well as the so-called Geneva-Saclay experiment [270]. In recent years, our knowledge of low-energy pion-pion scattering has improved in a very significant way and in several respects. Firstly, the high precision K^+_{e4} experiments performed at the BNL AGS by the E865 experiment [271, 272] and, more recently, by the NA48/2 collaboration [273, 274] at the CERN SPS, have provided very accurate determinations of the difference $\delta^0_0 - \delta^1_1$ of the pion-pion phase shifts in the S and P waves in the energy range between threshold and the kaon mass. Next, one should mention the measurement of the invariant mass distribution in $K^\pm \to \pi^\pm\pi^0\pi^0$ decays [275, 276], that gives information on the S-wave $\pi\pi$ scattering lengths [277] (see also [278–280]). Finally, forthcoming analyses of the data collected by the NA48/2 experiment on the K^+_{e4} decay channel into a pair of neutral pions (for a preliminary report, see ref. [281]), or on the $K^0_L \to \pi^0\pi^0\pi^0$ decay mode [282], together with the measurement of the pionium lifetime by the DIRAC collaboration [283,284], should provide additional information, and might sharpen the picture even more. In the meantime, the accuracy obtained on $K_{\ell 4}$ decays from NA48/2 implies that these data clearly drive the current determination of the difference between the S- and P-wave phase shifts at low energies.

$K_{\ell 4}$ data can be analyzed using a parametric representation of the solution of Roy equations written in the isospin limit for the $\pi\pi$ phase shifts δ^I_ℓ (where I and ℓ denote the isospin and angular momentum of the pion pair). A set of dispersion relations derived by Roy [251, 285] allows one to relate the phase shifts δ^0_0, δ^1_1 and δ^2_0 in the region $4M^2_\pi \leq s \leq s_0$ (with $\sqrt{s_0} \sim$ 0.8 GeV) to data at intermediate energies ($\sqrt{s_0} \leq \sqrt{s} \leq 2$ GeV) and to two subtraction constants. The latter can be identified with the two S-wave scattering lengths a^0_0 and a^2_0, which provide a particularly stringent test of two-flavour chiral perturbation theory [20, 42, 286]. We will recall the discussion that occurred at the time where the E865 data appeared, as the data themselves were not precise enough to constrain both S-wave scattering lengths and additional experimental information/theoretical constraints were needed to extract reasonably accurate information on the pattern of two-flavour chiral symmetry breaking. Mild differences (at the $1 - \sigma$ level) arose between the different determinations, which can be translated in slightly different values of the two-flavour leading-order (LO) parameters and the related next-to-leading-order (NLO) low-energy counterterms (LECs).

The recent experiments made it mandatory to take isospin violations into account in order to extract relevant information on low-energy pion-pion scattering from the above processes. This is quite easy to understand in the case of the $K^\pm \to \pi^\pm\pi^0\pi^0$ decay, where one exploits the presence of a unitarity cusp in the invariant $\pi^0\pi^0$ mass distribution, which occurs only if the masses of the charged and neutral pions differ [277]. Perhaps somewhat more unexpectedly, isospin-violating corrections proved also of importance [287] in the analysis of the K^+_{e4} data, in order to account for the high precision reached by the recent NA48/2 experiment, and to make contact with theory [288, 289]. Indeed, we will show that the analysis of the NA48/2 data lead to surprising results if one does include the corrections related to isospin breaking.

A NLO computation of isospin corrections is available [287], but it is performed in the

framework of χPT, and thus is strictly valid only in a limited range of (a_0^0, a_0^2). In this chapter, we will also propose an alternative treatment of this problem, starting from a dispersive and iterative reconstruction of the K_{e4}^+ decay amplitude in order to isolate the contribution due to $\pi\pi$ and πK rescatterings in the isospin-breaking corrections. We can then express these contributions in terms of the S-wave scattering lengths (a_0^0, a_0^2), even for values that are very different from those predicted by χPT. The estimate obtained, even though similar in size to ref. [287], has a slightly different dependence on the energy. Once applied to the NA48/2 data, one observes that the determinations of the two S-wave scattering lengths according to the different experimental/theoretical constraints get in a better agreement with each other and with the expectations of χPT. This yields the conclusion that the two-flavour order parameters (quark condensate and pseudoscalar decay constant) almost saturate the two-flavour chiral series. [1]

6.1 Dispersive constraints on low-energy $\pi\pi$ scattering

6.1.1 Roy equations

We recall elements of the analysis of Roy equations made in ref. [251], and we consider elastic $\pi\pi$ scattering in the isospin symmetry limit, where the masses of the up and down quarks are taken equal and the electromagnetic interaction is ignored[2]. In this case, the scattering process is described by a single Lorentz invariant amplitude $A(s,t,u)$:

$$\langle \pi^d(p_4)\pi^c(p_3)\,\mathrm{out}|\pi^a(p_1)\pi^b(p_2)\,\mathrm{in}\rangle = \delta_{fi} + (2\pi)^4 i\,\delta^4(P_f - P_i) \times\{\delta^{ab}\delta^{cd}A(s,t,u) + \delta^{ac}\delta^{bd}A(t,u,s) + \delta^{ad}\delta^{bc}A(u,s,t)\}\,. \tag{6.1}$$

The amplitude A depends on the Mandelstam variables s, t, u with $s+t+u = 4M_\pi^2$, and is crossing symmetric: $A(s,t,u) = A(s,u,t)$. The s-channel isospin components of the amplitude are given by:

$$T^0(s,t) = 3A(s,t,u) + A(t,u,s) + A(u,s,t)\,, \tag{6.2}$$

$$T^1(s,t) = A(t,u,s) - A(u,s,t)\,, \qquad T^2(s,t) = A(t,u,s) + A(u,s,t)\,. \tag{6.3}$$

The partial-wave decomposition reads:

$$T^I(s,t) = 32\,\pi \sum_\ell (2\ell+1)\,P_\ell\left(1 + \frac{2t}{s-4M_\pi^2}\right) t_\ell^I(s)\,,$$

$$t_\ell^I(s) = \frac{1}{2i\sigma(s)}\left\{\eta_\ell^I(s)\,e^{2i\delta_\ell^I(s)} - 1\right\}\,. \qquad \sigma(s) = \sqrt{1 - \frac{4M_\pi^2}{s}}\,.$$

The threshold parameters are the coefficients of the expansion in q^2 (with $s = 4(M_\pi^2 + q^2)$): $\mathrm{Re}\,t_\ell^I(s) = q^{2\ell}\{a_\ell^I + q^2\,b_\ell^I + q^4\,c_\ell^I + \ldots\}$. The isospin amplitudes $\vec{T} = (T^0, T^1, T^2)$ obey fixed-t

[1] This chapter is based on the following articles:

[I] SDG, N. Fuchs, L. Girlanda, and J. Stern, Analysis and interpretation of new low-energy $\pi\pi$ scattering data, Eur. Phys. J. C24 (2002) 469 [42]

[J] SDG, M. Knecht, V. Bernard, in preparation [43]

[2] In our numerical work, we identify the value of M_π with the mass of the charged pion, in agreement with our definition of the isospin limit $M_{\pi^0} \to M_{\pi^\pm}$. We will thus omit the superscript $\pm$, unless absolutely necessary, in the rest of this chapter.

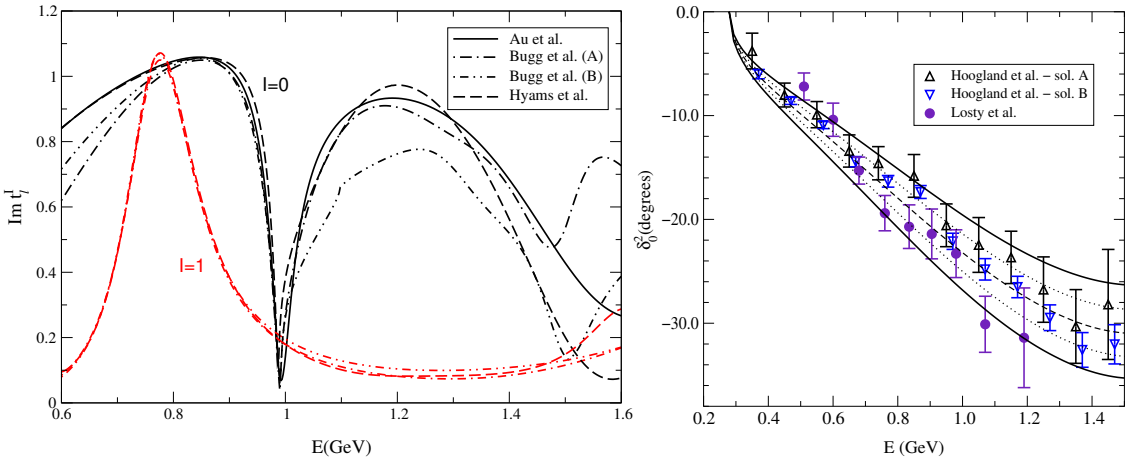

Figure 6.1: *Inputs for the Roy equation analysis of low-energy $\pi\pi$ scattering amplitude for $I = \ell = 0, 1$ (left) and $I = 2, \ell = 0$ (right). Taken from ref. [251].*

dispersion relations, valid in the interval $-28M_\pi^2 < t < 4M_\pi^2$ [290] with subtraction terms chosen to be the two S-wave scattering lengths: $\vec{T}(4M_\pi^2, 0) = 32\,\pi\,(a_0^0, 0, a_0^2)$. Performing the partial wave projections of these fixed-t dispersion relations, one obtains Roy's representation [285] for the partial wave amplitudes t_l^I:

$$t_\ell^I(s) = k_\ell^I(s) + \sum_{I'=0}^{2} \sum_{\ell'=0}^{\infty} \int_{4M_\pi^2}^{\infty} ds'\, K_{\ell\ell'}^{II'}(s, s')\, \mathrm{Im}\, t_{\ell'}^{I'}(s')\,, \tag{6.4}$$

where I and ℓ denote isospin and angular momentum, respectively and $k_\ell^I(s)$ is the partial wave projection of the subtraction term, arising only in the S- and P-waves:

$$k_\ell^I(s) = a_0^I\,\delta_\ell^0 + \frac{s - 4M_\pi^2}{4M_\pi^2}\,(2a_0^0 - 5a_0^2)\left(\frac{1}{3}\,\delta_0^I\,\delta_\ell^0 + \frac{1}{18}\,\delta_1^I\,\delta_\ell^1 - \frac{1}{6}\,\delta_2^I\,\delta_\ell^0\right). \tag{6.5}$$

The kernels $K_{\ell\ell'}^{II'}(s, s')$ are explicitly known functions which contain a diagonal, singular Cauchy kernel that generates the right hand cut in the partial wave amplitudes, as well as a logarithmically singular piece that accounts for the left-hand cut. The validity of these equations has been established on the interval $-4M_\pi^2 < s < 60M_\pi^2$ [251].

The relations (6.4) are consequences of the analyticity properties of the $\pi\pi$ scattering amplitude, of the Froissart bound and of crossing symmetry. Combined with unitarity, the Roy equations amount to an infinite system of coupled, singular integral equations for the phase shifts. One can actually use these constraints to determine the low-energy behaviour of the amplitudes close to threshold, as was shown in detail in ref. [251]. For small values of s and t, the scattering amplitude $\vec{T}(s, t)$ is dominated by the contributions from the subtraction constants and from the low-energy part of the dispersion integral over the imaginary parts of the S- and P-waves. One can thus split the integration in several parts:

- In the low-energy interval $4M_\pi^2 < s' < s_0$, S and P waves are dominant and their value will be the object of the analysis of the Roy equations. s_0 is called the matching point which is chosen appropriately in the range of validity of the Roy equations.
- In the intermediate-energy regime $s_0 < s' < s_2$, the currently available data is exploited. This is the essential experimental input to the analysis.

- In the high-energy region $s' > s_2$, an asymptotic parametrisation based on Regge theory [291] can be used, but the resulting background amplitude is very small.

The Roy equations for the S- and P-waves can then be recast under the form:

$$\begin{aligned}\mathrm{Re}\, t_\ell^I(s) = k_\ell^I(s) &+ \int\!\!\!\!\!\!-_{4M_\pi^2}^{s_0} ds' K_{\ell 0}^{I\,0}(s,s')\,\mathrm{Im}\, t_0^0(s') + \int\!\!\!\!\!\!-_{4M_\pi^2}^{s_0} ds' K_{\ell 1}^{I\,1}(s,s')\,\mathrm{Im}\, t_1^1(s') \\ &+ \int\!\!\!\!\!\!-_{4M_\pi^2}^{s_0} ds' K_{\ell 0}^{I\,2}(s,s')\,\mathrm{Im}\, t_0^2(s') + f_\ell^I(s) + d_\ell^I(s) \quad , \end{aligned} \tag{6.6}$$

where I and ℓ take only the values (I,ℓ) =(0,0), (1,1) and (2,0). The bar across the integral sign denotes the principal value integral. The functions $f_\ell^I(s)$ contain the part of the dispersive integrals over the three lowest partial waves that comes from the region between s_0 and s_2, where experimental data is used as input. The driving terms $d_\ell^I(s)$ account for the contributions that stem from the imaginary parts of the waves with $\ell = 2, 3, \ldots$ and those due to the imaginary parts of the S- and P-waves above s_2.

The two S-wave scattering lengths, the elasticity parameters below the matching point [3] and the imaginary parts above that point are treated as an external input. The mathematical problem consists in solving Roy integral equations for the region between $4M_\pi^2 < s < s_0$ with this input, determining $t_\ell^I(s)_{SP}$ from $d_\ell^I(s)$. The Roy equations yield a boundary value problem, and thus it is not surprising that the values of the phases at the matching point s_0 play an important role. In general, the Roy equations admit several solutions, depending on the values (modulo $\pi/2$) of the phases at the matching points. The solution does become unique if the value of s_0 is chosen between the ρ mass and the energy where the $I = 0$ S-wave phase passes through $\pi/2$ – this happens around 0.86 GeV. This explains the choices of the matching point and the start of the asymptotic regime made in ref. [251]:

$$\sqrt{s_0} = 0.8\,\mathrm{GeV}\,, \qquad \sqrt{s_2} = 2\,\mathrm{GeV}\,. \tag{6.7}$$

A further physical requirement beyond the mathematical uniqueness is the smoothness of the solutions, i.e., the absence of cusps at the matching point. This condition turns out to be rather stringent for the P-wave, but not for the S waves. This allows one to determine a_0^2 as a function of a_0^0, in principle in an unambiguous way.

The inputs used at intermediate energies in the $I = 0, 1$ channels came from $\pi N \to \pi\pi N$ experiments [247, 292–294], adopting the representation of ref. [247] for the S wave and that of ref. [293] for the P wave, as recalled in fig. 6.1. Unfortunately, the situation is not as good in the exotic $I = 2$ channel, where there is a large scatter of the data. In such a situation, solutions of the Roy equations with different choices of the $I = 2$ input were considered. This uncertainty is responsible for the so-called Universal Band, which corresponds to the region where a_0^0 and a_0^2 are constrained to lie for the solutions of the Roy equations to *a)* exhibit no cusp in the three lowest partial waves at the matching point and *b)* be in agreement with a reasonable choice for the $I = 2$ input. Several requirements were used to restrict the range of acceptable values for the scattering lengths, requiring the consistency between inputs and solutions above the matching point and using the Olson sum rule relating $2a_0^0 - 5a_0^2$ to a slowly convergent integral over imaginary part of T^0, T^1 and T^2, as well as the available information on the phase shifts at that time.

[3] The only inelastic channel below the matching point chosen comes from the 4π channel, strongly suppressed at low energies, so that all 3 channels $(I,\ell) = (0,0), (1,1), (2,0)$ are assumed to have no inelasticity below s_0.

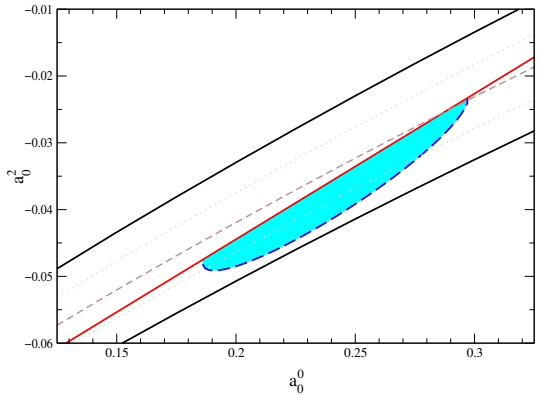

Figure 6.2: *Restriction on the values of the scattering lengths from the Universal Band (in black), the Olson sum rule (in red) and the $\pi\pi$ phase shifts known in year 2000 (in blue). Taken from ref. [251].*

Ref. [251] proposed solutions of the Roy equations, for energies below 800 MeV, expressed as:

$$\tan\delta_\ell^I(s) = \sqrt{1-\frac{4M_\pi^2}{s}}q^{2\ell}\left\{A_\ell^I + B_\ell^I q^2 + C_\ell^I q^4 + D_\ell^I q^6\right\}\left(\frac{4M_\pi^2 - s_\ell^I}{s - s_\ell^I}\right). \tag{6.8}$$

The dependence on a_0^0 and a_0^2 of the Schenk parameters $X = A, B, C, D$ in eq. (6.8) is well approximated by:

$$X_\ell^I = z_1 + z_2 u + z_3 v + z_4 u^2 + z_5 v^2 + z_6 uv + z_7 u^3 + z_8 u^2 v + z_9 uv^2 + z_{10} v^3\,, \tag{6.9}$$

where:

$$u = \frac{a_0^0}{p_0} - 1\,, \quad v = \frac{a_0^2}{p_2} - 1\,, \quad p_0 = 0.225\,, \quad p_2 = -0.03706\,, \tag{6.10}$$

and the values of the coefficients z_i are tabulated in ref. [251].

6.1.2 Alternative and extended treatments of Roy equations [I]

After the publication of ref. [251], there was a controversy concerning the experimental inputs used for the Roy equations. Ref. [295] criticised the inputs for the Regge model used for the region $\sqrt{s} \geq 1.4$ GeV, considering the choice of parameters as unconventional, in particular concerning the Pomeron exchange. The authors proposed a different model for this region, and considered several slowly-convergent sum rules exhibiting a sensitivity to the high-energy region. Dismissing the solutions of the Roy equations eq. (6.8) as spurious and not physical, the authors of ref. [295] proposed alternative parametrisations of the $\pi\pi$ phase shifts at low energies, leading to rather different values for the S-wave scattering lengths. In ref. [296], these claims were reexamined: using different inputs for the high-energy tail led to very little impact on the solutions of the Roy equations at low energies, which is not surprising as the Roy equations have enough subtractions to be dominated by the low-energy region. Moreover, the alternative input proposed in ref. [295] for the high energy region was shown to violate crossing symmetry, leading to inconsistencies in the slowly-convergent sum rules. More refined descriptions of the Regge asymptotics were considered in ref. [297].

Several features of the data in the intermediate region and of their impact on the analysis of the $\pi\pi$ scattering amplitude were discussed in refs. [298–300]. It turned out that the main

difference of these articles with respect to ref. [251] came from the region between 0.5 GeV and the $K\bar{K}$ threshold for the $I = \ell = 0$ partial wave. This led the authors of refs. [298–300] to criticise the rather narrow range of values taken for the phase shifts in the $I = 0$ S-wave at the matching point taken in ref. [251] ($82.3^\circ \pm 3.4^\circ$), which was considered as bearing too optimistic an error. On the other hand, in ref. [288], it was pointed out that these analyses included an input on the phase difference $\delta_0^0(M_K^2) - \delta_0^2(M_K^2)$ from $K \to 2\pi$ [178] which seemed difficult to reconcile with the rest of the available data. A reanalysis of this input in ref. [179] highlighted that this estimate suffers from significant theoretical uncertainties, as it involves assumptions on the structure of isospin-breaking effects as well as the NLO chiral expressions of the phase shifts. An alternative procedure for the determination (involving only estimates of the isospin-breaking effects as theoretical inputs) lowered the value of the phase-shift difference:

$$\delta_0^0(M_K^2) - \delta_0^2(M_K^2)\Big|_{K\to\pi\pi} = (60.8 \pm 2.2 \pm 3.1)^\circ \to (52.5 \pm 0.8 \pm 2.8)^\circ\,, \tag{6.11}$$

in good agreement with the analysis of Roy equations: $(47.7 \pm 1.5)^\circ$ (lattice simulations should soon provide more information on this issue [301]). This led to the latest analysis of ref. [302], consisting in taking a parametrisation (based on conformal mapping and respecting analyticity in the low-energy region) and to impose the fulfillment of dispersive constraints similar to Roy equations. The matching point is chosen at a much higher energy (around 1.42 GeV), above which a Regge parametrisation is used. Experimental phase shifts and inelasticities are included up to 1100 MeV. This choice of matching point prevents from providing a closed form for the solutions since there is no unicity of the latter, and the procedure does not make an optimal use of the dispersive constraints. Nevertheless this analysis obtained a very good agreement with the solutions in ref. [251], providing that they did not include the (controversial) input from $K \to \pi\pi$ in their data. For instance, the framework of ref. [302] allowed them to determine the values of the phase shifts at the matching point $\sqrt{s_0} = 0.8$ GeV, obtaining values that agree below 1σ with the ones used in ref. [251]. We will thus consider in the following that the analysis in ref. [251] can be essentially followed as far as low-energy $\pi\pi$ phase shifts are concerned.

The previous discussion should however highlight that it is necessary to discuss the sensitivity of the solutions to the inputs. If the high-energy tail is quite irrelevant for the low-energy solutions, this need not be the case for the intermediate region. Indeed, as explained above, the Roy equations yield a boundary-value problem: the solutions must interpolate between the phase shifts at the threshold, fixed by a_0^0 and a_0^2, and the three phases at the matching point s_0:

$$\theta_0 = \delta_0^0(s_0), \qquad \theta_1 = \delta_1^1(s_0), \qquad \theta_2 = \delta_0^2(s_0), \tag{6.12}$$

determined from data above s_0. As stated in ref. [251], the behaviour of the phases above s_0 is less important than the boundary values, because they only affect the slope and the curvature of the solutions. With the experimental input encountered in practice, the system of Roy equations admits a unique solution provided that the matching point s_0 is carefully chosen (0.78 GeV $\leq \sqrt{s_0} \leq$ 0.86 GeV). Moreover, for given boundary conditions $(a_0^0, \theta_0, \theta_1, \theta_2)$, arbitrary values of a_0^2 generate a strong cusp in the P-wave solution at the matching point s_0. If we require the phases to be smooth, a_0^2 is determined as a function of $(a_0^0, \theta_0, \theta_1, \theta_2)$. Since $\theta_{0,1,2}$ can only vary in their experimental range, this requirement leads to a correlation between a_0^0 and a_0^2, defining the so-called Universal Band (UB) in the (a_0^0, a_0^2) plane. Different choices for $\theta_{0,1,2}$ represent lines in the UB, $a_0^2 = F(a_0^0)$. Inverting the relation between a_0^2 and $(a_0^0, \theta_0, \theta_1, \theta_2)$, we can consider θ_2 as a function of the other parameters. This means the solutions of the Roy equations do depend eventually on $(a_0^0, a_0^2, \theta_0, \theta_1)$ only. The data in the

$I = 0, 1$ channels lead to:

$$\theta_0 = 82.3^\circ \pm 3.4^\circ, \qquad \theta_1 = 108.9^\circ \pm 2^\circ. \tag{6.13}$$

The authors of ref. [251] have provided explicit numerical solutions of the Roy equations for $\theta_0 = 82.0^\circ$ and $\theta_1 = 108.9^\circ$. In ref. [42], we have parametrised the solutions including an explicit dependence on θ_0 and θ_1, by generating solutions (with the same driving terms and experimental input above the matching point s_0) for nine different sets (θ_0, θ_1) and a few tens of (a_0^0, a_0^2) inside the UB. We parametrised our solutions in a similar way to eq. (6.9), with the additional ingredient that for each coefficient z_i, the dependence on the phase shifts at the matching point is parametrised by:

$$z_j = a_j + \delta\theta_0\, b_j + \delta\theta_1\, c_j\,, \qquad \delta\theta_0 = \theta_0 - 82.3^\circ\,, \qquad \delta\theta_1 = \theta_1 - 108.9^\circ\,. \tag{6.14}$$

The parameters s_0^0, s_1^1 and s_0^2 are fixed by the boundary conditions:

$$\delta_0^0(s_0) \equiv \theta_0\ , \qquad \delta_1^1(s_0) \equiv \theta_1\ , \qquad \delta_0^2(s_0) \equiv \theta_2\ , \tag{6.15}$$

where $\theta_2(a_0^0, a_0^2, \theta_0, \theta_1)$ is parametrised following eqs. (6.9) and (6.14). The coefficients a_j, b_j, c_j are collected in App. A.4.1. This parametrisation describes our solutions to better than 0.3° for the $I = 0, 2$, and 0.5° for the $I = 1$ partial waves in the Universal band.

By setting $\theta_0 = 82.0^\circ$ and $\theta_1 = 108.9^\circ$, we can compare with ref. [251]. We obtain slightly different Schenk parameters for the so-called reference point $a_0^0 = 0.225$ and $a_0^2 = -0.0371$, but the phase shifts are identical up to a few tenths of a degree. We obtain the same Universal Band, and only its lower half meets the consistency condition (Roy equations fulfilled in their range of validity $2M_\pi \leq \sqrt{s} \leq \sqrt{s_1} = 1.15$ GeV). In the range of interest for a_0^0, the gap between the parametrisation of ref. [251] and our Roy solutions is at most 0.3° in the $I = 0, 2$ channels and 0.7° in the $I = 1$ channel (for $\sqrt{s} \sim 0.7$ GeV and much smaller near threshold in all the channels).

6.1.3 Dispersive structure of low-energy $\pi\pi$ amplitude

The use of Roy equations allows one to reduce the description of low-energy $\pi\pi$ phase shifts to two subtraction constants, conveniently chosen as the two S-wave scattering lengths. Once the latter are determined from experiment, the whole low-energy $\pi\pi$ amplitude can be reconstructed, whose structure is strongly constrained by chiral symmetry, crossing and unitarity. As was first shown in ref. [303, 304], the amplitude depends on only six parameters up to and including terms of order $(p/\Lambda_H)^6$ in the low-energy expansion. In ref. [305], the amplitude was written as:

$$A_{\rm KMSF}(s|t,u) = A^{\rm cut}(s|t,u) + A^{\rm pol}(s|t,u) + O((p/\Lambda_H)^8)\,, \tag{6.16}$$

$$A^{\rm pol}(s|t,u) = \frac{\beta}{F_\pi^2}\left(s - \frac{4M_\pi^2}{3}\right) + \frac{\alpha}{F_\pi^2}\frac{M_\pi^2}{3} + \frac{\lambda_1}{F_\pi^4}(s-2M_\pi^2)^2 + \frac{\lambda_2}{F_\pi^4}\left[(t-2M_\pi^2)^2 + (u-2M_\pi^2)^2\right]$$
$$+\frac{\lambda_3}{F_\pi^6}(s-2M_\pi^2)^3 + \frac{\lambda_4}{F_\pi^6}\left[(t-2M_\pi^2)^3 + (u-2M_\pi^2)^3\right]\,,$$

$$\frac{1}{32\pi}A^{\rm cut}(s|t,u) = \frac{1}{3}[W_0(s) - W_2(s)] + \frac{1}{2}[3(s-u)W_1(t) + W_2(t)] + \frac{1}{2}[3(s-t)W_1(u) + W_2(u)] \tag{6.17}$$

The six parameters $\alpha, \beta, \lambda_1, \ldots, \lambda_4$ correspond to an expansion of the amplitude in the central region of the Mandelstam triangle, and are therefore called "subthreshold parameters". One can

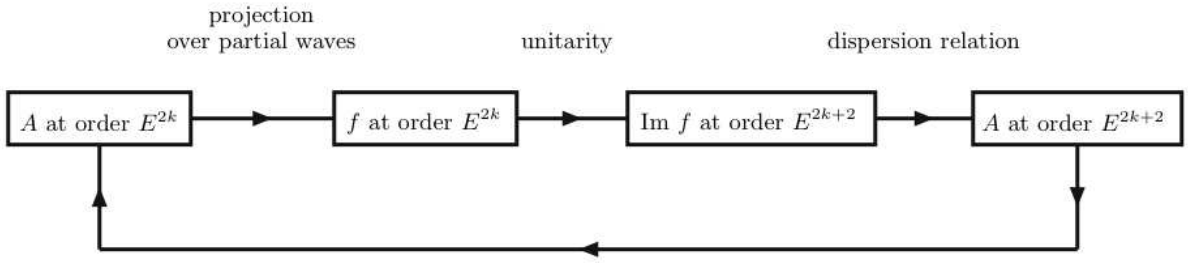

Figure 6.3: *Recursive construction of two-loop representations for the pion form factors and scattering amplitudes in the low-energy regime. One starts with polynomial expressions at order $\mathcal{O}(E^2)$ ($k = 1$ for the $\pi\pi$ amplitudes) and obtains the two-loop representation after two iterations.*

for instance reexpress the lowest order subthreshold parameters α, β to the S-wave scattering lengths up to higher-order corrections:

$$a_0^0 = \frac{M_\pi^2}{96\pi F_\pi^2}(5\alpha + 16\beta)\,, \qquad a_0^2 = \frac{M_\pi^2}{48\pi F_\pi^2}(\alpha - 4\beta)\,. \tag{6.18}$$

$A^{\rm cut}$ combines functions of the Mandelstam variables s, t, u that depend explictly on $\alpha, \beta, \lambda_1, \lambda_2$ and collect the unitarity cuts of the amplitude:

$$\text{Im } W_a(s) = (s - 4M_\pi^2)^{-\varepsilon_a}\text{Im } t_a(s)\theta(s - 4M_\pi^2)\,, \tag{6.19}$$

with $\epsilon_{0,2} = 0$, $\epsilon_1 = 1$, and t_a denote the three lowest partial-wave amplitudes for $\pi\pi$ scattering. This amplitude was constructed iteratively as the general solution of unitarity, analyticity and crossing symmetry up to and including $O(p^6)$, following the method sketched in fig. 6.3 and recalled in more detail in sec. 6.3.4.

A complete χPT calculation [306, 307] confirmed this result, allowing one to relate the six parameters to the quark masses and LECs of the chiral Lagrangian in addition. This last step is essential to translate the experimental information into knowledge of the LECs, which parametrise the chiral structure of the vacuum of QCD. The six parameters introduced in ref. [306, 307], $\bar{b}_1, \ldots, \bar{b}_6$, are dimensionless combinations of LECs in one-to-one (linear) correspondence with $\alpha, \beta, \lambda_1, \ldots, \lambda_4$ of ref. [305], or with $c_1, \ldots, c_6$, subsequently introduced in ref. [308]. Different choices for the set of six subthreshold parameters correspond to different parametrisations of solutions of unitarity, analyticity and crossing symmetry constraints, which are equivalent up to $O(p^6)$ and only differ at $O(p^8)$.

It is possible to match the χPT amplitude to the dispersive representation derived from the solutions of the Roy equations in their common domain of validity. Through the experimental determination of the scattering lengths, one can then obtain the six subthreshold parameters. Such a program was already advocated in ref. [309], leading to rapidly convergent sum rules for the parameters $\lambda_1, \ldots, \lambda_4$. A similar matching procedure (with different subtraction points) has been carried out in ref. [286], matching the dispersive subtraction constants $\bar{p}_{i=1\ldots6}$ and the chiral ones $c_{i=1\ldots6}$. Starting with particular values of a_0^0 and a_0^2, we can use the solutions of the Roy equations to determine the structure of the $\pi\pi$ amplitude at low-energy, compute the subtraction constants $\bar{p}_{i=1\ldots6}$ and reexpress them in terms of the chiral constants $c_{i=1\ldots6}$. App. A and B of ref. [286] can then be used to translate the chiral parameters $c_{i=1\ldots6}$ into α, β and $\lambda_{i=1\ldots4}$ in eq. (6.16), corresponding to a linear combination of these parameters.

6.1.4 The S-wave scattering lengths

The scattering lengths can be determined in principle from different methods. The first one consists in two-flavour χPT, where corrections to Weinberg's result [310]:

$$a_0^0 = \frac{7M_\pi^2}{32\pi F_\pi^2}\,, \qquad a_0^2 = -\frac{M_\pi^2}{16\pi F_\pi^2}\,, \tag{6.20}$$

have been worked out at NLO [249]:

$$a_0^0 = \frac{7M_\pi^2}{32\pi F_\pi^2} + \frac{M_\pi^4}{3072\pi^3 F_\pi^4}[105 + 40\bar{\ell}_1 + 80\bar{\ell}_2 - 15\bar{\ell}_3 + 84\bar{\ell}_4]\,, \tag{6.21}$$

$$a_0^2 = -\frac{M_\pi^2}{16\pi F_\pi^2} + \frac{M_\pi^4}{1536\pi^3 F_\pi^4}[3 + 8\bar{\ell}_1 + 16\bar{\ell}_2 - 3\bar{\ell}_3 - 12\bar{\ell}_4] \tag{6.22}$$

then NNLO [306], with the issue of determining the low-energy constants (LECs) from other observables or from resonance saturation. The results are mainly sensitive to the choice of $\bar{\ell}_3$, which governs the m-dependence of the pion mass at NLO. Taking the NLO inputs described in sec. 3.3.3, and in particular $\bar{\ell}_3 = 2.9$, one obtains the LO, NLO and NNLO results [286]:

$$a_0^0 = 0.159 \to 0.200 \to 0.216\,, \qquad a_2^0 = -0.0454 \to -0.0445 \to -0.0445\,. \tag{6.23}$$

We see that the convergence is somehow slow for a_0^0. This is expected from a quantity defined at threshold, and thus very sensitive to the exact description of the unitarity corrections due to $\pi\pi$ (re)scattering, very significant in the $I = \ell = 0$ channel (and much milder for $I = 2$). In ref. [286], an alternative determination was made, by computing combinations of c_i's equivalent to the coefficients α and β defined in eq. (6.16):

$$a_0^0 = 0.197 \to 0.2195 \to 0.220\,, \qquad a_2^0 = -0.0402 \to -0.0446 \to -0.0444\,. \tag{6.24}$$

One can see that this determination converges much more quickly, since the chiral expansion is performed for quantities defined away from any kinematic singularities.

Another, more recent, avenue is provided by lattice simulations. A direct lattice QCD determination of threshold scattering is difficult for two different reasons. The $I = \ell = 0$ channel involves disconnected diagrams that make lattice computations very costly in terms of computer time, and thus very difficult to tackle (even though such disconnected diagrams start being explored for $K \to 2\pi$ matrix elements [301]), leading lattice collaborations to focus on the $I = 2$, $\ell = 0$ channel. The second difficulty comes from the fact that lattice QCD calculations are performed on an Euclidean lattice. According to the Maiani-Testa theorem, S-matrix elements cannot be determined from lattice calculations of Green functions at infinite volume, except at kinematic thresholds [311]. This difficulty was overcome in refs. [312, 313], where the energy levels of two-particle states at finite volume were shown to encode information on two-meson scattering amplitudes. Indeed, the energy levels of the two interacting particles were found to deviate from those of two non-interacting particles by a quantity depending on the scattering amplitude and inversely on the the lattice spatial volume.

After many attempts in quenched QCD, the first full-QCD calculation of scattering (scattering length and phase shifts) was carried through by the CP-PACS collaboration, which exploited the finite-volume strategy to study $I = 2$ S-wave scattering with two flavours ($N_f = 2$) of improved Wilson fermions [316] with rather large pion masses. This work was followed by

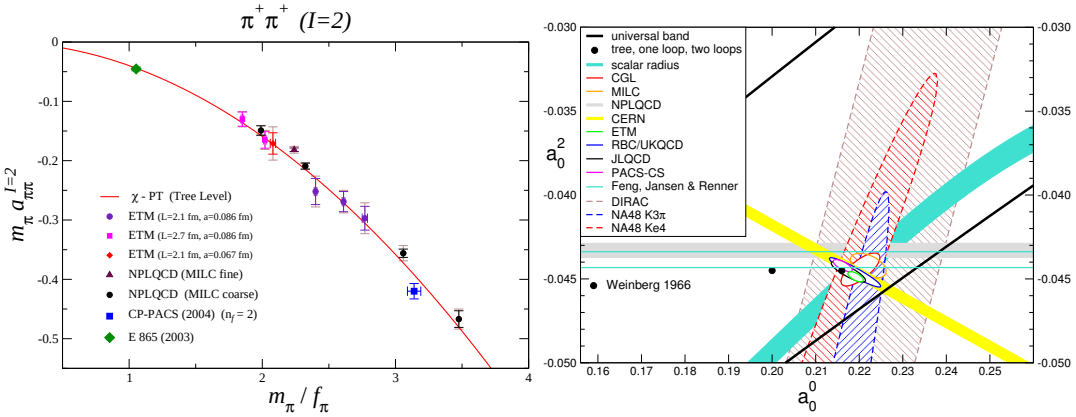

Figure 6.4: *On the left: compilation of lattice results for the $I = 2, \ell = 0$ $\pi\pi$ scattering length as a function of the pion mass, compared to the current algebra prediction (red). Taken from ref. [314]. On the right: compilation of lattice results for the scattering lengths, compared to the constraints of the Roy equations and the predictions of χPT. Taken from ref. [315].*

calculations with $N_f = 2 + 1$ dynamical quarks with mixed actions (domain-wall valence and rooted staggered sea) [317], later updated in ref. [318], leading to the extrapolated value

$$a_0^2 = -0.04330 \pm 0.00042 \text{ [NPLQCD]}\,. \tag{6.25}$$

Another estimation, performed by the ETM collaboration using $N_f = 2$ dynamical quarks with a twisted-mass action, led to:

$$a_0^2 = -0.04385 \pm 0.0028 \pm 0.0038 \text{ [ETM]}\,. \tag{6.26}$$

The results are gathered in fig. 6.4, where all data line up along the LO χPT result, which is quite surprising considering the expected convergence of the corresponding chiral series in eq. (6.23). This coincidence suggests either a fortunate cancellation between NLO chiral logarithms and counterterms, or lattice artefacts still to be understood.

Another possibility offered by lattice simulations consists in exploiting (and trusting) $N_f = 2$ χPT much more, by extracting some of the LECs (in particular $\bar{\ell}_3$ and $\bar{\ell}_4$) from the quark-mass dependence of observables (pion mass and decay constant) and reinjecting this piece of information into the chiral expansion of the scattering lengths. This approach relies much more on the assumed convergence of χPT, and has been followed for instance in ref. [197]. A summary of the situation is provided in fig. 6.4, showing very good agreement with the predictions of NNLO χPT. One should also note encouraging studies of phase shifts (and not only scattering lengths) in the $I = \ell = 1$ channel, with variations indicative of the ρ-meson [319].

In spite of this progress, the most important source of information on $\pi\pi$ scattering is experiment. One can distinguish several sources of information:

- the first breakthrough comes from the high-precision K_{e4}^+ experiments performed at the BNL AGS by the E865 experiment [271, 272] and, more recently, by the NA48/2 collaboration [273, 274] at the CERN SPS.

- the measurement of the invariant mass distribution in $K^\pm \to \pi^\pm\pi^0\pi^0$ decays [275, 276], that gives information on the S-wave $\pi\pi$ scattering lengths. Indeed, this invariant mass distribution features a cusp where the rescattering channel $\pi^+\pi^- \to \pi^0\pi^0$ opens [277–280].

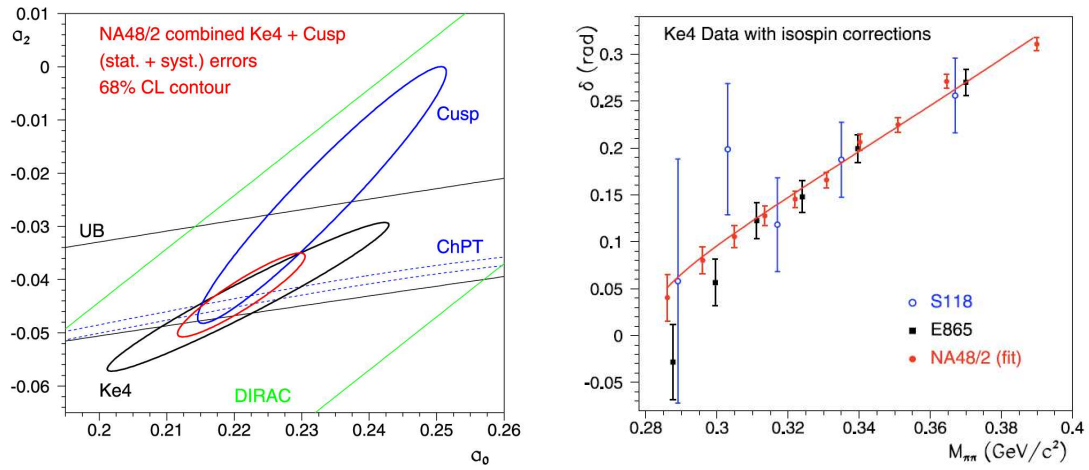

Figure 6.5: *On the left, constraints on the scattering lengths from the analysis of various experimental measurements. On the right, summary of the phase shift measurements $\delta_s - \delta_p$ from $K_{\ell 4}$ decays, applying a specific model for isospin-breaking corrections, discussed later in this chapter. Taken from ref. [276].*

- The measurement of the pionium lifetime by the DIRAC collaboration [283] should ultimately provide also interesting information on the difference of scattering lengths [284, 320].

For the time being, the most precise source of information comes from K^+_{e4} experiments (as can be seen in fig. 6.5) and these will be the main object of our discussion in the following. The decay $K^\pm \to \pi^+\pi^- e^\pm \nu$ is conveniently described using three different rest frames: the $K^\pm$ rest frame, the dipion rest frame and the dilepton rest frame. The kinematics is then fully described by the five Cabibbo-Maksymowicz variables [321–323] as shown in fig. 6.6: the square of the dipion invariant mass s, the square of the dilepton invariant mass s_ℓ, the angle of the $\pi^\pm$ in the dipion rest frame with respect to the flight direction of the dipion in the $K^\pm$ rest frame θ, the angle of the $e^\pm$ in the dilepton rest frame with respect to the flight direction of the dilepton in the $K^\pm$ rest frame θ_ℓ, and the angle between the dipion and the dilepton rest frames ϕ. The decay amplitude is expressed in terms of the hadronic matrix element $\langle \pi^+\pi^-|(V-A)|K^+\rangle$ which is decomposed in three axial-vector form factors F, G, R and a vector one H. These form factors can be expanded assuming the dominance of low partial waves:

$$F = F_s e^{i\delta_{fs}} + F_p e^{i\delta_{fp}} \cos\theta + F_d e^{i\delta_{fd}} \cos^2\theta + \ldots \tag{6.27}$$

$$G = G_p e^{i\delta_{fp}} + G_d e^{i\delta_{fd}} \cos\theta + \ldots \qquad H = H_p e^{i\delta_{fp}} + H_d e^{i\delta_{fd}} \cos\theta + \ldots \tag{6.28}$$

In the isospin limit, due to Watson theorem [324], a partial-wave amplitude of definite angular momentum ℓ and isospin I must have the same phase δ^I_ℓ as the corresponding $\pi\pi$ amplitude. The partial decay width can be expressed as [274]:

$$d^5\Gamma = \frac{G_F^2 |V_{us}|^2}{2(4\pi)^6 M_K^5} \rho(s, s_l) I(s, s_l, \cos\theta, \cos\theta_l, \phi) ds\ ds_l\ d\cos\theta\ d\cos\theta_l\ d\phi \tag{6.29}$$

where $\rho(s, s_l)$ is a phase space factor and I is a linear combination of 9 different angular functions of θ_l and ϕ, each coefficient corresponding to moduli of form factors or interferences between form factors. One then assumes that in the limited kinematic range for $K_{\ell 4}$ decays,

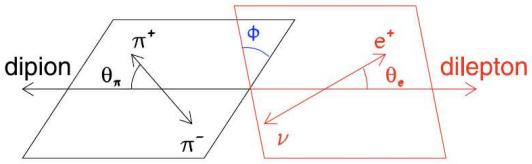

Figure 6.6: *Kinematics of K_{e4} decay. Taken from ref. [276].*

the moduli of the form factors in each partial wave varies slowly, and can be expanded in a low-order series in powers of s and s_l [4]. The data is then distributed in equally populated bins in the 5 kinematic variables and fitted to extract the coefficients of the form factor moduli as well as the values of the phase shifts δ_ℓ^I (assumed to be constant over each bin in s). This allows one to study the interference between S- and P-waves and to extract the difference of phase shifts $\delta_0^0 - \delta_1^1$ at the barycenter of the bin [325]. The corresponding phase shifts (corrected for isospin-breaking corrections discussed in sec. 6.3.2) are indicated in fig. 6.5, where one can see a steady increase in the accuracy on $\pi\pi$ phase shifts.

6.2 The two S-wave scattering lengths from E865 [I]

6.2.1 Model-independent determination of a_0^0 and a_0^2 [I]

We first recall the discussion of the scattering lengths before the publication of the NA48/2 results [42], in order to set the notation and highlight the impact of the most recent data. The E865 data on $\delta_0^0 - \delta_1^1$ were analyzed in ref. [271] in order to extract a_0^0. While two different (although compatible) results were quoted in this reference for a_0^0, no results were given for a_0^2, which is harder to pin down from K_{e4} data alone. Indeed, in order to extract both scattering lengths additional information has to be provided. The first constraint arises from the necessary consistency of the Roy solutions with the $I = 2$ data above the matching point. This forces the S-wave scattering lengths to lie within the so-called Universal Band. Unfortunately, this model-independent constraint is rather weak. We make use of additional information by fitting a broader set of data below 800 MeV, namely Geneva-Saclay and E865 sets for $I = 0, 1$ [270,271] and Hoogland (sol. A) and Losty sets for $I = 2$ [326, 327]. Notice that a similar fit has been considered in ref. [251] but without the E865 data (cf. figs. 11 and 12 in this reference).

We first perform a fit using the solutions of the Roy equations of ref. [251]. The χ^2 is defined as:

$$\chi^2_{\rm Global}(a_0^0, a_0^2) = \sum_{j=1}^{9} \left(\frac{(\delta_0^2)^{\rm ACGL}(s_j^{\rm exp}) - (\delta_0^2)_j^{\rm exp}}{\sigma_j^{\rm exp}} \right)^2 + \sum_{i=1}^{11} \left(\frac{[\delta_0^0 - \delta_1^1]^{\rm ACGL}(s_i^{\rm exp}) - [\delta_0^0 - \delta_1^1]_i^{\rm exp})}{\sigma_i^{\rm exp}} \right)^2, \tag{6.30}$$

where $[\delta_\ell^I]^{\rm ACGL}(a_0^0, a_0^2, s)$ is the parametrisation of Roy solutions proposed in ref. [251]. i and j are the indices of the experimental points for $I = (0, 1)$ and $I = 2$ respectively. This fitting procedure, referred to as Global, yields:

$$\text{Global:} \quad a_0^0 = 0.228 \pm 0.012, \quad a_0^2 = -0.0382 \pm 0.0038. \tag{6.31}$$

[4] In ref. [274], a good description of the data was achieved with F_s quadratic in s and linear in s_e, G_p linear in s only, and F_p and H_p constant, whereas F_d was found consistent with zero.

with $\chi^2_{\rm min} = 16.45/18$ d.o.f and a correlation coefficient of 0.788. Including data on the P-wave below 800 MeV reported by Protopopescu *et al.* [328] does not change the result of the fit, yielding[5] $\chi^2_{\rm min} = 23.1/28$ d.o.f. and $a_0^0 = 0.228 \pm 0.012$, $a_0^2 = -0.0392 \pm 0.0038$.

A second fitting procedure can be followed, in which we use our solutions of the Roy equations to include the dependence on the phase shifts at the matching point (θ_0, θ_1). The χ^2 is then defined as:

$$\chi^2_{\rm Extended}(a_0^0, a_0^2, \theta_0, \theta_1) = \sum_{j=1}^{9} \left(\frac{(\delta_0^2)^{\rm ext}(s_j^{\rm exp}) - (\delta_0^2)_j^{\rm exp}}{\sigma_j^{\rm exp}} \right)^2 + \sum_{i=1}^{11} \left(\frac{[\delta_0^0 - \delta_1^1]^{\rm ext}(s_i^{\rm exp}) - [\delta_0^0 - \delta_1^1]_i^{\rm exp})}{\sigma_i^{\rm exp}} \right)^2 + \left(\frac{\theta_0 - 82.3^\circ}{3.4^\circ} \right)^2 + \left(\frac{\theta_1 - 108.9^\circ}{2^\circ} \right)^2 \quad (6.32)$$

where $[\delta_\ell^I]^{\rm ext}(a_0^0, a_0^2, \theta_0, \theta_1, s)$ is our extended parametrisation of Roy solutions. This fit, called Extended, leads to the same S-wave scattering lengths as the Global fit:

$$\begin{aligned} \text{Extended: } a_0^0 = 0.228 \pm 0.013,\ a_0^2 = -0.0380 \pm 0.0044, \\ \theta_0 = 82.1^\circ \pm 3.3^\circ, \quad \theta_1 = 108.9^\circ \pm 2.0^\circ\,, \end{aligned} \quad (6.33)$$

with $\chi^2_{\rm min} = 16.48/18$ d.o.f and a correlation coefficient between a_0^0 and a_0^2 of 0.799 (the other correlations being rather weak, between 0 and 0.3) The results of these analyses are shown in fig. 6.7, where we have indicated the 1- and 2-σ contours for both determinations. These contours are defined [6] respectively as $\chi^2 = \chi^2_{\rm min} + 1$ and $\chi^2 = \chi^2_{\rm min} + 4$. We see that our fitting result lies slightly below the center of the UB, where the consistency condition for Roy equations is met.

A comment is in order here concerning our use of the ACM(A) $I = 2$ phase shifts by Hoogland *et al.* These were extracted following the method A, which is a conventional Chew-Low extrapolation to the pion pole of the measured t-channel ($m = 0$) helicity moments [326] (the beam momentum was 14 GeV/c). A similar method was used by Losty *et al.* [327]. A second method (B) is presented in ref. [326], which is based on an overall fit of an (absorption) model for the amplitude to all non-negligible s-channel helicity moments ($m = 0$ and $m = 1$). The method B involves extra assumptions and parameters, some of which exhibit unexpectedly rapid energy variations. No χ^2 is given in ref. [326] (in a preliminary analysis [326], based on a third of the data, a poor χ^2 was reported for method B). We have tried to use in our fit solution B of ref. [326] instead of solution A. Due to the small error bars of the former, we did not succeed in obtaining a consistent description of both ACM(B) and E865-K_{e4} data within the solutions of Roy equations [251]. The minimum has $\chi^2 = 68/18$ d.o.f. and is situated far outside the Universal Band. Such a fit has little meaning, since the Roy solutions are valid exclusively inside the Universal Band. Solution ACM(A) is free from such difficulties.

It has been suggested in ref. [251] that the difference between the phase shifts ACM(A) and (B) indicates sizeable systematic errors, and that the errors associated with ACM(A) solution should consequently be enlarged. It is not obvious to us that method B yields a correct estimate of the systematic errors inherent to method A – especially since the two methods do not use the same sample of data. We find it nevertheless useful to show in fig. 6.10 how our results would

[5] Specifically we have used the energy-independent solution, which has larger error bars. The P-wave production data at low energy have been often criticized, most recently in ref. [251]. Therefore we prefer not to include them in the analysis, but instead use our results to predict the P-wave at low energy.

[6] We recall that in the case of the simultaneous determination of two variables, this definition of the contours correspond to 39% and 86% confidence level.

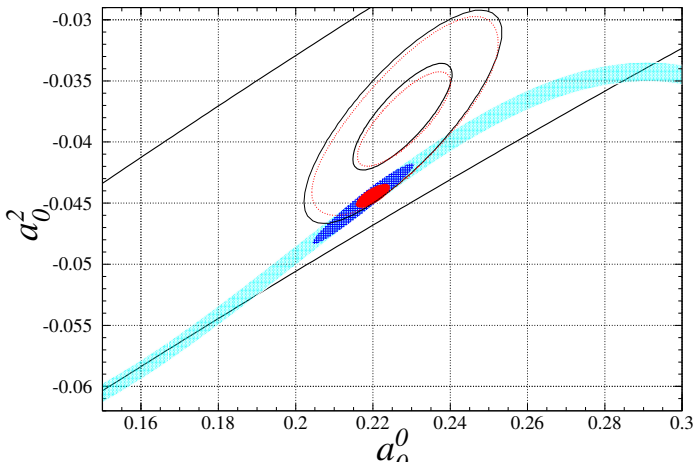

Figure 6.7: *Fit results using either the Roy solutions of ref. [251] (red, dotted ellipse – Global) or our parameterization of the Roy solutions (black, solid ellipse – Extended). In each case, the thicker lines indicate the 1-σ ellipse, and the thinner ones the 2-σ contour. The Universal Band (delimited by the two straight lines) is drawn according to ref. [251], and the narrow strip (shaded region, cyan) related to the scalar radius of the pion is taken from ref. [329]. We have indicated the result of the fit Scalar (blue, hatched ellipse) and the χPT prediction of ref. [286] (red, filled small ellipse).*

be modified if the errors in ACM(A) phase shifts were increased according to the prescription advocated in ref. [251], but these modifications barely affect the main conclusion and will not be discussed further.

6.2.2 Comparison with the χPT prediction for $2a_0^0 - 5a_0^2$ [I]

In the theoretical prediction of a_0^0 and a_0^2 based on two-loop χPT [286, 306–308, 329], one may distinguish two steps. The first step concerns the relation between the combination $2a_0^0 - 5a_0^2$ and the scalar radius of the pion $\langle r^2\rangle_s$ [286, 329]. This step is practically independent of the badly known $O(p^4)$ constant $\bar{\ell}_3$ but it requires an independent phenomenological determination of $\langle r^2\rangle_s$ and it is rather sensitive to the two-loop corrections (a more detailed discussion of this theoretical prediction can be found in sec. 6.2.4). If one takes the value $\langle r^2\rangle_s = 0.61 \pm 0.04$ fm^2, the prediction amounts to a narrow strip in the $a_0^0 - a_0^2$ plane, given in ref. [329] and reproduced in fig. 6.7:

$$a_0^2 = G(a_0^0) \pm .0008, \qquad G(a_0^0) = -.0444 + .236(a_0^0 - .22) - .61(a_0^0 - .22)^2 - 9.9(a_0^0 - .22)^3\,, \quad (6.34)$$

where the parametrisation of G and the error bar are estimated within the theoretical framework defined in refs. [286, 329]. The second step of the prediction procedure then consists in locating the actual position inside the narrow strip eq. (6.34) and it involves, among other things, an estimate of the constant $\bar{\ell}_3$.

The analysis performed in the previous subsection makes use only of the E865 and Geneva-Saclay data on $\delta_0^0 - \delta_1^1$, the Hoogland and Losty data on δ_0^2 together with the solution of Roy equations, and does not use χPT or a particular value of $\langle r^2\rangle_s$. It provides thus a sensitive experimental test of the theoretical prediction represented by the correlation eqs. (6.34). It is seen from fig. 6.7 that the 1-σ ellipses resulting from both fits Global and Extended are

situated outside the narrow strip despite the fact that they are entirely contained within the Universal Band required by the consistency of Roy equations solution. On the other hand, the 2-σ contours intersect the narrow strip. We thus conclude that there is a marginal (1-σ deviation) discrepancy between the theoretical prediction of the scalar radius and the result of the Global and Extended fits. This discrepancy will be further commented on in sec. 6.2.4.

In order to make the comparison more quantitative, we can perform a fit to the E865 data alone, imposing by hand the correlation described by the narrow strip. A similar fit has been performed in ref. [329], leading to the central value $a_0^0 = 0.218$ (no uncertainty was indicated in that reference). Our fitting procedure is defined by:

$$\chi^2_{\rm Scalar}(a_0^0, a_0^2) = \left(\frac{a_0^2 - G(a_0^0)}{.0008}\right)^2 + \sum_{k=1}^{6}\left(\frac{[\delta_0^0-\delta_1^1]^{\rm ACGL}(s_k^{\rm exp}) - [\delta_0^0-\delta_1^1]_k^{\rm exp}}{\sigma_k^{\rm exp}}\right)^2, \qquad (6.35)$$

where k runs only through the E865 points. We obtain:

$$\text{Scalar:}\quad a_0^0 = 0.218 \pm 0.013, \qquad a_0^2 = -0.0449 \pm 0.0033. \qquad (6.36)$$

with $\chi^2_{\rm min} = 5.89/5$ d.o.f., compatible with the results of E865 [271] for a_0^0, and a correlation coefficient of 0.972. The corresponding 1-σ contour is indicated in fig. 6.7. We refer to this fit and to the corresponding 1-σ ellipse as Scalar to be compared with the Global and Extended fits. The meaning of χ^2 and of the standard deviation in the Scalar fit should be taken with caution: The error bar 0.0008 arises from uncertainties in the experimental input, while the theoretical errors inherent in the estimate of $O(p^6)$ corrections are more difficult to quantify. On the other hand, the fits Global and Extended are fully based on experimental data and corresponding errors.

Finally, we would like to briefly comment on the Olsson sum rule for $2a_0^0 - 5a_0^2$, as discussed in ref. [251]. This sum rule converges slowly and demands good control over the asymptotic contribution, which is hard to obtain outside specific models. According to the model used for this purpose in ref. [251], the asymptotic contribution to $2a_0^0 - 5a_0^2$ is $O_{\rm as} = 0.102 \pm 0.017$. Even with such small error bar, the final result shown in eq. (11.2) of ref. [251] is consistent with our Global fit, which leads to $(2a_0^0 - 5a_0^2)_{\rm Global} = 0.647 \pm 0.015$. If the actual error bar in $O_{\rm as}$ is bigger, the impact of the Olsson sum rule on our fit becomes completely negligible.

6.2.3 Determination of $N_f = 2$ LECs and order parameters [I]

We can determine the subthreshold parameters associated with each fit by using the procedure outlined in sec. 6.1.3. In order to take full account of the theoretical and experimental correlations among the six parameters, we proceed in the following way: we generate random sets of (a_0^0, a_0^2) or $(a_0^0, a_0^2, \theta_0, \theta_1)$, distributed according to the 2- or 4-dimensional Gaussian obtained from the covariance matrix of the fit. We then fit the resulting distributions for the subthreshold parameters by Gaussians, leading[7] to tab. 6.1. $\rho_{a_0^0,a_0^2}$ and $\rho_{\alpha\beta}$ denote the correlation coefficients between the respective quantities.

The slightly larger error bars of the Extended fit, compared to the ones of the Global fit, reflect the influence of the uncertainties in θ_0 and θ_1, which in the Global fit are not explicitly

[7]The phenomenological moments J_n^I are integrals of the $I = 0, 1, 2$ phase shifts from threshold to $\sqrt{s_2} = 2$ GeV. The solutions of the Roy equations are used for $s \leq s_0$, and experimental input is used above the $K\bar{K}$ threshold. An interpolation is necessary in the intermediate region $[s_0, 4M_K^2]$. We have observed a weak sensitivity of λ_1 and λ_2 on the interpolation prescription. On the other hand, the values of α and β are independent of this procedure.

	Global (I)	Extended (I)	Scalar (I)
Inputs	E865 [272]	E865 [272] G.-Saclay [270] Hoogland(A) [326] Losty [327]	E865 [272] G.-Saclay [270] Hoogland(A) [326] Losty [327]
a_0^0	0.228 ± 0.012	0.228 ± 0.013	0.218 ± 0.013
a_0^2	-0.0382 ± 0.0038	-0.0380 ± 0.0044	-0.0449 ± 0.0033
$\rho_{a_0^0,a_0^2}$	0.788	0.799	0.972
χ^2/d.o.f	16.4/18	16.5/18	5.9/5
α	1.381 ± 0.242	1.384 ± 0.267	1.034 ± 0.248
β	1.081 ± 0.023	1.077 ± 0.025	1.116 ± 0.010
$\rho_{\alpha\beta}$	-0.14	-0.23	0.53
$\lambda_1 \cdot 10^3$	-4.40 ± 0.28	-4.18 ± 0.63	-3.97 ± 0.12
$\lambda_2 \cdot 10^3$	9.04 ± 0.10	8.96 ± 0.12	9.17 ± 0.06
$\lambda_3 \cdot 10^4$	2.21 ± 0.10	2.22 ± 0.16	2.32 ± 0.06
$\lambda_4 \cdot 10^4$	-1.40 ± 0.04	-1.38 ± 0.04	-1.46 ± 0.02
$\bar{\ell}_3$	-17.3 ± 15.3	-18.5 ± 16.7	2.8 ± 10.0
$\bar{\ell}_4$	4.1 ± 0.9	4.0 ± 0.9	4.9 ± 0.5
$X(2)$	0.81 ± 0.07	0.81 ± 0.08	0.88 ± 0.08
$Z(2)$	0.89 ± 0.02	0.90 ± 0.03	0.85 ± 0.02

Table 6.1: *Subthreshold and LECs for the three different fits considered in ref. [42].*

taken into account. The differences in the central values between these two fits (although compatible within the errors) may be ascribed to the fact that the Extended parametrisation is not as accurate as the one from ref. [251], due to the fact that the former has to account for the dependence on two more variables. The column referring to the Scalar fit should be understood as originating from a mixture of E865 data and χPT-based theoretical predictions that rely on assumptions about the size of $O(p^6)$ counterterms. For this reason the associated errors should not be interpreted in the strict statistical sense. The corresponding 1- and 2-σ ellipses in the $(\alpha - \beta)$ plane are drawn in fig. 6.8.

It is worth stressing that a rather small difference between a_0^0 and a_0^2 resulting from the Scalar fit, on the one hand, and from the Global and Extended fits on the other hand, results in a more pronounced difference in the corresponding values of the subthreshold parameters α, β. Whereas the Scalar fit is characterized by values of α close to (or smaller than) 1 and β well above 1.10, the Global and Extended fits lead to central values of $\alpha \sim 1.4$ and relatively smaller values of β.

In order to investigate the consequences of the results obtained so far for the parameters of the effective Lagrangian, we start with the Ward identity satisfied by the two-point function of the divergence of the axial current $\bar{u}\gamma_\mu\gamma_5 d$ and of its conjugate at zero momentum transfer, which were already written in eqs. (3.124)-(3.124), in terms of the two-flavour condensate $\Sigma(2)$, decay constant $F(2)$ and the ratio $B(2) = \Sigma(2)/F^2$. The fundamental order parameters, in

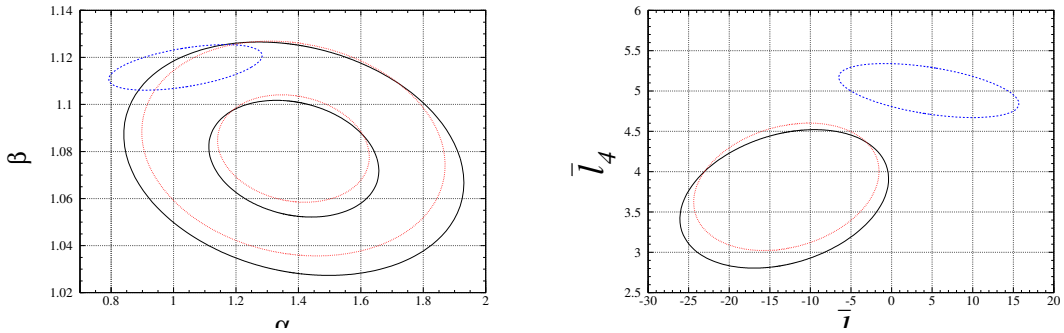

Figure 6.8: *On the left: correlation between α and β for the different fits considered: Scalar (blue, dashed), Global (red, dotted), Extended (black, solid). The thicker lines correspond to the 1-σ ellipses, whereas the thinner ones indicate the 2-σ ellipses (not shown for the Scalar fit). On the right: 1-σ ellipse in the $\bar{\ell}_3 - \bar{\ell}_4$ plane with the same conventions, using the linearised formulae.*

appropriate units, the condensate and the decay constant defined as:

$$X(2) = \frac{2m\Sigma(2)}{F_\pi^2 M_\pi^2}\,, \quad Y(2) = \frac{2mB}{M_\pi^2}\,, \quad Z(2) = \frac{F^2}{F_\pi^2} = \frac{X(2)}{Y(2)}\,, \tag{6.37}$$

are related to the observables M_π, F_π, to the LECs $\bar{\ell}_3$ and $\bar{\ell}_4$ and to the higher-order remainders δ, ε by the following identities:

$$Y(2) = \frac{2(1-\delta)}{1-\varepsilon+[(1-\varepsilon)^2 - 2\bar{\ell}_3\xi(1-\delta)]^{(1/2)}}\,, \tag{6.38}$$

$$X(2) = 1-\delta-(4\bar{\ell}_4-\bar{\ell}_3)\xi Y(2)^2/2\,, \qquad Z(2) = 1-\varepsilon-2\bar{\ell}_4\xi Y(2)\,. \tag{6.39}$$

The $\pi\pi$ subthreshold parameters α and β can be expressed similarly. Reading the LO and NLO perturbative contributions to $F_\pi^2 M_\pi^2\alpha$ and to $F_\pi^2\beta$ from ref. [249], one obtains the identities:

$$\alpha = 1-(1+3\bar{\ell}_3-4\bar{\ell}_4)\xi Y(2)^2/2+\delta_\alpha\,, \qquad \beta = 1+2(\bar{\ell}_4-1)\xi Y(2)+\varepsilon_\beta\,. \tag{6.40}$$

It may be expected that the higher-order remainders δ_α and ε_β are not more important than the uncertainties in the determination of the parameters α and β from experimental data.

If we expand the previous expressions of α and β in powers of ξ, we obtain the following (linearized) expressions in term of the LECs $\bar{\ell}_3$ and $\bar{\ell}_4$:

$$\alpha-\beta = 3\xi(1-\bar{\ell}_3)/2\,, \qquad \beta-1 = 2\xi(\bar{\ell}_4-1)\,. \tag{6.41}$$

This is an excellent approximation, unless $\bar{\ell}_3$ or $\bar{\ell}_4$ become "too" large. However, even if one of them were large, the non-linear equations (6.40) and (6.40) of the previous section would still be exact identities; moreover, the definition of $\bar{\ell}_3$ and $\bar{\ell}_4$ in terms of two-point functions is independent of their magnitudes. We can use eqs. (6.41) and (6.41) to translate our determination of (α,β) into a 1-σ contour plot in the $\bar{\ell}_3 - \bar{\ell}_4$ plane. In fig. 6.8, we show three ellipses corresponding to those in the $\alpha-\beta$ plane displayed in fig. 6.8 above.

If we use the formulae eqs. (6.38), (6.40) and (6.40), but now without linearising, the previous ellipses are deformed, as shown in fig. 6.9 (solid lines). The corresponding contours in the $X(2)-Z(2)$ plane are plotted in fig. 6.9. Up to now, we have neglected the indirect

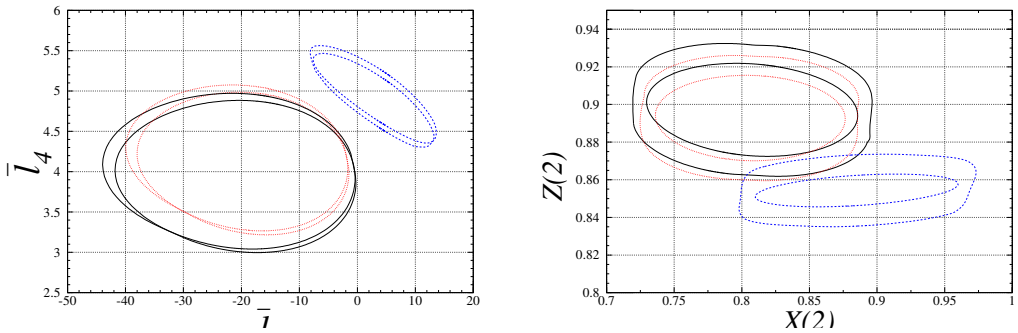

Figure 6.9: *1-σ ellipse in the $\bar{\ell}_3-\bar{\ell}_4$ (left) and $X(2)-Z(2)$ (right) planes, for the different fits considered: Scalar (blue, dashed), Global (red, dotted), Extended (black, solid). The thinner lines indicate the domains allowed if $\varepsilon, \delta \leq 1\%$.*

remainders δ and ε as well as direct remainders δ_α and ε_β. In the case $N_f = 2$, we expect these NNLO quantities to be less than 1%, since eqs. (3.124) and (3.124) are obtained by an expansion in powers of the *nonstrange* quark mass. This leads to a (small) additional broadening of the 1-σ regions, as seen in the plots with thinner lines in Figs. 6.9 and 6.9 (δ_α and ε_β are negligible compared to the present uncertainty in the parameters α and β).

It is clear from fig. 6.9 and tab. 6.1 that we obtain rather large and negative values of $\bar{\ell}_3$, compared to the standard expectation of 2.9 ± 2.4. This can be interpreted as a consequence of an important OZI-rule violating transition $\bar{s}s \leftrightarrow \bar{u}u + \bar{d}d$ leading to a larger value of the $N_f = 3$, large-N_c suppressed constant $L_6^r(M_\rho)$, than usually assumed. In fig. 6.9, we see that the two-flavour GOR ratio $X(2)$ is constrained (at one sigma): $X(2) = 0.81 \pm 0.09$, and F/F_π is also limited to a rather narrow band, $(F/F_\pi)^2 = 0.90 \pm 0.03$. Let us mention that the difference seen in the (α, β) plane between the various fits reappears clearly here. The Scalar fit favours larger values of $X(2)$ and lower values of $Z(2)$ than the Global/Extended fit.

6.2.4 The theoretical constraint of the scalar radius of the pion [I]

A relation between $2a_0^0 - 5a_0^2$ and the scalar radius of the pion based on two-loop χPT has been derived in refs. [286,329]. For the current value of the scalar radius $\langle r^2 \rangle_s = 0.61 \pm 0.04$ fm^2, this prediction results in the narrow strip in the $a_0^0 - a_0^2$ plane shown in ref. [329] and reproduced here in fig. 6.7. The accuracy of this prediction is not only conditional on the experimental error, but also on theoretical assumptions and "rules", which are a priori reasonable and natural, but not necessarily true.

It is usually assumed that $O(p^6)$ counterterms at a suitable scale can be estimated via the narrow resonance saturation [250, 286, 306, 307]. In fact, already at $O(p^4)$ this assumption fails in channels where $1/N_c$-corrections are large and/or the OZI-rule is strongly violated. This is what likely happens in the scalar channel, which is particularly relevant for the present discussion. Furthermore, the existing resonance estimates of $O(p^6)$ counterterms are often based on a "resonance effective Lagrangian $\mathcal{L}_{\rm res}$" involving (and missing) the same resonances with the same "minimal resonance couplings" as in ref. [23], originally used to estimate the $O(p^4)$ LECs. But non-minimal couplings are necessary to avoid conflicts with the QCD short-distance behaviour of two- and three-point functions, especially if the latter involve (pseudo)scalar currents [23, 24, 26, 28, 72, 110, 111, 116, 120–126, 330]. The estimates of the corresponding $O(p^6)$ counterterms can be affected by these new resonance couplings. Finally a remark should be

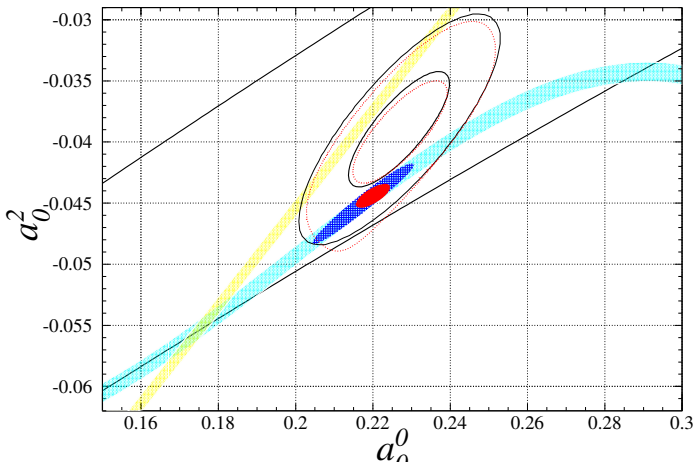

Figure 6.10: *Correlation eq. (6.42) between a_0^0 and a_0^2, obtained from the relation between $2a_0^0 - 5a_0^2$ and the scalar radius of the pion. The shaded oblique band (yellow) corresponds to the $O(p^4)$ level [eq. (6.42) with $\delta_a = 0$], using the dispersive estimate of ref. [238]: $\langle r^2\rangle_s = 0.61 \pm 0.04$ fm^2. The shaded curved strip (cyan) represents the effect of $O(p^6)$ corrections δ_a according to the prediction of ref. [329] using the same input value of $\langle r^2\rangle_s$. The contours correspond to fits using either the Roy solutions of ref. [251] (red, dotted ellipse – Global) or our parameterization of the Roy solutions (black, solid ellipse – Extended), with the errors of ACM(A) data enlarged to take into account potential systematics reflected by the differences between ACM(A) and ACM(B) data. In each case, the thicker lines indicate the 1-σ ellipse, and the thinner ones the 2-σ contour. The other elements are identical to fig. 6.7.*

made about the dispersive estimate of $\langle r^2\rangle_s$ in ref. [238], and the uncertainty related to it. The pion scalar form factor and radius are not experimentally measurable quantities – information about them can only come from indirect theoretical constructions (as discusssed in sec. 4). In contrast to the case of the (observable) vector form factor, QCD does not restrict very much the high momentum behaviour of the scalar form factor. It even does not guarantee that the latter satisfies an unsubtracted dispersion relation. Consequently, the dispersive evaluation of $\langle r^2\rangle_s$ suffers from a certain model dependence concerning the higher momentum contributions; this is usually not discussed in the literature. The quoted uncertainty should not be interpreted outside the framework of the model used in evaluating the scalar radius.

Most of these critical remarks are obviously not new, and could also be applied to the work presented in sec. 4. It might however be useful to keep them in mind when discussing the origin of the discrepancy between our model-free determination of scattering lengths from the data (Global/Extended fit) and the narrow strip prediction (Scalar) [329]. The origin of the narrow strip is more easily understood from eq. (3) of ref. [329]:

$$2a_0^0 - 5a_0^2 = \frac{3M_\pi^2}{4\pi F_\pi^2}\left(1 + \frac{1}{3}M_\pi^2\langle r^2\rangle_s + \frac{41}{12}\xi\right) + \delta_a = 0.57158 + 0.05541\left(\frac{\langle r^2\rangle_s}{0.61\ \text{fm}^2}\right) + \delta_a\,, \quad (6.42)$$

where $\delta_a = O(m^3)$. It is worth stressing that the $O(p^6)$ contribution δ_a is essential for the numerical coherence of eq. (6.42). If the $O(p^6)$ contribution δ_a is dropped, eq. (6.42) reduces to the $O(p^4)$ low-energy theorem [249] relating $2a_0^0 - 5a_0^2$ and $\langle r^2\rangle_s$. This model-independent $O(p^4)$ relation is represented in fig. 6.10 as a straight oblique band corresponding to the estimate of the scalar radius $\langle r^2\rangle_s = 0.61 \pm 0.04$ fm^2.

	Scalar			Global		
a_0^0	0.218	$\pm$	0.013	0.2279	$\pm$	0.012
a_0^2	-0.0449	$\pm$	0.0033	-0.0382	$\pm$	0.0038
$2a_0^0 - 5a_0^2$	0.660	$\pm$	0.011	0.647	$\pm$	0.015
δ_a	0.033	$\pm$	0.012	0.020	$\pm$	0.015

Table 6.2: *Values of δ_a required for satisfying eq. (6.42) and the estimate $\langle r^2\rangle_s = 0.61 \pm 0.04$ fm^2. The correlation between a_0^0 and a_0^2 has been taken into account to compute the error on $2a_0^0 - 5a_0^2$.*

In order to reproduce the prediction of ref. [286]: $2a_0^0 - 5a_0^2 = 0.663 \pm 0.006$, either the scalar radius should be as large as 1.01 fm^2, or the $O(p^6)$ correction δ_a should move the $O(p^4)$ straight oblique band up to the curved strip along the bottom of the Universal Band, reproduced in fig. 6.10 from ref. [329]. If we believe the estimate $\langle r^2\rangle_s = 0.61 \pm 0.04$ fm^2, and if eq. (6.42) should hold inside the Scalar or the Global ellipse, δ_a should take the values indicated in tab. 6.2. The $O(p^6)$ correction amounts thus to 5% in the Scalar case, and 3% in the Global one. As shown in more detail in ref. [42], this is still consistent with the crude order of magnitude estimate from resonance saturation, provided the effective mass scale M_S characteristic of the scalar channel contributions is reduced by a factor 2: $M_S \sim 500$ MeV. This could indeed be a rather natural (though rough and qualitative) way how to account for the exceptional role of the $\pi\pi$ continuum and of the OZI-rule violation in the scalar channel.

6.3 The two S-wave scattering lengths from NA48/2

6.3.1 First series of fits and the importance of isospin breaking

In 2007, the NA48/2 collaboration [273, 274] issued a series of new, and much more accurate measurements. These data exhibited a discrepancy with the E865 phase shifts at high $\pi\pi$ invariant mass $s_{\pi\pi}$. This question is of importance, as the main sensitivity of the fit on a_0^0 comes from these points at high hadronic invariant mass which are well determined experimentally and constrain the curvature of the solution. It turned out that this discrepancy could be solved if one corrects the prescription adopted in refs. [271,272] to determine the value of $s_{\pi\pi}$ at which each measured bin should be considered: rather than taking the expectation value of the $\pi\pi$ mass distribution $\langle s_{\pi\pi}\rangle$, one should consider the barycenter of the bin (including effects from other kinematic variables) [325]. This correction shifts the position in the highest mass bin downward by 11.4 MeV, in the second highest bin downward by 0.8 MeV, and in the lowest mass bin upward by 2.4 MeV, bringing E865 and NA48/2 data to a better agreement.

If one performs a fit of the corresponding inputs, neglecting correlations between two bins in the same experiment, we obtain the results displayed in fig. 6.11 and tab. 6.3 [8]. One can see that the values of the scattering lengths are significantly different from those expected from two-loop estimates, leading to very low values of the two-flavour quark condensate and pseudoscalar decay constant. On the other hand, the two fits (Extended and Scalar) are brought in closer agreement than previously.

[8] In the following, we do not consider the Global fit, which is essentially equivalent to the Extended one. We denote the different versions of the fits with roman numbers I,II,III, according to the added/modified $K_{\ell 4}$ inputs.

	Extended (II)	Scalar (II)
Inputs	E865 (correct.) [272] NA48/2 [274] G.-Saclay [270] Hoogland(A) [326] Losty [327]	E865 (correct.) [272] NA48/2 [274]
a_0^0	0.245 ± 0.008	0.241 ± 0.005
a_0^2	-0.0357 ± 0.0037	-0.0398 ± 0.0015
$\rho_{a_0^0,a_0^2}$	0.842	0.850
χ^2/d.o.f	24.0/28	13.2/15
α	1.63 ± 0.21	1.44 ± 0.010
β	1.10 ± 0.02	1.13 ± 0.01
$\rho_{\alpha\beta}$	0.337	0.021
$\lambda_1 \cdot 10^3$	-3.70 ± 0.57	-3.74 ± 0.10
$\lambda_2 \cdot 10^3$	9.02 ± 0.11	9.21 ± 0.04
$\lambda_3 \cdot 10^4$	2.36 ± 0.15	2.40 ± 0.04
$\lambda_4 \cdot 10^4$	-1.40 ± 0.04	-1.45 ± 0.02
$\bar{\ell}_3$	-37.9 ± 16.8	-18.3 ± 7.3
$\bar{\ell}_4$	5.2 ± 0.6	5.9 ± 0.4
$X(2)$	0.72 ± 0.06	0.76 ± 0.04
$Z(2)$	0.88 ± 0.03	0.85 ± 0.02

Table 6.3: *Subthreshold and LECs once NA48/2 data is included. The central values of the bins in hadronic invariant mass of E865 have been corrected according to the erratum of ref. [272]. Correlations between the bins are neglected.*

At that stage, it seemed necessary to include isospin-violating corrections [287] in the analysis of the K_{e4}^+ data, in order to account for the high precision reached by the recent NA48/2 experiment, and to compare with Roy equations built in the isospin limit [288, 289]. It was supposed then that the effects due to isospin breaking could be factorised into three different pieces: *i)* a Coulomb factor resumming effects of virtual photons [276], *ii)* the Photos program dealing with the emission of real photons [331, 332], *iii)* corrections due to the mass difference of charged and neutral particles (in particular pions). This last factor must be assessed theoretically. A first step in this direction was performed in refs [287, 289], by computing the mass corrections using the strong chiral Lagrangian with a mass term of electromagnetic origin, but without including photons as dynamical degrees of freedom [333–335], since these corrections were already treated by the Coulomb factor and the Photos program.

Once these corrections are applied to the results of NA48/2 [273, 274], they restore the agreement between the data and the expectations from NNLO χPT. However, this computation was performed in the framework of χPT itself, and thus is strictly valid only in a limited range of (a_0^0, a_0^2). We will now propose an alternative treatment of this problem, starting from a dispersive and iterative reconstruction of the K_{e4}^+ decay amplitude, in order to isolate the contribution due to $\pi\pi$ and πK rescatterings in the isospin-breaking corrections without

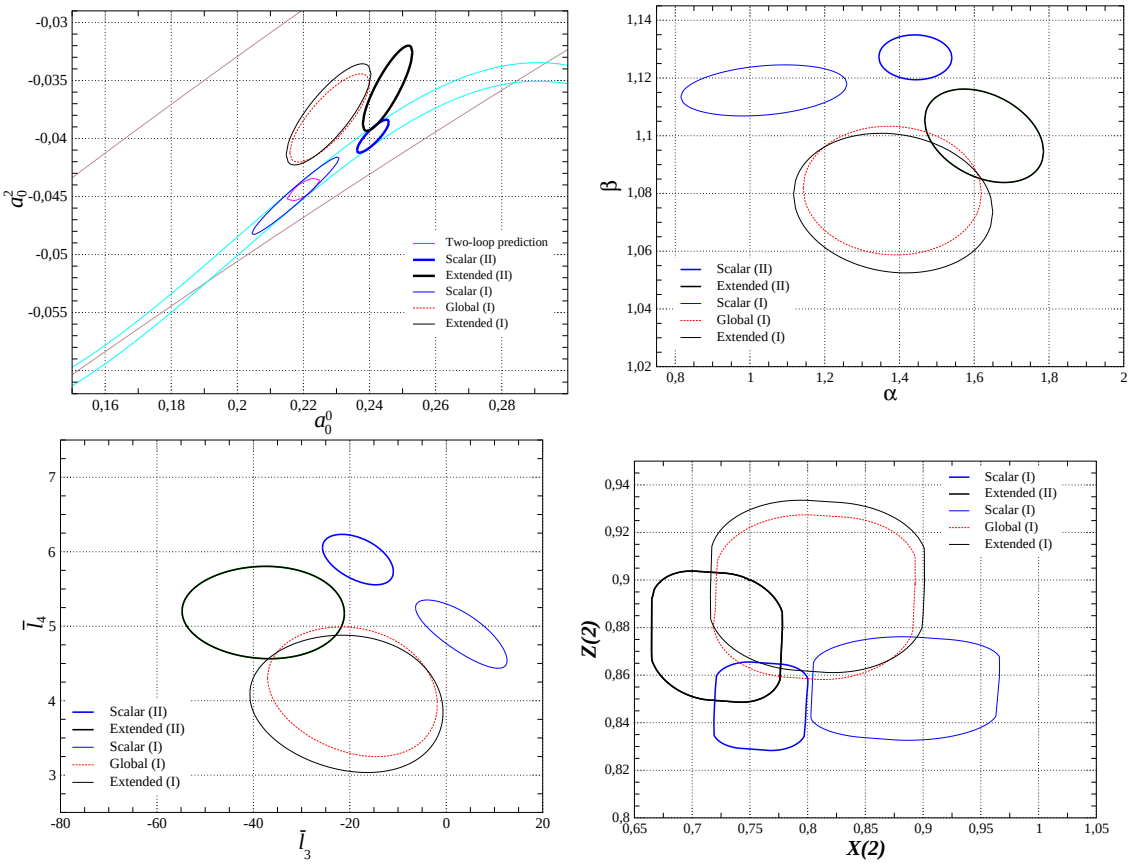

Figure 6.11: *Results for the Scalar and Extended fits once the NA48/2 data are included. For comparison, the previous results obtained without NA48/2 data are drawn with thin lines (Scalar (blue, dashed), Global (red, dotted), Extended (black, solid)). The central values of the bins in hadronic invariant mass of E865 have been corrected according to the erratum of ref. [272]. Correlations between the bins are neglected.*

assuming specific values of the scattering lengths.

6.3.2 Phase-shift analysis of $K_{e4}^{\pm}$ in presence of isospin breaking [J]

In the Standard Model, the amplitudes corresponding to K_{e4}^{+} decays are defined from the matrix element:

$$\mathcal{A}_{\mu}^{ab}(p_a, p_b; k) = \langle \pi^a(p_a)\pi^b(p_b)|iA_{\mu}^{4-i5}(0)|K(k)\rangle\,, \tag{6.43}$$

of the $\Delta S = \Delta Q = 1$ axial current between a (charged or neutral) kaon state and a corresponding two-pion state, specifically $(K, a, b) \in \{(K^+, +, -), (K^+, 0, 0), (K^0, 0, -)\}$. This matrix element is usually decomposed into form factors [9]:

$$\mathcal{A}_{\mu}^{ab}(p_a, p_b; k) = \frac{1}{M_K}\left[F^{ab}(s,t,u)(p_a+p_b)_{\mu} + G^{ab}(s,t,u)(p_a-p_b)_{\mu} + R^{ab}(s,t,u)(k-p_a-p_b)_{\mu}\right], \tag{6.44}$$

[9] In the present study, we shall not consider the matrix element of the vector current, related to the axial anomaly, and described by a single form factor H^{ab}. Moreover, we recall that we define the isospin limit as $M_{\pi^0} \to M_{\pi^\pm}$ and we neglect the superscript $\pm$ unless mandatory.

where $s=(p_a+p_b)^2,\ t=(k-p_a)^2,\ u=(k-p_b)^2$ and $s+t+u\,=\,M_a^2+M_b^2+M_K^2+s_\ell$, with $s_\ell\equiv(k-p_a-p_b)^2$ the square of the dilepton invariant mass. One can define the partial-wave projections of these different form factors, and study the impact of crossing symmetry. One notices that form factors of "F" and "G" types transform into themselves under crossing. and the form factors of the "R" type transform into themselves. This result follows from the fact that the form factors of the "R" type are related to the matrix elements of the divergence of the current $A_\mu^{4-i5}(x)$, and it allows us to focus on "F"- and "G"-type form factors which are those accessible experimentally. In terms of the form factors $F^{ab}(s,t,u)$ and $G^{ab}(s,t,u)$, this translates into the decomposition:

$$F^{ab}(s,t,u)=F_S^{ab}(s,s_\ell)+F_P^{ab}(s,s_\ell)\cos\theta+F^{ab}s_>(s,t,u)\,,\qquad G^{ab}(s,t,u)=G_P^{ab}(s,s_\ell)+G_>^{ab}(s,t,u)\,. \tag{6.45}$$

The contributions from higher partial waves are $\mathrm{Re}F_>^X(s,t,u)$, $\mathrm{Re}G_>^X(s,t,u)\sim\mathcal{O}(E^2)$ and $\mathrm{Im}F_>^X(s,t,u)$, $\mathrm{Im}G_>^X(s,t,u)\sim\mathcal{O}(E^6)$, while the contributions from S and P waves are collected in

$$F_S^{ab}(s,s_\ell)\,=\,f_0^{ab}(s,s_\ell)\,-\,\frac{M_a^2-M_b^2}{s}\,g_1^{ab}(s,s_\ell)\,, \tag{6.46}$$

$$F_P^{ab}(s,s_\ell)\,=\,f_1^{ab}(s,s_\ell)\,-\,\frac{M_K^2-s-s_\ell}{s}\,\frac{\lambda_{ab}^{1/2}(s)}{\lambda_{\ell K}^{1/2}(s)}\,g_1^{ab}(s,s_\ell)\,,\qquad G_P^{ab}(s,s_\ell)=g_1^{ab}(s,s_\ell) \tag{6.47}$$

In these expressions, $\lambda_{ab}(s)\equiv\lambda(s,M_a^2,M_b^2)$, $\lambda_{\ell K}(s)\equiv\lambda(s,M_K^2,s_\ell)$, where $\lambda(x,y,z)=x^2+y^2+z^2-2xy-2yz-2xz$ denotes the Källen function. In the data analysis of $K_{e4}^\pm$ decays, these form factors are expressed as:

$$F_S^{+-}(s,s_\ell)\,\equiv\,f_0(s,s_\ell)\,=\,e^{i\delta_{\rm s}(s,s_\ell)}\,f_{\rm s}(s,s_\ell), \tag{6.48}$$

$$F_P^{+-}(s,s_\ell)\,\equiv\,f_1(s,s_\ell)\,-\,\frac{M_{K^\pm}^2-s-s_\ell}{\lambda^{1/2}(s,s_\ell,M_{K^\pm}^2)}\,\sigma_\pm(s)\,g_1(s,s_\ell)\,=\,e^{i\delta_{\rm p}(s)}\,f_{\rm p}(s,s_\ell), \tag{6.49}$$

$$G_P^{+-}(s,s_\ell)\,\equiv\,g_1(s,s_\ell)\,=\,e^{i\delta_{\rm p}(s)}\,g_{\rm p}(s,s_\ell), \tag{6.50}$$

where $\sigma(s)=\sqrt{\lambda(s,M_\pi^2,M_\pi^2)}/s=\sqrt{1-4M_\pi^2/s}$. One should note that the phases may depend on the two invariant masses s and s_ℓ. In practice the P-wave does depend only on s. Indeed for that particular wave, in the available kinematical range and due to Bose symmetry, there can only be one single intermediate state produced by a $\pi^+\pi^-$ pair. Consequently, the Watson theorem does apply even in the presence of isospin breaking and it explains also the appearance of a common phase $\delta_{\rm p}(s)$ for F_P and G_P.

In the isospin limit, the phase $\delta_{\rm s}(s,s_\ell)$ does not depend on s_ℓ either, and following Watson theorem, it can be identified with the $I=0$, S-wave phase $\delta_0(s)$ of pion-pion scattering carried by the partial wave $f_0(s,s_\ell)$, On the other hand $\delta_{\rm p}(s)$ is the $I\,=\,1$, P-wave phase $\delta_1(s)$, carried by the partial waves $f_1(s,s_\ell)$ and $g_1(s,s_\ell)$, respectively. It should be stressed that, even in the isospin limit, this identification holds only upon neglecting the contributions from higher partial waves. This issue has been addressed in ref. [336], where it was found that the corresponding error from higher partial waves on $\delta_0-\delta_1$ measured in K_{e4}^+ decay is less than 1 mrad. Isospin-breaking effects will certainly not modify this result in a substantial manner, since the kinematical and chiral suppressions of the higher partial waves responsible for the smallness of this correction will remain operative. We will thus consider that:

$$\delta_{\rm s}(s,s_\ell)=\delta_0(s)\,+\,\Delta\delta_{\rm s}(s,s_\ell)\,,\quad \delta_{\rm p}(s)=\delta_1(s)\,+\,\Delta\delta_{\rm p}(s), \tag{6.51}$$

where $\Delta\delta_{\rm s,p}$ represent isospin-breaking corrections.

6.3.3 Isospin-breaking contributions to the phase shifts [J]

As detailed earlier, one can extract the difference $\delta_{\rm s}(s,s_\ell)-\delta_{\rm p}(s)$ from the angular analysis of the K^+_{e4} decay. In order to access the phase difference $\delta_0(s)-\delta_1(s)$ defined in the isospin limit, it is necessary to evaluate the correction term $\Delta\delta_{\rm s}(s)-\Delta\delta_{\rm p}(s)$, which can be computed at two-loop order as a function of the $\pi\pi$ scattering lengths. As an illustration, let us consider the (S or P) partial wave projection of a form factor describing the decay into the $\pi^+\pi^-$ channel, assuming a chiral expansion of the form:

$$f^{+-}(s) \,=\, e^{i\delta^{+-}(s)}\,|f^{+-}(s)| \,=\, \overset{(0)}{f}{}^{+-} \,+\, \overset{(2)}{f}{}^{+-}(s) + \,\overset{(4)}{f}{}^{+-}(s)\,, + \mathcal{O}(E^6)\,, \tag{6.52}$$

where $\overset{(n)}{f}{}^{+-}(s) = \mathcal{O}(E^n)$. The LO contribution $\overset{(0)}{f}$ is a real number. The phase of the form factor has itself a chiral expansion starting at $\mathcal{O}(E^2)$:

$$\delta^{+-}(s) \,=\, \frac{\mathrm{Im}\,\overset{(4)}{f}{}^{+-}(s)}{\overset{(0)}{f}{}^{+-}(s)} \,+\, \left[\frac{\mathrm{Im}\,\overset{(2)}{f}{}^{+-}(s)}{\overset{(0)}{f}{}^{+-}(s)} \,-\, \frac{\mathrm{Im}\,\overset{(2)}{f}{}^{+-}(s)]}{\overset{(0)}{f}{}^{+-}(s)}\,\frac{\mathrm{Re}\,\overset{(2)}{f}{}^{+-}(s)]}{\overset{(0)}{f}{}^{+-}(s)}\right] \,+\, \mathcal{O}(E^6)\,. \tag{6.53}$$

The imaginary part of the form factor is given by unitarity in terms of the relevant $\pi\pi$ intermediate states, i.e., in the present case, the two channels $\pi^+\pi^-$ and $\pi^0\pi^0$:

$$\mathrm{Im}\, f^{+-}(s) \,=\, \mathrm{Re}\,\{t^{+-}(s)(f^{+-})^*(s)\}\,\sigma_\pm(s) \,+\, \mathrm{Re}\left\{t^x(s)(f^{00})^*(s)\right\}\frac{1}{2}\sigma_0(s), \tag{6.54}$$

where $\sigma_0(s)=\sqrt{\lambda(s,M^2_{\pi^0},M^2_{\pi^0})}/s=\sqrt{1-4M^2_{\pi^0}/s}$, while t^{+-} and t^x represent the $\pi\pi$ partial waves for the $\pi^+\pi^-\to\pi^+\pi^-$ and $\pi^0\pi^0\to\pi^+\pi^-$ amplitudes, and are defined from the amplitude as[10]:

$$A^X(s,t) \,=\, 16\pi\sum_l (2l+1)t^X_l(s)P_l(\cos\theta). \tag{6.55}$$

The S and P $\pi\pi$ partial waves have a chiral expansion starting at $\sim\mathcal{O}(E^2)$:

$$\mathrm{Re}\,t^X(s)=\varphi^X(s) \,+\, \psi^X(s) \,+\, \mathcal{O}(E^6)\,, \quad \mathrm{Im}\,t^X(s)\sim\mathcal{O}(E^4)\,. \tag{6.56}$$

The phase shifts read:

$$\delta_{\rm s}(s) = \sigma(s)\,[\varphi_0^{+-}(s) \,+\, \psi_0^{+-}(s)] \tag{6.57}$$
$$+\,\frac{1}{2}\sigma_0(s)\,\frac{\overset{(0)}{f}{}^{00}_0}{\overset{(0)}{f}{}^{+-}_0}\left\{\varphi_0^x(s)\left[1 \,+\, \frac{\mathrm{Re}\,\overset{(2)}{f}{}^{00}_0(s,s_e)}{\overset{(0)}{f}{}^{00}_0} \,-\, \frac{\mathrm{Re}\,\overset{(2)}{f}{}^{+-}_0(s,s_e)}{\overset{(0)}{f}{}^{+-}_0}\right] \,+\, \psi_0^x(s)\right\} \,+\, \mathcal{O}(E^6)\,,$$

$$\delta_{\rm p}(s) = \sigma(s)\,[\varphi_1^{+-}(s) \,+\, \psi_1^{+-}(s)] + \mathcal{O}(E^6)\,. \tag{6.58}$$

We thus see that the phase of the two-loop form factor only depends on the real part on the form factors at one loop (first line of eq. (6.57), and on the real part of the (S and P) $\pi\pi$ partial-waves at two loops (eq. (6.58) and second line of eq. (6.57)). Moreover, eqs. (6.57)-(6.58) confirm that in presence of isospin breaking, i.e. Re $f^{00}(s,s_\ell)\neq$ Re $f^{+-}(s,s_\ell)$, the phase of the form factors is not only a function of the hadronic invariant mass s, but depends also on the leptonic invariant mass s_ℓ. Typical diagrams contributing to the discontinuities of the form factors and of the scattering amplitudes are drawn in figs. 6.12 and 6.13.

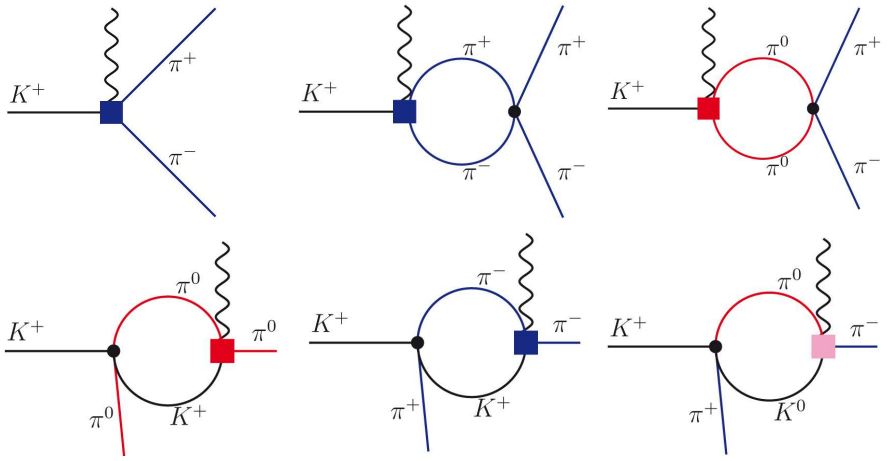

Figure 6.12: K^+_{e4} form factors. First row: LO contribution, and contribution at one loop from unitarity in the s-channel. Second row: typical rescattering diagrams involved in the reconstruction of the K^+_{e4} form factors in the t- and u-channels.

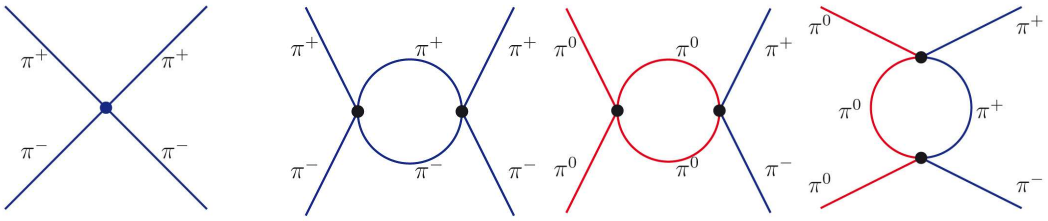

Figure 6.13: $\pi\pi$ scattering: LO contribution and some of the contributions at one loop from unitarity.

In the isospin limit (and denoting the quantities in this limit with a tilde), these expressions reduce to

$$\delta_0(s) = \sigma(s)\left[\left(\tilde{\varphi}\,{}^{+-}_{0}(s) - \frac{1}{2}\,\tilde{\varphi}\,{}^{x}_{0}(s)\right) + \left(\tilde{\psi}\,{}^{+-}_{0}(s) - \frac{1}{2}\,\tilde{\psi}\,{}^{x}_{0}(s)\right)\right] + \mathcal{O}(E^6),$$
$$\delta_1(s) = \sigma(s)\left[\tilde{\varphi}\,{}^{+-}_{1}(s) + \tilde{\psi}\,{}^{+-}_{1}(s)\right] + \mathcal{O}(E^6). \tag{6.59}$$

Therefore the corrections to the phases generated by isospin-breaking corrections are:

$$\begin{aligned}\Delta\delta_{\rm s}(s) = {}& \sigma(s)\left[\left(\varphi_0^{+-}(s) - \tilde{\varphi}\,{}^{+-}_{0}(s)\right) - \frac{1}{2}\left(\varphi_0^{x}(s) - \tilde{\varphi}\,{}^{x}_{0}(s)\right)\right] \\ & + \sigma(s)\left[\left(\psi_0^{+-}(s) - \tilde{\psi}\,{}^{+-}_{0}(s)\right) - \frac{1}{2}\left(\psi_0^{x}(s) - \tilde{\psi}\,{}^{x}_{0}(s)\right)\right] \\ & + \frac{1}{2}\left[\sigma_0(s) - \sigma(s)\right]\frac{{}^{(0)}_{}f\,{}^{00}_{0}}{{}^{(0)}_{}f\,{}^{+-}_{0}}\left[\varphi_0^{x}(s) + \psi_0^{x}(s)\right] + \frac{1}{2}\left(1 + \frac{{}^{(0)}_{}f\,{}^{00}_{0}}{{}^{(0)}_{}f\,{}^{+-}_{0}}\right)\sigma(s)\left[\varphi_0^{x}(s) + \psi_0^{x}(s)\right]\end{aligned}$$

[10]Notice that the normalisation factor is 16π, instead of the usual 32π, due to the loss of generalised Bose symmetry in the presence of isospin breaking; in the case of states composed of two identical pions, the corresponding symmetry factor is included in the phase-space term occurring in the expression of the discontinuity of the partial waves.

$$+\frac{1}{2}\sigma_0(s)\,\frac{\overset{(0)}{f}{}^{00}_{0}}{\overset{(0)}{f}{}^{+-}_{0}}\,\varphi_0^x(s)\left[\frac{\mathrm{Re}\,\overset{(2)}{f}{}^{00}_{0}(s,s_e)}{\overset{(0)}{f}{}^{00}_{0}}-\frac{\mathrm{Re}\,\overset{(2)}{f}{}^{+-}_{0}(s,s_e)}{\overset{(0)}{f}{}^{+-}_{0}}\right]+\mathcal{O}(E^6), \tag{6.60}$$

$$\Delta\delta_{\rm p}(s)=\sigma(s)\left[\left(\varphi_1^{+-}(s)-\tilde{\varphi}\,{}^{+-}_{1}(s)\right)+\left(\psi_1^{+-}(s)-\tilde{\psi}\,{}^{+-}_{1}(s)\right)\right]+\mathcal{O}(E^6). \tag{6.61}$$

In the case of the P-wave phase, Bose symmetry precludes a contribution from the $\pi^0\pi^0$ intermediate state, and the isospin-breaking corrections are therefore universal: they only involve the phase of the $\pi\pi$ scattering amplitudes and they can be expressed in terms of the $\pi\pi$ scattering lengths. The situation is more involved in the case of the phase of the S wave, since in addition to the universal, process-independent, contribution from $\pi\pi$ rescattering (first two lines in eq. (6.60)), there is also a piece which depends on the form factors of the process under consideration, due to the presence of a second intermediate two-pion state (last two lines in eq. (6.60)). In particular, we notice the presence of the ratio of normalisations:

$$\frac{\overset{(0)}{f}{}^{00}_{0}}{\overset{(0)}{f}{}^{+-}_{0}}=-\left(1+\frac{3}{2R}\right),\qquad R=\frac{m_s-\hat{m}}{m_d-m_u}, \tag{6.62}$$

which in ref. [288] is seen as arising from $\pi^0-\eta$ mixing induced by the difference m_d-m_u.

We need therefore two different ingredients from our dispersive analysis of isospin-breaking corrections for K^+_{e4} form factors: the two-loop $\pi\pi$ scattering amplitudes and the one-loop K^+_{e4} form factors, both in presence of isospin breaking. At this stage, we should stress the difference between our work and one-loop computations of K^+_{e4} form factors performed within χPT including isospin breaking [337, 338]. We study these form factors focusing on rescattering effects, in order to extract information on the $\pi\pi$ scattering lengths with as few assumptions as possible. The dispersive framework that we adopt here allows us to single out the terms corresponding to $\pi\pi$ rescattering in the chiral expansions, and thus to determine the impact of rescattering even when the $\pi\pi$ scattering lengths do not have values close to the ones expected in χPT. We will match this description to the chiral expression of the K^+_{e4} amplitude in order to assess the size of the contributions whose dynamics is not related to $\pi\pi$ rescattering. This separation allows a more general treatment of $\pi\pi$ rescattering compared to the chiral computations currently available, and it is the main outcome of our dispersive analysis.

6.3.4 Illustration of the reconstruction theorem [J]

These results set the stage for the construction of two-loop representations of the pion form factors and scattering amplitudes in the low-energy regime. This is achieved trough a two-step recursive process summarised in fig. 6.3. Chiral counting provides the initial seed, namely that at lowest order the form factors reduce to real constants, to be identified by their values at $s=0$, while the $\pi\pi$ scattering amplitudes consist of $\mathcal{O}(E^2)$ polynomials of at most first order in the Mandelstam variables. This initial input, together with unitarity, fixes the discontinuities of the form factors and of the amplitudes at next-to-leading order. One can easily build functions exhibiting the same cuts, identified with the complete one-loop expressions up to a subtraction polynomial of at most first order (second order) in s (in the Mandelstam variables) in the case of the form factors (scattering amplitudes). In turn, these one-loop expressions provide the discontinuities at next-to-next-to-leading order through unitarity, and thus the form factors and amplitudes themselves at order $\mathcal{O}(E^6)$, up to a polynomial ambiguity of second order in s (third order in the Mandelstam variables). In the case of the $\pi\pi$ scattering amplitudes, crossing

imposes further restrictions on the possible terms that may appear in these polynomials. Notice that the presence of these polynomials reflect the fact that the cut functions are only specified by their analytical properties (in particular, their discontinuities). This leaves room for polynomial ambiguities in the expressions of these functions, and the maximal degree of the polynomials is then limited by chiral power counting.

As an illustration of the method, let us take $\pi^+\pi^- \to \pi^+\pi^-$ scattering:

$$A^{+-}(s,t,u) = P^{+-}(s,t,u) \tag{6.63}$$
$$+ [W_0^{+-}(s) + 3(t-u)W_1^{+-}(s)] + [W_0^{+-}(t) + 3(s-u)W_1^{+-}(t)] + W_0^{++}(u) + \mathcal{O}(E^8),$$

where the third order polynomial $P^{+-}(s,t,u)$ is symmetric under exchange of s and t. The three functions $W_{0,1}^{+-}(s)$ and $W_0^{++}(s)$, similar to those introduced in eq. (6.16), have cut singularities along the real s axis, starting at $s = 4M_{\pi^0}^2$ and at $s = 4M_\pi^2$, respectively. The corresponding discontinuities read:

$$\mathrm{Im}W_{0,1}^{+-}(s) = 16\pi \mathrm{Im}\; t_{0,1}^{+-}(s)\; \theta(s - 4M_{\pi^0}^2)\,, \qquad \mathrm{Im}W_0^{++}(s) = 16\pi \mathrm{Im}\; t_0^{++}(s)\; \theta(s - 4M_\pi^2)\,. \tag{6.64}$$

The unitarity condition for the three $\pi\pi$ partial waves involved then leads to:

$$\begin{aligned}
\frac{1}{16\pi}\,\mathrm{Im}W_0^{+-}(s) &= \sigma(s)\;|t_0^{+-}(s)|^2\,\theta(s-4M_\pi^2) \;+\; \frac{1}{2}\,\sigma_0(s)\;|t_0^x(s)|^2\,\theta(s-4M_{\pi^0}^2) \;+\; \mathcal{O}(E^8)\,,\\
\frac{1}{16\pi}\,\mathrm{Im}W_1^{+-}(s) &= \sigma(s)\;|t_1^{+-}(s)|^2\,\theta(s-4M_\pi^2) \;+\; \mathcal{O}(E^8)\,,\\
\frac{1}{16\pi}\,\mathrm{Im}W_0^{++}(s) &= \frac{1}{2}\,\sigma(s)\;|t_0^{++}(s)|^2\,\theta(s-4M_\pi^2) \;+\; \mathcal{O}(E^8).
\end{aligned} \tag{6.65}$$

where t_ℓ^x denote the $\pi^+\pi^- \to \pi^0\pi^0$ partial-wave amplitudes and t^{+-} and t^{++} denote the corresponding elastic amplitudes. The reason why only the lowest S and P partial waves play a role in these expressions follows from the chiral counting for the partial waves:

$$\mathrm{Re}\,t_\ell(s) \sim \mathcal{O}(E^2),\;\; \ell = 0,1, \qquad \mathrm{Re}\,t_\ell(s) \sim \mathcal{O}(E^4),\;\; \ell \geq 2, \tag{6.66}$$

$$\mathrm{Im}\,t_\ell(s) \sim \mathcal{O}(E^4),\;\; \ell = 0,1, \qquad \mathrm{Im}\,t_\ell(s) \sim \mathcal{O}(E^8),\;\; \ell \geq 2. \tag{6.67}$$

We can make use of the chiral expansion for the real parts of the $\ell = 0,1$ partial waves, for values of s corresponding to the cut on the positive real axis,

$$\mathrm{Re}t_\ell(s) \;=\; \varphi_\ell(s) + \psi_\ell(s) + \mathcal{O}(E^6), \qquad |t_\ell(s)|^2 \;=\; [\varphi_\ell(s)]^2 + 2\varphi_\ell(s)\psi_\ell(s) \;+\; \mathcal{O}(E^8)\,, \tag{6.68}$$

for $\ell = 0,1$, with $\varphi_\ell(s) \sim \mathcal{O}(E^2)$ and $\psi_\ell(s) \sim \mathcal{O}(E^4)$. The functions $W(s)$ only have a right-hand cut, that coincides with the right-hand cut of the corresponding S and P $\pi\pi$ partial-wave projections. This structure is in agreement with the analyticity properties of the $\pi\pi$ scattering amplitudes $A(s,t,u)$ required by unitarity and crossing.

At the lowest order in the chiral expansion, the $\pi\pi$ scattering amplitudes in the relevant channels read:

$$A^x(s,t) = -\frac{\beta_x}{F_\pi^2}\left(s - \frac{2}{3}M_\pi^2 - \frac{2}{3}M_{\pi^0}^2\right) - \frac{\alpha_x M_{\pi^0}^2}{3F_\pi^2} \qquad A^{+-}(s,t) = \frac{\beta_{+-}}{F_\pi^2}\left(s + t - \frac{8}{3}M_\pi^2\right) + \frac{2\alpha_{+-}M_{\pi^0}^2}{3F_\pi^2}. \tag{6.69}$$

The various parameters, like β_x, that occur in these expressions are free, in the sense that they are not fixed by general principles (analyticity, unitarity, crossing, and chiral symmetry).

From these amplitudes, the partial wave projections are obtained as $\mathrm{Re} f_\ell(s) = \varphi_\ell(s) + \mathcal{O}(E^4)$, $\ell = 0, 1$, with:

$$\varphi_0^x(s) = -\frac{\beta_x}{16\pi F_\pi^2}\left(s - \frac{2}{3}M_\pi^2 - \frac{2}{3}M_{\pi^0}^2\right) - \frac{\alpha_x M_{\pi^0}^2}{48\pi F_\pi^2}\,, \quad \varphi_0^{+-}(s) = \frac{\beta_{+-}}{32\pi F_\pi^2}\left(s - \frac{4}{3}M_\pi^2\right) + \frac{\alpha_{+-} M_{\pi^0}^2}{24\pi F_\pi^2}\,,$$

$$\varphi_1^{+-}(s) = \frac{\beta_{+-}}{96\pi F_\pi^2}\left(s - 4M_\pi^2\right)\,, \qquad \varphi_0^{++}(s) = -\frac{\beta_{+-}}{16\pi F_\pi^2}\left(s - \frac{4}{3}M_\pi^2\right) + \frac{\alpha_{+-} M_{\pi^0}^2}{24\pi F_\pi^2}. \tag{6.70}$$

Applying the formulae given above, and recalling that at the one-loop order $|t_\ell(s)|^2 = [\varphi_\ell(s)]^2 + \mathcal{O}(E^6)$, one easily obtains the expressions for the unitarity parts of the various amplitudes, up to a polynomial ambiguity that can be reabsorbed into the corresponding subtraction polynomial $P^{+-}(s,t,u)$:

$$W_0^{+-}(s) = [16\pi\varphi_0^{+-}(s)]^2\,\bar{J}(s) + \frac{1}{2}\,[16\pi\varphi_0^x(s)]^2\,\bar{J}_0(s)\,,$$

$$W_1^{+-}(s) = \frac{\beta_{+-}^2}{36F_\pi^4}\left(s - 4M_\pi^2\right)\bar{J}(s)\,, \qquad W_0^{++}(s) = \frac{1}{2}\,[16\pi\varphi_0^{++}(s)]^2\,\bar{J}(s)\,. \tag{6.71}$$

We have introduced the well-known functions $\bar{J}_0(s)$ and $\bar{J}(s)$ defined by the following dispersive integrals

$$\bar{J}_0(s) = \frac{s}{16\pi^2}\int_{4M_{\pi^0}^2}^\infty \frac{dx}{x}\,\frac{1}{x - s - i0}\,\sigma_0(x), \qquad \bar{J}(s) = \frac{s}{16\pi^2}\int_{4M_\pi^2}^\infty \frac{dx}{x}\,\frac{1}{x - s - i0}\,\sigma(x). \tag{6.72}$$

These functions correspond to the standard one-loop integrals subtracted at $s = 0$ [21] introduced in sec. 3.3.2.Taking into account the symmetry properties of the corresponding amplitudes, the polynomial ambiguity of this representation may be written as:

$$P^{+-}(s,t,u) = \frac{\beta_{+-}}{F_\pi^2}\left(s + t - \frac{8}{3}M_\pi^2\right) + \frac{2\alpha_{+-}M_{\pi^0}^2}{3F_\pi^2} + \frac{\lambda_{+-}^{(1)} + \lambda_{+-}^{(2)}}{F_\pi^4}\left[(s - 2M_\pi^2)^2 + (t - 2M_\pi^2)^2\right] + \frac{2\lambda_{+-}^{(2)}}{F_\pi^4}(u - 2M_\pi^2)^2 \tag{6.73}$$

At this stage, we have therefore obtained the amplitude A^{+-} at one loop in terms of a few subtraction constants ($\alpha_X, \beta_X, \lambda$'s), by inserting eqs. (6.71) and (6.73) in eq. (6.63). At this stage, we have completed one whole cycle of the procedure described in fig. 6.3.

For the computation of the isospin-breaking correction to the phase shifts eqs. (6.60)-(6.61), we need to determine not only the one-loop amplitude, but more specifically the one-loop corrections $\psi_0^{+-}(s)$, $\psi_1^{+-}(s)$ to the $\pi\pi$ S and P partial wave projections. The starting point of this less straightforward computation is provided by the following formulae, obtained as the partial-wave expansion of eq. (6.63):

$$\psi_0^{+-}(s) = \frac{\lambda_{+-}^{(1)} + \lambda_{+-}^{(2)}}{F_\pi^4}\left(s - 2M_\pi^2\right)^2 + \frac{\lambda_{+-}^{(1)} + 3\lambda_{+-}^{(2)}}{3F_\pi^4}\left(s^2 - 2sM_\pi + 4M_\pi^4\right) \tag{6.74}$$
$$+ \frac{1}{32\pi}\,[16\pi\varphi_0^x(s)]^2\,\mathrm{Re}\,\bar{J}_0(s) + \frac{1}{16\pi}\,[16\pi\varphi_0^{+-}(s)]^2\,\mathrm{Re}\,\bar{J}(s)$$
$$+ \frac{1}{32\pi}\,\frac{1}{s - 4M_\pi^2}\int_{t_-(s)}^0 dt\,[16\pi\varphi_0^x(t)]^2\,\bar{J}_0(t)$$

$$
\begin{aligned}
&+\frac{1}{32\pi}\,\frac{1}{s-4M_\pi^2}\int_{t_-(s)}^{0}dt\,\left\{2\left[16\pi\varphi_0^{+-}(t)\right]^2+\left[16\pi\varphi_0^{++}(t)\right]^2\right\}\bar{J}(t)\\
&+\frac{1}{16\pi}\,\frac{1}{s-4M_\pi^2}\int_{t_-(s)}^{0}dt\,\frac{\beta_{+-}^2}{12F_\pi^4}\,(t-4M_\pi^2)(2s+t-4M_\pi^2)\bar{J}(t),\\
\psi_1^{+-}(s)\,=\,&-\frac{\lambda_{+-}^{(1)}-\lambda_{+-}^{(2)}}{96\pi F_\pi^4}\,s(s-4M_\pi^2)\,+\,\frac{1}{16\pi}\,\frac{\beta_{+-}^2}{36F_\pi^4}\,(s-4M_\pi^2)^2\,\mathrm{Re}\,\bar{J}(s)\\
&+\frac{1}{32\pi}\,\frac{1}{s-4M_\pi^2}\int_{t_-(s)}^{0}dt\,\left[16\pi\varphi_0^{x}(t)\right]^2\left(1+\frac{2t}{s-4M_\pi^2}\right)\bar{J}_0(t)\\
&+\frac{1}{32\pi}\,\frac{1}{s-4M_\pi^2}\int_{t_-(s)}^{0}dt\,\left\{2\left[16\pi\varphi_0^{+-}(t)\right]^2-\left[16\pi\varphi_0^{++}(t)\right]^2\right\}\left(1+\frac{2t}{s-4M_\pi^2}\right)\bar{J}(t)\\
&+\frac{1}{16\pi}\,\frac{1}{s-4M_\pi^2}\int_{t_-(s)}^{0}dt\,\frac{\beta_{+-}^2}{12F_\pi^4}\,(t-4M_\pi^2)(2s+t-4M_\pi^2)\left(1+\frac{2t}{s-4M_\pi^2}\right)\bar{J}(t),
\end{aligned}
\tag{6.75}
$$

with $t_-(s)=-(s-4M_\pi^2)$. The partial-wave projection integrals can actually be performed analytically [43, 305, 339]. We obtain thus the $\pi^+\pi^-\to\pi^+\pi^-$ in terms of a set of subtraction constants $(\alpha_X,\beta_X,\lambda)$. We may use the same framework to consider other amplitudes relevant for the phase-shift analysis of K_{e4}^+ decays in eqs. (6.57)-(6.58), namely the various $\pi\pi\to\pi\pi$ scattering amplitudes (up to one loop, and their partial-wave projection) as well as the $K_{\ell 4}$ form factors up to one loop (and their partial-wave projection). The latter will involve not only the $\pi\pi\to\pi\pi$ scattering amplitudes, but also the (tree-level) $\pi K\to\pi K$ scattering amplitudes, which will involve new subtraction constants.

The previous dispersive constructions generate subtraction polynomials with unspecified coefficients. In the case of the form factors, these coefficients may be identified with their slopes and curvatures. In the case of the $\pi\pi$ scattering amplitudes, they can be expressed in terms of the subthreshold parameters occurring in the expansions of these amplitudes as Taylor series around the center of the Mandelstam triangle. This was the option considered in the isospin symmetric case in ref. [305] and briefly recalled in sec. 6.1.3. By no means, however, is this choice a necessity. It has, for instance, become customary to rather let the scattering lengths play a prominent role. They have a more direct physical interpretation than the subthreshold parameters, and are thus considered as more "experimentalist friendly". We can therefore also provide expressions where the subtraction polynomials are given in terms of the two S-wave $I=0$ and $I=2$ scattering lengths, a_0^0 and a_0^2, in the isospin limit. In the isospin symmetric situation, this provides an alternative to the choice made in ref. [305]. The two formulations are equivalent, up to corrections that are of higher order. In the situation where isospin is broken, this allows us to discuss the size of the corresponding corrections to the phases of the form factors in terms a_0^0 and a_0^2. This second option is of course the most interesting in the present context, where these scattering lengths are the quantities one would eventually like to determine from the data.

6.3.5 Dispersive estimate of the isospin-breaking corrections [J]

We have now all the elements needed to compute the isospin-breaking corrections encoded in eqs. (6.60)-(6.61), expressed in terms of (integrals of) loop integrals and a set of subtraction constants related to $\pi\pi$ scattering, πK scattering and K_{e4}^+ form factors. The phase shifts $\delta_{\mathrm{s,ps}}(s,s_\ell)$ are thus functions of several types of subtraction parameters [43]:

- the $\pi\pi \to \pi\pi$ subtraction constants $a_X, b_X, \lambda_X^{(1)}, \lambda_X^{(2)}$ for $X = 00, x, +-, +0, ++$ can be obtained by matching the dispersive representation of $\pi\pi$ scattering amplitudes with the one-loop chiral expansion of the amplitudes including isospin breaking [340, 341]. The subtraction constants are then expressed in terms of a_0^0, a_0^2 and $N_f = 2$ LECs ($\bar{l}_{1,2,6}$ and $\hat{k}_i$). We trade $\bar{l}_{3,4}$ for a_0^0 and a_0^2 in the evaluation of the scattering amplitude, using eqs. (6.21)-(6.22), since we want to investigate values of (a_0^0, a_0^2) different from the χPT predictions.

- the $K^+ \to \pi\pi\ell\nu$ subtraction constants $\pi_{0,1,2,3}^Y$ for $Y = +-, 00$ can be obtain by matching the dispersive representation with the one-loop expression of the form factors with isospin breaking [337, 338, 341]. One gets the subtraction constants in terms of $N_f = 3$ LECs L_i, $\hat{K}_i$ and the ratio $R = \frac{m_s - \hat{m}}{m_d - m_u}$.

- the $\pi K \to \pi K$ subtraction constants $\tilde{a}_Z, \tilde{b}_Z$ for $Z = x, +-, 00$ (where x denotes the channel $\pi^0\bar{K}^0 \to \pi^+K^-$) are obtained by considering πK scattering at tree level including isospin breaking. They are expressed in terms of $a_0^{1/2}, a_0^{3/2}$, (πK), a_0^0, a_0^2 $(\pi\pi)$, and the ratio R.

With a very large set of data in the various decay channels for both the moduli and the phases of the form factors, one could in principle imagine to determine all the subtraction constants involved in the previous expressions. Our goal here will be more modest. We will assume that the values of the subtraction constants can be determined with a reasonable accuracy using one-loop χPT in the same way as in ref. [287], i.e., a strong chiral Lagrangian supplemented with counterterms responsible for the mass difference between neutral and charge pseudoscalar mesons, but without dynamical photons. One has thus to (re)compute the one-loop $\pi\pi$ scattering amplitudes and K_{e4}^+ form factors in this setting, and match onto the dispersive representation to obtain the expression of the subtraction constants. For our evaluation, we use estimates for the involved various LECs, which are collected in tab. 6.4. For the strong LECs $\bar{\ell}_i$ and L_i, we take the estimates in refs. [158, 183], taking $\log M_{\pi^\pm}$ in the definition of $\bar{\ell}_i$. For the $N_f = 3$ counterterms L_i, we take the central values of the so-called $O(p^4)$ fit in ref. [183], and assign an uncertainty of $\pm 0.5 \cdot 10^{-3}$ to each of the LECs. For the electromagnetic counterterms $\hat{k}_i$ and $\hat{K}_i$, we use resonance estimates obtained in χPT [118, 342] even though virtual photons are not included in the theory considered here. Since the $N_f = 3$ electromagnetic counterterms $\hat{K}_i$ have only a very limited impact on Δ, we keep them fixed and do not assume any range of variation. Finally, for the scattering parameters $a_0^{1/2}, a_0^{3/2}$, we use the values from the analysis of Roy-Steiner equations for πK scattering [44]. All our analysis involves values of the subtraction constants computed at the first order in isospin breaking.

We compute the difference with respect to the isospin limit case $M_{\pi^0} \to M_{\pi^\pm}$: $\Delta = [\delta_\mathrm{s} - \delta_0^0] - [\delta_\mathrm{p} - \delta_1^1]$ (in milliradians), where we identify the LO and NLO contributions $\Delta_2\delta$ and $\Delta_4\delta$. Moreover, in $\Delta_4\delta_\mathrm{s}$ we separate the part stemming from unitarity and involving only $\pi\pi$ scattering, $\Delta_4^U\delta_\mathrm{s}$, and the process-dependent part depending on the form factors $\Delta_4^F\delta_\mathrm{s}$:

$$\Delta = [\Delta_2\delta_\mathrm{s} + \Delta_4^U\delta_\mathrm{s} + \Delta_4^F\delta_\mathrm{s}] - [\Delta_2\delta_\mathrm{p} + \Delta_4\delta_\mathrm{p}]\,, \tag{6.76}$$

keeping only the first order in isospin breaking. In the kinematical regime accessible to K_{e4}^+ experiments, the contributions to the isospin-breaking correction are collected in tab. 6.5 and the resulting correction plotted in fig. 6.14 for the reference values:

$$s_\ell = 0\,, \quad a_0^0 = 0.225\,, \quad a_0^2 = -0.0382\,, \quad a_1^{1/2} = 0.144\,, \quad a_3^{1/2} = -0.0287\,, \qquad R = 37\,. \tag{6.77}$$

i	$\bar{\ell}_i$ [158]	i	$\hat{k}_i \cdot 10^3$ [342]	i	$L_i(M_\rho) \cdot 10^3$ [183]	i	$\hat{K}_i(M_\rho) \cdot 10^3$ [118]
1	-0.4± 0.6	1	8.4 ± 6.3	1	1.12 ± 0.5	1	-2.71
2	4.3±0.1	2	3.4± 6.3	2	1.23 ± 0.5	2	0.69
6	16.0 ± 0.9	3	2.7± 6.3	3	-3.98± 0.5	3	2.71
		4	1.4± 6.3	4	1.50± 0.5	4	1.38
		5	11.6± 6.3	5	1.21± 0.5	5	11.59
		6	3.9± 6.3	6	1.17± 0.5	6	2.77
		8	-1.4± 6.3	8	-0.36± 0.5	12	-4.2
		12	0	9	0.62± 0.5		

Table 6.4: *Values of the LECs used for the estimate of the subtraction constants. Note that we have expressed $\bar{\ell}_{3,4}$ in terms of a_0^0 and a_0^2 as explained in the text, and consequently these quantities do not appear here.*

E (MeV)	$\Delta_2\delta_\mathrm{s}$	$\Delta_4^U\delta_\mathrm{s}$	$\Delta_4^F\delta_\mathrm{s}$	$\Delta_2\delta_\mathrm{p}$	$\Delta_4\delta_\mathrm{p}$	Δ [43]	NA48/2 corr. [274]
286	15.75	0.06	-0.82	0.01	-0.00	14.98	12.54
296	12.91	0.07	-1.33	0.02	-0.00	11.62	11.56
305	12.52	0.06	-1.73	0.04	-0.01	10.80	11.54
313	12.60	0.03	-2.09	0.07	-0.01	10.47	11.76
322	12.88	-0.01	-2.45	0.09	-0.02	10.32	12.07
331	13.27	-0.06	-2.83	0.12	-0.03	10.25	12.44
340	13.75	-0.13	-3.25	0.15	-0.04	10.21	12.87
351	14.36	-0.23	-3.76	0.19	-0.05	10.17	13.38
365	15.17	-0.37	-4.43	0.25	-0.07	10.12	14.04
390	16.80	-0.72	-5.82	0.37	-0.12	9.90	15.32

Table 6.5: *Decomposition of the isospin-breaking correction to the difference of phase shifts $\delta_s - \delta_p$, with the S- and P-wave contribution at one and two loops according to our dispersive approach. All values are in milliradians. The reference values $a_0^0 = 0.225$, $a_0^2 = -0.0382$, $R = 37$ were used for the evaluation of the subtraction constants (see the text for more details). For comparison, the correction used in ref. [274] and based on the χPT estimate in ref. [289] is indicated in the last column.*

corresponding to central points in the analysis of Roy and Roy-Steiner equations for $\pi\pi$ and πK scatterings respectively [42, 44, 251] as well as the value for the isospin breaking in quark masses covering the range of values obtained from various sources (Dashen theorem [186], $\rho - \omega$ mixing [343] and baryon spectrum [344], $\eta \to 3\pi$ [345, 346]). We observe that the contribution from the P-wave is very small. Moreover a cancellation occurs between the NLO contributions due to unitarity and form factors, which brings Δ close to the LO asymptotic value $\frac{7}{32\pi F_\pi^2}[M_{\pi^\pm}^2 - M_{\pi^0}^2]$ ($\sim$ 10 mrad) for energies above 0.3 GeV. In the reference point eq. (6.77), the agreement with ref. [289] is good at intermediate energies, but our prediction at the higher end of the allowed range for hadronic invariant mass is smaller in magnitude than that in ref. [289].

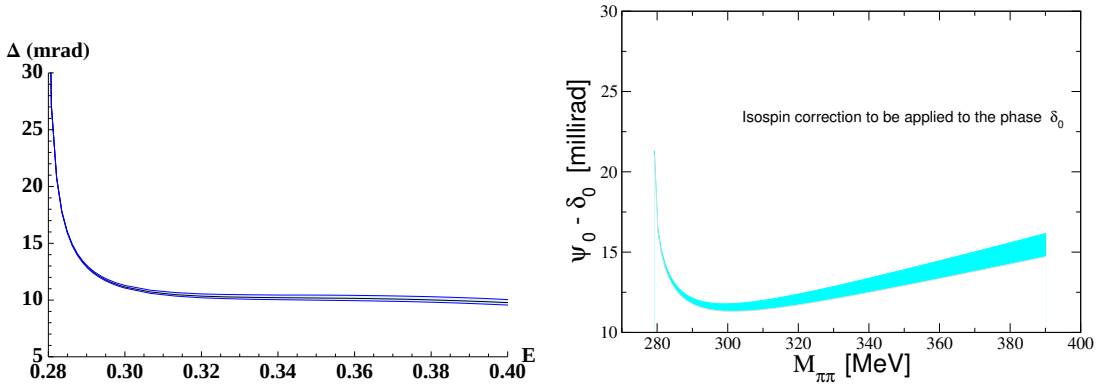

Figure 6.14: *On the left : isospin-breaking correction* Δ *for the reference values eq. (6.77) of the input parameters. The small variation corresponds to the variation of* $R = 35 \pm 7$*. On the right :* χPT *estimate of the same correction from ref. [289].*

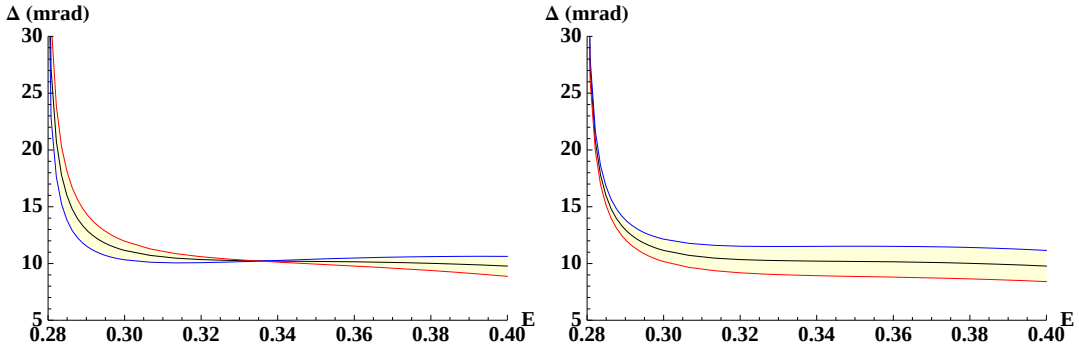

Figure 6.15: *Variation of the isospin-breaking correction* Δ *when varying* a_0^0 *(top) and* a_0^2 *(bottom) by 20% respectively compared to their reference values eq. (6.77).*

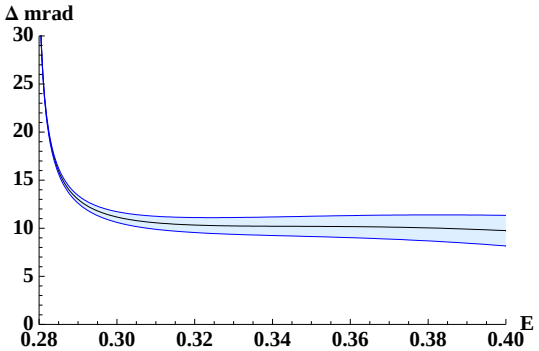

Figure 6.16: *Uncertainty on the isospin-breaking correction* Δ *from the variation of the LECs for the reference values eq. (6.77).*

The dependence of Δ on $a_0^{1/2}$ and $a_0^{3/2}$ turns out to be negligible, and that on R is rather weak. We are now in a position to rediscuss the dependence on s_ℓ, already stressed in sec. 6.3.2 in the case of the phase shifts. There is indeed a dependence on s_ℓ in the partial-wave projection

of the K_{e4} form factors, and more precisely, a singularity at the edge of the allowed kinematic range $s_\ell \to (M_K - \sqrt{s})^2$. In this limit, the hadronic and the leptonic pairs have both a vanishing three-momentum in the rest frame of the decaying kaon, and the projection over the partial waves cannot be defined in a meaningful way (since the angle involves the line of flight of the $\pi\pi$ pair in the K rest frame). However, this singularity blows up only very close to the edge of the available range for s_ℓ, and it should affect only weakly the experiments whose acceptance decreases as one gets closer to the endpoints of the kinematic ranges. For instance, at the reference point eq. (6.77), if we vary s between $4M_\pi^2$ and 0.19 GeV^2 (which is the range for which NA48/2 has enough acceptance to collect data) and s_ℓ between m_e^2 and $0.95\cdot(M_K - \sqrt{s})^2$, Δ does not change by more than 11%. Even though the dependence of Δ on s_ℓ is not very strong, it would be interesting to have the NA48/2 phase shifts by bins of s and s_ℓ in order to apply the isospin-breaking correction that we have just computed.

The dependence of Δ on a_0^0 and a_0^2 is not negligible, as can be seen in fig. 6.15. The uncertainties related to the inputs of the LECs are indicated in fig. 6.16, and come mostly from the $SU(2)$ electromagnetic LECs $\hat{k}_i$ and the $SU(3)$ strong LECs $L_{1,2,3}$. A numerical parametrisation of the correction Δ and the uncertainty stemming from LECs is provided in app. A.4.2 under the form $\Delta(s, s_\ell, a_0^0, a_0^2, R) \pm \delta\Delta(s)$.

6.3.6 Re-analysis of NA48 results

We can use our computation of the isospin-breaking correction $\Delta = [\delta_\mathrm{s} - \delta_0^0] - [\delta_\mathrm{p} - \delta_1^1]$ to perform an analysis of the available phase shifts from K_{e4}^+ decays, namely the old Geneva-Saclay experiment, BNL-E865 experiment and NA48/2 [270, 271, 273, 274]. We perform the two Scalar and Extended fits, correcting through a χ^2 function including the isospin-breaking corrections:

$$\chi^2_{\mathrm{iso-corr}}(a_0^0, a_0^2, \theta_0, \theta_1) = \sum_i \frac{([\delta_0^0 - \delta_1^1]^{\mathrm{Roy}}(s_i^{\mathrm{exp}}) - [\delta_\mathrm{s} - \delta_\mathrm{p}]_i^{\mathrm{exp}}) + \Delta)^2}{(\sigma_i^{\mathrm{exp}})^2 + (\delta\Delta)^2}$$
$$+ \left(\frac{\theta_0 - 82.3^\circ}{3.4^\circ}\right)^2 + \left(\frac{\theta_1 - 108.9^\circ}{2^\circ}\right)^2 + \left(\frac{R - 37}{5}\right)^2 + \chi^2_{\mathrm{intial}}\,, (a_0^0, a_0^2, \theta_0, \theta_1)\,, \quad (6.78)$$

where $\chi^2_{\mathrm{initial}}$ contains either the constraint of the scalar radius of the pion eq. (6.35) or $I = 2$ data eq. (6.32). We evaluated Δ at $s_\ell = 0$, since it has a negligible impact on the value of Δ in most of the kinematic range. We have corrected only $I = \ell = 0$ and $I = \ell = 1$ partial waves for isospin-breaking corrections. A similar correction should also be performed for $I = 2, \ell = 0$ data if data of sufficiently good quality were obtained in this channel – however the discussion of isospin correction would be quite different from the one presented here, as this kind of data can be obtained only from production experiments. The results of the fit are presented in fig. 6.17, and tab. 6.6. We notice several appealing features in the results. First, the inclusion of isospin-breaking corrections brings back the scattering length a_0^0 into the domain of χPT expectations. Moreover, we see that the two types of fits are getting in closer agreement, and the previous 1-σ disagreement observed previously has disappeared.

We have also performed a fit including the constraint from the cusp in $K^\pm \to \pi^\pm\pi^0\pi^0$ decays [275, 276], based on the theoretical treatment of ref. [347] of a non-relativistic theory including real and virtual photons:

$$a_0^0 - a_0^2 = 0.2571(48)(29)\,, \qquad a_0^2 = -0.0241(129)(96)\,, \qquad \rho_{a_0^0 - a_0^2, a_0^2} = -0.774\,, \qquad (6.79)$$

where we combined statistics and systematics in quadrature to include this piece information in the fit called "All", also described in fig. 6.17, and tab. 6.6, in good agreement with the Scalar

and Extended fits, and slightly more accurate. The three fits all point towards a saturation of $N_f = 2$ chiral series by their leading orders (two-flavour quark condensate and decay constant), even though the value of $\bar{\ell}_3$ remains a bit low compared to its estimates around 4, described in sec. 3.3.5.

It is quite interesting to compare these results with the ones obtained by the NA48/2 collaboration [276]:

$$\text{[NA48/2]} \qquad K_{\ell 4}: \qquad a_0^0 = 0.2220 \pm 0.0128_{\rm stat} \pm 0.0050_{\rm syst} \pm 0.0037_{\rm th}\,, \tag{6.80}$$

$$a_0^2 = -0.0432 \pm 0.0086_{\rm stat} \pm 0.0034_{\rm syst} \pm 0.0028_{\rm th}\,, \tag{6.81}$$

$$\text{[NA48/2]} \quad K_{\ell 4} + (K \to 3\pi): \qquad a_0^0 = 0.2210 \pm 0.0047_{\rm stat} \pm 0.0040_{\rm syst}\,, \tag{6.82}$$

$$a_0^2 = -0.0429 \pm 0.0044_{\rm stat} \pm 0.0028_{\rm syst}\,, \tag{6.83}$$

using the isospin-breaking corrections in ref. [274], based on the χPT estimate in ref. [289] One should also recall the result obtained in ref. [302] following a different approach, detailed in sec. 6.1.2: each partial wave was parametrised through a conformal mapping on which dispersive constraints similar to Roy equations were imposed, including experimental data up to 1100 MeV:

$$\text{[GarciaMartin et al.]}: \qquad a_0^0 = 0.221 \pm 0.009\,, \qquad a_0^2 = -0.043 \pm 0.008\,. \tag{6.84}$$

We see that all fits lead to the same constraints on a_0^0 and a_0^2 and thus, on the pattern of $N_f = 2$ chiral symmetry breaking. As indicated in sec. 3.6.1, this puts strong constraints on the values of r, that cannot be too close to $r_1 \simeq 8$, indicating that the framework of Generalized χPT [159] is not particularly suited to deal with $\pi\pi$ scattering.

6.4 Summary

We have discussed the determination of the pattern of chiral symmetry breaking in the $N_f = 2$ chiral limit, which is tested essentially through $\pi\pi$ scattering. Several pieces of information are available, from production experiment and processes involving the rescattering of $\pi\pi$ final states. A particularly efficient tool to exploit these data consists in Roy equations, a set of dispersion relations that exploits unitarity and crossing symmetry to constrain the structure of the low-energy $\pi\pi$ amplitude, dominated by S- and P-waves. Given inputs at higher energies, one can solve these equations and provide solutions in terms of two subtraction constants identified with the S-wave scattering lengths a_0^0 and a_0^2. In this boundary-value problem, an essential input consists in the values of the $\pi\pi$ phase shifts at the matching point, i.e. the frontier between low energy (where the Roy equations are solved) and high energy (where data is available). We extended the framework of ref. [251] to include explicitly the dependence of the solutions on the phase shifts at the matching point.

These solutions can be compared to different sources of experimental information for low-energy $\pi\pi$ scattering, in particular the cusp in the invariant mass plot of the Dalitz plot for $K^\pm \to \pi^\pm\pi^0\pi^0$, the lifetime of pionium atoms, and the angular analysis of $K_{\ell 4}$ decays. The latter play a prominent role due to the accuracy reached successively by the E865 and NA48/2 experiments, which were able to determine the difference of the phase shifts between $I = \ell = 0$ and $I = \ell = 1$ partial waves. One can combine this piece of information either with a theoretical input (the scalar radius of the pion and its connection with a_0^0 and a_0^2 at NNLO in $N_f = 2$ χPT) or with some experimental information (for instance, the available data in the $I = 2$,

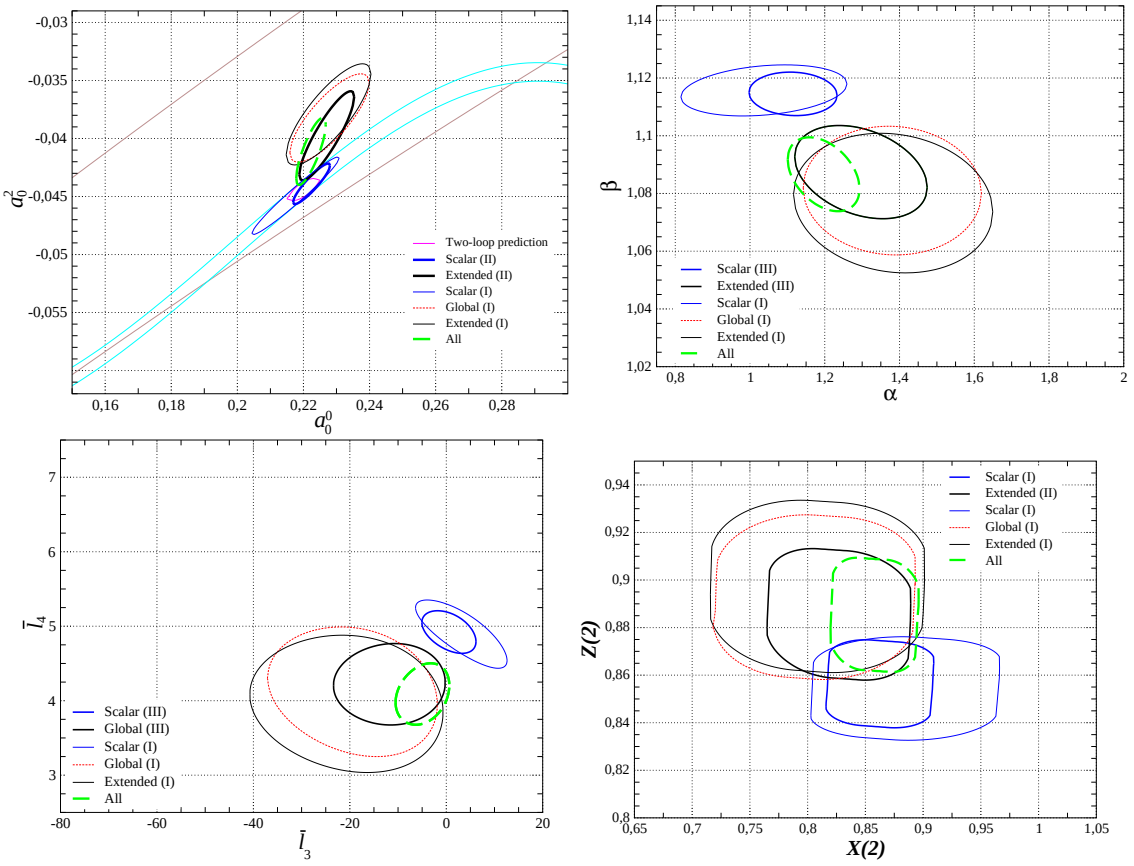

Figure 6.17: *Results for the Scalar and Extended fits once NA48/2 data is included and isospin-breaking corrections are taken into account. For comparison, the previous results obtained without NA48/2 data are drawn with thin lines (Scalar (blue, dashed), Global (red, dotted), Extended (black, solid)). The central values of the bins in hadronic invariant mass of E865 have been corrected according to the erratum of ref. [272]. Correlations between the bins are neglected.*

$\ell = 0$ channel). At the time of the first E865 analysis, the two methods led to slightly different results (1-σ discrepancy) especially concerning the value of a_0^2. Once the scattering lengths are determined, one can reconstruct the $\pi\pi$ scattering amplitude in the subthreshold region where Chiral Perturbation Theory is expected to converge quickly. The fit including data from the $I = 2$ $\ell = 0$ channel led to rather low values of the two-flavour quark condensate ($X(2) = 0.81 \pm 0.08$) compared to the fit including the theoretical constraint coming from the scalar radius of the pion.

The advent of new data from the NA48/2 collaboration led to a reassessment of these conclusions at several levels. First, there was a discrepancy between the two experiments at high $\pi\pi$ invariant mass, which turned out to be related to an inappropriate definition of the center of the bins by the E865 collaboration. Second, the accuracy of the data of the NA48/2 collaboration obliged to consider effects that had been neglected before, namely radiative corrections. In particular, if the effect of virtual and real photons is taken into account in the experimental analysis, one has also to correct for the isospin-breaking difference of mass between the neutral and the charged pions, and the corresponding breakdown of Watson's theorem. It becomes mandatory to correct the data for such an effect before comparing them with the solutions of

	Extended (III)	Scalar (III)	All
Isospin brkg	Corrected	Corrected	Corrected
Inputs	E865 corr. [272] NA48/2 [274] G.-Saclay [270] Hoogland(A) [326] Losty [327]	E865 corr. [272] NA48/2 [274]	E865 corr. [272] NA48/2 [274] G.-Saclay [270] Hoogland(A) [326] Losty [327] NA47/2 Cusp [276]
a_0^0	0.227 ± 0.009	0.222 ± 0.006	0.222 ± 0.005
a_0^2	-0.0398 ± 0.0039	-0.0439 ± 0.0018	-0.0411 ± 0.0029
$\rho_{a_0^0,a_0^2}$	0.873	0.906	0.802
χ^2/d.o.f	27.2/28	15.7/15	28.6/30
α	1.30 ± 0.21	1.12 ± 0.12	1.19 ± 0.14
β	1.09 ± 0.02	1.11 ± 0.01	1.09 ± 0.02
$\rho_{\alpha\beta}$	0.329	0.068	0.408
$\lambda_1 \cdot 10^3$	-3.71 ± 0.59	-3.92 ± 0.10	-3.48 ± 0.50
$\lambda_2 \cdot 10^3$	8.93 ± 0.11	9.13 ± 0.04	8.90 ± 0.10
$\lambda_3 \cdot 10^4$	2.31 ± 0.15	2.31 ± 0.03	2.37 ± 0.13
$\lambda_4 \cdot 10^4$	-1.39 ± 0.04	-1.45 ± 0.02	-1.40 ± 0.04
$\bar{\ell}_3$	-11.8 ± 11.6	0.6 ± 5.6	-4.9 ± 4.6
$\bar{\ell}_4$	4.2 ± 0.6	4.9 ± 0.3	4.1 ± 0.4
$X(2)$	0.83 ± 0.06	0.86 ± 0.05	0.86 ± 0.04
$Z(2)$	0.88 ± 0.03	0.86 ± 0.02	0.89 ± 0.02

Table 6.6: *Subthreshold and LECs once NA48/2 data is included and isospin-breaking corrections are taken into account. The central values of the bins in hadronic invariant mass of E865 have been corrected according to the erratum of ref. [272]. Correlations between the bins are neglected.*

the Roy equations derived in the isospin limit. We illustrated the importance of this effect by performing fits including the NA48/2 and E865 data without applying any further correction: the various fits get in better agreement than before, but with values of a_0^0 much larger than expected in two-flavour χPT: the two-flavour condensate contributes only by 3/4 to the chiral series of $F_\pi^2 M_\pi^2$, and $F(2)^2$ is 15% below F_π^2.

Isospin breaking corrections due to mass effects have been computed within χPT [289] and indicate that they would restore the agreement with chiral expectations. However, these corrections, being computed within χPT, are strictly valid only in a limited region of (a_0^0, a_0^2), and may change significantly when the scattering lengths are varied. We have adopted a slightly different approach, incorporating the effect of rescattering (governed by a_0^0 and a_0^2) up to two loops through a dispersive framework, and we match the resulting amplitude to the chiral expansion to estimate the size of the subtraction constants. In the S-wave, we can identify two different isospin-breaking corrections to the phase shifts: a universal part, due to isospin-breaking in $\pi\pi$ rescattering, and a process-dependent one, coming from the isospin-breaking

in the form factors. In the case of $K_{\ell 4}$ the two contributions tend to compensate, leading to a correction for $\delta_{\rm s} - \delta_{\rm p}$ in broad agreement with the χPT evaluation of ref. [289] for the values of the scattering lengths where they can be compared, even though our estimate tends to be smaller at large invariant masses.

Once applied to the $K_{\ell 4}$ data, the isospin-breaking correction brings back the scattering lengths in very good agreement with two-loop χPT predictions whichever fit procedure is chosen. One can also include information from the cusp in $K \to 3\pi$ in order to narrow the uncertainty on the scattering lengths further. In all case, the two-flavour order parameters saturate the pion mass and decay constants chiral series very efficiently, even though the value of $\bar{\ell}_3$ remains a bit low compared to the original estimates. This disfavours clearly the Generalized scenario with a small $N_f = 2$ quark condensate, and indicates that the pattern of chiral symmetry breaking two-flavour chiral limit $m_u = m_d = 0$ and m_s physical is dominated by the $N_f = 2$ quark condensate.

Curiouser and curiouser !
Alice

7

πK scattering: experimental and dispersive constraints

After having investigated the pattern of chiral symmetry breaking in the $N_f = 2$ chiral limit, we turn to the $N_f = 3$ chiral limit $m_u = m_d = m_s = 0$, and focus on πK scattering in order to determine the corresponding chiral order parameters. The situation is less favourable than for $\pi\pi$ scattering: at the theoretical level, the predictions involve more low-energy constants (LECs) are potentially affected by larger higher-order corrections, and at the experimental level, low-energy data is more scarce.

However, the same dispersive approach as in the previous chapter can be used to constrain the structure of the πK scattering amplitudes at low energies. The situation is more complicated because of the existence of two different scattering amplitudes, and the crossed channel ($\pi\pi \to K\bar{K}$) is different from the one considered here ($\pi K \to \pi K$). We can write down two different kinds of dispersion relations, keeping t fixed or the product us fixed, and project them onto partial waves in the s- and t-channels to determine the low partial waves in terms of high-energy data. In analogy to the $\pi\pi$ scattering, we express everything in terms of two subtraction constants, identified to the S-wave scattering lengths $a_0^{1/2}$ and $a_0^{3/2}$. The corresponding Roy-Steiner equations prove powerful to extract information on πK scattering from data at intermediate energies. One can study the range of validity of these dispersion relations (validity of the Mandelstam double spectral representation, range of the partial-wave expansion). We choose appropriate matching points for $\pi K \to \pi K$ and $\pi\pi \to K\bar{K}$ scatterings separating the low- and high-energy regions, so that there is only one solution for both kinds of partial waves in the low-energy region. Physical requirements put further constraints on $a_0^{1/2}$ and $a_0^{3/2}$ so that the solutions are not only continuous, but also smooth at the matching points. Once these constraints have been derived, it is possible to determine the shape of the πK scattering amplitudes including non-physical (subthreshold) regions, where it can be matched to the chiral expansions of these amplitudes. We can then extract information on some of the LECs of $N_f = 3$ Chiral Perturbation Theory (χPT), and in particular on L_4 and L_6.

The elastic $\pi\pi$- and πK-scattering amplitudes enjoy rather unique properties because pions and kaons are the lightest particles in the QCD spectrum. The analytic structure of the amplitudes is simple, free from anomalous thresholds, and elastic unitarity holds in both direct and crossed channels in the low-energy region. An additional useful property of the S matrix element for elastic scattering is that a resonance manifests itself not only as a pole on the second Riemann sheet, but also as a zero on the first sheet. This has been used as in conjunction with $\pi\pi$ Roy equations to confirm the existence of the σ meson in the $\pi\pi$ scattering amplitude and its mass and width have been determined quite accurately [133]. We will follow here the same method as in ref. [133] and show from Roy-Steiner equations that the existence of the scalar $K_0^*(800)$ resonance (also called κ), corresponding to a pole in the S matrix, can be established using *a)* the available experimental data and *b)* general properties of analyticity, unitarity and crossing symmetry of two-body scattering amplitudes. [1]

[1] This chapter is based on the following articles:

[K] P. Büttiker, SDG, and B. Moussallam, *A new analysis of πK scattering from Roy and Steiner type equations*, Eur. Phys. J. C33 (2004) 409 [44]

[L] SDG and B. Moussallam, *The $K^*0(800)$ scalar resonance from Roy-Steiner representations of πK scattering*, Eur.Phys.J. C33 (2004) 409-432 [45]

7.1 Derivation of the Roy-Steiner equations

7.1.1 Definitions [K]

Firstly, we define from the pion and kaon masses [348]:

$$m_\pm = M_K \pm M_\pi,\ \Sigma = M_K^2 + M_\pi^2,\ \Delta = M_K^2 - M_\pi^2\ . \tag{7.1}$$

Isospin symmetry will always be assumed here, so that there are two independent πK amplitudes $F^I(s,t)$, with isospin $I = 1/2$ and $I = 3/2$. Making use of $s-u$ crossing, the $I = 1/2$ amplitude can be expressed in terms of the $I = 3/2$ one:

$$F^{1/2}(s,t,u) = -1/2F^{3/2}(s,t,u) + 3/2F^{3/2}(u,t,s)\ . \tag{7.2}$$

It is convenient to introduce the amplitudes F^+ and F^- which are, respectively, even and odd under $s-u$ crossing. In terms of isospin amplitudes, they are defined as:

$$F^+(s,t,u) = \frac{1}{3}F^{1/2}(s,t,u) + \frac{2}{3}F^{3/2}(s,t,u)\,, F^-(s,t,u) = \frac{1}{3}F^{1/2}(s,t,u) - \frac{1}{3}F^{3/2}(s,t,u)\ . \tag{7.3}$$

The partial-wave expansion of the πK isospin amplitudes is defined as:

$$F^I(s,t) = 16\pi \sum_l (2l+1) P_l(z_s) f_l^I(s)\ . \tag{7.4}$$

where $P_l(z)$ are the standard Legendre polynomials and z_s is the cosine of the s-channel scattering angle:

$$z_s = 1 + \frac{2st}{\lambda_s} \quad \text{with } \lambda_s = (s-m_+^2)(s-m_-^2)\ . \tag{7.5}$$

In a similar way we can expand F^+ and F^-, and the corresponding partial-wave projections are denoted by $f_l^+(s)$ and $f_l^-(s)$. The amplitudes can be projected over the partial waves through:

$$f_l^I(s) = \frac{s}{16\pi\lambda_s} \int_{-\lambda_s/s}^{0} dt\ P_l(z_s) F^I(s,t)\ . \tag{7.6}$$

The values of the amplitudes at threshold define the S-wave scattering lengths, with the following conventional normalization $a_0^I = 2f_0^I(m_+^2)/m_+$ (and similarly for $a_0^\pm$ in terms of $f_0^\pm(m_+^2)$). Under $s-t$ crossing, one generates the $I = 0$ and $I = 1$ $\pi\pi \to K\overline{K}$ amplitudes:

$$G^0(t,s,u) = \sqrt{6}F^+(s,t,u)\,, \qquad G^1(t,s,u) = 2F^-(s,t,u)\ . \tag{7.7}$$

The partial-wave expansion of the $\pi\pi \to K\overline{K}$ amplitudes is defined as:

$$G^I(t,s) = 16\pi\sqrt{2} \sum_l (2l+1)[q_\pi(t)q_K(t)]^l P_l(z_t) g_l^I(t)\ , \tag{7.8}$$

where the summation runs over even (odd) values of l for $I = 0$ ($I = 1$) due to Bose symmetry in the $\pi\pi$ channel. In this expression the momenta q_π, q_K and the cosine of the t-channel scattering angle z_t are given by:

$$q_P(t) = \frac{1}{2}\sqrt{t - 4m_P^2}, \quad z_t = \frac{s-u}{4q_\pi(t)q_K(t)}\ . \tag{7.9}$$

The relations between these partial-wave amplitudes and the S-matrix elements are easily worked out:

$$\left[S_l^I(s)\right]_{\pi K\to\pi K} = 1 + 2i\frac{\sqrt{\lambda_s}}{s}\theta(s-m_+^2) f_l^I(s)\,, \tag{7.10}$$

$$\left[S_l^I(t)\right]_{\pi\pi\to K\overline{K}} = 4i\frac{(q_\pi(t)q_K(t))^{l+1/2}}{\sqrt{t}}\theta(t-4M_K^2) g_l^I(t)\ . \tag{7.11}$$

7.1.2 Fixed-t based dispersive representation [K]

To derive Roy-Steiner equations, we assume the validity of the Mandelstam double-spectral representation [349]:

$$A(s,t,u) = \frac{1}{\pi^2}\int_{(M_\pi+M_K)^2}^{\infty} dt' \int_{4M_\pi^2}^{\infty} dt' \frac{\rho_{st}(s',t')}{(s'-s)(t'-t)} \tag{7.12}$$

$$+\frac{1}{\pi^2}\int_{(M_\pi+M_K)^2}^{\infty} du' \int_{4M_\pi^2}^{\infty} dt' \frac{\rho_{tu}(t',u')}{(t'-t)(u'-u)} + \frac{1}{\pi^2}\int_{(M_\pi+M_K)^2}^{\infty} ds' \int_{(M_\pi+M_K)^2}^{\infty} du' \frac{\rho_{tu}(t',u')}{(t'-t)(u'-u)}\,,$$

from which one can derive a variety of dispersion relations (DRs) for one variable [2]. According to the Froissart bound [350], two subtractions are needed at most for F^+ and one subtraction for F^- (because $s-u$ can be factored out in the latter case). More detailed information about asymptotic behaviour is provided by Regge phenomenology [291], according to which two subtractions are indeed necessary for F^+ while an unsubtracted DR is expected to converge for F^-. However, convergence is rather slow in the latter case since the integrand behaves like $(s')^{-3/2}$ asymptotically. Therefore, we choose to make use of a once-subtracted DR for F^- in order to improve the convergence and reduce the sensitivity to the high-energy domain.

Fixed-t DRs for F^+ and F^- can be written in the following form:

$$F^+(s,t) = c^+(t) + \frac{1}{\pi}\int_{m_+^2}^{\infty} ds' \left[\frac{1}{s'-s} + \frac{1}{s'-u} - \frac{2s'-2\Sigma-t}{\lambda_{s'}}\right] \mathrm{Im}\, F^+(s',t)\ .$$

$$\frac{F^-(s,t)}{s-u} = c^-(t) + \frac{1}{\pi}\int_{m_+^2}^{\infty} ds' \left[\frac{1}{(s'-s)(s'-u)} - \frac{1}{\lambda_{s'}}\right] \mathrm{Im}\, F^-(s',t)\ . \tag{7.13}$$

These expressions involve two unknown functions of t: $c^+(t)$ and $c^-(t)$. The basic idea for determining these functions is to invoke crossing [285,351], which can be implemented in various ways: for instance, one can use fixed-s or fixed-$(s-u)$ DRs. It turns out that DRs at fixed us provide the largest domain of applicability (these relations, sometimes called hyperbolic DRs, were exploited in ref. [352]). We start with a special set of hyperbolic DRs (more general hyperbolic DRs will be considered later) in which $us=\Delta^2$, along the trajectory:

$$s \equiv s_\Delta(t) = 1/2\left(2\Sigma - t + \sqrt{(t-4M_\pi^2)(t-4M_K^2)}\right)\ ,$$

$$u \equiv u_\Delta(t) = 1/2\left(2\Sigma - t - \sqrt{(t-4M_\pi^2)(t-4M_K^2)}\right)\ . \tag{7.14}$$

According to Regge theory [291], the function $F^+(s_\Delta,t)$ satisfies a once-subtracted DR which is slowly converging. Like in the case of the fixed-t DR for F^-, we choose to improve the convergence by using a twice-subtracted representation, whereas the function $F^-(s_\Delta,t)$ is expected to satisfy an unsubtracted DR which is well converging:

$$F^+(s_\Delta,t) = 8\pi m_+ a_0^+ + b^+ t + \frac{1}{\pi}\int_{m_+^2}^{\infty} ds' \left[\frac{2s'-2\Sigma+t}{\lambda_{s'}+s't} - \frac{2s'-2\Sigma-t}{\lambda_{s'}}\right] \mathrm{Im}\, F^+(s',t'_\Delta)$$

$$+\frac{t^2}{\sqrt{6}\pi}\int_{4M_\pi^2}^{\infty} \frac{dt'}{(t')^2(t'-t)} \mathrm{Im}\, G^0(t',s'_\Delta)\,,$$

[2] For the πK amplitude, the existence of fixed-t DR can be established on more general grounds in a finite domain of t [290].

$$\frac{F^-(s_\Delta,t)}{s_\Delta-u_\Delta}=\frac{8\pi m_+a_0^-}{m_+^2-m_-^2}+\frac{1}{\pi}\int_{m_+^2}^\infty ds'\left[\frac{1}{\lambda_{s'}+s't}-\frac{1}{\lambda_{s'}}\right]\mathrm{Im}\,F^-(s',t'_\Delta)$$
$$+\frac{t}{2\pi}\int_{4M_\pi^2}^\infty\frac{dt'}{t'(t'-t)}\mathrm{Im}\,\frac{G^1(t',s'_\Delta)}{\sqrt{(t'-4M_\pi^2)(t'-4M_K^2)}}\ . \qquad (7.15)$$

In these equations, we have used the following notation: $s'_\Delta=s_\Delta(t')$ and $t'_\Delta=2\Sigma-s'-\Delta^2/s'$, together with the relation $(s'-s_\Delta(t))(s'-u_\Delta(t))=\lambda_{s'}+s't$.

These representations involve three subtraction constants: the two scattering lengths a_0^+, a_0^- and an additional parameter denoted b^+. One can eliminate the latter by combining two slowly convergent sum rules for a_0^- and b^+ into a rapidly convergent sum rule:

$$b^+=\frac{8\pi m_+a_0^-}{m_+^2-m_-^2}-\frac{1}{\pi}\int_{m_+^2}^\infty\frac{ds'}{\lambda_{s'}}\mathrm{Im}\,\left[F^+(s',t'_\Delta)+F^-(s',t'_\Delta)\right]$$
$$+\frac{1}{\pi}\int_{4M_\pi^2}^\infty\frac{dt'}{t'}\mathrm{Im}\,\left[\frac{G^0(t',s'_\Delta)}{\sqrt{6}t'}-\frac{G^1(t',s'_\Delta)}{2\sqrt{(t'-4M_\pi^2)(t'-4M_K^2)}}\right]\ . \qquad (7.16)$$

Why does this sum rule converge more quickly ? In the first integral, the combination F^++F^- appears, which is the amplitude for the process $\pi^+K^-\to\pi^+K^-$. The asymptotic region of the integrand corresponds to $s\to\infty$, $u\to 0$. The amplitude in this region is controlled by the Regge trajectories in the $u-$channel which is exotic, leading to a fast decrease of the integrand. In the second integral, the high-energy tail involves the combination $\frac{1}{\sqrt{6}}G^0(t',s')-1/2G^1(t',s')$ for $t'\to\infty$ and $s'\to 0$. The leading Regge contributions are generated by the K^{**} and K^* trajectories [291]:

$$\lim_{t\to\infty,\ s\to 0}\mathrm{Im}\,\left[\frac{1}{\sqrt{6}}G^0(t,s)-1/2G^1(t,s)\right]=\beta_{K^{**}}(s)t^{\alpha_{K^{**}}(s)}-\beta_{K^*}(s)t^{\alpha_{K^*}(s)}\ . \qquad (7.17)$$

This difference would vanish if Regge trajectories satisfied exactly the property of exchange degeneracy. In nature, this property is not exact but it has long been observed to be approximately fulfilled, which should lead to a significant suppression of the integrand at high energies. Therefore, the two integrals involved in eq. (7.16) are expected to converge quickly, providing a determination of b^+ with only a mild sensitivity to high energies.

Combining the two dispersive representations eqs. (7.13) and (7.15) for the amplitudes F^+ and F^-, the subtraction functions in eqs. (7.13) get determined in terms of the two S-wave scattering lengths and we obtain the following representation for the two amplitudes:

$$F^+(s,t)=8\pi m_+a_0^++b^+t+\frac{1}{\pi}\int_{m_+^2}^\infty ds'\left[\frac{1}{s'-s}+\frac{1}{s'-u}-\frac{2s'-2\Sigma+t}{\lambda_{s'}+s't}\right]\mathrm{Im}\,F^+(s',t) \qquad (7.18)$$
$$+\frac{1}{\pi}\int_{m_+^2}^\infty ds'\left[\frac{2s'-2\Sigma+t}{\lambda_{s'}+s't}-\frac{2s'-2\Sigma-t}{\lambda_{s'}}\right]\mathrm{Im}\,F^+(s',t'_\Delta)+\frac{t^2}{\sqrt{6}\pi}\int_{4M_\pi^2}^\infty\frac{dt'}{(t')^2(t'-t)}\mathrm{Im}\,G^0(t',s'_\Delta)\ ,$$

$$F^-(s,t)=\frac{8\pi m_+a_0^-}{m_+^2-m_-^2}(s-u)+\frac{1}{\pi}\int_{m_+^2}^\infty ds'\left[\frac{1}{s'-s}-\frac{1}{s'-u}-\frac{s-u}{\lambda_{s'}+s't}\right]\mathrm{Im}\,F^-(s',t) \qquad (7.19)$$
$$+(s-u)\left\{\frac{1}{\pi}\int_{m_+^2}^\infty ds'\left[\frac{1}{\lambda_{s'}+s't}-\frac{1}{\lambda_{s'}}\right]\mathrm{Im}\,F^-(s',t'_\Delta)+\frac{t}{2\pi}\int_{4M_\pi^2}^\infty\frac{dt'}{t'(t'-t)}\mathrm{Im}\,\frac{G^1(t',s'_\Delta)}{\sqrt{(t'-4M_\pi^2)(t'-4M_K^2)}}\right\},$$

where the parameter b^+ is to be expressed in the terms of the sum rule eq. (7.16). The domain of applicability of this representation is limited by the domain of validity of the fixed$-t$ DRs, eq. (7.13). In sec. 7.2, we will show that the fixed-t DRs hold for $t < 4M_\pi^2$, which enables us to perform the projection of eq. (7.18) on $\pi K \to \pi K$ partial waves. We will also need a representation which is valid for $t \geq 4M_\pi^2$ in order to obtain equations for the $\pi\pi \to K\bar{K}$ partial waves. For this purpose, we now consider a family of hyperbolic DRs.

7.1.3 Fixed us dispersive representation [K]

Let us consider a general family of hyperbolic DRs for which $us = b$ is fixed. b is a parameter with (a priori) arbitrary values and should not be confused with the subtraction constant b^+ introduced in the previous section. We write down a twice-subtracted representation for $F^+(s_b, t)$ and a once-subtracted one for $F^-(s_b, t)$:

$$F^+(s_b,t) = f^+(b) + th^+(b) + \frac{1}{\pi}\int_{m_+^2}^{\infty} ds' \left[\frac{2s'-2\Sigma+t}{\lambda^b_{s'}+s't} - \frac{2s'-2\Sigma-t}{\lambda^b_{s'}}\right] \mathrm{Im}\, F^+(s',t'_b) \\ + \frac{t^2}{\sqrt{6}\pi}\int_{4m_\pi^2}^{\infty} \frac{dt'}{t'^2(t'-t)} \mathrm{Im}\, G^0(t',s'_b)\ , \tag{7.20}$$

$$\frac{F^-(s_b,t)}{s_b-u_b} = f^-(b) + \frac{1}{\pi}\int_{m_+^2}^{\infty} ds' \left[\frac{1}{\lambda^b_{s'}+s't} - \frac{1}{\lambda^b_{s'}}\right] \mathrm{Im}\, F^-(s',t'_b) + \frac{t}{2\pi}\int_{4m_\pi^2}^{\infty} \frac{dt'}{t'(t'-t)} \mathrm{Im}\, \frac{G^1(t',s'_b)}{s'_b-u'_b}\ ,$$

with the notation $s'_b = \left(2\Sigma - t' + \sqrt{(2\Sigma-t')^2-4b}\right)/2$, $t'_b = 2\Sigma - s' - b/s'$, $\lambda^b_{s'} = (s')^2 - 2\Sigma s' + b$. The representations eqs. (7.20) are a generalization of the DRs eqs. (7.15) derived for $us = \Delta^2$. They involve three unknown functions of b: $f^+(b)$, $f^-(b)$ and $h^+(b)$ (which generalize the subtraction constants of eqs. (7.15)). The two functions $f^+(b)$, $f^-(b)$ can be determined by matching eqs. (7.20) with the representations eqs. (7.18) at the point $t = 0$ (which lies inside their domain of validity). Next, the function $h^+(b)$ can be expressed as a rapidly convergent sum rule analogous to eq. (7.16). Putting things together, one finally obtains the following representations involving the two S-wave scattering lengths a_0^+, a_0^- as the only arbitrary constants:

$$F^+(s_b,t) = 8\pi m_+ \left(a_0^+ + t\frac{a_0^-}{m_+^2-m_-^2}\right) + \frac{t}{\pi}\int_{4m_\pi^2}^{\infty}\frac{dt'}{t'}\left[\frac{\mathrm{Im}\, G^0(t',s'_b)}{\sqrt{6}(t'-t)} - \mathrm{Im}\,\frac{G^1(t',s'_b)}{2(s'_b-u'_b)}\right] \\ + \frac{1}{\pi}\int_{m_+^2}^{\infty} ds' \left\{\frac{2s'-2\Sigma+t}{\lambda^b_{s'}+s't}\mathrm{Im}\, F^+(s',t'_b) - \frac{2s'-2\Sigma}{\lambda^b_{s'}}\mathrm{Im}\,[F^+(s',t'_b)-F^+(s',0)]\right. \\ \left. - \frac{t}{\lambda^b_{s'}}\mathrm{Im}\,[F^-(s',t'_b)-F^-(s',0)] - \frac{2s'-2\Sigma}{\lambda_{s'}}\mathrm{Im}\, F^+(s',0) - \frac{t}{\lambda_{s'}}\mathrm{Im}\, F^-(s',0)\right\},$$

$$\frac{F^-(s_b,t)}{s_b-u_b} = \frac{8\pi m_+ a_0^-}{m_+^2-m_-^2} + \frac{t}{2\pi}\int_{4m_\pi^2}^{\infty}\frac{dt'}{t'(t'-t)}\mathrm{Im}\,\frac{G^1(t',s'_b)}{s'_b-u'_b} \tag{7.21}$$

$$+\frac{1}{\pi}\int_{m_+^2}^{\infty} ds' \left\{\frac{1}{\lambda^b_{s'}+s't}\mathrm{Im}\, F^-(s',t'_b) - \frac{1}{\lambda_{s'}}\mathrm{Im}\, F^-(s',0) - \frac{1}{\lambda^b_{s'}}\mathrm{Im}\,[F^-(s',t'_b)-F^-(s',0)]\right\}.$$

These representations will allow us to perform projections on the t-channel partial waves for $t \geq 4M_\pi^2$.

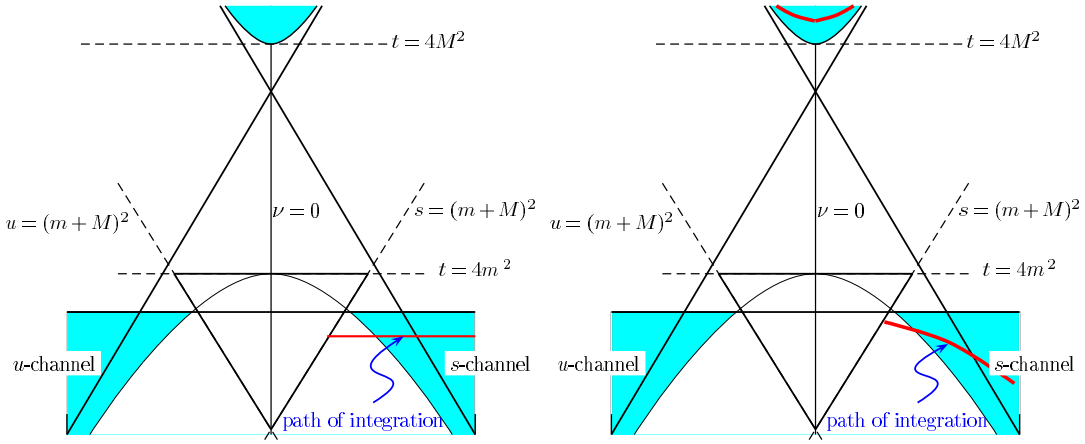

Figure 7.1: *Representation of the integration paths in the Mandelstam plane, used in the dispersive representations at fixed t (left) and the hyperbolic ones at fixed $u \cdot s$ (right). In both cases, m denotes M_π and M denotes M_K.*

7.1.4 Roy-Steiner equations [K]

Roy-Steiner equations can now be obtained by performing the partial-wave projections of the dispersive representations obtained above. Projecting eqs. (7.18) on the $l = 0, 1$ $\pi K \to \pi K$ amplitude we get the first four equations:

$$\begin{aligned}
\mathrm{Re}\, f_l^{1/2}(s) &= k_l^{1/2}(s) + \frac{1}{\pi}\int_{4M_\pi^2}^{\infty} dt' \Big\{ K_{l0}^0(s,t')\mathrm{Im}\, g_0^0(t') + 2K_{l1}^1(s,t')\mathrm{Im}\, g_1^1(t') \Big\} + d_l^{1/2}(s) \qquad (7.22)\\
&+\frac{1}{\pi}\!\!\int\!\!\!\!\!\!-_{m_+^2}^{\infty} ds' \sum_{l'=0,1} \left\{ \left(\delta_{ll'} \frac{\lambda_s}{(s'-s)\lambda_{s'}} - \frac{1}{3} K_{ll'}^{\alpha}(s,s') \right) \mathrm{Im}\, f_{l'}^{1/2}(s') + \frac{4}{3} K_{ll'}^{\alpha}(s,s') \mathrm{Im}\, f_{l'}^{3/2}(s') \right\},\\
\mathrm{Re}\, f_l^{3/2}(s) &= k_l^{3/2}(s) + \frac{1}{\pi}\int_{4M_\pi^2}^{\infty} dt' \Big\{ K_{l0}^0(s,t')\mathrm{Im}\, g_0^0(t') - K_{l1}^1(s,t')\mathrm{Im}\, g_1^1(t') \Big\} + d_l^{3/2}(s)\\
&+\frac{1}{\pi}\!\!\int\!\!\!\!\!\!-_{m_+^2}^{\infty} ds' \sum_{l'=0,1} \left\{ \left(\delta_{ll'} \frac{\lambda_s}{(s'-s)\lambda_{s'}} + \frac{1}{3} K_{ll'}^{\alpha}(s,s') \right) \mathrm{Im}\, f_{l'}^{3/2}(s') + \frac{2}{3} K_{ll'}^{\alpha}(s,s') \mathrm{Im}\, f_{l'}^{1/2}(s') \right\},
\end{aligned}$$

The domain of validity in s of these equations is given by eq. (7.32) below. In these equations, the terms $k_l^I(s)$ contain the contributions associated with the subtraction constants:

$$\begin{aligned}
k_0^I(s) &= 1/2 m_+ a_0^I + \frac{\lambda_s}{32\pi s}\left(-b^+ + (-3I + \frac{7}{2}) \frac{8\pi m_+ a_0^-}{m_+^2 - m_-^2} \frac{3s + m_-^2}{s - m_-^2} \right),\\
k_1^I(s) &= \frac{\lambda_s}{96\pi s}\left(b^+ + (-3I + \frac{7}{2}) \frac{8\pi m_+ a_0^-}{m_+^2 - m_-^2} \right) . \qquad (7.23)
\end{aligned}$$

The equations involve three kinds of kernels $K_{ll'}^{\alpha}(s,s')$, $K_{ll'}^{I}(s,t')$, and $K_{ll'}^{\sigma}(s,s')$ (which appear only in the driving terms d_l^I), and their expression can be found in ref. [44]. The analyticity properties of the partial-wave amplitudes $f_l^I(s)$ can be recovered by considering these various kernels. The terms $d_l^I(s)$ are the so-called driving terms in which the contributions

from the partial waves with $l' \geq 2$ are collected:

$$d_l^I(s) = \frac{1}{\pi}\int_{4M_\pi^2}^\infty dt' \sum_{l'\geq 1}\left\{K^0_{l2l'}(s,t')\mathrm{Im}\, g^0_{2l'}(t') + (-3I+\frac{7}{2})K^1_{l2l'+1}(s,t')\mathrm{Im}\, g^1_{2l'+1}(t')\right\} \tag{7.24}$$

$$+\frac{1}{\pi}\int_{m_+^2}^\infty ds' \sum_{l'\geq 2}\left\{\left(K^\sigma_{ll'}(s,s') + \frac{2}{3}(I-1)\,K^\alpha_{ll'}(s,s')\right)\mathrm{Im}\, f_{l'}^{1/2}(s') + \frac{1}{3}(-2I+5)\,K^\alpha_{ll'}(s,s')\mathrm{Im}\, f_{l'}^{3/2}(s')\right\}.$$

with further kernels $K^\sigma_{ll'}(s,s')$ appearing in the driving terms only [44].

In order to obtain a closed system of equations we now need two equations yielding the real parts of $g_0^0(t)$ and $g_1^1(t)$ valid for positive values of t. They can be obtained by projecting the family of fixed$-us$ DRs of eqs. (7.21). Using the relation between the cosine of the t-channel scattering angle z_t and the parameter b:

$$z_t^2 = \frac{(2\Sigma - t)^2 - 4b}{(2\Sigma - t)^2 - 4\Delta^2}\,, \tag{7.25}$$

the projection is carried out by using:

$$g_0^0(t) = \frac{\sqrt{3}}{16\pi}\int_0^1 dz_t\, F^+(s_b,t)\,, \qquad g_1^1(t) = \frac{4\sqrt{2}}{16\pi}\int_0^1 dz_t\, z_t^2\,\frac{F^-(s_b,t)}{s_b - u_b}\,. \tag{7.26}$$

This yields the following two equations for g_0^0, g_1^1:

$$\begin{aligned} g_0^0(t) &= \frac{\sqrt{3}m_+}{2}\left(a_0^+ + \frac{ta_0^-}{m_+^2 - m_-^2}\right) + \frac{t}{\pi}\int_{4m_\pi^2}^\infty \frac{dt'}{t'}\frac{\mathrm{Im}\, g_0^0(t')}{t'-t} - \frac{3\sqrt{6}}{8}\frac{t}{\pi}\int_{4m_\pi^2}^\infty \frac{dt'}{t'}\mathrm{Im}\, g_1^1(t') \\ &\quad + \sum_{l'=0}^1 \frac{1}{\pi}\int_{m_+^2}^\infty ds'\left[G^+_{0l'}(t,s')\mathrm{Im}\, f^+_{l'}(s') + t\,G^-_{0l'}(t,s')\mathrm{Im}\, f^-_{l'}(s')\right] + d_0^0(t)\,. \\ g_1^1(t) &= \frac{2\sqrt{2}m_+a_0^-}{3(m_+^2 - m_-^2)} + \frac{t}{\pi}\int_{4m_\pi^2}^\infty \frac{dt'}{t'}\frac{\mathrm{Im}\, g_1^1(t')}{(t'-t)} \\ &\quad + \frac{1}{\pi}\int_{m_+^2}^\infty ds'\left[G^-_{10}(t,s')\mathrm{Im}\, f_0^-(s') + G^-_{11}(t,s')\mathrm{Im}\, f_1^-(s')\right] + d_1^1(t)\,. \end{aligned} \tag{7.27}$$

The two equations (7.27) together with the four equations (7.22) form a complete set of Roy-Steiner type equations. The domain of validity of the equations for g_0^0, g_1^1 is given in eq. (7.33) below. The corresponding kernels and driving terms can be found in ref. [44].

7.2 Domains of validity [K]

It is important to assess the domains of validity of the dispersive representations discussed in the preceding section precisely . There are two restrictions for the domain of validity of the Roy-Steiner equations, both coming from constraints on the values of the arguments of the spectral functions: they must be real, and they must be defined in unphysical regions through their partial-wave expansions.

The discussion is based on the assumption that the scattering amplitudes satisfy the Mandelstam double spectral representation eq. (7.12) [349], i.e., a spectral representation in terms of two variables which involves three spectral functions $\rho_{st}(s',t')$, $\rho_{ut}(u',t')$ and $\rho_{us}(u',s')$. The

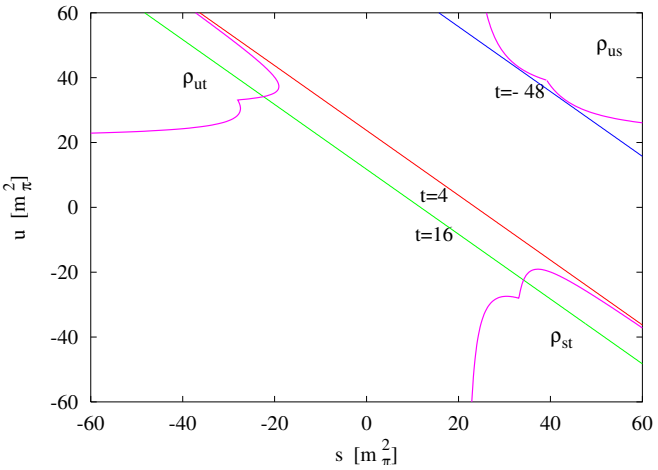

Figure 7.2: *Boundaries of the support of the Mandelstam double spectral functions for the πK system. The variables s, t, u are displayed in units of M_π^2.*

boundaries of the support of these spectral functions are shown in fig.7.2, with expressions obtained from the consideration of box diagrams, of the form $t = T_X(s)$ for the boundary $X = st, ut, us$ (the expressions can be found in refs. [44, 45]).

Let us consider first the fixed$-t$ DRs. First, the spectral functions arising in these DRs are obtained by taking the double spectral Mandelstam representation eq. (7.12) along a particular path in the Mandelstam plane. In other words, the imaginary parts involved in the single-spectral representations of the Roy-Steiner equations can be actually written as dispersive integrals over the double spectral functions $\rho_{st}, \rho_{ut}, \rho_{su}$. Since the spectral functions involved in the Roy-Steiner equations must remain real, the lines of constant t must not cross the double-spectral boundaries. From fig. 7.2 one sees that this condition confines t in the region: $-48M_\pi^2 < t < 4M_\pi^2$, where the lower bound comes from the boundary associated with ρ_{us} and the upper bound from the one associated with ρ_{st}.

The second restriction on the domain of validity arises from the fact that the spectral function $\mathrm{Im}\, F(s', t)$ is needed in an unphysical region (except if $t = 0$) and must thus be defined using the partial-wave expansion:

$$\mathrm{Im}\, {}_sF^+(s', t) \equiv 16\pi \sum_l (2l+1)\ \mathrm{Im}\, {}_sf_l^+(s')\ P_l(z(s', t))\,, \qquad z(s', t) = 1 + \frac{2s't}{\lambda_{s'}}. \tag{7.28}$$

As shown by Lehmann [353], the series of Legendre polynomials (7.28) converges when $z(s', t)$ lies inside an ellipse whose focal points are located at $z(s', t) = \pm 1$ and whose boundary touches the nearest singularity of $\mathrm{Im}\, {}_sF^+(s', t)$:

$$z_{s'}^{\max} = 1 + \frac{2s'T_{st}(s')}{\lambda_{s'}}\ . \tag{7.29}$$

The point $-z_{s'}^{\max}$ of the ellipse corresponds to another value of t given by $T'_{st}(s) = -\lambda_s/s - T_{st}(s)$. For each value of s', the convergence of the partial-wave expansion is ensured if $-z_{s'}^{\max} \leq z_{s'} \leq z_{s'}^{\max}$, i.e., $T'_{st}(s') < t < T_{st}(s')$. The us boundary provides another similar constraint, but it turns out to be weaker than that obtained from the st boundary.

The conjunction of the two constraints (reality of the spectral functions and convergence of the partial expansion) leads to the fact that the fixed-t dispersion relation for πK scattering

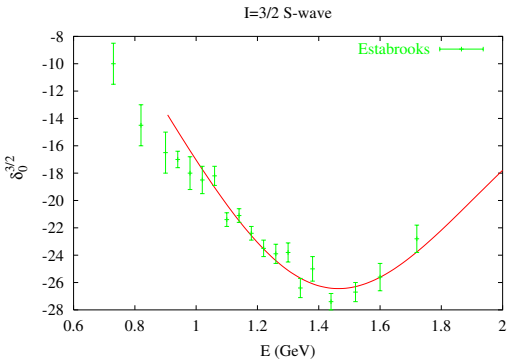

Figure 7.3: *Experimental data from ref. [354] for the $I = 3/2$ S-wave phase shift.*

is valid in the range:

$$[\text{fixed } t]: \qquad -23M_\pi^2 < t < 4M_\pi^2 \ . \tag{7.30}$$

A similar discussion can be carried out for the set of dispersion relations with $us = b$ fixed. Firstly, the criterion that the hyperbolas $us = b$ do not intersect a spectral function boundary yields $-700M_\pi^4 < b < 1420M_\pi^4$, where the lower bound comes from the st boundary and the upper bound from the us boundary. For the hyperbolic DRs, the spectral functions $\mathrm{Im}\, F^\pm(s', t'_b)$, $\mathrm{Im}\, G^I(t', s'_b)$ are also needed in unphysical regions (unless $b = \Delta^2$), so that the values of b must be restricted to ensure the convergence of the partial-wave expansion. Considering the Lehman ellipse related to $\mathrm{Im}\, F^\pm(s', t'_b)$ restricts the range to:

$$[\text{fixed } us]: \qquad -700M_\pi^4 < b < 450M_\pi^4 \ , \tag{7.31}$$

and no further restriction arises from the Lehman ellipse related to $\mathrm{Im}\, G^I(t', s'_b)$.

We can now derive the ranges of validity of the Roy-Steiner equations, which are obtained by projecting the DRs over partial waves. Let us start with the fixed-t DRs, the projection over πK partial waves is legitimate provided the range of integration of eq. (7.6) is included inside the range of validity in t of the DRs. One deduces that the Roy-Steiner equations for s-channel partial waves (7.22) are valid for:

$$[f_l^I]: \qquad 3M_\pi^2 \leq s \leq 48M_\pi^2 \ . \tag{7.32}$$

In the same way, the projection on $\pi\pi \to K\bar{K}$ partial waves is allowed only if the range of integration of eq. (7.26) lies within the range of validity in b of the fixed$-us$ DRs. The last two Roy-Steiner equations eq. (7.27) are thus valid for:

$$[g_l^I]: \qquad -15M_\pi^2 \leq t \leq 70M_\pi^2 \ . \tag{7.33}$$

7.3 Experimental input [K]

In the previous sections, we have derived a set of Roy-Steiner equations for the s-channel partial waves for $I = 1/2, 3/2$ and $l = 0, 1$, and the t-channel partial waves for $(I, l) = (0, 0)$ and $(1, 1)$, which we call "lowest" partial waves from now on. We want now to perform a numerical resolution of these equations following the same approach as that adopted for $\pi\pi$ scattering in

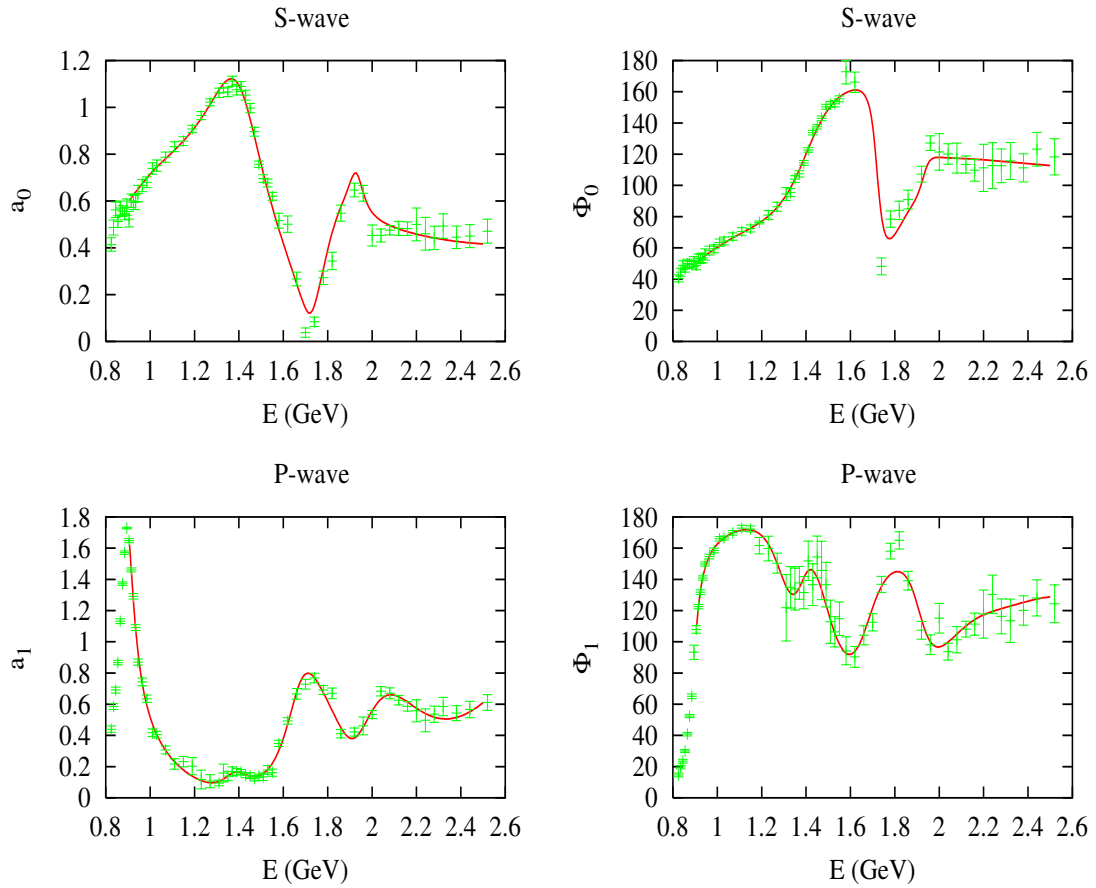

Figure 7.4: *Modulus and phase of the S- and P-partial-waves amplitudes from ref. [354] and the fits in the region $0.9 \leq E \leq 2.5$ GeV which are used in the calculations.*

sec. 6.1.1. Let us consider these equations in the ranges $m_+^2 \leq s \leq s_m$ and $4M_\pi^2 \leq t \leq t_m$. The upper limits of s_m, t_m (which will be taken such that the equations are valid i.e. $s_m \leq 48M_\pi^2$, $t_m \leq 70M_\pi^2$) are the matching points of the Roy-Steiner equations. In order to be able to solve for the lowest partial waves below the matching points the following input must be provided: 1) the imaginary part of the lowest partial waves for $s \geq s_m$, $t \geq t_m$, 2) the imaginary parts of the $l \geq 2$ partial waves above the thresholds and 3) the phases of $g_0^0(t)$, $g_1^1(t)$ in the range $4M_\pi^2 \leq t \leq t_m$.

For the s-channel partial waves, we choose the matching point at the border of the range of validity:

$$s_m = 0.935 \text{ GeV}^2 \ . \tag{7.34}$$

The reason for this choice is that the experimental data available at present comes from production experiments, and one expects the precision to decrease as the energy goes down below 1 GeV (and we will see, for instance, that the $I = 3/2$ S-wave phase shifts seem rather unreliable below 1 GeV). In the $t-$channel the range of validity extends, as we have seen, up to $t_{val} \simeq 1.36$ GeV^2 and one could, in principle, choose the matching point anywhere between the $K\overline{K}$ threshold and t_{val}. In practice, we choose a value slightly above the $K\bar{K}$ threshold (see

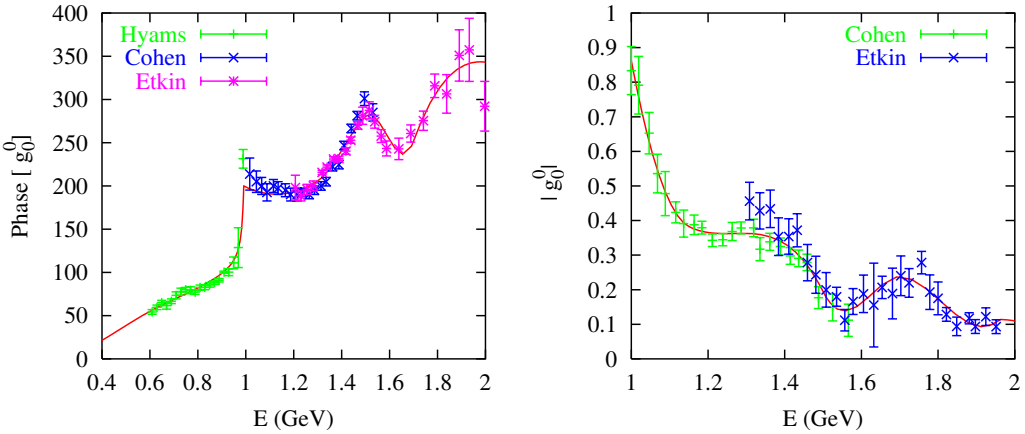

Figure 7.5: *Inputs for the phase of g_0^0 above the $\pi\pi$ threshold and its modulus above the $K\overline{K}$ threshold. The data are from refs. [355–357].*

sec. 7.4.3):

$$t_m = 1.04 \text{ GeV}^2 \ . \tag{7.35}$$

For the lowest partial waves above the matching point, and for the higher partial waves, we exploit experimental data at intermediate energies $E \leq \sqrt{s_2} = 2.5$ GeV and Regge models for $E > \sqrt{s_2}$. We aim at determining the lowest partial waves below the matching point. For this purpose, an additional information is needed concerning unitarity. We will make the usual assumption that elastic unitarity holds exactly below the matching points [358]. In other terms, in the πK channel the possible couplings to $\pi\pi K$ and $\pi\pi\pi K$ are assumed to be negligibly small in the low-energy region. For the S-wave the validity of elastic unitarity was observed experimentally up to the $\eta' K$ threshold. In principle, the P-wave can couple to the $\pi\pi K$ state but no such coupling has been detected for the K^* [137], and potentially important two-body channels like $K^*\pi$, $K\rho$ lie above the matching point. Similarly, in the $\pi\pi$ channel we assume that the coupling to 4π can be neglected below the $K\overline{K}$ threshold.

Phase shift analyses of the $\pi K \to \pi K$ amplitude have been performed based on high-statistics production experiments $KN \to K\pi N$ by Estabrooks *et al.* [359] and by Aston *et al.* [354]. Earlier results are much less precise and we will not use them in our analysis. The amplitude $\pi^+K^+ \to \pi^+K^+$ which is purely $I = 3/2$ has been measured by Estabrooks *et al.* [359]. In practice the $I = 3/2$ phase shifts are very small in the range $E \lesssim 2$ GeV except for the S-wave. The amplitude $\pi^+K^- \to \pi^+K^-$ which involves the isospin combination $F^c \equiv F^{1/2} + F^{3/2}/2$, was measured both in ref. [359] and ref. [354] – the latter experiment has better statistics and covers a larger energy range. The amplitude F^c can be expanded over partial-waves in the same way as eq. (7.4) and refs. [354, 359] provide the phase $\Phi_l(s)$ and the modulus $a_l(s)$ of these partial waves: $f_l^c(s) \equiv \sqrt{2l+1}\, a_l(s) \mathrm{e}^{i\Phi_l(s)}$.

Performing a combined fit of the $I = \frac{3}{2}$ partial waves [359] and of the parameters a_l, Φ_l [354, 359] one can separate the two isospin partial waves. The fits correspond to a parametrisation of the partial-wave S-matrices as products of Breit-Wigner S-matrices, allowing for inelasticity in the $I = \frac{1}{2}$ amplitude to set in at the ηK threshold. Inelasticity is found to remain quite small up to $E \simeq 1.5$ GeV. The data of Aston *et al.* and the fits for both a_l and Φ_l for $l = 0$ to

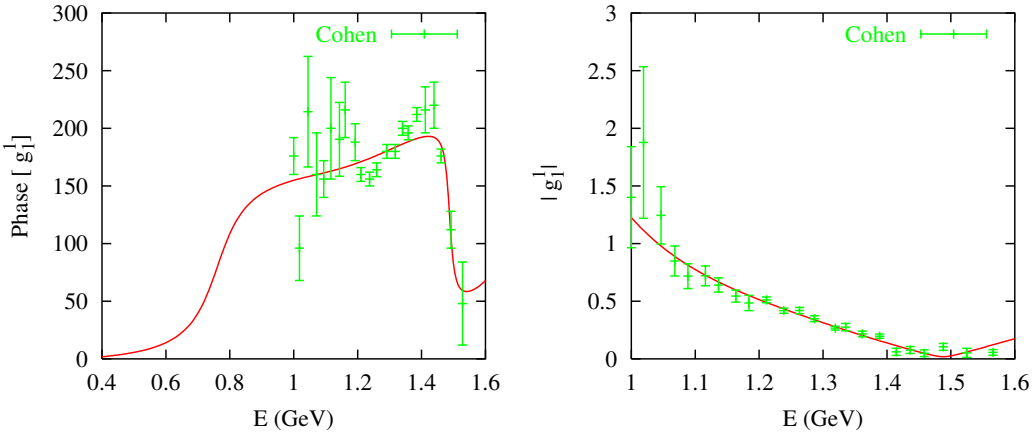

Figure 7.6: *Input for the phase and the magnitude of* g_1^1. *The data shown are from ref. [356] and the curve is the fit.*

$l = 5$ and energy up to $E = 2.5$ GeV are shown in fig. 7.4.

A key role is also played by the $l = 0$ and $l = 1$ $\pi\pi \to K\overline{K}$ amplitudes, which can be determined from $\pi N \to K\overline{K}N$ production experiments in the range $t \geq 4M_K^2$. We will make use of the two high-statistics experiments described in Cohen *et al.* [356] and Etkin *et al.* [357,360]: The experiment of Cohen *et al.* [356] determines the charged amplitude $\pi^+\pi^- \to K^+K^-$, thereby providing results for both g_0^0 and g_1^1. There are several possible solutions but physical requirements select a single one, called solution II b in ref. [356]. Close to the $K\overline{K}$ threshold, the presence of the $l = 1$ phase allows the authors to accurately determine the $l = 0$ phase. The experiment of Etkin *et al.* concerns the amplitude $\pi^+\pi^- \to K_SK_S$ which is purely $I = 0$. Because of the absence of the P-wave in this channel, their determination of the phase of g_0^0 close to the threshold (where the D-wave phase is very small) is likely to be less reliable than that of ref. [356]. Their determination of the magnitude of g_0^0 close to the threshold disagrees with that of Cohen *et al.* and also with earlier experiments [361]. Consequently, we make the choice to use the results of Etkin *et al.* only in the range $\sqrt{t} \geq 1.2$ GeV. Our input for the phase of g_0^0 is determined as follows:

- Below the $K\overline{K}$ threshold this phase is identical to the $\pi\pi$ phase shift because of the elastic unitarity assumption.
- In the range $2M_\pi \leq E \leq 0.8$ GeV we use solutions of the $\pi\pi$ Roy equations. We use the parametrisation recalled in sec. 6.1.2, together with the scattering lengths corresponding to the Global fit, with the central values $a_0^0 = 0.228$, $a_0^2 = -0.0382$ [3].
- In the range $E \geq 2M_K$ we perform piecewise-polynomial fits of the data of refs. [356,357]

[3] These values correspond to the fit Global (I) to E865 data alone, see tab. 6.1. The results quoted below are only marginally affected if we replace this input with the outcome of the fits Extended (III) or All including NA48/2 data and corrected for isospin-breaking corrections, see tab. 6.6. The main difference occurs in the uncertainty for $a_0^{1/2}$, that gets reduced by a factor 3 ($a_0^{3/2}$ is barely affected) if one uses the fit All instead of Global (I). A similar reduction in the uncertainties occur for the threshold and subthreshold coefficients considered here

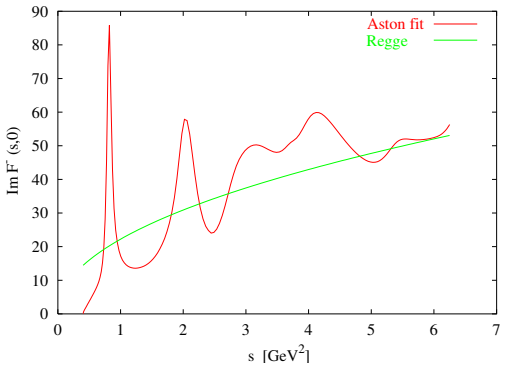

Figure 7.7: *Comparison of* $\mathrm{Im}\, F^-(s,0)$ *constructed from experimental data and our Regge asymptotic form.*

and fixing the threshold value to $\Phi_0^0 = 200 \pm 15$ degrees. This range is an educated guess based on considering the data of Cohen *et al.* as well as $\pi\pi$ data.

- Finally in the range 0.8 GeV $\leq E \leq 2M_K$ we perform a fit to the CERN-Munich data as given by Hyams *et al.* [355] and to the polarised target production data analyzed by Kaminski *et al.* [362].

For the modulus of g_0^0, we have performed piecewise polynomial fits to the data of refs. [356,357].

As far as g_1^1 is concerned, we use the experimental determination of the $\pi\pi$ P-wave phase in the range $2M_\pi \leq E \leq 2M_K$ obtained from the pion vector form factor measured by CLEO [363]. This determination is compatible with the results of the analysis of $\pi\pi$ Roy equations and has a comparable accuracy. At larger energies, we use the experimental results from Cohen *et al.* for the phase and the magnitude of g_1^1. The data and the fits are shown in fig. 7.6.

The amplitudes with $l \geq 2$ play a much less significant role in our analysis and are suppressed at low energies. They will be described by simple Breit-Wigner parametrisations associated with the resonances $f_2(1200)$, $f_2'(1525)$, $\rho_3(1690)$, $f_4(2050)$. Masses and partial decay widths of these resonances were taken from the PDG [137].

As discussed above, we can make use of the partial-wave expansion and experimental data up to energies $E = \sqrt{s_2} = 2.5$ GeV for the s- as well as the t-channel. Above that point we use a description of the amplitudes based on Regge phenomenology. We will content ourselves with very unsophisticated models (similar to that in ref. [358], including the ρ, K^* and Pomeron trajectories) because this energy region turns out to play a very minor role in our analysis. For illustration we compare in fig. 7.7 the imaginary part of $F^-(s,0)$ resulting from our fit to the experimental data and the Regge asymptotic form chosen for this analysis.

7.4 Resolution

7.4.1 Solving for $\pi\pi \to K\bar{K}$ partial waves [K]

We have now all the ingredients to solve the set of Roy-Steiner equations. The first step consists in solving eqs. (7.27) for g_0^0, g_1^1. This problem was discussed a long time ago [352, 364] and we recall the main ideas here for completeness. Elastic unitarity implies that the phases Φ_l^I of these amplitudes:

$$g_l^I(t) \equiv \mathrm{e}^{i\Phi_l^I(t)} |g_l^I(t)|\,, \tag{7.36}$$

can be identified with the $\pi\pi$ phase shifts δ_l^I in the unphysical region $t < 4M_K^2$ according to Watson's theorem, and therefore they are known in principle. In the physical region $t \geq 4M_K^2$ the phases are determined from experiment as discussed above.

On the other hand, the modulus of the t-channel partial waves is not known below the $K\bar{K}$ threshold, and must be determined using the equations satisfied by g_0^0 and g_1^1 which have the following simple form:

$$g_0^0(t) = \Delta_0^0(t) + \frac{t}{\pi}\int_{4M_\pi^2}^{\infty} \frac{dt'}{t'}\frac{\mathrm{Im}\, g_0^0(t')}{t'-t}, \qquad g_1^1(t) = \Delta_1^1(t) + \frac{t}{\pi}\int_{4M_\pi^2}^{\infty} \frac{dt'}{t'}\frac{\mathrm{Im}\, g_1^1(t')}{t'-t}\ . \tag{7.37}$$

In sec. 7.2, we have shown that these relations can be used up to $t \simeq 1.4$ GeV^2, which includes the whole region inaccessible to experiment where $|g_0^0|$, $|g_1^1|$ are needed. The quantities $\Delta_l^I(t)$ are analytic functions with a left-hand cut along the negative t axis and no right-hand cut, as can be verified using eqs. (7.27) and the explicit form of the kernels. Determining the moduli $|g_l^I(t)|$ in the range $4M_\pi^2 \leq t \leq t_m$ from eqs. (7.27) while the phase is known is a standard Muskhelishvili-Omnès problem [241]. The most general solution involves arbitrary parameters, the number of which depend on the value of the phase at the matching point. We have chosen t_m to be slightly larger than $4M_K^2$. The $l = 1$ phase $\Phi_1^1(t_m)$ is lower than π, which implies that the solution for g_1^1 involves no free parameter. The $l = 0$ phase, as we argued in the previous section, satisfies $\pi \leq \Phi_0^0(t_m) < 2\pi$, such that one free parameter is involved in the solution. Let us recall the explicit form of the solutions. One first introduces the Omnès function:

$$\Omega_l^I(t) = \exp\left(\frac{t}{\pi}\int_{4M_\pi^2}^{t_m} \frac{\Phi_l^I(t')\,dt'}{t'(t'-t)}\right) \equiv \Omega_{l\,R}^I(t)\exp[i\Phi_l^I(t)\theta(t-4M_\pi^2)\theta(t_m-t)]\,, \tag{7.38}$$

where $\Omega_{l\,R}^I(t)$ is real. Then, the solutions of eqs. (7.37) read:

$$\begin{aligned} g_0^0(t) = \Delta_0^0(t) + \frac{t\Omega_0^0(t)}{t_m-t}\Bigg[\alpha_0 + \frac{t}{\pi}\int_{4M_\pi^2}^{t_m} dt'\,\frac{(t_m-t')\Delta_0^0(t')\sin\Phi_0^0(t')}{\Omega_{0\,R}^0(t')(t')^2(t'-t)} \\ + \frac{t}{\pi}\int_{t_m}^{\infty} dt'\,\frac{(t_m-t')|g_0^0(t')|\sin\Phi_0^0(t')}{\Omega_{0\,R}^0(t')(t')^2(t'-t)}\Bigg], \end{aligned} \tag{7.39}$$

$$g_1^1(t) = \Delta_1^1(t) + t\Omega_1^1(t)\left[\frac{1}{\pi}\int_{4M_\pi^2}^{t_m} dt'\,\frac{\Delta_1^1(t')\sin\Phi_1^1(t')}{\Omega_{1\,R}^1(t')t'(t'-t)} + \frac{1}{\pi}\int_{t_m}^{\infty} dt'\,\frac{|g_1^1(t')|\sin\Phi_1^1(t')}{\Omega_{1\,R}^1(t')t'(t'-t)}\right], \tag{7.40}$$

It can be shown that the solution satisfies automatically the first matching condition:

$$\lim_{\epsilon\to 0} g_l^I(t_m \pm \epsilon)|_{\mathrm{sol}} = g_l^I(t_m)|_{\mathrm{input}}\ . \tag{7.41}$$

At this stage, the formulae (7.39)-(7.40) for $g_0^0(t)$, $g_1^1(t)$ involve three parameters: the two S-wave scattering lengths $a_0^{1/2}$, $a_0^{3/2}$ that appear in the expressions for $\Delta_0^0(t)$, $\Delta_1^1(t)$ and an additional parameter α_0 which plays a role to be clarified now.

7.4.2 Matching conditions and uniqueness [K]

Once $g_0^0(t)$, $g_1^1(t)$ are expressed according to eqs. (7.39) and (7.40), the set of four Roy-Steiner equations 7.22 becomes a closed set of equations for the four πK partial waves $f_l^I(s)$, $l = 0, 1$, $I = 1/2,\ 3/2$. The structure of these equations is similar to that of $\pi\pi$ Roy equations: the kernels consist of a singular Cauchy part and a regular part, and elastic unitarity provides

a non-linear relation between $\mathrm{Re}\, f_l^I(s)$ and $\mathrm{Im}\, f_l^I(s)$. The equations must be solved with the boundary condition that the solution phase shifts must equate the input phase shifts at the frontier of the region of resolution (matching condition). Therefore, we can apply the results in refs. [365, 366] concerning the number of independent solutions in the vicinity of a given solution. The multiplicity index of one solution is determined by the values of the input phase shifts at the matching point $s = s_m$ (with $s_m \simeq 0.935$ GeV^2). The experimental phase shifts at $s = s_m$ lie in the following ranges:

$$0 < \delta_0^{1/2}(s_m) < \frac{\pi}{2}, \quad \frac{\pi}{2} < \delta_1^{1/2}(s_m) < \pi, \quad \delta_0^{3/2}(s_m) < 0, \quad \delta_1^{3/2}(s_m) < 0. \tag{7.42}$$

According to the discussion in ref. [366], the multiplicity index in this situation is $m = 0 + 1 - 1 - 1 = -1$, to be compared with $m = 0$ in the case of $\pi\pi$. This means that our situation corresponds to a constrained system: a solution will not exist unless the two S-wave scattering lengths lie on a one dimensional curve.

In practice, however, the phase shift for the $I = 3/2$, P-wave is extremely small below 1 GeV and the experimental input is not precise enough to implement matching conditions in this channel in any meaningful way (see fig. 7.13 below). This leads us to treat the $I = 3/2$ P-wave on the same footing as the partial waves with $l \geq 2$. For instance, the dispersive representations can be projected on $l = 2$ and used to compute the real part of $f_2^{1/2}(s)$ for $s \leq s_m$ while the contribution of $\mathrm{Im}\, f_2^{1/2}(s')$ for $s' \leq s_m$ in the integrands is negligibly small compared to contributions from S- and P-waves; it can be evaluated approximately or even ignored [4]. Dropping one matching condition, the effective multiplicity index becomes $m = 0$ for πK. The fact that the multiplicity index vanishes means that solutions should exist for arbitrary values of the two S-wave scattering lengths $a_0^{1/2}$, $a_0^{3/2}$ lying in some two-dimensional region, and each solution is unique.

However, not all solutions are physically acceptable. An acceptable solution must satisfy the further requirement that it displays no cusp at the matching point [358]. This condition leads to constraints on the subtraction parameters. First, let us consider the t-channel, for which we choose the matching point t_m to be slightly larger than the $K\overline{K}$ threshold. As discussed in the previous section, the solution for $g_0^0(t)$ involves one parameter α_0. While the continuity $g_0^0|_{\mathrm{sol}} = g_0^0|_{\mathrm{input}}$ is automatically guaranteed by eq. (7.39), the solution $g_0^0|_{\mathrm{sol}}$ exhibits a sharp cusp at the matching point in general. Therefore, the no-cusp condition fixes the value of α_0. The same reasoning can be applied to the πK partial waves: imposing the no-cusp condition to the $I = 1/2$ S- and P-waves provides two equations which should determine, in principle, the two scattering lengths $a_0^{1/2}$, $a_0^{3/2}$. In other words, given ideal experimental input data[5] with no errors in the ranges $s \geq s_m$ and $t \geq t_m$, one should be able to fix exactly the two scattering lengths by solving the Roy-Steiner equations with the appropriate boundary conditions on the values and the derivatives of the phase shifts. Obviously, the actual situation is different from that ideal view: the input data are known with errors and only for discrete values of the energy, which introduces uncertainties on the boundary conditions and thus on the solutions of the Roy-Steiner equations.

[4] A second argument to neglect the low-energy contribution of the imaginary part of this partial wave is provided by the chiral counting $\mathrm{Im}\, f_1^{3/2} = O(\mathrm{Im}\, f_{l\geq 2}^I) = O(p^8)$.

[5] The data are assumed to be ideal also in the sense that they ensure the existence of a solution to the equations [366].

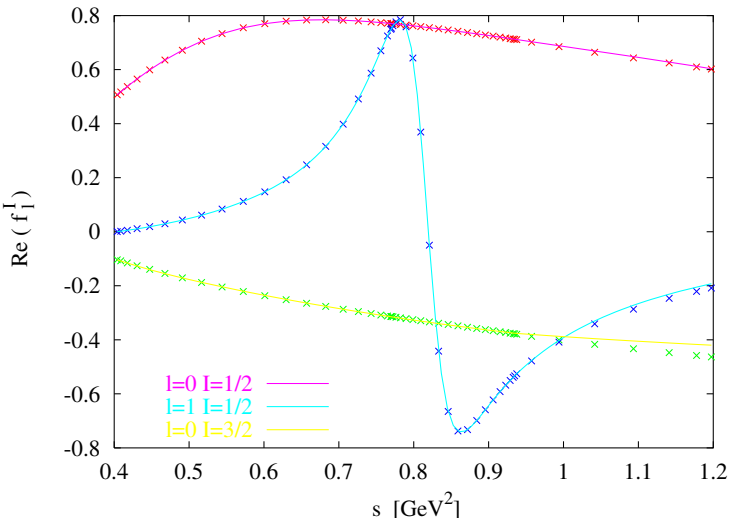

Figure 7.8: *Left-hand sides of the Roy-Steiner equations eqs. (7.22) (lines) compared to the right-hand sides (points) after minimization in the range* $m_+^2 \leq s \leq 0.93$ *GeV*^{2} .

7.4.3 Numerical determination of the solutions [K]

We have described how to solve the Roy-Steiner equations for the $\pi\pi \to K\bar{K}$ partial waves. Assuming that the input for $s > s_m$ is given as well as the input for $l \geq 2$ at all energies, our purpose is to determine the three phase shifts:

$$\delta^0(s) \equiv \delta_0^{1/2}(s), \quad \delta^1(s) \equiv \delta_1^{1/2}(s) \quad \delta^2(s) \equiv \delta_0^{3/2}(s) \tag{7.43}$$

in the range $m_+^2 \leq s \leq s_m$, so that the Roy-Steiner equations represented symbolically as:

$$\mathrm{Re}\, f^a(s) \equiv \frac{s}{\lambda_s} \sin(2\delta^a(s)) = \Phi^a[\delta^b, s]\,, \tag{7.44}$$

are satisfied up to a certain accuracy. We introduce a set of N mesh points $m_+^2 < s_i \leq s_m$ (N was varied between 16 and 30, the results were very stable) and characterize the accuracy of an approximate solution by the measure:

$$\epsilon = \max_{i,a} |\mathrm{Re}\, f^a(s_i) - \Phi^a[\delta^b, s_i]|\ . \tag{7.45}$$

An exact solution, of course, satisfies $\epsilon = 0$. While it is possible to search directly for minima of ϵ, a more appropriate quantity for minimization algorithms is the chi-square:

$$\chi^2 = \sum_{i=1}^{N} \sum_{a=0}^{2} |\mathrm{Re}\, f^a(s_i) - \Phi^a[\delta^b, s_i]\,|^2\ , \tag{7.46}$$

which we have minimised using the MINUIT package. Approximations to the πK phase shifts $\delta^a(s)$ are constructed in the form of polynomials or piecewise polynomial parametrisations similar to that proposed by Schenk [367]. This is essentially the same method as in ref. [358] for the $\pi\pi$ Roy equations. The parameters are constrained so that the phase shifts are continuous at the matching point and the no-cusp condition applies to $\delta^0(s)$ and $\delta^1(s)$. As discussed in

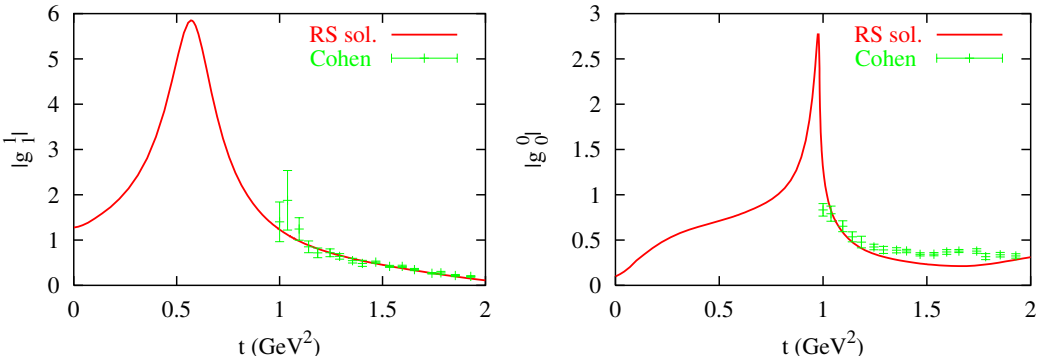

Figure 7.9: *Comparison of the absolute values of g_0^0 and g_1^1 obtained from solving the Roy-Steiner equations and the corresponding experimental input from ref. [356].*

sec. 7.4.2, these additional conditions fix the values of the two S-wave scattering lengths, which are therefore included as two additional parameters in the minimization of the chi-square. The minimisation yields a χ^2 at a few per mille. Seeking a much higher accuracy would be difficult: all integrals must be evaluated with a numerical precision better than ϵ, and the computation of the phase shifts involve up to three successive numerical integrations, see eqs. (7.22), (7.38), (7.39), (7.40)).

The accuracy of the solutions is illustrated in fig. 7.8. In particular, the figure shows that the left- and right-hand sides of the Roy-Steiner equations still agree with a good accuracy well above the matching point[6]. This constitutes a consistency condition as discussed in ref. [358]. We have checked that its fulfillment is a direct consequence of imposing the no-cusp conditions. At this level, there is a notable difference between the $\pi\pi$ and the πK Roy-Steiner equations. In the case of $\pi\pi$ scattering [358], it is found that imposing a *single* no-cusp condition for the P-wave is sufficient to ensure that the no-cusp condition holds to a good approximation for the S-waves as well, and the consistency conditions are well satisfied. In the πK case, we find that it is necessary to impose no-cusp conditions for the two phase shifts $\delta_0^{1/2}(s)$ and $\delta_1^{1/2}(s)$. In fact, even after doing so, we find that a (small) cusp remains for the third phase shift $\delta_0^{3/2}(s)$. This does not represent a serious problem, in practice, because this phase shift is not determined very precisely in the vicinity of the matching point.

Further consistency conditions ought to be considered in the $\pi\pi \to K\overline{K}$ sector. Here as well, one expects that the Roy-Steiner equations should be approximately satisfied above the matching point. This point is illustrated in fig.7.9 which compares the moduli of $g_0^0(t)$ and $g_1^1(t)$ computed from the Roy-Steiner equations to the experimental input for these quantities. Very good agreement is observed for $g_1^1(t)$. In contrast, we find that the agreement for $g_0^0(t)$ is moderately good. In the range $t \geq 4M_K^2$ we have checked that the unitarity bound $|S_{\pi\pi\to K\overline{K}}| \leq 1$ is obeyed. Adopting a larger value for the matching point t_m improves the input-output agreement for $t > t_m$ but leads to violation of unitarity for $t < t_m$ close to the $K\overline{K}$ threshold.

Our general procedure for evaluating the errors consists in performing variations of the parameters which enter in the description of the input – making use of the errors on these

[6]We are then exceeding the strict domain of applicability of the equations but they are still expected to be satisfied approximately.

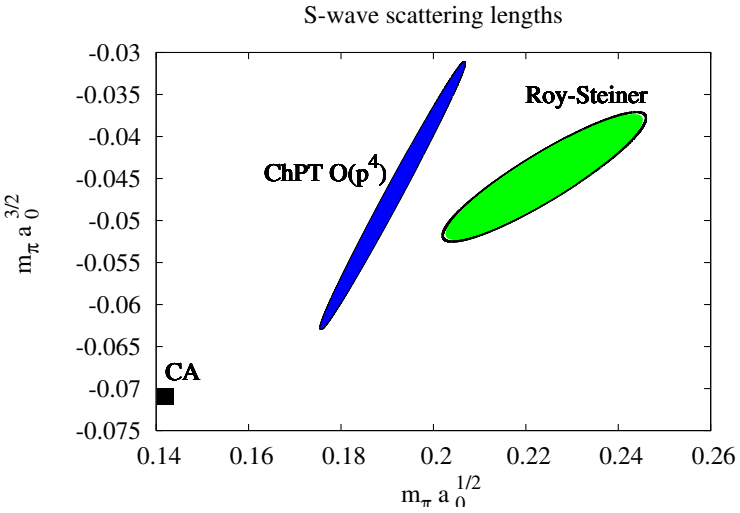

Figure 7.10: *Standard error ellipse for the S-wave scattering lengths obtained from solving the Roy-Steiner equations with boundary conditions. The corresponding ellipse in the χPT calculation at $O(p^4)$ and the current-algebra result are also plotted.*

parameters and their covariance matrices as provided by running the MINUIT package. The experimental errors are assumed to be essentially of statistical origin and the errors at different energy points are assumed to be independent. Let us discuss first the case of the $I = 1/2$ S- and P-waves. It is clear that this part of the input plays a crucial role as it controls the boundary conditions which determine the two S-wave scattering lengths. To begin with, one notes that variations of the input in the energy region $E \gtrsim 1.5$ GeV has a negligibly small influence, so we will consider only the energy region $\sqrt{s_m} \leq E \leq 1.5$ GeV. We have performed two different kinds of fits in order to check the validity of the determination of the phase shifts, their derivatives, and the errors obtained from varying the parameters at the matching point $E = \sqrt{s_m}$. Firstly, we perform "global" fits based on a K-matrix parametrisation with six parameters for the S-wave and seven parameters for the P-wave (determined such as to minimize the chi-square in the energy region $0.90 \leq E \leq 1.50$ GeV). Secondly, we have performed "local" fits in which one considers separately a small energy region surrounding the matching point $0.90 \leq E \leq 1.1$ GeV and the remaining energy region, where we approximate the S-wave phase shift by a quadratic polynomial. Comparing the two fits, the determinations of the phases at the matching point are in good agreement as well as that of the errors. The determinations of the derivative of the P-wave agree while those of the derivative of the S-wave are only in marginal agreement. In this case, we consider the determination from the global fit to be somewhat more reliable as it has continuity and smoothness built in.

7.5 Results

7.5.1 The πK S-wave scattering lengths [K]

We can now derive the constraints on the S-wave scattering lengths which arise upon solving the Roy-Steiner equations, making use of the available experimental input above the matching

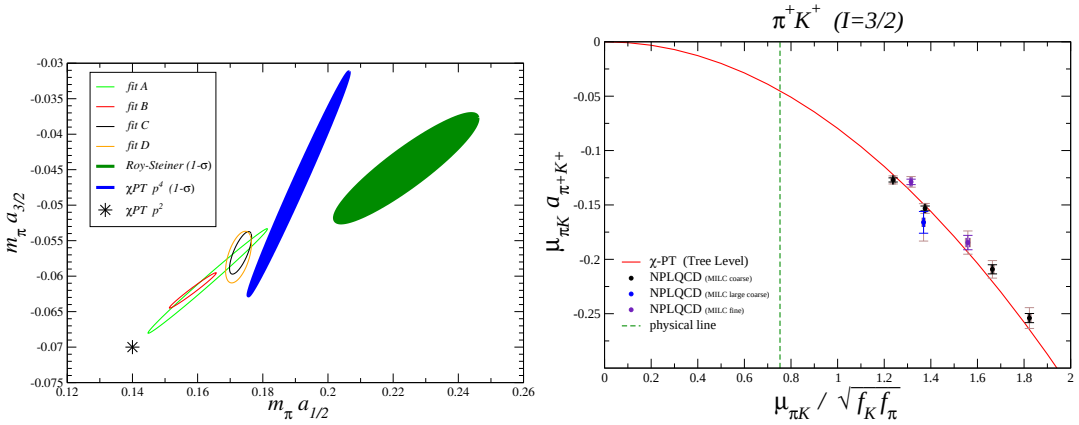

Figure 7.11: *On the left: compilation of lattice results for the $I = 3/2, \ell = 0$ πK scattering length as a function of the pion mass, compared to the current algebra prediction (red). On the right: Results of different NLO fits to the lattice data, compared to χPT and Roy-Steiner equations. Taken from refs. [314, 368].*

point. This analysis generates the following results for the scattering lengths a_0^I:

$$M_\pi\, a_0^{1/2} \simeq 0.224 \pm 0.022, \quad M_\pi\, a_0^{3/2} \simeq (-0.448 \pm 0.077)\, 10^{-1}, \quad \rho_{1/2,3/2} = 0.908\,. \tag{7.47}$$

The one-sigma error ellipse corresponding to the above results for the S-wave scattering lengths is represented in fig.7.10. The two main sources of uncertainty are *a)* the πK $I = 1/2$ S-wave and *b)* the $\pi\pi \to K\overline{K}$ $I = 0$ S-wave. In contrast, the influence of the partial waves with $l \geq 2$ (in which the Regge region is also included) is rather modest.

Our results are compatible with the band obtained for $a_0^{1/2}$, $a_0^{3/2}$ in ref. [352]. We find a much smaller allowed region for the scattering lengths simply because we have used considerably better experimental input for the S- and P-waves: in the work of ref. [352] no data at all were available for $E \geq 1.1$ GeV. Predictions from χPT at $O(p^4)$ for the S-wave scattering lengths were presented in ref. [369]:

$$\text{[Bernard et al.]}: \qquad M_\pi a_0^{1/2} = 0.19 \pm 0.02\,, \quad M_\pi a_0^{3/2} = -0.05 \pm 0.02\,. \tag{7.48}$$

Within the errors these results appear compatible with those from the Roy-Steiner equations. A more refined comparison, however, should take the correlation into account. Computing the correlation parameter under the same assumptions as used in ref. [369] for the evaluation of the errors one obtains the standard error ellipse shown in fig. 7.10. One observes that the χPT ellipse is very narrow and does not intersect the corresponding error ellipse resulting from the Roy-Steiner equations [7]. If one judges from the size of the $O(p^4)$ corrections as compared to the current algebra result, it seems not unreasonable to attribute the remaining discrepancy to $O(p^6)$ effects. We quote also our results for the two combinations of scattering lengths proportional to a_0^-, a_0^+:

$$M_\pi\, (a_0^{1/2} - a_0^{3/2}) \simeq 0.269 \pm 0.015, \quad M_\pi\, (a_0^{1/2} + 2a_0^{3/2}) \simeq 0.134 \pm 0.037\,, \tag{7.49}$$

[7] This particular shape reflects two features of the scattering lengths a_0^- and a_0^+ in the chiral expansion at order p^4: a) they are essentially uncorrelated (the correlation parameter is $\rho_{-+} \simeq -0.15$), b) the error on a_0^- is very small because it involves a single chiral LEC (L_5) which is multiplied by M_π^4 while a_0^+ involves seven chiral parameters which are multiplied by $M_\pi^2 M_K^2$.

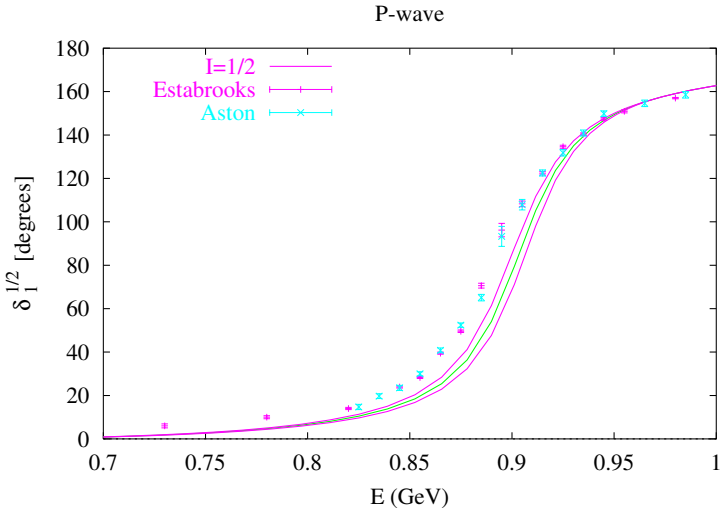

Figure 7.12: *The $I = 1/2$ P-wave phase shift obtained from solving the Roy-Steiner equations. The central curve corresponds to solving with $a_0^{1/2}$, $a_0^{3/2}$ taken at the center of the ellipse fig. 7.10. The upper (lower) curves are obtained by using the points with the maximal (minimal) values for $a_0^{1/2}$ on this ellipse.*

which are of interest in connection with the πK atom: the square of the first combination is proportional to the inverse lifetime of the atom and the sum of the two combinations is proportional to the energy shift of the lowest atomic level [370]. For comparison, let us mention the results for the combinations proportional to a_0^-, a_0^+ in χPT:

$$[\chi\text{PT } O(\text{p}^4)]: \qquad M_\pi\,(a_0^{1/2} - a_0^{3/2}) \simeq 0.238 \pm 0.002, \quad M_\pi\,(a_0^{1/2} + 2a_0^{3/2}) \simeq 0.097 \pm 0.047\ . \tag{7.50}$$

The uncertainty affecting a_0^- is remarkably small. This, however, could be an artifact of the $O(p^4)$ approximation. It remains to investigate how $O(p^6)$ corrections affect this result.

We can also compare these results with the lattice determinations performed in ref. [368] and detailed in fig. 7.11. As in the $\pi\pi$ $I = 2$ $\ell = 0$ case, the results are found to be in very good agreement with leading-order (LO) χPT, which seems again a rather fortunate coincidence. Different fits to next-to-leading-order (NLO) χPT were used in ref. [368] in order to determine the combinations of LECs involved in the two scattering lengths and reinject this piece of information:

$$[\text{Beane et al.}]: \quad M_\pi a_0^{1/2} = 0.1725 \pm 0.0017^{+0.0023}_{-0.0156}\,, \qquad M_\pi a_0^{3/2} = -0.0574 \pm 0.0016^{+0.0024}_{-0.0058}\,. \tag{7.51}$$

Before we present the results for the amplitudes in the threshold region, a few remarks are in order concerning the intermediate energy region, that ranges from the threshold up to the matching point. Experimental data from production experiments exist below 1 GeV, but one has to keep in mind the possibility that systematic errors may have been underestimated in this energy region in such experiments. Fig. 7.12 shows the $I = 1/2$ P-wave phase shift from the Roy-Steiner equations compared to experiment. The central curve correspond to solving with $a_0^{1/2}$, $a_0^{3/2}$ taken at the center of the ellipse fig.7.10 while the upper and lower curves are obtained by using the points on the ellipse with the maximal and the minimal values for $a_0^{1/2}$ respectively. The experimental results are seen to deviate from the solutions as the energy decreases from

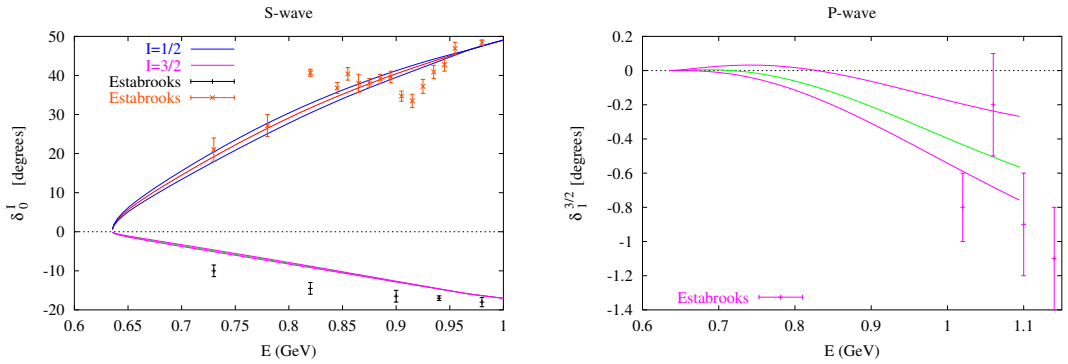

Figure 7.13: *On the left : Same as fig. 7.12 for the $I = 1/2$ S-wave phase shift (curves in the upper half of the figure) and the $I = 3/2$ S-wave phase shift (curves in lower half). On the right: Same as fig. 7.12 for the $I = 3/2$ P-wave phase shift.*

the matching point. In particular, the mass of the K^* (defined such that $\delta_1^{1/2}(M_{K^*}) = \pi/2$)) is predicted from the Roy-Steiner equations as $M_{K^*} = (905 \pm 2)$ MeV. This result is nearly 10 MeV larger than the mass quoted in ref. [354] ($M_{K^{*0}} = 896 \pm 0.7$ MeV), which is in agreement with the current values quoted by the PDG review [137] for both neutral and charged mesons: $M_{K^{*0}} = 896 \pm 0.3$ MeV and $M_{K^{*+}} = 896 \pm 0.2 \pm 0.8$ MeV (determination from $\tau \to K_S \pi \nu_\tau$, free from final state interaction problems [371]). This discrepancy is caused in part by isospin breaking which is not taken into account by the Roy-Steiner equations and could generate an uncertainty of a few MeV as to the value of the K^* mass that should come out from solving the equations[8]. Besides, even though the K^* resonance is rather narrow, a slight shift is also possible depending on the exact mass definition used (Breit-Wigner parametrisation, pole in the complex plane, particular value of the phase shift...). We will come back to this issue in sec. 7.6 in the case of the scalar $K_0^*(800)$ resonance.

The two S-wave phase shifts predicted by the Roy-Steiner equations are shown in fig. 7.13. For the isospin $I = 1/2$ the Roy-Steiner solution does not exhibit any of the oscillations appearing in the data of ref. [359]. For the isospin $I = 3/2$ phase shift, the experimental data for $E < 0.9$ GeV lie systematically below the Roy-Steiner curve, by 2-3 standard deviations. The Roy-Steiner equations also predict the $I = 3/2$ P-wave phase shift, the result is shown in fig.7.13. This phase shift displays the unusual feature that it is positive at very low energy and changes sign as the energy increases. In the region around 1 GeV the results are in qualitative agreement with the experimental data of Estabrooks *et al.*

7.5.2 Threshold and sub-threshold expansion parameters [K]

The behaviour of amplitudes at very small energies is conveniently characterised by sets of expansion parameters, which are particularly useful for making comparisons with chiral expansions. We consider first the set obtained by performing an expansion around the πK threshold. These parameters are conventionally defined from the partial-wave amplitudes:

$$\frac{2}{\sqrt{s}} \mathrm{Re} f_l^I(s) = q^{2l} \left(a_l^I + b_l^I q^2 + c_l^I q^4 + \dots \right) . \tag{7.52}$$

[8] For instance, the result depends on the input values for M_π and M_K for which we used $M_\pi = 0.13957$ GeV, $M_K = 0.4957$ GeV.

	$I=1/2$	$I=3/2$	$(I=1/2)-(I=3/2)$
$M_\pi^3\, a_1^I$	$(0.19\pm0.01)10^{-1}$	$(0.65\pm0.44)10^{-3}$	$(0.18\pm0.01)10^{-1}$
$M_\pi^5\, a_2^I$	$(0.47\pm0.03)10^{-3}$	$(-0.11\pm0.27)10^{-4}$	$(0.48\pm0.01)10^{-3}$
$m_\pi^7\, a_3^I$	$(0.23\pm0.03)10^{-4}$	$(0.91\pm0.30)10^{-5}$	$(0.14\pm0.01)10^{-4}$
$M_\pi^3\, b_0^I$	$(0.85\pm0.04)10^{-1}$	$(-0.37\pm0.03)10^{-1}$	0.12 ± 0.01
$M_\pi^5\, b_1^I$	$(0.18\pm0.02)10^{-2}$	$(-0.92\pm0.17)10^{-3}$	$(0.27\pm0.01)10^{-2}$
$M_\pi^7\, b_2^I$	$(-0.14\pm0.03)10^{-3}$	$(-0.96\pm0.26)10^{-4}$	$(-0.48\pm0.02)10^{-4}$
$M_\pi^5\, c_0^I$	$(-0.45\pm0.04)10^{-1}$	$(0.18\pm0.02)10^{-1}$	$(-0.62\pm0.06)10^{-1}$
$M_\pi^7\, c_1^I$	$(0.71\pm0.11)10^{-3}$	$(0.51\pm0.09)10^{-3}$	$(0.20\pm0.03)10^{-3}$

Table 7.1: *Results for the threshold expansion parameters (see eq. (7.52)) computed from the dispersive representations and the Roy-Steiner equations solutions. The third column shows the difference of the $I=1/2$ and the $I=3/2$ parameters.*

Once a solution of the Roy-Steiner equations is obtained, all the threshold parameters are predicted. The two S-wave scattering lengths are determined from the matching conditions, as explained above. The other threshold parameters may be obtained from the dispersive representation eq. (7.18). The results for the threshold parameters are summarised in tab.7.1. The values of the P-waves scattering lengths in χPT at NLO was given in ref. [369]:

$$\text{[Bernard et al.]}: \qquad M_\pi^3 a_1^{1/2} = 0.016 \pm 0.003\,, \quad M_\pi^3 a_1^{3/2} = (1.13 \pm 0.57)\, 10^{-3}\,. \tag{7.53}$$

Within the errors, these values are compatible with our corresponding results displayed in tab. 7.1.

χPT expansions of the amplitude are expected to have best convergence properties in unphysical regions away from any threshold singularity. The dispersive representations derived in sec. 7.1 allow us to evaluate the amplitude in such regions. A first domain considered in the literature is the neighbourhood of the point $s=u$, $t=0$. The following set of expansion parameters are conventionally introduced:

$$F^+(s,t) = \sum \tilde{C}_{ij}^+\, t^i \nu^{2j}\,, \qquad F^-(s,t) = \nu \left\{ \sum \tilde{C}_{ij}^-\, t^i \nu^{2j} \right\}\,, \tag{7.54}$$

where $\nu = (s-u)/(4M_K)$. It is customary to quote the values of the dimensionless parameters $C_{ij}^\pm$ which are related to $\tilde{C}_{ij}^\pm$:

$$C_{ij}^+ = (m_{\pi^+})^{2i+2j}\, \tilde{C}_{ij}^+, \quad C_{ij}^- = (m_{\pi^+})^{2i+2j+1}\, \tilde{C}_{ij}^-\,. \tag{7.55}$$

The results for the subthreshold expansion parameters are collected in tab. 7.2. The table also shows for comparison results from ref. [372], which used fits to the experimental data of Estabrooks *et al.* [359] combined with earlier sets of data (taking into account the data points below 1 GeV as well as above). The authors of ref. [372] observed that the low-energy part of the data of Estabrooks *et al* leads to inconsistencies with a dispersive representation of F^-. The agreement with our results is reasonable for the coefficients C_{ij}^-. For the coefficients C_{ij}^+ the results are compatible within the errors, except for the coefficient C_{10}^+, for which we find a somewhat larger value. Another point of interest is the Cheng-Dashen point $s=u$, $t=2M_\pi^2$. The value of the amplitude F^+ at this point can be related to the kaon sigma-term [373] (see [374] for a recent review), for which we obtain $F^+(M_K^2, 2M_\pi^2) = 3.90 \pm 1.50$.

				ref. [372]	$SU(3)$	$SU(2)$
		C_{00}^-	8.92 ± 0.38	7.31 ± 0.90	2	1
C_{00}^+	2.01 ± 1.10			-0.52 ± 2.03	2	2
C_{10}^+	0.87 ± 0.08			0.55 ± 0.07	2	2
C_{01}^+	2.07 ± 0.10			2.06 ± 0.22	4	2
		C_{10}^-	0.31 ± 0.01	0.21 ± 0.04	4	3
C_{20}^+	$(0.24 \pm 0.06)10^{-1}$				4	4
		C_{01}^-	0.62 ± 0.06	0.51 ± 0.10	6	3
C_{11}^+	$(-0.66 \pm 0.10)10^{-1}$			-0.04 ± 0.02	6	4
		C_{20}^-	$(0.85 \pm 0.01)10^{-2}$		6	5
C_{30}^+	$(0.34 \pm 0.08)10^{-2}$				6	6
C_{02}^+	0.34 ± 0.03				8	4

Table 7.2: *Results for the dimensionless subthreshold expansion parameters defined in eqs. (7.54) and (7.55). The last two columns indicate the chiral order of the leading tree-level contribution to each parameter in $SU(3)$ and $SU(2)$ χPT respectively.*

7.5.3 Implications for the low-energy constants [K]

In this section we present some results on the NLO LECs of the $N_f = 3$ chiral expansion, which are easily derived from the subthreshold parameters obtained above. More detailed comparisons between chiral expansions and dispersive representations of the πK scattering amplitude should be performed, but this is left for future work. The expression for this amplitude in χPT at order p^4 was presented in ref. [375]. More specifically, we will make use of a reformulation of the expression of ref. [375] in which F_0 is expressed in terms of F_π only (and not F_K) as in ref. [358] (a factor $\bar{J}_{\pi K}(s)$ is missing in eq. (41) of that reference). From this, it is straightforward to obtain the chiral formulas in χPT at NLO:

$$C_{00}^+ = 0.14985 + \frac{8M_\pi^2 M_K^2}{F_\pi^4}\left[4L_1 + L_3 - (4L_4 + L_5) + 2(L_8 + 2L_6)\right] ,$$

$$C_{10}^+ = 0.45754 + \frac{4(M_K^2 + M_\pi^2)M_\pi^2}{F_\pi^4}\left[-(4L_1 + L_3) + 2L_4\right] + \frac{2M_\pi^4}{F_\pi^4}L_5 ,$$

$$C_{20}^+ = 0.02554 + \frac{2M_\pi^4}{F_\pi^4}\left[4L_1 + L_2 + \frac{5}{4}L_3\right] , \qquad C_{01}^+ = 1.67285 + \frac{8M_K^2 M_\pi^2}{F_\pi^4}\left[4L_2 + L_3\right] ,$$

$$C_{00}^- = 8.42568 + \frac{8M_K M_\pi^3}{F_\pi^4}L_5 , \qquad C_{10}^- = -0.02533 - \frac{4M_K M_\pi^3}{F_\pi^4}L_3 . \tag{7.56}$$

In order to lighten the notation we have denoted the renormalised LECs $L_i^r(\mu = 0.77)$ simply by L_i. It is now easy to solve for the L_i's making use of the results from tab. 7.2, the results for $L_1, \ldots, L_4$ are collected in tab. 7.3. The errors are obtained, as before, by varying all the parameters of the fits to the input data and taking into account the correlations. These errors appear to be rather small but they only reflect the uncertainty coming from the input data. The dominant source of uncertainty in the determination of the L_i's comes from the unknown higher-order terms in the chiral expansion, this uncertainty is expected to be of the

	πK Roy-Steiner	πK sum-rules	$Kl_4,\ O(p^4)$	$Kl_4,\ O(p^6)$
$10^3\, L_1$	1.05 ± 0.12	0.84 ± 0.15	0.46 ± 0.24	0.53 ± 0.25
$10^3\, L_2$	1.32 ± 0.03	1.36 ± 0.13	1.49 ± 0.23	0.71 ± 0.27
$10^3\, L_3$	-4.53 ± 0.14	-3.65 ± 0.45	-3.18 ± 0.85	-2.72 ± 1.12
$10^3\, L_4$	0.53 ± 0.39	0.22 ± 0.30		-0.2 ± 0.9

Table 7.3: *LECs $L_i^r(\mu)$, $\mu = 0.77$ GeV obtained by matching the dispersive results for the subthreshold expansion parameters (see tab. 7.2) with their chiral expansion at order p^4. Also shown are the results from ref. [358] (col. 3) as well as those from ref. [189] in which fits to the Kl_4 form factors were performed using chiral expansions at order p^4 (col. 4) as well as p^6 (col. 5).*

order of 30-40% . This can be seen from the table which shows the results of some alternative determinations based on the Kl_4 form factors [189, 376, 377] and on πK sum rules [189][9]. We also quote the results that we get for L_5 and for $L_8 + 2L_6$ which have rather large errors:

$$10^3 L_5^r(M_\rho) = 3.19 \pm 2.40, \quad 10^3 (L_8^r(M_\rho) + 2L_6^r(M_\rho)) = 3.66 \pm 1.52\ . \tag{7.57}$$

The LEC L_5 is determined, in principle, from C_{00}^- but its contribution turns out to be suppressed, as it appears multiplied by a factor M_π^2. In order to determine $L_8 + 2L_6$ we used C_{00}^+ and the value $L_5 \simeq 1.4 \cdot 10^{-3}$ derived from F_K/F_π. The large uncertainty for $L_8 + 2L_6$ reflects that affecting the coefficient C_{00}^+ or, alternatively, the uncertainty in the combination of scattering lengths $a_0^{1/2} + 2a_0^{3/2}$. This could improve considerably once experimental results from πK atoms are available. Our result for L_4, though affected by a sizeable error, agrees with the evaluations [218, 219] based on a dispersive method for constructing scalar form factors [238] and is suggestive of a significant violation of the OZI rule in the scalar sector. A similar statement holds for L_6.

7.5.4 Experimental prospects

In the near future, we may hope to obtain more precise information on πK scattering from $\tau \to K\pi\nu_\tau$ as well as from $D \to K\pi\ell\nu$ decays. There has been a steady improvement in the measurement of the differential branching ratio of $\tau \to K\pi\nu_\tau$ [371, 378–380], allowing more and more sophisticated descriptions of the vector $K\pi$ form factors in this energy range, taking into account the effect of inelastic channels, either by solving dispersion relations [381], or unitarising the chiral expansion exploiting Resonance Chiral Theory [382, 383] (the latter approach has proved already very efficient to describe the S-wave πK scattering amplitude [384]). Ultimately, one should be able to connect these accurate descriptions of the $K\pi$ form factors with the $I = 1/2$ P-wave phase shifts discussed here, even though the presence of a sizeable S-wave contribution makes the analysis more complicated than initially thought [381, 384]. The resulting models for the $K\pi$ form factors have anyway be exploited in sum rules for the pseudoscalar correlator to determine the strange quark mass [385], to improve the accuracy on the normalisation of the $K_{\ell 3}$ form factor to determine of $|V_{us}|$ [260, 262, 263, 386–388] and to exploit $K_{\ell 3}$ decays as a test of right-handed currents [223, 258, 259, 389].

The $D \to K\pi\ell\nu$ analysis follows closely the K_{e4} case detailed in sec. 6.1.4, as discussed in refs. [390, 391]. The hadronic matrix element can be decomposed into four form factors

[9] In that paper, terms of order p^6 were dropped in the dispersive representations and the phase shifts used below 1 GeV in the sum rules were not constrained to obey the Roy-Steiner equations.

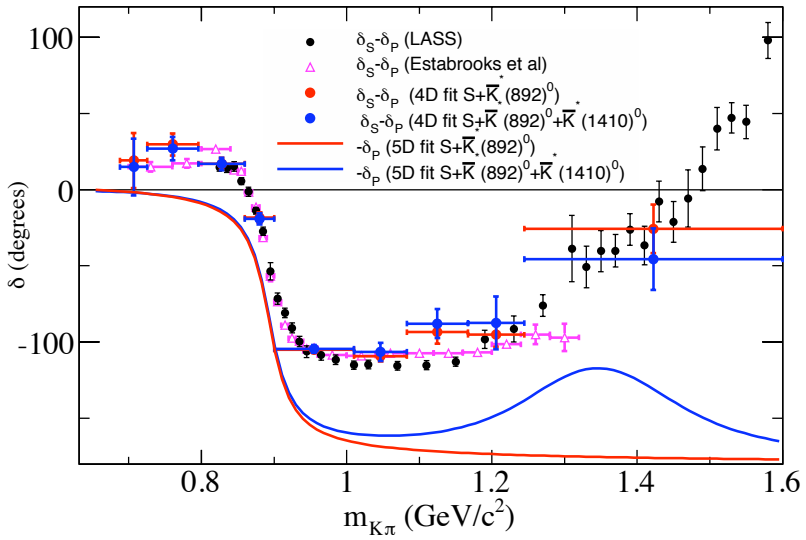

Figure 7.14: *Results on $K\pi$ phase shifts from the analysis of $D^+ \to K^-\pi^+e^+\nu_e$ from the Babar collaboration. Difference between the $I = 1/2$ S- and P-wave phase versus the $K\pi$ mass. Measurements are similar whether or not the $\bar{K}^{*0}(1410)$ resonance is included in the P-wave parameterization. Results are compared with measurements from $K\pi$ scattering [354, 359]. The continuous and dashed lines give the phase variation with a minus sign ($-\delta_P$) for the $\bar{K}^{*0}(892)$ and $\bar{K}^{*0}(892) + \bar{K}^{*0}(1410)$, respectively. The difference between these curves and the measured points corresponds to the S-wave contribution. Taken from ref. [398].*

involved in the partial decay width. Once again, one should perform an angular analysis to extract interference terms between S- and P-waves, and ultimately the corresponding phase shifts, up to two main modifications. First, the $K\pi$ mass difference in the final state yields a complication of the expressions (even though it does not modify the conceptual description of the decay). Second, the kinematic range of the decay involves the $K^*(892)$ meson in the P-wave, meaning that one cannot describe the P-wave form factors as slowly-varying functions of s – one has to rely on more model-dependent descriptions. At the experimental level, the FOCUS collaboration reported the first indications of a significant S-wave component in the decay $D^+ \to K^-\pi^+\mu^+\nu_\mu$ in the $K^*(892)$ energy range [392–394]. The form factors were further studied by the CLEO collaboration [395, 396] finding no indication of partial waves $\ell \geq 2$. A more complete study was performed by the Babar collaboration [397, 398], leading to a first determination of the difference between $I = 1/2$ S- and P-wave phase shifts. The results recalled in fig. 7.14 are obviously not competing yet with production experiments, but they are already an encouraging indication that such measurements can be considered at dedicated charm-factories [399].

Study of the low-energy interactions between kaons and pions with πK bound-states has been proposed by the DIRAC collaboration, to study πK atoms at CERN, J-PARC and GSI, the results of which would provide direct measurements or constraints on combinations of the scattering lengths [283, 284]. Considering the accuracy currently reached by pionium experiments for the $\pi\pi$ scattering lengths, this seems however to a rather long-term option.

7.6 The lightest scalar meson in the strange sector

7.6.1 Roy-Steiner representations in the complex plane [L]

We want to investigate the analytic structure of the Roy-Steiner representation of the πK amplitudes. In particular, we would like to identify the poles in the complex energy plane related to low-energy resonances, such as the scalar $K_0^*(800)$ meson. We have then to extend the analysis of sec. 7.2, considering now that s is a complex variable. As before, we assume that the scattering amplitude satisfies Mandelstam's double spectral representation [349], so that the nearest singularity is given by the boundary of the support of the double spectral functions ρ_{st}, ρ_{us}. We recall that these boundaries are generated by considering the lightest contributions in the unitarity relations. It turns out that the representation of the partial waves derived from the fixed-t representation eq. (7.13) does not have a satisfying domain of validity in the complex plane. Indeed, a Roy-Steiner representation is generated by projecting eq. (7.13) on the $l = 0$ partial wave:

$$f_0^+(s) = \frac{s}{16\pi\lambda_s} \int_{-\frac{\lambda_s}{s}}^{0} dt\, F^+(s,t) \ . \tag{7.58}$$

This projection can be performed only if the segment of integration remains inside the region of validity. The boundary of the domain of validity of the Roy-Steiner representation in the s-plane is therefore obtained, in parametric form, by solving:

$$\lambda_s + s\ T(\theta)\exp(i\theta) = 0 \ . \tag{7.59}$$

The result is displayed in fig. 7.15 where the two cuts along the real axis as well as the circular cut of the partial wave amplitude are also drawn. As can be seen on this figure, the validity region of the Roy-Steiner representation based on fixed-t dispersion relation gets squeezed when $\mathrm{Re}\,(s)$ is close to the πK threshold, which makes it a priori unfit to search for a wide resonance like the κ.

Let us now investigate the second kind of dispersion relation, eq. (7.20), denoted $\mathrm{RS_b}$. We must ensure that the discontinuity functions $\mathrm{Im}\,{}_sF^+(s', t_b(s'))$ and $\mathrm{Im}\,{}_tF^+(s'_b(t'), t')$ are defined inside the s' and the t' integration ranges, once these functions are expanded on $\pi K \to \pi K$ and $\pi\pi \to K\overline{K}$ partial waves respectively. As done before, we consider each Mandelstam boundary (st and us) and we determine the region for the parameter b inside which the representation 7.20 is valid. $B(\theta)$ the description (in polar coordinates) for the boundary of such a region.

The S-wave component of this representation is then taken:

$$f_0^+(s) = \frac{1}{16\pi\lambda_s} \int_{\Delta^2}^{(2\Sigma-s)s} db\, F^+\left(s, 2\Sigma - s - \frac{b}{s}\right) \ . \tag{7.60}$$

The segment of integration (i.e., its end at $(2\Sigma - s)s$) must remain within the region of validity in b, so that the boundary in the s plane for the $\mathrm{RS_b}$ representation is obtained as a solution to:

$$s^2 - 2\Sigma s + B(\theta)\exp(i\theta) = 0 \ . \tag{7.61}$$

The domains of validity which result from the consideration of the s' and t' integrals are shown in fig. 7.15. In the case of the t' integral, the st Mandelstam boundary is the only one relevant. In the case of the s' integral, one must consider both the us and the st Mandelstam boundaries. The last domain is included into all the others and therefore defines the region in the complex plane where the $\mathrm{RS_b}$ representation is valid. The shape of this domain is

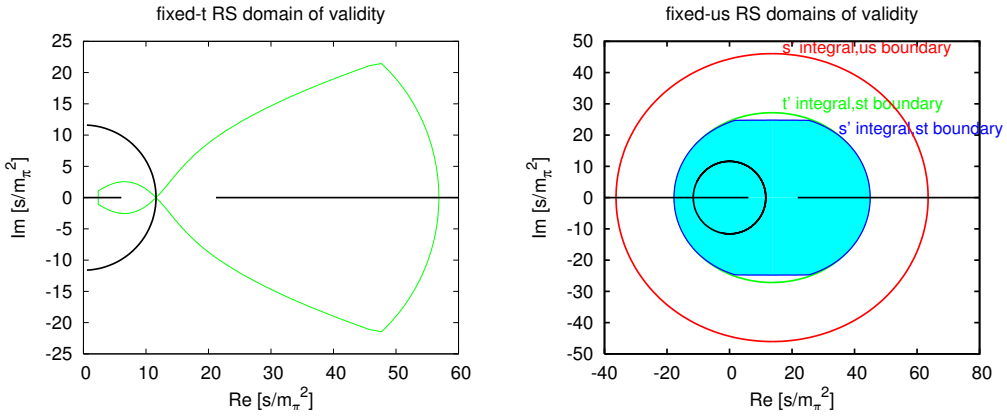

Figure 7.15: *On the left: domain of validity of the Roy-Steiner representation based on fixed-t dispersion relation. On the right: domains of validity associated with the s' and t' integrals in the fixed-us representation 7.20 and resulting from the conditions that the Lehmann ellipses do not touch the st or the us Mandelstam boundaries. The energy variables are expressed in units of $m_{\pi^+}^2$.*

quite different from fig. 7.15 corresponding to the fixed-t Roy-Steiner representation. The latter exhibits a more extended validity along the real axis, whereas the former is significantly broader along the imaginary direction. Indeed, the domain of validity for $\mathrm{RS_b}$ extends up to $\mathrm{Im}\,(s) \simeq 0.39$ GeV^2 when $\mathrm{Re}\,(s)$ is close to the threshold, which will turn out to be sufficient for the $K_0^*(800)$ resonance.

7.6.2 Is there a $K_0^*(800)$? [L]

We have for the $\pi K \to \pi K$ amplitude of isospin $I = 1/2$ for the partial wave $l = 0$:

$$
\begin{aligned}
f_0^{1/2}(s) = 1/2 m_+ a_0^{1/2} + \frac{1}{12} m_+ (a_0^{1/2} - a_0^{3/2}) \frac{(s - m_+^2)(5s + 3m_-^2)}{(m_+^2 - m_-^2)\, s} \\
+ \frac{1}{\pi} \int_{m_+^2}^{\infty} ds' \sum_{l=0}^{\infty} \left\{ K_{0l}^{1/2}(s,s') \mathrm{Im}\, f_l^{1/2}(s') + K_{0l}^{3/2}(s,s') \mathrm{Im}\, f_l^{3/2}(s') \right\} \\
+ \frac{1}{\pi} \int_{4M_\pi^2}^{\infty} dt' \sum_{l=0}^{\infty} \left\{ K_{02l}^{0}(s,t') \mathrm{Im}\, g_{2l}^{0}(t') + K_{02l+1}^{1}(s,t') \mathrm{Im}\, g_{2l+1}^{1}(t') \right\} \ , \qquad (7.62)
\end{aligned}
$$

This is the key expression which enables us to compute the amplitude $f_0^{1/2}(s)$ for complex values of s. In the formula 7.62, the integrands are evaluated using the description of πK scattering (and its crossed channel) along the real axis obtained by solving Roy-Steiner equations.Whenever the integration variables s', t' are larger than approximately 1 GeV^2, the imaginary parts $\mathrm{Im}\, f_l^I(s')$, $\mathrm{Im}\, g_l^I(t')$ are taken from fits to the experimental data For the evaluation of the integrands, experimental information is available for values of l up to $l = 5$ and in a range of energies up to $s'_{max} \simeq t'_{max} \simeq 6$ GeV^2. The integrals involved here converge quickly and we restrict ourselves to values of s such that $|s| \lesssim 1$ GeV^2. We can conclude that we only need qualitative estimates for the imaginary parts in the higher integration region. For this purpose, the simple Regge pole models used in ref. [44] are appropriate. In the lower parts of the integration ranges, $\mathrm{Im}\, f_l^I(s')$, $\mathrm{Im}\, g_l^I(t')$ with $l = 0, 1$ are taken from the solutions of the Roy-Steiner equations, as well as the scattering lengths $a_0^{1/2}$ and $a_0^{3/2}$.

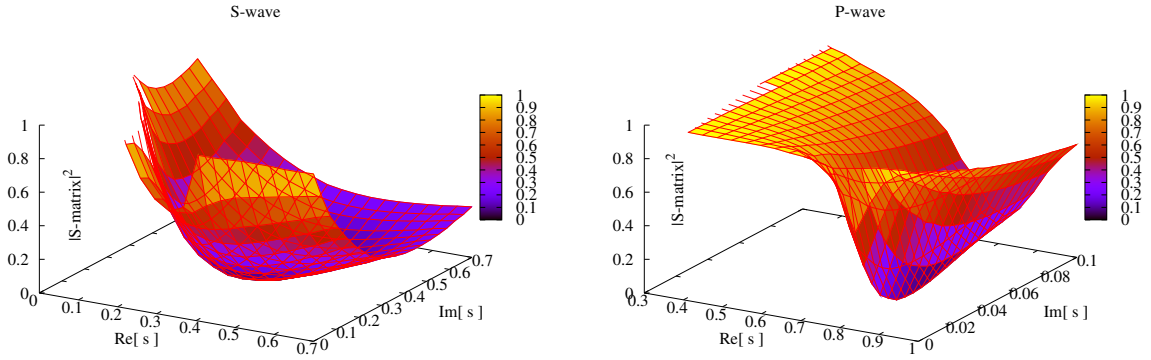

Figure 7.16: *Plot of* $|S_0^{1/2}(s)|^2$ *and* $|S_1^{1/2}|^2$ *for complex values of* s *(in units of* GeV^2*), computed from the* $\mathrm{RS_b}$ *representation (7.62).*

Therefore, we have a representation for $f_0^{1/2}(s)$ which is valid in the complex region of s shown in fig.7.15 and lies on the first Riemann sheet with respect to all the cuts. Let us recall that the elastic $S_l^{1/2}$ matrix element, defined in eq. (7.10), exhibits a resonance as a zero on the first sheet as well as as a pole on the second sheet. This fortunate property stems from the unitarity relation which can be recast, using the analyticity properties, as an equation between the values of the amplitude on both sides of the cut:

$$f_l^{1/2}(s-i\epsilon) - f_l^{1/2}(s+i\epsilon) = 2i\frac{\sqrt{(s-m_+^2)(s-m_-^2)}}{s} f_l^{1/2}(s+i\epsilon) f_l^{1/2}(s-i\epsilon)\ . \tag{7.63}$$

This relation holds for real values of s along the elastic cut below the first inelastic threshold. It can be translated into a relation for the S matrix:

$$S_l^{1/2}(s+i\epsilon) S_l^{1/2}(s-i\epsilon) = 1\ . \tag{7.64}$$

Introducing a variable $z = -\sqrt{m_+^2 - s}$ which maps the first sheet of the s plane onto the upper part of the z plane, we can rewrite eq. (7.64) as:

$$S_l^{1/2}(z) S_l^{1/2}(-z) = 1\ . \tag{7.65}$$

The relation 7.65 holds on a finite portion of the positive real axis. By analytic continuation, it must also hold everywhere in the complex z plane. This relation immediately shows that a resonance pole z_0 on the second Riemann sheet [$\mathrm{Im}\,(z_0) < 0$] is automatically associated to a zero at $-z_0$, which lies on the first sheet. Computing $S_0^{1/2}(s)$ from the $\mathrm{RS_b}$ representation described above for the central values of our experimental input, we find that it does feature a zero:

$$S_0^{1/2}(s_0) = 0\,, \qquad s_0 = 0.356 + i \cdot 0.366\ \mathrm{GeV}^2\ . \tag{7.66}$$

The global shape of the S matrix for complex values of s is illustrated in fig. 7.16, which displays the squared modulus of $S_0^{1/2}(s)$ resulting from our computation. The figure shows that the modulus is constant and equal to one over a portion of the real axis (in accordance with unitarity) and drops when one leaves this axis, eventually becoming zero at $s = s_0$. We

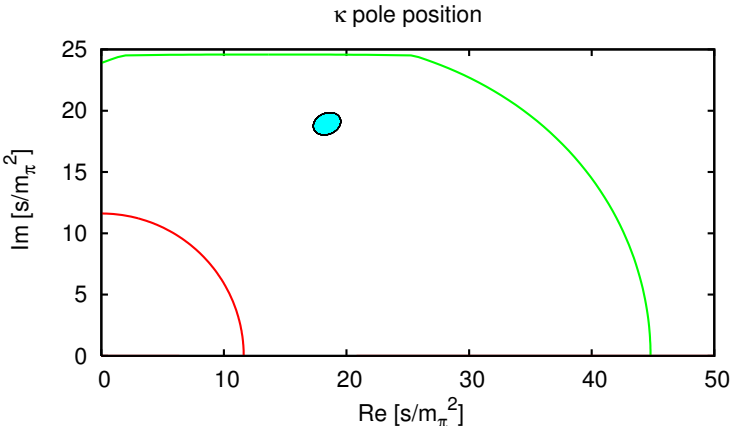

Figure 7.17: *Position of the κ pole s_0 and its one-sigma error ellipse (in units of M_π^2). We also show the boundary of the region of validity of the* $\mathrm{RS_b}$ *representation and the left-hand cuts of the amplitude.*

notice the similarity of the global behaviour of the S matrix with the case of an ordinary narrow resonance. Indeed, fig. 7.16 shows the squared modulus of the P-wave S matrix computed using the same apparatus, which exhibits the well-known $K^*(890)$ resonance as a zero. According to these results, the existence of the $K_0^*(800)$ scalar resonance is established on the same footing as that of the vector $K^*(890)$ resonance.

As stated earlier, the point s_0 is located inside the domain of validity of the $\mathrm{RS_b}$ representation. This is illustrated in fig. 7.17 which shows the one-sigma error ellipse on s_0 computed by varying the parameters describing our input data (see ref. [44] for more detail). In addition the figure shows that s_0 is located at about the same distance from the physical cut as from the circular cut. This feature confirms that a representation of the amplitude accounting for the left-hand cuts correctly is needed in order to determine s_0 in a reliable way. The mass and width of the κ resonance, as defined from the square root of s_0, $M_\kappa + i \cdot \Gamma_\kappa/2 = \sqrt{s_0}$, are:

$$M_\kappa = 658 \pm 13 \text{ MeV}\,, \quad \Gamma_\kappa = 557 \pm 24 \text{ MeV}\,. \tag{7.67}$$

We can summarise the results of a few other determinations of the $K_0^*(800)$ resonance parameters in the recent literature. These are derived from input experimental data on πK scattering, except for the result of Aitala et al. [401] which is based on $D \to K\pi\pi$ decays and the one from Bugg [402, 403] who uses the same data combined with BES II data on $J/\psi \to K^*(890)K\pi$. Our results are compatible with those of ref. [400] who have also employed dispersive methods. The mass which we find is lighter than in previous calculations. A similar effect was observed in ref. [133] in the case of the σ and it was traced to a more complete treatment of the left-hand cuts in Roy-type representations. Our errors are rather small and of the same size as the errors affecting the σ-meson mass and width as obtained in ref. [133]. This reflects the good quality of the experimental data used as input, which is exploited in an optimal way. In ref. [133] the following results were found for the σ meson:

$$M_\sigma = 441^{+16}_{-8} \text{ MeV}, \quad \Gamma_\sigma = 544^{+18}_{-25} \text{ MeV}. \tag{7.68}$$

	M_κ (MeV)	Γ_κ (MeV)
This work	658 ± 13	557 ± 24
Zhou, Zheng [400]	694 ± 53	606 ± 89
Jamin et al. [384]	708	610
Aitala et al. [401]	$721 \pm 19 \pm 43$	$584 \pm 43 \pm 87$
Pelaez [298]	750 ± 18	452 ± 22
Bugg [402, 403]	750^{+30}_{-55}	684 ± 120
Ablikim et al. [404]	$841 \pm 23^{+64}_{-55}$	$618 \pm 52^{+55}_{-87}$
Ishida et al. [405]	877^{+65}_{-30}	668^{+235}_{-110}

Table 7.4: *The mass and width of the $K_0^*(800)$ from our work and some other recent determinations. Refs. [401, 404, 405] quote Breit-Wigner parameters from which we have computed the corresponding pole positions.*

Comparing M_κ and M_σ suggests that the κ meson is the $S = 1$ partner of the σ meson. If one formed a nonet by associating together the σ, the κ, the iso-singlet $f_0(980)$ and the iso-triplet $a_0(980)$, its mass pattern would be clearly at variance with the usual $Q\bar{Q}$ picture (which is also what is expected in the large-N_c limit of QCD). In contrast, it would be conspicuously similar to the pattern predicted by Jaffe from a $Q^2\bar{Q}^2$ picture a long time ago [406]. The correct values for the widths seem more difficult to reproduce in simple quark models [407]. Many different models, multiplet assignments and interpretations of the light scalar mesons have been proposed in the literature (see sec. 2.5.1 and ref. [138] for a review).

7.7 Summary

We have set up and then solved a system of equations à la Roy and Steiner for the S- and P-partial waves of the $\pi K \to \pi K$ and the $\pi\pi \to K\overline{K}$ amplitudes. These equations are necessary consequences of analyticity and crossing, together with plausible assumptions concerning the range of effective applicability of elastic unitarity. In treating these equations, the approach advocated recently in ref. [251] was followed, which consists in choosing a matching point around 1 GeV and enforcing a set of boundary conditions at this point. As input for this analysis, we have exploited the high-statistics data which are now available from $KN \to K\pi N$ as well as $\pi N \to K\overline{K}N$ production experiments.

The main result obtained from solving the Roy-Steiner equations together with the boundary conditions is the determination of an allowed region for the two S-wave scattering lengths which is shown, as a one-sigma ellipse, in fig. 7.10. This region is much smaller than the ones resulting from older analyses, e.g. ref. [352]; this reflects the better accuracy of the experimental input data used here. Using this result together with the dispersive representations one can determine the πK scattering amplitude in regions of very low energies inaccessible to experiment. We have computed a set of sub-threshold expansion parameters and then matched the result with the $SU(3)$ χPT expansion of the amplitude at NLO [369, 375], leading to the LECs L_1, L_2, L_3, and L_4. The bounds that we have obtained for the S-wave scattering lengths constrain the combination $2L_6 + L_8$. These values suggest a significant departure of L_4 and L_6 from the critical values corresponding to an operative Zweig suppression in the scalar sector, inducing a significant competition between leading- and next-to-leading-order terms in the chiral series. More detailed comparisons with χPT expansions will be discussed in the next

chapter.

As an additional outcome of this study, we have showed the existence of the scalar $K_0^*(800)$ or sκ meson. Previously, the same conclusion was derived by similar means in the case of the σ meson [133]. A major advantage of the methods used here and in ref. [133] lies in the control of their range of validity as one moves away from the physical energy region into the complex plane. No such control exists for naive parametrisations of the Breit-Wigner type or even for more sophisticated ones like chiral-unitarised approaches. The combination of experimental and theoretical information leads to a zero of the S matrix on the first sheet, and therefore a pole on the second one, which confirms the existence of the $K_0^*(800)$ resonance. We have observed that the behaviour of the S matrix when the energy variable s becomes complex is qualitatively the same as in the case of a narrow resonance

This discussion closes the study of the experimental pieces of information on $\pi\pi$ and πK scatterings. We can now turn to the combination of elements to extract some information on the low-energy constants of the three-flavour chiral Lagrangian.

Now, I give you fair warning, either you or your head must be off, and that in about half no time ! Take your choice !

The Queen

8

Three-flavour chiral symmetry breaking according to $\pi\pi$ and πK scatterings

We have been discussing the possibility of significant differences in the pattern of chiral symmetry breaking as one sends the strange quark mass to zero, i.e., from the two-flavour chiral limit to the three-flavour one. This was hinted at by a dispersive estimate of L_6 as well as by the pseudoscalar spectrum obtained through lattice simulations. However, a more powerful test consists in comparing pion and kaon scatterings, using the description provided by χPT, in order to extract some information on the leading-order parameters of the three-flavour chiral Lagrangian, i..e the quark condensate, the pseudoscalar decay constant and the quark mass ratio:

$$X(3) = \frac{2m\Sigma(3)}{F_\pi^2 M_\pi^2}\,, \qquad Z(3) = \frac{F^2(3)}{F_\pi^2}\,, \qquad r = \frac{m_s}{m}\,. \tag{8.1}$$

In the previous chapters, we have discussed experimental information obtained on $\pi\pi$ and πK scattering amplitudes thanks to dispersive methods, and we have provided a framework (Resummed χPT or ReχPT) that hopefully will deal with a numerical competition between LO and NLO (or instabilities) in the chiral series, as well as with the possibility of their saturation by the quark condensate and the pseudoscalar decay constant. We have now to combine these elements: this is the purpose of the present chapter. Such a discussion was started in ref. [38], with three ingredients: the subthreshold parameters $\alpha_{\pi\pi}$ and $\beta_{\pi\pi}$ describing the $\pi\pi$ scattering amplitude in the unphysical region where χPT is expected to converge well, the expressions of these parameters obtained in the framework of ReχPT, and a Bayesian statistical framework to update prior beliefs on the quantities in eq. (8.1) through experimental knowledge. By comparing the p.d.f's before and after including $\alpha_{\pi\pi}$ and $\beta_{\pi\pi}$, one could check that $\pi\pi$ scattering puts a lower bound on the value of r, but is not enough to constrain the chiral order parameters.

One could object to this first attempt that it could make use of Chiral Perturbation Theory in a very limited way: even though the $\pi\pi$ amplitude should be well described in the (unphysical) region around the center of the Mandesltam plane and can be reconstructed (using Roy equations) from the available experimental information, only two subtraction constants are actually exploited. Another, more general, issue consists in the use of the Bayesian approach, as it proves difficult to disentangle the effects of the prior p.d.f's and of the experimental likelihood in the outcome of the analyses (for instance, in ref. [38], one could see that the priors tended to suppress small values of $Z(3)$ before adding any experimental data). A related problem stems from the treatment of the nuisance parameters, such as the higher-order remainders, taken as Gaussian random variables, even though they are rather to be considered as fixed parameters constrained in a given range (for instance, from resonance saturation). The respective merits of the Bayesian and frequentist approaches are obviously a recurrent subject of discussion, as can be seen in other areas of particle physics (e.g., the determination of the CKM matrix elements [14, 408–411]).

In this chapter, we will update the work in ref. [46], adopting a frequentist approach together with a dedicated scheme to handle theoretical uncertainties. We will build a χ^2 comparing the values of the $\pi\pi$ and πK scattering amplitudes with their ReχPT expansions in the subthreshold region(s). Minimising this χ^2 allows us to derive p-values corresponding to the hypothesis that one of the parameter of interest eq. (8.1) has a given value. We thus obtain confidence intervals for each parameter, analysing separately $\pi\pi$ and πK scatterings before combining them, updating the values given in ref. [46]. [1]

[1] This chapter is based on the following article:

[M] SDG, *Low-energy $\pi\pi$ and πK scatterings revisited in three-flavour resummed chiral perturbation theory*, Eur. Phys. J. C52 (2007) 141 [46]

8.1 $\pi\pi$ and πK scattering amplitudes

8.1.1 One-loop expression in ReχPT [M]

In the isospin symmetry limit, the low-energy $\pi\pi$ scattering is described by a single Lorentz-invariant amplitude:

$$A(\pi^a(p_1)+\pi^b(p_2)\to\pi^c(p_3)+\pi^d(p_4))=\delta^{ab}\delta^{cd}A(s,t,u)+\delta^{ac}\delta^{bd}A(t,u,s)+\delta^{ad}\delta^{bc}A(u,t,s) \quad (8.2)$$

where the usual Mandelstam variables are: $s=(p_1+p_2)^2, t=(p_1-p_3)^2, u=(p_1-p_4)^2$ and A is symmetric under $t\leftrightarrow u$ exchange. In a similar way, we consider the low-energy πK scattering, which can be decomposed into two amplitudes according to isospin in the s-channel $I=3/2$ and $I=1/2$:

$$A(\pi^a(p_1)+K^i(p_2)\to\pi^b(p_3)+K^j(p_4))=F^I_{\pi K}(s,t,u)\,, \quad (8.3)$$

from which one can define two amplitudes, respectively even and odd under $s\leftrightarrow u$ exchange:

$$B(s,t,u)=\frac{2}{3}F^{3/2}_{\pi K}(s,t,u)+\frac{1}{3}F^{1/2}_{\pi K}(s,t,u)\,, \quad C(s,t,u)=-\frac{1}{3}F^{3/2}_{\pi K}(s,t,u)+\frac{1}{3}F^{1/2}_{\pi K}(s,t,u)\,. \quad (8.4)$$

Crossing symmetry provides a relation between the two amplitudes:

$$F^{1/2}_{\pi K}(s,t,u)=\frac{3}{2}F^{3/2}_{\pi K}(u,t,s)-\frac{1}{2}F^{3/2}_{\pi K}(s,t,u)\,. \quad (8.5)$$

We can apply the prescriptions described in sec. 5.1 to determine the one-loop ReχPT expansions of A, B and C. The relevant observables with good convergence properties can be derived from Green functions of vector/axial currents: $F_\pi^4 A$, $F_\pi F_K F$ and $F_\pi F_K G$. We start by determining the one-loop bare expansions of these quantities. This can be done using the generating functional of $N_f=3$ χPT [21], with the essential difference that we keep the distinction between $O(p^2)$ truncated masses and physical masses of the Goldstone bosons. This was performed in the case of πK scattering in ref. [369, 375]. A similar work can be done in the case of $\pi\pi$ scattering. From ref. [305], we obtain, with the same notation in ch. 3:

$$\begin{aligned}
F_\pi^4 A_{\pi\pi} &= \frac{2}{3}mB_0F_0^2+F_0^2\left(s-\frac{4}{3}M_\pi^2\right) \quad (8.6)\\
&+\mu_\pi F_0^2\left[-4\left(s-\frac{4}{3}M_\pi^2\right)-2B_0m\right]+\mu_K F_0^2\left[-2\left(s-\frac{4}{3}M_\pi^2\right)-\frac{4}{3}B_0m\right]-\frac{2}{9}\mu_\eta F_0^2B_0m\\
&+16B_0mL_4^r\left[\left(s-\frac{4}{3}M_\pi^2\right)(r+4)-\frac{4}{3}M_\pi^2\right]+32B_0mL_5^r\left(s-\frac{5}{3}M_\pi^2\right)+\frac{64}{3}B_0^2m^2L_6^r(r+8)\\
&+\frac{256}{3}B_0^2m^2L_8^r+4\left(2L_1^r+L_3^r\right)\left(s-2M_\pi^2\right)^2+4L_2^r\left[(t-2M_\pi^2)^2+(u-2M_\pi^2)^2\right]\\
&+\frac{1}{2}\left[(s-2M_\pi^2)^2+8B_0m(s-2M_\pi^2)+12B_0^2m^2\right]J^r_{\pi\pi}(s)\\
&+\frac{1}{4}\left[(t-2M_\pi^2)^2J^r_{\pi\pi}(t)+(u-2M_\pi^2)^2J^r_{\pi\pi}(u)\right]\\
&+\frac{1}{8}\left[(s-2M_\pi^2)^2+8B_0m(s-2M_\pi^2)+16B_0^2m^2\right]J^r_{KK}(s)+\frac{2}{9}B_0^2m^2J^r_{\eta\eta}(s)\\
&+\frac{1}{2}\left[(s-u)t\left(2M^r_{\pi\pi}+M^r_{KK}\right)(t)+(s-t)u\left(2M^r_{\pi\pi}+M^r_{KK}\right)(u)\right]\,,
\end{aligned}$$

where $\overset{\circ}{M}{}^2_P$ denotes the leading-order pseudoscalar squared mass of the Goldstone boson P and the tadpole logarithm is:

$$\mu_P = \frac{\overset{\circ}{M}{}^2_P}{32\pi^2 F_0^2} \log \frac{\overset{\circ}{M}{}^2_P}{\mu^2} \,. \tag{8.7}$$

We recast the amplitude as:

$$\begin{aligned}
F_\pi^4 A_{\pi\pi} &= \mathcal{A}^r + \left(s - \frac{4}{3}M_\pi^2\right)\mathcal{B}^r + 4(2L_1^r + L_3)(s-2M_\pi^2)^2 + 4L_2^r[(t-2M_\pi^2)^2 + (u-2M_\pi^2)^2] \\
&+\frac{1}{2}[(s-2M_\pi^2)^2 + 8mB_0(s-2M_\pi^2) + 12m^2B_0^2]J_{\pi\pi}^r(s) \\
&+\frac{1}{4}[(t-2M_\pi^2)^2 J_{\pi\pi}^r(t) + (u-2M_\pi^2)^2 J_{\pi\pi}^r(u)] \\
&+\frac{1}{8}[(s-2M_\pi^2)^2 + 8mB_0(s-2M_\pi^2) + 16m^2B_0^2]J_{KK}^r(s) + \frac{1}{18}4m^2B_0^2 J_{\eta\eta}^r(s) \\
&+\frac{1}{2}[(s-u)t \times (2M_{\pi\pi}^r + M_{KK}^r)(t) + (s-t)u \times (2M_{\pi\pi}^r + M_{KK}^r)(u)] \,,
\end{aligned} \tag{8.8}$$

where $\mathcal{A}^r$ and $\mathcal{B}^r$ are scale-dependent combinations of low-energy constants (LECs):

$$\begin{aligned}
3\times\mathcal{A}^r &= 2mB_0F_0^2 + 64m^2B_0^2[(r+8)L_6^r + 4L_8^r] - 32mB_0M_\pi^2[2L_4^r + L_5^r] \\
&\quad -\frac{1}{32\pi^2}4m^2B_0^2\left[3\log\frac{\overset{\circ}{M}{}^2_\pi}{\mu^2} + (r+1)\log\frac{\overset{\circ}{M}{}^2_K}{\mu^2} + \frac{1}{9}(2r+1)\log\frac{\overset{\circ}{M}{}^2_\eta}{\mu^2}\right] \,, \\
\mathcal{B}^r &= F_0^2 + 16mB_0[(r+4)L_4^r + 2L_5^r] - \frac{1}{32\pi^2}2mB_0\left[4\log\frac{\overset{\circ}{M}{}^2_\pi}{\mu^2} + (r+1)\log\frac{\overset{\circ}{M}{}^2_K}{\mu^2}\right] \,,
\end{aligned} \tag{8.9}$$

which correspond to $F_\pi^2 M_\pi^2 \alpha_{\pi\pi}^r/3$ and $\mathcal{B}$ to $F_\pi^2\beta_{\pi\pi}^r$ respectively, as defined in ref. [305]. In the above expressions, we have replaced the LO masses $\overset{\circ}{M}{}^2_P$ by the physical masses in the loop function $\bar{J}$ involved in J^r and M^r [2]. One can check explicitly that there is no μ dependence in the above expression of the amplitude: for each polynomial in $s-2M_\pi^2, t-2M_\pi^2, u-2M_\pi^2$, the dependence of the LECs on the renormalisation scale μ cancels that of J^r and M^r.

We recall the expression obtained in ref. [369, 375] for the $I = 3/2$ πK amplitude:

$$\begin{aligned}
F_\pi^2 F_K^2 F_{\pi K}^{3/2} &= \frac{F_0^2}{6}\Bigg[2M_\pi^2 + 2M_K^2 + \overset{\circ}{M}{}^2_\pi + \overset{\circ}{M}{}^2_K - 3s + \frac{\mu_\pi}{8}[66s - 34M_\pi^2 - 54M_K^2 - 15\overset{\circ}{M}{}^2_\pi - 21\overset{\circ}{M}{}^2_K] \\
&+\frac{\mu_K}{4}[30s - 22M_\pi^2 - 18M_K^2 - 11\overset{\circ}{M}{}^2_\pi - 9\overset{\circ}{M}{}^2_K] + \frac{\mu_\eta}{24}[54s - 54M_\pi^2 - 18M_K^2 - 17\overset{\circ}{M}{}^2_\pi - 11\overset{\circ}{M}{}^2_K] \\
&+8L_1^r(t-2M_\pi^2)(t-2M_K^2) + 4L_2^r[(s-M_\pi^2-M_K^2)^2 + (u-M_\pi^2-M_K^2)^2] \\
&+2L_3[(u-M_\pi^2-M_K^2)^2 + (t-2M_\pi^2)(t-2M_K^2)] \\
&+8L_4^r[\overset{\circ}{M}{}^2_\pi(t - \frac{1}{2}s + \frac{1}{3}M_\pi^2 - \frac{5}{3}M_K^2) + \overset{\circ}{M}{}^2_K(t - s - \frac{4}{3}M_\pi^2 + \frac{2}{3}M_K^2)]
\end{aligned}$$

[2] This is in agreement with the general discussion of resummed χPT in sec. 5.1, but slightly different from the original discussion in ref. [46], where the replacement was also performed in M^r and in the tadpole diagrams. We will see that this change had a limited impact on the results of the analysis.

$$+\frac{4}{3}L_5^r[\overset{\circ}{M}{}_\pi^2(2M_\pi^2-3s)+\overset{\circ}{M}{}_K^2(2M_K^2-3s)]+\frac{8}{3}L_6^r[\overset{\circ}{M}{}_\pi^4+15\overset{\circ}{M}{}_\pi^2\overset{\circ}{M}{}_K^2+2\overset{\circ}{M}{}_K^4]$$

$$+\frac{8}{3}L_8^r[\overset{\circ}{M}{}_\pi^4+6\overset{\circ}{M}{}_\pi^2\overset{\circ}{M}{}_K^2+\overset{\circ}{M}{}_K^4]+\frac{t}{2}(u-s)[M_{\pi\pi}^r(t)+\frac{1}{2}M_{KK}^r(t)]$$

$$+\frac{3}{8}\{(s-t)[L_{\pi K}(u)-uM_{\pi K}^r(u)]+(M_K^2-M_\pi^2)^2M_{\pi K}^r(u)\}$$

$$+\frac{3}{8}\{(s-t)[L_{K\eta}(u)-uM_{K\eta}^r(u)]+(M_K^2-M_\pi^2)^2M_{K\eta}^r(u)\}$$

$$+\frac{1}{8}(M_K^2-M_\pi^2)K_{\pi K}(u)[5(u-M_\pi^2-M_K^2)+3\overset{\circ}{M}{}_\pi^2+3\overset{\circ}{M}{}_K^2]$$

$$+\frac{1}{8}(M_K^2-M_\pi^2)K_{K\eta}(u)[3(u-M_\pi^2-M_K^2)+\overset{\circ}{M}{}_\pi^2+\overset{\circ}{M}{}_K^2]+\frac{1}{4}J_{\pi K}^r(s)(s-M_\pi^2-M_K^2)^2$$

$$+\frac{1}{32}J_{\pi K}^r(u)[11(u-M_\pi^2-M_K^2)^2+10(u-M_\pi^2-M_K^2)(\overset{\circ}{M}{}_\pi^2+\overset{\circ}{M}{}_K^2)+3(\overset{\circ}{M}{}_\pi^2+\overset{\circ}{M}{}_K^2)^2]$$

$$+\frac{1}{32}J_{K\eta}^r(u)[u-M_\pi^2-M_K^2+\frac{1}{3}(\overset{\circ}{M}{}_\pi^2+\overset{\circ}{M}{}_K^2)]^2+\frac{1}{8}J_{\pi\pi}^r(t)[4M_\pi^2-2t-3\overset{\circ}{M}{}_\pi^2][2M_K^2-t-2\overset{\circ}{M}{}_K^2]$$

$$+\frac{3}{16}J_{KK}^r(t)[2M_\pi^2-t-2\overset{\circ}{M}{}_\pi^2][2M_K^2-t-2\overset{\circ}{M}{}_K^2]+\frac{1}{8}J_{\eta\eta}^r(t)\overset{\circ}{M}{}_\pi^2[t-2M_K^2+\frac{10}{9}\overset{\circ}{M}{}_K^2]\,. \tag{8.10}$$

This expression is renormalisation-scale independent. In both $\pi\pi$ and πK scatterings, the one-loop expressions obtained with the usual treatment of three-flavour χPT [21] are recovered if we treat chiral series perturbatively and neglect the (potentially large) difference between the truncated $O(p^2)$ expressions and the physical values of the pseudoscalar masses and decay constants.

The second step consists in using eqs. (3.79)-(3.78) to reexpress the $O(p^4)$ LECs L_4, L_5, L_6, L_8 in terms of r, $X(3)$ and $Z(3)$, and higher-order remainders related to π and K masses and decay constants. We denote with the superscript $LO+NLO$ the resulting expressions, which include the LO and NLO expansions of the relevant good observables and resum the vacuum fluctuations encoded in L_4 and L_6.

The last step to obtain the ReχPT expansions of the $\pi\pi$ and πK scattering amplitudes requires adding the resulting expressions a polynomial modeling higher-order contributions:

$$\begin{aligned}F_\pi^4A^{Re\chi PT} &= F_\pi^4A^{LO+NLO}+F_\pi^2(s_A-M_\pi^2)a_1+F_\pi^2(s-s_A)a_2 \\ &\quad +(s-s_A)^2a_3+[(t-t_A)^2+(u-u_A)^2]a_4\,,\end{aligned} \tag{8.11}$$

$$\begin{aligned}F_\pi^2F_K^2B^{Re\chi PT} &= F_\pi^2F_K^2B^{LO+NLO}+F_\pi F_Kt_Bb_1+F_\pi F_K(t-t_B)b_2 \\ &\quad +(t-t_B)^2b_3+[(s-s_B)^2+(u-u_B)^2]b_4\,,\end{aligned} \tag{8.12}$$

$$F_\pi^2F_K^2C^{Re\chi PT} = F_\pi^2F_K^2C^{LO+NLO}+F_\pi F_K(s-u)c_1+(t-t_B)(s-u)c_2\,, \tag{8.13}$$

where (s_A,t_A,u_A), (s_B,t_B,u_B), (s_C,t_C,u_C) denote the points around which we perform the expansion of the NNLO polynomial. The first remainder is multiplied by a constant estimating roughly the value of the amplitude at the expansion point (obtained from the LO chiral expression). The other remainders are multiplied by polynomials in the Mandelstam variables which vanish at the expansion point and respect the crossing properties of the amplitude.

For our purposes, we take:

$$(s_A,t_A,u_A) = (4/3M_\pi^2,4/3M_\pi^2,4/3M_\pi^2)\,, \tag{8.14}$$

$$(s_B, t_B, u_B) = (s_C, t_C, u_C) = (M_K^2 + 1/3M_\pi^2, 4/3M_\pi^2, M_K^2 + 1/3M_\pi^2)\,. \tag{8.15}$$

The remainders a_i, b_i, c_i include only NNLO terms or higher: we expect therefore these contributions to be suppressed by $1/\Lambda_H^4$ where Λ_H is a typical hadronic scale [23]. On the other hand, the numerator may depend on the remainder considered, but the contribution to the polynomial must be order $O(p^6)$ in the usual chiral counting. This means that the remainders have a typical size of order:

$$a_1, a_2, b_1, b_2, c_1 \sim \frac{M_K^4}{\Lambda_H^4}\,, \qquad a_3, a_4, b_3, b_4, c_2 \sim \frac{F_\pi^2 M_K^2}{\Lambda_H^4}\,. \tag{8.16}$$

Remainders associated with higher-order polynomials would be of order F_π^4/Λ_H^4, much suppressed compared to the terms considered here, and thus neglected in the following analysis.

In the case of $\pi\pi$ scattering, we can exploit the behaviour of the amplitude in the $N_f = 2$ chiral limit in order to constrain the size of higher-order remainders further. Indeed, from $N_f = 2$ chiral perturbation theory, we know that:

$$F_\pi^4 A(s,t,u) - F_\pi^2(s - M_\pi^2) = O(\epsilon^4) \quad \text{with} \quad \epsilon^2 \sim p^2 \sim m\,. \tag{8.17}$$

ϵ counts only powers of $m = m_u = m_d$ but not those of m_s. If we compare this relation with $F_\pi^4 A$ expressed in $N_f = 3$ ReχPT in eqs. (8.11) and (8.8), we see that the relation (8.17) implies a constrain on the higher-order remainders: $a_1 - e_\pi - (d_\pi - e_\pi)/3/(s_A/M_\pi^2 - 1)$ and $a_2 - e_\pi$ must be proportional to m. Therefore, we can expect the remainders to exhibit the typical sizes:

$$a_1 - e - \frac{d-e}{3(s_A/M_\pi^2 - 1)}, a_2 - e \sim \frac{M_\pi^2 M_K^2}{\Lambda_H^4}\,, \qquad b_1, b_2, c_1 \sim \frac{M_K^4}{\Lambda_H^4}\,, \qquad a_3, a_4, b_3, b_4, c_2 \sim \frac{F_\pi^2 M_K^2}{\Lambda_H^4}\,. \tag{8.18}$$

According to this discussion, we take the following ranges for the direct remainders:

$$a_1 - e - \frac{F_\pi^2 M_\pi^2}{3(s_A - M_\pi^2)}(d-e), a_2 - e \in \left[-\frac{2M_\pi^2 M_K^2}{\Lambda_H^4}, \frac{2M_\pi^2 M_K^2}{\Lambda_H^4}\right]\,, \tag{8.19}$$

$$b_1, b_2, c_1 \in \left[-\frac{M_K^4}{\Lambda_H^4}, \frac{M_K^4}{\Lambda_H^4}\right]\,, \qquad a_3, a_4, b_3, b_4, c_2 \in \left[-\frac{F_\pi^2 M_K^2}{\Lambda_H^4}, \frac{F_\pi^2 M_K^2}{\Lambda_H^4}\right]\,,$$

with $\Lambda_H = 0.85$ GeV. This choice for the numerical value of Λ_H provides a good agreement of our estimates with those used in the preceeding chapter for energy-independent quantities: higher-order remainders were taken of order $O(m_s^2) = (30\%)^2 = 10\%$ of the leading-order value, unless they were suppressed by one power of m and thus of order $O(mm_s) = 30\% \times 10\% = 3\%$. According to this work, the same remainders must remain respectively of order $M_K^4/\Lambda_H^4 = 12\%$ and $2M_\pi^2 M_K^2/\Lambda_H^4 = 2\%$. In addition, one can check that the definition and size of remainders given in this section can be applied to the two-point correlators related to F_P^2 and $F_P^2 M_P^2$ ($P = \pi, K$) with an expansion around the point of vanishing transfer momentum, leading to remainders identical to those defined in sec. 3.5.1.

8.1.2 Input from Roy and Roy-Steiner equations [M]

The above theoretical expressions for low-energy $\pi\pi$ and πK scattering must be compared to experimental information in order to extract the parameters of three-flavour chiral symmetry breaking. Fortunately, dispersion relations provide an appropriate framework to analyse

experimental data and extract the low-energy behaviour of the amplitude, through Roy and Roy-Steiner equations that have been described in Chs. 6 and 7. We will consider two different cases

For $\pi\pi$ scattering, we will first consider the situation described in ref. [46], where only the E865 results (without corrections) were available: this corresponds to the fit "Extended (I)" in in tab. 6.1 in ch. 6). At a second stage, we will update these results by considering the fit "All" in tab. 6.6 in ch. 6, which include the NA48/2 and E865 results on $K_{\ell 4}$ after correction together with the NA48/2 results from the cusp in $K \to 3\pi$, For πK scattering, we will consider the results of ch. 7 in both cases [3] It is a straightforward, if tedious, exercise, to exploit the dispersive representations of the amplitudes A,B,C found in sec. 3 of ref. [251] and in sec. 2 of ref. [44], and to compute them in subthreshold regions, where none of the dispersion integrals exhibit singularities. We checked in particular that our representation of the low-energy πK amplitude was in good numerical agreement with the subthreshold expansion presented in sec 7.5.2.

We define the subthreshold region of interest for $\pi\pi$ scattering as a triangle in the Mandelstam plane delimited by points with (s,t,u):

$$(2M_\pi^2, M_\pi^2, M_\pi^2)\,, \qquad (M_\pi^2/2, 3/2M_\pi^2, 3/2M_\pi^2)\,, \qquad (M_\pi^2/2, 3M_\pi^2, M_\pi^2/2)\,, \tag{8.20}$$

taking into account the symmetry of the amplitude under $t-u$ exchange. Similarly, we define for πK scattering a triangle in the Mandelstam plane with:

$$(M_K^2, 2M_\pi^2, M_K^2)\,, \qquad (M_K^2, 0, M_K^2 + 2M_\pi^2)\,, \qquad (M_K^2 + M_\pi^2, 0, M_K^2 + M_\pi^2)\,, \tag{8.21}$$

exploiting the symmetry or antisymmetry under $s-u$ exchange. These triangles are defined so that each point inside their area is $2M_\pi^2$ away from an opening channel ($4M_\pi^2$ for s,t,u in the $\pi\pi$ case, $4M_\pi^2$ for t and $(M_\pi + M_K)^2$ for u,s in the πK case). In each triangle, we defined 15 points regularly spaced where we compute the scattering amplitudes. Some aspects of the computation, and of the correlations among the points, are covered in app. A.5.1.

8.2 Matching in a frequentist approach

8.2.1 Likelihood [M]

We must match the chiral expansions of the scattering amplitudes with the experimental values described in the previous section. We perform this matching in a frequentist statistical framework, with a treatment of theoretical uncertainties (or systematics) inspired by the Rfit scheme advocated to constrain the Cabibbo-Kobayashi-Maskawa matrix [14].

We start by collecting in a vector V our $3n$ observables:

$$V^T = [A(s_1,t_1), \dots A(s_n,t_n), B(s'_1,t'_1), \dots B(s'_n,t'_n), C(s''_1,t''_1), \dots C(s''_n,t''_n)]\ . \tag{8.22}$$

Since we use the masses and decay constant identities for pions and kaons to reexpress the $O(p^4)$ LECs in terms of F_P^2 and $F_P^2 M_P^2$ through eqs. (3.77)-(3.80), our set of theoretical parameters

[3] As discussed in ch. 7, the $\pi\pi$ scattering lengths are among the inputs needed to determine the πK scattering lengths from the Roy-Steiner equations. This particular input has actually a very limited impact on the solutions of the Roy equations: using the $\pi\pi$ S-wave scattering lengths from fit "All" leads to values of πK scattering lengths which are very close to those quoted in ch. 7. We will however include the impact of this change in the numerical analysis of sec. 8.3.2.

is:

$$\text{Parameters} : r, X(3), Z(3), L_1^r, L_2^r, L_3\,, \tag{8.23}$$

$$\text{Direct remainders} : a_1, a_2, a_3, a_4, b_1, b_2, b_3, b_4, c_1, c_2\,, \tag{8.24}$$

$$\text{Indirect remainders} : d, d', e, e', d_X, d_Z\,. \tag{8.25}$$

We have separated the direct remainders, attached to the bare expansions of the observables, and the indirect remainders, arising through the reexpression of $O(p^4)$ LECs thanks to mass and decay constant equalities. The latter include also the remainders d_X and d_Z, whose expressions will be given in sec. 8.2.2 and which are required to express the paramagnetic constraints on X and Z, eq. (2.63).

We construct the experimental likelihood $\mathcal{L}_{\rm exp}$, i.e. the probability of observing the data for a given choice of theoretical parameters T_n:

$$\mathcal{L}_{\rm exp}(T_n) = P(\text{data}|T_n) \propto \exp\left(-\frac{1}{2}(V_{th}-V_{exp})^T C^{-1}(V_{th}-V_{exp})\right)/\sqrt{\det C}\,. \tag{8.26}$$

To avoid a proliferation of (purely numerical) normalisation factors of no significance for our discussion, we use the sign $\propto$ meaning "proportional to". C is the covariance matrix between the experimental values V_{exp} computed through eq. (A.67), whereas V_{th} denote the theoretical values computed with the particular choice of T_n. Since we expect strong correlations among the parameters, the covariance matrix must be treated with some care, as described in app. A.5.2.

The theoretical likelihood $\mathcal{L}_{\rm th}(T_n)$ describes our current knowledge on the theory parameters. In agreement with the Rfit prescription [14], we consider that $\mathcal{L}_{\rm th}(T_n) = 1$ if each theoretical parameter lies within its allowed range described in the next section, otherwise the likelihood vanishes.

8.2.2 Constraints on the theoretical parameters [M]

To build the theoretical likelihood, we impose a list of constraints on the theoretical parameters, most of them coming from the analysis presented in sec. 3.6.1. Some constraints are fairly simple:

- We take the following range for the ratio of quark masses r:

$$r_1 \le r \le r_2\,, \qquad r_1 = 2\frac{F_K M_K}{F_\pi M_\pi} - 1\,, \qquad r_2 = 2\left(\frac{F_K M_K}{F_\pi M_\pi}\right)^2 - 1\,. \tag{8.27}$$

- Vacuum stability yields constraints on the $N_f = 3$ chiral order parameters:

$$X(3) \ge 0\,, \qquad Z(3) \ge 0\,. \tag{8.28}$$

- We allow the three $O(p^4)$ LECs $L_1^r(M_\rho), L_2^r(M_\rho), L_3$ in the range $[-F_\pi^2/\Lambda_H^2, F_\pi^2/\Lambda_H^2]$, i.e. lower than $12\cdot 10^{-3}$ in absolute value.

- The direct remainders are constrained to remain in the range given in eq. (8.19).

- The indirect remainders must lie in the ranges discussed in sec. 8.1.1:

$$d', e', d_X, e_X \in \left[-\frac{2M_\pi^2 M_K^2}{\Lambda_H^4}, \frac{2M_\pi^2 M_K^2}{\Lambda_H^4}\right]\,, \qquad d, e \in \left[-\frac{M_K^4}{\Lambda_H^4}, \frac{M_K^4}{\Lambda_H^4}\right]\,, \tag{8.29}$$

  i.e. 3% for the first and 12% for the latter.

A second set of constraints translates into bounds on combinations of remainders:

- Vacuum stability for $N_f = 2$ chiral order parameters yields:

$$X(2) \geq 0 \leftrightarrow d \leq d_{\max} \equiv 1 - \epsilon(r) - Y(3)^2 \times f_1 \,, \tag{8.30}$$

$$Z(2) \geq 0 \leftrightarrow e \leq e_{\max} \equiv 1 - \eta(r) - Y(3) \times g_1 \,, \tag{8.31}$$

  where f_1 and g_1 are small combinations of chiral logarithms introduced in sec. 3.6.1

- The paramagnetic inequalities yields:

$$X(3) \leq X(2) \leftrightarrow d_X \geq d_{X,\min} \equiv 1 - \frac{d_{\max} - d}{X(3)(1-d)} \,, \tag{8.32}$$

$$Z(3) \leq Z(2) \leftrightarrow e_Z \geq e_{Z,\min} \equiv 1 - \frac{e_{\max} - e}{Z(3)(1-e)} \,. \tag{8.33}$$

- The ratio of order parameters $Y(3) = X(3)/Z(3) = 2mB_0/M_\pi^2$ is bound:

$$Y(3) \leq Y^{\max} = 2\frac{1 - \epsilon(r) - d}{1 - \eta(r) - e} \,. \tag{8.34}$$

8.2.3 Computation of the confidence levels [M]

Contrary to ref. [38] which adopted a Bayesian approach to deal with $\pi\pi$ scattering, we follow the (frequentist) approach advocated in ref. [14] for the analysis of the CKM matrix, and used the corresponding Rfit scheme to deal with theoretical uncertainties. From the theoretical and experimental likelihoods we define the function of theoretical parameters:

$$\chi^2(T_n) = -2\log\mathcal{L}(T_n) = -2\log[\mathcal{L}_{\rm th}(T_n)\mathcal{L}_{\rm exp}(T_n)] \,. \tag{8.35}$$

We start by computing the absolute minimum of χ^2, letting all theoretical parameters vary freely: we denote $\chi^2_{\rm min;all}$ this value. Then we focus on one theoretical parameter T_i, set it to a particular value compute the minimum:

$$\chi^2_{\rm min;fixed\ }{}_i(t_i) = \min\{\chi^2(T_n); T_i = t_i\} \,. \tag{8.36}$$

which by definition is larger than the absolute minimum. Then we compute the corresponding p-value corresponding to the hypothesis $T_i = t_i$:

$$\mathcal{P}(t_i) = {\rm Prob}[\chi^2_{\rm min;not\ }{}_i(t_i) - \chi^2_{\rm min;all}, 1] \,, \tag{8.37}$$

where ${\rm Prob}(c^2, N_{\rm dof})$ is the routine from the CERN library providing the probability that a random variable having a χ^2-distribution with $N_{\rm dof}$ degrees of freedom assumes a value which is larger than c^2. Admittedly, we are simplifying the statistical problem at hand, since we assume that the function $\chi^2(t_i)$ has indeed a χ^2-distribution. This should be a correct assumption if the experimental component is free from non Gaussian contributions and inconsistent measurements [14].

This method provides an upper bound on the marginal confidence level (CL) of the hypothesis $T_i = t_i$ for the optimal set of theoretical parameters: the CL value is the probability that a new series of measurements will agree with the most favourable set of theoretical parameters (at $T_i = t_i$) in a worse way than the experimental results actually used in the analysis. The

value of t_i for which $\mathcal{P}(t_i)$ is maximal provides an estimator of T_i: in the ideal case of very accurate data in excellent agreement with theoretical expectations, $\mathcal{P}(t_i)$ should exhibit a sharp peak indicating the "true" value of T_i. These marginal CLs can be used to derive confidence intervals at the desired level [14].

We have implemented this procedure numerically in a Fortran code. Before turning to Goldstone boson scattering, we checked the validity of our code using "fake" observables. We designed observables with very simple chiral representations (linear or quadratic dependence on $r, X(3), Z(3)$) and we simulated a set of data with a certain choice of $r, X(3), Z(3)$, adding some random noise. We plugged these "data" into our program and computed the confidence level for each theoretical parameter $r, X(3), Z(3)$. When the chiral representation of the observables depended on this parameter, we obtained a function $\mathcal{P}(t_i)$ showing a peak in agreement with the value used to simulate the data (i.e., we recovered the information contained in the data). When the chiral series for the observables had no dependence on the parameter, the function $\mathcal{P}(t_i)$ was flat (i.e., we did not extract information absent from the data).

8.3 Results

8.3.1 Confidence levels for leading-order parameters [M]

We start by considering the situation described in ref. [46], where only the E865 results (without corrections) were available for $\pi\pi$ scattering – this corresponds to the fit "Extended (I)" in in tab. 6.1 in ch. 6). For πK scattering, we take the results from Roy-Steiner equations described in ch. 7. Following the procedure described above, we can plot the confidence levels obtained for the order parameters $X(3)$, $Y(3)$ and $Z(3)$, as well as the quark mass ratio r in figs. 8.1 and 8.2. In each case, the dashed line indicates the results obtained from $\pi\pi$ scattering, the dotted line from πK scattering, while the solid line stems from the combination of both pieces of information.

If we consider $\pi\pi$ scattering only, we see that small values of r, below 13, are disfavoured (this is also the case for large values of r above 25, but not at a significant level): $r \geq 12.7$ at 68 % CL. The CL for $X(3)$ is rather flat up to 0.85, where it suddenly drops, as well as that for $Z(3)$ up to 0.95. $Y(3)$, which is related to B_0 and measures the fraction of the LO contribution to M_π^2, is essentially not constrained, even though values close to 2 are slightly disfavoured. If we consider πK scattering only, r and $Y(3)$ are essentially not constrained. Flat CLs are observed for $X(3)$ and $Z(3)$, with a steep decrease respectively for 0.85 and 1. Finally, if we combine both pieces of information, intermediate values of r are clearly favoured (between 20 and 25), in agreement with the information contained in $\pi\pi$ and πK scattering data. Low values of $X(3)$ and $Y(3)$ are slightly preferred, whereas the CL for $Z(3)$ peaks around 0.6. We see that the combination of the two data sets provides more stringent constraints on the various theoretical parameters of interest, even though these results have still a limited statistical significance.

We recall that the frequentist method given here provides an upper bound on the confidence level (CL) for the optimal set of theoretical parameters assuming $T_i = t_i$ [14]. In the ideal case, we would expect the CL to peak in a very limited interval of t_i, providing the "true" value of the corresponding theoretical parameter. In practice, we see that the chosen set of data is not accurate enough to provide very stringent constraints on the theoretical parameters. In such a case, the CL profiles can be exploited to extract a confidence interval, say at 68 % CL, i.e. a range of values so that the probability that the range contains the true value of the parameter is 68 %. This can be obtained by determining the region of parameter space where the CL

Ref.	Inputs	$10^3 \cdot L_1^r(M_\rho)$	$10^3 \cdot L_2^r(M_\rho)$	$10^3 \cdot L_3^r(M_\rho)$
Sec. 8.3.1	$\pi\pi$	[-12;5.1]	[-12;3.0]	n.d.
	πK	[-8.3;4.5]	[-12;6.0]	n.d.
	Both	[-6.6;2.5]	[-12;2.5]	[-9.0;2.0]
Sec. 8.3.2	$\pi\pi$	[-12;5.1]	[-12;3.0]	n.d.
	πK	[-7.5;4.3]	[-12;6.4]	n.d.
	Both	[-5.3;3.0]	[-12;2.5]	[-9.5;0]
Ref. [44]	Roy-Steiner	1.05 ± 0.12	1.32 ± 0.03	-4.53 ± 0.14
Ref. [183]	Fit All $O(p^4)$	1.12	1.23	-3.98
Ref. [183]	Fit All $O(p^6)$	0.88 ± 0.12	0.61 ± 0.20	-3.04 ± 0.43

Table 8.1: *Derivative chiral couplings $L^r_{1,2,3}$ obtained in our approach, using for πK scattering the outcome of the Roy-Steiner equations and for $\pi\pi$ scattering either E865 data only ("Extended fit (I)" in tab. 6.1) or corrected E865 and NA48/2 data ("All" in tab. 6.6). The confidence intervals correspond to a 68 % CL. "n.d." means that the corresponding CL is flat over the whole range imposed by the theoretical likelihood, and thus the coupling is not determined. Results obtained assuming small vacuum fluctuations of $s\bar{s}$ pairs are also shown: ref. [44] recalls the results described in ch. 7, whereas ref. [183] performed fits to the observables using chiral expansions at NLO as well as NNLO.*

curve lies above 0.32.

From the CL profiles obtained from the combined analysis of $\pi\pi$ and πK scattering, we obtain the following confidence intervals at 68 % CL:

$$r \geq 12.7\,, \qquad X(3) \leq 0.92\,, \qquad Y(3) \leq 1.65, \qquad Z(3) \leq 0.98\,. \qquad [68\%\ \text{CL}] \qquad (8.38)$$

The values for L_1, L_2, L_3 can also be determined in each case, and the corresponding confidence intervals are collected in tab. 8.1.

As a cross-check, we have also studied the case where the higher-order direct remainders are removed, i.e. eqs. (8.11)-(8.13) is set to zero. The corresponding CLs are sharper, but very similar in shape to those presented here. Therefore, the polynomial terms modeling higher order contributions tend to push CLs towards 1, but the qualitative features shown in figs. 8.1 and 8.2 stem mainly from the matching of LO and NLO terms of the ReχPT expansion to experimental information.

8.3.2 Update using NA48/2 data

We can now proceed to the update of ref. [46], including the corrected E865 and NA48/2 results for $\pi\pi$ scattering – this corresponds to the fit "All" in in tab. 6.6 in ch. 6). For πK scattering, we take again the results from Roy-Steiner equations described in ch. 7. The results are plotted in figs. 8.1 and 8.2 as well as in tab. 7.3. We can see the changes induced by the reduced uncertainty on the two $\pi\pi$ S-wave scattering lengths. In particular the favoured values of r are slightly pushed towards higher values, and the preferred values of $X(3)$ and $Z(3)$ sightly pushed towards lower values. The upper bound on $X(3)$ and $Z(3)$ shifts a bit because of the change in the two-flavour chiral order parameters involved in paramagnetic inequalities.

We see that in both cases, the scenario mildly favoured from the matching of both $\pi\pi$ and πK scatterings would correspond to a value of $r = m_s/m$ quite close to the canonical value $r = 25$. However, we emphasise that this agreement is rather coincidental: the latter value

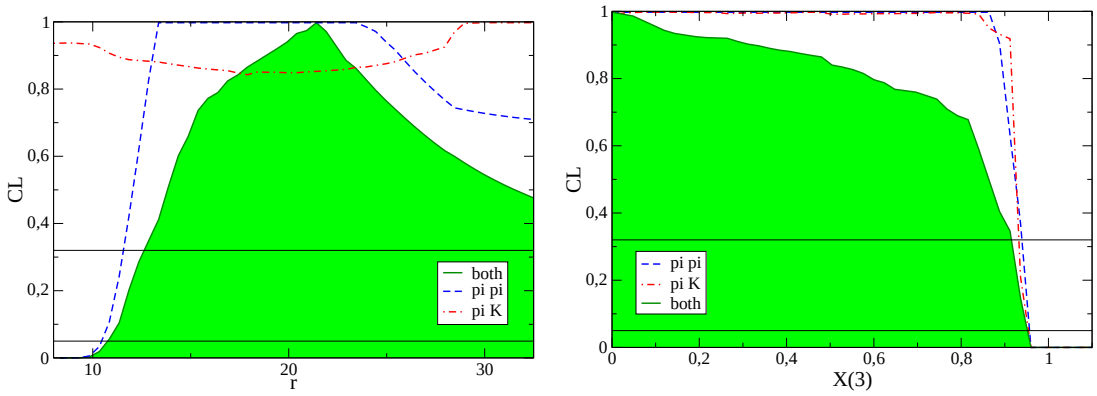

Figure 8.1: *CL profiles for $r = m_s/m$ (left) and $X(3) = 2m\Sigma(3)/(F_\pi^2 M_\pi^2)$ (right), using E865 data for $\pi\pi$ scattering and Roy-Steiner equations for πK scattering ("Extended fit (I)" in tab. 6.1). The (blue) dashed line corresponds to experimental information on $\pi\pi$ scattering, the (red) dashed-dotted line to πK scattering, and the (green) solid line to the combination of both sets. The two horizontal lines indicate the confidence intervals at 68 and 95% CL.*

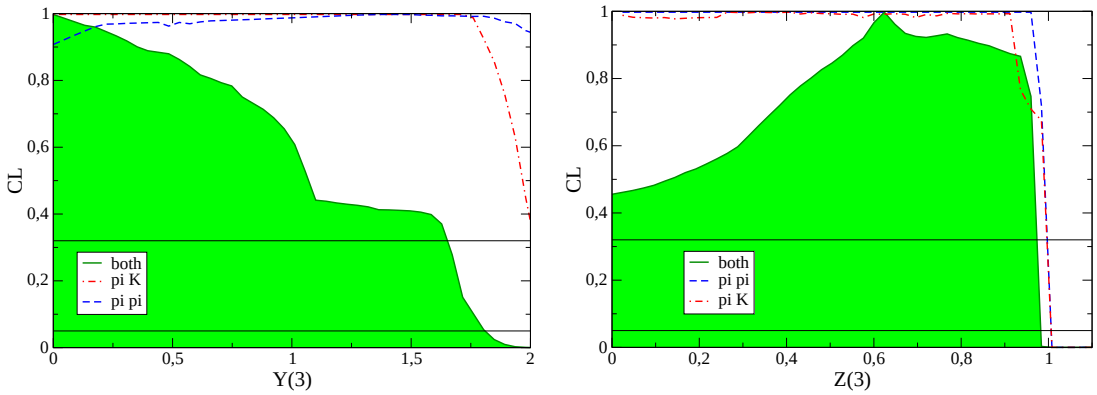

Figure 8.2: *CL profiles for $Y(3) = 2mB_0/M_\pi^2$ (left) and $Z(3) = F_0^2/F_\pi^2$ (right), using E865 data for $\pi\pi$ scattering and Roy-Steiner equations for πK scattering ("Extended fit (I)" in tab. 6.1). The (blue) dashed line corresponds to experimental information on $\pi\pi$ scattering, the (red) dashed-dotted line to πK scattering, and the solid line to the combination of both sets. The two horizontal lines indicate the confidence intervals at 68 and 95% CL.*

comes from the (perturbative) reexpression of M_K^2/M_π^2 in terms of r, assuming that the chiral expansions of the two squared masses converge quickly. This assumption is not supported by our results for the quark condensate (or X), which exhibits some suppression when one moves from the $N_f = 2$ chiral limit to the $N_f = 3$ one, i.e., when m_s decreases from its physical value down to zero. On the other hand, the pion decay constant (or Z) seems quite stable from $N_f = 2$ to $N_f = 3$, see eqs. (8.41).

From the CL profiles obtained from the combined analysis of $\pi\pi$ and πK scattering, we obtain the following confidence intervals at 68 % CL:

$$r \geq 17.9\,, \qquad X(3) \leq 0.94\,, \qquad Y(3) \leq 1.75\,, \qquad Z(3) \leq 0.97\,. \qquad [68\%\ \text{CL}] \qquad (8.39)$$

The values for L_1, L_2, L_3 can also be determined in each case, and the corresponding confidence intervals are collected in tab. 8.1. Actually, the indetermination of L_1, L_2, L_3 is an important

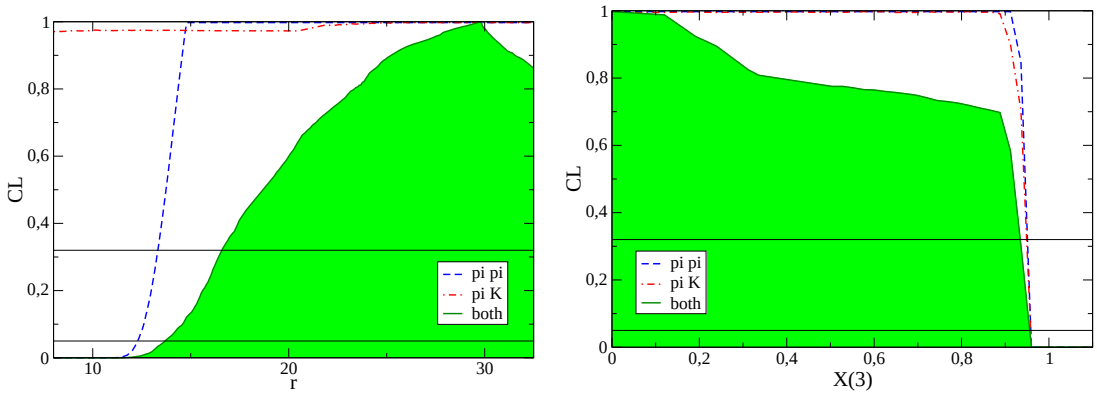

Figure 8.3: *CL profiles for $r = m_s/m$ (left) and $X(3) = 2m\Sigma(3)/(F_\pi^2 M_\pi^2)$ (right), using E865 and NA48 data for $\pi\pi$ scattering and Roy-Steiner equations for πK scattering ("All" in tab. 6.6). The dashed line corresponds to experimental information on $\pi\pi$ scattering, the dahshed-dotted line to πK scattering, and the solid line to the combination of both sets. The two horizontal lines indicate the confidence intervals at 68 and 95% CL.*

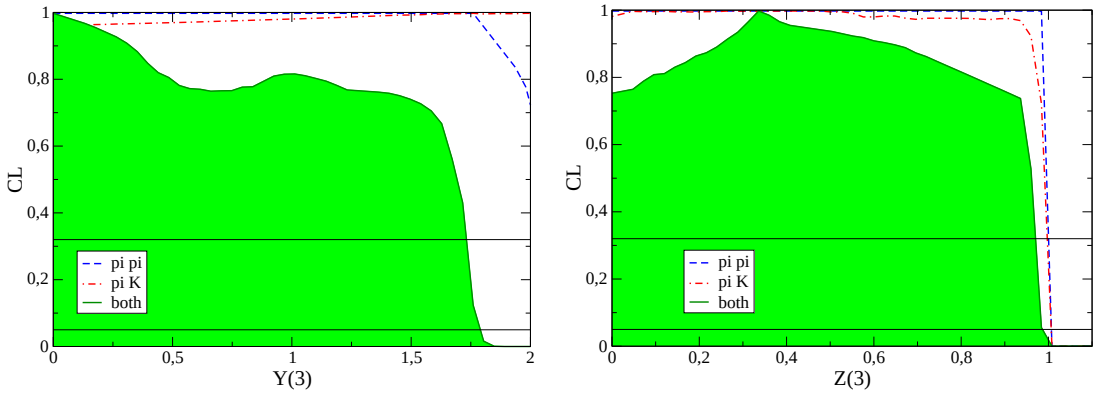

Figure 8.4: *CL profiles for $Y(3) = 2mB_0/M_\pi^2$ (left) and $Z(3) = F_0^2/F_\pi^2$ (right), using E865 and NA48 data for $\pi\pi$ scattering and Roy-Steiner equations for πK scattering ("All" in tab. 6.6). The dashed line corresponds to experimental information on $\pi\pi$ scattering, the dahshed-dotted line to πK scattering, and the solid line to the combination of both sets. The two horizontal lines indicate the confidence intervals at 68 and 95% CL.*

limiting factor: imposing a smaller range of variation on these three LECs would improve the CL profiles for the parameters r, $X(3)$, $Y(3)$ and $Z(3)$. For instance, we illustrate what would be the results imposing the following ranges of L_1, L_2, L_3:

$$L_1^r(M_\rho) = (1.0 \pm 0.1)\cdot 10^{-3}\,, \qquad L_2^r(M_\rho) = (1.0 \pm 0.1)\cdot 10^{-3}\,, \qquad L_3^r(M_\rho) = (-5.0 \pm 0.1)\cdot 10^{-3}\,. \tag{8.40}$$

We see in figs. 8.5 and 8.6 that adding an input fixing the values of these three LECs with a good accuracy would impact quite significantly the CL profiles for all the parameters, even if the 68% and 95% confidence intervals would not be affected directly. This improvement could be obtained by an analysis of the $K_{\ell 4}$ form factors in our framework, whose energy dependence is directly related to the three LECs L_1, L_2, L_3 [43, 189], and which are used for this purpose in NNLO fits of chiral series [183].

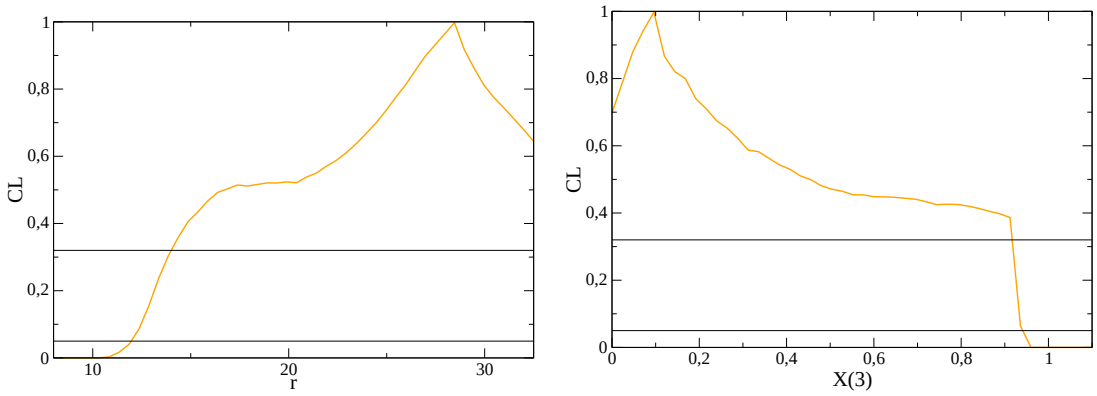

Figure 8.5: *CL profiles for $r = m_s/m$ (left) and $X(3) = 2m\Sigma(3)/(F_\pi^2 M_\pi^2)$ (right), using E865 and NA48 data for $\pi\pi$ scattering and Roy-Steiner equations for πK scattering ("All" in tab. 6.6), assuming a narrow range eq. (8.40) for $L_{1,2,3}$ to illustrate potential improvements of the procedure.*

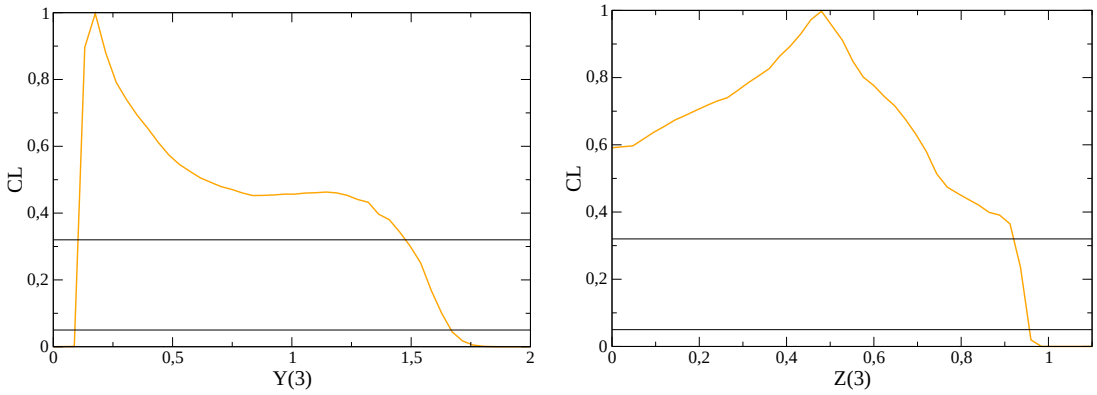

Figure 8.6: *CL profiles for $Y(3) = 2mB_0/M_\pi^2$ (left) and $Z(3) = F_0^2/F_\pi^2$ (right), using E865 and NA48 data for $\pi\pi$ scattering and Roy-Steiner equations for πK scattering ("All" in tab. 6.6), assuming a narrow range eq. (8.40) for $L_{1,2,3}$ to illustrate potential improvements of the procedure.*

8.3.3 Comparison with other works [M]

$\pi\pi$ scattering

This work differs on three points from ref. [38]: we include πK scattering in our analysis, we choose as observables the scattering amplitudes in subthreshold regions rather than the subtraction constants involved in their dispersive representations, we perform the statistical analysis in a frequentist framework rather than a Bayesian one.

We observe the same qualitative features in both analyses. As expected, low values of r are strongly disfavoured. Indeed, the analysis of currently available data on $\pi\pi$ scattering in sec. 6.3.6 provides a value of $X(2)$ and $Z(2)$:

$$X(2) = 0.86 \pm 0.04\,, \qquad Z(2) = 0.89 \pm 0.02\,. \tag{8.41}$$

As illustrated in fig. 3.8, $X(2)$ is related to r through the pion and kaon mass and decay constant identities, eqs. (3.66)-(3.69): the value of $X(2)$ favours the same range for the quark mass ratio as the upper plot in fig. 8.1. On the other hand, we find that $X(3)$ and $Z(3)$ are

only constrained through an upper bound, in agreement with the paramagnetic inequalities.

This agreement was not built in our procedure, since the method of analysis of the present work does not require computing $N_f = 2$ chiral order parameters or related subtraction constants like refs. [38, 42]. Moreover, one can see an improvement compared to the latter references, thanks to the frequentist approach chosen here. In ref. [38], it was difficult to disentangle the effect of the data from that of the Bayesian priors inside a posterior p.d.f. : the so-called "reference profiles" (p.d.f.s from priors but no data) had to be compared to the posterior p.d.f.s (p.d.f.s from priors and data) to judge the impact of $\pi\pi$ data. In the present paper, this intricate procedure and the arbitrariness induced by Bayesian priors are avoided : it is clearly seen that $\pi\pi$ data constrains $X(3)$ and $Z(3)$ essentially through the values of $X(2)$ and $Z(2)$ and the corresponding paramagnetic upper bounds.

πK scattering

For πK scattering, we can compare our results with ref. [44], where the solutions of the Roy-Steiner dispersion relations were used to reconstruct the amplitudes in the subthreshold region. These amplitudes were expanded around the point $s = u$, $t = 0$, and the coefficients of the polynomials, C_{ij}^+ and C_{ij}^-, were matched with their NLO chiral expansions in order to determine some $O(p^4)$ LECs. This led to a determination of L_1, L_2, L_3 recalled in the previous section, and to a value of L_4 suggesting a significant suppression of $Z(3)$. The value of L_6, though affected by large uncertainties, indicated also a suppression of $X(3)$, stronger than that of $Z(3)$:

$$\text{[Buettiker et al.]}: \qquad L_4^r(M_\rho) = (0.53 \pm 0.39) \cdot 10^{-3}\,, \qquad [2L_6^r + L_8^r](M_\rho) = (3.66 \pm 1.52) \cdot 10^{-3}\,. \tag{8.42}$$

Using eq. (3.94) and the other results of Ch. 3, and taking $L_8^r(M_\rho) = (0.9 \pm 0.3) \cdot 10^{-3}$ [21] we can convert these results into the parameters of interest: following these results, $X(3)$ would stand between 0.15 and 0.41, $Z(3)$ between 0.14 and 0.92, and $Y(3)$ between 0.44 and 1.05. Obviously, the low values of $X(3)$ and $Z(3)$ indicate that the values obtained in ref. [44], relying on the assumption of small vacuum fluctuations and on $X(3)$ and $Z(3)$ close to 1, should be reassessed relaxing this hypothesis.

If our results for the combined $\pi\pi$ and πK data point towards a similar pattern, our analysis of πK data alone provides weaker constraints than that of ref. [44]. At least two different reasons lead us to weaker constraints. First, we have explicitly take into account the presence of NNLO contributions which were neglected in the $O(p^4)$ analysis of ref. [44] and which may affect significantly the energy-dependent part of the amplitudes. Secondly, the analysis in ref. [44] assumes explicitly the smallness of vacuum fluctuations: once we drop this assumption, a smaller value of L_4 (and thus a value of $Z(3)$ close to 1) can be compensated by the variation of other parameters, such as the quark mass ratio r. These two phenomena may explain the weaker constraints observed in our analysis.

Combined analyses

For the combined analysis of $\pi\pi$ and πK scatterings, we can compare our results with refs. [183, 187, 188], recalled in sec. 3.3.3. The authors took a different approach from ours, computing NNLO chiral expansions to $\pi\pi$ and πK scattering amplitudes, and matching with results on $\pi\pi$ scattering (scattering lengths) and πK scattering (scattering lengths and subthreshold expansion coefficients), supplemented with information on $K_{\ell 4}$ form factors. In agreement with

the one-loop framework of ref. [21], these two-loop computations assume a numerical dominance of LO contributions and a quick convergence of $N_f = 3$ chiral expansions.

In previous studies in this NNLO framework, the authors performed fits to pseudoscalar masses and decay constants [189], $K_{\ell 3}$ decays [190], and scalar form factors [191]. In each case, the values of the Zweig-rule suppressed $O(p^4)$ LECs L_4 and L_6 had to be fixed by hand: fits of similarity quality could be obtained with values of these two constants corresponding either to small or large vacuum fluctuations of $s\bar{s}$ pairs. For scalar form factors, values of L_4 and L_6 larger than conventionally assumed led to an improvement in the convergence of observables (fits A,B,C compared to fit 10, in Table 2 of ref. [191]).

In the case of refs. [187,188], the authors analysed $\pi\pi$ and πK scattering amplitudes in the same NNLO framework. The fits were not able to reproduce some observables, in particular among πK subthreshold coefficients. A particular subset of subthreshold coefficients and scattering lengths led to $L_4^r(M_\rho) \simeq 0.2 \cdot 10^{-3}$ and $L_6(M_\rho)$ negative. These results were confirmed in ref. [183], where the authors doubled the errors associated to the scattering lengths in order to ease some of the discrepancies arising in ref. [187,188]. The results, recalled in tab.3.1, led to values of L_4 and L_6 that are positive. Consistently, these results yield a significant decrease of $F_0 = 65$ MeV compared to $F_\pi = 92.2$ MeV, and a peculiar pattern of convergence for masses and decay constants (for Fit All $O(p^6)$) recalled in tab. 3.2. NLO and NNLO contributions are of similar size and cancel each other for some of the contributions, as expected if we have instabilities in chiral series as discussed more extensively in sec. 3.4.3. Even though it is not possible to compare directly our results to those in ref. [183], since the frameworks adopted are quite different, but they point both towards a suppression of the leading-order chiral parameters in the three-flavour chiral limit, and a numerical competition between LO and NLO contributions.

8.4 Summary

We wanted to combine the information gathered on $\pi\pi$ and πK scatterings in order to put constraints on the three leading-order parameters eq. (8.1). In order to perform this combination, we have chosen a frequentist framework allowing a specific treatment of the nuisance parameters for which only theoretical estimates are available (e.g., the higher-order remainders). The χ^2 is built by comparing the meson-meson amplitudes with their chiral expansion in Resummed χPT for a set of points located in the subthreshold region, including polynomials in the Mandelstam parameters corresponding to higher-order contributions explicitly.

The output of this analysis are marginal CL curves, providing an upper bound on the p-value for the optimal set of theoretical parameters at fixed $T_i = t_i$: the p value is the probability that a new series of measurements will agree with the most favourable set of theoretical parameters (at $T_i = t_i$) in a worse way than the experimental results actually used in the analysis [14]. This allows ultimately to determine confidence intervals for the various parameters considered.

Unfortunately, the marginal CL profiles do not provide sharp peaks and thus stringent constraints on theoretical parameters at a statistically significant level. However, our results point towards some favoured regions of parameter space, see figs. 8.1 and 8.2. If only $\pi\pi$ scattering is included, the results obtained in earlier works [38] are recovered: small values of r are disfavoured, whereas $X(3)$ and $Z(3)$ are only constrained to remain below their $N_f = 2$ counterpart due to paramagnetic inequalities eq. (2.63). πK scattering alone does not constrain strongly the various theoretical parameters, apart from setting bounds on $X(3)$ and $Z(3)$. The combination of the two pieces of information proves more interesting, with a sharpening of the CL profile for r, and a slight preference for low values of $Y(3)$. From the CL curves ob-

tained from the combined analysis of $\pi\pi$ and πK scattering, we obtain the following confidence intervals at 68 % CL:

$$r \geq 17.9\,, \qquad X(3) \leq 0.84\,, \qquad Y(3) \leq 1.75\,, \qquad Z(3) \leq 0.97\,. \qquad [68\%\ \text{CL}] \qquad (8.43)$$

corresponding to the regions of parameter space where the marginal CL profiles lie above 0.32 [14]. A major limitation at this stage comes from the LECs $L_{1,2,3}$ which are constrained only very weakly: the CL profiles would be significantly improved by the consideration of other energy-dependent quantities, in particular $K_{\ell 4}$ form factors.

Such a situation is reminiscent of the scenario proposed in sec. 2.5.3. The quark condensate $\Sigma(N_f)$ and the decay constant $F(N_f)$ depend on the way small eigenvalues of the Dirac operator accumulate around zero in the thermodynamic limit. It was conjectured that the two order parameters could decrease at a different rate when the number of massless flavours N_f increases: the quark condensate would vanish first, followed later by the vanishing of the decay constant related to the restoration of chiral symmetry. The trend of our results for $N_f = 3$ order parameters, compared to $N_f = 2$ results, could fit such a scenario.

At this point, we should stress again that our framework allows for any size of fluctuations, i.e. for both small and large leading-order chiral order parameters. We see that the pattern of the marginal CL profiles is consistent with the scenario of significant vacuum fluctuations of $s\bar{s}$ pairs, with the corresponding implications for the convergence of chiral series, in agreement with the points raised by the previous chapter. Unfortunately, the uncertainties concerning πK scatterings are still large enough to prevent from an accurate determination of $X(3)$ and $Z(3)$ at this stage. More observables ($K_{\ell 4}$ form factors on the theoretical side, πK scattering on the experimental side) are needed to sharpen the determination of the pattern of three-flavour chiral symmetry breaking.

- You're thinking about something, my dear, and that makes you forget to talk. I can't tell you just now what the moral of that is, but I shall remember it in a bit.
- Perhaps it hasn't one.
- Tut, tut, child! Everything's got a moral, if only you can find it.

The Duchess and Alice

9 Outlook

9.1 End of Part One

This *Habilitation à Diriger les Recherches* has been focused on QCD at low energies (below 1 GeV), where the theory becomes strongly coupled and our ability to predict its behaviour very limited, even though its equations in terms of quantum field theory are perfectly known. One of the main phenomena taking place at these energies is the breakdown of chiral symmetry, explaining the existence of an octet of light pseudoscalar mesons π, K, η. The dynamics of these states is related to the actual pattern of chiral symmetry breaking, and offers us the possibility to understand it in deeper details. The particular mass hierarchy of the light quark masses allows one to consider (and compare) two different chiral limits of interest, with $m_u = m_d = 0$ and m_s kept at its physical value ($N_f = 2$ massless flavours) or $m_u = m_d = m_s = 0$ ($N_f = 3$ massless flavours). Are these patterns equivalent, or do they differ significantly ? And what are the implications for the low-energy effective theory of QCD ? A significant part of my research activities over the last decade has been devoted to this issue, and the purpose of this *habilitation* was to provide an overview of the picture arising from my work on the subject.

A first step (ch. 2) consisted in discussing the chiral order parameters (and in particular the quark condensate and the pseudoscalar decay constant) in terms of the Euclidean Dirac operator, highlighting the role of the fermion determinant. The potential dependence of the order parameters on vacuum light-quark loops and on the number of massless fermions of the theory was emphasised. In particular, a bound on the eigenvalues of the Dirac operator, derived by Vafa and Witten, indicates that the order parameters should decrease when one goes from $N_f = 2$ to $N_f = 3$ chiral limits (one may speculate what would occur if the number of light (or massless) quarks increased, and how chiral symmetry would eventually be restored). One may then (ch. 3) explore the consequences of this suppression for the effective theory of QCD at low energies, i.e., Chiral Perturbation Theory. A significant suppression of the three-flavour quark condensate and/or decay constant raises the issue of the convergence of the chiral expansions. One must in particular determine the conditions under which the chiral expansions of pseudoscalar masses and decay constants are saturated by their leading-order. The next-to-leading order low-energy constants L_4 and L_6, suppressed by the Zweig rule but enhanced by the large value of the strange quark, are shown to play an essential role in the discussion. If they deviate from very specific values, this might lead to a significant competition between formal leading- and next-to-leading orders in the three-flavour chiral expansions. I discussed also the two-flavour limit chiral expansions, and showed that the matching with three-flavour chiral series provides interesting correlations between $N_f = 2$ order parameters and the quark mass ratio $r = 2m_s/(m_u + m_d)$.

In ch. 4, I estimated the two-point correlator $\langle(\bar{u}u)(\bar{s}s)\rangle$ related to the dependence of the $N_f = 2$ chiral condensate on the strange-quark mass. This estimation is performed through rapidly convergent sum rules, which are saturated by pion and kaon scalar form factors (reconstructed from coupled-channel dispersive equations involving models for the scattering between $\pi\pi$ and $K\bar{K}$ states). The sum rule yields finally constraints between the values of three-flavour order parameters and the quark mass ratio r, indicating a significant suppression of the quark condensate (and the pseudoscalar decay constant) from the two- to the three-flavour chiral limits: for instance, for $r \simeq 25$, one would expect $X(2) - X(3) \geq 0.3$ (see figs. 4.8-4.11). A second hint of such a decrease was given in Ch. 5, by considering lattice determinations of the masses, decay constants, and form factors by the RBC/UKQCD and PACS-CS collaborations. It gave me the opportunity to discuss in more detail how to treat chiral series when the pattern of chiral symmetry breaking yields a numerical competition between leading- and next-to-leading-order chiral perturbation theory. I proposed a framework to deal with chiral series in such a

situation of instabilities (Resummed χPT), and applied it to the case of several form factors of phenomenological interest (electromagnetic pion and kaon ones, $K_{\ell 3}$ vector and scalar form factors). This led to a determination of three-flavour chiral order parameters suggesting once again a significant decrease from $N_f = 2$ to $N_f = 3$ (see tabs. 5.2 and 5.3).

Ch. 6 and ch. 7 were focused on the experimental and dispersive constraints on $\pi\pi$ and πK scatterings. In both cases, one can write and solve dispersive equations (Roy and Roy-Steiner equations) making use of unitarity, analyticity and crossing symmetry to constrain the low-energy parts of these amplitudes in terms of high-energy data. In both cases, two S-wave scattering lengths are chosen as subtraction constants, and their knowledge is enough to fix the whole low-energy amplitudes up to a very good accuracy. In the $\pi\pi$ case, the existence of accurate $K_{\ell 4}$ data from two different collaborations (E865 and NA48/2) offers the possibility to determine the two scattering lengths (a_0^0, a_0^2) very precisely. One has in particular to take into account isospin-breaking effects inducing mass differences between neutral and charged mesons. I have presented a dispersive approach to deal with this problem, more suited than χPT alone for arbitrary values of (a_0^0, a_0^2), and used it to determine the S-wave scattering lengths (see tab. 6.6). The πK case is less satisfying than the $\pi\pi$ case due to the more complicated analytic structure and the lack of accurate data at low energies, leading to a fair determination of the S-wave scattering lengths $a_0^{1/2}, a_0^{3/2}$ (see eq. (7.47)). I also recall how the existence and the parameters of the scalar $K_0^*(800)$ resonance can be inferred from the same dispersion relations as the Roy-Steiner equations in the complex plane.

These two chapters suggest that two-flavour order parameters saturate the $N_f = 2$ chiral series, but that L_4 and L_6 induce a significant suppression once the strange quark mass is sent to zero. These elements are combined in ch. 8: the $\pi\pi$ and πK amplitudes are reconstructed in the subthreshold region (below the opening of physical channels) and matched to a representation allowing for a competition between leading and next-to-leading orders. The extraction of the values of the various low-energy constants is obtained within a frequentist approach, allowing to define confidence intervals for the three-flavour chiral order parameters as well as the quark mass ratio r. A lower bound is obtained on the latter, in agreement with the correlation observed between $X(2)$ and r. On the other hand, the data on πK scattering alone is not precise enough to determine whether $X(3)$ and $Z(3)$ are significantly smaller than their $N_f = 2$ counterparts (see eq. (8.43)), but the inclusion of $K_{\ell 4}$ form factors in this framework could improve the accuracy of this determination.

9.2 What's next ?

From the previous overview, we have witnessed recent progress in our understanding of the pattern of two-flavour chiral symmetry breaking, indicating that two-flavour chiral series are almost saturated by their leading order. It is the encouraging sign that progress is possible (if slow) in the field if significant efforts are made on both experimental and theoretical sides. On the other hand, we see that there remains a significant uncertainty on the situation concerning three-flavour χPT, as could be expected from an effect related to the elusive scalar sector of QCD. Several aspects of this question are still under scrutiny and should be studied in deeper detail.

A first way of accessing consists in studying other processes involving K and η mesons. One can in particular investigate $K \to 3\pi$ [412–416] and $\eta \to 3\pi$ decays [339,345,346,417,418], for which accurate measurements are available [419–422]. These processes can be dealt with similarly to $\pi\pi$ and πK scatterings within the framework of Resummed χPT. In the same way,

the scalar form factors of the pion and the kaon, already described in ch. 4, are in principle an interesting source of information. Even though they cannot be measured experimentally, their low-energy behaviour can be constructed starting from two-channel models for scattering, and their slope can give access to interesting information on the dynamics of the scalar sector [191, 218, 219]. NNLO computations of many observables are available [185–192], and can be matched onto the one-loop expressions used in ReχPT. It would in particular be interesting to identify the contributions of L_4 and L_6 in these NNLO expressions to compare them with the corresponding contributions resummed in ReχPT. Through this matching, the structure of the higher-order remainders could also be investigated. One should also consider how the suppression of three-flavour chiral order parameters would impact the interaction of soft Goldstone bosons with other systems. First candidates for this study would be the light baryons, for which high-quality data are available or expected from experiment as well as from lattice simulations [22, 161, 423–430].

As far as lattice simulations are concerned, many quantities probing chiral symmetry breaking, such as the scalar form factors of Goldstone bosons and the topological susceptibility, can be investigated simultaneously on the lattice and in Resummed χPT. Even though they are technically much more demanding to evaluate, quantities related to Zweig-suppressed correlators should be accessible with a good accuracy in a near future (all-to-all propagators) [264]. It will be exciting to compare these results, probing directly the strange sea-quark effects on chiral dynamics, with the expectations of Chiral Perturbation Theory, whether in its usual form or its resummed version. A related issue concerns the systematic uncertainties attached to lattice results from the light mass extrapolation and the determination of the lattice spacing. Both rely often on three-flavour χPT in order to connect the observables measured at unphysical values of m_u and m_d to the physical case. One could have to reassess the size of the uncertainties if the extrapolation formulae must be modified to account for suppressed leading-order chiral parameters [194]. Conversely, it would be interesting to investigate the effect of lattice artefacts in Resummed Chiral Perturbation Theory, starting from the Wilson action for fermions that includes an $O(a)$ term breaking explicitly chiral symmetry. Beyond that, one may expect significant progress in the coming years concerning lattice simulations. They may make obsolete the discussions of chiral extrapolations, as they should eventually be able to perform simulations at physical quark masses with large volumes and fine lattices. This should however not stop investigations on the pattern of chiral symmetry breaking, since simulations reaching such a mature stage should then be able to determine not only physical quantities but also chiral order parameters. It will be quite fascinating to discover which pattern comes out of the simulations in a near-physical regime, playing with the variations in the quark masses as well as studying the spectrum of Dirac eigenvalues.

A proper assessment of radiative corrections is central to the analysis of many rare physical processes, as they constitute an important source of systematic uncertainties. This is particularly relevant for the determination of the CKM matrix elements $|V_{us}|$ through $K_{\ell 2}$ and $K_{\ell 3}$ decays (where a high accuracy is achievable) [431, 432], $|V_{ub}|$ via $B \to \tau\nu_\tau$ (currently in disagreement with other determinations based on semileptonic $b \to u$ transitions) [433, 434]. This area stands at the frontier between experiment and theory, since parts of the electromagnetic effects are studied via Monte Carlo simulations, whereas other effects, such as those induced by the differences between neutral and charged masses require theoretical analyses. In the specific case of $K_{\ell 4}$ decays, one should check that all sources of isospin breaking are properly taken into account through the separation between the correction for virtual and real and photons applied experimentally (Coulomb factor and Monte-Carlo generation) [332] and the mass effects treated theoretically (through a chiral Lagrangian including operators inducing

the difference between neutral and charged mesons) [289]. A longer-term effort would consist in performing the separation between universal and process-dependent radiative corrections in a field-theoretical language [435], without relying on specific parametrisation/models of the relevant form factors and amplitudes.

As always in physics, the last word should come from experiment, and one should hope news very soon. The analysis of $K^+ \to \pi^0\pi^0 e^+\nu_e$ is under way [436] and should provide more information on isospin breaking among form factors. These $K_{\ell 4}$ data should also be compared with our NNLO dispersive representation of the form factors, providing an interesting handle on the counterterms $L_{1,2,3}$ (one of the main sources of uncertainties in our estimate of isospin-breaking corrections, as well as our determination of LO chiral parameters). One should also note that the curvature of the scalar form factor is not well reproduced by NNLO χPT and could prove another interesting observable [183]. The upcoming NA62 experiment should also bring improvements on the measurement of rare K decayst [436]. Moreover, our knowledge on πK scattering could be improved through the analysis of the decay $D \to K\pi\ell\nu$, accessible to charm factories like BES [399] – the accuracy of this analysis could benefit from a more accurate description of the form factors thanks to a dispersive reconstruction similar to that performed for $K_{\ell 4}$ decays.

In any case, the short history told in these pages clearly stresses the importance of bringing theory and experiment together, if one is to unveal the features of the strong interaction in its non-perturbative regime. Indeed, low-energy QCD is full of experimental surprises, bad and good, and proves often more complicated (and more difficult) than the theorists would consider (like ?) it to be. This comes as a warning not only for our investigations on the patterns chiral symmetry breaking, but more generally for flavour physics. Indeed the field is becoming a tool of choice to constrain physics beyond the Standard Model through tiny deviations, but this ambitious goal requires a particularly good understanding of low-energy QCD and its interplay with electroweak interactions, both conceptually and numerically. Such an exciting prospect highlights all the more the importance of phenomenology, and of phenomenologists, to ensure that particle physics theory and experiment can progress together.

10 Thanks

I am deeply honoured that Michel for having accepted to be the president of this jury. It has always been an enlightening pleasure to discuss physics with him, as a teacher or as a colleague, on theoretical as well as on experimental matters.

I would like to thank Marc, Ulf and Toni very sincerely for having accepted the burden of refereeing this Habilitation, in spite of their very busy schedules and their many commitments. I am sorry that my viva prevented them from accepting other invitations attending more exciting conferences and workshops, and I apologize for this annoyance.

I am very glad that Chris could be a member of this jury, because of his deep knowledge of (continuum and lattice) flavour physics, but also because of the highly enjoyable time I spent in Southampton during my post-doctoral stay, from the research and personal points of view.

It is also a pleasure for me that Brigitte Bloch-Devaux was able to take part in this committee, considering our very enjoyable interactions on the NA48/2 results. We promised a dispersive estimate of the isospin-breaking corrections in the $K_{\ell 4}$ analysis (several years ago !), and it seemed natural to invite her to discuss the first estimates included in this manuscript.

While writing these words, I think of all the people with whom I interacted on the subjects presented in this document, and in particular Luca, Norman, Bachir, Paul, Véronique and Guillaume. I do not forget (how could I ?) the role played by Jan Stern in the shaping of this subject and in my career.

I have to thank Henk Hilhorst, Philippe Boucaud and Jean-Pierre Leroy for the pleasant environment that has been provided at the Laboratoire de Physque Théorique over all these years. This has been all the more pleasant thanks to the researchers of the LPT laboratory, and in particular, Olivier, Alain, Luis, Damir, Asmaa, Benoît, as well as the technical and administrative staff of the laboratory.

More generally, I have really enjoyed my time on the Orsay campus, in spite of all its defaults. I can only hope that the poorly planned actions of the politicians will not destroy completely a campus, a university and a research system that took so long to build.

I should also thank all the people with whom I worked or discussed over the years on various physics subjects, in particular Patrick, Marie-Hélène, Nicolas, Ji-bo, Patrick, Emi, Joao, Niels, Bogdan, Andreas, Sacha, Quim, Javier, Marc, Hai-bo, Xian-Wei, as well as all the members of the CKMfitter group.

I must say that over the years, I learned also a lot during my "other" activities beyond pure research, whether in popular science (CVC, Élémentaire), teaching (Paris-Sud, ENS) or research administration (Comité National du CNRS), and I thank all those with whom I shared special – and sometimes very intense – moments.

Finally, I would like to thank my friends and family for their help and support during all these years of a researcher's life – a life which is not always easy to comprehend or to follow. My life would be quite different without their affectionate presence at my side. It is only natural to dedicate this manuscript to Jean, Anny and Jean-Luc, for their love and understanding.

A
Appendix

A.1 Chiral symmetry breaking and the number of light flavours

A.1.1 Fermions in an Euclidean metric

In sec. 2.3.1, a Wick rotation eq. (2.27) was discussed to go from a Minkowskian metric to an Euclidean one. This transformation applied on a Lagrangian $\mathcal{L}$ yields its Euclidean version $\mathcal{L}_e$:

$$\exp\left[i\int d^4x\ \mathcal{L}\right] \to \exp\left[-\int d^4\bar{x}\ \mathcal{L}_e\right] \tag{A.1}$$

For instance, the ϕ^4 theory with a source term J is:

$$i\int d^4x\left[\frac{1}{2}(\partial_\mu\phi)^2-\frac{1}{2}m^2\phi^2-\frac{\lambda}{4!}\phi^4+J\phi\right] \to -\int d^4\bar{x}\left[\frac{1}{2}\bar{\partial}_\mu\phi)^2+\frac{1}{2}m^2\phi^2+\frac{\lambda}{4!}\phi^4-J\phi\right] \tag{A.2}$$

The Euclidean counterpart of the quadratic part of a bosonic theory is definite positive. The analytic structure of the Green functions is assumed to be unchanged by this rotation, so that poles and cuts are just rotated from the Minkowski theory to its Euclidean counterpart. However, the Wick rotation is not limited to using an imaginary time coordinate. Indeed, the Lorentz transformations constitute the non-compact group $SO(3,1)$ in a Minkowskian metric, whereas their Euclidean equivalents form the compact group $SO(4)$. The construction of invariants for scalar and vector fields yield the same results in the same metric since the corresponding representations have similar covariance properties, and the naive "complexification" of the time coordinate such as eq. (A.2) is well justified.

Spinors are more subtle [437]. In both metrics, one can collect the generators of the Lorentz group into two commuting SU(2) sub-algebras, and to classify all their representations by two half-integer indices (m,n). For SO(4) (Euclidean case), the generators are Hermitian and the two sub-algebras are independent. The left-handed $(1/2,0)$ and right-handed $(0,1/2)$ spinors transform as:

$$\psi_L^e \to \Lambda_L^e\psi_L^e\,, \qquad \psi_R^e \to \Lambda_R^e\psi_R^e\,, \qquad \Lambda_L^e(\Lambda_L^e)^\dagger = \Lambda_R^e(\Lambda_R^e)^\dagger = 1. \tag{A.3}$$

In the Minkowskian case SO$(3,1)$, the transformation for left-handed and right-handed spinors are not independent anymore:

$$\psi_L \to \Lambda_L\psi_L\,, \qquad \psi_R \to \Lambda_R\psi_R\,, \qquad \Lambda_L^{-1} = \Lambda_R^\dagger, \tag{A.4}$$

where Λ_L and Λ_R are not unitary. This topological difference between SO(4) and SO$(3,1)$ a is exemplified by Majorana spinors. From a single (two-component) spinor, say left-handed, in Minkowskian space, it is possible to build a four-component spinor, self-charge conjugate, called Majorana spinor. Such an object cannot be build in an Euclidean metric. On the other hand, in both metrics, one can build Dirac spinors $(1/2,0)\oplus(0,1/2)$. In Minkowski space, one can obtain from a spinor ψ its conjugate $\bar{\psi}=\psi^\dagger\gamma_0$. Since left- and right-handed spinors have independent transformation laws in an Euclidean metric, the conjugation operation is not defined, and $\bar{\psi}$ is an independent spinor from ψ. This yields the dictionary:

$$g_{\mu\nu} = (1,-1,-1,-1) \to \bar{g}_{\mu\nu} = (1,1,1,1), \tag{A.5}$$

$$\epsilon^{\mu\nu\rho\sigma} \to \epsilon_{\mu\nu\rho\sigma}, \tag{A.6}$$

$$\bar{\psi} \to \psi^\dagger, \tag{A.7}$$

$$\gamma_0 \to \bar{\gamma}_0 = i\gamma_0, \tag{A.8}$$

$$\gamma_i \to \bar{\gamma}_i = \gamma_i \ (i = 1, 2, 3), \tag{A.9}$$

$$\gamma_5 \to \bar{\gamma}_5 = \gamma_5, \tag{A.10}$$

$$\{\gamma_\mu, \gamma_\nu\} = 2g_{\mu\nu} \to \{\bar{\gamma}_\mu, \bar{\gamma}_\nu\} = -2\bar{g}_{\mu\nu}, \tag{A.11}$$

so that covariant quantities in SO(4) can be build similarly to those in SO(3, 1). The usual relations on the Dirac matrices are obviously modified due to their changed anticommutation relations. In particular, in the Euclidean metric, all four $\bar{\gamma}_\mu$ ($\mu = 0 \dots 3$) are anti-Hermitian, the distinction between $\epsilon^{\mu\nu\rho\sigma}$ and $\epsilon_{\mu\nu\rho\sigma}$ becomes pointless. The combination $d^4x\ \tilde{G}G$ is invariant under a Wick rotation, since $\tilde{G}G$ contains a single time derivative canceling the rotation of the integration element.

Let us remark in particular that the couplings between spinors of different helicities are modified by the description in the Euclidean metric. Indeed, the Euclidean action for the quarks read:

$$S_{D,e} = -\int d^4\bar{x}\psi^\dagger(-i\bar{\gamma}_\mu\bar{D}_\mu + \tilde{M})\psi\,, \qquad \tilde{M} = M\frac{1-\gamma_5}{2} + M^\dagger\frac{1+\gamma_5}{2}\,, \tag{A.12}$$

for a general mass matrix $\tilde{M}$. We can therefore write down the Euclidean Lagrangian splitting into left- and right-handed chiralities $\psi_{L,R} = (1 \mp \gamma_5)/2$, leading to:

$$S_{D,e} = -\int d^4\ \bar{x}[\psi_R^\dagger(-i\bar{\gamma}_\mu\bar{D}_\mu)\psi_L + \psi_L^\dagger(-i\bar{\gamma}_\mu\bar{D}_\mu)\psi_R + \psi_L^\dagger M\psi_L + \psi_R^\dagger M\psi_R]\,. \tag{A.13}$$

One may introduce an action looking more like the Minkowskian one by introducing the notation $\bar{\psi}_L = \psi_R^\dagger$ and $\bar{\psi}_R = \psi_L^\dagger$, keeping in mind that the label does not carry information on the chirality of $\bar{\psi}$.

Introducing the eigenvectors and eigenvalues of the Dirac operator, the Dirac matrix has then the following structure for a positive winding number ν corresponding to ν left-handed zero eigenvalues:

$$-i\bar{\gamma}\mu + \tilde{M} = \left[\begin{array}{c|c|c|c} \begin{array}{c} M \\ (\nu\ times) \\ M \end{array} & & & \\ \hline & \begin{array}{cc} M & -i\lambda_1 \\ -i\lambda_1 & M^\dagger \end{array} & & \\ \hline & & \begin{array}{cc} M & -i\lambda_2 \\ -i\lambda_2 & M^\dagger \end{array} & \\ \hline & & & \begin{array}{c} \cdots\ \cdots \\ \cdots\ \cdots \end{array} \end{array}\right] \tag{A.14}$$

If ν is negative, one has $|\nu|$ copies of $M^\dagger$ in the first block of the matrix. One gets therefore the following expression for the fermionic determinant (see eq. (2.44)):

$$\det(-i\bar{\gamma}_\mu\bar{D}_\mu + \tilde{M}) = \begin{cases} (\det_f M)^\nu \prod_{n=1}^{+\infty} \det_f(\lambda_n^2 + MM^\dagger) & [\nu \geq 0] \\ (\det_f M^\dagger)^{-\nu} \prod_{n=1}^{+\infty} \det_f(\lambda_n^2 + MM^\dagger) & [\nu \leq 0]\,. \end{cases} \tag{A.15}$$

A.1.2 Weingarten inequalities

There are constraints on the pattern of chiral symmetry breaking that can be derived using the formalism of developed in Ch. 2. One can use in particular the Weingarten inequalities [65], obtained by considering the Euclidean two-point correlators of the form:

$$C_\Gamma(x,y) = \langle 0|(\bar{u}\Gamma d)(x)(\bar{d}\Gamma u)(y)|0\rangle\,, \qquad \Gamma = 1, \bar{\gamma}_5, i\bar{\gamma}_\mu, \bar{\gamma}_\mu\bar{\gamma}_5, i\bar{\sigma}_{\mu\nu}\,, \tag{A.16}$$

with a vanishing vacuum angle $\theta = 0$. One can provide inequalities between the correlators, by exploiting the Dirac representation of the propagator eq. (2.41), and by projection the 4×4 fermion propagator over the full basis of Dirac matrices:

$$S(x,y|G) = s(x,y) + \bar{\gamma}_5 p(x,y) + i\bar{\gamma}_\mu v_\mu(x,y) + \bar{\gamma}_\mu\bar{\gamma}_5 a_\mu(x,y) + \frac{1}{2} i\bar{\sigma}_{\mu\nu} t_{\mu\nu}(x,y)\,, \tag{A.17}$$

where the dependence on the gluonic configuration G is implicit. We get for the axial correlator:

$$C_{\gamma_5(x,y)} = - \ll \mathrm{Tr}[\gamma_5 S(x,y|G)\gamma_5 S(y,x|G)] \gg = - \ll \mathrm{Tr}[S(x,y|G)S^\dagger(x,y)] \gg \tag{A.18}$$

$$= -4 \ll |s|^2 + |p|^2 + |v_\mu|^2 + |a_\mu^2| + \frac{1}{2}|t_{\mu\nu}|^2 \gg\,, \tag{A.19}$$

using the fact that $\gamma_5 S(x,y|G)\gamma_5 = S^\dagger(y,x|G)$ which can be proven easily using the representation of the propagator in terms of Dirac eigenvectors and eigenvalues eq. (2.42). Similarly, we obtain for the scalar correlator:

$$C_1(x,y) = - \ll \mathrm{Tr}[S(x,y|G)S(y,x|G)] \gg = - \ll \mathrm{Tr}[\gamma_5 S(x,y|G)\gamma_5 S^\dagger(x,y)] \gg \tag{A.20}$$

$$= -4 \ll |s|^2 + |p|^2 - |v_\mu|^2 - |a_\mu^2| + \frac{1}{2}|t_{\mu\nu}|^2 \gg\,, \tag{A.21}$$

and the other choices for Γ yields other linear combinations with alternating signs. We see that $\Gamma = \gamma_5$ is the only one obtained by adding up positive contributions only (indeed, the positive functions $|s|^2$ and the like are averaged over a positive measure if $\theta = 0$). This means that for any separation $|x-y|$, we expect the following Weingarten inequalities [65]:

$$|C_{\gamma_5}(x-y)| \geq |C_\Gamma(x-y)|\,, \qquad \forall |x-y|\,. \tag{A.22}$$

Let us add that these relationships were derived between bare correlators, regularised by introducing some ultraviolet cut-off Λ in a scheme respecting chiral symmetry. We should therefore read the previous statement as:

$$|C_{\gamma_5}^{(\Lambda)}(x-y)| \geq |C_\Gamma^{(\Lambda)}(x-y)|\,, \qquad \lim_{\Lambda\to\infty} \left|\frac{Z_{\gamma_5}(\mu,\Lambda)}{Z_\Gamma(\mu,\Lambda)}\right| \times |C_{\gamma 5}^r(x-y;\mu)| \geq |C_\Gamma^r(x-y;\mu)|\,, \tag{A.23}$$

where the superscript Λ denote bare quantities regularised by the (chirally-symmetric) cut-off Λ and the superscript r denote renormalised quantities considered at a renormalisation scale μ. The factor Z corresponds to the renormalisation factor associated with the correlator Z_Γ.

Let us consider the Weingarten inequalities eq. (eq:Weingarten) for regularised bare correlators at large $|x-y|$. The finite ultraviolet cut-off Λ is taken significantly larger than the mass scales of the light states of the theory. We know that the correlators will decay exponentially like:

$$|C_\Gamma^{(\Lambda)}(x-y)| \sim A_\Gamma^{(\Lambda)} \exp[-M_\Gamma|x-y|]\,, \tag{A.24}$$

where M_Γ is the mass of the physical lightest state coupling to the relevant channel, and $A_\Gamma(\Lambda)$ the (potentially Λ-dependent) coupling of the state to the current/density considered. The Weingarten inequalities state that the exponential decay of the pseudoscalar vector must beat any other state, i.e. the lightest pseudoscalar state must be lighter than the lightest states in the other channels. This is in particular used to prove the Vafa-Witten theorem [64]: let us take QCD in the isospin limit $m_u = m_d \neq 0$, and let us assume that some of the vector symmetries of the theory are spontaneously broken, we should have scalar massless Goldstone bosons (even out of the chiral limit), and thus should also have pseudoscalar massless states since $M_{\gamma_5} \leq M_1$. But where would these latter states come from ? A natural answer would be the spontaneous breakdown of the axial isospin symmetry, which unfortunately is not a symmetry of the theory for massive quarks. We have actually no good interpretation for such pseudoscalar massless states. This strongly suggests that our initial hypothesis is wrong, and that the vector symmetries of the theory cannot be spontaneously broken for any mass of the quarks, which is the content of the Vafa-Witten theorem.

We could imagine to get more information from the inequalities eq. (A.23), as was proposed in refs. [438, 439], by considering the expression of the correlators at large separation, where they are dominated by Goldstone bosons, allowing us to compare their couplings to different currents/densities. The only non-trivial case requires to compare correlators with one-particle intermediate states as their lightest contributions, i.e. the axial and pseudoscalar propagators. One gets:

$$\left| F_\pi^2 \partial_\mu \partial_\nu \left[\frac{M_\pi}{z} K_1(M_\pi z) \right] \right| \leq F_\pi^2 [B^{(\Lambda)}(M_\pi)]^2 \left[\frac{M_\pi}{z} K_1(M_\pi z) \right] , \tag{A.25}$$

for $|z| = |x - y| \gg 1/M_H$ where M_H is the mass scale for higher, non-Goldstone, excitations coupling to axial currents and/or pseudoscalar densities. The bracketed term containing the Bessel function K_1 is the Fourier transform of the pion propagator. $F_\pi B^{(\Lambda)}(M_\pi^2)$ denotes the coupling of the pion to the pseudoscalar current.

We can consider eq. (A.25) in two different non-trivial cases. Let us take $z_1 = z$, $z_{i\neq 1} = 0$, and consider first $\mu = \nu = 1$:

$$\frac{[B^{(\Lambda)}(M_\pi)]^2}{M_\pi^2} \geq \left| \frac{2}{z^2 M_\pi} [K_1(M_\pi z) - M_\pi z K_1'(M_\pi z)] + K_1''(M_\pi z) \right| \frac{1}{|K_1(M_\pi z)|} \geq 1 , \quad \forall z \gg 1/M_H . \tag{A.26}$$

For a non-vanishing quark condensate, at small M_π, one has:

$$B^{(\Lambda)}(M_\pi) = B^{(\Lambda)} + O(m) . \qquad M_\pi^2 = 2m^{(\Lambda)} B^{(\Lambda)} + O(m^2) , \qquad 2m^{(\Lambda)} \leq B^{(\Lambda)} . \tag{A.27}$$

If we put explicitly the appropriate renormalisation factors $Z(\Lambda, \mu)$ and send the cut-off to infinity, we obtain an RG-invariant constraint [438]:

$$2m(\mu) Z^{-1/2}(\mu) \leq B^r(\mu) Z^{1/2}(\mu) , \tag{A.28}$$

with $B^r(\mu) = \Sigma^r(N_f; \mu)/F^2(N_f)$ and the quark mass renormalisation constant: $Z(\mu) = \lim_{\Lambda\to\infty} Z_{\gamma_5}/Z_{\gamma_\mu\gamma_5}$. But eq. (A.26) does not prevent an alternative possibility that $B^{(\Lambda)}(M_\pi)$ vanishes like M_π in the chiral limit, corresponding to a situation where the renormalised quark condensate vanishes, and $B^{(\Lambda)}(M_\pi) \sim M_\pi \sim m$ at small quark mass.

Let us now consider $\mu = \nu \neq 1$. We obtain then [439]:

$$B^{(\Lambda)}(M_\pi) \geq \left| \frac{1}{z^2} K_1(M_\pi z) \right| \frac{1}{|K_1(M_\pi z)|} = \frac{1}{z^2} \qquad \forall z \gg 1/M_H . \tag{A.29}$$

This constraint indicates that $B^{(\Lambda)}(M_\pi)$ is bounded by a value related to the distance at which one can neglect safely higher states than the Goldstone bosons. In particular, one can take the chiral limit and obtain that:

$$B^{(\Lambda)} > 0\,, \qquad \forall \Lambda \text{ large}\,. \tag{A.30}$$

which indicates that the bare quark condensate cannot vanish at finite cut-off. However, the issue remains open to know what will be the behaviour of the renormalised quantity as one sends the cut-off to infinity:

$$B^r(\mu) = \lim_{\Lambda\to\infty} \frac{B^{(\Lambda)}}{\sqrt{Z_{\gamma_5}(\mu;\Lambda)/Z_{\gamma_\mu\gamma_5}(\mu;\Lambda)}}\,, \tag{A.31}$$

since one can expect divergences from both the numerator and the denominator when $\Lambda \to \infty$, but without knowing their relative rate. The Weingarten inequalities indicate that $B^{(\Lambda)} > 0$, but this does not allow to determine its behaviour as $\Lambda \to \infty$ and thus the value of the renormalised quantity $B^r(\mu)$ and that of the renormalised quark condensate (zero or non-vanishing).

Let us emphasize that the Weingarten inequalities provide useful information between bare correlators, and therefore quantities before renormalisation. They are therefore useful to derive inequalities between quantities unaffected by renormalisation (such as the masses of the physical states) or between quantities with the same RG evolution (such as between $mZ^{-1/2}$ and $BZ^{1/2}$). Unfortunately, they are not well suited to derive absolute bounds on quantities subjected to renormalisation, such as the quark condensate, and thus to discuss the phases described in sec. 2.5.3.

A.2 Chiral perturbation theory and its limits

A.2.1 Chiral Ward identities

The generating functional of QCD is given by eq. (3.5):

$$\begin{aligned} e^{i\Gamma[v,a,s,p,\theta]} &= \int [DG][D\psi][D\bar\psi] \exp\left\{ i \int d^4x \mathcal{L}_{\text{QCD}}[v,a,s,p,\theta] \right\}, \\ \mathcal{L}_{\text{QCD}}[v,a,s,p,\theta] &= \mathcal{L}_f + \sum_Q (i\not{D} - M_Q)Q - \frac{1}{4} G^{\alpha;\mu\nu} G^\alpha_{\mu\nu} - \frac{g^2}{32\pi^2}\theta\ \tilde{G}^{\alpha;\mu\nu} G^\alpha_{\mu\nu} \\ &\quad + \sum_q \bar\psi[\gamma^\mu(iD_\mu + v_\mu + \gamma_5 a_\mu) - s + \gamma_5 p]\psi. \end{aligned} \tag{A.32}$$

We can promote the chiral symmetry to a local form in order to obtain chiral Ward identities in a simple way. We impose the following transformation laws:

$$\psi(x) \to \psi'(x) = V_R(x)\psi_R(x) + V_L(x)\psi_L(x), \tag{A.33}$$

with

$$V_L(x) = \exp\left\{ i \sum_{a=0}^{N_f^2-1} \alpha_L^a(x)\lambda^a \right\}, \qquad V_R(x) = \exp\left\{ i \sum_{a=0}^{N_f^2-1} \alpha_R^a(x)\lambda^a \right\}. \tag{A.34}$$

Under (A.33), only the source terms of (A.32) are modified:

$$\bar\psi'[\gamma^\mu(v_\mu + \gamma_5 a_\mu) - s + i\gamma_5 p]\psi' = \bar\psi[\gamma^\mu(v'_\mu + \gamma_5 a'_\mu) - s' + i\gamma_5 p']\psi, \tag{A.35}$$

with:

$$(v'_\mu + a'_\mu)(x) = V_R(x)(v_\mu + a_\mu)(x)V_R^\dagger(x) + iV_R(x)\partial_\mu V_R^\dagger(x) \tag{A.36}$$

$$(v'_\mu - a'_\mu)(x) = V_L(x)(v_\mu - a_\mu)(x)V_L^\dagger(x) + iV_L(x)\partial_\mu V_L^\dagger(x) \tag{A.37}$$

$$(s' + ip')(x) = V_R(x)(s + ip)(x)V_L^\dagger(x) \tag{A.38}$$

$$(s' - ip')(x) = V_L(x)(s - ip)(x)V_R^\dagger(x). \tag{A.39}$$

Eq. (A.33) is equivalent to a local source transformation. However, the integration measure over fermions is not invariant under (A.33). Therefore, we must introduce a Jacobian Δ taking into account all the effects of this local transformation. For infinitesimal rotations, we have:

$$V_L(x) = 1 + i\alpha(x) + i\beta(x) + \dots \qquad V_R(x) = 1 + i\alpha(x) - i\beta(x) + \dots \tag{A.40}$$

$$v'_\mu = v_\mu + \partial_\mu\alpha + i[\alpha, v_\mu] + i[\beta, a_\mu]\,, \qquad s' = s + i[\alpha, s] - \{\beta, p\}\,, \tag{A.41}$$

$$a'_\mu = a_\mu + \partial_\mu\beta + i[\alpha, a_\mu] + i[\beta, v_\mu]\,, \qquad p' = p + i[\alpha, p] + \{\beta, s\}\,, \tag{A.42}$$

yielding the relation ($\mathcal{S}$ denoting v, a, s, p, θ):

$$\Gamma[\mathcal{S}'] = \Gamma[\mathcal{S}] + \Delta[\mathcal{S}, V_L V_R^\dagger], \qquad \Delta[\mathcal{S}, V_L V_R^\dagger] = -\int d^4x\ \langle\beta(x)\Omega(x)\rangle, \tag{A.43}$$

$$\Omega(x) = \frac{N_C}{16\pi^2}\epsilon^{\alpha\beta\mu\nu}\left[v_{\alpha\beta}v_{\mu\nu} + \frac{4}{3}\nabla_\alpha a_\beta \nabla_\mu a_\nu + \frac{2i}{3}\{v_{\alpha\beta}, a_\mu a_\nu\} + \frac{8i}{3}a_\mu v_{\alpha\beta}a_\nu + \frac{4}{3}a_\alpha a_\beta a_\mu a_\nu\right],$$

$$v_{\mu\nu} = \partial_\mu v_\nu - \partial_\nu v_\mu - i[v_\mu, v_\nu], \qquad \nabla_\mu a_\nu = \partial_\mu a_\nu - i[v_\mu, a_\nu], \tag{A.44}$$

if we add to the transformation laws of external sources (A.36)-(A.39) that of the vacuum angle:

$$\theta'(x) = \theta(x) - 2\langle\beta(x)\rangle. \tag{A.45}$$

Ω flags the presence of anomalies in the theory. (A.43) must apply for all infinitesimal transformations and we can write the Ward identities as:

$$-\partial_\mu^x\frac{\delta\Gamma}{\delta v_\mu^a(x)} + f_{abc}v_\mu^c(x)\frac{\delta\Gamma}{\delta v_\mu^b(x)} + f_{abc}a_\mu^c(x)\frac{\delta\Gamma}{\delta a_\mu^b(x)} + f_{abc}s^c(x)\frac{\delta\Gamma}{\delta s^b(x)} + f_{abc}p^c(x)\frac{\delta\Gamma}{\delta p^b(x)} = 0, \tag{A.46}$$

for $a = 0 \dots N_f^2 - 1$,

$$-\partial_\mu^x\frac{\delta\Gamma}{\delta a_\mu^a(x)} + f_{abc}v_\mu^c(x)\frac{\delta\Gamma}{\delta a_\mu^b(x)} + f_{abc}a_\mu^c(x)\frac{\delta\Gamma}{\delta v_\mu^b(x)} - d_{abc}p^c(x)\frac{\delta\Gamma}{\delta s^b(x)} + d_{abc}s^c(x)\frac{\delta\Gamma}{\delta p^b(x)} = -\Omega^a(x), \tag{A.47}$$

for $a = 1 \dots N_f^2 - 1$, and because of the presence of θ for β_0,

$$-\partial_\mu^x\frac{\delta\Gamma}{\delta a_\mu^0(x)} + \sqrt{\frac{2}{N_f}}\sum_{a=0\dots N_f^2-1}\left[s^a(x)\frac{\delta\Gamma}{\delta p^a(x)} - p^a(x)\frac{\delta\Gamma}{\delta s^a(x)}\right] - \sqrt{2N_f}\frac{\delta\Gamma}{\delta\theta(x)} = -\Omega^0(x), \tag{A.48}$$

These three expressions encode the constraints among Green functions of vector/axial currents and scalar/pseudoscalar densities imposed by chiral symmetry. All Ward identities can be obtained by taking the derivatives of one of these three relations with respect to some external

sources, then to set $v = a = p = 0$, $s = M_q$, $\theta = \theta_0$ in the resulting equality. The structure of Ω indicates that anomalous Ward identities involve correlators like $\partial_x^\mu \langle \Omega | T\{A_\mu(x) X\} | \Omega \rangle$ with $X = VV$, AA, VVV, AAV, $VVVV$, $AAVV$ et $AAAA$. The non-conservation of the singlet axial current (related to the peculiar status of the η' with respect to chiral symmetry) arises through the derivative with respect to θ in eq. (A.48).

A.2.2 $1/N_c$ power counting

If the number of colours is taken large, the quark loop graph which gives rise to the $U(1)$ anomaly is suppressed [104, 105, 107, 440–442]. In the limit $N_c \to \infty$, the singlet axial current is also conserved and the theory acquires a higher degree of symmetry. Since the operator $\bar{q}q$ fails to be invariant under the extra $U(1)$ symmetry, the formation of a quark condensate, $\langle \bar{q}q \rangle \neq 0$, implies that this symmetry is also spontaneously broken [443] (the argument can also be applied for other order parameters taking part in the breakdown of chiral symmetry). The spectrum of QCD contains a ninth state, the η' meson, which becomes massless if the chiral limit $m_u = m_d = m_s = 0$ and the large-N_c limit $N_c \to \infty$ are both taken. The existence of an additional Goldstone boson in this limit can be implemented within an effective Lagrangian, so that the Green functions of QCD are expressed by means of a simultaneous expansion in powers of momenta, quark masses and $1/N_c$ [21, 157]. Conversely, large-N_c arguments have been used to fix some of the low-energy counterterms of $N_f = 3$ chiral perturbation theory, based on the fact that the corresponding correlators were suppressed in the limit of a large number of colours.

One has to define a counting in powers of $1/N_c$ associated to the correlators [21, 444]. The well-known leading logarithmic formula for the strong coupling constant:

$$\frac{g^2}{(4\pi)^2} = \frac{1}{\beta_0 \ln(\mu^2/\Lambda^2_{\rm QCD})}\,, \qquad \beta_0 = \frac{1}{3}\,(11 N_c - 2 N_f)\,, \tag{A.49}$$

implies that the running coupling constant tends to zero when N_c becomes large, $g^2 \sim 1/N_c$. Let us consider the connected correlation function formed with n_j quark currents $j_i = barq\,\Gamma_i q$ and n_ω winding number densities $\omega = \mathrm{tr}_c G_{\mu\nu}\tilde{G}^{\mu\nu}/(16\pi^2)$:

$$G_{n_j n_\omega} = \langle 0 | T j_1(x_1) \cdots j_{n_j}(x_{n_j})\, \omega(y_1) \cdots \omega(y_{n_\omega}) | 0 \rangle\,, \tag{A.50}$$

and let us denote the contribution of the graphs graphs with ℓ quark loops by $G^\ell_{n_j n_\omega}$. The large-N_c counting rules of perturbation theory imply that this quantity represents at most (for the planar graph) a term of order:

$$G^\ell_{n_j n_\omega} = O\left(N_c^\ell \times \frac{1}{N_c^{2(\ell-1)}} \times \frac{1}{N_c^{n_\omega}} \right) = O(N_c^{2-\ell-n_\omega}) \qquad \ell = 0, 1, \ldots \tag{A.51}$$

where the first term corresponds to the ℓ closed quark loops, the second term to the vertex of the gluons attached between quark loops, the third term to the winding densities (a similar rule can be obtained by topological considerations on the Euler character of the diagrams [444]). The leading power is independent of the number n_j of quark currents, but decreases with n_ω and with the number of quark loops. If we have several flavours in the theory, we see that depending on the flavours carried by the quark currents (and whether we can build a single trace out of all the flavours involved), we may or may not be able to close the loop. In particular, we see that Zweig-rule violating correlators:

$$\langle (\bar{u}u)(x)(\bar{s}s)(0) \rangle\,, \qquad \langle (\bar{u}\gamma_\mu\gamma_5 u)(x)(\bar{d}\gamma_\mu\gamma_5 d)(y)(\bar{s}s)(0) \rangle\,, \tag{A.52}$$

count as $O(N_c^0)$ (see fig. 2.4 for a diagrammatic representation of the first correlators), compared to the non-suppressed correlators:

$$\langle(\bar{u}u)(0)\rangle\,, \qquad \langle(\bar{u}\gamma_\mu\gamma_5 u)(0)(\bar{d}\gamma_\mu\gamma_5 d)(x)\rangle\,, \tag{A.53}$$

which count as $O(N_c)$. It is not surprising that eqs. (A.52) are related to L_6 and L_4 in the effective theory, which correspond to operators with two traces over flavour as seen in eq. (3.34) (rather than a single trace like L_8 and L_5). Moreover, the second correlator in eq. (A.53) shows that $F_0^2 = O(N_c)$. An effective Lagrangian can be built to combine the expansion in powers of momenta, quark masses and $1/N_c$ [21, 157, 445, 446], including the η'-meson as an additional degree of freedom. This led in particular to the conclusion that L_7 was the only NLO counterterm to receive a contribution from the η' meson, of the form $F_0^2/M_{\eta'}^2 = O(N_c^2)$ in the chiral limit, since $M_{\eta'}^2 = O(1/N_c, m_q)$.

A.3 An alternative treatment of three-flavour chiral series

A.3.1 Inputs from the RBC/UKQCD Collaboration [H]

We first consider the RBC/UKQCD Collaboration simulations with 2+1 dynamical flavours [207–209] performed with domain-wall fermions at one lattice spacing $a^{-1} = 1.729(28)$ GeV. The calculations are performed on two volumes, $16^3 \times 32$ and $24^3 \times 64$ (with a fifth dimension of length 16), at each quark mass, except the lightest mass which is only simulated on the larger volume. They performed a non-perturbative renormalisation to relate the lattice quark masses to those in the RI-MOM scheme.

The only points that we will use are those where the sea and valence quark masses are identical, for the largest volume (which corresponds to a spatial volume of $(2.74)^3\text{fm}^3$) . There are four sets corresponding to such a situation for pseudoscalar masses and decay constants in Ref. [207], corresponding to $a(\tilde{m}^{lat} - m_{res})$ and $a(\tilde{m}_s^{lat} - m_{res})$ being respectively $(0.005, 0.040)$, $(0.010, 0.040)$, $(0.020, 0.020)$, $(0.030, 0.030)$. where $am_{res} = 0.00315(2)$, but we will consider only the first two sets where the pseudoscalar masses are light enough for $N_f = 3$ χPT to hold. The quark masses are given in the RI-MOM scheme, but they can be related to the $\overline{MS}$ scheme through a multiplicative factor $\bar{m}(2\text{ GeV}) = Z_m a^{-1}(a\tilde{m}^{lat})$.

We obtain the following values expressed in units of 10^{-3} GeV^{-2} for the pseudoscalar masses and decay constants [207]. The uncertainties here are purely statistical and do not include those induced by the uncertainty on the value of the lattice spacing.

Masses	(p, q)	F_π^2	$F_\pi^2 M_\pi^2$	F_K^2	$F_K^2 M_K^2$
$(0.005, 0.040)$	$(1.15, 0.189)$	10.98 ± 0.16	1.196 ± 0.022	14.11 ± 0.19	4.644 ± 0.076
$(0.010, 0.040)$	$(1.15, 0.304)$	12.85 ± 0.16	2.249 ± 0.036	15.59 ± 0.18	5.730 ± 0.082

In two papers [208, 209], the RBC/UKQCD collaboration investigated the $K_{\ell 3}$ form factors f_0 and f_+ using in particular twisted boundary conditions to obtain a sample transfer momenta, with the same two sets of values corresponding to nondegenerate masses $(a(\tilde{m}^{lat} - m_{res}), a(\tilde{m}_s^{lat} - m_{res})) = (0.005, 0.040), (0.010, 0.040)$. The set with the lighter u, d quark masses yields the following values:

t	60.7	59.87	38.1	21.6	0.30	-44.00	-129.3
$F_\pi F_K f_0(t)$	12.68 ± 0.17	12.73 ± 0.17	12.49 ± 0.17	12.32 ± 0.17	12.15 ± 0.16	11.68 ± 0.21	10.95 ± 0.32
$F_\pi F_K f_+(t)$	$\times$	$\times$	12.71 ± 0.176	12.42 ± 0.175	12.15 ± 0.17	$\times$	$\times$

r	$28.8 \pm 0.4 \pm 1.6$
$\tilde{m}_{s,ref}/m_s$	1.150
F_K/F_π	$1.205 \pm 0.018 \pm 0.062$
$m_s(2\text{ GeV})$[MeV]	$107.3 \pm 4.4 \pm 9.7 \pm 4.9$
$m(2\text{ GeV})$[MeV]	$3.72 \pm 0.16 \pm 0.33 \pm 0.18$
$B(2\text{ GeV})$[GeV]	$2.52 \pm 0.11 \pm 0.23 \pm 0.12$
F[MeV]	$81.2 \pm 2.9 \pm 5.7$
$\bar{\ell}_3$	$3.13 \pm 0.33 \pm 0.24$
$\bar{\ell}_4$	$4.43 \pm 0.14 \pm 0.77$

(A.54)

Table A.1: *Results obtained by the RBC/UKQCD collaboration in ref. [207].*

The set with the heavier value leads to the following values for the scalar form factor:

t	35.42	-90.51	-195.3
$F_\pi F_K f_0(t)$	14.28 ± 0.17	13.05 ± 0.21	11.64 ± 0.38

We have considered only a subset of the available data where the convergence of chiral series is expected to be particularly good. This amounts to considering only non-degenerate u, d, s quark masses, and to drop the points for $t \leq -0.2$ Gev^{-2} [i.e., the two points for f_0 in ref. [208] corresponding to the lowest values of transfer momentum].

The values of the physical quark masses (m and m_s) and the lattice spacing are obtained by studying the dependence of the mass of π, K and Ω hadrons on these three parameters and tuning them to reproduce the physical hadron masses. If we call $\tilde{m}_{s,ref}$ the value of the strange quark mass corresponding to the set (0.005,0.040), the RBC/UKQCD collaboration obtained $\tilde{m}_{s,ref}/m_s = 1.150$. Considering the uncertainty associated with such a determination (in particular the role played by the form of the chiral extrapolation used for π and K), we will not assume this value in our fit, but rather include this quantity as a parameter of our fit, and scale the other ratios involving a simulated strange quark mass over the physical value.

Fits to the $N_f = 2$ and $N_f = 3$ NLO chiral series for pseudoscalar masses and decay constants were performed in ref. [207]. It turned out that the $N_f = 3$ chiral expansions led to rather poor fits (large χ^2 per d.o.f), in particular for decay constants, unless they put stringent cuts on the values of quark masses where such expansions should hold. This led the authors in ref. [207] to perform fits to $N_f = 2$ NLO chiral expansions. In addition, in ref. [447], NNLO $SU(2)$ chiral expansions were shown to have only a limited utility to extrapolate the data: many more data points would be needed to fix the size of the combinations of $O(p^6)$ counterterms involved The results obtained in ref. [207] that are relevant for our discussion are summarised in tab. A.1.

In addition, two different values for $f_+(0)$ were obtained in refs. [208, 209] from the same gauge configurations, using either data for the scalar form factor or data for both form factors, and applying a pole ansatz based on either $N_f = 3$ or $N_f = 2$ chiral perturbation theory for $K_{\ell 3}$ form factors [211]:

$$[\text{RBC/UKQCD 2007}]: \quad f_+(0) = 0.964 \pm 0.033 \pm 0.0034 \pm 0.0014\,, \tag{A.55}$$

$$[\text{RBC/UKQCD 2010}]: \quad f_+(0) = 0.960(^{+5}_{-6})\,. \tag{A.56}$$

A.3.2 Inputs from the PACS-CS collaboration [H]

The PACS-CS collaboration [127] has investigated the pseudoscalar masses and decay constants with a large sample of light quark masses, for one particular value of lattice spacing $a^{-1} = 2.176(31)$ GeV, on a $32^3 \times 64$ volume. They used a non-perturbatively $O(a)$-improved Wilson quark action and performed the renormalisation of quark masses perturbatively at one loop (with tadpole improvement), with the following results:

$(am_{ud}^{\overline{MS}}, am_s^{\overline{MS}})$	(p, q)	F_π^2	$F_\pi^2 M_\pi^2$	F_K^2	$F_K^2 M_K^2$
$(0.001, 0.040)$	$(1.410, 0.040)$	10.19 ± 1.09	0.247 ± 0.035	14.29 ± 0.48	4.385 ± 0.151
$(0.006, 0.041)$	$(1.456, 0.138)$	11.51 ± 0.26	1.007 ± 0.031	15.49 ± 0.22	5.459 ± 0.088
$(0.010, 0.036)$	$(1.256, 0.271)$	12.48 ± 0.21	1.846 ± 0.041	15.37 ± 0.16	5.200 ± 0.067

Once again, the uncertainties are of purely statistical origin, and they do not include the uncertainty coming from the determination of the lattice spacing. We have considered only a subset of data, where the convergence of the chiral series is expected to be particularly good. This amounts to considering the three lightest values of the pion masses.

The values of the physical quark masses (m and m_s) and the lattice spacing are obtained by studying the dependence of the mass of π, K and Ω hadrons on these three parameters and tuning them to reproduce the physical hadron masses. If we call $\tilde{m}_{s,ref}$ the value of the strange quark mass corresponding to the set (0.0016,0.0399), we obtain $\tilde{m}_{s,ref}/m_s = 1.19$. Considering the uncertainty associated with such a determination (in particular the role played by the form of the chiral extrapolation used for π and K), we will not assume this value in our fit, but rather include this quantity as a parameter of our fit, and scale the other ratios involving a simulated strange quark mass over the physical value.

Fits to the $N_f = 2$ and $N_f = 3$ NLO chiral series for pseudoscalar masses and decay constants were performed in ref. [127]. It turned out that the $N_f = 3$ chiral expansions led to rather poor fits, related to very significant NLO contributions compared to LO terms, in particular for the decay constants, related to large contributions from kaon loops. In other words, the dependence of these quantities on the strange quark mass seen in these simulations is not accounted for properly by NLO $SU(3)$ chiral perturbation theory. This led the authors in ref. [127] to perform fits to $N_f = 2$ chiral expansions. The results obtained in ref. [127] that are relevant for our discussion are summarised in tab. A.2.

A latter article of the same collaboration [268] considered simulations directly performed at the physical point including non-perturbative renormalisation. This has induced a significant modification for the quark mass renormalisation factor, becoming $Z_m = 1.441(15)$ (non-perturbative) instead of $Z_m = 1.114$ (one-loop perturbation theory) leading to an increase (decrease) in the values of quark masses (condensates) by a factor 1.30. This should be taken into account when comparing the results obtained from the PACS and RBC/UKQCD sets in this article. The results obtained in ref. [268] that are relevant for our discussion are summarised in tab. A.3. Since the simulation was performed at the physical point, there is no further information on LECs describing the pattern of $N_f = 2$ and $N_f = 3$ chiral symmetry breakings.

A.3.3 Update of the inputs from the RBC/UKQCD Collaboration

Since the publication of ref. [41], the RBC/UKQCD Collaboration simulations has issued new data with 2+1 dynamical flavours [194] performed with domain-wall fermions at a different volume $32^3 \times 64$ and lattice spacing $a^{-1} = 2.28(3)$ GeV. The points of interest for our analysis

r	28.8 ± 0.4
$Y(3)$	0.88 ± 0.01
$Z(3)$	0.76 ± 0.04
F_K/F_π	1.189 ± 0.020
$\tilde{m}_{s,ref}/m_s$	1.19
m_s(2 GeV)[MeV]	72.72 ± 0.78
m(2 GeV)[MeV]	2.527 ± 0.047
B_0(2 GeV)[GeV]	3.869 ± 0.092
F_0[MeV]	83.8 ± 6.4
$L_4(\mu) \cdot 10^3$	-0.06 ± 0.10
$L_5(\mu) \cdot 10^3$	1.45 ± 0.07
$L_6(\mu) \cdot 10^3$	0.03 ± 0.05
$L_8(\mu) \cdot 10^3$	0.61 ± 0.04
$Y(2)$	0.96 ± 0.01
$Z(2)$	0.88 ± 0.01
B(2 GeV)[GeV]	0.96 ± 0.01
F[MeV]	88.2 ± 3.4
$\bar{\ell}_3$	3.14 ± 0.23
$\bar{\ell}_4$	4.04 ± 0.19
Σ/Σ_0	1.205 ± 0.014
B/B_0	1.073 ± 0.055
F/F_0	1.065 ± 0.058

(A.57)

Table A.2: *Results obtained by the CP-PACS collaboration with one-loop perturbative renormalisation and extrapolation to the physical limit [127]. The values for the quantities in the $N_f = 2$ chiral limit correspond to $N_f = 2$ fits to the so-called Range I with finite-size effects included.*

r	31.2 ± 2.7
F_K/F_π	1.333 ± 0.072
m_s(2 GeV)[MeV]	$92.75 \pm 0.58 \pm 0.95$
m(2 GeV)[MeV]	$2.97 \pm 0.28 \pm 0.03$

(A.58)

Table A.3: *Results obtained by the CP-PACS collaboration [268] with non-perturbative renormalisation and simulation at the physical point.*

are those where the sea and valence quark masses are identical, for the largest volume. There are three new sets corresponding to such a situation for pseudoscalar masses and decay constants in Ref. [207], corresponding to $a(\tilde{m}^{lat} - m_{res})$ and $a(\tilde{m}_s^{lat} - m_{res})$ being respectively $(0.004, 0.030)$, $(0.006, 0.030)$, $(0.008, 0.030)$. where $am_{res} = 0.0006664(8)$. The quark masses are given in the RI-MOM scheme, but they can be related to the $\overline{MS}$ scheme through a multiplicative factor $\bar{m}(2\text{ GeV}) = Z_m a^{-1}(a\tilde{m}^{lat})$. We have also updated the values of the renormalisation constants,

r	$26.8 \pm 0.8 \pm 1.1$
F_K/F_π	$1.204 \pm 0.007 \pm 0.025$
$m_s(2\text{ GeV})[\text{MeV}]$	$96.2 \pm 1.6 \pm 0.2 \pm 2.1$
$m(2\text{ GeV})[\text{MeV}]$	$3.59 \pm 0.13 \pm 0.14 \pm 0.08$
$B(2\text{ GeV})[\text{GeV}]$	$2.64 \pm 0.06 \pm 0.06 \pm 0.06$
$F[\text{MeV}]$	79.2 ± 0.2

(A.59)

Table A.4: *Results obtained by the RBC/UKQCD collaboration in ref. [194].*

residual mass and inputs for the $24^3 \times 64$ volume, keeping the same sets of quark masses.

We obtain the following values expressed in units of 10^{-3} GeV^{-2} for the pseudoscalar masses and decay constants. The uncertainties here are purely statistical and do not include those induced by the uncertainty on the value of the lattice spacing.

Masses	(p, q)	F_π^2	$F_\pi^2 M_\pi^2$	F_K^2	$F_K^2 M_K^2$
$(0.004, 0.030)$	$(1.10, 0.15)$	9.799 ± 0.096	0.821 ± 0.010	12.99 ± 0.11	3.988 ± 0.036
$(0.006, 0.030)$	$(1.10, 0.22)$	10.65 ± 0.10	1.265 ± 0.013	13.51 ± 0.11	4.390 ± 0.038
$(0.008, 0.030)$	$(1.10, 0.29)$	11.53 ± 0.10	1.787 ± 0.018	14.16 ± 0.12	4.895 ± 0.043

Values obtained by fits to sets of data from both volumes are gathered in tab. A.4. As explained in sec. 5.6.4, the almost linear behaviour of F_π as a function of $m_{u,d}$ led the RBC/UKQCD collaboration to consider two different kinds of extrapolation formulae, either $N_f = 2$ χPT (with a curvature due to chiral logarithms in disagreement with the data) or analytic (in good agreement with the data, but not supported by our understanding of low-energy QCD). The errors quoted in tab. A.4 include as a systematic uncertainty the difference of results between the two approaches.

A.4 $\pi\pi$ scattering: experimental and dispersive constraints

A.4.1 Parametrisation of the Roy solutions [I]

In ref. [251], the solutions of Roy equations have been described according to the Schenk parametrisation eq. (6.8). The Schenk parameters X_ℓ^I ($X = A, B, C, D, s$) are functions of the scattering lengths, a_0^0 and a_0^2, and the phase shifts at the matching point, $\delta_0^0(s_0) \equiv \theta_0$ and $\delta_1^1(s_0) \equiv \theta_1$. In ref. [251], the Roy equations were solved for the particular choice of phase shifts at the matching point: $\theta_0 = 82.0°$ and $\theta_1 = 108.9°$, and the dependence on a_0^0 and a_0^2 of the parameters $X = A, B, C, D, s$ was parametrised according to eq. (6.9).

We have followed the same procedure as in ref. [251], with the only difference that θ_0 and θ_1 are explicitly treated as variables. After generating Roy solutions for $\theta_0 \in \{78.9°, 82.3°, 85.7°\}$ and $\theta_1 \in \{106.9°, 108.9°, 110.9°\}$, we then performed a fit of the form of eqs. (6.8), (6.9) and (6.14) with our solutions, in order to obtain the parameters a_i, b_i, c_i of eq. (6.14). The Schenk parameters s_0^0, s_1^1 and s_0^2 are not parametrised in the form of eq. (6.9), but are fixed by the condition at the matching point $\delta_\ell^I(s_0) = \theta_I$.

The parameters a_i are obtained by considering only the solution $(\theta_0 = 82.3°, \theta_1 = 108.9°)$. The parameters b_i have then been obtained by fitting Roy solutions with $\delta\theta_0 \neq 0$ and $\delta\theta_1 = 0$, and the parameters c_i with $\delta\theta_0 = 0$ and $\delta\theta_1 \neq 0$. At each step, the fit has been performed at

the level of the phase shifts, and not of the Schenk parameters, in order to ensure a smooth dependence on $(a_0^0, a_0^2, \theta_0, \theta_1)$. We have checked that this parametrisation was adequate, even for solutions with both non-vanishing $\delta\theta_0$ and $\delta\theta_1$. The maximal gap between any solution and our parametrisation is at most 1% in the $I = 0, 1, 2$ channels.

The coefficients resulting from the fit are expressed in units of M_π, and the phase shifts $\theta_{0,1,2}$ are in radians. For A_0^0 and A_0^2, all the coefficients a_i, b_i, c_i vanish, apart from:

$$A_0^0 : a_1 = a_2 = 0.225\,, \qquad A_0^2 : a_1 = a_3 = -0.03706\,. \tag{A.60}$$

Par.	z_i	a_i	b_i	c_i	Par.	z_i	a_i	b_i	c_i
	1	$.3617 \cdot 10^{-1}$	$-.1716 \cdot 10^{-2}$	$-.3860 \cdot 10^{-2}$		1	.2482	$.4902 \cdot 10^{-1}$	$.1282 \cdot 10^{-1}$
	2	$.1574 \cdot 10^{-1}$	$-.2448 \cdot 10^{-2}$	$-.3384 \cdot 10^{-3}$		2	.1997	.1630	$-.3179 \cdot 10^{-3}$
	3	$.1057 \cdot 10^{-1}$	$-.1774 \cdot 10^{-2}$	$-.2510 \cdot 10^{-4}$		3	.1285	.1137	$.1640 \cdot 10^{-3}$
	4	$-.1782 \cdot 10^{-2}$	$-.1025 \cdot 10^{-1}$	$-.4312 \cdot 10^{-2}$		4	$.1831 \cdot 10^{-1}$	$-.1185$	$.6305 \cdot 10^{-1}$
A_1^1	5	$.2572 \cdot 10^{-3}$	$-.4649 \cdot 10^{-2}$	$-.1705 \cdot 10^{-2}$	B_0^0	5	$.9970 \cdot 10^{-2}$	$-.6395 \cdot 10^{-2}$	$.1104 \cdot 10^{-1}$
	6	$-.2872 \cdot 10^{-3}$	$.1046 \cdot 10^{-2}$	$-.3467 \cdot 10^{-2}$		6	$.4846 \cdot 10^{-1}$	.3431	$-.1661 \cdot 10^{-1}$
	7	$.8311 \cdot 10^{-2}$	$-.9152 \cdot 10^{-2}$	$-.3637 \cdot 10^{-2}$		7	$-.3888 \cdot 10^{-2}$	$-.1598$	$.4322 \cdot 10^{-1}$
	8	$-.2603 \cdot 10^{-2}$	$-.1489 \cdot 10^{-1}$	$.2188 \cdot 10^{-2}$		8	$-.8912 \cdot 10^{-2}$	.5183	$-.3067 \cdot 10^{-1}$
	9	$.1247 \cdot 10^{-2}$	$.7639 \cdot 10^{-3}$	$-.1340 \cdot 10^{-2}$		9	$-.4265 \cdot 10^{-2}$	$.4161 \cdot 10^{-1}$	$.8623 \cdot 10^{-2}$
	10	$-.1186 \cdot 10^{-3}$	$.4371 \cdot 10^{-2}$	$.1128 \cdot 10^{-4}$		10	$-.3232 \cdot 10^{-2}$	$-.1073$	$.2976 \cdot 10^{-2}$

Par.	z_i	a_i	b_i	c_i	Par.	z_i	a_i	b_i	c_i
	1	$.1135 \cdot 10^{-3}$	$-.1685 \cdot 10^{-3}$	$-.6043 \cdot 10^{-3}$		1	$-.8567 \cdot 10^{-1}$	$-.5496 \cdot 10^{-2}$	$.1526 \cdot 10^{-2}$
	2	$-.2094 \cdot 10^{-2}$	$-.3429 \cdot 10^{-3}$	$-.5583 \cdot 10^{-4}$		2	$-.1561 \cdot 10^{-1}$	$.1510 \cdot 10^{-2}$	$-.6254 \cdot 10^{-3}$
	3	$-.8626 \cdot 10^{-3}$	$-.2467 \cdot 10^{-3}$	$-.2205 \cdot 10^{-4}$		3	$-.8722 \cdot 10^{-2}$	$.9679 \cdot 10^{-3}$	$.2538 \cdot 10^{-3}$
	4	$.2911 \cdot 10^{-3}$	$-.8897 \cdot 10^{-3}$	$-.5793 \cdot 10^{-3}$		4	$.9872 \cdot 10^{-2}$	$.1001 \cdot 10^{-1}$	$.2140 \cdot 10^{-1}$
B_1^1	5	$.7343 \cdot 10^{-4}$	$-.4099 \cdot 10^{-3}$	$-.2258 \cdot 10^{-3}$	B_0^2	5	$.2176 \cdot 10^{-1}$	$.3724 \cdot 10^{-2}$	$.3595 \cdot 10^{-2}$
	6	$.2063 \cdot 10^{-3}$	$-.4832 \cdot 10^{-3}$	$-.6376 \cdot 10^{-3}$		6	$.3338 \cdot 10^{-1}$	$-.1050 \cdot 10^{-1}$	$-.5945 \cdot 10^{-2}$
	7	$.5294 \cdot 10^{-3}$	$-.6346 \cdot 10^{-3}$	$-.3879 \cdot 10^{-3}$		7	$-.2051 \cdot 10^{-1}$	$.4012 \cdot 10^{-1}$	$.1157 \cdot 10^{-1}$
	8	$-.3372 \cdot 10^{-3}$	$-.2347 \cdot 10^{-2}$	$.9292 \cdot 10^{-5}$		8	$-.5171 \cdot 10^{-1}$	$.7078 \cdot 10^{-2}$	$.1593 \cdot 10^{-2}$
	9	$-.1564 \cdot 10^{-3}$	$.1032 \cdot 10^{-4}$	$-.1169 \cdot 10^{-4}$		9	$-.5929 \cdot 10^{-1}$	$-.6046 \cdot 10^{-2}$	$.1382 \cdot 10^{-2}$
	10	$-.1301 \cdot 10^{-4}$	$.8137 \cdot 10^{-3}$	$-.1051 \cdot 10^{-3}$		10	$-.2247 \cdot 10^{-1}$	$.4017 \cdot 10^{-2}$	$-.1490 \cdot 10^{-2}$

Par.	z_i	a_i	b_i	c_i	Par.	z_i	a_i	b_i	c_i
	1	$-.1652 \cdot 10^{-1}$	$.2246 \cdot 10^{-1}$	$.3320 \cdot 10^{-2}$		1	$-.7257 \cdot 10^{-4}$	$-.1076 \cdot 10^{-4}$	$-.8750 \cdot 10^{-4}$
	2	$.3280 \cdot 10^{-2}$	$.5387 \cdot 10^{-1}$	$.9391 \cdot 10^{-4}$		2	$.2234 \cdot 10^{-3}$	$-.4577 \cdot 10^{-4}$	$-.8053 \cdot 10^{-5}$
	3	$.1127 \cdot 10^{-1}$	$.2911 \cdot 10^{-1}$	$.2303 \cdot 10^{-3}$		3	$.3718 \cdot 10^{-4}$	$-.3531 \cdot 10^{-4}$	$-.6497 \cdot 10^{-5}$
	4	$.1367 \cdot 10^{-1}$	.1198	$.9361 \cdot 10^{-2}$		4	$.2259 \cdot 10^{-4}$	$.2031 \cdot 10^{-4}$	$-.7306 \cdot 10^{-4}$
C_0^0	5	$.1606 \cdot 10^{-1}$	$.5107 \cdot 10^{-1}$	$.1440 \cdot 10^{-3}$	C_1^1	5	$.1216 \cdot 10^{-4}$	$-.2042 \cdot 10^{-4}$	$-.2856 \cdot 10^{-4}$
	6	$.2990 \cdot 10^{-1}$	$-.1170 \cdot 10^{-1}$	$.1345 \cdot 10^{-2}$		6	$.4075 \cdot 10^{-4}$	$-.1625 \cdot 10^{-3}$	$-.1121 \cdot 10^{-3}$
	7	$-.5982 \cdot 10^{-2}$	$.9021 \cdot 10^{-1}$	$.1428 \cdot 10^{-1}$		7	$-.1238 \cdot 10^{-4}$	$-.3676 \cdot 10^{-4}$	$-.2568 \cdot 10^{-4}$
	8	$.1923 \cdot 10^{-2}$	$.9601 \cdot 10^{-1}$	$-.4036 \cdot 10^{-2}$		8	$.1103 \cdot 10^{-3}$	$-.3679 \cdot 10^{-3}$	$-.5010 \cdot 10^{-4}$
	9	$.1106 \cdot 10^{-1}$	$.2148 \cdot 10^{-1}$	$-.1501 \cdot 10^{-2}$		9	$.3813 \cdot 10^{-4}$	$-.5706 \cdot 10^{-5}$	$.3202 \cdot 10^{-4}$
	10	$.3809 \cdot 10^{-2}$	$-.2854 \cdot 10^{-1}$	$.2780 \cdot 10^{-2}$		10	$.3531 \cdot 10^{-4}$	$.1373 \cdot 10^{-3}$	$-.3439 \cdot 10^{-4}$

Par.	z_i	a_i	b_i	c_i	Par.	z_i	a_i	b_i	c_i
	1	$-.7557 \cdot 10^{-2}$	$.2648 \cdot 10^{-2}$	$-.5166 \cdot 10^{-3}$		1	$-.6396 \cdot 10^{-3}$	$.7978 \cdot 10^{-3}$	$.6667 \cdot 10^{-3}$
	2	$.3425 \cdot 10^{-1}$	$-.2038 \cdot 10^{-2}$	$.5412 \cdot 10^{-3}$		2	$-.4143 \cdot 10^{-2}$	$.5649 \cdot 10^{-2}$	$-.5508 \cdot 10^{-4}$
	3	$.2830 \cdot 10^{-1}$	$-.9686 \cdot 10^{-3}$	$.2995 \cdot 10^{-3}$		3	$-.3708 \cdot 10^{-2}$	$.5227 \cdot 10^{-2}$	$.1462 \cdot 10^{-3}$
	4	$.3342 \cdot 10^{-2}$	$.5536 \cdot 10^{-2}$	$-.5538 \cdot 10^{-2}$		4	$-.4016 \cdot 10^{-2}$	$-.6414 \cdot 10^{-2}$	$-.8673 \cdot 10^{-3}$
C_0^2	5	$.1391 \cdot 10^{-1}$	$.7956 \cdot 10^{-3}$	$-.2012 \cdot 10^{-2}$	D_0^0	5	$-.3159 \cdot 10^{-2}$	$-.3022 \cdot 10^{-2}$	$-.9427 \cdot 10^{-3}$
	6	$.2375 \cdot 10^{-1}$	$.1775 \cdot 10^{-2}$	$.2675 \cdot 10^{-2}$		6	$-.7352 \cdot 10^{-2}$	$.1584 \cdot 10^{-1}$	$.2274 \cdot 10^{-2}$
	7	$-.3024 \cdot 10^{-1}$	$-.1924 \cdot 10^{-1}$	$.6680 \cdot 10^{-4}$		7	$-.1305 \cdot 10^{-2}$	$-.1363 \cdot 10^{-1}$	$.3488 \cdot 10^{-2}$
	8	$-.9323 \cdot 10^{-1}$	$-.2108 \cdot 10^{-2}$	$.2173 \cdot 10^{-2}$		8	$-.4523 \cdot 10^{-2}$	$.1960 \cdot 10^{-1}$	$.1146 \cdot 10^{-2}$
	9	$-.8813 \cdot 10^{-1}$	$.4251 \cdot 10^{-2}$	$-.2462 \cdot 10^{-2}$		9	$-.4581 \cdot 10^{-2}$	$-.2917 \cdot 10^{-3}$	$-.1778 \cdot 10^{-2}$
	10	$-.2679 \cdot 10^{-1}$	$-.3504 \cdot 10^{-2}$	$.1984 \cdot 10^{-2}$		10	$-.1272 \cdot 10^{-2}$	$-.4082 \cdot 10^{-2}$	$.1184 \cdot 10^{-2}$

Par.	z_i	a_i	b_i	c_i	Par.	z_i	a_i	b_i	c_i
	1	$.6607 \cdot 10^{-7}$	$-.1767 \cdot 10^{-6}$	$-.1271 \cdot 10^{-4}$		1	$.1980 \cdot 10^{-3}$	$.1510 \cdot 10^{-3}$	$-.2527 \cdot 10^{-4}$
	2	$-.1750 \cdot 10^{-4}$	$-.5895 \cdot 10^{-5}$	$-.8847 \cdot 10^{-6}$		2	$-.2572 \cdot 10^{-2}$	$-.5907 \cdot 10^{-4}$	$.1149 \cdot 10^{-4}$
	3	$-.6507 \cdot 10^{-5}$	$-.5144 \cdot 10^{-5}$	$-.1517 \cdot 10^{-5}$		3	$-.2024 \cdot 10^{-2}$	$-.2137 \cdot 10^{-4}$	$.1067 \cdot 10^{-4}$
	4	$-.3851 \cdot 10^{-5}$	$.1657 \cdot 10^{-4}$	$-.7559 \cdot 10^{-5}$		4	$.1600 \cdot 10^{-2}$	$.5689 \cdot 10^{-3}$	$-.2189 \cdot 10^{-3}$
D_1^1	5	$.4987 \cdot 10^{-6}$	$.2201 \cdot 10^{-5}$	$-.3089 \cdot 10^{-5}$	D_0^2	5	$.1790 \cdot 10^{-3}$	$.1280 \cdot 10^{-3}$	$-.7452 \cdot 10^{-4}$
	6	$.1953 \cdot 10^{-6}$	$-.3159 \cdot 10^{-4}$	$-.1827 \cdot 10^{-4}$		6	$.1228 \cdot 10^{-2}$	$-.3551 \cdot 10^{-4}$	$.9342 \cdot 10^{-4}$
	7	$-.2797 \cdot 10^{-4}$	$.3893 \cdot 10^{-5}$	$.1194 \cdot 10^{-5}$		7	$.9168 \cdot 10^{-3}$	$-.7961 \cdot 10^{-3}$	$-.1405 \cdot 10^{-3}$
	8	$.1604 \cdot 10^{-4}$	$-.5762 \cdot 10^{-4}$	$-.1570 \cdot 10^{-4}$		8	$.4960 \cdot 10^{-2}$	$-.1981 \cdot 10^{-3}$	$.7174 \cdot 10^{-4}$
	9	$-.1183 \cdot 10^{-4}$	$-.9919 \cdot 10^{-6}$	$.9930 \cdot 10^{-5}$		9	$.5225 \cdot 10^{-2}$	$.2966 \cdot 10^{-3}$	$-.8173 \cdot 10^{-4}$
	10	$-.7835 \cdot 10^{-5}$	$.2179 \cdot 10^{-4}$	$-.7949 \cdot 10^{-5}$		10	$.1550 \cdot 10^{-2}$	$-.1694 \cdot 10^{-3}$	$.6938 \cdot 10^{-4}$

We determine s_0^0, s_1^1 and s_0^2 by the conditions:

$$\delta_0^0(s_0) \equiv \theta_0 \ , \qquad \delta_1^1(s_0) \equiv \theta_1 \ , \qquad \delta_0^2(s_0) \equiv \theta_2 \tag{A.61}$$

where $\theta_2(a_0^0, a_0^2, \theta_0, \theta_1)$ is parametrised following eqs. (6.9) and (6.14), with the coefficients:

Par.	z_i	a_i	b_i	c_i
	1	$-.3160$	$.7038 \cdot 10^{-1}$	$-.2480 \cdot 10^{-1}$
	2	$-.2355$	$.2380 \cdot 10^{-1}$	$.6701 \cdot 10^{-2}$
	3	$-.2021$	$.1687 \cdot 10^{-1}$	$.5869 \cdot 10^{-2}$
	4	$.4885 \cdot 10^{-1}$	$.6057 \cdot 10^{-1}$	$-.2094 \cdot 10^{-1}$
θ_2	5	$-.1106 \cdot 10^{-1}$	$.2317 \cdot 10^{-1}$	$-.1128 \cdot 10^{-1}$
	6	$.8406 \cdot 10^{-2}$	$.7702 \cdot 10^{-1}$	$-.2254 \cdot 10^{-1}$
	7	$.3569 \cdot 10^{-2}$	$.1531$	$.1103$
	8	$.3021 \cdot 10^{-1}$	$.1027 \cdot 10^{-2}$	$-.4945 \cdot 10^{-2}$
	9	$.2762 \cdot 10^{-1}$	$.2859 \cdot 10^{-2}$	$-.1297 \cdot 10^{-1}$
	10	$.7229 \cdot 10^{-2}$	$.1513 \cdot 10^{-1}$	$.1340 \cdot 10^{-1}$

We have introduced the function $\theta_2(a_0^0, a_0^2, \theta_0, \theta_1)$ to improve the accuracy on s_0^2. The dependence of θ_2 on the S-wave scattering lengths and on the phases at the matching point is smoother than the analogous dependence of s_0^2. A direct fit of s_0^2 using the form of eqs. (6.9) and (6.14) would therefore induce a loss of accuracy, compared to the procedure we follow here.

A.4.2 Parametrisation of isospin-breaking corrections [J]

We can parametrise Δ, i.e., the isospin breaking in $\delta_s - \delta_p$ with a good accuracy as a polynomial in

$$\Delta = \sum c_{ijklm} \left(\frac{s-4M_{\pi^\pm}^2}{M_{\pi^\pm}^2}\right)^{i-1/2} \left(\frac{\sqrt{\lambda(s,s_\ell,M_K^2)}}{M_K^2}\right)^{j-1} \left(\frac{a_0^0}{0.225}-1\right)^k \left(\frac{a_0^2}{-0.0382}-1\right)^l \left(\frac{37}{R}-1\right)^m ,$$
$$\text{with } i=0\ldots4, \quad j=0\ldots3, \quad k=0\ldots2, \quad l=0\ldots2, \quad m=0\ldots1\,, \tag{A.62}$$

where $\lambda(x,y,z) = x^2+y^2+z^2-2xy-2yz-2xz$ denotes the Källen function, and the coefficients are collected in tabs. A.5 and A.6. The remaining uncertainty coming from our pour knowledge of the low-energy constants can be parametrised as a quadratic function of $(s-4M_{\pi^\pm}^2)/M_{\pi^\pm}^2$:

$$\delta\Delta = \sum_{n=0\ldots2} d_n \left(\frac{s-4M_{\pi^\pm}^2}{M_{\pi^\pm}^2}\right)^n , \tag{A.63}$$

with

$$d_0 = 0.733278, \qquad d_1 - 0.0457505, \qquad d_2 = 0.0132922 \tag{A.64}$$

We obtained these coefficients by computing Δ for a large sample of $(s, s_\ell, a_0^0, a_0^2, R)$ in the kinematic range allowed for s and s_ℓ and for

$$0.16 \le a_0^0 \le 0.3\,, \qquad -0.06 \le a_0^2 \le -0.02\,, \qquad 25 \le R \le 50\,, \tag{A.65}$$

keeping the low-energy constants at their central values, then we performed a polynomial fit of these points [1]. The difference between the fitted value of Δ and its actual value remained always smaller than 0.5 mrad (i.e. small compared to the uncertainties coming from the low-energy constants). In the case of the $\delta\Delta$, we performed a similar analysis, adding in quadrature the uncertainties from the various low-energy constants when the latter are varied in their ranges indicated in Tab. 6.4. The difference between the fitted value of $\delta\Delta$ and its actual value remained below the 1% level.

A.5 Three-flavour chiral symmetry breaking according to $\pi\pi$ and πK scatterings

A.5.1 Computation of the amplitudes [M]

The amplitudes are smooth functions of the various experimental inputs. This means in particular that there will be significant correlations among the value of the same scattering amplitude at different points in the Mandelstam plane. We compute these correlations according to the following procedure. Let us call a_k $(k = 1\ldots n)$ the parameters describing the variations of the experimental inputs. To each of these parameters is attached an uncertainty (σ_k), and the correlations among them are encoded in a covariance matrix D_{kl}, or equivalently, a reduced covariance matrix $H_{kl} = D_{kl}/(\sigma_k\sigma_l)$. We compute the mean value m_i of the observables x_i's by setting all the parameters a_k to their central value $\bar{a}_k$: $m_i \equiv x_i(\bar{a}_k)$. Then, we vary the parameters one by one (the others being kept at their central value) and compute each time:

$$\Delta_i^k \equiv x_i\left(\bar{a}_k + \frac{\sigma_k}{\rho}\right) - m_i = \frac{\sigma_k}{\rho} \times \frac{\partial x_i}{\partial a_k} + \ldots \tag{A.66}$$

[1] We also varied the πK scattering lengths, but the impact on Δ was small compared to the error coming from the LECs in $\delta\Delta$, and could be well accommodated by a constant.

j	k	l	m	c_{0jklm}	c_{1jklm}	c_{2jklm}	c_{3jklm}	c_{4jklm}
0	0	0	0	0.00408075	-0.037109	0.0256052	-0.00102641	-0.000132779
0	0	0	1	-0.000396782	0.00515833	-0.00317269	0.000557488	-0.0000301507
0	0	1	0	0.00172858	-0.0207691	0.01245	-0.00121942	0.0000157535
0	0	1	1	-0.00019949	0.00278162	-0.00169132	0.000295475	-0.0000159236
0	0	2	0	-0.000352405	0.00506193	-0.00304836	0.000529188	-0.0000283819
0	0	2	1	0	-0.0000919988	0.0000555492	0	0
0	1	0	0	0.00222772	-0.0143104	0.0117905	0.000543864	-0.000173075
0	1	0	1	-0.000285096	0.00363627	-0.00224116	0.000394058	-0.000021315
0	1	1	0	0.000543846	-0.00781044	0.0047014	-0.000815728	0.0000437279
0	1	1	1	-0.0000270461	0.000388231	-0.000233305	0.0000404037	0
0	2	0	0	-0.000034258	0.000490918	-0.000293745	0.0000506198	0
0	2	0	1	-0.0000419505	0.000602546	-0.000363017	0.0000630481	0
1	0	0	0	5.6326	5.69856	-0.520896	-0.0475999	0.00402889
1	0	0	1	0.00296164	1.08293	0.0539793	-0.0281812	0.000987649
1	0	1	0	0.809083	5.49273	-0.668947	0.0206698	-0.00025277
1	0	1	1	0.00144958	0.104885	0.0505555	-0.0108245	0.000450808
1	0	2	0	0.00244321	-0.0329271	0.0844347	-0.0139556	0.000592634
1	0	2	1	-0.0000461274	-0.00548283	-0.00612487	0.000957791	-0.0000161492
1	1	0	0	4.82437	-2.38606	-0.0246789	-0.0842424	0.00494047
1	1	0	1	0.00212653	0.667555	-0.0261395	-0.0149657	0.000666723
1	1	1	0	-0.00374025	0.0371545	-0.271428	0.0228138	-0.000890091
1	1	1	1	0.000181815	-0.0752042	-0.0129246	0.00209766	0.0000233248
1	2	0	0	0.000209764	-0.27961	-0.0121203	0.000602476	0.0000343068
1	2	0	1	0.000294063	-0.227759	-0.0118032	0.00170368	0.0000557709

Table A.5: *First part of the coefficients for the parametrisation of the isospin-breaking correction* Δ.

where ρ is a largish parameter (around 10), and the ellipsis denotes higher derivatives. Once this is done for all the parameters, we compute the covariance matrix for the observables:

$$V_{ij} \equiv \rho^2 \sum_{kl} \Delta_i^k \Delta_j^l H_{kl} = \sum_{kl} \frac{\partial x_i}{\partial a_k} \frac{\partial x_j}{\partial a_l} D_{kl} + \dots \tag{A.67}$$

A.5.2 Treatment of correlated data [M]

We expect strong correlations among the data points. This is reflected by the fact that the covariance matrix C in eq. (8.26) is nearly degenerate, and therefore cannot be inverted easily. In order to treat this problem, one can diagonalize the matrix C:

$$C = UDU^T\,, \qquad D = \mathrm{diag}(\lambda_1, \dots, \lambda_n)\,, \qquad UU^T = U^T U = 1\,, \tag{A.68}$$

j	k	l	m	c_{0jklm}	c_{1jklm}	c_{2jklm}	c_{3jklm}	c_{4jklm}
2	0	0	0	0.064777	-0.329443	-0.752549	0.329432	-0.00493116
2	0	0	1	-0.00810965	0.0703793	0.0122972	-0.0184276	0.00181876
2	0	1	0	0.0300777	-0.241158	-0.216191	0.117539	-0.00435461
2	0	1	1	-0.00398709	0.0424437	0.00454033	-0.0093948	0.000937616
2	0	2	0	-0.00694273	0.0798882	0.00793341	-0.0168085	0.00165269
2	0	2	1	0.000127674	-0.00148408	-0.000112044	0.000299676	-0.0000300626
2	1	0	0	0.0317176	-0.0418002	-0.556006	0.21019	0.000438524
2	1	0	1	-0.00585148	0.0477542	0.00972068	-0.0132276	0.00129526
2	1	1	0	0.0106913	-0.122801	-0.0126945	0.0260116	-0.00254856
2	1	1	1	-0.00052736	0.00601697	0.000719098	-0.00130958	0.000126754
2	2	0	0	-0.000654829	0.00734259	0.00116208	-0.00169482	0.000158666
2	2	0	1	-0.000827849	0.00953291	0.000922877	-0.00199909	0.0001972
3	0	0	0	-0.0551633	0.236287	0.14803	0.226778	-0.105781
3	0	0	1	0.00676711	-0.130306	0.00598503	0.00302712	0.00143925
3	0	1	0	-0.0253551	0.217623	0.019838	0.0600479	-0.0308006
3	0	1	1	0.00334818	-0.047997	0.000649354	0.00174378	0.00075468
3	0	2	0	0.00592331	-0.074042	0.0092368	0	0.00172281
3	0	2	1	-0.000107209	0.00133079	-0.000117648	-0.0000316854	-0.0000264796
3	1	0	0	-0.0273058	-0.0202905	0.135118	0.17567	-0.0771778
3	1	0	1	0.00488996	-0.100599	0.00674336	0.00154108	0.00108788
3	1	1	0	-0.00914914	0.114557	-0.0150928	0.000509847	-0.00273471
3	1	1	1	0.000455604	-0.00572319	0.000868521	-0.000103778	0.000148124
3	2	0	0	0.000583594	-0.00747208	0.00166134	-0.000459851	0.000235585
3	2	0	1	0.000703795	-0.008788	0.00101315	0.0000467118	0.000198545

Table A.6: *Second part of the coefficients for the parametrisation of the isospin-breaking correction* Δ.

which yields the corresponding likelihood:

$$\mathcal{L}(\Delta V) = \exp\left[-\frac{1}{2}\Delta V^T\ C^{-1}\ \Delta V\right] / \sqrt{\det(2\pi C)} \tag{A.69}$$

$$= \exp\left[-\frac{1}{2}\Delta V^T\ U D^{-1} U^T\ \Delta V\right] / \sqrt{\det(2\pi C)}\,. \tag{A.70}$$

Let us split the set of eigenvalues in two categories: large eigenvalues of order 1, collected in the diagonal matrix $\tilde{D}$, and almost vanishing eigenvalues, smaller than a cut-off and gathered in the diagonal matrix D_0:

$$D = \tilde{D} + D_0\,, \qquad \tilde{C} = U\tilde{D}U^T\,, \qquad C_0 = UD_0U^T\,. \tag{A.71}$$

The eigenvalues in D_0 are responsible for the near degeneracy of the matrix. In the corresponding directions, the exponential could be approximated with a Dirac distribution and

would yield constrains on NNLO and higher-order remainders. Our approximation by a low-degree polynomial is expected to hold at the level of a few percent: numerically, a perfect agreement between data and experiment occurs already if $\Delta V = O(1\%)$. Therefore, we cannot make much use of eigenvalues of the covariance matrix much smaller than $(1\%)^2 = 10^{-4}$. This leads us to limit the analysis to the subspace where $\tilde{D}$ is non-vanishing, and to define on this subspace $D^{-1} \equiv \tilde{D}^{-1}$ (see ch. 2.6 in ref. [448] for a more detailed discussion on the relationships between singular value decomposition and matrix inversion). We chose to set the limit between small and large eigenvalues of order 10^{-8} (with only a very mild dependence of our results on the exact value of the cutoff).

B
Bibliography

Bibliography

[1] C. Itzykson and J. Zuber, *Quantum Field Theory*, . New York, USA: Mcgraw-hill (1980) 705 p. (International Series In Pure and Applied Physics).

[2] M. E. Peskin and D. V. Schroeder, *An Introduction to quantum field theory*, . Reading, USA: Addison-Wesley (1995) 842 p.

[3] S. Weinberg, *The Quantum theory of fields. Vol. 1: Foundations*, . Cambridge, UK: Univ. Pr. (1995) 609 p.

[4] A. Pich, *The Standard model of electroweak interactions*, arXiv:0705.4264.

[5] **ALEPH** Collaboration, *et. al.*, *Precision Electroweak Measurements and Constraints on the Standard Model*, arXiv:1012.2367.

[6] M. Davier, A. Hoecker, B. Malaescu, and Z. Zhang, *Reevaluation of the Hadronic Contributions to the Muon $g-2$ and to $\alpha(M_Z)$*, *Eur.Phys.J.* **C71** (2011) 1515, [arXiv:1010.4180].

[7] M. Knecht and A. Nyffeler, *Hadronic light by light corrections to the muon g-2: The Pion pole contribution*, *Phys.Rev.* **D65** (2002) 073034, [hep-ph/0111058].

[8] M. Knecht, A. Nyffeler, M. Perrottet, and E. de Rafael, *Hadronic light by light scattering contribution to the muon g-2: An Effective field theory approach*, *Phys.Rev.Lett.* **88** (2002) 071802, [hep-ph/0111059].

[9] M. Knecht, S. Peris, M. Perrottet, and E. De Rafael, *Electroweak hadronic contributions to the muon (g-2)*, *JHEP* **0211** (2002) 003, [hep-ph/0205102].

[10] D. Gross and F. Wilczek, *Ultraviolet Behavior of Nonabelian Gauge Theories*, *Phys.Rev.Lett.* **30** (1973) 1343–1346.

[11] D. Gross and F. Wilczek, *Asymptotically Free Gauge Theories. 1.*, *Phys.Rev.* **D8** (1973) 3633–3652.

[12] D. Gross and F. Wilczek, *Asymptotically Free Gauge Theories. 2.*, *Phys.Rev.* **D9** (1974) 980–993.

[13] H. Politzer, *Asymptotic Freedom: An Approach to Strong Interactions*, *Phys.Rept.* **14** (1974) 129–180.

[14] **CKMfitter Group** Collaboration, J. Charles *et. al.*, *CP violation and the CKM matrix: Assessing the impact of the asymmetric B factories*, *Eur.Phys.J.* **C41** (2005) 1–131, [hep-ph/0406184].

[15] R. Chivukula, *Models of electroweak symmetry breaking: Course*, hep-ph/9803219.

[16] K. Lane, *Two lectures on technicolor*, hep-ph/0202255.

[17] A. Nyffeler and A. Schenk, *The Electroweak chiral Lagrangian reanalyzed*, *Phys.Rev.* **D62** (2000) 113006, [hep-ph/9907294].

[18] S. Weinberg, *Phenomenological Lagrangians*, *Physica* **A96** (1979) 327. Festschrift honoring Julian Schwinger on his 60th birthday.

[19] A. Pich, *Effective field theory*, hep-ph/9806303.

[20] J. Gasser and H. Leutwyler, *Chiral Perturbation Theory to One Loop*, *Annals Phys.* **158** (1984) 142.

[21] J. Gasser and H. Leutwyler, *Chiral Perturbation Theory: Expansion in the Mass of the Strange Quark*, *Nucl.Phys.* **B250** (1985) 465.

[22] U. G. Meißner, *Recent developments in chiral perturbation theory*, *Rept.Prog.Phys.* **56** (1993) 903–996, [hep-ph/9302247].

[23] G. Ecker, J. Gasser, A. Pich, and E. de Rafael, *The Role of Resonances in Chiral Perturbation Theory*, *Nucl.Phys.* **B321** (1989) 311.

[24] M. Knecht and A. Nyffeler, *Resonance estimates of O(p**6) low-energy constants and QCD short distance constraints*, *Eur.Phys.J.* **C21** (2001) 659–678, [hep-ph/0106034].

[25] V. Cirigliano, G. Ecker, M. Eidemuller, A. Pich, and J. Portoles, *The Green function in the resonance region*, *Phys. Lett.* **B596** (2004) 96–106, [hep-ph/0404004].

[26] I. Rosell, J. J. Sanz-Cillero, and A. Pich, *Towards a determination of the chiral couplings at NLO in $1/N_c$: $L_8^r(\mu)$*, *JHEP* **01** (2007) 039, [hep-ph/0610290].

[27] V. Cirigliano *et. al.*, *Towards a consistent estimate of the chiral low-energy constants*, *Nucl. Phys.* **B753** (2006) 139–177, [hep-ph/0603205].

[28] A. Pich, I. Rosell, and J. J. Sanz-Cillero, *Form-factors and current correlators: chiral couplings $L_{10}(\mu)$ and $C_{87}(\mu)$ at NLO in $1/N_c$*, *JHEP* **07** (2008) 014, [arXiv:0803.1567].

[29] J. Bijnens and J. Prades, *Two and three point functions in the extended NJL model*, *Z.Phys.* **C64** (1994) 475–494, [hep-ph/9403233].

[30] J. Bijnens, *Chiral Lagrangians and Nambu-Jona-Lasinio - like models*, *Phys.Rept.* **265** (1996) 369–446, [hep-ph/9502335].

[31] J. Erlich, E. Katz, D. T. Son, and M. A. Stephanov, *QCD and a holographic model of hadrons*, *Phys.Rev.Lett.* **95** (2005) 261602, [hep-ph/0501128].

[32] L. Da Rold and A. Pomarol, *The Scalar and pseudoscalar sector in a five-dimensional approach to chiral symmetry breaking*, *JHEP* **0601** (2006) 157, [hep-ph/0510268].

[33] M. Knecht, S. Peris, and E. de Rafael, *On Anomaly Matching and Holography*, arXiv:1101.0706.

[34] S. Descotes-Genon, L. Girlanda, and J. Stern, *Paramagnetic effect of light quark loops on chiral symmetry breaking*, *JHEP* **0001** (2000) 041, [hep-ph/9910537].

[35] S. Descotes-Genon and J. Stern, *Finite volume analysis of N_f induced chiral phase transitions*, *Phys.Rev.* **D62** (2000) 054011, [hep-ph/9912234].

[36] S. Descotes-Genon and J. Stern, *Vacuum fluctuations of $\bar{q}q$ and values of low-energy constants*, *Phys.Lett.* **B488** (2000) 274–282, [hep-ph/0007082].

[37] S. Descotes-Genon, L. Girlanda, and J. Stern, *Chiral order and fluctuations in multiflavor QCD*, *Eur.Phys.J.* **C27** (2003) 115–134, [hep-ph/0207337].

[38] S. Descotes-Genon, N. Fuchs, L. Girlanda, and J. Stern, *Resumming QCD vacuum fluctuations in three flavor chiral perturbation theory*, *Eur.Phys.J.* **C34** (2004) 201–227, [hep-ph/0311120].

[39] S. Descotes-Genon, *Zweig rule violation in the scalar sector and values of low-energy constants*, *JHEP* **0103** (2001) 002, [hep-ph/0012221].

[40] S. Descotes-Genon, *The Role of strange sea quarks in chiral extrapolations on the lattice*, *Eur.Phys.J.* **C40** (2005) 81–96, [hep-ph/0410233].

[41] V. Bernard, S. Descotes-Genon, and G. Toucas, *Chiral dynamics with strange quarks in the light of recent lattice simulations*, *JHEP* **1101** (2011) 107, [arXiv:1009.5066].

[42] S. Descotes-Genon, N. Fuchs, L. Girlanda, and J. Stern, *Analysis and interpretation of new low-energy $\pi\pi$ scattering data*, *Eur.Phys.J.* **C24** (2002) 469–483, [hep-ph/0112088].

[43] V. Bernard, S. Descotes-Genon, and M. Knecht. work in progress.

[44] P. Buettiker, S. Descotes-Genon, and B. Moussallam, *A new analysis of πK scattering from Roy and Steiner type equations*, *Eur.Phys.J.* **C33** (2004) 409–432, [hep-ph/0310283].

[45] S. Descotes-Genon and B. Moussallam, *The $K_0^*(800)$ scalar resonance from Roy-Steiner representations of πK scattering*, *Eur.Phys.J.* **C48** (2006) 553, [hep-ph/0607133].

[46] S. Descotes-Genon, *Low-energy $\pi\pi$ and πK scatterings revisited in three-flavour resummed chiral perturbation theory*, *Eur.Phys.J.* **C52** (2007) 141–158, [hep-ph/0703154].

[47] M. Gell-Mann, *A Schematic Model of Baryons and Mesons*, *Phys.Lett.* **8** (1964) 214–215.

[48] G. Zweig, *An $SU(3)$ model for strong interaction symmetry and its breaking. 2.*, . Published in 'Developments in the Quark Theory of Hadrons'. Volume 1. Edited by D. Lichtenberg and S. Rosen. Nonantum, Mass., Hadronic Press, 1980. pp. 22-101.

[49] M. Han and Y. Nambu, *Three Triplet Model with Double $SU(3)$ Symmetry*, *Phys.Rev.* **139** (1965) B1006–B1010.

[50] O. Greenberg, *Spin and Unitary Spin Independence in a Paraquark Model of Baryons and Mesons*, *Phys.Rev.Lett.* **13** (1964) 598–602.

[51] H. Fritzsch, M. Gell-Mann, and H. Leutwyler, *Advantages of the Color Octet Gluon Picture*, *Phys.Lett.* **B47** (1973) 365–368. Introduces the term 'color'.

[52] J. Callan, Curtis G., R. F. Dashen, and D. J. Gross, *The structure of the gauge theory vacuum*, *Phys. Lett.* **B63** (1976) 334–340.

[53] R. Jackiw and C. Rebbi, *Vacuum periodicity in a Yang-Mills quantum theory*, *Phys. Rev. Lett.* **37** (1976) 172–175.

[54] B. Borasoy, *The electric dipole moment of the neutron in chiral perturbation theory*, *Phys. Rev.* **D61** (2000) 114017, [hep-ph/0004011].

[55] R. D. Peccei and H. R. Quinn, *CP Conservation in the Presence of Instantons*, *Phys. Rev. Lett.* **38** (1977) 1440–1443.

[56] R. D. Peccei and H. R. Quinn, *Constraints Imposed by CP Conservation in the Presence of Instantons*, *Phys. Rev.* **D16** (1977) 1791–1797.

[57] Y. Nambu, *Quasiparticles and Gauge Invariance in the Theory of Superconductivity*, *Phys.Rev.* **117** (1960) 648–663.

[58] Y. Nambu, *Axial vector current conservation in weak interactions*, *Phys.Rev.Lett.* **4** (1960) 380–382.

[59] Y. Nambu and G. Jona-Lasinio, *Dynamical Model of Elementary Particles Based on an Analogy with Superconductivity. 1.*, *Phys.Rev.* **122** (1961) 345–358.

[60] Y. Nambu and G. Jona-Lasinio, *Dynamical Model of Elementary Particles Based on an Analogy with Superconductivity. 2*, *Phys.Rev.* **124** (1961) 246–254.

[61] S. Glashow and S. Weinberg, *Breaking chiral symmetry*, *Phys.Rev.Lett.* **20** (1968) 224–227.

[62] J. Goldstone, *Field Theories with Superconductor Solutions*, *Nuovo Cim.* **19** (1961) 154–164.

[63] J. Goldstone, A. Salam, and S. Weinberg, *Broken Symmetries*, *Phys.Rev.* **127** (1962) 965–970.

[64] C. Vafa and E. Witten, *Restrictions on Symmetry Breaking in Vector-Like Gauge Theories*, *Nucl. Phys.* **B234** (1984) 173.

[65] D. Weingarten, *Mass Inequalities for QCD*, *Phys.Rev.Lett.* **51** (1983) 1830. Second revised version.

[66] G. 't Hooft *et. al.*, *Recent Developments in Gauge Theories. Proceedings, Nato Advanced Study Institute, Cargese, France, August 26 - September 8, 1979*, . New York, Usa: Plenum (1980) 438 p. (Nato Advanced Study Institutes Series: Series B, Physics, 59).

[67] C. Vafa and E. Witten, *Eigenvalue inequalities for fermions in gauge theories*, *Commun. Math. Phys.* **95** (1984) 257.

[68] S. Weinberg, *The quantum theory of fields. Vol. 2: Modern applications*, . Cambridge, UK: Univ. Pr. (1996) 489 p.

[69] C. P. Burgess, *Goldstone and pseudo-Goldstone bosons in nuclear, particle and condensed-matter physics*, *Phys. Rept.* **330** (2000) 193–261, [hep-th/9808176].

[70] H. Leutwyler, *Principles of chiral perturbation theory*, hep-ph/9406283.

[71] M. A. Shifman, A. Vainshtein, and V. I. Zakharov, *QCD and Resonance Physics. Sum Rules*, *Nucl.Phys.* **B147** (1979) 385–447.

[72] E. de Rafael, *An Introduction to sum rules in QCD: Course*, hep-ph/9802448.

[73] V. Novikov, M. A. Shifman, A. Vainshtein, and V. I. Zakharov, *Are All Hadrons Alike?*, *Nucl.Phys.* **B191** (1981) 301.

[74] H. Leutwyler and A. V. Smilga, *Spectrum of Dirac operator and role of winding number in QCD*, *Phys. Rev.* **D46** (1992) 5607–5632.

[75] L. D. Faddeev and A. A. Slavnov, *Gauge fields. Introduction to quantum theory*, *Front. Phys.* **50** (1980) 1–232.

[76] A. V. Smilga, *Lectures on the foundations of QCD*, hep-ph/9901412.

[77] M. F. Atiyah and I. M. Singer, *Dirac Operators Coupled to Vector Potentials*, *Proc. Nat. Acad. Sci.* **81** (1984) 2597–2600.

[78] J. Schwinger, *The Theory of Quantized Fields. 5*, *Phys. Rev.* **93** (1954) 615–628.

[79] H. Hogreve, R. Schrader, and R. Seiler, *A conjecture on the spinor functional determinant*, *Nucl. Phys.* **B142** (1978) 525.

[80] D. Brydges, J. Frohlich, and E. Seiler, *On the construction of quantized gauge fields. I. General results*, *Annals Phys.* **121** (1979) 227–284.

[81] R. Schrader and R. Seiler, *A uniform lower bound on the renormalized scalar euclidean functional determinant*, *Commun. Math. Phys.* **61** (1978) 169.

[82] G. Colangelo *et. al.*, *Review of lattice results concerning low energy particle physics*, arXiv:1011.4408.

[83] L. Lellouch, *Flavor physics and lattice quantum chromodynamics*, arXiv:1104.5484.

[84] J. Stern, *Two alternatives of spontaneous chiral symmetry breaking in QCD*, hep-ph/9801282.

[85] T. Banks and A. Casher, *Chiral Symmetry Breaking in Confining Theories*, *Nucl. Phys.* **B169** (1980) 103.

[86] A. V. Smilga and J. Stern, *On the spectral density of Euclidean Dirac operator in QCD*, *Phys. Lett.* **B318** (1993) 531–536.

[87] J. Gasser and H. Leutwyler, *Light Quarks at Low Temperatures*, *Phys.Lett.* **B184** (1987) 83.

[88] J. Gasser and H. Leutwyler, *Thermodynamics of Chiral Symmetry*, *Phys.Lett.* **B188** (1987) 477.

[89] J. Gasser and H. Leutwyler, *Spontaneously Broken Symmetries: Effective Lagrangians at Finite Volume*, *Nucl.Phys.* **B307** (1988) 763.

[90] J. Verbaarschot, *QCD, chiral random matrix theory and integrability*, hep-th/0502029.

[91] M. Stephanov, J. Verbaarschot, and T. Wettig, *Random matrices*, hep-ph/0509286. Article originally published in the Wiley Encyclopedia of Electrical and Electronics Engineering, Supplement 1 (2001).

[92] J. Verbaarschot and T. Wettig, *Random matrix theory and chiral symmetry in QCD*, *Ann.Rev.Nucl.Part.Sci.* **50** (2000) 343–410, [hep-ph/0003017].

[93] **JLQCD Collaboration, TWQCD** Collaboration, T. Chiu *et. al.*, *Topological susceptibility in (2+1)-flavor lattice QCD with overlap fermion*, *PoS* **LATTICE2008** (2008) 072, [arXiv:0810.0085].

[94] **TWQCD** Collaboration, T.-W. Chiu, T.-H. Hsieh, and P.-K. Tseng, *Topological susceptibility in 2+1 flavors lattice QCD with domain-wall fermions*, *Phys.Lett.* **B671** (2009) 135–138, [arXiv:0810.3406].

[95] A. Bazavov, D. Toussaint, C. Bernard, J. Laiho, C. DeTar, *et. al.*, *Nonperturbative QCD simulations with 2+1 flavors of improved staggered quarks*, *Rev.Mod.Phys.* **82** (2010) 1349–1417, [arXiv:0903.3598].

[96] **MILC** Collaboration, A. Bazavov *et. al.*, *Topological susceptibility with the asqtad action*, *Phys.Rev.* **D81** (2010) 114501, [arXiv:1003.5695].

[97] T.-W. Chiu, T.-H. Hsieh, and Y.-Y. Mao, *Topological Susceptibility in Two Flavors Lattice QCD with the Optimal Domain-Wall Fermion*, *Phys.Lett.* **B702** (2011) 131–134, [arXiv:1105.4414].

[98] S. Aoki, H. Fukaya, S. Hashimoto, and T. Onogi, *Finite volume QCD at fixed topological charge*, *Phys.Rev.* **D76** (2007) 054508, [arXiv:0707.0396].

[99] P. H. Damgaard and H. Fukaya, *The Chiral Condensate in a Finite Volume*, *JHEP* **0901** (2009) 052, [arXiv:0812.2797].

[100] S. Aoki and H. Fukaya, *Chiral perturbation theory in a theta vacuum*, *Phys.Rev.* **D81** (2010) 034022, [arXiv:0906.4852].

[101] **TWQCD** Collaboration, Y.-Y. Mao and T.-W. Chiu, *Topological Susceptibility to the One-Loop Order in Chiral Perturbation Theory*, *Phys.Rev.* **D80** (2009) 034502, [arXiv:0903.2146].

[102] **JLQCD and TWQCD** Collaboration, H. Fukaya *et. al.*, *Determination of the chiral condensate from QCD Dirac spectrum on the lattice*, *Phys. Rev.* **D83** (2011) 074501, [arXiv:1012.4052].

[103] K. G. Chetyrkin, J. H. Kuhn, and A. Kwiatkowski, *QCD corrections to the e+ e- cross-section and the Z boson decay rate: Concepts and results*, *Phys. Rept.* **277** (1996) 189–281.

[104] G. 't Hooft, *A Planar Diagram Theory for Strong Interactions*, *Nucl.Phys.* **B72** (1974) 461.

[105] G. Veneziano, *Some Aspects of a Unified Approach to Gauge, Dual and Gribov Theories*, *Nucl.Phys.* **B117** (1976) 519–545.

[106] E. Witten, *Current Algebra Theorems for the U(1) Goldstone Boson*, *Nucl. Phys.* **B156** (1979) 269.

[107] E. Witten, *Baryons in the 1/n Expansion*, *Nucl.Phys.* **B160** (1979) 57.

[108] M. Knecht and E. de Rafael, *Patterns of spontaneous chiral symmetry breaking in the large N_c limit of QCD-like theories*, *Phys. Lett.* **B424** (1998) 335–342, [hep-ph/9712457].

[109] M. Golterman and S. Peris, *Large-N_c QCD meets Regge theory: The example of spin-one two-point functions*, *JHEP* **01** (2001) 028, [hep-ph/0101098].

[110] M. Golterman, S. Peris, B. Phily, and E. De Rafael, *Testing an approximation to large-N_c QCD with a toy model*, *JHEP* **01** (2002) 024, [hep-ph/0112042].

[111] E. de Rafael, *Analytic approaches to kaon physics*, *Nucl. Phys. Proc. Suppl.* **119** (2003) 71–83, [hep-ph/0210317].

[112] V. Cirigliano, G. Ecker, H. Neufeld, and A. Pich, *Meson resonances, large N_c and chiral symmetry*, *JHEP* **0306** (2003) 012, [hep-ph/0305311].

[113] M. Golterman and S. Peris, *On the relation between low-energy constants and resonance saturation*, *Phys. Rev.* **D74** (2006) 096002, [hep-ph/0607152].

[114] P. Masjuan, S. Peris, and J. J. Sanz-Cillero, *Vector Meson Dominance as a first step in a systematic approximation: the pion vector form factor*, arXiv:0807.4893.

[115] B. Moussallam, *A sum rule approach to the violation of Dashen's theorem*, *Nucl. Phys.* **B504** (1997) 381–414, [hep-ph/9701400].

[116] G. Ecker, J. Gasser, H. Leutwyler, A. Pich, and E. de Rafael, *Chiral Lagrangians for Massive Spin 1 Fields*, *Phys. Lett.* **B223** (1989) 425.

[117] B. Ananthanarayan and B. Moussallam, *Electromagnetic corrections in the anomaly sector*, *JHEP* **05** (2002) 052, [hep-ph/0205232].

[118] B. Ananthanarayan and B. Moussallam, *Four-point correlator constraints on electromagnetic chiral parameters and resonance effective Lagrangians*, *JHEP* **06** (2004) 047, [hep-ph/0405206].

[119] S. Descotes-Genon and B. Moussallam, *Radiative corrections in weak semi-leptonic processes at low energy: A Two-step matching determination*, *Eur.Phys.J.* **C42** (2005) 403–417, [hep-ph/0505077].

[120] J. J. Sanz-Cillero and A. Pich, *Rho meson properties in the chiral theory framework*, *Eur. Phys. J.* **C27** (2003) 587–599, [hep-ph/0208199].

[121] A. Pich and J. Portoles, *Vector form factor of the pion: A model-independent approach*, *Nucl. Phys. Proc. Suppl.* **121** (2003) 179–182, [hep-ph/0209224].

[122] P. D. Ruiz-Femenia, A. Pich, and J. Portoles, *Phenomenology of the Green's function within the resonance chiral theory*, *Nucl. Phys. Proc. Suppl.* **133** (2004) 215–218, [hep-ph/0309345].

[123] J. J. Sanz-Cillero and A. Pich, *Rho meson properties*, *Nucl. Phys. Proc. Suppl.* **133** (2004) 219–222, [hep-ph/0310174].

[124] I. Rosell, J. J. Sanz-Cillero, and A. Pich, *Quantum loops in the resonance chiral theory: The vector form factor*, *JHEP* **08** (2004) 042, [hep-ph/0407240].

[125] D. Dumm, P. Roig, A. Pich, and J. Portoles, *Hadron structure in $\tau \to KK\pi\nu_\tau$ decays*, *Phys.Rev.* **D81** (2010) 034031, [arXiv:0911.2640].

[126] D. Dumm, P. Roig, A. Pich, and J. Portoles, *$\tau \to \pi\pi\pi\nu_{tau}$ decays and the $a_1(1260)$ off-shell width revisited*, *Phys.Lett.* **B685** (2010) 158–164, [arXiv:0911.4436].

[127] **PACS-CS** Collaboration, S. Aoki *et. al.*, *2+1 Flavor Lattice QCD toward the Physical Point*, *Phys.Rev.* **D79** (2009) 034503, [arXiv:0807.1661].

[128] C. Bernard, C. E. DeTar, L. Levkova, S. Gottlieb, U. Heller, *et. al.*, *Status of the MILC light pseudoscalar meson project*, *PoS* **LAT2007** (2007) 090, [arXiv:0710.1118].

[129] **The MILC** Collaboration, A. Bazavov *et. al.*, *Results from the MILC collaboration's SU(3) chiral perturbation theory analysis*, *PoS* **LAT2009** (2009) 079, [arXiv:0910.3618].

[130] U.-G. Meißner and J. Oller, *$J/\psi \to \phi\pi\pi(K\bar{K})$ decays, chiral dynamics and OZI violation*, *Nucl.Phys.* **A679** (2001) 671–697, [hep-ph/0005253].

[131] T. A. Lahde and U.-G. Meißner, *Improved Analysis of J/ψ Decays into a Vector Meson and Two Pseudoscalars*, *Phys.Rev.* **D74** (2006) 034021, [hep-ph/0606133].

[132] M. Pennington, *Light 0^{++} Mesons: Scalargators in Florida*, *AIP Conf.Proc.* **1257** (2010) 27–36, [arXiv:1003.2549].

[133] I. Caprini, G. Colangelo, and H. Leutwyler, *Mass and width of the lowest resonance in QCD*, *Phys.Rev.Lett.* **96** (2006) 132001, [hep-ph/0512364].

[134] J. Ruiz de Elvira, J. Pelaez, M. Pennington, and D. Wilson, *Chiral Perturbation Theory, the $1/N_c$ expansion and Regge behaviour determine the structure of the lightest scalar meson*, arXiv:1009.6204.

[135] M. Doring, U.-G. Meißner, E. Oset, and A. Rusetsky, *Unitarized Chiral Perturbation Theory in a finite volume: Scalar meson sector*, arXiv:1107.3988.

[136] V. Bernard, M. Lage, U.-G. Meißner, and A. Rusetsky, *Scalar mesons in a finite volume*, *JHEP* **1101** (2011) 019, [arXiv:1010.6018].

[137] **Particle Data Group** Collaboration, K. Nakamura *et. al.*, *Review of particle physics*, *J.Phys.G* **G37** (2010) 075021.

[138] C. Amsler and N. Tornqvist, *Mesons beyond the naive quark model*, *Phys.Rept.* **389** (2004) 61–117.

[139] T. Banks and A. Zaks, *On the Phase Structure of Vector-Like Gauge Theories with Massless Fermions*, *Nucl. Phys.* **B196** (1982) 189.

[140] Z.-y. Duan, P. S. Rodrigues da Silva, and F. Sannino, *Enhanced global symmetry constraints on epsilon terms*, *Nucl. Phys.* **B592** (2001) 371–390, [hep-ph/0001303].

[141] T. Appelquist, P. S. Rodrigues da Silva, and F. Sannino, *Enhanced global symmetries and the chiral phase transition*, *Phys. Rev.* **D60** (1999) 116007, [hep-ph/9906555].

[142] E. Gardi and G. Grunberg, *The conformal window in QCD and supersymmetric QCD*, *JHEP* **03** (1999) 024, [hep-th/9810192].

[143] T. Appelquist, A. Ratnaweera, J. Terning, and L. C. R. Wijewardhana, *The phase structure of an SU(N) gauge theory with N_f flavors*, *Phys. Rev.* **D58** (1998) 105017, [hep-ph/9806472].

[144] T. Schafer and E. V. Shuryak, *Instantons in QCD*, *Rev. Mod. Phys.* **70** (1998) 323–426, [hep-ph/9610451].

[145] M. Velkovsky and E. V. Shuryak, *QCD with large number of quarks: Effects of the instanton anti-instanton pairs*, *Phys. Lett.* **B437** (1998) 398–402, [hep-ph/9703345].

[146] T. Appelquist and S. B. Selipsky, *Instantons and the chiral phase transition*, *Phys. Lett.* **B400** (1997) 364–369, [hep-ph/9702404].

[147] L. Del Debbio, *The conformal window on the lattice*, arXiv:1102.4066.

[148] L. Girlanda, J. Stern, and P. Talavera, *η' mass and chiral symmetry breaking at large N_c and N_f*, *Phys. Rev. Lett.* **86** (2001) 5858–5861, [hep-ph/0103221].

[149] H. Leutwyler, *On the foundations of chiral perturbation theory*, *Ann. Phys.* **235** (1994) 165–203, [hep-ph/9311274].

[150] G. Colangelo and G. Isidori, *An introduction to CHPT*, hep-ph/0101264.

[151] B. Moussallam, *Chiral perturbation theory: A basic introduction*, hep-ph/0407246.

[152] G. Buchalla, A. J. Buras, and M. E. Lautenbacher, *Weak decays beyond leading logarithms*, *Rev. Mod. Phys.* **68** (1996) 1125–1144, [hep-ph/9512380].

[153] E. D'Hoker and S. Weinberg, *General effective actions*, *Phys.Rev.* **D50** (1994) 6050–6053, [hep-ph/9409402].

[154] K. Fujikawa, *Path Integral Measure for Gauge Invariant Fermion Theories*, *Phys.Rev.Lett.* **42** (1979) 1195.

[155] W. A. Bardeen, *Anomalous Ward identities in spinor field theories*, *Phys.Rev.* **184** (1969) 1848–1857.

[156] J. Wess and B. Zumino, *Consequences of anomalous Ward identities*, *Phys. Lett.* **B37** (1971) 95.

[157] R. Kaiser and H. Leutwyler, *Large N_c in chiral perturbation theory*, *Eur.Phys.J.* **C17** (2000) 623–649, [hep-ph/0007101].

[158] J. Bijnens, *Chiral perturbation theory beyond one loop*, *Prog.Part.Nucl.Phys.* **58** (2007) 521–586, [hep-ph/0604043].

[159] M. Knecht and J. Stern, *Generalized chiral perturbation theory*, hep-ph/9411253.

[160] M. Gell-Mann, R. Oakes, and B. Renner, *Behavior of current divergences under $SU(3) \times SU(3)$*, *Phys.Rev.* **175** (1968) 2195–2199.

[161] U.-G. Meißner, *Chiral QCD: baryon dynamics*, hep-ph/0007092. Essay for the Festschrift in honor of Boris Ioffe, to appear in the 'Encyclopedia of Analytic QCD', edited by M. Shifman, to be published by World Scientific.

[162] N. Fettes, U.-G. Meißner, M. Mojzis, and S. Steininger, *The Chiral effective pion nucleon Lagrangian of order p^4*, *Annals Phys.* **283** (2000) 273–302, [hep-ph/0001308].

[163] V. Bernard and U.-G. Meißner, *Chiral perturbation theory*, *Ann.Rev.Nucl.Part.Sci.* **57** (2007) 33–60, [hep-ph/0611231]. Commissioned article for Ann.Rev.Nucl.Part.Sci.

[164] V. Bernard, *Chiral Perturbation Theory and Baryon Properties*, *Prog.Part.Nucl.Phys.* **60** (2008) 82–160, [arXiv:0706.0312].

[165] B. Grinstein, *An Introduction to the theory of heavy mesons and baryons*, hep-ph/9411275.

[166] C. W. Bernard and M. F. Golterman, *Chiral perturbation theory for the quenched approximation of QCD*, *Phys.Rev.* **D46** (1992) 853–857, [hep-lat/9204007].

[167] C. W. Bernard and M. F. Golterman, *Partially quenched gauge theories and an application to staggered fermions*, *Phys.Rev.* **D49** (1994) 486–494, [hep-lat/9306005].

[168] S. R. Sharpe and N. Shoresh, *Physical results from unphysical simulations*, *Phys.Rev.* **D62** (2000) 094503, [hep-lat/0006017].

[169] M. Golterman, *Applications of chiral perturbation theory to lattice QCD*, arXiv:0912.4042.

[170] M. Knecht and J. Stern, *Exact results on mass dependence and chiral limit of supersymmetric QCD*, *Phys.Lett.* **B155** (1985) 167.

[171] T. Appelquist, A. Nyffeler, and S. B. Selipsky, *Analyzing chiral symmetry breaking in supersymmetric gauge theories*, *Phys.Lett.* **B425** (1998) 300–308, [hep-th/9709177].

[172] S. R. Sharpe and J. Singleton, Robert L., *Spontaneous flavor and parity breaking with Wilson fermions*, *Phys.Rev.* **D58** (1998) 074501, [hep-lat/9804028].

[173] O. Bar, G. Rupak, and N. Shoresh, *Chiral perturbation theory at $O(a^2)$ for lattice QCD*, *Phys.Rev.* **D70** (2004) 034508, [hep-lat/0306021].

[174] C. Sachrajda and G. Villadoro, *Twisted boundary conditions in lattice simulations*, *Phys.Lett.* **B609** (2005) 73–85, [hep-lat/0411033].

[175] O. Bar, S. Necco, and S. Schaefer, *The Epsilon regime with Wilson fermions*, *JHEP* **0903** (2009) 006, [arXiv:0812.2403].

[176] J. Kambor, J. H. Missimer, and D. Wyler, *The Chiral Loop Expansion of the Nonleptonic Weak Interactions of Mesons*, *Nucl.Phys.* **B346** (1990) 17–64.

[177] C. W. Bernard, T. Draper, A. Soni, H. Politzer, and M. B. Wise, *Application of Chiral Perturbation Theory to $K \to 2\pi$ Decays*, *Phys.Rev.* **D32** (1985) 2343–2347.

[178] V. Cirigliano, G. Ecker, H. Neufeld, and A. Pich, *Isospin breaking in $K \to \pi\pi$ decays*, *Eur.Phys.J.* **C33** (2004) 369–396, [hep-ph/0310351].

[179] V. Cirigliano, G. Ecker, and A. Pich, *Reanalysis of pion pion phase shifts from $K \to \pi\pi$ decays*, *Phys.Lett.* **B679** (2009) 445–448, [arXiv:0907.1451].

[180] J. Hirn and J. Stern, *The Role of spurions in Higgsless electroweak effective theories*, *Eur.Phys.J.* **C34** (2004) 447–475, [hep-ph/0401032].

[181] J. Bijnens and J. Lu, *Technicolor and other QCD-like theories at next-to-next-to-leading order*, *JHEP* **0911** (2009) 116, [arXiv:0910.5424].

[182] M. Davier, L. Girlanda, A. Hocker, and J. Stern, *Finite energy chiral sum rules and tau spectral functions*, *Phys.Rev.* **D58** (1998) 096014, [hep-ph/9802447].

[183] J. Bijnens and I. Jemos, *A new global fit of the L_i^r at next-to-next-to-leading order in Chiral Perturbation Theory*, arXiv:1103.5945.

[184] A. Gomez Nicola and J. Pelaez, *Meson meson scattering within one loop chiral perturbation theory and its unitarization*, *Phys.Rev.* **D65** (2002) 054009, [hep-ph/0109056].

[185] G. Amoros, J. Bijnens, and P. Talavera, *Two point functions at two loops in three flavor chiral perturbation theory*, *Nucl.Phys.* **B568** (2000) 319–363, [hep-ph/9907264].

[186] G. Amoros, J. Bijnens, and P. Talavera, *QCD isospin breaking in meson masses, decay constants and quark mass ratios*, *Nucl.Phys.* **B602** (2001) 87–108, [hep-ph/0101127].

[187] J. Bijnens, P. Dhonte, and P. Talavera, *$\pi\pi$ scattering in three flavor ChPT*, *JHEP* **0401** (2004) 050, [hep-ph/0401039].

[188] J. Bijnens, P. Dhonte, and P. Talavera, *πK scattering in three flavor ChPT*, *JHEP* **0405** (2004) 036, [hep-ph/0404150].

[189] G. Amoros, J. Bijnens, and P. Talavera, *$K_{\ell 4}$ form-factors and $\pi\pi$ scattering*, *Nucl.Phys.* **B585** (2000) 293–352, [hep-ph/0003258].

[190] J. Bijnens and P. Talavera, *Pion and kaon electromagnetic form-factors*, *JHEP* **0203** (2002) 046, [hep-ph/0203049].

[191] J. Bijnens and P. Dhonte, *Scalar form-factors in SU(3) chiral perturbation theory*, *JHEP* **0310** (2003) 061, [hep-ph/0307044].

[192] J. Bijnens and P. Talavera, *$K_{\ell 3}$ decays in chiral perturbation theory*, *Nucl.Phys.* **B669** (2003) 341–362, [hep-ph/0303103].

[193] K. Kampf and B. Moussallam, *Tests of the naturalness of the coupling constants in ChPT at order p^6*, *Eur.Phys.J.* **C47** (2006) 723–736, [hep-ph/0604125].

[194] **RBC Collaboration, UKQCD** Collaboration, Y. Aoki *et. al.*, *Continuum Limit Physics from 2+1 Flavor Domain Wall QCD*, *Phys.Rev.* **D83** (2011) 074508, [arXiv:1011.0892].

[195] **ETM** Collaboration, R. Baron *et. al.*, *Kaon and D meson masses with N_f = 2+1+1 twisted mass lattice QCD*, arXiv:1009.2074. Long author list - awaiting processing.

[196] **TWQCD Collaboration, JLQCD** Collaboration, J. Noaki *et. al.*, *Chiral properties of light mesons with N_f = 2+1 overlap fermions*, *PoS* **LAT2009** (2009) 096, [arXiv:0910.5532].

[197] **MILC** Collaboration, C. Aubin *et. al.*, *Light pseudoscalar decay constants, quark masses, and low energy constants from three-flavor lattice QCD*, *Phys.Rev.* **D70** (2004) 114501, [hep-lat/0407028].

[198] M. Creutz, *Flavor extrapolations and staggered fermions*, hep-lat/0603020.

[199] M. Creutz, *Chiral anomalies and rooted staggered fermions*, *Phys.Lett.* **B649** (2007) 230–234, [hep-lat/0701018].

[200] M. Creutz, *Reply to: 'Comment on: 'Chiral anomalies and rooted staggered fermions'*, *Phys.Lett.* **B649** (2007) 241–242, [arXiv:0704.2016]. Rebuttal to hep-lat/0603027.

[201] C. Bernard, M. Golterman, Y. Shamir, and S. R. Sharpe, *'t Hooft vertices, partial quenching, and rooted staggered QCD*, *Phys.Rev.* **D77** (2008) 114504, [arXiv:0711.0696].

[202] M. Creutz, *Comment on "'t Hooft vertices, partial quenching, and rooted staggered QCD"*, *Phys.Rev.* **D78** (2008) 078501, [arXiv:0805.1350].

[203] C. Bernard, *Order of the chiral and continuum limits in staggered chiral perturbation theory*, *Phys.Rev.* **D71** (2005) 094020, [hep-lat/0412030].

[204] S. R. Sharpe and R. S. Van de Water, *Staggered chiral perturbation theory at next-to-leading order*, *Phys.Rev.* **D71** (2005) 114505, [hep-lat/0409018].

[205] **MILC** Collaboration, *et. al.*, *Results for light pseudoscalar mesons*, *PoS* **LATTICE2010** (2010) 074, [arXiv:1012.0868].

[206] **UKQCD** Collaboration, K. Bowler, B. Joo, R. Kenway, C. Maynard, and R. Tweedie, *Lattice QCD with mixed actions*, *JHEP* **0508** (2005) 003, [hep-lat/0411005].

[207] **RBC-UKQCD** Collaboration, C. Allton *et. al.*, *Physical Results from 2+1 Flavor Domain Wall QCD and SU(2) Chiral Perturbation Theory*, *Phys.Rev.* **D78** (2008) 114509, [arXiv:0804.0473].

[208] P. Boyle, A. Juttner, R. Kenway, C. Sachrajda, S. Sasaki, *et. al.*, *$K_{\ell 3}$ semileptonic form-factor from 2+1 flavour lattice QCD*, *Phys.Rev.Lett.* **100** (2008) 141601, [arXiv:0710.5136].

[209] P. Boyle, J. Flynn, A. Juttner, C. Kelly, C. Maynard, *et. al.*, *$K \to \pi$ form factors with reduced model dependence*, *Eur.Phys.J.* **C69** (2010) 159–167, [arXiv:1004.0886].

[210] U.-G. Meißner, *Chiral dynamics with strange quarks: Mysteries and opportunities*, *Phys.Scripta* **T99** (2002) 68–83, [hep-ph/0201078].

[211] **RBC Collaboration, UKQCD** Collaboration, J. Flynn and C. Sachrajda, *SU(2) chiral perturbation theory for $K_{\ell 3}$ decay amplitudes*, *Nucl.Phys.* **B812** (2009) 64–80, [arXiv:0809.1229].

[212] J. Pelaez and G. Rios, *Chiral extrapolation of light resonances from one and two-loop unitarized Chiral Perturbation Theory versus lattice results*, *Phys.Rev.* **D82** (2010) 114002, [arXiv:1010.6008].

[213] J. Gasser, C. Haefeli, M. Ivanov, and M. Schmid, *Relations between SU(2)- and SU(3)-LECs in chiral perturbation theory*, *Phys.Part.Nucl.* **41** (2010) 939–941.

[214] M. A. Ivanov and M. Schmid, *Integrating out the heaviest quark in N–flavour ChPT*, arXiv:1107.0598.

[215] A. Roessl, *Pion kaon scattering near the threshold in chiral SU(2) perturbation theory*, *Nucl.Phys.* **B555** (1999) 507–539, [hep-ph/9904230]. Ph.D. Thesis.

[216] S. Durr, Z. Fodor, C. Hoelbling, S. Katz, S. Krieg, *et. al.*, *Lattice QCD at the physical point: Simulation and analysis details*, arXiv:1011.2711.

[217] **ETM** Collaboration, B. Blossier *et. al.*, *Average up/down, strange and charm quark masses with Nf=2 twisted mass lattice QCD*, *Phys.Rev.* **D82** (2010) 114513, [arXiv:1010.3659].

[218] B. Moussallam, *N_f dependence of the quark condensate from a chiral sum rule*, *Eur.Phys.J.* **C14** (2000) 111–122, [hep-ph/9909292].

[219] B. Moussallam, *Flavor stability of the chiral vacuum and scalar meson dynamics*, *JHEP* **0008** (2000) 005, [hep-ph/0005245].

[220] J. Bijnens, G. Colangelo, and G. Ecker, *Double chiral logs*, *Phys. Lett.* **B441** (1998) 437–446, [hep-ph/9808421].

[221] J. Bijnens, G. Colangelo, and G. Ecker, *The mesonic chiral Lagrangian of order p^6*, *JHEP* **02** (1999) 020, [hep-ph/9902437].

[222] J. Bijnens, G. Colangelo, and G. Ecker, *Renormalization of chiral perturbation theory to order p^6*, *Annals Phys.* **280** (2000) 100–139, [hep-ph/9907333].

[223] **FlaviaNet Working Group on Kaon Decays** Collaboration, M. Antonelli *et. al.*, *Precision tests of the Standard Model with leptonic and semileptonic kaon decays*, arXiv:0801.1817.

[224] I. Towner and J. Hardy, *The evaluation of V_{ud} and its impact on the unitarity of the Cabibbo-Kobayashi-Maskawa quark-mixing matrix*, *Rept.Prog.Phys.* **73** (2010) 046301.

[225] S. Okubo, *Note on unitary symmetry in strong interactions*, *Prog. Theor. Phys.* **27** (1962) 949–966.

[226] M. Gell-Mann, *Symmetries of baryons and mesons*, *Phys. Rev.* **125** (1962) 1067–1084.

[227] S. Narison, *QCD spectral sum rules*, *World Sci.Lect.Notes Phys.* **26** (1989) 1–527.

[228] S. Narison, *Light and heavy quark masses, flavor breaking of chiral condensates, meson weak leptonic decay constants in QCD*, hep-ph/0202200. Adapted from a chapter of the forthcoming book 'QCD as a Theory of Hadrons: From Partons to Confinement, Monograph series in Physics, Cambridge Univ. Press (to appear in 2002).

[229] J. Kambor and K. Maltman, *The Strange quark mass from flavor breaking in hadronic tau decays*, *Phys.Rev.* **D62** (2000) 093023, [hep-ph/0005156].

[230] M. Jamin, J. A. Oller, and A. Pich, *Light quark masses from scalar sum rules*, *Eur.Phys.J.* **C24** (2002) 237–243, [hep-ph/0110194].

[231] E. Braaten, S. Narison, and A. Pich, *QCD analysis of the tau hadronic width*, *Nucl.Phys.* **B373** (1992) 581–612.

[232] F. Le Diberder and A. Pich, *Testing QCD with τ decays*, *Phys.Lett.* **B289** (1992) 165–175.

[233] F. Le Diberder and A. Pich, *The perturbative QCD prediction to R_τ revisited*, *Phys.Lett.* **B286** (1992) 147–152.

[234] M. Davier, A. Hocker, and Z. Zhang, *The Physics of hadronic tau decays*, *Rev.Mod.Phys.* **78** (2006) 1043–1109, [hep-ph/0507078].

[235] M. Davier, S. Descotes-Genon, A. Hocker, B. Malaescu, and Z. Zhang, *The Determination of α_s from Tau Decays Revisited*, *Eur.Phys.J.* **C56** (2008) 305–322, [arXiv:0803.0979].

[236] A. I. Davydychev, V. A. Smirnov, and J. Tausk, *Large momentum expansion of two loop selfenergy diagrams with arbitrary masses*, *Nucl.Phys.* **B410** (1993) 325–342, [hep-ph/9307371].

[237] V. A. Smirnov, *Asymptotic expansions in limits of large momenta and masses*, *Commun.Math.Phys.* **134** (1990) 109–137.

[238] J. F. Donoghue, J. Gasser, and H. Leutwyler, *The decay of a light Higgs boson*, *Nucl.Phys.* **B343** (1990) 341–368.

[239] A. Efremov and A. Radyushkin, *Asymptotical Behavior of Pion Electromagnetic Form-Factor in QCD*, *Theor.Math.Phys.* **42** (1980) 97–110.

[240] G. Lepage and S. J. Brodsky, *Exclusive Processes in Perturbative Quantum Chromodynamics*, *Phys.Rev.* **D22** (1980) 2157.

[241] R. Omnes, *On the Solution of certain singular integral equations of quantum field theory*, *Nuovo Cim.* **8** (1958) 316–326.

[242] N. Muskhelishvili, *Singular integral equations*, *P. Noordhoff* (1953).

[243] J. Gasser and U. G. Meißner, *Chiral expansion of pion form-factors beyond one loop*, *Nucl.Phys.* **B357** (1991) 90–128.

[244] J. Oller, E. Oset, and J. Pelaez, *Meson meson interaction in a nonperturbative chiral approach*, *Phys.Rev.* **D59** (1999) 074001, [hep-ph/9804209].

[245] R. Kaminski, L. Lesniak, and J. Maillet, *Relativistic effects in the scalar meson dynamics*, *Phys.Rev.* **D50** (1994) 3145–3157, [hep-ph/9403264].

[246] R. Kaminski, L. Lesniak, and B. Loiseau, *Three channel model of meson meson scattering and scalar meson spectroscopy*, *Phys.Lett.* **B413** (1997) 130–136, [hep-ph/9707377].

[247] K. Au, D. Morgan, and M. Pennington, *Meson Dynamics Beyond the Quark Model: A Study of Final State Interactions*, *Phys.Rev.* **D35** (1987) 1633.

[248] A. Pich, *QCD predictions for the tau hadronic width: Determination of $\alpha_S(M_\tau^2)$*, *Nucl.Phys.Proc.Suppl.* **39BC** (1995) 326, [hep-ph/9412273].

[249] J. Gasser and H. Leutwyler, *Low-Energy Theorems as Precision Tests of QCD*, *Phys.Lett.* **B125** (1983) 325.

[250] J. Bijnens, G. Colangelo, and P. Talavera, *The vector and scalar form factors of the pion to two loops*, *JHEP* **05** (1998) 014, [hep-ph/9805389].

[251] B. Ananthanarayan, G. Colangelo, J. Gasser, and H. Leutwyler, *Roy equation analysis of $\pi\pi$ scattering*, *Phys.Rept.* **353** (2001) 207–279, [hep-ph/0005297].

[252] F. Yndurain, *The Quadratic scalar radius of the pion and the mixed πK radius*, *Phys.Lett.* **B578** (2004) 99–108, [hep-ph/0309039].

[253] B. Ananthanarayan, I. Caprini, G. Colangelo, J. Gasser, and H. Leutwyler, *Scalar form-factors of light mesons*, *Phys.Lett.* **B602** (2004) 218–225, [hep-ph/0409222].

[254] J. Gasser and H. Leutwyler, *Low-Energy Expansion of Meson Form-Factors*, *Nucl.Phys.* **B250** (1985) 517–538.

[255] S. Descotes-Genon, *Chiral extrapolations on the lattice with strange sea quarks*, *Nucl.Phys.* **A755** (2005) 645–648.

[256] F.-K. Guo, C. Hanhart, F. J. Llanes-Estrada, and U.-G. Meißner, *Quark mass dependence of the pion vector form factor*, *Phys.Lett.* **B678** (2009) 90–96, [arXiv:0812.3270].

[257] C. Callan and S. Treiman, *Equal Time Commutators and K Meson Decays*, *Phys.Rev.Lett.* **16** (1966) 153–157.

[258] V. Bernard, M. Oertel, E. Passemar, and J. Stern, *$K^L_{\mu 3}$ decay: A Stringent test of right-handed quark currents*, *Phys.Lett.* **B638** (2006) 480–486, [hep-ph/0603202].

[259] V. Bernard, M. Oertel, E. Passemar, and J. Stern, *Dispersive representation and shape of the K(l3) form factors: Robustness*, *Phys.Rev.* **D80** (2009) 034034, [arXiv:0903.1654].

[260] **NA48** Collaboration, A. Lai *et. al.*, *Measurement of $K^0_{\mu 3}$ form factors*, *Phys.Lett.* **B647** (2007) 341–350, [hep-ex/0703002].

[261] M. Veltri, *$K^{+-}_\mu 3$ Form Factors Measurement at NA48/2*, arXiv:1101.5031.

[262] **KLOE** Collaboration, F. Ambrosino *et. al.*, *Measurement of the $K_L \to \pi\mu\nu$ form-factor parameters with the KLOE detector*, *JHEP* **0712** (2007) 105, [arXiv:0710.4470].

[263] **KTeV** Collaboration, E. Abouzaid *et. al.*, *Dispersive analysis of $K^L_{\mu 3}$ and K^L_{e3} scalar and vector form factors using KTeV data*, *Phys.Rev.* **D81** (2010) 052001, [arXiv:0912.1291].

[264] C. Sachrajda, *Phenomenology from the Lattice*, *PoS* **LATTICE2010** (2010) 018, [arXiv:1103.5959].

[265] S. Durr, Z. Fodor, C. Hoelbling, S. Katz, S. Krieg, *et. al.*, *The ratio FK/Fpi in QCD*, *Phys.Rev.* **D81** (2010) 054507, [arXiv:1001.4692].

[266] S. Durr, Z. Fodor, J. Frison, C. Hoelbling, R. Hoffmann, *et. al.*, *Ab-Initio Determination of Light Hadron Masses*, *Science* **322** (2008) 1224–1227, [arXiv:0906.3599].

[267] R. Baron, P. Boucaud, J. Carbonell, A. Deuzeman, V. Drach, *et. al.*, *Light hadrons from lattice QCD with light (u,d), strange and charm dynamical quarks*, *JHEP* **1006** (2010) 111, [arXiv:1004.5284].

[268] **PACS-CS** Collaboration, S. Aoki *et. al.*, *Physical Point Simulation in 2+1 Flavor Lattice QCD*, *Phys.Rev.* **D81** (2010) 074503, [arXiv:0911.2561].

[269] V. Bernard and E. Passemar, *Chiral Extrapolation of the Strangeness Changing $K\pi$ Form Factor*, *JHEP* **1004** (2010) 001, [arXiv:0912.3792].

[270] L. Rosselet, P. Extermann, J. Fischer, O. Guisan, R. Mermod, *et. al.*, *Experimental Study of 30,000 K_{e4} Decays*, *Phys.Rev.* **D15** (1977) 574.

[271] **BNL-E865** Collaboration, S. Pislak *et. al.*, *A New measurement of K^+_{e4} decay and the s wave $\pi\pi$ scattering length a^0_0*, *Phys.Rev.Lett.* **87** (2001) 221801, [hep-ex/0106071].

[272] S. Pislak, R. Appel, G. Atoyan, B. Bassalleck, D. Bergman, *et. al.*, *High statistics measurement of K_{e4} decay properties*, *Phys.Rev.* **D67** (2003) 072004, [hep-ex/0301040].

[273] **NA48/2** Collaboration, J. Batley *et. al.*, *New high statistics measurement of K_{e4} decay form factors and $\pi\pi$ scattering phase shifts*, *Eur.Phys.J.* **C54** (2008) 411–423.

[274] **NA48-2** Collaboration, J. Batley *et. al.*, *Precise tests of low energy QCD from K_{e4}decay properties*, *Eur.Phys.J.* **C70** (2010) 635–657.

[275] **NA48/2** Collaboration, J. Batley *et. al.*, *Observation of a cusp-like structure in the $\pi^0\pi^0$ invariant mass distribution from $K^\pm \to \pi^\pm\pi^0\pi^0$ decay and determination of the $\pi\pi$ scattering lengths*, *Phys.Lett.* **B633** (2006) 173–182, [hep-ex/0511056].

[276] J. Batley, A. Culling, G. Kalmus, C. Lazzeroni, D. Munday, *et. al.*, *Determination of the S-wave $\pi\pi$ scattering lengths from a study of $K^\pm \to \pi^\pm\pi^0\pi^0$ decays*, *Eur.Phys.J.* **C64** (2009) 589–608, [arXiv:0912.2165].

[277] N. Cabibbo, *Determination of the a_0-a_2 pion scattering length from $K^+ \to \pi^+\pi^0\pi^0$ decay*, *Phys.Rev.Lett.* **93** (2004) 121801, [hep-ph/0405001].

[278] N. Cabibbo and G. Isidori, *Pion-pion scattering and the $K \to 3\pi$ decay amplitudes*, *JHEP* **0503** (2005) 021, [hep-ph/0502130].

[279] E. Gamiz, J. Prades, and I. Scimemi, *$K \to 3\pi$ final state interactions at NLO in CHPT and Cabibbo's proposal to measure a_0-a_2*, *Eur.Phys.J.* **C50** (2007) 405–422, [hep-ph/0602023].

[280] J. Gasser, B. Kubis, and A. Rusetsky, *Cusps in $K \to 3\pi$ decays: a theoretical framework*, *Nucl.Phys.* **B850** (2011) 96–147, [arXiv:1103.4273].

[281] L. Masetti, *K_{e4} decays and Wigner cusp*, arXiv:0704.1307.

[282] **NA48/2** Collaboration, D. Madigozhin, *Probing non perturbative QCD with the cusp effect in kaon decays by NA48*, *PoS* **KAON09** (2009) 032.

[283] **DIRAC** Collaboration, V. Yazkov, *Investigation of $\pi^+\pi^-$ and πK atoms at DIRAC*, *PoS* **CD09** (2009) 003.

[284] J. Gasser, V. Lyubovitskij, and A. Rusetsky, *Hadronic Atoms*, *Ann.Rev.Nucl.Part.Sci.* **59** (2009) 169–190, [arXiv:0903.0257].

[285] S. Roy, *Exact integral equation for pion pion scattering involving only physical region partial waves*, *Phys.Lett.* **B36** (1971) 353.

[286] G. Colangelo, J. Gasser, and H. Leutwyler, *$\pi\pi$ scattering*, *Nucl.Phys.* **B603** (2001) 125–179, [hep-ph/0103088].

[287] J. Gasser, *Theoretical progress on cusp effect and $K_{\ell 4}$ decays*, *PoS* **KAON** (2008) 033, [arXiv:0710.3048].

[288] G. Colangelo, *Theoretical progress on $\pi\pi$ scattering lengths and phases*, *PoS* **KAON** (2008) 038, [arXiv:0710.3050].

[289] G. Colangelo, J. Gasser, and A. Rusetsky, *Isospin breaking in $K_{\ell 4}$ decays*, *Eur.Phys.J.* **C59** (2009) 777–793, [arXiv:0811.0775].

[290] A. Martin, *Extension of the axiomatic analyticity domain of scattering amplitudes by unitarity. 1.*, *Nuovo Cim.* **A42** (1965) 930–953.

[291] T. Regge, *Introduction to complex orbital momenta*, *Nuovo Cim.* **14** (1959) 951.

[292] J. Baton, G. Laurens, and J. Reignier, *$\pi^+\pi^-$ elastic cross-section from chew-low extrapolations of $\pi^-p \to \pi^+\pi^-n$ reaction at 2.77 Gev/c*, *Phys.Lett.* **B33** (1970) 525–527.

[293] B. Hyams, C. Jones, P. Weilhammer, W. Blum, H. Dietl, *et. al.*, *$\pi\pi$ Phase Shift Analysis from 600 MeV to 1900 MeV*, *Nucl.Phys.* **B64** (1973) 134–162.

[294] **CERN-Munich** Collaboration, H. Becker *et. al.*, *Measurement and analysis of the reaction $\pi^-p \to \rho^0 n$ on a polarised target*, *Nucl.Phys.* **B150** (1979) 301.

[295] J. Pelaez and F. Yndurain, *On the precision of chiral dispersive calculations of pi pi scattering*, *Phys.Rev.* **D68** (2003) 074005, [hep-ph/0304067].

[296] I. Caprini, G. Colangelo, J. Gasser, and H. Leutwyler, *On the precision of the theoretical predictions for pi pi scattering*, *Phys.Rev.* **D68** (2003) 074006, [hep-ph/0306122].

[297] J. Pelaez and F. Yndurain, *Regge analysis of pion pion (and pion kaon) scattering for energy $\sqrt{s} > 1.4$ GeV*, *Phys.Rev.* **D69** (2004) 114001, [hep-ph/0312187].

[298] J. Pelaez and F. Yndurain, *The Pion-pion scattering amplitude*, *Phys.Rev.* **D71** (2005) 074016, [hep-ph/0411334].

[299] R. Kaminski, J. Pelaez, and F. Yndurain, *The pion-pion scattering amplitude. II. Improved analysis above $K\bar{K}$ threshold*, *Phys.Rev.* **D74** (2006) 014001, [hep-ph/0603170].

[300] F. Yndurain, R. Garcia-Martin, and J. Pelaez, *Experimental status of the $\pi\pi$ isoscalar S wave at low energy: $f_0(600)$ pole and scattering length*, *Phys.Rev.* **D76** (2007) 074034, [hep-ph/0701025].

[301] T. Blum, P. Boyle, N. Christ, N. Garron, E. Goode, *et. al.*, *$K \to \pi\pi$ Decay amplitudes from Lattice QCD*, arXiv:1106.2714. * Temporary entry *.

[302] R. Garcia-Martin, R. Kaminski, J. Pelaez, J. Ruiz de Elvira, and F. Yndurain, *The Pion-pion scattering amplitude. IV: Improved analysis with once subtracted Roy-like equations up to 1100 MeV*, *Phys.Rev.* **D83** (2011) 074004, [arXiv:1102.2183].

[303] N. Fuchs, H. Sazdjian, and J. Stern, *How to probe the scale of $\bar{q}q$ in chiral perturbation theory*, *Phys.Lett.* **B269** (1991) 183–188.

[304] J. Stern, H. Sazdjian, and N. Fuchs, *What $\pi\pi$ scattering tells us about chiral perturbation theory*, *Phys.Rev.* **D47** (1993) 3814–3838, [hep-ph/9301244].

[305] M. Knecht, B. Moussallam, J. Stern, and N. Fuchs, *The Low-energy $\pi\pi$ amplitude to one and two loops*, *Nucl.Phys.* **B457** (1995) 513–576, [hep-ph/9507319].

[306] J. Bijnens, G. Colangelo, G. Ecker, J. Gasser, and M. Sainio, *Elastic $\pi\pi$ scattering to two loops*, *Phys.Lett.* **B374** (1996) 210–216, [hep-ph/9511397].

[307] J. Bijnens, G. Colangelo, G. Ecker, J. Gasser, and M. Sainio, *Pion pion scattering at low-energy*, *Nucl.Phys.* **B508** (1997) 263–310, [hep-ph/9707291].

[308] G. Colangelo, J. Gasser, and H. Leutwyler, *The $\pi\pi$ S wave scattering lengths*, *Phys.Lett.* **B488** (2000) 261–268, [hep-ph/0007112].

[309] M. Knecht, B. Moussallam, J. Stern, and N. Fuchs, *Determination of two loop $\pi\pi$ scattering amplitude parameters*, *Nucl.Phys.* **B471** (1996) 445–470, [hep-ph/9512404].

[310] S. Weinberg, *Pion scattering lengths*, *Phys.Rev.Lett.* **17** (1966) 616–621.

[311] L. Maiani and M. Testa, *Final state interactions from Euclidean correlation functions*, *Phys.Lett.* **B245** (1990) 585–590.

[312] M. Luscher, *Volume Dependence of the Energy Spectrum in Massive Quantum Field Theories. 2. Scattering States*, *Commun.Math.Phys.* **105** (1986) 153–188.

[313] M. Luscher, *Two particle states on a torus and their relation to the scattering matrix*, *Nucl.Phys.* **B354** (1991) 531–578.

[314] S. Beane, W. Detmold, K. Orginos, and M. Savage, *Nuclear Physics from Lattice QCD*, *Prog.Part.Nucl.Phys.* **66** (2011) 1–40, [arXiv:1004.2935].

[315] H. Leutwyler, *Light quark masses*, *PoS* **CD09** (2009) 005, [arXiv:0911.1416].

[316] **CP-PACS** Collaboration, T. Yamazaki *et. al.*, *$I = 2$ $\pi\pi$ scattering phase shift with two flavors of O(a) improved dynamical quarks*, *Phys.Rev.* **D70** (2004) 074513, [hep-lat/0402025].

[317] **NPLQCD** Collaboration, S. R. Beane, P. F. Bedaque, K. Orginos, and M. J. Savage, *$I = 2$ $\pi\pi$ scattering from fully-dynamical mixed-action lattice QCD*, *Phys.Rev.* **D73** (2006) 054503, [hep-lat/0506013].

[318] S. R. Beane, T. C. Luu, K. Orginos, A. Parreno, M. J. Savage, *et. al.*, *Precise Determination of the I=2 $\pi\pi$ Scattering Length from Mixed-Action Lattice QCD*, *Phys.Rev.* **D77** (2008) 014505, [arXiv:0706.3026].

[319] X. Feng, K. Jansen, and D. B. Renner, *Resonance Parameters of the rho-Meson from Lattice QCD*, *Phys.Rev.* **D83** (2011) 094505, [arXiv:1011.5288].

[320] J. Gasser, V. Lyubovitskij, and A. Rusetsky, *Hadronic atoms in QCD + QED*, *Phys.Rept.* **456** (2008) 167–251, [arXiv:0711.3522].

[321] N. Cabibbo and A. Maksymowicz, *Angular Correlations in K_{e4} Decays and Determination of Low-Energy $\pi\pi$ Phase Shifts*, *Phys. Rev.* **137** (1965) B438–B443.

[322] F. A. Berends, A. Donnachie, and G. C. Oades, *Theoretical Study of K_{l4} Decay*, *Phys. Rev.* **171** (1968) 1457–1465.

[323] A. Pais and S. Treiman, *Pion Phase-Shift Information from K_{l4} Decays*, *Phys.Rev.* **168** (1968) 1858–1865.

[324] K. M. Watson, *Some general relations between the photoproduction and scattering of π mesons*, *Phys.Rev.* **95** (1954) 228–236.

[325] G. Lafferty and T. Wyatt, *Where to stick your data points: The treatment of measurements within wide bins*, *Nucl.Instrum.Meth.* **A355** (1995) 541–547.

[326] W. Hoogland, S. Peters, G. Grayer, B. Hyams, P. Weilhammer, *et. al.*, *Measurement and Analysis of the $\pi^+\pi^+$ System Produced at Small Momentum Transfer in the Reaction $\pi^+p \to \pi^+\pi^+n$ at 12.5 GeV*, *Nucl.Phys.* **B126** (1977) 109.

[327] M. Losty, V. Chaloupka, A. Ferrando, L. Montanet, E. Paul, *et. al.*, *A Study of $\pi^-\pi^-$ scattering from π^-p interactions at 3.93 GeV/c*, *Nucl.Phys.* **B69** (1974) 185–204.

[328] S. D. Protopopescu *et. al.*, *$\pi\pi$ Partial Wave Analysis from Reactions $\pi^+p \to \pi^+\pi^-\Delta^{++}$ and $\pi^+p \to K^+K^-\Delta^{++}$ at 7.1 GeV/c*, *Phys. Rev.* **D7** (1973) 1279.

[329] G. Colangelo, J. Gasser, and H. Leutwyler, *The Quark condensate from K_{e4} decays*, *Phys.Rev.Lett.* **86** (2001) 5008–5010, [hep-ph/0103063].

[330] B. Moussallam and J. Stern, *Chiral symmetry aspects of the scalars*, hep-ph/9404353.

[331] E. Barberio and Z. Was, *PHOTOS: A Universal Monte Carlo for QED radiative corrections. Version 2.0*, *Comput.Phys.Commun.* **79** (1994) 291–308.

[332] Q. Xu and Z. Was, *News on PHOTOS Monte Carlo: $\gamma^* \to \pi^+\pi^-(\gamma)$ and $K^\pm \to \pi^+\pi^-e^\pm\nu(\gamma)$*, *Chin.Phys.* **C34** (2010) 889–895, [arXiv:1001.0070].

[333] M. Knecht and R. Urech, *Virtual photons in low-energy $\pi\pi$ scattering*, *Nucl.Phys.* **B519** (1998) 329–360, [hep-ph/9709348].

[334] U.-G. Meißner, G. Muller, and S. Steininger, *Virtual photons in SU(2) chiral perturbation theory and electromagnetic corrections to $\pi\pi$ scattering*, *Phys.Lett.* **B406** (1997) 154–160, [hep-ph/9704377].

[335] J. Schweizer, *Explicit generating functional for pions and virtual photons*, *JHEP* **0302** (2003) 007, [hep-ph/0212188].

[336] G. Colangelo, M. Knecht, and J. Stern, *On the Pais-Treiman method to measure $\pi\pi$ phase shifts in K_{e4} decays*, *Phys.Lett.* **B336** (1994) 543–548, [hep-ph/9406211].

[337] A. Nehme, *Isospin breaking in $K_{\ell 4}$ decays of the neutral kaon*, *Nucl.Phys.* **B682** (2004) 289–346, [hep-ph/0311113].

[338] A. Nehme and P. Talavera, *Isospin breaking corrections to low-energy πK scattering*, *Phys.Rev.* **D65** (2002) 054023, [hep-ph/0107299].

[339] K. Kampf, M. Knecht, J. Novotny, and M. Zdrahal, *Analytical dispersive construction of $\eta \to 3\pi$ amplitude: first order in isospin breaking*, arXiv:1103.0982.

[340] M. Knecht and A. Nehme, *Electromagnetic corrections to charged pion scattering at low-energies*, *Phys.Lett.* **B532** (2002) 55–62, [hep-ph/0201033].

[341] V. Cuplov. PhD thesis, unpublished.

[342] C. Haefeli, M. A. Ivanov, and M. Schmid, *Electromagnetic low-energy constants in χPT*, *Eur.Phys.J.* **C53** (2008) 549–557, [arXiv:0710.5432].

[343] J. Bijnens, P. Gosdzinsky, and P. Talavera, *Vector meson masses in chiral perturbation theory*, *Nucl.Phys.* **B501** (1997) 495–517, [hep-ph/9704212].

[344] B. Borasoy and U.-G. Meißner, *Chiral expansion of baryon masses and sigma terms*, *Annals Phys.* **254** (1997) 192–232, [hep-ph/9607432].

[345] J. Gasser and H. Leutwyler, *$\eta \to 3\pi$ to One Loop*, *Nucl.Phys.* **B250** (1985) 539.

[346] J. Bijnens and K. Ghorbani, *$\eta \to 3\pi$ at Two Loops In Chiral Perturbation Theory*, *JHEP* **0711** (2007) 030, [arXiv:0709.0230].

[347] M. Bissegger, A. Fuhrer, J. Gasser, B. Kubis, and A. Rusetsky, *Radiative corrections in $K \to 3\pi$ decays*, *Nucl.Phys.* **B806** (2009) 178–223, [arXiv:0807.0515].

[348] C. Lang, *Meson Meson Scattering Amplitudes in the Modified K-Matrix Formalism*, *Nuovo Cim.* **A41** (1977) 73.

[349] S. Mandelstam, *Determination of the pion - nucleon scattering amplitude from dispersion relations and unitarity. General theory*, *Phys.Rev.* **112** (1958) 1344–1360.

[350] M. Froissart, *Asymptotic behavior and subtractions in the Mandelstam representation*, *Phys.Rev.* **123** (1961) 1053–1057.

[351] F. Steiner, *Partial wave crossing relations for meson-baryon scattering*, *Fortsch.Phys.* **19** (1971) 115–159.

[352] N. Johannesson and G. Nilsson, *An Analysis of Low-Energy πK Scattering*, *Nuovo Cim.* **A43** (1978) 376.

[353] H. Lehmann *Nuovo Cim.* **10** (1958).

[354] D. Aston, N. Awaji, T. Bienz, F. Bird, J. D'Amore, *et. al.*, *A Study of $K^-\pi^+$ Scattering in the Reaction $K^-p \to K^-\pi^+n$ at 11 GeV/c*, *Nucl.Phys.* **B296** (1988) 493.

[355] B. Hyams, C. Jones, P. Weilhammer, W. Blum, H. Dietl, *et. al.*, *A Study of All the $\pi\pi$ Phase Shift Solutions in the Mass Region 1.0 GeV to 1.8 GeV from $\pi^- p \to \pi^- \pi^+ n$ at 17.2 GeV*, *Nucl.Phys.* **B100** (1975) 205.

[356] D. H. Cohen, D. Ayres, R. Diebold, S. Kramer, A. Pawlicki, *et. al.*, *Amplitude Analysis of the $K^- K^+$ System Produced in the Reactions $\pi^- p \to K^- K^+ n$ and $\pi^+ n \to K^- K^+ p$ at 6 GeV/c*, *Phys.Rev.* **D22** (1980) 2595.

[357] A. Etkin *et. al.*, *Amplitude Analysis of the $K^0_S K^0_S$ System Produced in the Reaction $\pi^- p \to K^0_S K^0_S n$ at 23 GeV/c*, *Phys. Rev.* **D25** (1982) 1786.

[358] B. Ananthanarayan, P. Buettiker, and B. Moussallam, *πK sum rules and the SU(3) chiral expansion*, *Eur.Phys.J.* **C22** (2001) 133–148, [hep-ph/0106230].

[359] P. Estabrooks, R. Carnegie, A. D. Martin, W. Dunwoodie, T. Lasinski, *et. al.*, *Study of $K\pi$ Scattering Using the Reactions $K^\pm p \to K^\pm \pi^+ n$ and $K^\pm p \to K^\pm \pi^- \Delta^{++}$ at 13 GeV/c*, *Nucl.Phys.* **B133** (1978) 490.

[360] S. Lindenbaum and R. Longacre, *Coupled channel analysis of J(PC) = 0++ and 2++ isoscalar mesons with masses below 2 GeV*, *Phys.Lett.* **B274** (1992) 492–497.

[361] W. Wetzel, K. Freudenreich, F. Gentit, P. Muhlemann, W. Beusch, *et. al.*, *A Study of $\pi\pi \to K\bar{K}$ Using an Experiment on $\pi^- p \to K^0_S K^0_S n$ at 8.9 GeV/c*, *Nucl.Phys.* **B115** (1976) 208.

[362] R. Kaminski, L. Lesniak, and K. Rybicki, *Separation of S-wave pseudoscalar and pseudovector amplitudes in $\pi^- p$(pol.) $\to \pi^+ \pi^- n$ reaction on polarized target*, *Z. Phys.* **C74** (1997) 79–91, [hep-ph/9606362].

[363] **CLEO** Collaboration, S. Anderson *et. al.*, *Hadronic structure in the decay $\tau^- \to \pi^- \pi^0 \nu_\tau$* , *Phys.Rev.* **D61** (2000) 112002, [hep-ex/9910046].

[364] N. Hedegaard-Jensen, *A Phenomenological Investigation of $\pi + \pi \to K + \bar{K}$ Partial Wave Amplitudes from Hyperbolic Dispersion Relations*, *Nucl.Phys.* **B77** (1974) 173.

[365] J. Gasser and G. Wanders, *One channel Roy equations revisited*, *Eur.Phys.J.* **C10** (1999) 159–173, [hep-ph/9903443].

[366] G. Wanders, *The Role of the input in Roy's equations for $\pi\pi$ scattering*, *Eur.Phys.J.* **C17** (2000) 323–336, [hep-ph/0005042].

[367] A. Schenk, *Absorption and dispersion of pions at finite temperature*, *Nucl.Phys.* **B363** (1991) 97–116.

[368] S. R. Beane, K. Orginos, and M. J. Savage, *Hadronic Interactions from Lattice QCD*, *Int. J. Mod. Phys.* **E17** (2008) 1157–1218, [arXiv:0805.4629].

[369] V. Bernard, N. Kaiser, and U. G. Meißner, *πK scattering in chiral perturbation theory to one loop*, *Nucl.Phys.* **B357** (1991) 129–152.

[370] S. Deser, M. Goldberger, K. Baumann, and W. E. Thirring, *Energy level displacements in pi mesonic atoms*, *Phys.Rev.* **96** (1954) 774–776.

[371] **Belle** Collaboration, D. Epifanov *et. al.*, *Study of $\tau \to K_S \pi^- \nu_\tau$ decay at Belle*, *Phys. Lett.* **B654** (2007) 65–73, [arXiv:0706.2231].

[372] C. Lang and W. Porod, *Symmetry breaking and the πK amplitudes in the unphysical region*, *Phys.Rev.* **D21** (1980) 1295.

[373] T. Cheng and R. F. Dashen, *Is SU(2) x SU(2) a better symmetry than SU(3)?*, *Phys.Rev.Lett.* **26** (1971) 594.

[374] J. Gasser and M. E. Sainio, *Sigma term physics*, hep-ph/0002283.

[375] V. Bernard, N. Kaiser, and U. G. Meißner, *Threshold parameters of πK scattering in QCD*, *Phys.Rev.* **D43** (1991) 2757–2760.

[376] C. Riggenbach, J. Gasser, J. F. Donoghue, and B. R. Holstein, *Chiral symmetry and the large N_c limit in $K_{\ell 4}$ decays*, *Phys.Rev.* **D43** (1991) 127–139.

[377] J. Bijnens, *$K_{\ell 4}$ and the low-energy expansion*, *Nucl.Phys.* **B337** (1990) 635.

[378] **ALEPH** Collaboration, R. Barate *et. al.*, *Study of tau decays involving kaons, spectral functions and determination of the strange quark mass*, *Eur.Phys.J.* **C11** (1999) 599–618, [hep-ex/9903015].

[379] **OPAL** Collaboration, G. Abbiendi *et. al.*, *Measurement of the strange spectral function in hadronic tau decays*, *Eur.Phys.J.* **C35** (2004) 437–455, [hep-ex/0406007].

[380] **BABAR** Collaboration, B. Aubert *et. al.*, *Measurement of the $\tau^- \to K^- \pi^0 \nu_{tau}$ branching fraction*, *Phys.Rev.* **D76** (2007) 051104, [arXiv:0707.2922].

[381] B. Moussallam, *Analyticity constraints on the strangeness changing vector current and applications to $\tau \to K\pi\nu_\tau, \tau \to K\pi\pi\nu_\tau$", journal =, .*

[382] M. Jamin, A. Pich, and J. Portoles, *Spectral distribution for the decay $\tau \to \nu_\tau K\pi$*, *Phys.Lett.* **B640** (2006) 176–181, [hep-ph/0605096].

[383] D. Boito, R. Escribano, and M. Jamin, *$K\pi$ vector form factor constrained by $\tau \to K\, pi\nu_\tau$ and K_{l3} decays*, *JHEP* **1009** (2010) 031, [arXiv:1007.1858].

[384] M. Jamin, J. A. Oller, and A. Pich, *S-wave $K\pi$ scattering in chiral perturbation theory with resonances*, *Nucl.Phys.* **B587** (2000) 331–362, [hep-ph/0006045].

[385] M. Jamin, J. Oller, and A. Pich, *Scalar $K\pi$ form factor and light quark masses*, *Phys.Rev.* **D74** (2006) 074009, [hep-ph/0605095].

[386] **NA48** Collaboration, A. Lai *et. al.*, *Measurement of K^0_{e3} form-factors*, *Phys.Lett.* **B604** (2004) 1–10, [hep-ex/0410065].

[387] **KLOE** Collaboration, F. Ambrosino *et. al.*, *Measurement of the form-factor slopes for the decay $K_L \to \pi^\pm e^\mp \nu$ with the KLOE detector*, *Phys.Lett.* **B636** (2006) 166–172, [hep-ex/0601038].

[388] **KTeV** Collaboration, E. Abouzaid *et. al.*, *Improved $K_L \to \pi^\pm e^\mp \nu$ form factor and phase space integral with reduced model uncertainty*, *Phys.Rev.* **D74** (2006) 097101, [hep-ex/0608058].

[389] **FlaviaNet Kaon Working Group** Collaboration, B. Sciascia, *Precision tests of the SM with leptonic and semileptonic kaon decays*, *Nucl.Phys.Proc.Suppl.* **181-182** (2008) 83–88, [arXiv:0812.1112].

[390] C. L. Lee, M. Lu, and M. B. Wise, *B_{l4} and D_{l4} decay*, *Phys.Rev.* **D46** (1992) 5040–5048.

[391] B. Ananthanarayan and K. Shivaraj, *Comment on evidence for new interference phenomena in the decay $D^+ \to K^-\pi^+\mu^+\nu$*, *Phys.Lett.* **B628** (2005) 223–227, [hep-ph/0508116].

[392] **FOCUS** Collaboration, J. Link *et. al.*, *Evidence for new interference phenomena in the decay $D^+ \to K^-\pi^+\mu^+\nu$*, *Phys.Lett.* **B535** (2002) 43–51, [hep-ex/0203031].

[393] **FOCUS** Collaboration, J. Link *et. al.*, *Analysis of the semileptonic decay $D^0 \to \bar{K}^0\pi^-\mu^+\nu$*, *Phys.Lett.* **B607** (2005) 67–77, [hep-ex/0410067].

[394] **FOCUS** Collaboration, J. Link *et. al.*, *A Non-parametric approach to the $D^+ \to \bar{K}^{*0}\mu^+\nu$ form-factors*, *Phys.Lett.* **B633** (2006) 183–189, [hep-ex/0509027].

[395] **CLEO** Collaboration, M. Shepherd *et. al.*, *Model independent measurement of form-factors in the decay $D^+ \to K^-\pi^+e^+\nu_e$*, *Phys.Rev.* **D74** (2006) 052001, [hep-ex/0606010].

[396] **CLEO** Collaboration, R. Briere *et. al.*, *Analysis of $D^+ \to K^-\pi^+e^+\nu_e$ and $D^+ \to K^-\pi^+\mu^+\nu_\mu$ Semileptonic Decays*, *Phys.Rev.* **D81** (2010) 112001, [arXiv:1004.1954].

[397] J. Firmino da Costa, *Study of the semileptonic decay $D^+ \to K^-\pi^+e^+\nu_e$ with the BaBar experiment*, . PhD. Thesis (Advisor: Patrick Roudeau).

[398] **The BABAR** Collaboration, P. del Amo Sanchez *et. al.*, *Analysis of the $D^+ \to K^-\pi^+e^+\nu_e$ decay channel*, *Phys.Rev.* **D83** (2011) 072001, [arXiv:1012.1810].

[399] D. Asner, T. Barnes, J. Bian, I. Bigi, N. Brambilla, *et. al.*, *Physics at BES-III*, arXiv:0809.1869.

[400] H. Zheng, Z. Zhou, G. Qin, Z. Xiao, J. Wang, *et. al.*, *The κ resonance in s wave πK scatterings*, *Nucl.Phys.* **A733** (2004) 235–261, [hep-ph/0310293].

[401] **E791** Collaboration, E. Aitala *et. al.*, *Dalitz plot analysis of the decay $D^+ \to K^-\pi^+\pi^+$ and indication of a low-mass scalar $K\pi$ resonance*, *Phys.Rev.Lett.* **89** (2002) 121801, [hep-ex/0204018].

[402] D. Bugg, *The κ in $J/\psi \to K^+\pi^-K^-\pi^+$*, *Eur.Phys.J.* **A25** (2005) 107–114, [hep-ex/0510026].

[403] D. Bugg, *The Kappa in E791 data for $D \to K\pi\pi$*, *Phys.Lett.* **B632** (2006) 471–474, [hep-ex/0510019].

[404] **BES** Collaboration, M. Ablikim *et. al.*, *The σ pole in $J/\psi \to \omega\pi^+\pi^-$*, *Phys.Lett.* **B598** (2004) 149–158, [hep-ex/0406038].

[405] S. Ishida, M. Ishida, T. Ishida, K. Takamatsu, and T. Tsuru, *Analysis of $K\pi$ scattering phase shift and existence of $\kappa(900)$ particle*, *Prog.Theor.Phys.* **98** (1997) 621–629, [hep-ph/9705437].

[406] R. L. Jaffe, *Multi-Quark Hadrons. 1. The Phenomenology of (2 Quark 2 anti-Quark) Mesons*, *Phys.Rev.* **D15** (1977) 267.

[407] L. Maiani, F. Piccinini, A. Polosa, and V. Riquer, *A New look at scalar mesons*, *Phys.Rev.Lett.* **93** (2004) 212002, [hep-ph/0407017].

[408] J. Charles, A. Hocker, H. Lacker, F. Le Diberder, and S. T'Jampens, *Bayesian statistics at work: The Troublesome extraction of the CKM phase α*, hep-ph/0607246.

[409] J. Charles, A. Hocker, H. Lacker, F. Le Diberder, and S. T'Jampens, *Reply to: 'Improved determination of the CKM angle α from $B \to \pi\pi$ decays'*, hep-ph/0703073.

[410] **UTfit** Collaboration, M. Bona *et. al.*, *Improved Determination of the CKM Angle α from $B \to \pi\pi$ decays*, *Phys.Rev.* **D76** (2007) 014015, [hep-ph/0701204].

[411] **UTfit** Collaboration, A. Bevan *et. al.*, *Update of the Unitarity Triangle Analysis*, *PoS* **ICHEP2010** (2010) 270, [arXiv:1010.5089].

[412] J. Kambor, J. H. Missimer, and D. Wyler, *$K \to 2\pi$ and $K \to 3\pi$ decays in next-to-leading order chiral perturbation theory*, *Phys.Lett.* **B261** (1991) 496–503.

[413] J. Bijnens, P. Dhonte, and F. Borg, *$K \to 3\pi$ decays in chiral perturbation theory*, *Nucl.Phys.* **B648** (2003) 317–344, [hep-ph/0205341].

[414] J. Bijnens and F. Borg, *Isospin breaking in $K \to 3\pi$decays III: Bremsstrahlung and fit to experiment*, *Eur.Phys.J.* **C40** (2005) 383–394, [hep-ph/0501163].

[415] J. Bijnens and F. Borg, *Isospin breaking in $K \to 3\pi$ decays. II. Radiative corrections*, *Eur.Phys.J.* **C39** (2005) 347–357, [hep-ph/0410333].

[416] J. Bijnens and F. Borg, *Isospin breaking in $K \to 3\pi$ decays. 1. Strong isospin breaking*, *Nucl.Phys.* **B697** (2004) 319–342, [hep-ph/0405025].

[417] C. Ditsche, B. Kubis, and U.-G. Meißner, *Electromagnetic corrections in $\eta \to 3\pi$ decays*, *Eur.Phys.J.* **C60** (2009) 83–105, [arXiv:0812.0344].

[418] S. P. Schneider, B. Kubis, and C. Ditsche, *Rescattering effects in $\eta \to 3\pi$ decays*, *JHEP* **1102** (2011) 028, [arXiv:1010.3946].

[419] I. Ajinenko, S. Akimenko, G. Britvich, K. Datsko, A. Filin, *et. al.*, *Measurement of the Dalitz plot slope parameters for $K^- \to \pi^0\pi^0\pi^-$ decay using ISTRA+ detector*, *Phys.Lett.* **B567** (2003) 159–166, [hep-ex/0205027].

[420] **KLOE** Collaboration, A. Aloisio *et. al.*, *Measurement of the branching ratio for the decay $K^+ \to \pi^\pm\pi^0\pi^0$ with the KLOE detector*, *Phys.Lett.* **B597** (2004) 139–144, [hep-ex/0307054].

[421] **Crystal Ball Collaboration at MAMI, A2** Collaboration, S. Prakhov *et. al.*, *Measurement of the Slope Parameter alpha for the $\eta \to 3\pi^0$ decay with the Crystal Ball at MAMI-C*, *Phys.Rev.* **C79** (2009) 035204, [arXiv:0812.1999].

[422] **KLOE** Collaboration, F. Ambrosino *et. al.*, *Determination of $\eta \to \pi^+\pi^-\pi^0$ Dalitz plot slopes and asymmetries with the KLOE detector*, *JHEP* **0805** (2008) 006, [arXiv:0801.2642].

[423] B. Kubis and U. G. Meißner, *Baryon form-factors in chiral perturbation theory*, *Eur.Phys.J.* **C18** (2001) 747–756, [hep-ph/0010283].

[424] M. Frink and U.-G. Meißner, *Chiral extrapolations of baryon masses for unquenched three flavor lattice simulations*, *JHEP* **0407** (2004) 028, [hep-lat/0404018].

[425] M. Frink, U.-G. Meißner, and I. Scheller, *Baryon masses, chiral extrapolations, and all that*, *Eur.Phys.J.* **A24** (2005) 395–409, [hep-lat/0501024].

[426] U.-G. Meißner, U. Raha, and A. Rusetsky, *Kaon-nucleon scattering lengths from kaonic deuterium experiments*, *Eur.Phys.J.* **C47** (2006) 473–480, [nucl-th/0603029].

[427] B. Borasoy, U.-G. Meißner, and R. Nissler, *Kp scattering length from scattering experiments*, *Phys.Rev.* **C74** (2006) 055201, [hep-ph/0606108].

[428] A. Lacour, B. Kubis, and U.-G. Meißner, *Hyperon decay form-factors in chiral perturbation theory*, *JHEP* **0710** (2007) 083, [arXiv:0708.3957].

[429] M. Mai, P. C. Bruns, B. Kubis, and U.-G. Meißner, *Aspects of meson-baryon scattering in three and two-flavor chiral perturbation theory*, *Phys.Rev.* **D80** (2009) 094006, [arXiv:0905.2810].

[430] M. Lage, U.-G. Meißner, and A. Rusetsky, *A Method to measure the antikaon-nucleon scattering length in lattice QCD*, *Phys.Lett.* **B681** (2009) 439–443, [arXiv:0905.0069].

[431] V. Cirigliano and I. Rosell, *Two-loop effective theory analysis of $\pi(K) \to e\bar{\nu}_e(\gamma)$ branching ratios*, *Phys.Rev.Lett.* **99** (2007) 231801, [arXiv:0707.3439].

[432] V. Cirigliano, M. Giannotti, and H. Neufeld, *Electromagnetic effects in $K_{\ell 3}$ decays*, *JHEP* **0811** (2008) 006, [arXiv:0807.4507].

[433] G. Burdman, J. Goldman, and D. Wyler, *Radiative leptonic decays of heavy mesons*, *Phys.Rev.* **D51** (1995) 111–117, [hep-ph/9405425].

[434] D. Becirevic, B. Haas, and E. Kou, *Soft Photon Problem in Leptonic B-decays*, *Phys.Lett.* **B681** (2009) 257–263, [arXiv:0907.1845].

[435] W. Marciano and A. Sirlin, *Radiative Corrections to Neutrino Induced Neutral Current Phenomena in the $SU(2)_L \times U(1)$ Theory*, *Phys.Rev.* **D22** (1980) 2695.

[436] **NA62** Collaboration, T. Spadaro, *The NA62 experiment at CERN: status and perspectives*, arXiv:1101.5631.

[437] P. Ramond, *Field Theory. A modern primer.*, *Front.Phys.* **51** (1981) 1–397.

[438] J. Comellas, J. I. Latorre, and J. Taron, *Constraints on chiral perturbation theory parameters from QCD inequalities*, *Phys. Lett.* **B360** (1995) 109–116, [hep-ph/9507258].

[439] I. I. Kogan, A. Kovner, and M. A. Shifman, *Chiral symmetry breaking without bilinear condensates, unbroken axial $Z(N)$ symmetry, and exact QCD inequalities*, *Phys. Rev.* **D59** (1999) 016001, [hep-ph/9807286].

[440] G. 't Hooft, *A Two-Dimensional Model for Mesons*, *Nucl.Phys.* **B75** (1974) 461.

[441] G. Veneziano, *U(1) Without Instantons*, *Nucl.Phys.* **B159** (1979) 213–224.

[442] P. Nath and R. L. Arnowitt, *The U(1) Problem: Current Algebra and the Theta Vacuum*, *Phys.Rev.* **D23** (1981) 473.

[443] S. R. Coleman and E. Witten, *Chiral Symmetry Breakdown in Large N Chromodynamics*, *Phys.Rev.Lett.* **45** (1980) 100.

[444] A. V. Manohar, *Large N QCD*, `hep-ph/9802419`. From 'Probing the Standard Model of Particle Interactions', F. David & R. Gupta eds.

[445] P. Herrera-Siklody, J. Latorre, P. Pascual, and J. Taron, *Chiral effective Lagrangian in the large N_c limit: The Nonet case*, *Nucl.Phys.* **B497** (1997) 345–386, [`hep-ph/9610549`].

[446] P. Herrera-Siklody, J. Latorre, P. Pascual, and J. Taron, *$\eta\eta'$ mixing from $U(3)_L \times U(3)_R$ chiral perturbation theory*, *Phys.Lett.* **B419** (1998) 326–332, [`hep-ph/9710268`].

[447] **RBC Collaboration, UKQCD** Collaboration, R. Mawhinney, *NLO and NNLO chiral fits for 2+1 flavor DWF ensembles*, *PoS* **LAT2009** (2009) 081, [`arXiv:0910.3194`].

[448] W. H. Press, S. A. Teukolsky, W. T. Vetterling, and B. P. Flannery, *Numerical Recipes in FORTRAN: The Art of Scientific Computing*, . Cambridge University Press.